The Hydrology and Hydrogeology of Heron Island, The Great Barrier Reef: Modelling Natural Recharge and Tidal Groundwater Flow in a Coral Cay

A Thesis submitted to the University of Queensland
as a requirement for admission to the degree of

DOCTOR OF PHILOSOPHY

by

Delton Benjamin Chen BE (Hons)

Department of Chemical Engineering
University of Queensland
St. Lucia 4067
Australia
January, 2000

DEDICATION

I dedicate this thesis to Diane.

STATEMENT

The work embodied in this thesis is, to the best of my knowledge and belief, original, except as acknowledged in the text, and has not been submitted for a degree at any university either in whole or in part.

D.B. Chen

ABSTRACT

Heron Island is a coral cay located on a platform reef, Heron Reef, in the southern region of Australia's Great Barrier Reef. Although the island is only 0.2 km^2 in area, it is ecologically significant because it supports a stand of the now uncommon *Pisonia grandis* tree and is a seasonal breeding site for seaturtles and many thousands of seabirds. It also supports concentrated social and economic activity being the site of a tourist resort and a scientific research station. Whilst Heron Island's groundwater is brackish and non-potable, the hydrology and hydrogeology of the island has attracted recent interest from researchers pioneering the study of nutrient dynamics on coral cays (circa 1990) and from government agents concerned with the disposal of treated sewage in the Great Barrier Reef.

Previous research has identified an ecologically-significant store of water-soluble nutrients, particularly nitrates and phosphates, in the cay's soil and groundwater. Most of this nitrate was leached from fresh bird guano that was deposited at the island. To better understand the dynamics of water-soluble nutrients at Heron Island an improved understanding of natural recharge and tidally-influenced groundwater flow is required. This study examines these processes with particular emphasis given to field investigations and the development of conceptual and mathematical models. The study is therefore comprised of two major parts: Part I examines natural recharge hydraulics, and Part II examines tidal groundwater hydraulics.

In Part I, hydrometeorological data, including throughfall, soil moisture levels and soil matric potentials, were collected intensively over a ten month period from an instrumented study site in the *Pisonia grandis* forest. This data, in combination with data obtained from laboratory and field tests on soil samples, are used to estimate the water retention and the unsaturated hydraulic conductivity functions of Heron Island soil at the site. A finite-difference numerical model is developed from Richard's equation and the Moving Mean Slope (MMS) method to simulate non-hysteretic soil-water redistribution in the vertical dimension and thus help interpret the unsaturated hydraulic conductivity functions of the soil.

By applying approximate techniques to the hydrometeorological field data, an estimate of the local hydrologic balance is obtained; including throughfall, soil-water storage, deep drainage, evapotranspiration and surface runoff estimates. This ten-month-long hydrologic balance is used to calibrate a one-dimensional hydrologic model for Heron Island: called the Soil-Water Transport and Evapotranspiration Model (STEM). The STEM model was used to simulate natural recharge as a function of daily rainfall, and as such is applied to a ten-year-long historical rainfall record. The model results are examined at hourly, daily, and yearly time-scales to improve understanding of natural recharge at Heron Island. Because field measurements of natural recharge were beyond the resources of the current study, the accuracy of STEM's predictions is not established and the model is only used interpretatively.

In Part II, groundwater tides at Heron Island and ocean tides at Heron Reef were monitored intensively over a number of weeks using piezometers, pressure transducers and electronic data-logging equipment. The amplitude-decay and phase-shift of the tidal signal are determined for fixed positions in the island's aquifer. The data also indicate that the groundwater movement directly below Heron Island was unconfined and essentially vertical. Analytical and semi-analytical expressions for this type of flow are derived and applied to the field data to estimate the aquifer's effective vertical hydraulic diffusivity at a number of locations. At one location near the shoreline, distortions of the tidal-pressure signal are interpreted as a seawater intrusion process that involves the beach face and the tide over the reef flat.

A conceptual hydrogeological model for Heron Island and Reef is proposed based on the 'dual-aquifer' concept which involves a moderately permeable upper-layer of Holocene-age limestone overlaying a highly permeable lower-layer Pleistocene-age limestone: a concept that is commonly associated with low atoll islands. Further, to validate the conceptual hydrogeological model, a two-dimensional finite-element groundwater model is developed using a general-purpose groundwater transport simulation model (SUTRA). The results of the SUTRA simulations are compared with the field observations made at the centre of the cay to show that the simulations and the conceptual hydrogelogical models are reasonable.

The results of this study will be of interest to hydrologists, hydrogeologists and biogeochemists who study low carbonate islands, and scientists interested in nutrient dynamics in the vadose and phreatic zones at Heron Island. Furthermore, environmental implications are highlighted by the study which should be of interest to island managers. These include: (a) a high potential for nutrient enrichment of the reef ecosystem as a result of disturbing natural groundwater flow, especially in the vicinity of the cay's shoreline, and (b) a low immediate risk associated with the current approach to aquifer-disposal of treated sewage effluent.

PUBLICATIONS ARISING FROM THESIS

Journals

Chen D., and Krol A., (1997). Hydrogeology of Heron Island, Great Barrier Reef, Australia. In: Geology and Hydrogeology of Carbonate Islands, Developments in Sedimentology 54, Elsevier, Amsterdam, 948 pp. Edited by H.L. Vacher and T.M. Quinn.

Conferences

Krol A., Noordink M., Jell J., and Chen D (1992). The Heron Island Groundwater Project. In: National Conference on Environmental Engineering, Gold Coast, Australia, 17-19 June 1992, Reprints of Papers. The Institute of Engineers Australia, National Conference Publication No 92/5.

Chen, D. (1993). Nutrient Dynamics of Heron Island: Groundwater Quality and Movement. Australian Coral Reef Society National Conference, The University of Queensland, Brisbane, 21-22 August 1993.

Chen, D. (1995). Using Tensiometers to Investigate the Water Balance of a Forested Sandy Island: The Heron Island Groundwater Project. Environmental Engineering Postgraduate Conference, The University of Queensland, Brisbane, 3 November 1995.

Unpublished Reports

Noordink, M., A. Krol, and D. Chen (1992). Heron Island Groundwater Programme, status report following field trip 31 January - 9 February 1992. Department of Chemical Engineering, The University of Queensland (for departmental use).

Chen, D. (1992). Heron Island Groundwater Project, groundwater quality status report following field trip 7 March - 19 February 1995. Department of Chemical Engineering, The University of Queensland (for departmental use).

ACKNOWLEDGMENTS

CONTENTS

LIST OF FIGURES

LIST OF TABLES

1. GENERAL INTRODUCTION

1.1 INTRODUCTION

Heron Island (23° 26' S and 15° 57' E) is a coral cay located on the western fringe of Heron Reef - a platform reef situated about 70 km off the east coast of Australia and near the southern limit of Australia's Great Barrier Reef (see Figure 1-1). The cay, despite its modest size (0.2 km^2), supports a variety of flora including a major stand of *Pisonia grandis* trees. It is also an important breeding site for a variety of fauna, including seabirds and sea-turtles, and is currently occupied by a human population of about 300 persons on average. Visitors to the island are mostly resort staff, tourists, scientists and students attracted to the splendour of the reef and the conveniences of P&O's tourist resort (established 1932) and The University of Queensland's scientific research station (established 1951).

Groundwater at Heron Island is brackish, non-potable and receives natural recharge and anthropogenic waste-waters (Chen and Krol, 1997). This groundwater has attracted the attention of scientists interested in nutrient capital and dynamics at the island (e.g., Charley et al., 1990) and the environmental impacts of treated-sewage disposal in the Great Barrier Reef (Chen and Krol, 1997). Previous research conducted by Charley et al. (1990) and Chen and Krol (1997) shows that the island's vadose and phreatic zones contain an 'ecologically significant' store of water-soluble nutrients, but lacking from these studies is a general description of nutrient transport in the reef-cay system. This is due, in part, to a lack of knowledge regarding water movement in the island's soil and aquifer (a carrier of soluble nutrients). Original knowledge provided herein includes the first detailed description of Heron Island's hydrology and hydrogeology (Parts I and II, respectively) with balanced attention given to natural recharge dynamics and tidal groundwater hydraulics. Novel aspects of the work include the detailed monitoring and modelling of unsaturated soil-water movement and tidal groundwater flow in a coral cay. Implications for nutrient transport are discussed in a concluding chapter.
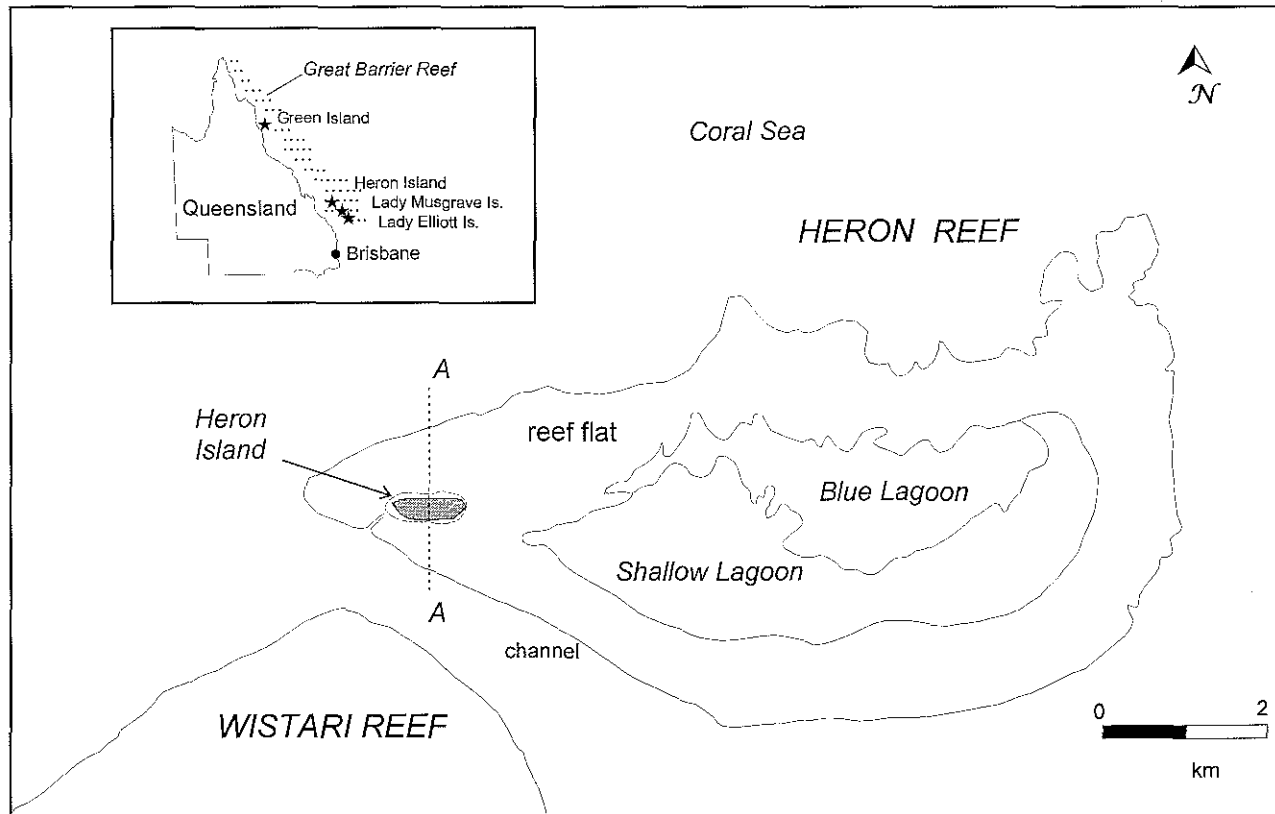
Figure 1-1. Heron Reef and locality map (see inset).

1.1.1 Introduction to Part I: The Hydrologic Study

The natural recharge rate, G, is usually of great interest for islands where a potable groundwater resource occurs and is utilised by local communities. Quite different is the situation at Heron Island where groundwater is brackish and is not utilised by man. The current study of recharge at Heron Island is related to scientific interest in groundwater dynamics and associated transport of dissolved nutrients through the aquifer and its potential impact on the surrounding reef ecosystem (Krol et al., 1992). Recharge introduces water and solutes to the aquifer and thus could affect groundwater chemistry, density and movement. In particular, recharge at Heron Island is known to be a major carrier of nitrates from fresh bird guano to the aquifer (Charley et al., 1990; Staunton Smith, 1992). The degree to which recharge influences the groundwater system is difficult to determine without first estimating its long-term rate: the main topic of Part I of the study.

A broader scientific justification for the current research is that natural recharge in low carbonate islands, including carbonate atoll islands, is critical in controlling the size and shape of freshwater lenses (Underwood, 1990). The hydrodynamics of the vadose zone at Heron Island may have implications for resource estimation on atoll islands assuming major hydrogeological similarities exist. Natural recharge on atoll islands is poorly described due to difficulties with its observation and measurement (Chapman, 1985; Carpenter and Margos, 1989). Underwood (1990, page 36) further assumes that the recharge hydrodynamics on atoll islands is probably not important due to the shallow depth and sandy composition of atoll soils:

"There have been no studies reported on unsaturated flow in atoll islands, but the unsaturated zone in atoll islands typically is only a few meters thick and is not thought to be a complicating factor in ground-water recharge".

Because the current study attempts to describe the process of natural recharge at Heron Island (a coral cay) it will also help to improve understanding of natural

recharge dynamics in low-lying atoll islands that have a soil structure similar to Heron Island's.

To help satisfy the objectives of this study, the direct and accurate *in situ* measurement of the recharge rate (G) was sought. However, at the time of the study, such measurements were beyond reach due to technical and logistical constraints. This being a common problem, hydrologists often resort to estimating average annual G indirectly from the hydrologic balance (eg, Falkland, 1991):

$$\overline{G} = \overline{P} - \overline{E_t} - \overline{R} \qquad : \overline{R} = 0 \qquad \textbf{(Equation 1-1)}$$

where $\overline{G}$, $\overline{P}$, $\overline{E_t}$ and $\overline{R}$ are the average annual recharge, precipitation, evapotranspiration and surface runoff, respectively. By applying Equation 1-1 to low-lying sedimentary carbonate islands it is generally assumed that surface infiltration is uniform, that soil-water storage change is negligible (on a yearly basis), and that $\overline{R}$ is negligible (eg, Anthony et al., 1989; Underwood, 1990). Whilst these assumptions may be intuitive for low carbonate islands in certain climates, evidence supporting them is often scant. The application of Equation 1-1 may ignore important spatial and temporal properties of soil-water redistribution in the vadose zone and the statistical irregularities of the soil-plant-atmosphere continuum.

Shallow soils of vegetated low carbonate islands (such as Heron Island) also contain organic material and that may be significantly less permeable than clean coral sediment. Consequently, surface water ponding and surface runoff on vegetated low carbonate islands could be significant. Rainfall is also more irregular in some sub-tropical regions of the Pacific (such as at Heron Reef) due to the irregular occurrence of tropical storms and cyclones (Nolan & Cameron, 1989). Intense and irregular rainfall tends to increase surface ponding and runoff during individual rainfall events and on an annual basis. Hence there exists conceptual uncertainty regarding the application of Equation 1-1 to Heron Island and possibly elsewhere.

Another major hindrance to the application of Equation 1-1 is the fact that it is difficult and often impossible to measure evapotranspiration (Et) in the field to the accuracy often required by hydrologists (Stewart, 1984). Because of this problem, empirical equations which relate $\overline{G}$, to standard meteorological data are often used. Consider for example (Falkland, 1991):

$$\overline{G} = A\overline{P}$$ (Equation 1-2)

where A is an empirical averaging factor that accounts for surface runoff and evapotranspiration.

Rather than employing empirical equations (eg, Equation1-2) which do little to enhance our understanding of physical processes, an attempt was made to investigate natural recharge at Heron Island by tensiometry. The overall approach of Part I is to develop a finite-difference model for groundwater recharge by combining a published algorithm for vertical unsaturated fluid flow with empirical sub-models for the soil's unsaturated moisture-pressure relationship, the soil's unsaturated hydraulic conductivity relationship, surface runoff, evapotranspiration, infiltration and surface ponding. The model is calibrated from field data and then used interpretively to provide new information on the timing and magnitude of natural recharge at Heron Island. Whilst the approach is data intensive, the resulting model has on-going scientific value as a mathematical tool.

1.1.2 Introduction Part II: The Hydrogeologic Study

The primary goals of Part II are to provide the first reliable conceptual hydrogeological model of Heron Island and Reef, and to provide the first deterministic tidal groundwater flow model for Heron Island. The tidal nature of groundwater flow was identified in previous groundwater investigations by Charley et al. (1990) and Krol et al. (1991). These researchers show that groundwater movement at Heron Island is influenced by the ocean tide but fail to explain the major trends

evident in their field data: such as a general increase in strength and decrease in lag of the tidal pressure-signal with depth below the water-table.

As a prelude to the field investigations, the governing differential equations for groundwater flow are outlined and the literature on reef-island groundwater models are reviewed. From the literature it is found that some rather fundamental hydrogeological concepts pertaining to tidally affected groundwater flow in low carbonate atoll islands may be applied to Heron Reef.

In the current study, electronic water-level sensors and automated data recorders were used to obtain time-series piezometric data that are considerably more detailed than that previously obtained at Heron Island. A major asset to the current study was the piezometer network installed by Krol et al. (1991). Water-levels in nine piezometer-nests were monitored over periods of greater than 14 days. These water-levels are presented and analysed in Chapter 8.

To help interpret the field data, mathematical models for vertical tidal unconfined groundwater flow (VTUGF) are derived for the first time in Chapter 9 for single- and two-layered aquifers. These models are used to estimate the average vertical hydraulic diffusivity of the Holocene aquifer at the investigation wells. The short-term groundwater hydraulics that were observed at Heron Island are further analysed in Chapter 10 in terms of a 'first-pass' numerical model of groundwater flow in the reef-cay system.

Also investigated is the potential for groundwater and seawater to seep across the shoreline as a result of tidal variations. Any seepage at the shoreline will have implications for groundwater nutrient fluxing into the reef ecosystem. Whilst the groundwater piezometers used in this study were not specifically designed for this purpose, in Chapter 10 some compelling new interpretations are made regarding the hydrogeology of the shoreline and seawater intrusion rates from the previously mentioned field data.

1.2 BACKGROUND TO THE STUDY

1.2.1 Nutrient Enrichment in the Great Barrier Reef

Urban and agricultural runoff are linked to nutrient enrichment in the coastal waters of Australia's Great Barrier Reef (GBR) (Bell & Elmetri, 1995). This is of concern because such nutrient enrichment may eventually lead to eutrophication on a regional scale (e.g., Bell, 1991; Bell & Elmetri, 1995). The relationship between seawater nutrient levels in the GBR and coral reef eutrophication on a large-scale is not adequately understood and is currently a topic of intense scientific research and debate (e.g., Walker, 1991c; Kinsey, 1991). Despite uncertainty in the matter, Bell (1992) suggests that the levels of dissolved orthophosphate (P-PO4) and dissolved inorganic nitrogen (DIN) associated with the onset of such eutrophication are relatively low: 1 μM for DIN and 0.1-0.2 μM for P-PO$_4$. These eutrophication threshold levels are only marginally higher than current mean levels in the outer GBR lagoon: about 0.05-1.0 μM for DIN and about 0.1-0.3 μM for P-PO$_4$ (interpreted from Bell, 1992).

Sea grass beds adjacent to Green Island (16° 45' S, 145° 59' E; see inset of Figure 1-1) have expanded rapidly since 1945 (Hopley, 1982). Although not widely reported in the literature, this is an example of localised eutrophication caused by the ocean discharge of treated-sewage from a tourist resort on a coral cay (Bell, pers. comm., 1997). To help prevent localised eutrophication from occurring in the GBR, government agencies have, in more recent times, imposed water-quality standards on effluent discharges and receiving waters in the Great Barrier Reef Marine Park (Gersekowski, 1992; Woodley, 1989; Henry, 1989).

Heron Island (see Figure 1-1), like Green Island, is a coral cay with a tourist resort. However at Heron Island treated sewage is discharged into the island's aquifer rather than into the sea. Staunton Smith (1992) also showed that nutrient fluxing by the local avian population is much greater than nutrient fluxing by humans. In the avian nutrient cycle, seabirds feed on fish over wide-ranging areas and then concentrate nutrient-rich guano on and around their roosting area (ie, Heron Island) (Charley et al., 1990; Staunton Smith, 1992). Charley et al. (1990) showed that nitrogen (N) species

in guano are leached by rain into the vadose zone and thence into the aquifer. Groundwater monitoring by Charley et al. (1990) and Chen and Krol (1997) show that average groundwater DIN concentrations at Heron Island are very high: typically three orders-of-magnitude greater than the DIN eutrophication threshold level of 1 μM. Chen and Krol (1997) show that average groundwater P-PO$_4$ concentrations are also high: typically one order-of-magnitude greater than the P-PO$_4$ eutrophication threshold level of 0.1-0.2 μM. Charley et al. (1990) and Chen and Krol (1997) suggest that the groundwater P-PO$_4$ concentrations are controlled by mineralisation activity in the limestone aquifer.

From the preliminary investigations of Charley et al. (1990), it is suggested that the fluxing of dissolved nutrients from the beach aquifer to the reef-flat may represent a locally significant source of nutrients for the reef ecosystem. However, Charley et al. (1990) stop short of estimating the actual flow of groundwater and associated nutrients to the reef-flat due to a lack of pertinent field data. Moreover, previous conceptual hydrogeological models of Heron Island are speculative and the potential for groundwater to influence the reef in the vicinity of Heron Island is by-and-large unknown.

1.2.2 Nutrient Dynamics at Heron Island

Heron Island's avian populations vary seasonally; with a great many more birds roosting there during the summer for habitual breeding (Staunton Smith, 1992). Staunton Smith (1992) estimates that 164 000 shearwaters (*Puffinus pacificus*) and white-capped noddies (*Anous minutus*) occupied Heron Island during the peak of the 1992 breeding period. Staunton Smith (1992) further estimates that seabirds delivered, in the form of guano, a gross nutrient load of about 9.8 tonnes of nitrogen (N) per year and 2.0 tonnes of phosphorus (P) per year to the cay surface.

Ammonium (NH$_4^+$) in the fresh guano accounts for about 15% of the total guano-N, with the balance being present in organic form. Significant loss of N from the guano to the atmosphere occurs due to the ammonification of organic N to NH$_4^+$ by bacteria

and the subsequent volatilisation of ammonia (NH_3) (Staunton Smith, 1992). Moisture from rainfall increases bacterial activity in the guano. Under simulated rainfall conditions Staunton Smith (1992) observed a 58% decrease in the total N of fresh guano within 4 days and a 87% decrease within 28 days. However, a considerable portion of NH_4^+ is not volatilised, but is nitrified by bacteria to nitrite ($N-NO_2$) and then to nitrate ($N-NO_3$) (Charley et al., 1991; Chen and Krol, 1997). It appears that most of this $N-NO_3$ is readily leached by rainfall, enters the vadose zone, and is eventually transported to Heron Island's groundwater system (Chen and Krol, 1997).

Shearwaters and white-capped noddies void guano over open waters as well as over land. Staunton Smith (1992), who investigated seawater quality at Heron Reef, found that eutrophication was unlikely although marine nutrient concentrations were extremely variable in space and time. Staunton Smith (1992) further suggests that seasonal changes in avian activity may result in generally lower marine nutrient concentrations in winter.

Heron Island is the site of a tourist resort and research station (see Figure 1-2). At the time of writing, most of the raw sewage produced by the island's inhabitants (about 300 persons on average) was treated to a secondary level at a sewage treatment plant prior to being discharged to the aquifer via soakage trenches located in shallow soil near the centre of the island (see Figure 1-2). A smaller amount of raw sewage was treated in septic tanks prior to being released into the vadose zone. Sludge from the sewage treatment process was dried and either buried on the cay or transported to the mainland for disposal. The sludge from the septic tanks was transported to the mainland for disposal. Nutrient loading to the cay's vadose zone in the form of treated sewage effluent has been estimated to be 300 kg of N and 300 kg of P annually (Staunton Smith, 1992).

Chen and Krol (1997) suggest that the calcium carbonate ($CaCO_3$) of the vadose and saturated zones adsorbed most of the P contained in the anthropogenic waste-water that was discharged into the island. Soil-P profiles obtained by Charley et al. (1991) also indicate that guano-P is leached downward but is generally adsorbed by the

$CaCO_3$ soil. Furthermore, despite the P loading from various sources, observed P-PO$_4$ concentrations in Heron Island's groundwater are of the same order of magnitude as the P-PO$_4$ concentrations found in the ambient groundwaters of other reefs and the interstitial waters of individual corals. Hence, it is suggested by Chen and Krol (1997) that further removal of P from the sewage (ie, tertiary treatment) at Heron Island is unlikely to provide any tangible benefit with regards to nutrient control.

With regards to N and P dynamics, Charley et al. (1990, p.197) describe the island as "...a nutrient sink of high chemical potential within a matrix of general scarcity...". This is more true for P than N because naturally occurring P has a relatively low solubility and is readily adsorbed by $CaCO_3$, whereas naturally occurring N has a relatively high solubility and is not readily adsorbed by $CaCO_3$ (Charley et al., 1990).

1.2.3 The Heron Island Groundwater Project (HIGP)

The Heron Island Groundwater Project (HIGP) is a research study that was initiated by the Department of Chemical Engineering at the University of Queensland in 1991. The HIGP was to investigate the significance of natural and anthropogenic nutrients at Heron Island in terms of aquifer storage, groundwater transport and potential for reef eutrophication. The objectives of the HIGP are (adapted from Krol et al., 1992):

1.   To quantify and compare the nutrient loads introduced to the aquifer of Heron Island by the local human and avian populations.

2.   To describe the hydrogeology of Heron Island. This includes the development of conceptual and numeric models for groundwater movement and groundwater-solute transport as they apply to Objectives 3 and 4.

3.   To quantify the nutrient fluxing into the marine environment from the cay's aquifer, and to evaluate the potential impact of these nutrient fluxes on the marine ecosystem.

4.   To review the rationale for waste-water treatment and disposal at Heron Island, with particular reference to potential environmental impacts.

The aims and objectives of this study partially address Objective 2 of the HIGP. Due to the relevance of this study to the HIGP, some of the issues raised by the HIGP are discussed in Chapter 11. For further information regarding the HIGP, the reader is referred to Krol et al. (1992).

1.2.4 Groundwater Investigation Wells and Nested Piezometers

Thirteen groundwater investigation wells with a total of 44 piezometers were installed at Heron Island in 1991 for the HIGP (Krol et al., 1992). The wells were designed to facilitate groundwater sampling and to provide information on groundwater dynamics. The following account of the installation is adapted from Krol et al. (1992):-

> The drilling of the groundwater investigations wells at Heron Island was carried out in 1991 by Afrac Drilling Pty Ltd using a truck mounted Jacro 200 top drive rotary rig powered by a 1600 cc Volkswagen engine. During the first stage of the drilling, a 5 inch auger was advanced in half-metre steps followed by retraction so that material could be removed. On reaching the water-table, the hole was enlarged using a 6 inch four-way chevron blade bit that received steel casings to a depth of 2-3 metres. Drilling to greater depths involved use of a *tricone* roller bit (without cores beings recovered) or a tungsten carbide triple core *HQ3* (with cores being recovered). A biodegradable mud (Revert) was injected during drilling with the triple core to stabilise the surrounding material. In general, the maximum depth of the drill holes were limited by excessive mud loss which occurred when cavities in the reef rock were encountered. The maximum well depth achieved was -16.7 m RGL (at well #6). The retrieved cores were somewhat mixed and fragmented due to the brittleness of the reef rock and intermittent layers of unconsolidated sediment. The material that was recovered was not described in any great detail, although sediment samples were sieved for particle-sizing.

Either 2, 3 or 4 piezometers were installed into each hole immediately after drilling. Each piezometer was constructed from 25 mm diameter Class 9 PVC tube with the bottom 20 cm slotted to allow free interchange with the groundwater at a discrete level in the aquifer. Each of these slotted sections of tubing was wrapped in a fibreglass screen and packed in a cell of washed river sand. The top and bottom of most of the sand cells were capped by bentonite clay to limit the vertical region of the aquifer from which groundwater was to be sampled. The piezometers nearest the water-table of each piezometer-nest were constructed so that water-table heads could be measured. This was achieved by capping the sand cells of these piezometers from below only. Due to installation variations, the thickness of the sand cells varied from 50 cm to 2.3 m. When not in use, the tops of the piezometers were covered with PVC caps to reduce the risk of nutrient contamination. Each cap had air-holes to allow the interchange of air associated with changing water-levels in the piezometers. The exposed ends of each piezometer-nest was physically protected by a steel collar and steel lid which was locked when not in use.

Overall, the positioning of the piezometers was such that a 3-dimensional network of piezometers was constructed comprising two irregular transects across the cay: one running approximately east-west and one running approximately north-south (see Figure 1-2). Wells #1, #2, #4, and #7 were located in the Heron Island Research Station lease, wells #5, #8, #9, and #10 were located in the P&O resort lease, and wells #3, #6, #11, #12 and #13 were located in the Australian National Parks and Wildlife reserve (see Figure 1-2). Wells #4, #5 and #7 were located near the waste-water soakage trench.

1.3 GEOGRAPHIC SETTING

The Great Barrier Reef Marine Park (GBRMP) extends from 9° 15' S to 24° 7' S, and encompasses an area of 344 000 km^2 (Hopley, 1997). Within the GBRMP are about 2900 individual reefs and about 750 fringing reefs (Hopley, 1997). Associated with these reefs are more than 300 sedimentary islands, although about 160 of these are only ephemeral cays or submerging sandbanks. Reef islands of the GBR have been classified into four main types by Hopley et al. (1989): unvegetated cays, vegetated sand cays, vegetated shingle cays and low wooded islands, of which there are 213, 40, 3 and 44, respectively. Only 25 coral cays are found south of 18°S, and Heron Island at latitude 23° 26' S and longitude 151° 57' E is one of these.

Heron Island is a vegetated sand cay that is supported by a platform reef, Heron Reef (see Figure 1-1). In relation to its host reef, Heron Island is only a minor morphological feature: a sedimentary deposit of reef-detritus stabilised by vegetation and beachrock. Heron Island is roughly oval-shaped with a supra-tidal area of 0.20 km^2 and a maximum lateral dimension of about 850 m (orientated east-west; see Figure 1-3). It is much smaller than its host reef which has a plan area of about 26 km^2 and a maximum lateral dimension of nearly 9 km. The cay itself is located on the leeward (western) margin of Heron Reef, and as such the cay is less than 1 km from the reef edge to the north, west, and south.

Heron Reef is situated in the Coral Sea, about 75 km due-east of the Australian coastline and is close to the Tropic of Capricorn (23° 26.5' S). Heron Reef is also a neighbour to 21 other major reefs and a number of shoals. These reefs and shoals comprise the Capricorn Group, the Bunker Group and Lady Elliott Reef: the most southerly group of reefs in the GBR system.
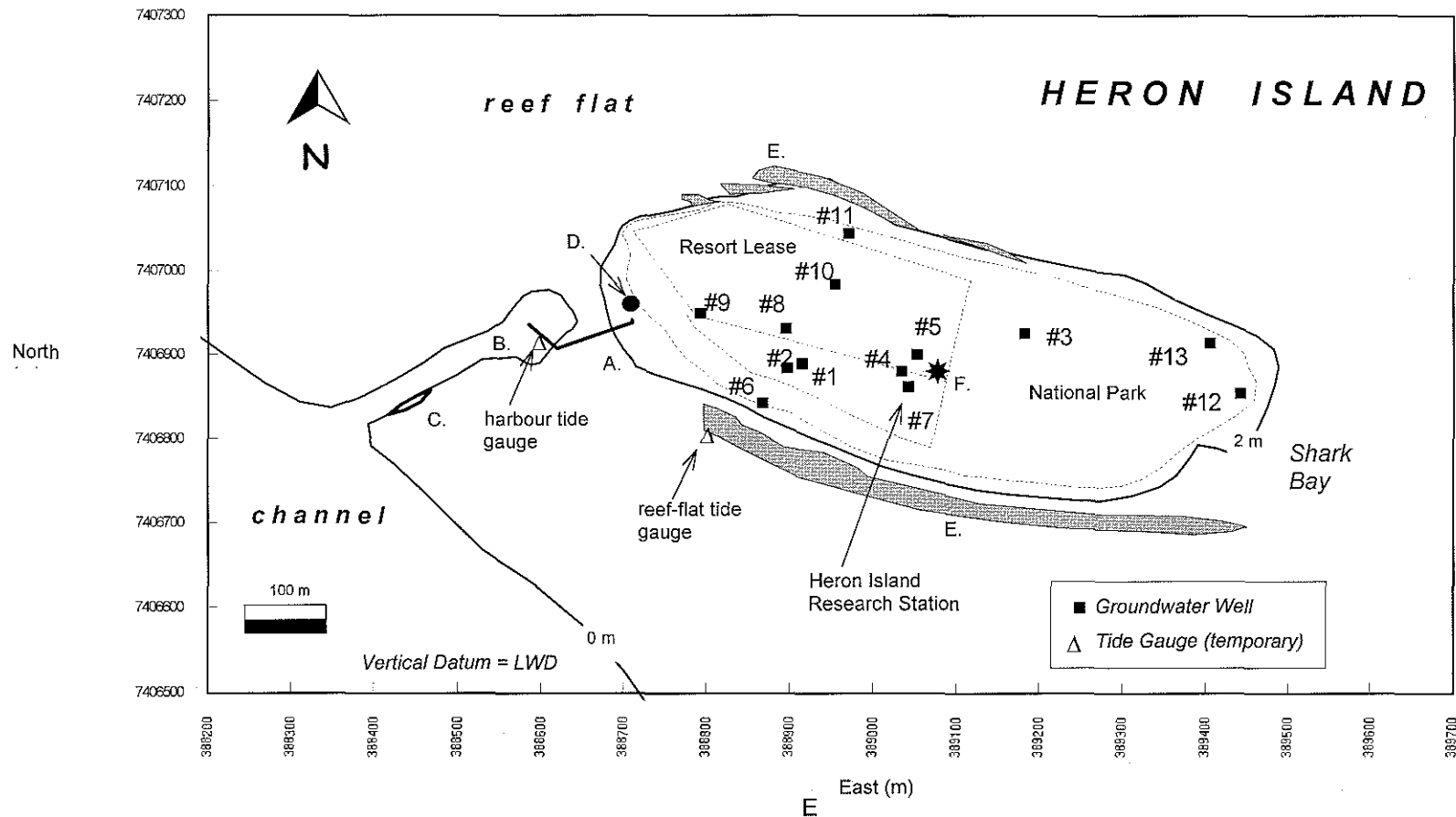
Figure 1-2. Heron Island land-use, groundwater investigation wells and temporary tide gauges (KEY: A, jetty; B, harbour; C, shipwreck; D, helipad and survey benchmark PSM61221; E, beachrock; F, sewage treatment plant).
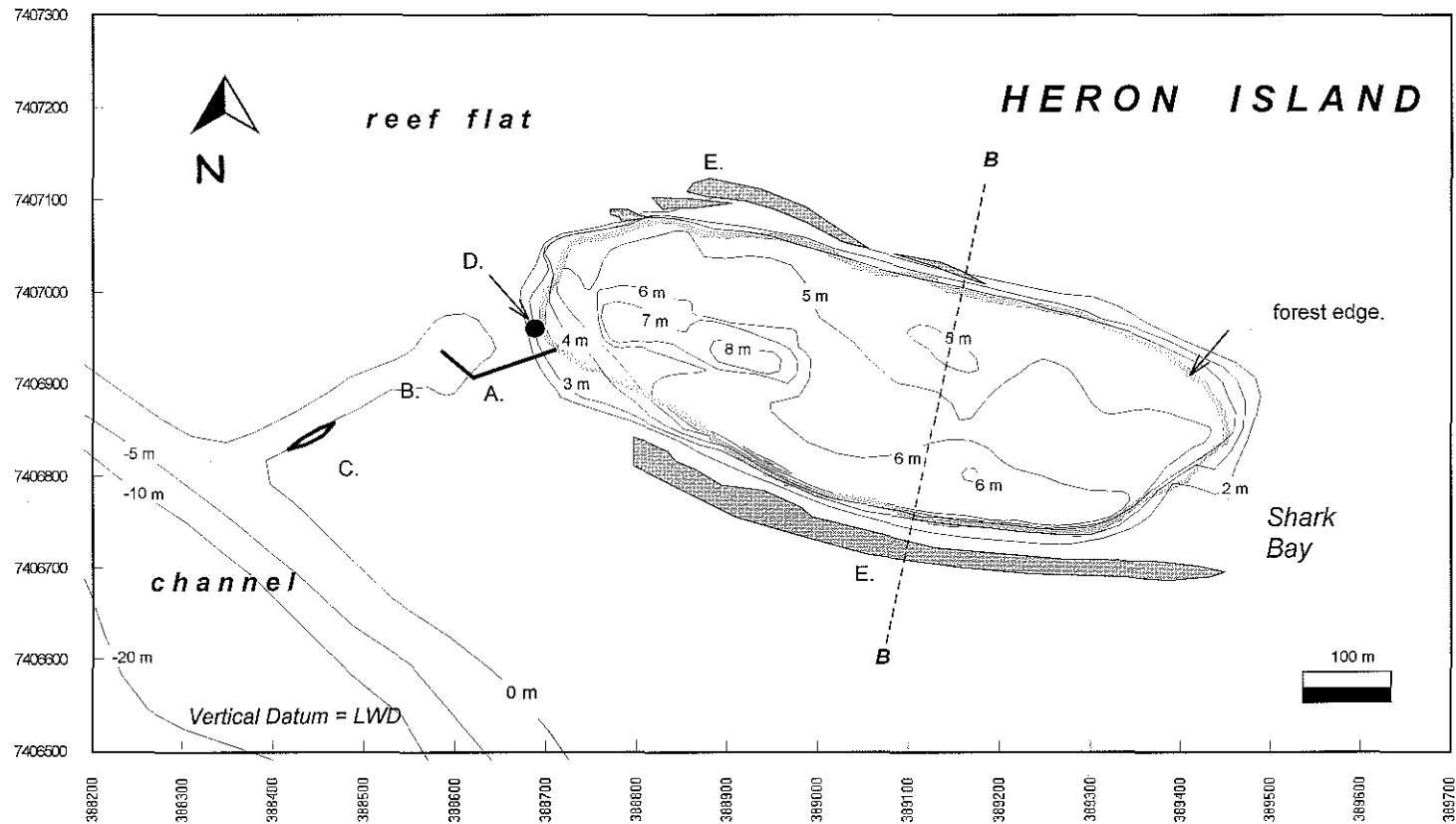
Figure 1-3. Heron Island topography (KEY: A, jetty; B, harbour; C, shipwreck; D, helipad and survey benchmark PSM61221; E, beachrock).

1.3.1 Climate

Heron Island has a subtropical maritime climate with a seasonal pattern of hot wet summers and warm and moderately dry winters. The average annual rainfall is 1.07 m a^{-1}; most of which falls during the months of January to July (refer Table A-2). Although annual rainfall off the Queensland coastline is greatest in the northern areas, the most variable rainfall occurs between latitudes 18° and 25°S. This variability is due to the occurrence of dry spells and the irregularity of extreme rainfall associated with cyclones and storms. On average 14 cyclones occur per decade within the area bounded by 150°-155°E and 20°-25°S (Lourensz, 1977). ESE to SE winds dominate at Heron Island with more variable N to NW winds also occurring between September and January (Flood, 1986). A further discussion of the island's climate is provided in Chapter 3.

1.3.2 Tide

Ocean tides in the GBR are semi-diurnal. At Heron Reef the tide has an average range of 2.3 m for the spring tide and 1.1 m for the neap tide (QDT, 1991). Further information on tides at Heron Reef is provided in Chapter 8.

1.3.3 Flora and Fauna

Heron Island is ecologically significant in that it is one of Eastern Australia's ten largest nesting sites for the green sea turtle (*Chelonia mydas*) and supports the third largest surviving stand in Australia of a now uncommon tree, the *Pisonia grandis* (Walker, 1991a). During the summer breeding season of 1991-92, Staunton Smith (1992) observed that the island surface and its vegetation provided a habitat for as many as 34 000 wedgetail shearwaters (*Puffinus pacificus*) and 130 000 white-capped noddies (*Anous minutus*). Published estimates of seabird populations for Heron Island indicate that there has been a dramatic increase in arrivals of wedgetail shearwaters and white-capped noddies since the 1930's. The reason for this increase is uncertain, although it has been suggested by Walker (1991a) that previous mass mortalities of

white-capped noddies may have occurred as a consequence of cyclonic activity, epidemics, or predation by introduced species. Although Heron Island still sustains abundant flora and fauna, human occupation over the last seven decades has resulted in substantial ecological degradation.

1.3.4 Human Influence

The island was first occupied in 1925 when a turtle soup factory was established. The closure of the factory in 1928 was followed by the founding of a resort in 1932 (now owned by P&O Resorts Pty Ltd) and a research station in 1951 (The University of Queensland's Heron Island Research Station). To improve access to the island, a boat channel was blasted through the reef in 1945 and was subsequently deepened in 1966 to provide a safe harbour (Hopley, 1982). Sand spoil from the harbour has been used to reclaim land on the western beaches and a retaining wall has been built along the north-western corner to stabilise the resort foreshore. Numerous buildings, water tanks, and unpaved roads have been constructed on the western half of the cay. The eastern half of the island is designated a national park.

Heron Island is a popular tourist destination being one of only four tourist cays in the Great Barrier Reef (GBR): the others are Green Island (16° 45' S, 145° 59' E), Lady Elliott Island (24° 7' S, 152° 43' E) and Lady Musgrave Island (23° 54' S, 152° 23' E). Since the 1960's visitation has tripled, reaching nearly 100 000 user nights per year in 1991. Currently the island supports a human population which averages about 300, about two thirds of which are tourists. Almost all of the food and beverages consumed by the island's inhabitants are imported from the mainland and potable water is provided by the reverse osmosis desalination of seawater. Although roof rainwater is collected and stored in tanks, this water is not considered potable because of contamination by bird guano. Some of this rainwater is mixed with seawater prior to desalination whilst the remainder is either used for irrigation or is saved for emergencies. The island's groundwater does not provide a freshwater resource (Charley et al., 1991; Chen and Krol, 1997).

1.4 GEOLOGIC SETTING

The reef structures of the GBR are mostly discrete carbonate slabs less than 250 m thick and less than 500 000 years of age: quite young in geologic time (Davies, 1992). The geologic structure and climate are major factors controlling coral reef distribution along eastern Queensland. Most of the reefs in the GBR are concentrated on the outer one-third of the continental shelf, in the warm, shallow, oligotrophic waters of the Coral Sea (Hopley, 1982; Hopley, 1997). The Capricorn-Bunker Group is located in an area of the Queensland shelf that is known as the Bunker High. The Bunker High is relatively narrow (about 60 km wide), unrimmed and only 20-40 m below sea level. About 50-70 km to the west of the Bunker High is the Queensland coast. Just to the east of the Bunker High the Queensland shelf slopes down about 300 m into the Capricorn Basin.

Eustatic changes in sea level during the Quaternary period are responsible for profound heterogeneities within the geologic record. It is believed that rising sea levels (ie, transgressions) have resulted in reef build-up, whilst falling sea levels (ie, regressions) have resulted in reef emergence and subaerial erosion. Due to these eustatic fluctuations, the stratigraphic record has become somewhat intermingled, although at certain levels solution unconformities are sharply defined. Solution unconformities may be evidenced by contrasts in chemical composition, mineralogy, colour, porosity, and permeability. In particular, the Pleistocene reef material has been subject to substantial sub-aerial weathering and diagenesis during emergence, whilst the Holocene coral cap is composed mostly of the original reef material that is poorly consolidated and rich in unstable aragonite. Hence, the Holocene-Pleistocene contact is a solution unconformity delineated by rather sharp contrasts in porosity, permeability and aragonite/calcite composition. The geology of the GBR has been complicated by continuous subsidence and warping of the continental shelf (Hopley, 1997).

Most of reef islands in the GBR are less than 5000 years old; corresponding to a stabilisation in sea level off the coast circa 6500 years ago (Hopley, 1997). Reef islands are sedimentary accumulations that rise above the general reef-flat level. Two

periods of Holocene cay development coinciding with different sea levels have been reported for some islands (Hopley, 1997). The sediment is biogenetic calcium carbonate and mostly sand-sized fragments of coralline debris, shells and other skeletal remains, and the tests of *Foraminifera* and *Halimeda* and other plants and animals. For a more detailed account of the geology of reefs in the GBR, the reader is referred to Hopley (1982; 1997).

1.4.1 Geologic Structure

In simple geologic terms, a coral reef is a rigid limestone framework which is formed *in situ* by hermatypic (reef-building) organisms, the most common of which are the scleractinian corals and the carboniferous algae. A usually minor contribution to the total mass of a coral reef is the material chemically precipitated *in situ* and the material transported to the reef from elsewhere. The coral reef framework is mostly dimorphous calcium carbonate ($CaCO_3$) which exists either as calcite (a rhombohedral crystal system) or aragonite (a orthorhombic crystal system). Aragonite may be the original form in which most of the $CaCO_3$ was deposited, especially in shallow waters, converting with time to the more stable calcite (Whitten and Brooks, 1987). Various proportions of the Ca^{2+} cations in the reef have been replaced by magnesium or iron, giving rise to carbonate minerals such as dolomite ($CaMg(CO_3)_2$), magnesite ($MgCO_3$), and siderite ($FeCO_3$). The most common minerals in reef rock are aragonite, high-Mg calcite, and low-Mg calcite (Hopley, 1982).

Deep drilling at Heron Island in 1937 (Richards, 1938; Richards and Hill, 1942) revealed a geologic sequence consisting of calcareous sands, *in situ* reef rock, foraminiferal and quartz sands, and lime muds. Maxwell (1962) generalised this geologic sequence into three zones: shallow reef rock (0-30 m), intermediate reef rock (30-150 m), and subreef sands (150-223 m) (see Figure 1-6). The top 15-20 m of Heron Reef comprises a veneer of Holocene reef growth covering a Pleistocene limestone basement (Jell and Flood, 1977). The pre-Holocene reef rock has experienced a series of eustatic sea-level changes, as is evidenced by mineralogic

alteration, marked cementation, and brown staining. Solution unconformities at 20 m, 35 m, and possibly at 75 m, 95 m, and 140 m were reported by Davies (1974).

Deep drilling operations were also carried out in 1926 to a depth of 183 m in the northern region of the GBR at Michaelmas Cay (Richards and Hill, 1942). Despite the 1000 km distance between Heron Island and Michaelmas Cay, the drill cores retrieved from the two islands were rather similar. At Michaelmas Cay, coralline material was found to a depth of 120 m, whilst at Heron Island coralline material was found to a depth of 150 m. In both instances, the coralline material was poorly lithified, lacked dolomite and was underlain by a foundation of loosely coherent terrigenous sands.

Since 1978, at least 24 other reefs throughout the GBR have been shallow drilled, including One Tree, Fairfax and Fitzroy Islands in the Capricorn-Bunker Group (Davies & Hopley, 1983). Solution unconformities in these reefs of the southern GBR were encountered at depths of 7.4-14.3 m, and were easily delineated on the basis of the appearance of *Halimedia*-rich limestone which is often found in the cavities of the coral framework (Marshall, 1983).

1.4.2 Karst Induced Antecedent Platform Hypothesis

Current thinking is that the morphology of modern reefs is determined by a combination of Holocene growth patterns and Pleistocene karst morphology (Hopley, 1982). Because the Pleistocene foundations have been subject to karst processes during at least one glacial period, they have been subject to (i) case hardening of exposed surfaces and (ii) gradual erosion of flatter and lower-lying surfaces. Certain morphologic features of the Holocene reefs, including saucer-shaped surfaces, raised rims, spur and groove structures and isolated depressions, are therefore likely to be inherited from their Pleistocene foundations (Hopley, 1982).

The karst induced antecedent platform hypothesis is commonly used to explain the conical topography of atolls and the presence of solution rims, deep central lagoons and sink holes (Hopley, 1982). It is believed that during the marine regression, the

steep surfaces of reef edges were more resistant to solution, giving rise to their elevation above more central areas. The hypothesis may be similarly applied to reefs of the Capricorn-Bunker Group where the Pleistocene contact is deeper below lagoonal areas (ie, 13-18 m) as compared with reef flat areas (ie, 6-12 m) (Hopley, 1982).

Much of the antecedent platform morphology of Heron Reef has been masked by Holocene reef growth and by infilling with sediments. This level of reef development appears to lie between the classification of 'mature' and 'senile', as described by Hopley (1982).

1.4.3 Geomorphology

Heron Reef is separated from Wistari Reef by an inter-reef channel (see Figure 1-1). It is not clear how this channel formed, although surface erosion during low sea level periods is a likely explanation. Off the eastern edge of Heron Reef is a submerged shoal: an area of reef which has been drowned during a period of marine transgression. Heron Reef itself has six major physiographic zones (refer Figure 1-1): reef slope, reef flat, reef rim, Shallow Lagoon, Blue Lagoon and Heron Island. The following zone descriptions are adapted from Jell and Flood (1977) and other sources of information:

1. Reef Slope
The reef slope marks the transition between the channel floor and the reef rim. It is steep with gradients between 1:20 and 1:4, and exhibits spur-and-groove structures due to the erosional effects of wave scour and tidal runoff in conjunction with coral growth over karst foundations.

2. Reef Flat

The reef flat is that portion of the reef top which may be exposed during low tides. The surface of the reef flat around Heron Island consists mainly of bioclastic sands and living corals with encrustations of coralline algae.

3. Reef Rim

The reef rim marks the highest part of the intertidal portion of the reef and is generally continuous with only a few channels to the open sea. During low tides, the flow of seawater off the reef is impeded by the topography and surface permeability of the reef rim and reef flat. Dredging of a man-made harbour through the reef and close to the cay has altered the hydrodynamics of the waters around the cay (Gourlay, pers. comm. 1993).

4. Shallow Lagoon

The shallow lagoon has a low-tide water depth of 0.3-1 m. Corals are sparser and smaller than on either the reef flat or the reef rim.

5. Blue Lagoon

The Blue Lagoon makes up the central physiographic unit of Heron Reef. It is delineated by an abrupt increase in water depth to an average of 3.5 m. This lagoon is characterised by numerous small patch reefs and a floor of fine sediment.

6. Heron Island

Heron Island is a sedimentary deposit located at a focal zone of wind-induced waves. Gourlay (1988) explains that the position of the focal zone and the size and shape of the cay are governed primarily by reef size and shape and the direction of prevailing winds and wind-induced waves. Tides modulate the sedimentary processes and vegetative cover and beachrock formations play a further role in trapping and stabilising sediments. The shoreline of Heron Island is dynamic, as is evidenced by observed changes to the cay's shoreline and exposed beachrock formations which outline earlier shorelines (Flood, 1986). According to Flood (1986), decadal-scale oscillations of annual wind-energy vectors are a major factor in shoreline dynamics.
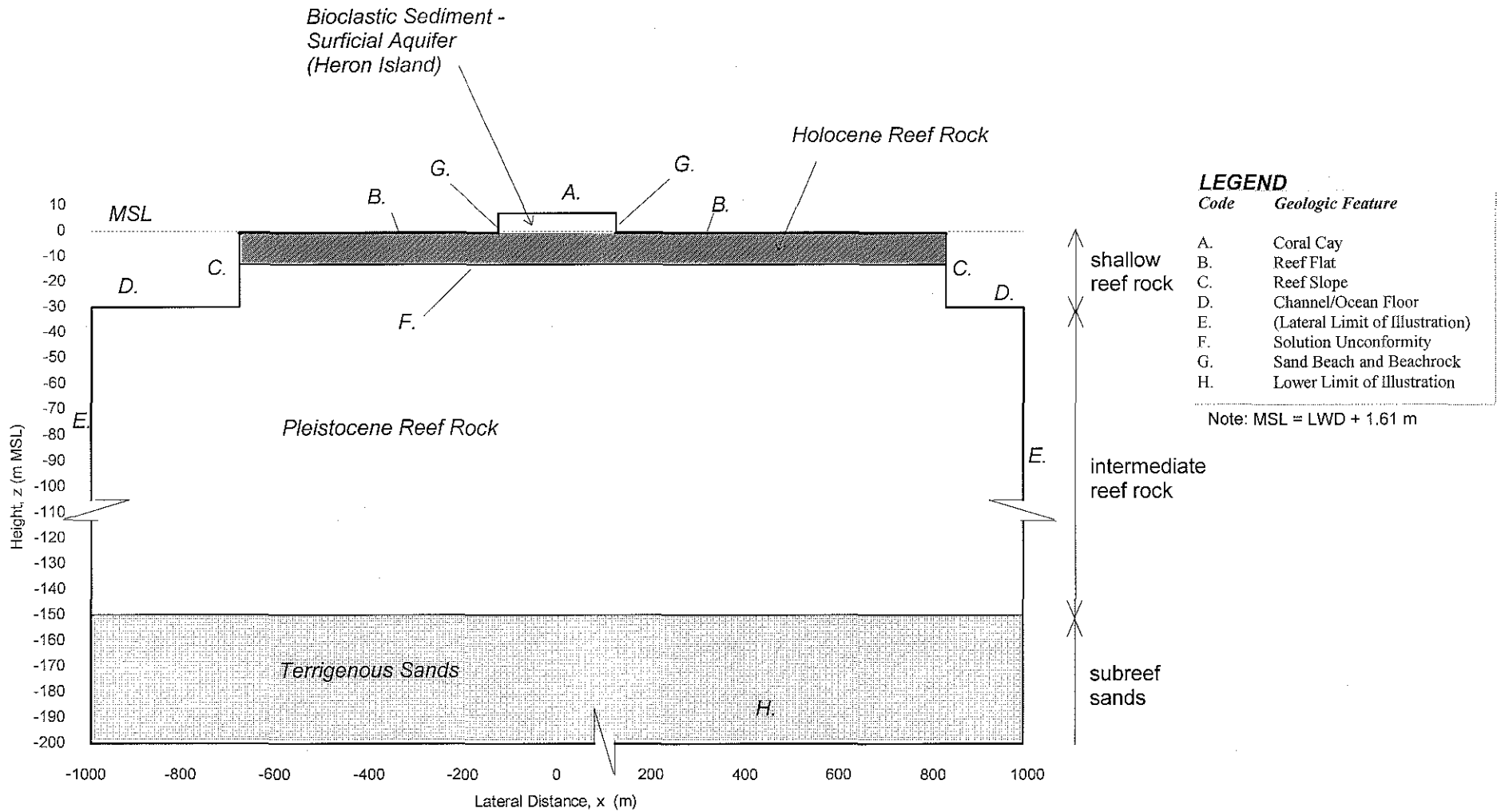
Figure 1-4. The major known stratigraphic units of Heron Reef (after Maxwell (1962); refer section A-A of Figure 1-1).

1.4.4 Stratigraphy

An incomplete picture of Heron Reef's stratigraphy is provided by drill core and other information (see Figures 1-6 and 1-7). There is evidence for at least six major stratigraphic units: (1) beachrock, (2) unconsolidated surficial aquifer (ie, the cay), (3) lagoonal sediment, (4) Holocene reef rock aquifer, (5) Pleistocene reef rock aquifer and (6) a terrigenous sediment foundation. It is hypothesised that a seventh major stratigraphic unit, reef plate, covers the reef-flat at Heron Reef. Reef plate is the upper layer of indurated Holocene-age reef rock that behaves as an impermeable 'cap' or barrier to groundwater flow (see Section 1.5.4.5). An argument for the reef-plate hypothesis is provided in Part II in terms of hydraulic observations and interpretive mathematical modelling.

1.4.4.1 Beachrock

Beachrock is a firmly cemented sedimentary rock that is formed *in situ* by precipitation of $CaCO_3$ from seawater. The mechanisms controlling this precipitation process are still the topic of research and debate, however one popular theory is that the precipitation process is driven by evaporation on the inter-tidal zone (Hopley, 1982). The beachrock at Heron Island is seaward sloping and is mostly found between MHWS and the reef flat. The surface of the beachrock is pitted, probably due to the influence of water chemistry in the intertidal zone. A major factor controlling beachrock formation and geomorphology is the general pattern of sediment migration. Younger beachrock strikes can form either shoreward or seaward of previous strikes, depending on the direction of long-term sediment movement (Coote, 1984).

1.4.4.2 Surficial aquifer

The surficial aquifer is the sand cay above the general level of the reef flat. The surficial aquifer is comprised of cream-coloured and mostly medium-to-coarse grained coralline sediment (bioclastic grainstone devoid of quartz) and very minor amounts of pumice. To investigate the stratigraphy of the surficial aquifer, particle size data from 87 drill samples were analysed for silt-, sand-, and gravel-size fractions and geometric

means and standard deviations as a function of level (see Figures 1-6 and 1-7, respectively). Sieve-sizing of the sand samples was carried out by the Department of Geology at the University of Queensland using the sieve sizes shown in Appendix A. Figure 1-7 shows that the inter-tidal sediments are mostly larger than and not as well sorted as the supra-tidal sediments. From Figures 1-6 and 1-7 and the author's personal observations, it is concluded that Heron Island is comprised of three major stratigraphic units (refer Figure 1-7):

A. Silty-Sand Layer (above -1.0 m RGL; Pisonia grandis rooting zone)
B. Gravelly-Sand Layer (supra-tidal; above 2.5-3 m LWD but below -1.0 m RGL)
C. Sand-and-Gravel Layer (inter-tidal; between about 0.8 m and 2.5-3 m LWD)

The silty-sand layer is a soft, light-brown humic sand with about 0-15% silt-sized material by weight. This layer extends to a depth of about 0.9-1.3 m below ground level in most areas (corresponding to the rooting zone of Pisonia grandis) and is overtopped by a layer of leaf litter. A colour transition, of light brown to creamy-white, indicates the position of the silty-sand layer/gravelly-sand layer interface. The gravelly-sand layer is generally clean, well-sorted, contains as much as 15% by weight gravel-sized sediment (see Figure 1-8), and has a chemical composition of 91-93% $CaCO_3$, 1-5% $MgCO_3$ and 2-3% organic matter by weight (Richards and Hill, 1942).

At about 2.5-3 m LWD, the gravelly-sand layer grades into the sand-and-gravel layer. The sediment in the sand-and-gravel layer is moderately sorted (presumably of beach origin) and is more rounded, whiter, coarser and usually wetter than above. Coral shingle (often as large as 1-3 cm), shells, coralline algae and nodules and some pumice are found in the sand-and- gravel layer. Although the shingle has a strong influence on the particle-size distributions of the inter-tidal sediment (see Figure 1-8), it is not expected to greatly influence the bulk hydraulic properties of the sediment as the pore-size distributions will tend to be controlled by the smaller granular material which can pack around the shingle pieces. Below the level approximately defined by MHWN (2.15 m LWD), there is limited hardening/cementing of sediment, especially

near the shoreline where antecedent beachrock may be present. This hardening is more intensive at greater depths below MHWN.

It should be noted that the samples obtained from below the water table were subject to water flushing during drilling, thus the actual silt-size fractions of these samples may be under-represented. However, the data indicate that the silt fractions of the sand-and-gravel layer are generally less than 0.7% by weight. Hence a naturally low silt content gives confidence in the results despite the possible flushing of the sediment samples during drilling (Krol, pers. commun. 1996).
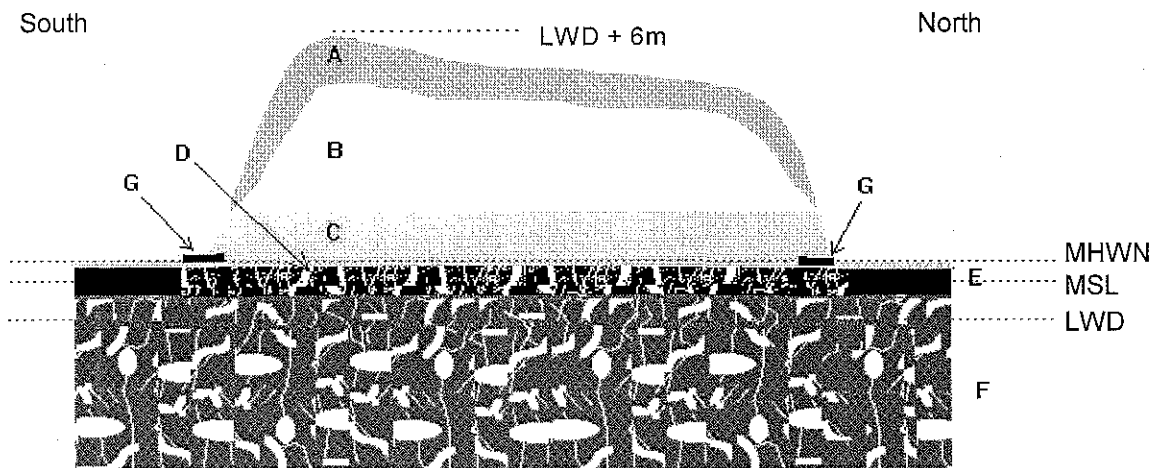
Figure 1-5. Hydrostratigraphic layering of Heron Island: interpreted from particle-size data, bore logs, and the literature (not to scale; refer Section B-B of Figure 1-3)

LEGEND

A. Silty-Sand Layer (*Pisonia grandis* rooting zone; humic material)
B. Gravelly-Sand Layer (medium-to-coarse grained sand; some gravel-sized)
C. Sand-and-Gravel Layer (coral shingle, shells and nodules present)
D. Irregular Layering of Sediment and Limestone (interconnected porosity)
E. Reef Plate (cemented framework of coral, algae and sediment)
F. Reef Rock (interconnected cavities, karst, loose infilling material)
G. Beachrock (geochemically cemented coralline rock; antecedent structures)
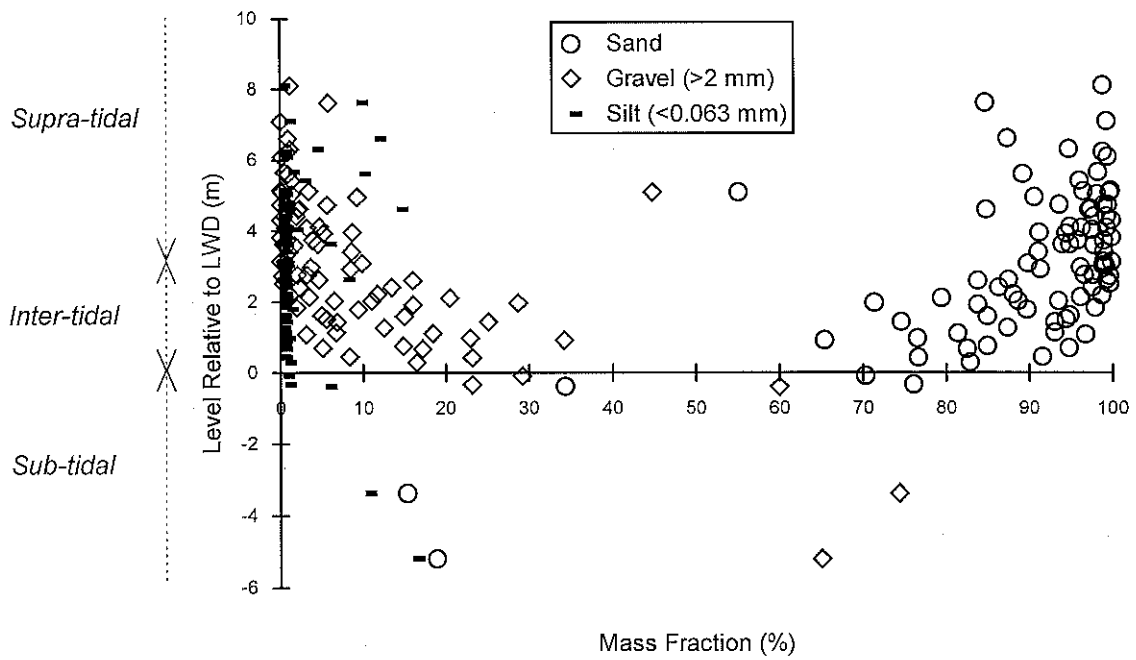
Figure 1-6. Heron Island sand particle size classifications as a function of level.

Geometric Mean Size (mm) or Geometric Standard Deviation (mm)
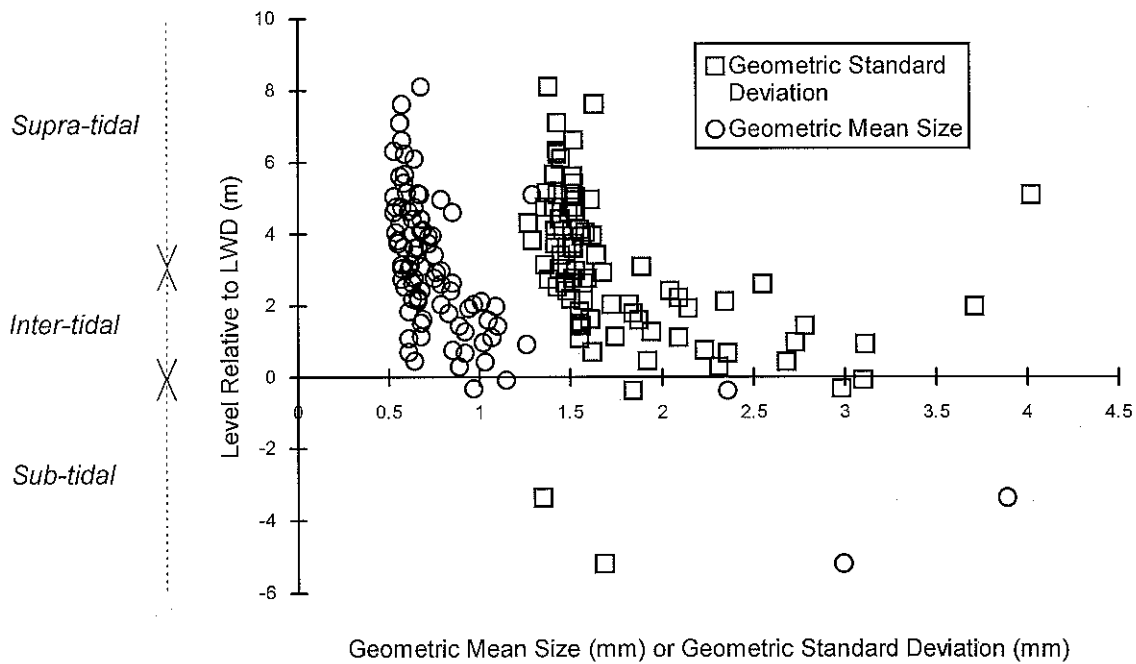
Figure 1-7. Heron Island sand particle size distribution parameters as a function of level.

1.4.4.3 Holocene Reef Rock

The Holocene reef rock beneath Heron Island was drilled and cored at the thirteen sites shown in Figure 1-2 (Krol et al., 1992). Due to the drilling techniques employed, megapores in the reef rock limited the subsurface investigations to depths above about -7±3 m LWD. The reef rock consisted of irregular layers of limestone with thicknesses varying between 0.2 and 2.5 m approximately. Loose material, including gravel- and sand-sized sediment, nodules, shells, and mud, in-filled the layers.

Sediments excavated at Heron Island from the approximate level of the reef flat and below the reef flat were mostly gravel-sized due to the inclusion of loose nodules, shells and coral shingle. It is apparent that the three sub-tidal sediment samples that were taken from well #9 contained some of the highest silt-sized fractions. However, there is scant particle-size data from which to draw conclusions about the sub-tidal sediments. The three sub-tidal sediment samples that were obtained were a silty-sandy gravel consisting of at least 60% by weight gravel-sized material.

The drilling logs of Noordink et al. (1992) describe a transition from irregular hard layers to what appears to be a series of interconnected or large cavities. Although this transition was not always clear, the general trend was that "banded layering with porous vents" and "interconnected cavities and preferential pathways" overtopped cavities. Richard and Hill (1942) encountered a 2-m-thick cavity at Heron Island at a depth of -2.9 m LWD. Marshall & Davies (1982) also found cavities of up to 1 m thick in the Holocene reef of nearby One Tree Reef (23° 30' S, 152° 5' E). This Holocene reef rock of One Tree Reef had an open framework and branching-coral facies, typical of a low-energy or leeward environment. Heron Island, too, is in the leeward margin of its reef, and the predominant corals in the Heron Island borehole were, similarly, the branching Acropora spp. (Richards & Hill, 1942). A high but variable permeability for the Holocene reef rock aquifer is expected due to the presence of megapores and irregular layering.

1.4.4.4 Pleistocene Reef Rock

Richards and Hill (1942) describe the Pleistocene material as being mostly a "soft, porous reef rock", often containing chalky muds and large fragments, and showing some evidence of cementation and cavities. It is believed that the Pleistocene component of the reef aquifer is highly permeable because of solution during sea level lowstands (Hopley, 1982).

1.4.4.5 Reef Plate

As mentioned previously, the internal geology of the reef-flat at Heron Reef was not investigated *in situ* during this study. Nonetheless, it is assumed that reef plate is ubiquitous to the reef flat at Heron Reef on the basis that Holocene age indurated layers are commonly found within or below the reef flats of other reefs (e.g., Lam, 1974; Hunt and Peterson, 1980; Ayers and Vacher, 1986). According to Underwood (1990), indurated layers may include buried beachrock, reef-flat facies and diagenetically lithified layers. Geochemical studies by Boucher (1977) at Barbados show that a processes of cementation can be very active in the upper 1.5 m of Holocene reefs. Boucher (1977) concludes that diagenetic modification within the reef surface involves micritization of skeletal material, deposition of internal sediments, and precipitation of calcite and aragonite cements.

Underwood (1990, p.42) claims that "... reef flat facies (of atolls) most generally have reduced effective porosity and are nearly impermeable, ...". These hard layers, according to Underwood (1990), occur slightly below mean sea level on the ocean sides of atoll islands and can protrude into the interior of atoll islands. Where reef-plate extends into an island aquifer the freshwater lens can be physically affected (e.g., Hunt and Peterson, 1980; Ayers and Vacher, 1986). Studies of platform reefs also show reef-plate to be a relatively impermeable layer. Buddemeier and Oberdorfer (1986) described the reef plate at Davies Reef, GBR, as a 0.5- to 1.5-m-thick layer of cemented corals, coralline algae encrustations, and sediments. According to Buddemeier and Oberdorfer (1986) the reef plate at Davies Reef behaved as a "leaky confining layer".

1.5 AIMS AND SCOPE OF THE STUDY

The main objectives of this study are to describe the groundwater hydrology at Heron Island through field and laboratory investigations and mathematical modelling. By elucidating the processes of natural recharge and tidal groundwater flow in particular, other researchers and managers who are interested in the hydrogeology, geochemistry and nutrient dynamics of Heron Island (e.g., Charley et al., 1990; Chen and Krol, 1997; Brock and Waterhouse, 1990; Staunton Smith, 1992) should be in a better position to understand and interpret information provided by groundwater investigations and related studies. A broader objective of this research is to expand on current undertsanding of natural recharge dynamics as it occurs in low atoll and reef islands. For the benefit of future researchers, the groundwater recharge and movement models developed herein are designed in such a way that they can be applied to atoll island situations with some modification.

Because groundwater recharge and groundwater movement involve different physical processes, their study demands different theoretical and experimental techniques. Subsequently the current dissertation is divided into Parts I and II which relate to the vadose and phreatic zones, respectively:

The Hydrologic Study (Part I)

The main aims of Part I are to characterise the timing and magnitude of natural recharge at Heron Island over the short-term (ie, over hours and days) and the long-term (ie, over months and years). Because direct measurement of recharge in the field was believed too difficult, natural recharge was to be interpreted indirectly using a mathematical model that can realistically simulate unsaturated soil-water flow and the field water-balance. Importantly, the realistic modelling of natural recharge also requires the simulation of rainfall infiltration, evapotranspiration, deep drainage and surface runoff terms. Calibration data for the model are to include time-series hydrometeorological field observations/measurements spanning about one year and other laboratory measurements as required.

The Hydrogeologic Study (Part II)

The main aim of Part II is to describe and explain the short-term patterns of tidal groundwater movement at Heron Island and Reef. This involves the development of conceptual and mathematical hydrogeological models where necessary. New field investigations were designed and executed and the results combined with existing geological knowledge to assist with the interpretations and model development. The main field data to be obtained include: (1) groundwater piezometric water-levels, (2) ocean seawater levels (ie, the ocean tide), (3) seawater levels over the reef-flat (ie, the reef-flat tide), and (4) groundwater salinities. An existing network of groundwater investigation wells was utilised for the piezometric investigations (refer Section 1.2.3).

1.6 RESEARCH PLAN

1.6.1 The Hydrologic Study (Part I)

The general research plan shown in Figure 1-8 was adopted to meet the stated objectives of Part I. The main objectives being the development of a groundwater recharge model, the characterisation of natural recharge, and the discussion of implications for nutrient transport. The research plan is strategic in that it involves a number of inter-related steps to produce the final model and long-term recharge predictions. The plan begins with the collection of hydrometeorological data in the field over a 10 month period (Chapters 3) and the collection of related information in the field and laboratory (Chapters 3 & 4). Some of this data are used to evaluate the soil's characteristic curves (Chapters 3 & 4) and water storage history in the study site (Chapter 3). In Chapter 4, a finite-difference soil-water transport model is developed. A unsaturated hydraulic conductivity function employed by the model is calibrated by matching simulated soil matric potentials with those that were observed (Chapter 4). The empirically calibrated soil-water transport model is then used to estimate deep drainage from the study site for the study period (Chapter 5). Surface runoff and evapotranspiration from the study site are then estimated using an empirical approach as described in Chapter 5. The resulting field-water balance for the study period and a

preliminary estimate of potential evapotranspiration (Chapter 2) are then used as calibration data for a Soil-water Transport and Evapotranspiration Model (STEM). This model, once calibrated, is then finally used to simulate natural recharge at Heron Island over a ten year period (Chapter 6) using the existing long-term rainfall record as the driving variable (Chapter 1). Implications for the hydrology of Heron Island including implications for nutrient transport are discussed in Chapters 6 and 11. Details of the research methodology are provided in the relevant chapters.
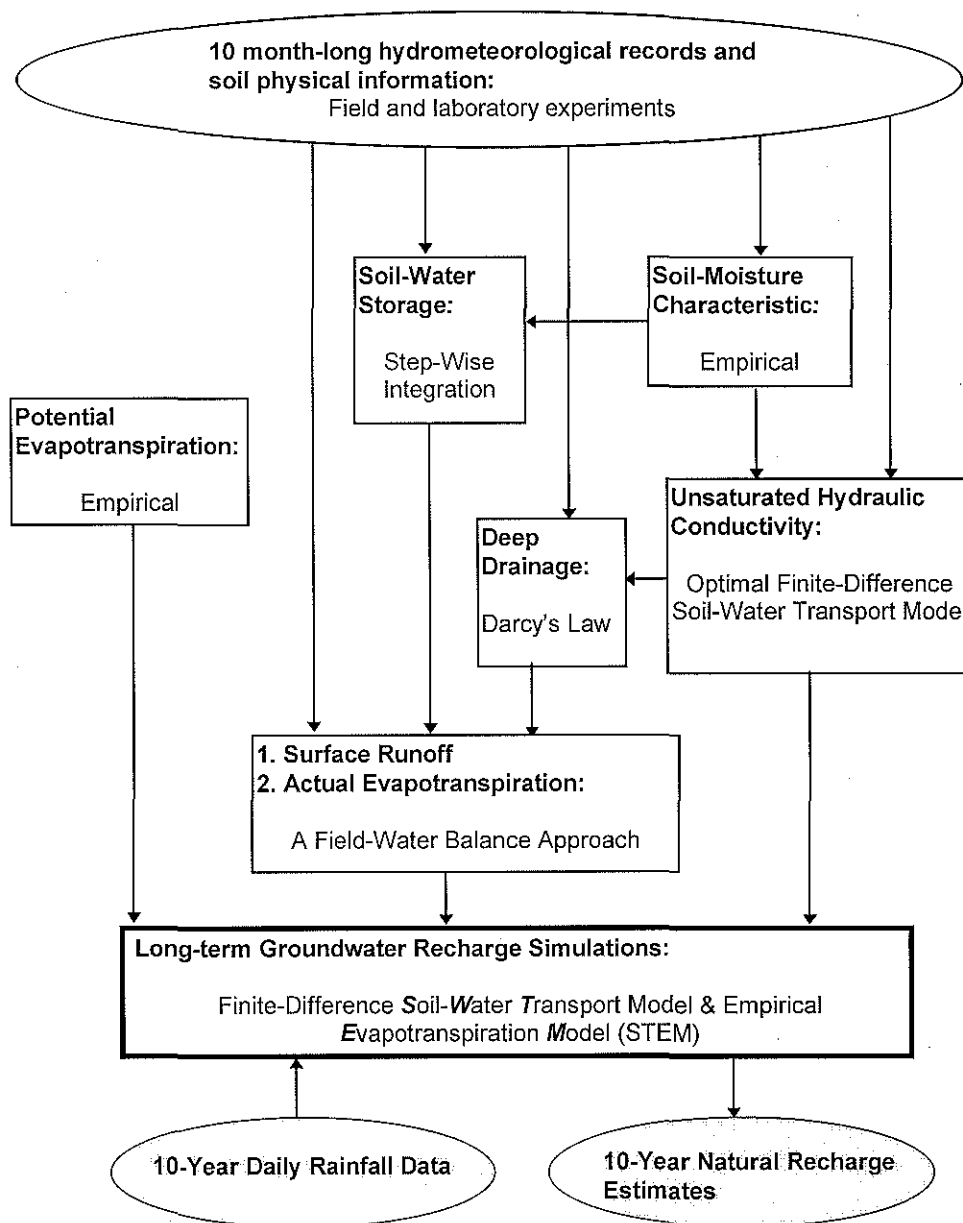
Figure 1-8. The research plan for the investigation of natural recharge at Heron Island: Part I of this study.

1.6.2 The Hydrogeologic Study (Part II)

The general research plan shown in Figure 1-9 was adopted to meet the stated objectives of Part II. The plan involves some well-defined steps, including a literature review, field investigations, model conceptualisations, and model development, verifications and calibrations. Model evolution is prone to iterative and concurrent analyses (see Figure 1-9). For details of the research methodology the following chapters should be consulted: piezometric field investigations are described in Chapter 8, localised unconfined tidal groundwater flow within the cay is considered in Chapter 9, large-scale tidal groundwater flow through the reef-cay system is considered in Chapter 10, and tidal groundwater flow through the beach is considered in Chapter 10. The main results and implications for nutrient dynamics at Heron Island are discussed in Chapter 11.
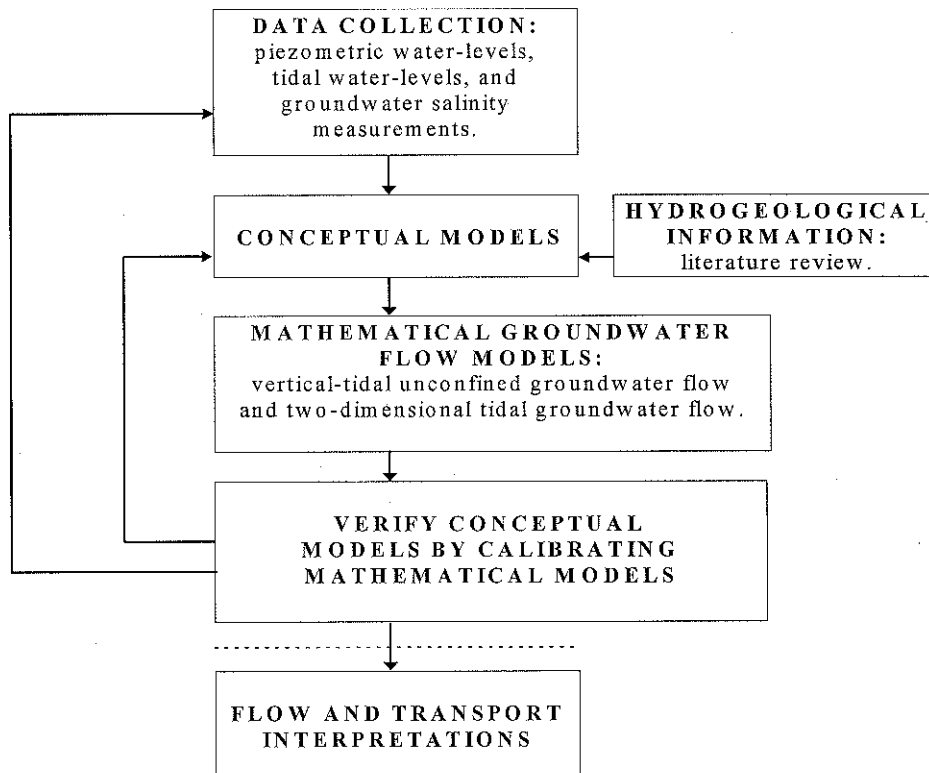
Figure 1-9. The general research plan for the investigation of groundwater movement at Heron Island: Part II of this study.

2. HYDROLOGIC CYCLE AND BALANCE

2.1 INTRODUCTION

Significant components of the hydrological cycle on small low carbonate islands with permeable soil and vegetation are precipitation, evaporation, transpiration, throughfall, infiltration, groundwater recharge and possibly surface runoff and washover (Falkland, 1991). Each of these are introduced in the following paragraphs. The hydrologic cycle of Heron Island also includes man-induced components, such as roof runoff, tank storage, seawater desalination, irrigation and waste-water disposal. These are not considered in the current study of natural recharge (see Figure 2-1).
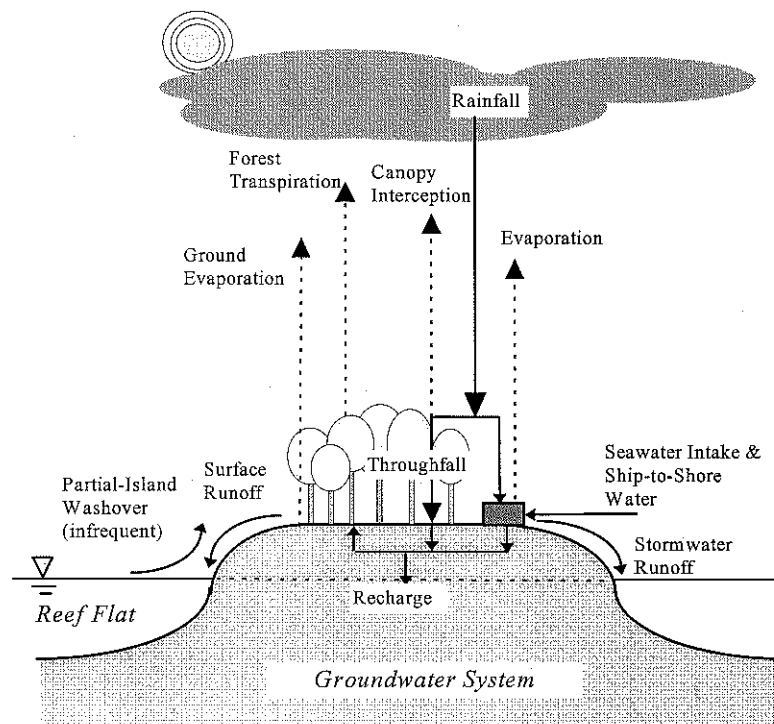
Figure 2-1. The main components of the hydrologic cycle at Heron Island: a small, low, vegetated coral cay on a platform reef (the box represents anthropogenic influences).

Precipitation, Throughfall and Interception   Rainfall is the only form of precipitation known to contribute to the hydrological cycle at Heron Island. Rainfall that is trapped by foliage either evaporates (canopy interception) or coalesces and flows to the ground via plant surfaces (stem flow). That portion of rainfall which eventually reaches the ground either directly or indirectly is called 'throughfall'. The interception-to-throughfall ratio tends to increase with lower rainfall intensities and greater vegetative cover.

Evapotranspiration   Evapotranspiration is the loss of water from the soil-plant continuum to the atmosphere by evaporation and plant transpiration. Although the term 'evapotranspiration' is often used in the literature, it is somewhat redundant[1] because plant transpiration is ultimately an evaporation process. The main factors influencing the rate of evaporation from vegetated surfaces are the radiant energy input and the water vapour transfer resistance (or conductance) of the atmospheric boundary layer (ABL). Evapotranspiration is also affected by soil-water availability and the biophysical properties of the vegetation (Stewart, 1984).

Evapotranspiration is considered a complex process because it is influenced by a number of interrelated environmental factors (eg, McIlroy). These factors act either 'internally' or 'externally' to the soil-plant system. External factors include (i) net radiant energy, (ii) air temperature, (iii) air humidity, (iv) wind velocity, (v) atmospheric stability and (vi) atmospheric heat and vapour conductance. Internal factors include (i) water content, (iii) plant physiology, (ii) plant-water and soil-water conductance, and (iii) plant and soil temperatures. When soil-water is freely available to the soil-plant system, the actual evapotranspiration rate is controlled more by external factors than by internal ones, and when water is scarce the opposite tends to be true (McIlroy, 1984).

Unsaturated Flow and Groundwater Recharge   By definition, vadose (unsaturated) soils have pore spaces filled with variable amounts of air and water. Typically the most moisture-variable zone is the top 1 to 3 m, the 'soil-water zone', where strong interactions with the atmosphere, rainwater and plants occur (Hornberger et al., 1998).

---

[1] McIlroy (1984) believes that the word evapotranspiration (and the symbol ET) is clumsy and should be replaced with the word evaporation (and the symbol E with subscripts that denote the different types of evaporation).

Processes controlling the flow of moisture through the unsaturated zone also control groundwater recharge behaviour, including surface infiltration, evaporation, plant-uptake of moisture, and unsteady unsaturated fluid flow: the later being a major topic of Part I.

Immediately above the water-table, capillary suction creates a highly saturated zone called the 'capillary fringe'. The soil matrix between the capillary fringe and the soil-water zone comprises an 'intermediate zone' (Hornberger et al., 1998): a zone that has comparatively slow and steady flow. Any moisture that passes through to the water-table is, by definition, groundwater recharge.

The two main factors causing moisture movement in unsaturated porous soil are gravity and capillary-pressures acting on the curved air-water interfaces. Gradients in total hydraulic head, h, drives the flow of moisture, where h is the sum of capillary-pressure head, ψ, and gravity head, z. Darcy's law may be applied to the estimation of this moisture flow as follows;

$$
\begin{aligned}
q_z &= -K\{\theta\}\frac{dh}{dz} \\
&= -K\{\theta\}\frac{d(\psi+z)}{dz} \\
&= -K\{\theta\}\left(\frac{d\psi}{dz}+1\right)
\end{aligned}
$$

(Equation 2-1)

An important relationship governing moisture flow in the unsaturated porous media is that which occurs between ψ and θ, called the soil moisture characteristic. As θ increases, ψ tends to become less negative in a highly non-linear fashion. A second and equally important relationship governing unsaturated moisture flow occurs between unsaturated hydraulic conductivity, K, and θ. As θ increases, so too does K, but in a highly non-linear fashion. The $\psi\{\theta\}$ and $K\{\theta\}$ relationships of Heron Island soils are examined in Chapter 4.

A full mathematical description of unsteady flow requires the continuity equation for moisture, ie:

$$\frac{\partial \theta}{\partial t} = -\frac{\partial q_z}{\partial z}$$
(Equation 2-2)

The above two equations are combined to form the governing differential equation for vertical unsteady water flow in unsaturated porous media, otherwise known as Richard's equation (Hornberger et al., 1998):

$$\frac{\partial \theta}{\partial t} = -\frac{\partial}{\partial z}\left[K\{\theta\}\left(\frac{\partial \psi}{\partial z}+1\right)\right]$$
(Equation 2-3)

In the above formula, *x*- and *y*-dimensions have been ignored because soil structures and moisture fluxes are assumed to be uniform in the lateral space-plane and because gravity acts vertically.

Certain processes can complicate vertical soil-water movement, including:

- hysteresis in $\psi\{\theta\}$;
- hysteresis in $K\{\theta\}$; and
- the influence of layering on moisture flow.

Hysteresis in $\psi\{\theta\}$ and $K\{\theta\}$ relationships is produced when a soil is drying as compared when it is wetting. Upon drying, soil moisture tends to be less mobile than when wetting as a result of capillary-pressure 'hurdles' associated with individual pore spaces. Soil moisture at Heron Island will be subject to hysteresis effects.

Layers of coarse soil inter-bedded with fine soil can have a counter-intuitive affect on vertical moisture flow. When saturated, moisture can move quickly in the coarse soil compared with the fine soil, however when unsaturated, the large pore spaces of a coarse soil tend to fill rapidly with air to essentially halt the flow of moisture. At a

similar matric potential, however, the pore spaces of a fine soil retain more moisture connectivity such that substantial flow can still occur. As a consequence, the conductivity of unsaturated coarse/gravelly soils can be much lower than the conductivity of fine/clayey soils at the same low moisture content. For this reason a layer of well-drained coarse gravel can act as a 'capillary barrier' to the downward movement of moisture in an otherwise fine-grained medium. The vadose zone at Heron Island is layered and so a capillary-barrier effect may be involved.

Both hysteresis and layering can be described using Richard's equation for idealised flow. There is a possibility, however, that non-ideal behaviour in soil-water movement can also occur because of (a) macropores, (b) organic material and (c) swelling soils. Macropores are the unusually large pores created biotically (eg, animal burrows, earthworm channels, and plant root spaces) or non-biotically (eg, soil pipes and shrinkage cracks). When moisture enters a macropore the small surrounding pores tend to fill with moisture first (due to their greater capillary suction), but when saturated the macropore can transfer moisture more quickly by 'pipe flow'. Macropores are unlikely to form in the lose unconsolidated sand at Heron Island, however there may be issue with the bird burrows in the island's surface soil. The irregular structure and surface physico-chemical action of organics in surface soils could also influence moisture movement unpredictably. Some clay soils change volume with variations in moisture content, but since Heron Island is devoid of clay this will not be an issue.

Infiltration   Infiltration of water at the soil surface is important in the recharge process. If water is freely applied to the surface at zero pressure head then infiltration will occur at a maximum rate called the infiltration capacity. Infiltration into a dry soil is initially very rapid because of initially large hydraulic gradients in the near-surface soil. However infiltration rates will decrease with time if the surface conditions remain constant and will approach asymptotically the saturated hydraulic conductivity, K_s, of the soil. Hence if the infiltration capacity is reduced below the rainfall rate then ponding and surface flow will occur.

Surface Water Retention   'Surface water retention' is that water held temporarily in depressions of the soil surface before infiltrating, evaporating or moving laterally.

Overland Flow and Surface Runoff   Ponding occurs if the rainfall rate is greater than the infiltration rate. 'Overland flow' is that surface water which flows laterally from areas of higher to lower gravitational head. Factors inhibiting the flow of ponded water include small-scale topographic relief and the hydraulic resistance of soil, surface mulch and vegetation. At Heron Island, the dirt tracks and paved areas, in contrast to the forest floor, pond water after light rain or irrigation. During tropical downpours the dirt tracks behave as channels for overland flow. 'Surface runoff' is that overland flow which discharges from the island to the ocean via the beach zone and stormwater drains.

Washover   On rare occasions, large waves and storm surges pass over the reef flat at high tide causing some washover at the island's shoreline. Although there is little historical data on washover, this component of the hydrologic cycle is believed to be insignificant due to its infrequency.

Anthropogenic Water   The vadose zone at Heron Island receives anthropogenic water, principally secondary treated sewage, septic tank effluent, irrigation water and pipe leakage. At the time of the study the treated sewage was discharged into the vadose zone via perforated pipes located near the centre of the island and below the rooting zone of *Pisonia grandis* (see Figure 1-2). The septic tank effluent derived from a number of septic tanks located within the research station, and the irrigation water was mostly tank water (ie, stored rainwater) that was sprayed on gardens in the resort and the research station. Finally, pipe leakage, as the name suggests, includes any freshwater and sewage that may have leaked from underground pipes. Falkland (1991) suggests that water losses from pipelines of 15-25% are normal in well maintained island water distribution networks, and that losses of 50% or more are common in poorly maintained island networks. Anecdotal evidence suggests that pipe leakage and major pipe failures have occurred at Heron Island on occasions. However most of the anthropogenic water discharged at Heron Island was not monitored, and so the flow of anthropogenic water

into the environment at Heron Island can only be estimated from crude water resource and human population figures.

2.1.1 The Field Water Balance

A general one-dimensional field water balance equation for Heron Island is as follows:

$$\int P\,dt + \int I\,dt = \int E_t\,dt + \int G\,dt + \int R\,dt + \int X\,dt + \Delta S \ : t_1 \rightarrow t_2 \qquad \textbf{(Equation 2-4)}$$

where,

P	= precipitation rate	(mm d^{-1})
I	= anthropogenic water input rate	(mm d^{-1})
R	= surface runoff rate	(mm d^{-1})
E_t	= evapotranspiration rate	(mm d^{-1})
G	= groundwater recharge rate	(mm d^{-1})
X	= combined washover and sea spray rate	(mm d^{-1})
ΔS	= total soil-water storage change	(mm)
t	= time	(d)

For the natural (ie, forested) portion of Heron Island, Equation 2-4 may be reduced to the following assuming areal uniformity, nil anthropogenic effects and nil washover:

$$\int P\,dt = \int E_t\,dt + \int G\,dt + \int R\,dt + \Delta S \ : t_1 \rightarrow t_2 \qquad \textbf{(Equation 2-5)}$$

The above equation is explained diagrammatically in Figure 2-2.
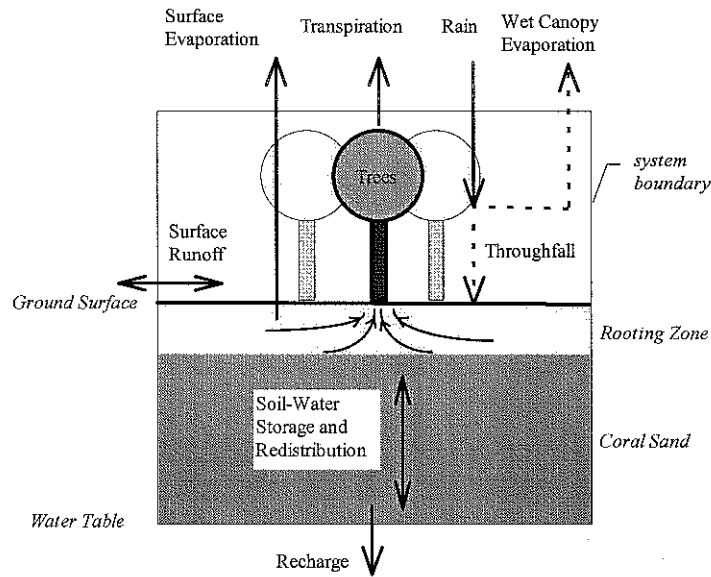
Figure 2-2. System boundary and flowstreams used to describe the field water balance of the natural forest at Heron Island.

Rainfall (P), evapotranspiration (E_t) and natural groundwater recharge (G) are usually[2] the largest and therefore the most important components of the hydrologic balance on small low islands. However, the accurate evaluation of the hydrologic balance is often a challenge because evaporation and drainage are very difficult to measure accurately in the field (Jury et al., 1991). Also, because it is difficult to measure and estimate E_t accurately, it is often the case that evapotranspiration is the least-quantified component of the water balance on small islands (Abell, 1993).

---

2 Abell (1993) claims that on some small islands in the southwest Pacific region, Et can actually exceed rainfall annually and often exceeds rainfall for consecutive months during seasonal dry periods and during droughts.

Because of inherent difficulties with measuring E_t and G, these terms are usually approximated from empirical methods which require standard hydrometeorological data as input (eg, Falkland, 1991). For this reason, detailed physical descriptions of evapotranspiration and groundwater recharge are usually not made. Furthermore, with regards to groundwater recharge on small low atoll islands, it is commonly assumed that soil-water redistribution is "...not a complicating factor..." (Underwood, 1990 p.36) in the recharge process. A closely related assumption is that unconsolidated coral sediments are 'well draining'. A problem with attempting to describe the recharge process *in situ*, is that the relevant field data are rather difficult and costly to obtain.

Total water stored in the soil profile, S, tends to vary about a central value governed by the hydrologic cycle and the water holding capacity of the soil matrix. Hence the relative magnitude of ΔS in Equation 2-4 & 2-5 reduces with increasing sample period. ΔS may be dropped from most hydrologic balances that extend for a year or longer without an appreciable loss of accuracy (Jury et al. 1991). On small low lying islands runoff, R, is often assumed negligible in the long-term balance despite the fact that R can actually be significant during individual storm events (Falkland, 991).

When evaluating the hydrologic balance, measurement and estimation techniques that average over large space-scales are preferred to small-scale techniques that do not account for areal variations in hydrology and geology. At Heron Island, the ideal space-scale is the size of the forest (ie, 100-1000 m) although smaller space-scales may be used if the soil-plant-atmosphere continuum is reasonably uniform. Suitable time intervals for the computation of the hydrologic balance are also important. A daily period is recommended for the soil-water balance and groundwater recharge calculations in most cases, whilst a monthly period is recommended for most groundwater studies (Falkland, 1991).

Experimental error in the balance can be quite large and may even be larger than some of the smaller components of the balance (eg, larger than R, I, X or ΔS). Hence the estimation of smaller components of the balance by difference is not recommended unless the errors are of relatively small magnitude.

2.2 ESTIMATION TECHNIQUES

2.2.1 Actual and Potential Evapotranspiration

The potential evapotranspiration rate, E_{tP}, is the theoretical evapotranspiration rate that can occur under the prevailing meteorological conditions assuming that water is freely available to the vegetation and to the soil surface. Of significance is whether E_{tP} is estimated assuming dry forest foliage or wet forest foliage, as the later situation can result in much higher E_{tP} values. Although actual evapotranspiration, E_t is more relevant to water balance studies than is E_{tP}, E_{tP} is more readily estimated in certain situations and so is often applied as an upper-bound estimate of E_t.

Complicating the estimation of forest evapotranspiration is the fact that most the available methods for measuring/estimating E_t and E_{tP} have been applied mainly on crops and have not been fully tested on forests (Spittlehouse and Black, 1981; Stewart, 1984). The better known approaches for estimating E_t and E_{tP} from forested sites generally require meteorological data to enable the evaluation of (a) water *lost* from the evaporating surface to the atmosphere, and/or (b) water *supplied* to the evaporating surface (Spittlehouse and Black, 1981). These approaches include:

(i) The vapour flux (or 'mass transfer' or 'aerodynamic') approach attempts to quantify vapour fluxes in the atmospheric boundary layer (ABL). This may involve measurement of horizontal wind speeds to characterise the ABL, or direct measurement of vertical eddy-fluxes of water vapour (ie, the eddy correlation method). The latter requires fast response equipment and is currently impractical for standard applications (Shaw, 1985).

(ii) The energy budgeting approach involves estimating latent heat loss from the evaporating system by quantifying every other term in an energy balance equation. The energy balance of the forested surface at Heron Island can be represented by Figure 2-3a and Equation 2-6. The various components of the balance include the energy flux densities of net radiation (R_n), latent heat (LE_t), sensible heat (H), and ground heat exchange (G_H). When studying vegetated surfaces it is commonly assumed, as in Equation 2-6, that energy storage in the biomass due to photosynthesis and heat adsorption has negligible impact on

the total energy balance (Campbell, 1977; Brutsaert, 1982). LE_t and H are difficult to measure in the field and are usually determined indirectly.

(a)   (b)
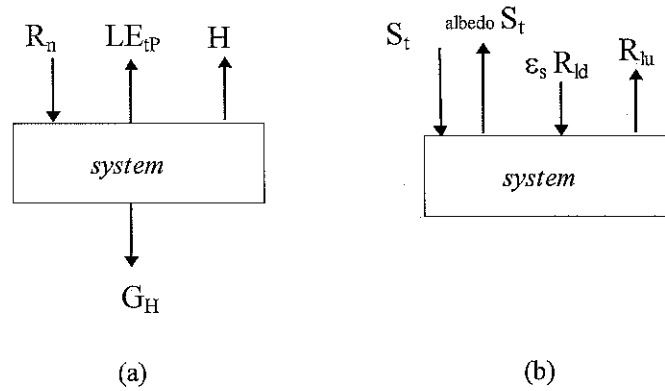
Figure 2-3. (a) The major energy fluxes affecting the energy balance of the soil-plant-atmosphere system, and (b) the short- and long-wave irradiance components affecting the soil-plant-atmosphere system (after Brusaert, 1982).

$$R_n - LE_t - H - G_H = 0$$ **(Equation 2-6)**

where,

$$R_n = S_t \, (1 - albedo) + \varepsilon_s R_{ld} - R_{lu}$$
$$= S_t \, (1 - albedo) + \varepsilon_s \, \varepsilon_a \, \sigma \, T_a^4 - \varepsilon_s \sigma \, T_s^4$$ **(Equation 2-7)**

and

albedo	= average surface albedo	(-)
E_t	= evapotranspiration rate	$(g \ m^{-2} \ s^{-1})$
G_H	= ground heat flux density	$(W \ m^{-2})$
H	= sensible heat flux density	$(W \ m^{-2})$
L	= 2450, latent heat of vaporisation of H_2O at 20 °C	$(J \ g^{-1})$
R_{ld}	= long-wave downward irradiance	$(W \ m^{-2})$
R_{lu}	= long-wave upward irradiance	$(W \ m^{-2})$
R_n	= net irradiance	$(W \ m^{-2})$
S_t	= global short wave irradiance	$(W \ m^{-2})$
T_a	= air temperature	(K)
T_s	= surface temperature	(K)
σ	= 5.6697x10^{-8}, Stephan-Boltzmann constant	$(W \ m^{-2} \ K^{-4})$
ε_a	= atmospheric emissivity	(-)
ε_s	= surface emissivity	(-)

The sensible heat flux density, H, flowing from a surface to the air can be estimated as follows (Campbell, 1977):

$$H = \frac{C_p (T_s - T_a)}{r_h}$$
(Equation 2-8)

where,

C_p = 1200, volumetric specific heat of air at 20°C and 1 atm $(J\ m^{-3}\ K^{-1})$
r_h = ABL resistance to sensible heat transfer $(s\ m^{-1})$

Energy fluxing through the ground, G_H, can occur as a result of radiation exchange, heat conduction, flowing water, gases convection, and latent heat convection (Jury, Gardener and Gardener, 1972). The ground-surface heat flux, $G_H\{0,t\}$, usually fluctuates with a 24 hour periodicity as a consequence of solar radiation exchange. Hence the integration of $G_H\{0,t\}$ over daily periods usually results in small net energy exchange and so is often ignored in long-term energy budgets (Campbell, 1977 p. 138).

(iii) The combined approach combines aspects of the aerodynamic and energy budgeting approaches. Two better known methods are the Penman and the Penman-Monteith formulae: the later being described as the 'best available' equation for describing evapotranspiration (Lerner, Issar & Simmers, 1990). Penman's (1948) formula for E_t utilises linear approximations for R_n and E_t and assumes that the air at the plant's surface is saturated with moisture. As shown in Appendix A, the Penman equation may be divided into two parts: an 'equilibrium' or 'energy' term and an 'aerodynamic' term.

Campbell (1977) argues that the Penman formula is not always useful because of R_n's implicit dependence on T_s (refer Equation 2-7) and the fact that R_n and T_s are rarely measured in the field. To help overcome these problems, Monteith (1965) provides a linearized model for the net long-wave radiation based upon air temperature in what is known as the Penman-Monteith formula (see Equation A-11 in Appendix A1 page A-8). The Penman-Monteith formula differs from the Penman formula because (a) net isothermal radiation, R_{ni}, is used instead of R_n, and (b) non-isothermal long-wave

radiation conductance and heat conductance are combined in a single conductance term, K_{hr}, ie:

In certain situations hydrologists may attempt to estimate actual evapotranspiration by scaling estimates of E_{tP}. But difficulty with measuring plant and aerodynamic resistances has been a major problem with the approach (Campbell, 1977). Another major problem which may render the approach "...futile..." (Campbell, 1977; p141), is that actual E_t can be functionally unrelated to E_{tP} when the soil-plant system is controlling water loss and not the atmospheric boundary layer.

(iv) The empirical approach may employ simplified energy budgeting, aerodynamic or combined equations.

(v) The field-water balancing approach involves measuring components of the field-water balance at a study site, eg:

$$\int E_t \, dt = \int P \, dt - \int R \, dt - \int D \, dt - \Delta S \quad :I = 0: \ X = 0: \ t_1 \rightarrow t_2 \qquad \textbf{(Equation 2-9)}$$

where D is the deep drainage rate from a control volume in units of mm d^{-1}. With Equation 2-9, the problem of estimating E_t is shifted to that of estimating P, D, R and ΔS. Lysimeters are particularly useful for measuring R, D and ΔS of control volumes; however, a lysimeter large enough to carry a whole tree was beyond the resources of this study. Soil-water profiling and integration techniques may also be used to estimate D and ΔS in a study plot (this technique is applied in Chapter 5).

(vi) The 'cut tree' and 'sap flow' methods can be used to estimate E_t from individual trees. The cut tree method involves cutting a tree trunk under water and measuring the amount of water adsorbed by the tree (Stewart, 1984). The cut tree method was considered impractical given the size of mature *Pisonia grandis*. The sap flow method involves the determination of a tree's sap flow-rate by monitoring the time taken for heat or radioactivity to pass between two points within the trunk (Stewart, 1984). Although Bartle (1987) and Falkland and Brunel (1989) have successfully used a sap

flow method to estimate the transpiration rate from coconut trees at Cocos Island, this method was not adopted because of biophysical uncertainties and potential difficultlies in applying the technique over extended periods.

2.2.2 Groundwater Recharge

As far as the author was aware, no techniques were available at the time of writing that could be used to directly, continuously, and accurately measure groundwater recharge (G) at Heron Island. The more common indirect and empirical techniques are discussed below (Lerner, Issar and Simmers, 1990):

(i) One-dimensional field-water balancing can be used to estimate groundwater recharge in an areally uniform site if all the remaining components of the balance can be estimated, ie:

$$\int G\,dt = \int P\,dt - \int R\,dt - \int E_t\,dt - \Delta S \quad :I = 0:\ X = 0:\ t_1 \rightarrow t_2 \qquad \textbf{(Equation 2-10)}$$

This approach shifts the problem of estimating G to that of estimating P, E_t, R and ΔS. Because P is readily measured, the main objectives of the field-water balancing approach are the estimation of E_t, R and ΔS. Unfortunately, the field-water balance technique is usually hampered by inaccurate estimates of E_t (refer Section 2.2.1).

(ii) Water-table hydrography has been used to interpret recharge events on certain islands by matching predicted water-table hydrographs with field observations (eg, Chapman, 1985). However the collection of the appropriate data and model calibration are major tasks with associated high cost. The viability of this approach for Heron Island is believed limited because tidal and barometric signals would tend to mask the recharge signal in the hydrographic record.

(iii) Environmental tracing has been used by Vacher and Ayers (1980) to estimate groundwater recharge on the island of Bermuda. Vacher and Ayers (1980) claim that total rainfall at Bermuda can be partitioned into evapotranspiration and recharge on the

basis of their respective chloride concentrations ([Cl⁻]) and the conservation of mass principle. In their study, a rainfall [Cl⁻] of 15 ppm, a evapotranspiration [Cl⁻] of 0 ppm, and a recharge [Cl⁻] of 60 ppm (ie, the salinity of the 'most fresh' groundwater in the freshwater lens) were recorded in the field. By assuming a constant chloride content for the vadose zone, they estimated that the average recharge rate was 25% of the average rainfall rate.

Whilst this method is attractive in its simplicity, there are two major reasons why it was considered unsuitable for application at Heron Island. Firstly, Heron Island (0.12 km^2) is more prone to saltation by aerosols than Bermuda (56 km^2) due to its relatively small size (thus increasing soil-moisture and recharge salinities). Secondly, Heron Island lacks a permanent freshwater lens and receives irregular groundwater recharge and so it seems unlikely that the [Cl⁻] of shallow groundwater and the [Cl⁻] of freshwater recharge at Heron Island will be consistently the same.

(iv) Empirical methods can be used to provide a first-approximation of monthly or annual groundwater recharge on small low-lying islands if the groundwater recharge correlates reasonably well with rainfall in a linear or near-linear fashion, ie (Falkland, 1991):

$$G = \alpha(P - P_o)^\beta \qquad :P \geq P_o$$
$$G = 0 \qquad\qquad\quad :P \leq P_o$$

(Equation 2-11)

where P_o is the threshold rainfall, α is a coefficient, and β is a coefficient with a value equal to or close to unity. P_o, α, and β are island specific parameters that are determined from measurements of P and best available estimates of G. The relationship between rainfall and recharge is usually more linear on islands that receive regular inter-annual rainfall (Falkland, 1991).

Chapman (1985, unpublished) and Falkland (1991) plot rainfall-recharge figures for a number of small low-lying islands to produce a general relationship between mean annual rainfall and mean annual recharge (see Figure 2-4). This type of general

relationship is better suited to islands that have uniform geology, homogeneous soil and vegetation and no orographic rainfall (Falkland, 1991). Figure 2-4 also shows that island catchments with high tree densities tend to have lower mean annual groundwater recharge rates in relation to local rainfall conditions.

(v) The indirect estimation of recharge by numeric groundwater modelling is technically possible in certain situations (eg, Vacher & Ayers, 1980). This involves estimating hydrogeological parameters by matching computer simulated salinity isochors to field observations. The approach may also involve the simulation of groundwater flow, advective-dispersive solute transport, density effects and tidal mixing in two or more dimensions (eg, Griggs and Peterson, 1993). Such an approach is data intensive and is usually not considered reliable until the numeric model is calibrated and independently validated. Most studies of reef island groundwater systems do not generate sufficient field data to justify the estimation of recharge by calibrating numeric groundwater models. Numeric groundwater models can, however, assist in validating estimates of G obtained by independent means.
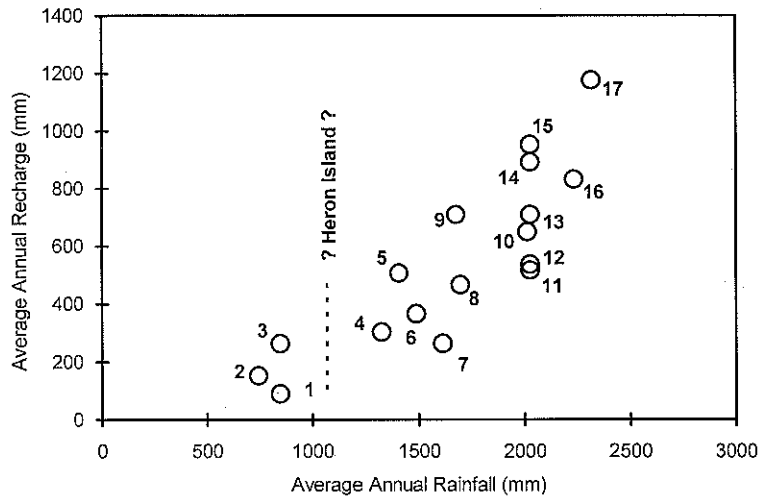
Figure 2-4. Published estimates of groundwater recharge for a number of flat islands as a function of average annual rainfall (modified from Falkland, 1991)

Legend

Ref. No.	Location
1	Christmas Is. (50% trees)
2	Rottnest Is.
3	Christmas Is. (no trees)
4	Bribie Is.
5	Yorke Is. (30% trees)
6	Bermuda
7	Grand Cayman
8	Tongatapu
9	Warraber Is. (30% trees)
10	Tarawa
11	Cocos Islands (100% trees)
12	Cocos Islands, West Island Northern (90% trees)
13	Cocos Islands (50% trees)
14	Cocos Islands, Home Is. (15% trees)
15	Cocos Islands, West Is. Airport (no trees)
16	North Guam
17	Kwajalein

Note: Modified from Falkland (1991).

2.2.3 Surface Runoff

Small reef islands are generally low-lying and have well draining soils, therefore it is often assumed that surface water movement is negligible even though this may not be true during heavy rainfall events (Falkland, 1991). Surface water movement is also difficult to measure at these islands because they are generally without surface water bodies and defined water courses that can be gauged. In this study surface runoff was not measured but was estimated indirectly from rainfall data and soil hydraulic properties to simplify the field experiments (refer Chapter 5).

2.2.4 Soil-Water

Technologies available for the *in situ* measurement of soil moisture are discussed widely (eg, Schmugge, Jackson & McKim, 1980). Major approaches include the gravimetric method, nuclear methods (eg, Carbon et al., 1982; Sophocleous and Perry, 1985), electromagnetic methods (eg, Dalton et al., 1984), tensiometry and hygrometric methods:

- The gravimetric method involves oven-dying, is the most reliable, but poses logistical problems as repeated hand auguring is required to obtain a time-series record. It is common practice to use the gravimetric method to calibrate other non-destructive measurement techniques. The gravimetric method is utilised in the curent study (refer Chapter 3).

- The neutron probe can be used under favourable conditions to indirectly measure soil-water on the basis of neutron scattering by water molecules (eg, Carbon et al., 1982). However it was anticipated that neutron interference by chloride ions in Heron Island soil would have rendered this method unreliable and so the method was not adopted.

- Time-domain reflectrometry (TDR) is a non-destructive method of measuring the dielectric constant of a soil. For most soils, the volumetric water content is uniquely

related to the dielectric constant thus enabling the determination of a calibration curve for repeated interpolation of moisture contents by TDR (Dalton et al., 1984). Whilst TDR technology may have been suitable, an automated TDR installation was beyond the resources of the current study and was not used.

- Tensiometry relates soil-moisture content to matric potentials via the characteristic curve. Because this curve is highly non-linear and hysteretic, the approach may not be suitable for studies requiring particularly accurate measurements. Tensiometry's main advantages are that it is non-destructive and can be automated to produce time-series records using pressure transducers and dataloggers (as in the case of this study; refer Chapter 3).

2.2.5 Rainfall and Throughfall

The measurement of rainfall in the field is standard hydrological practice (Falkland, 1991). This normally achieved using a manual raingauge (daily intervals) or a tipping-bucket raingauge and a datalogger (smaller intervals). The measurement of rainfall at Heron Island is discussed more fully in Chapter 3.

2.2.6 Deep Drainage

The techniques suited to the measurement of deep drainage are usually similar to those suited to the measurement of groundwater recharge (refer Section 2.2.2). In this study the Darcian approach is used with tensiometry to estimate deep drainage beneath the forest at Heron Island (refer Chapters 4 and 6).

2.3 A PRELIMINARY ESTIMATE OF THE LONG-TERM HYDROLOGIC BALANCE

2.3.1 Precipitation: Measured

The Bureau of Meteorology (1995) give Heron Island's average annual precipitation rate as 1069 mm a^{-1} for 1957-1975 (see Appendix A, Table A-2).

2.3.2 Throughfall and Interception: Empirical

Rainfall interception by forest canopies can be modelled as a function of wetting cycle and rainfall depth in an empirical fashion (eg, Lee, 1980), or simply by assuming that interception is a constant fraction of total rainfall. Rainfall interception is typically only 10-40% of total rainfall on a seasonal or annual basis and tends to decrease with greater rainfall intensity and thinner vegetative cover (Lee, 1980, p.113). Hence canopy interception at Heron Island should lie between 110-440 mm a^{-1} and throughfall between 950-620 mm a^{-1}. Average interception at Heron Island may be at the low end of this range due to the frequency of intense tropical storms in the wet season and canopy defoliation during the dry season.

2.3.3 Potential Evaporation: Empirical

Potential evaptranspiration (E_{tP}) was estimated from Nullet's (1987) map of E_{tP} isolines for low lying islands within the Pacific Ocean. These isolines were derived from the Priestly-Taylor (1972) equation; an equation which empirically relates potential evapotranspiration to the net radiation balance (Spittlehouse and Black, 1981; Crago and Brutsaert, 1992). An E_{tP} of about 1500 mm a^{-1} was extrapolated for Heron Island using Nullets' (1987) map. However this E_{tP} value probably an underestimates the 'true' forest E_{tP} at Heron Island as the Priestly-Taylor equation is most suited to crops in tropical regions: with crops the evaporative demand of the atmospheric boundary layer is usually not large compared to that of the net radiation balance whereas with forests the opposite tends to be true.

For comparative purposes, the long-term free-water evaporation rate (E_o) for coastal south-eastern Queensland is estimated from the daily class-A-pan evaporation depths (E_{pan}) recorded at Gladstone for the period 1967-92 (Bureau of Meteorology, 1995). The average E_{pan} were converted to daily E_o using Equation 2-12 and the commonly used annual pan factor (N) of 0.7 (Shaw, 1985).

$$E_o\{t\} = N\,E_{pan}\{t\}$$ (Equation 2-12)

The resulting long-term E_o is 1220 (± 80) mm y^{-1} (see also Figure 2-5). According to Shaw (1985), N can vary significantly between reservoirs and from month to month at the same reservoir hence this long-term E_o estimate and Figure 2-5 are only approximate.
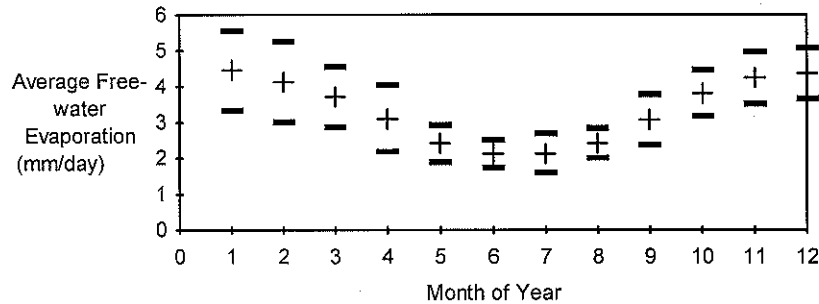
Figure 2-5. Free-water evaporation estimates for Gladstone derived from Class-A-pan depths recorded between 1967-92 and a pan factor of 0.7 (crosses are mean monthly values; lines are the 95% confidence intervals based upon annual variations).

2.3.4 Actual Evapotranspiration: Empirical Approach of Turc (1954)

An empirical formula for estimating mean annual evapotranspiration, E_t, was developed by Turc (1954) using data obtained from numerous catchments exposed to widely varying climatic conditions:

$$E_t = \frac{P}{\sqrt{0.9 + (P/L)^2}}$$

(Equation 2-13)

$$L = 300 + 25T + 0.05T^3$$

(Equation 2-14)

where,

E_t	= mean annual evapotranspiration	$(mm\ a^{-1})$
T	= 24, mean air temperature	(°C)
P	= 1069, average annual precipitation	$(mm\ a^{-1})$

The input data, which was obtained from the Bureau of Meteorology (1975) (see Table A-2), gives an average E_t estimate for Heron Island of 920 mm a^{-1}.

2.3.5 Groundwater Recharge

Given that the average rainfall at Heron Island is 1069 mm a^{-1}, a linear-regression estimate of average groundwater recharge at Heron Island is 240±270 mm a^{-1} based on the data in Figure 2-4. This is only a rough estimate because groundwater recharge is a function of many other variables besides rainfall (eg, climate, vegetation, surface topography and soil hydraulic properties).

Alternatively, Nullet (1987) gives a map of mean-annual-G isolines for low-lying atoll islands assuming rain-fed vegetation with rooting depth of 1 m and evapotranspiration rates determined from the Priestly-Taylor method. This map suggests G is ≤250 mm a^{-1} at Heron Island.

2.3.6 Surface Runoff: Assumed

As far as the author was aware, no direct measurements of surface runoff have been made at Heron Island. Long-term surface runoff, R, at Heron Island was initially assumed to be zero because the island is rather flat and has well draining medium-to-coarse grain soils.

2.3.7 Soil-Water Storage: Empirical Approach

The annual change in total soil-water-storage, ΔS, at Heron Island was initially assumed to be zero. This assumption is often found reasonable in long-term hydrologic studies because annual ΔS tends to vary around a long-term mean of zero (eg, Jury et al. 1991).

2.3.8 Washover and Sea-Spray: Assumed

Anecdotal evidence from Heron Island suggests that partial-washover of the foreshore had occurred when storm surges coincided with the high tide. Because of the rarity and peripheral nature of washover at Heron Island this term was assumed negligible in the current study. From the author's first hand experience, it appeared that sea spray at

Heron Island was negligible in terms of water loading and was also assumed zero in the hydrologic balance.

2.3.9 Anthropogenic Discharges: Approximate

The anthropogenic waste-water produced by the local population (typically 300-400 persons) was derived primarily from desalinated seawater, seawater and imported water and so is not directly associated with natural rainfall. By assuming a water consumption rate of 400-600 l per capita per day, which is typical for urban Australia (AWWA, 1995), the total anthropogenic water consumption rate at Heron Island is approximately 120-240 m^3 d^{-1}. Given that the cay's surface area is 0.2 km^2, the potential for anthropogenic discharge is equivalent to 220-440 mm a^{-1} on the basis of uniform spreading and zero evaporative loss. Unlike rainfall, however, anthropogenic waste-water was discharged at fixed points and beneath the soil surface.

Some of the roof-runoff at Heron Island was stored in tanks for miscellaneous purposes including the irrigation of ornamental gardens. This diversion and storage of water was not monitored but would have only affect the western half of the cay where the total roof catchment area comprised about 7-10% of the island's total plan area. Other anthropogenic effects, such as stormwater control and pipe leakages were not measured either and are assumed to have negligible impact on the hydrology of the forested areas (refer Table 2-1).

Table 2-1. A preliminary estimate of Heron Island's hydrologic balance for the forested areas.

Hydrologic Component	Value (mm a⁻¹)	Estimation Method	Reference
rainfall	1069	measured	Bureau of Meteorology (1975)
interception	110-440[a]	empirical	Lee (1980)
throughfall	960-630[b]	empirical	rainfall-interception
evapotranspiration	920	empirical	Turc (1954)
groundwater recharge	0-510	empirical	Chapman (1985) and Falkland (1991)
groundwater recharge	≤250	empirical	Nullet (1987)
surface runoff	0	assumed	
change in soil-water storage	0	assumed	
washover and sea-spray	0	assumed	
potential evaporation	1500[c]	empirical	Nullet (1987)
free-water evaporation	1220[c]	empirical	Class-A-Pan Evaporation Device
treated sewage effluent discharge (equivalent)	220-440 [c,d,e]	assumed on a per capita basis	AWWA (1995)

Notes:
(a) Evaporation of water from man-made and natural surfaces are not differentiated.
(b) The use of tank rainwater for irrigation is not differentiated from natural throughfall.
(c) For comparative purposes only.
(d) Calculations assume uniform spreading over the island although sewage effluent is actually released at fixed points (refer main text).
(e) The anthropogenic water cycle is fed primarily by desalinated seawater, seawater and imported water.

2.4 DISCUSSION

This chapter provides a brief description of the hydrologic cycle and a 'first-pass' estimate of the hydrologic balance at Heron Island. Whilst the rainfall figures are reliable, the preliminary hydrologic balance is only approximate, does not balance, and does not account for temporal variations (see Table 2-1). From Table 2-1 it appears that the island's average annual recharge is between 0-250 mm a⁻¹. Hence a rough estimate of the annual evaporation rate is 719-1069 mm a⁻¹ - which agrees with the method of Turc (1954). These figures indicate that natural recharge is limited by a rather high evapotranspiration-to-rainfall ratio. A basic relationship between average annual evaporation and recharge may be expressed as follows (units are mm a⁻¹):

$G \approx P - Et$

$\approx 1069 - Et$ **(Equation 2-15)**

A review of the literature indicates that no suitable methods were available that could provide for the direct, accurate and convenient measurement of groundwater recharge at Heron Island. Also, indirect estimates of G from the field-water balance approach are inhibited by difficulties with measuring Et (refer Equation 2-10). Lysimeters, if applied judiciously, could have been used to measure evapotranspiration at Heron Island, however a lysimeter large enough to carry *Pisonia grandis* was beyond the resources of the current investigation. The Penman and Penman-Monteith formulae, which have been used with some success to predict Et from other forest types, require detailed hydrometeorological and biophysical data (including canopy resistance to vapour transfer) that were beyond the resources of the current study.

Given the technical barriers to the quantification of natural recharge at Heron Island, one possible approach was to investigate natural recharge by developing a Darcian-type mathematical groundwater recharge model and applying that model to the simulation of natural recharge over a wide range of rainfall conditions; including periods of intense rainfall and prolonged dry weather. By doing so, rainfall and recharge patterns not included in a short-term study period could be interpreted, albeit approximately.

This approach is adopted in the remainder of Part I. It required the collection of hydrometeorological data in the laboratory and in the field to calibrate the groundwater recharge model (see Chapter 3). As shown in the following chapters, the model is used to simulate a decade of natural recharge at Heron Island using rainfall data as the driving variable (see Chapters 4, 5 and 6).

The disposal of treated sewage effluent, the artificial diversion of rainwater and stormwater, and all other anthropogenic impacts on the island's hydrology were not investigated further. This is because the current study was more concerned with describing natural systems including the hydrology of the *Pisonia* forest: the largest and most important land-use type at the time of writing.

3. HYDROMETEOROLOGICAL FIELD MEASUREMENTS

3.1 INTRODUCTION

This chapter describes the methods and materials that were used to collect hydrometeorological data for application with a Darcian approach for the purpose of investigating soil-water redistribution, evapotranspiration and groundwater recharge at Heron Island. Most of the data were collected intensively between January and October 1994 (ie, over a 'short-term' period) using three semi-automated monitoring stations located in the Heron Island Reseaerch Station (HIRS). These monitoring stations are (1) the 'wind station', (2) the 'soil-moisture station', and (3) the HIRS weather station (see Figure 3-1 for a locality guide). The data obtained from the three stations include measurements of rainfall, throughfall, and matric potentials and moisture contents of forest soil. In addition to the 'short-term' field data, a 'long-term' rainfall record is also utilised (see Section 3.1.1).

In this chapter the field data are presented graphically and are discussed. Some preliminary analyses are also undertaken to provide a time-series estimate of soil-water storage in the top 1.725 m of the vadose zone at one locality in the *Pisonia* forest. The combined short-term and long-term data are later utilised in Chapters 4, 5 and 6.

3.1.1 HIRS Weather Station

Standard weather data were recorded at the HIRS weather station for the duration of the short-term study period (see No.3 in Figure 3-1 for a locality guide). This data, which is not reproduced for reasons of brevity, include 9 a.m. values of rainfall spanning the 1st of June 1956 to the 31st December 1994 (ie, over the 'long-term'; refer Table 3-1). This data were provided by the HIRS and the Bureau of Meteorology in digital (ASCII) format.
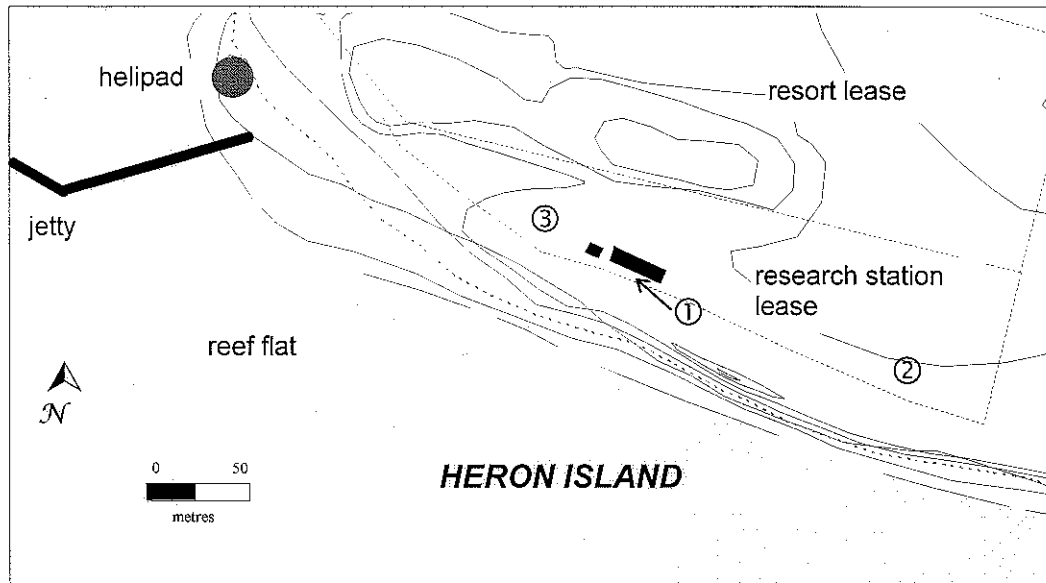
Figure 3-1. Locality guide for the short-term hydrometeorological monitoring stations and the long-term weather station at Heron Island (KEY: 1. The wind station. 2. The soil-moisture station. 3. The HIRS weather station.).

Table 3-1. Parameters stored in the HIRS weather station meteorological data files.

Col. No.	Data Type	Symbol	Units
1	Month (1-12)	-	month
2	Day (1-31)	-	day
3	Daily Rainfall	P	mm
4	Daily Minimum Air Temperature	T_{min}	°C
5	9 am Dry Bulb Temperature	T_d	°C
6	9 am Wet Bulb Temperature	T_w	°C
7	Daily Maximum Air Temperature	T_{max}	°C
8	9 am Relative Humidity	R.H.	%

Notes:

(a) Data for 1994 were provided by the University of Queensland's Heron Island Research Station.

(b) Computer file names are found in Table B-5 of Appendix B.

(c) 9 am R.H. are calculated from T_d and T_w of the same day.

(d) Temperature and relative humidity data are not directly used in this study.

There exist intermittent gaps in the rainfall record giving a total of 12 902 rainfall values over a total period of 14 093 days (ie, 91.5% complete). Of the 12902 days when rainfall measurements were made, a total of 4 496 days were recorded as being rainy days. Monthly averages and standard deviations of daily rainfall are plotted in Figure B-1 of Appendix B.

3.2 OBJECTIVES

The main objective of the field experiments was to obtain the hydrometeorological data listed in Table 3-1, Table 3-2 and Table 3-3. These data are to allow the estimation of the following terms in this and later chapters:-

- daily rainfall and throughfall,
- daily soil-water storage,
- soil matric potential functions (Chapters 3 & 4), and
- soil unsaturated hydraulic conductivity functions (Chapter 4),

and to allow the estimation of actual forest evapotranspiration (refer Chapter 5) and natural recharge on a daily basis (refer Chapters 4 and 6) during the study period and for the development of an interpretive soil-water transport and evapotranspiration model for Heron Island (refer Chapter 6).

3.3 SITE DESCRIPTIONS, EQUIPMENT AND METHODS

3.3.1 Wind Station

The wind station, which was owned and operated by the HIRS, was already in use prior to this study. It consisted of a wind anemometer, a tipping-bucket raingauge and a electronic weather station terminal (Heathkit ID-5001). For the purposes of this study the HIRS staff attached the raingauge to the outside of a two-storey building at roof level (ie, 6.1 m above ground level) and 0.5 m away from the roof gutter. The anemometer was already attached to a mast on the top of the same building at a height of 17.4 m RGL.

Because the Heathkit ID-5001 had no data recording capacity, the author developed a terminal emulation program (TEP) based on TELIX© software (*delta*Comm Development) to prompt the Heathkit ID-5001 for data at hourly intervals and save the data to computer in ASCII format (see Table 3-2). The TEP was executed continuously on an IBM compatible 286 personal computer. The electronic weather station terminal and the personal computer were housed in an air-conditioned room. Because mains power stop-started about once per month, the assistance of the HIRS staff was required to reboot the computer and TEP after power resumptions.
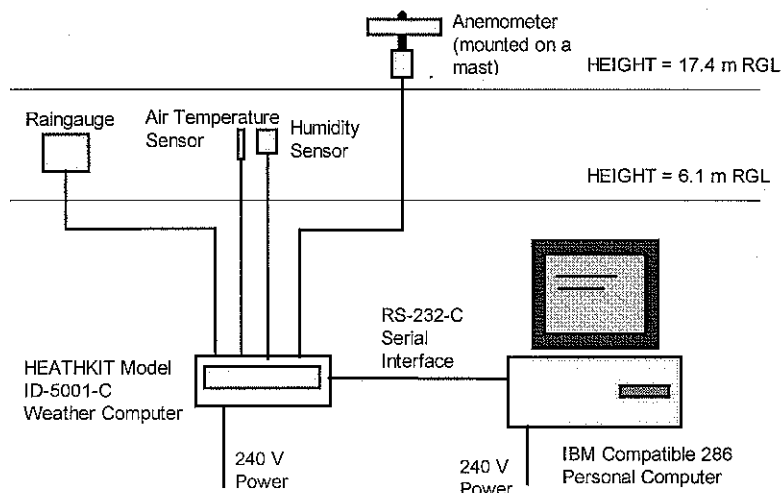
Figure 3-2. Schematic of the automatic wind station arrangement used in this study to record wind gust speeds at Heron Island.

Table 3-2. Parameters stored in the wind station meteorological data files.

Col. No.	Data Type	Symbol	Units
1	Year (0-99)	-	year
2	Month (1-12)	-	month
3	Day (1-31)	-	day
4	Hour (0-23)	-	hour
5	Air Temperature	T_a	°C
6	Relative Humidity	R.H.	%
7	Cumulative Rainfall	C.P.	mmx10^{-1}
8	Rainfall Rate	P	mm/hrx10^{-1}
9	Wind Gust Speed (1 Minute Sample Time)	U	knots

Notes:
(a) Files are in ASCII format.
(b) Filenames are found in Appendix B, Table B-5.
(c) Col. No. refers to column position in the computer data file.
(d) Data are recorded hourly on the hour.
(e) The wind speed data are not used in this study.
(f) The air temperature and humidity data recorded by the wind station are considered unreliable due to equipment failures and are not used in this study.

3.3.2 Soil-Moisture Station

The soil-moisture station was located within the *Pisonia grandis* forest (see No. 2 in Figure 3-1) to record on an hourly basis soil matric potentials at six different depths and throughfall (see Table 3-3). It occupied approximately 5 by 5 m of forest floor which was flat, covered by leaf litter and partially shaded by the canopy. Shearwater burrows were absent from the site during the study period (for reasons unknown) and the nearest burrows were at about 4-5 m away. By visual inspection it was estimated that the *Pisonia grandis* immediately around the study site were about 7-9 m tall.

The site was located within the HIRS lease about 30 m from a two storey dwelling, 40 m from the southern beach, and 40 m from walkways in the National Park. Separating the site and the dwelling was a narrow strip of lawn and some *Pisonia grandis* trees. Between the site and the beach the *Pisonia grandis* forest was low-lying and dense with a thick leaf litter layer, whereas on the inland side of the study site the *Pisonia grandis* forest was taller with only moderate leaf litter. A 90 mm diameter groundwater investigation well (non-operational) was found 17 m SW of the site. The site coincidently lay within the botanical study area of Ogden (1981).
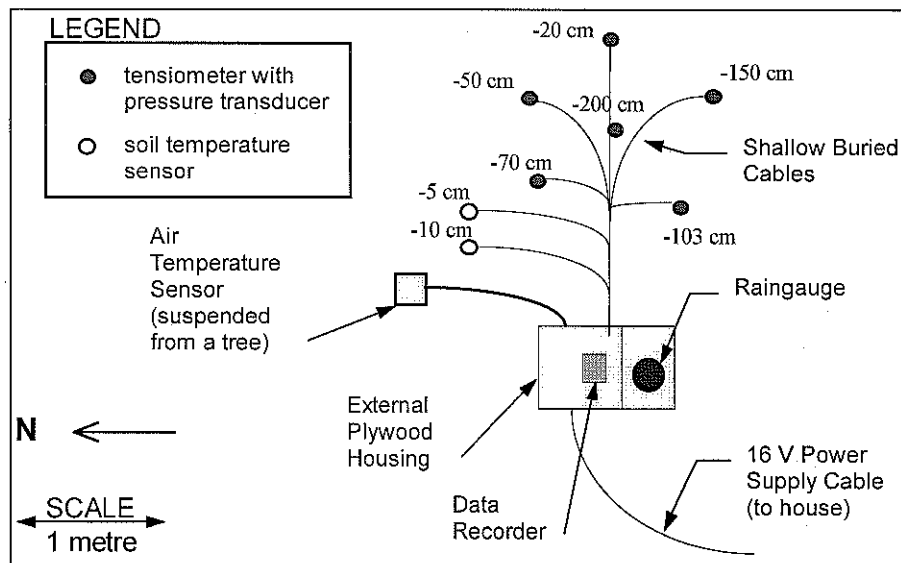
Figure 3-3. Plan layout of the soil-moisture station in the *Pisonia grandis* forest at Heron Island (vertical distances are relative to ground level).

<u>Datalogging</u>   A commercially available datalogger (Environdata, Easidata Mark 3) was used in the soil-moisture station to automatically record data signals from 10 different input channels at hourly intervals. Communications with the datalogger for the purposes of programming and downloading data were carried out using a laptop computer (Toshiba T1200XE), proprietary software (Environdata) and an RS232 cable. Because the datalogger's memory capacity was equivalent to 3 months of continuous data collection, a field trip was required at least once every 3 months to download data to the laptop computer.

<u>Protective Housings</u>   To protect the electronic equipment from the corrosive effects of the marine atmosphere and possible physical disturbance, the electronic equipment was stored in a 'inner-housing' constructed from a plastic box and lid, foam rubber

lining and compression bolts. To further protect the equipment the inner-housing was stored in a 1 m × 0.6 m × 0.4 m box constructed from marine-grade plywood and brass fittings (ie, the outer-housing). The outer-housing served four important purposes; (i) it protected the inner housing from falling branches, guano, moisture etc., (ii) it provided a stable and level platform for the raingauge, (iii) it provided some security against vandalism, and (iv) it provided safe storage for the equipment during transit. All cables to the datalogger passed through the outer-housing via small holes under its lid and through the inner-housing via compression glands. A vinyl cover over the outer-housing provided additional protection against dirt, guano, and rainwater.

Raingauge   A tipping bucket raingauge with a 203 cm diameter funnel was used to record throughfall in discrete 0.2 mm units to an upper limit of 150 mm h^{-1}. The raingauge was mounted on the top of the datalogger's outer housing (see Figure 3-3) in an area where the density of the forest canopy directly above was judged typical for the study site. The raingauge was factory calibrated and checked in the laboratory for accuracy. Because bird guano and leaf litter regularly fell on the study site, the raingauge funnel was covered by wire mesh (6 mm × 6 mm open spacings) and the tipping mechanism was covered by metal gauze (2 mm diameter spacings) to reduce the risk of blockages. The raingauge and covers were periodically checked and cleaned by HIRS staff.

Table 3-3. Parameters stored in the soil-moisture station meteorological data files.

Col. No.	Data Type	Symbol	Units
1	Year (0-99)	-	year
2	Month (1-12)	-	month
3	Day (1-31)	-	day
4	Hour (0-23)	-	hour
5	Canopy Air Temperature	T_c	°C
6	Soil Temperature at -5 cm	T_{-5}	°C
7	Soil Temperature at -10 cm	T_{-10}	°C
8	Throughfall	P_c	mm/hr
9	Soil-Water Pressure at -20 cm	p_1	-kPa
10	Soil-Water Pressure at -50 cm	p_2	-kPa
11	Soil-Water Pressure at -70 cm	p_3	-kPa
12	Soil-Water Pressure at -103 cm	p_4	-kPa
13	Soil-Water Pressure at -145 cm	p_5	-kPa
14	Soil-Water Pressure at -200 cm	p_6	-kPa

Notes:
(a) Files are in ASCII format.
(b) Computer filenames are found in Appendix B.
(c) Col. No. refers to column position in the computer file.
(d) Data are recorded hourly on the hour.
(e) Air and soil temperatures are not used in this study.

<u>Soil Tensiometers and Pressure Transducers</u> Polycarbonate tensiometers (Soilmoisture Equipment Corp.) of 30, 60, 90, 135, 150 and 210 cm lengths were used to measure soil matric potentials. This equipment was supplied by the manufacturer with screw-in vacuum dial gauges, porous ceramic cups and plastic 'jet-fill' water reservoirs (see Figure 3-4). The accuracy of the dial gauges were observed, during calibration, to be within ± 2 kPa. Each tensiometer also had a pressure transducer attached (Northern River Industrial Electronics, NSW) which had a capacity to give 0-1 V output relating directly to 0-100 (±0.5) kPa of vacuum pressure at 25 °C. Signal converters were required to convert this output to pulse frequencies (0-10 Hz). The electricity needed to power the six pressure transducers and the other equipment was supplied at 200 mA and 16 V via a single 30-m-long cable connected to the local electricity grid and shared via a junction box stored with the datalogger. Drift in the pressure transducer responses due to temperature changes were reported by the manufacturer as being only 0-1 kPa over 0-40 °C.
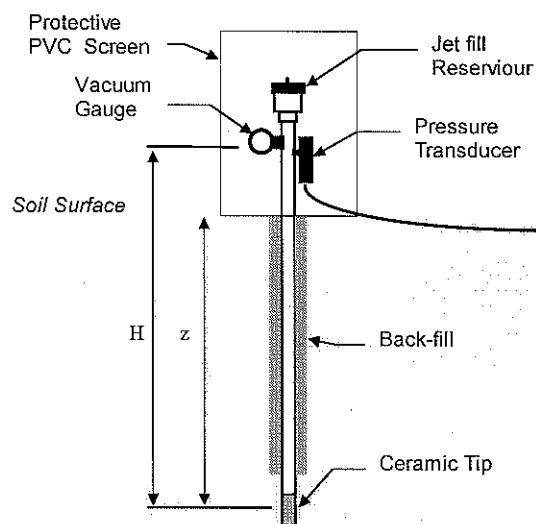
Figure 3-4. The soil tensiometer and pressure transducer arrangement (not to scale).

Calibration of the pressure transducers was undertaken in the Department of Mechanical Engineering workshop at the University of Queensland (refer Table B-4 of Appendix B). The transducers were calibrated using a vacuum pump, a mercury manometer (accurate to ± 0.05 in Hg) and a multi-way valve arrangement. Corrections to the tensiometers responses were determined in the laboratory to account for the negative pressure created by the water column within the tensiometers (ie, see H in Figure 3-4 and Table B-4).

Distilled water and an antifungal agent were used in the tensiometers to inhibit the growth of fungi and algae. The above-ground portions of the tensiometers were protected by covers constructed from PVC tubing and fly-screen (see Figure 3-4). Each cover had large side holes to allow air circulation and a fly-screen top to allow rainwater penetration. The soil-moisture site was cordoned with rope and signposted to restrict public access during the investigations.

The six soil tensiometers (2 cm diameter) were installed in the ground at different depths to a maximum depth of -2 m RGL (see igure 3-17). Holes for the tensiometers were dug with a hand auger to the required depth and with a diameter of 12-14 cm. During the digging, the excavated soil was placed in sequentially arranged piles on

plastic sheets. Backfilling of the tensiometer holes was then undertaken so as to approximate the original soil layering and density. To help establish good physical contact between the soil and the ceramic tip, each tensiometer was forced into the ground over the last 3-5 cm of vertical distance. Small soil samples were taken from the *Pisonia grandis* study site for the purposes of determining the soil-water profile *in situ* (see below).

<u>Soil-Moisture Measurements</u> The soil-water profiles in the study site were estimated by the gravimetric method. A 3 m long hand auger was used to excavate soil samples at 15 cm intervals to a maximum depth of -2.4 m RGL. At each sample depth, three soil samples were taken, stored in air-tight containers, and weighed (precise to ± 0.1 mg). The soil was dried at 110 degrees C overnight and dry weights were recorded. The frequency of the soil moisture profiling in the study site was restricted by the number of field trips to Heron Island during the study period. Between December 1993 and September 1994 soil-moisture profiles were obtained eight times.

3.4 RESULTS

For reasons of brevity the field data that were collected at Heron Island are only presented graphically in this chapter. If not enclosed with this document on floppy disk, the raw data may be obtained in digital format from the Dept. of Chemical Engineering at the University of Queensland (see Appendix B-5).

3.4.1 Rainfall and Throughfall

Total daily rainfall data was provided by the HIRS weather station (raingauge No. 1), hourly precipitation data was recorded by the wind station (raingauge No.2), and hourly throughfall was recorded by the soil-moisture station (raingauge No. 3) as indicated in Table 3-4. Erroneous entries and blanks that were detected in the HIRS rainfall record (see Table B-6) were substituted with data obtained by raingauge No. 2 (ie, raingauge No. 2 was used for cross-checking purposes). Rainfall and throughfall for 1994 are presented Figure 3-5 on a monthly basis and Figure 3-6 as cumulative totals on a daily basis. A class frequency and cumulative frequency analyses were also performed on the throughfall data (see Table 3-5).

Table 3-4. Raingauges used at Heron Island during the study period.

No.	Owners/ Operators	Raingauge Type	Raingauge Location	Data Type
1	HIRS	Manually Operated Raingauge	HIRS Weather Station (0 m RGL)	Daily 9 am precipitation.
2	HIRS	Electronic Tipping Bucket Raingauge	Wind Station (6.1 m RGL)	Hourly precipitation.
3	this study	Electronic Tipping Bucket Raingauge	Soil-Moisture Station (0.3 m RGL)	Hourly through-canopy precipitation (throughfall)

Notes:
a) The locations of the HIRS weather station, the wind station, and the soil-moisture station are shown in Figure 3-1.

Table 3-5. Throughfall intensity data collected at Heron Island between 1st January and 30th October 1994 (raingauge No. 3).

Throughfall ≥ (mm/hr)	Throughfall < (mm/hr)	Class Frequency (#)	Cumulative Frequency (%)	Throughfall Subtotal (mm)	Cumulative Throughfall (mm)	Cumulative Throughfall (%)
0+	1	138	54.12	67.5	67.5	8.75
1	2	37	68.63	52.2	119.7	15.53
2	3	22	77.25	51.9	171.6	22.26
3	4	13	82.35	43.8	215.4	27.94
4	5	10	86.27	45	260.4	33.77
5	6	6	88.63	32.7	293.1	38.02
6	7	3	89.80	19.5	312.6	40.54
7	8	1	90.20	7.2	319.8	41.48
8	9	4	91.76	32.7	352.5	45.72
9	10	5	93.73	46.2	398.7	51.71
10	20	8	96.86	125.7	524.4	68.02
20	30	6	99.22	143.1	667.5	86.58
30	40	0	99.22	0	667.5	86.58
40	50	1	99.61	43.5	711	92.22
50	60	0	99.61	0	711	92.22
60	70	1	100.00	60	771	100.00

3.4.2 Soil Moisture

The soil-moisture station was hand augured eight times during the study period. The laboratory determined water content profiles, w{z}, are presented in Figure 3-7 to Figure 3-9 (see Table B-10 for the raw data).

3.4.3 Soil Matric Potentials

Pressures in the six tensiometers were recorded hourly during most of the study period (ie, January-October 1994). Figure 3-11 to Figure 3-13 show daily values of ψ{z,t} converted to units of cm. The raw data are contained in the files referred to in Table B-5. Some equipment problems caused gaps to occur in the tensiometer records. On one occasion power was lost to the pressure transducers (due to a slipped power socket) resulting in complete data loss over a ten day period. On another occasion the datalogger's memory was overloaded resulting in two weeks of complete data loss. Two of the tensiometers also malfunctioned when they developed faulty o-rings (eg, see the dashed line in Figure 3-13). Gas purging of the tensiometers also produced false pressure readings due to sudden pressure equilibration with the atmosphere. From the time of purging, the tensiometers usually required 1 to 3 days to re-establish pressure equilibrium with the soil-water matrix. Hence tensiometer readings 1 to 3 days immediately after purging were omitted and replaced with interpolated data. The interpolated tensiometer records are considered adequate for daily analyses, however only the *bona fide* data were used for analyses sensitive to hourly changes in matric potential.
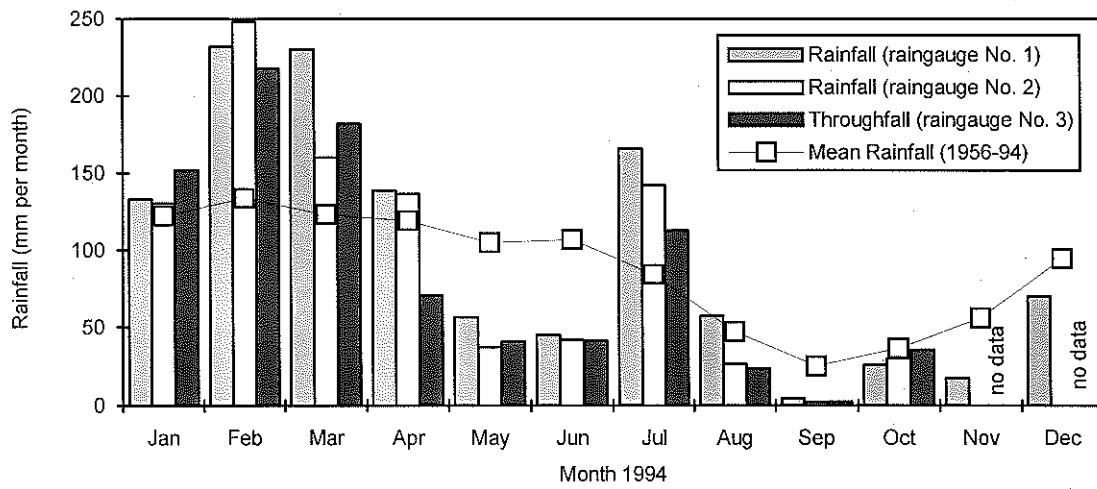
Figure 3-5. Monthly rainfall and throughfall at Heron Island during 1994 and long-term averages (refer Appendices A and B for details).
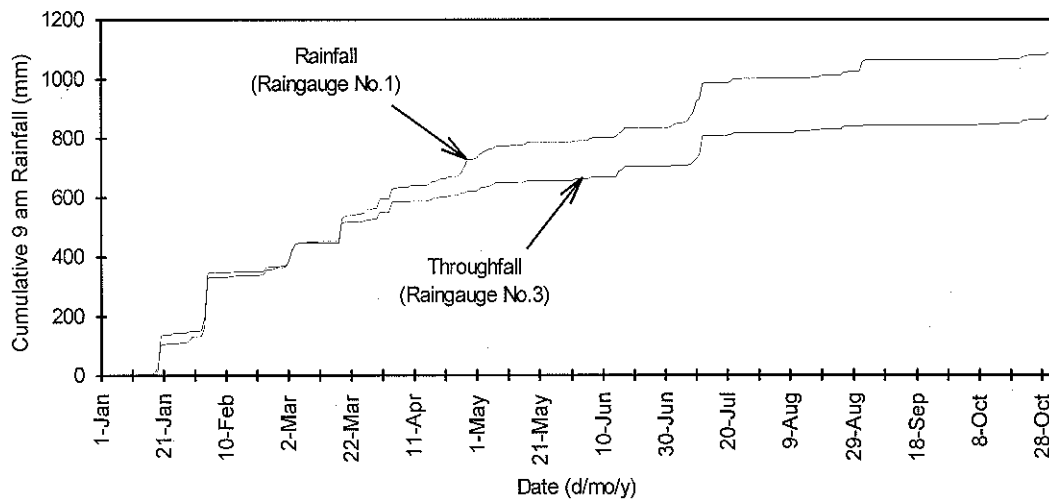
Figure 3-6. Cumulative rainfall and throughfall at Heron Island between 1st January - 31st October 1994 (the short-term study period).
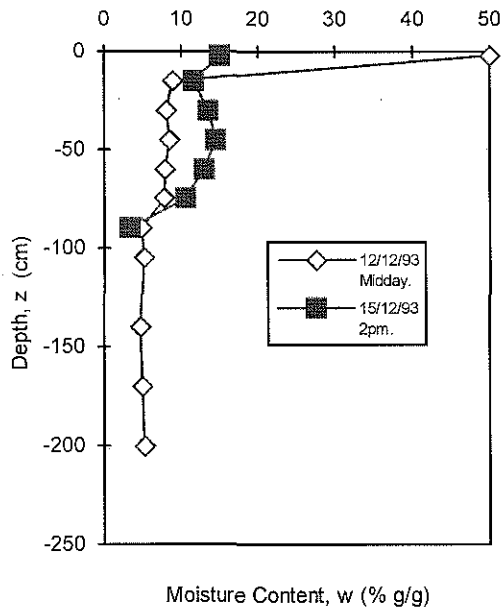
Figure 3-7. *In situ* soil moisture profiles from the study site 3 days apart (after 66 mm of rainfall on the 9th & 10th Dec. 1993).
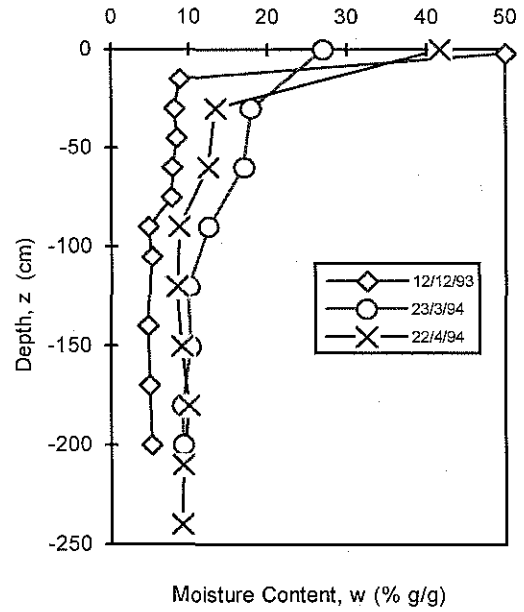
Figure 3-8. *In situ* soil moisture profiles from the study site.
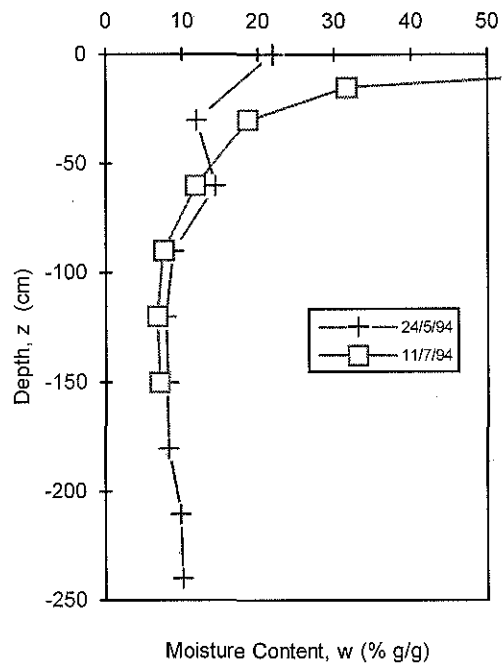
Figure 3-9. *In situ* soil moisture profiles from the study site.
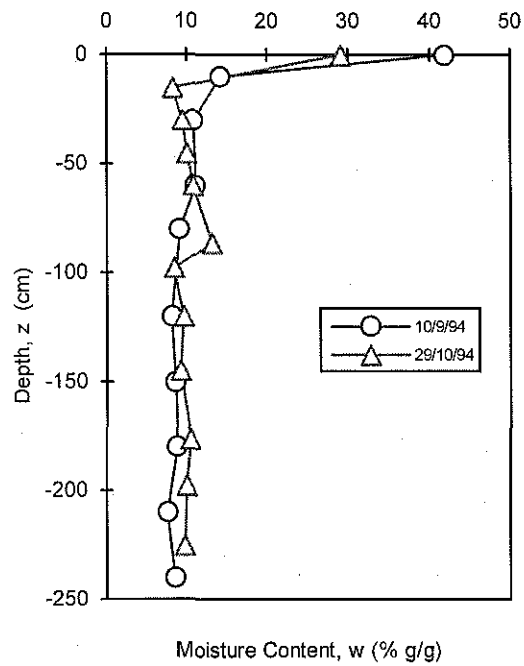
Figure 3-10. *In situ* soil moisture profiles from the study site.
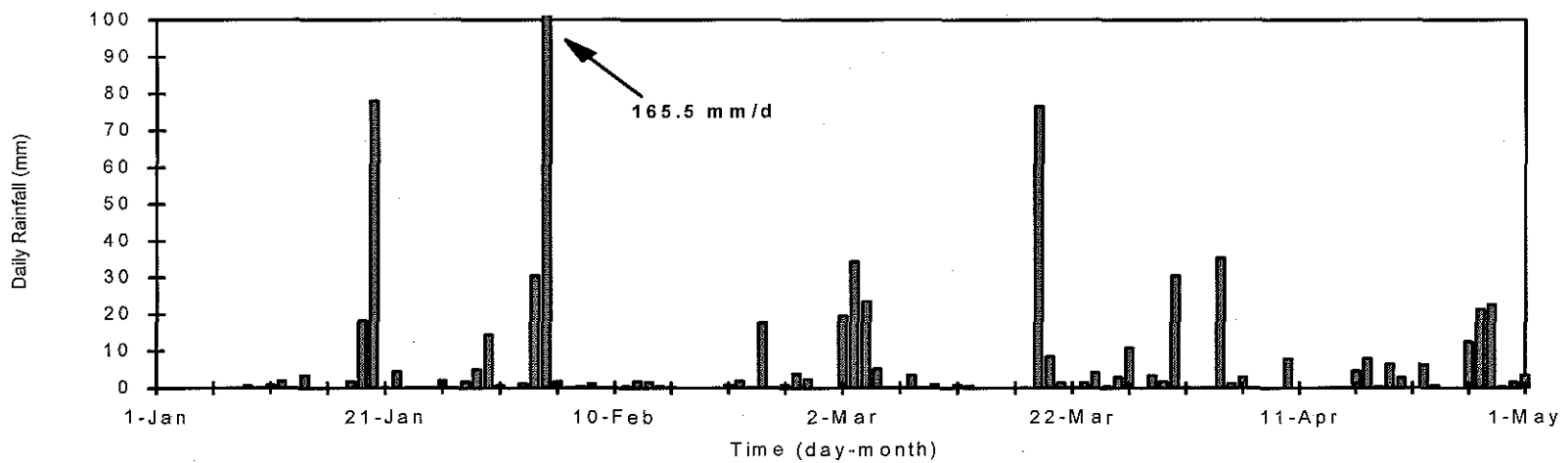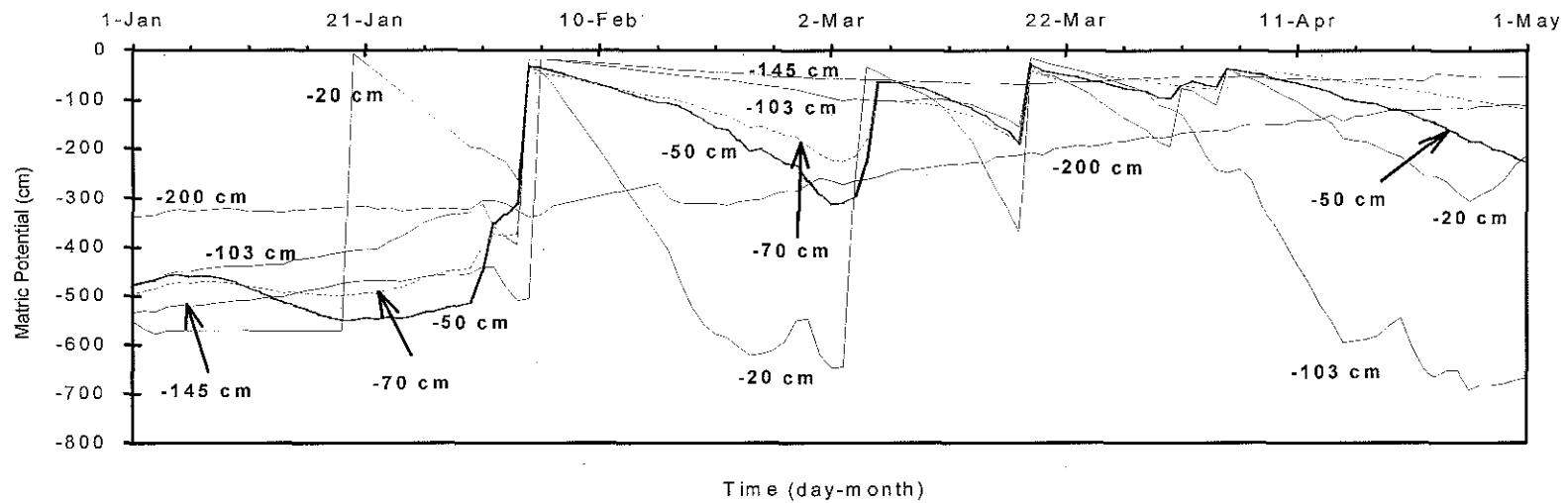
Figure 3-11. Soil matric potentials and rainfall at Heron Island during the first four months of 1994.
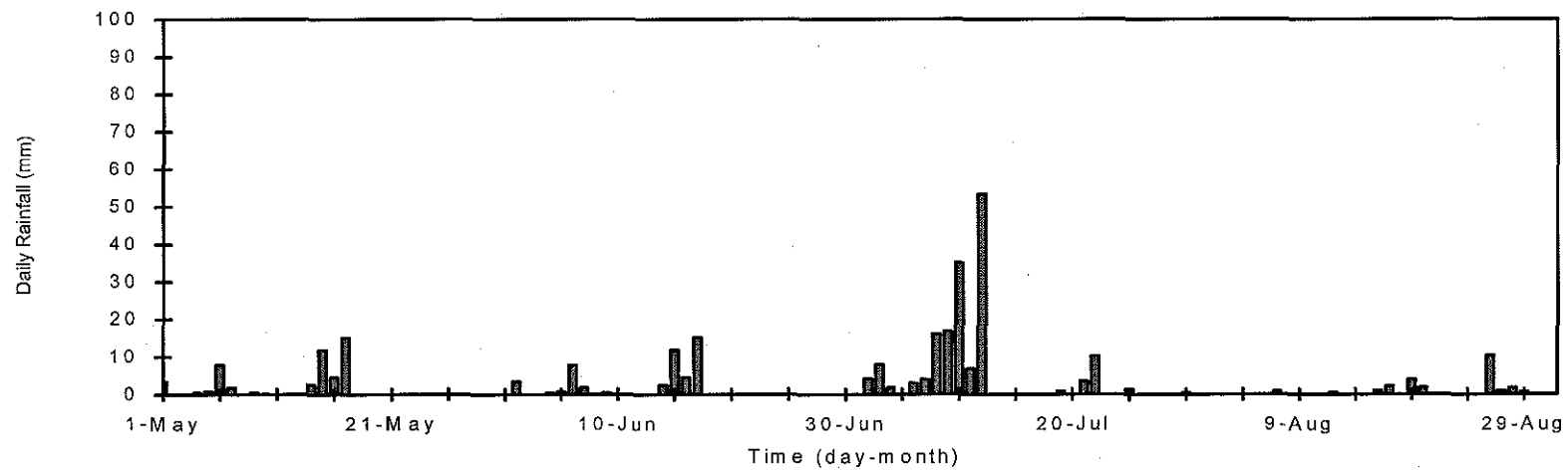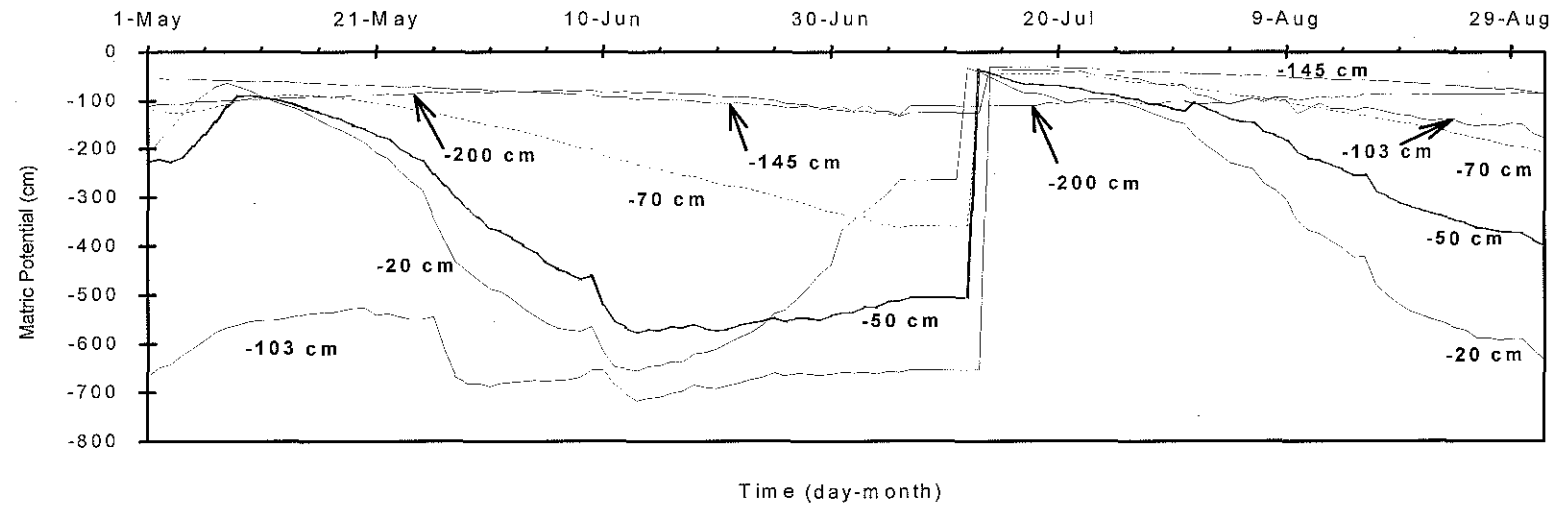
Figure 3-12. Soil matric potentials and rainfall at Heron Island during the second four months of 1994.
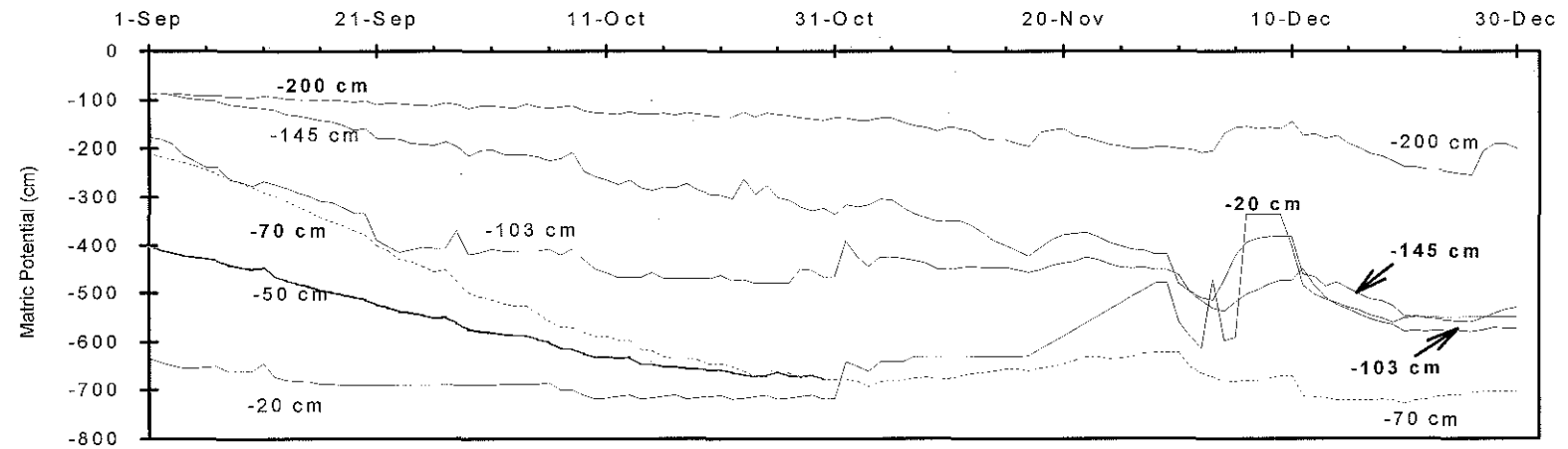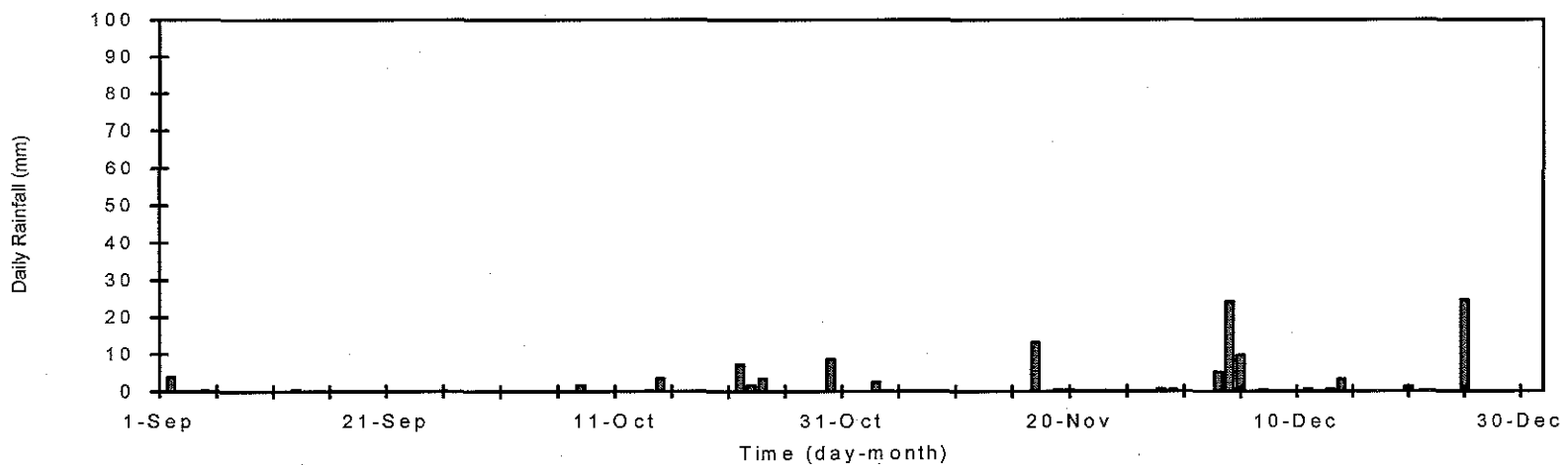
Figure 3-13. Soil matric potentials and rainfall at Heron Island during the third four months of 1994.

3.5 PRELIMINARY ANALYSIS

3.5.1 Tensiometer Readings

Matric potentials below the air entry pressure of the ceramic of the tensiometers (ie, below about -800 to -900 cm) could not be recorded. This is a physical limitation of tensiometers generally (Schmugge, Jackson & McKim, 1980). Hence, the matric potentials in Figure 3-11, Figure 3-12 and Figure 3-13 may over-estimate the actual potentials under dry conditions; possibly introducing error to the study.

Diurnal patterns of matric variation were recorded by all of the tensiometers to varying degrees and at various times. For example, consider the field results for the tensiometers at -103 and -200 cm RGL (see Figure B-2b). For convenience, these diurnal pressure changes, $\Delta p\{i,t\}$, are defined as follows:

$$\Delta p\{i,t\} = p_i - p_{i,t}$$ (Equation 3-1)

where $p_{i,t}$ is the tensiometer pressure at time t of day i, and p_i is the tensiometer pressure at midnight of day i. Whilst diurnal patterns of plant transpiration can induce $\Delta p\{i,t\}$ around plant roots, strong $\Delta p\{i,t\}$ were recorded well beneath the rooting zone of *Pisonia grandis*. Hence it appears that the cyclic $\Delta p\{i,t\}$ are a 'non-matric' phenomena. It is hypothesised that the cyclic heating and cooling of gases within the pressure transducers were responsible for $\Delta p\{i,t\}$. This hypothesis was tested by comparing $\Delta p\{i,t\}$ with variations in T_c and S_{ht} obtained over a ten day sample period in January 1994. Strong negative correlations between T_c and Δp_i, and between S_{ht} and Δp_i were computed from the field data (see Table B-8). To reduce the affect of $\Delta p\{i,t\}$ in the analyses that follow, the non-matric pressure variations are minimised by using only 9 am tensiometer records for anlayses requiring soil matric potential as input.

3.5.2 Soil-Water Retention Functions

Volumetric soil-moisture content profiles, $\theta\{z\}$, were evaluated from the gravimetric moisture content profiles, $w\{z\}$, and the dry density of the soil, ie:

$$\theta\{z,t\} = w\{z,t\} \frac{\rho_d\{z\}}{\rho_w}$$ **(Equation 3-2)**

where,

z = depth RGL   (cm)
$\rho_d\{z\}$ = dry density function for the soil profile   (kg/m^3)
ρ_w = density of water   (kg/m^3)

The soil's *in situ* bulk dry density, $\rho_d\{z\}$, is modelled as follows:

$\rho_d\{z\} = 1.0 - 0.004\,z$ $: 0 \geq z > -100$ **(Equation 3-3)**

$\rho_d\{z\} = 1.4$ $: -100 \geq z$

The above equation for $\rho_d\{z\}$ is based upon the field and laboratory data that are presented in Chapter 4.

The next step in evaluating the soil-water retention functions is to curve-fit the θ and ψ field data. Because this data were collected from different positions in the soil profile, the analyses were simplified by grouping the data into three vertical regions which delineate rather distinct changes in the soil's texture, ie: (1) above -60 cm RGL (ie, shallow humic silty sand), (2) between -60 cm and -100 cm RGL (ie, silty sand), and (3) below -100 cm RGL (ie, coral sand). The plots of $\psi\{\theta\}$ for the three regions are shown in Figure 3-14, 3-15 and 3-16. This water-retention data were curve fitted with the following power function which forces θ_s to a matric potential of -1 cm.

$$\theta(\psi) = \theta_s \, |\psi|^{\,b} \qquad : \psi < -1 \text{ cm}$$ **(Equation 3-4)**

where, ψ is the soil matric potential (units of cm), θ_s is the volumetric moisture content at saturation (units of ml ml^{-1}), and b is a fitted parameter (dimensionless). Sophocleous & Perry (1985), for example, similarly use this technique to average-out the affects of hysteresis in the soil water-retention relationship of a sandy loam.

The scatter in the field soil-water retention data indicates that the fitted power functions are only approximate. This is particularly true for the shallow humic silty sand (refer Figure 3-14). The scatter in Figure 3-14, 3-15 and 3-16 may be the result of a combination of (i) spatial variation in soil texture and hydraulic properties, (ii) hysteresis in the soil-water retention relationships, (iii) plasticity of the soil matrix due to soil organics, (iv) interaction between soil-water and organic surface films, and (iv) lateral variations in evapotranspiration and infiltration.
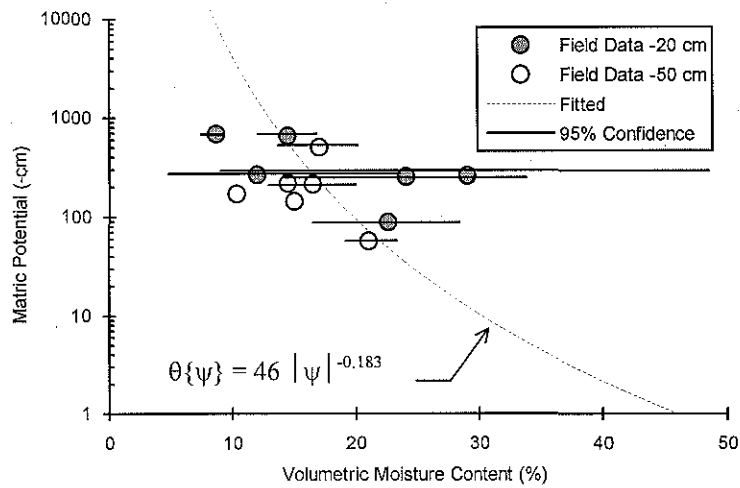
Figure 3-14. Field estimate of the soil-water retention function for shallow humic silty sand at Heron Island (95% probable error is less than the size of the symbols unless shown otherwise).
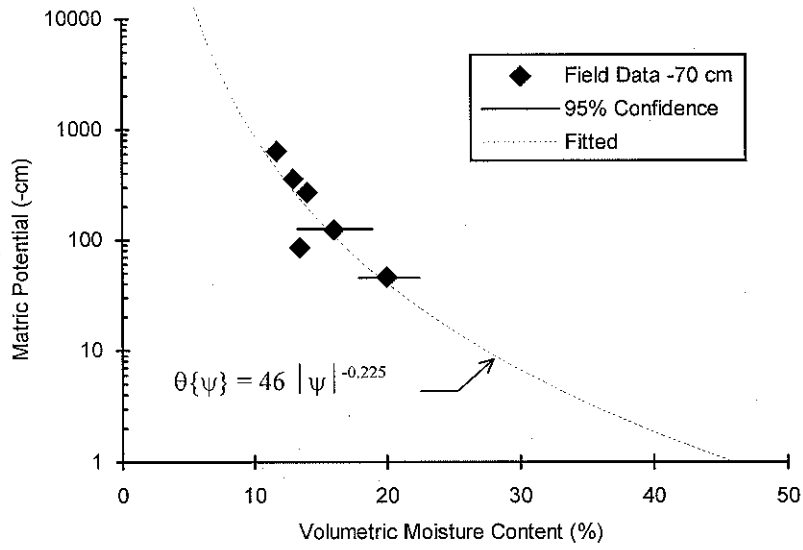
Figure 3-15. Field estimate of the soil-water retention function for silty sand at Heron Island (95% probable error is less than the size of the symbols unless shown otherwise).
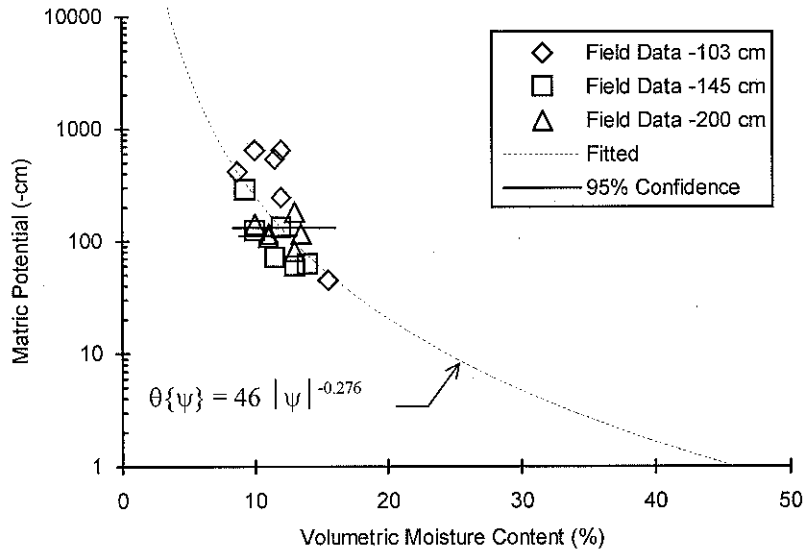
Figure 3-16. Field estimate of the soil-water retention function for coral sand at Heron Island (95% probable error is less than the size of the symbols unless shown otherwise).

Table 3-6. Average soil-water retention functions for Heron Island soil estimated from tensiometry data.

Soil Layer or Type	Layer Depth Range	Power Function Constant	Standard Error of Regression	Saturated Moisture Content
	z (cm)	b (-)	Δb (-)	θ_s (ml/ml)
Humic Silty Sand	0 to -60 cm	-0.183	0.036	0.46
Silty Sand	-60 to -100 cm	-0.225	0.018	0.46
Coral Sand	< -100 cm	-0.276	0.016	0.46

Notes:
(a) Curve fitting was to the power function, Equation 3-4.
(b) Curve fitting used the method of least squares (unweighted), with matric potentials as the independent variable.
(c) The estimates of saturated moisture content for the soil are discussed in Chapter 4.

3.5.3 Soil-Water Storage

The soil matric potential records shown in Figure 3-11, Figure 3-12 and Figure 3-13 and water-retention formulae described in Table 3-6 were used to approximate the total water stored in the soil profile, S, on a daily basis (see Figure 3-18). This was achieved by representing the soil profile in the study site as five discrete layers and assuming that the actual soil-moisture profile may be approximated in a stepwise fashion without appreciable loss of accuracy, ie:

$$S = \int_{z=0}^{z=-172.5cm} \theta\, dz$$

$$\cong \sum_{i=1}^{5} \theta\{\psi_i\}\, \Delta z_i$$

(Equation 3-5)

where i denotes the layer number, z, is the depth of layer i, and Δz is the thickness of layer i. The lower boundary of the integration is taken at -172.5 cm RGL which is central to the two deepest tensiometers (see Figure 3-17). The tensiometer estimates of $S\{t\}$ differ from the gravimetric (ie, direct) estimates by as much as 0-50 mm over the entire soil profile. It is therefore assumed that $\pm$ 50 mm is a reasonable approximation of standard error in the indirect estimates of S. Most of this uncertainty is derived from uncertainty in the moisture content and the density of the shallow humic silty sand.
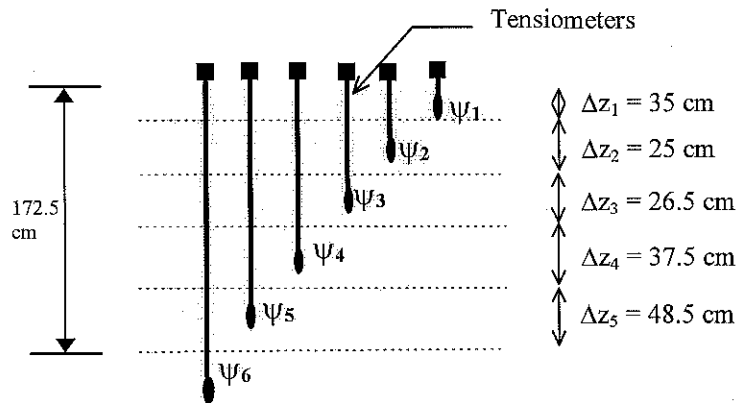
igure 3-17. Discretisation of the soil profile for estimating total soil-water storage from matric potentials and water-retention functions.
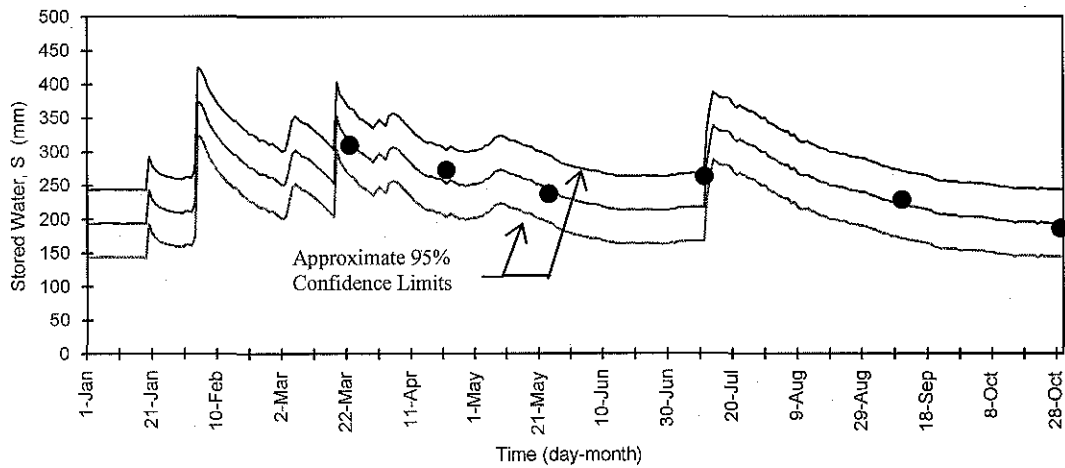
Figure 3-18. Soil-water stored in the top 172.5 cm of the soil profile during 1994 (lines are from tensiometry, dots are determined from the gravimetric method and Equations 3-2, 3-3 and 3-5).

3.6 DISCUSSION

Rainfall, Throughfall and Interception   Most of the rain that fell at Heron Island during 1994 was produced by tropical storms between January and April (see Figures 3-5 and Figure 3-6). Noteworthy also were the rains that fell during the first three weeks of July as they contributed greatly to a bimodal wet season. The largest rainfall and throughfall recorded during any 24 hour period were 165.5 mm d^{-1} and 159.3 mm d^{-1}, respectively, as a result of a storm between 10 am 3rd February and 9 am 4th February 1994 (see Figure 3-6 and Figure 3-11). A few other rainfall events in January, March and June were also quite large (ie, between 50 and 80 mm d^{-1}). However the 165.5 mm d^{-1} rainfall event in February stands out as being the 10th largest daily rainfall depth recorded at Heron Island between 1957 and 1994 (the largest recorded was 282.4 mm on the 21st February 1992). The total rainfall for 1994 is 1178 mm, which is greater than the island's long-term annual average rainfall of 1069 mm a^{-1}.

It is apparent from Table 3-5 that a large proportion of the throughfall fell in a very brief period. The records show that throughfall intensities $\geq$10 mm h^{-1} occurred in a total of only 16 hours (the study period was 7272 hours long) but contributed about 50% of the total throughfall (see Table 3-5). The cumulative throughfall recorded in the *Pisonia* forest (ie, raingauge No. 3) is 20% less than the cumulative rainfall recorded over the same period (ie, raingauge No. 1). This difference is believed to be partly due to interception losses above raingauge No. 3, however because of likely spatial variation in rainfall and throughfall and seasonal changes in canopy density, the 20% difference cannot be assumed to be a reliable measure of the average interception ratio.

Soil Matric Potentials   When the short-term study in the *Pisonia* forest began on the 1st January 1994, the top 2 m of the soil profile had low moisture levels and matric potentials between -300 and -600 cm (see Figure 3-11). Although some rain fell during the first two weeks of 1994, it was not until the third week that the soil profile was moistened substantially by heavy rains. During the fourth week of 1994 evapotranspiration exceeded rainfall. This dry period was broken in the 5th week when

197.3 mm of throughfall moistened the soil profile to a depth -103 cm RGL in one hour and moistened the soil profile to a depth of -145 cm RGL in another 19 hours. The wetting front then slowed considerably and soil matric potentials at -200 cm RGL were only affected weeks and months later as a result of soil-water redistribution.

During the months of March, April and May a number of significant rainfall events moistened the upper regions of the soil profile whilst evapotranspiration gradually dried the soil profile (see Figure 3-11 Figure 3-12). Meanwhile, the soil matric potentials at -145 and -200 cm RGL increased due to deep soil-water redistribution caused by antecedent rainfall. In April 1994, soil matric potentials at -103 cm RGL decreased somewhat unexpectedly. Whilst the cause of this change is uncertain, one possible explanation is that transpiration in the rooting zone forced moisture at the -103 cm level to flow upwards.

May and June was a net drying phase for the soil profile although intermittent rain caused the occasional wetting of the near-surface soil. By the end of May 1994, the matric potentials at -200 cm RGL had reached their highest values during the entire study period. In the second week of July a period of heavy rainfall caused the moistening of the soil profile to a depth of -145 cm RGL. The July wet period was followed by a long drying phase which lasted to the end of 1994 and possibly longer. Rainfall in December 1994 only had a marginal affect on the matric potentials in the soil profile, and matric potentials at -200 cm RGL were still falling at that time.

Soil-Water Storage   The S{t} values of Figure 3-18 reveal a pattern of sporadic wetting and gradual drying of the soil profile throughout the year. As mentioned previously, the sporadic wetting between January and April 1994 is attributable to irregular storm activity. May and June 1994 was a net drying phase whilst July was a brief wetting phase. August through to December 1994 was a net drying phase bringing S{t} to levels similar to that recorded in December 1993. From Figure 3-18 it appears that the 172.5 cm deep study site has a residual S of about 200 ± 50 mm and field capacity of about 370 ± 50 mm.

4. SOIL-WATER TRANSPORT MODEL

4.1 INTRODUCTION

A numeric model of one-dimensional unsaturated isothermal fluid flow in layered porous media is developed in this chapter for simulating soil-water redistribution in the vadose zone at Heron Island. The model is later utilised in Chapter 5 to estimate deep drainage in the study plot and in Chapter 6 to interpret the groundwater recharge process at Heron Island. The numeric model is based upon the moving mean slope (MMS) finite-difference algorithm of Moldrup et al. (1989), which, according to its developers, can provide relatively rapid, stable and accurate numerical solutions to a wide variety of unsaturated flow problems. The model/program that is presented in this chapter is written in the FORTRAN language and is verified against three published soil-water transport examples.

Fundamentally important to the application of the unsaturated fluid flow model is the reliable quantification of soil hydraulic properties: soil porosity, $\eta\{z\}$; soil bulk dry density, $\rho_d\{z\}$; matric potential as a function of soil-moisture, $\psi\{z,\theta\}$; and unsaturated hydraulic conductivity as a function of either matric potential or soil moisture, $K\{z,\theta\}$ or $K\{z,\psi\}$. In this study, as in most, the evaluation of soil hydraulic properties is challenging because the parameters K and ψ can vary by several orders of magnitude within the moisture (θ) range of interest, whilst most measurement systems have a limited range of θ (Klute, 1986; Dirksen, 1991). The hydraulic properties of Heron Island's main soil types were estimated using a combination of field, laboratory, and theoretical/computational techniques.

Klute (1972) and others argue that a high order of accuracy in $K\{\theta\}$ is not essential and may indeed be impractical given the variability of field soils. Hence for meaningful application of computed results to field problems; "The principle requirement is that $\theta\{\psi\}$ and saturated conductivity data adequately characterise the field soil volume of interest" (Klute, 1972; p. 273). Spatial variance in soil physical properties can also mean that the amount of data required to 'fully' describe $K\{x,y,z,\theta\}$ and $\psi\{x,y,z,\theta\}$ is prohibitive.

On the basis of the soil textural information presented in Chapter 1, it is reasoned that the soil profile at Heron Island is sufficiently uniform in the x- and y-dimensions that only z-dimensional (ie, vertical) variations need be considered. Another simplification in the model is that hysteresis in the field soil-water retention and conductivity functions is neglected. Thus a non-hysteretic model is assumed adequate when modelling bulk soil-water redistribution at Heron Island.

4.2 OBJECTIVES

The main objectives of this part of the study were to write and verify a numerical 1-D soil-water transport model for a layered soil and to quantify the hydraulic properties of Heron Island's vadose soils. The hydraulic properties of interest are:

1. bulk dry density,
2. porosity,
3. soil-water retention,
4. saturated hydraulic conductivity, and
5. unsaturated hydraulic conductivity.

4.3 THE MOVING MEAN SLOPE FINITE-DIFFERENCE METHOD

The Moving Mean Slope (MMS) method of Moldrup et al. (1989) is an explicit finite-difference scheme for approximating Richard's equation, the governing differential equation for unsaturated soil-water transport (see Equation 2-3). The MMS method relies on the exponential form of the hydraulic conductivity function, $K\{\psi\}$, to describe K at local values of matric potential, ψ:

$$K\{\psi\} = K_s\, e^{\alpha\psi}$$
(Equation 4-1)

where K_s is the saturated hydraulic conductivity (m s^{-1}) and α is a curve-fitted parameter (non-dimensional).

The MMS method calculates the constants $K_{L,i}$ and $\alpha_{L,i}$ at the current matric potential for each node point i (Equations 4-3 and 4-4; Figure 4-1). A small change in matric potential, x, is used to calculate $\alpha_{L,i}$. A value of $x > 0.2$ and < 3 cm was recommended by Moldrup et al (1989). In this study a value of 0.3 for x was found to be adequate and is used consistently.

$$K \{\psi_i\} = K_{L,i} \, e^{\alpha_{L,i} \psi_i} \qquad \textbf{(Equation 4-2)}$$

$$K_{L,i} = K \{\psi_i\} \, e^{-\alpha_{L,i} \psi_i} \qquad \textbf{(Equation 4-3)}$$

$$\alpha_{L,i} = \frac{\ln[\, K\{\psi_i + x/2\} \,] - \ln[\, K\{\psi_i - x/2\} \,]}{x} \qquad \textbf{(Equation 4-4)}$$

Soil-water flow velocities are calculated from Equation 4-5 and Equation 4-7, and cell moisture contents are updated after each time step using Equation 4-8. The constants, K_N and α_N, in Equations 4-5 and 4-6, represent the average exponential unsaturated hydraulic conductivity function between nodes i and i+1. K_N and α_N change by small amounts during the execution of the MMS method, giving rise to a relatively smooth changes in K between node points over time.
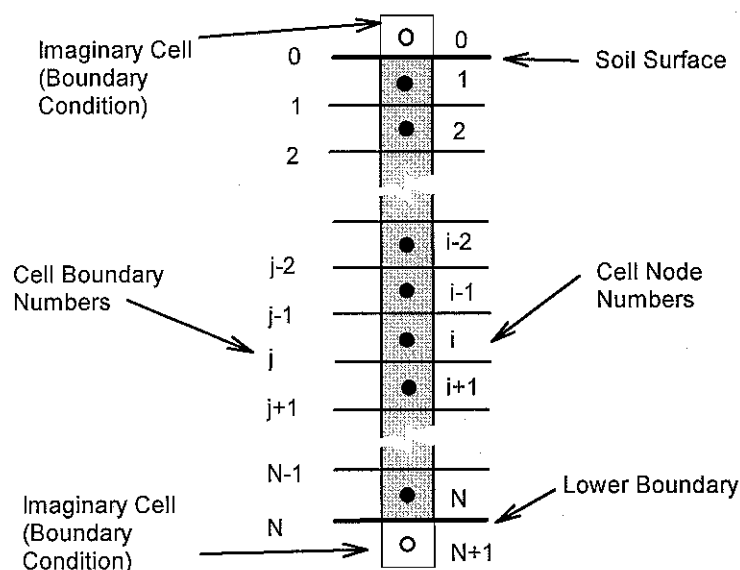
Figure 4-1. Cell boundary and node numbering conventions of the soil-water transport model.

$$\alpha_N = \frac{\alpha_{L,i} + \alpha_{L,i+1}}{2}$$

(Equation 4-5)

$$K_N = \frac{K_{L,i} + K_{L,i+1}}{2}$$

(Equation 4-6)

$$V_j = \frac{-K_N e^{\alpha_N \psi_{i+1}} - K_N e^{\alpha_N \psi_i}}{e^{\alpha_N \Delta z} - 1} + K_N e^{\alpha_N \psi_i}$$

(Equation 4-7)

$$\theta_{t+\Delta t,i} = \theta_{t,i} + \left(V_{t,j-1} - V_{t,j+1}\right)\frac{\Delta t}{\Delta z}$$

(Equation 4-8)

The solution to the finite-difference problem also requires a scheme to control numeric instability. Equation 4-9 and 4-10 were used by Moldrup et al. (1989) to avoid numeric instability, and are similarly used in this study.

$$5 < K_s\left(1 + \frac{1}{e^{\alpha_N \Delta z} - 1}\right)$$

(Equation 4-9)

$$\frac{\partial K}{\partial \theta}\frac{e^{\alpha_N \Delta z} + 1}{e^{\alpha_N \Delta z} - 1}\frac{\Delta t}{\Delta z} < 1$$

(Equation 4-10)

$$\Rightarrow \Delta t < \frac{\partial \theta}{\partial K}\frac{e^{\alpha_N \Delta z} - 1}{e^{\alpha_N \Delta z} + 1}\Delta z$$

The maximum stable time step, Δt, should be chosen such that Equation 4-10 is satisfied at all nodes. If a 'power-type' formulae are used to represent the $\psi\{\theta\}$ and $K\{\theta\}$ relationships of a homogenous soil, then the above equation for Δt simplifies to the following form:

$$\Delta t < \Phi_1 |\psi|^{\Phi_2}$$

(Equation 4-11)

where Φ_1 and Φ_2 are determined by investigation.

The above soil-water transport equations allow the soil profile to be comprised of any number of homogeneous layers with different hydraulic properties. Also, with the appropriate modifications, the surface boundary condition may be designated either a fixed or time-varying flow rate, moisture content, or pressure.

4.3.1 Program Coding and Verification

The soil-water transport model was written and compiled in F77L-FORTRAN 77 Version 4.01 (Copyright 1984-90; Lahey Computer Systems, Inc). The program pseudo-code and source code is presented in Appendix E. The soil-water transport model was verified by comparing model outcomes with three published examples: Problem A (experimental and numerical), Problem B (semi-analytical), and Problem C (semi-analytical and numerical). All three verification examples are reproduced from Haverkamp et al. (1977) and are shown in Appendix D.

4.4 HYDRAULIC PROPERTIES OF HERON ISLAND SAND

The soil that makes up Heron Island is mostly sand-sized coral sediment with significant amounts of carbonate gravel and shingle at inter-tidal elevations. The rooting zone of *Pisonia grandis* is a coffee-coloured organically-rich silty-sand, and covers most of the cay to a depth of about -1 m RGL. Below the rooting zone is a cream-coloured medium-to-coarse grained coral sand. As mentioned in Chapter 1, Heron Island has three major stratigraphic layers (refer Figure 1-5):

A. Silty-Sand Layer (above -1.0 m RGL; Pisonia grandis rooting zone)
B. Sand Layer (supra-tidal; above 2.5-3 m LWD but below -1.0 m RGL)
C. Sand-and-Gravel Layer (inter-tidal; between about 0.8 m and 2.5-3 m LWD

The silty-sand layer and the sand layer make up the vadose zone of Heron Island and as such are of most interest here. The particle mass-size relationships of the coral sand is described by the log-normal distribution on a mass basis with the geometric mean (d_{gm})

and the geometric standard deviation (σ_{gm}) defined as follows (Stockham and Fochtnian, 1977):

$$d_{gm} = \exp \{\Sigma\, m_i \log (d_i) / \Sigma\, m_i\}$$ **(Equation 4-12)**

$$\sigma_{gm} = d_{84.1} / d_{50}$$ **(Equation 4-13)**

where,

m_i	= mass retained on sieve-size class i	(g)
d_i	= sieve-size class i mid-range value	(mm)
$d_{84.1}$	= particle size for which 84.1% is smaller than by mass	(mm)
d_{50}	= particle size for which 50% is smaller than by mass	(mm)
d_{gm}	= geometric mean size	(mm)
σ_{gm}	= geometric standard deviation	(-)

To help illustrate the textural differences between the various soil layers, the cumulative particle size distributions, F{d}, of eleven different soil samples are plotted in Figure 4-2. The cumulative particle size distributions of five soil samples are also expressed mathematically for future reference (see Appendix D2; Equation D-13; Table D-1).
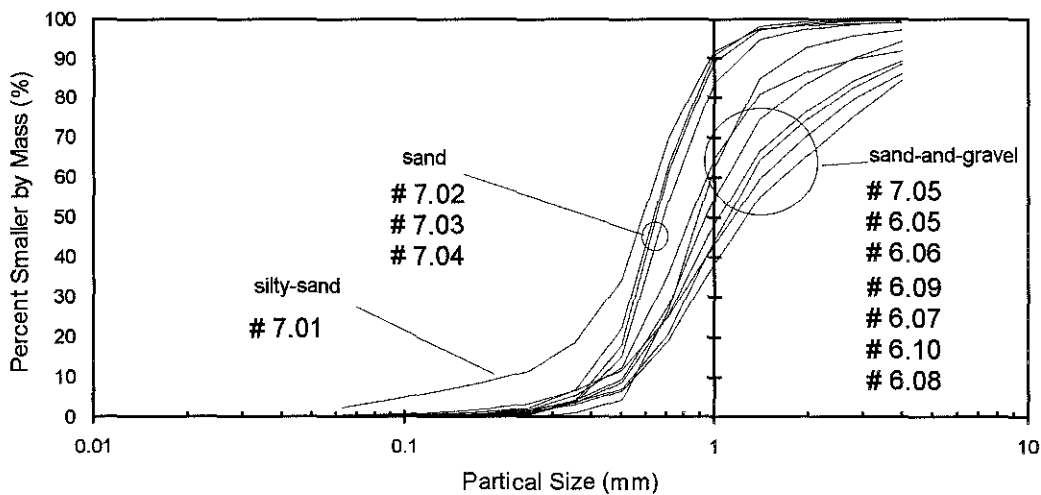
Figure 4-2. Cumulative particle size distributions of some Heron Island soil samples.

4.4.1 Methods and Equipment

4.4.1.1 Bulk Dry Density

<u>*In Situ* Cylinder Method</u>   Five minimally disturbed sand samples were tested *in situ* for bulk dry density. These *in situ* tests were all undertaken above -1.2 m RGL in a forested area of the cay. To reach the desired level in the soil profile, a pit with an area of about 80 cm by 80 cm (ie, wide enough to stand in) was hand dug. At a number of levels between -85 and -120 cm RGL a flat surface at the base of the pit was prepared in such a way as to minimise disturbance to the *in situ* soil structure. Individual sand cores were then taken from the pit floor by forcing a cylindrical metal container into the sand until it became full. Care was taken to ensure that the entire sand sample contained by the cylinder was removed intact.

The sand cores were placed in air-tight plastic bags and taken to the HIRS laboratory for weighing (scales accurate to ±0.5 g). The moisture contents of the sand samples were determined gravimetrically by oven-drying subsamples at 105 °C for 1-2 days. The volume of each metal cylinder was determined by measuring its water holding capacity on a mass basis (accurate to ±0.05 g) and assuming a water density of 1.000 g cm^{-3}. *In situ* bulk dry densities were then computed for the five sand samples, the details of which are presented in Table D-5.

<u>Disturbed Sand Samples</u>   About 87 soil samples were excavated at Heron Island using a drilling rig (refer Chapter 1 and Appendix A). These soil samples were physically disturbed and as such may have lost their natural grain-packing properties and bulk density. None-the-less, two of these sand samples were tested in the laboratory for bulk dry density using techniques similar to that described above (see Table D-4). The two sand samples examined were from between -1 and -4.5 m RGL. The sensitivity of the coral sand's bulk dry density to different packing conditions was also investigated by vibrating and compressing the sand and by submersing the sand in water.

4.4.1.2 Soil-Water Retention

The soil-water retention curves of Heron Island sand were estimated using four approaches: (1) the theoretical approach of Haverkamp and Parlange (1986) which requires particle size distributions as input data, (2) experimentally using a hanging column apparatus, (3) experimentally using pressure plate apparatus, and (4) experimentally using field tensiometry. The experimental Ψ and θ data were combined and curve-fitted using a number of published water-retention formulae. The theoretical approach was only applied to sand samples #7.01 (silty-sand), #7.04 (sand) and #6.08 (sand-and-gravel) for comparative purposes.

Theoretical Predictions   The model of Haverkamp and Parlange (1986) relates the degree of saturation of a soil to its particle size distribution, F{d}, as a function of equivalent pore radius (for a detailed discussion see Appendix D3). Haverkamp and Parlange (1986) claim that their model is able to describe the $\Psi(\theta)$ relationship of sand including the effects of air entrapment and hysteresis. Haverkamp and Parlange (1986) show that for ten different sandy soils their model results are in "excellent" agreement with their field and laboratory data. Model input includes F{d}, ρ_d, and θ_s. Errors associated with their predicted $\Psi(\theta)$ functions and their experiments were reported as being similar within an order-of-magnitude.

Detracting from the current application of the method of Haverkamp and Parlange (1986) is the fact that the particle density, ρ_d, of Heron Island sand is below recommended limits. Despite this shortcoming the method is applied to the silty-sand (#7.01), the sand (#7.04) and the sand-and-gravel (#6.08) using experimentally determined values of ρ_d (1.400 g cm^{-3}), porosity (0.45) and θ_s (0.45).

Hanging Column   A segmented hanging column constructed from clear perspex and stainless steel bolts was used to determine the characteristic curve of Heron Island sand for matric potentials between 0 and -28 cm of water head (see Figure 4-3). The hanging column was filled with the sand sample and its lower end placed in a static water reservoir. The entire arrangement was covered with plastic to inhibit evaporation. After one week it was assumed that the gravitational potential of the soil-water system was balanced by an equilibrating matric potential profile (ie, nil gravity drainage). To obtain

the main *wetting* curve, oven dried soil was used in the column. To obtain the main *drying* curve, the soil sample was saturated over its full length prior to draining. The average θ of each segment was determined gravimetrically. Each soil segment was 2 cm deep and circular, with a radius of 25 mm.
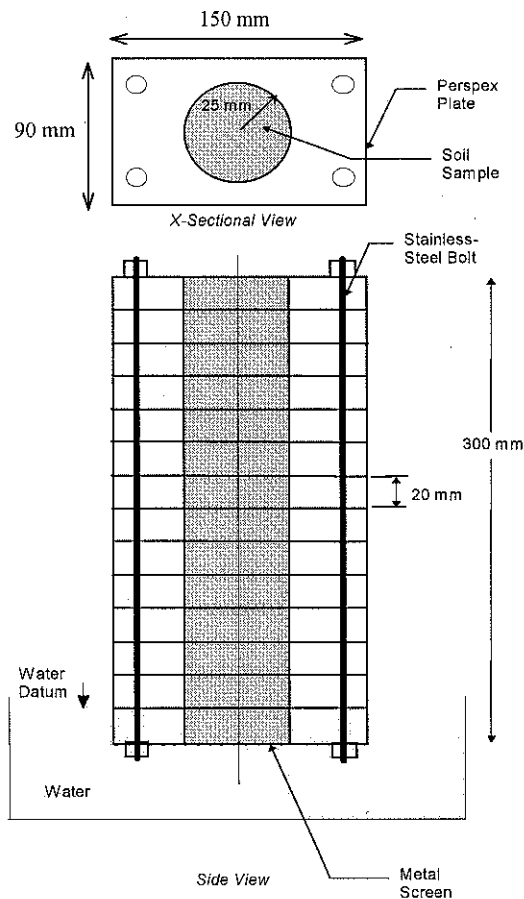
Figure 4-3. Schematic of the hanging column apparatus.

<u>Pressure Plates</u>   A pressure plate apparatus, on loan from the Department of Agriculture, the University of Queensland, was used to obtain Ψ-θ data from Heron Island sand samples. The main components of the pressure plate apparatus include (a) a number of steel pressure vessels, (b) a nitrogen gas tank, (c) a porous ceramic plate with rubber bladder for each pressure vessel, and (d) a valve-operated pressure regulator and control system (see Figure 4-4).

Sand subsamples of 15 to 30 ml volume were placed in metal rings, wet to saturation, and then placed on top of the ceramic plates which were saturated with water and placed inside the pressure vessels (one or two per vessel). The rubber bladder of each ceramic plate had a drainage tube which passed through the pressure vessels thus allowing water to drain from the soil samples and ceramic plates in response to the positive gas pressure within the vessels. The gas pressure within the vessels was maintained below that of the bubbling pressure of the ceramic to prevent gas from escaping via the drainage tubes. The gas pressure was controlled by a doubly-regulated valve system accurate to ±2 kPa. Pressures of 0-1 bar (ie, 'low' pressure) to 3-15 bar (ie, 'high' pressure) were investigated.

A pressure equilibrium between the soil-water and the gas was achieved in less than three days, after which time the sand samples were removed and their moisture contents determined gravimetrically. The average of three subsample θ values were used to determine each data point on the main drying curve of each soil sample tested.
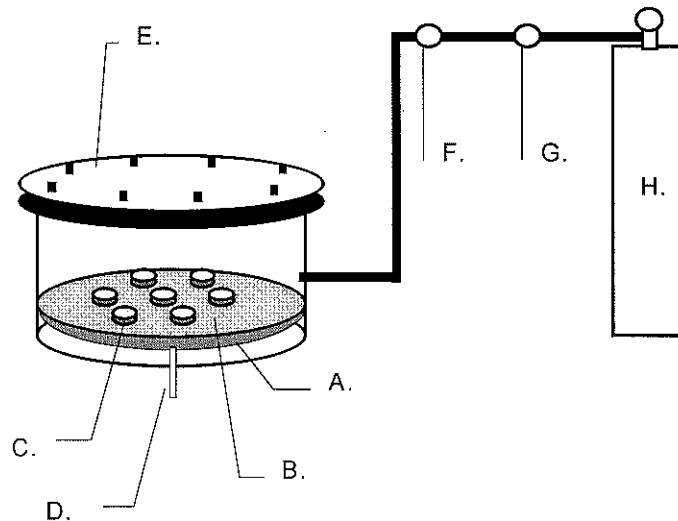
Figure 4-4.
Schematic of the pressure plate apparatus - not to scale (A. rubber diaphragm, B. porous ceramic plate, C. soil sample, D. water outlet, E. pressure vessel, F. high pressure gauge, G. low pressure gauge, H. gas cylinder).

4.4.1.3 Saturated Hydraulic Conductivity

The saturated hydraulic conductivity of Heron Island soil was estimated from a limited number of constant head permeameter tests on disturbed sand samples.

<u>Constant Head Permeameter Test</u>   The K_s of eight disturbed Heron Island soil samples were measured using a constant head permeameter constructed from rigid acrylic, metal gauze, geo-fabric and glass beads (see Figure 4-5). The experimental K_s values were computed from Darcy's principle as follows (Domenico & Schwartz, 1990):

$$Q = -A K_s \frac{\partial h}{\partial z}$$

$$\Rightarrow K_s \cong -\frac{Q}{A} \frac{\Delta z}{h_2 - h_1}$$

(Equation 4-14)

where h_1 and h_2 are the measured fluid heads immediately below and above the sample volume, respectively, Δz is the height of the sample volume, Q is the measured fluid flow-rate, and A is the cross-sectional area of the sample volume (ie, πR^2, where R is the sample radius; see Figure 4-5).

The soil samples were hand-compacted in the permeameter to approximate the bulk density found in the field and fully saturated with water prior to testing. Each test was conducted over a period of about 3-5 minutes using a head difference (h_1-h_2) of between 40 and 5 cm. Sample #7.09, which was gravel-sized, was tested with a h_1-h_2 of about 1.5 cm. Experimental details are presented in Appendix D and the results are given in Table 4-1. Replications were carried out using the same soils under the same packing conditions (refer Tables D-13 and D-14).
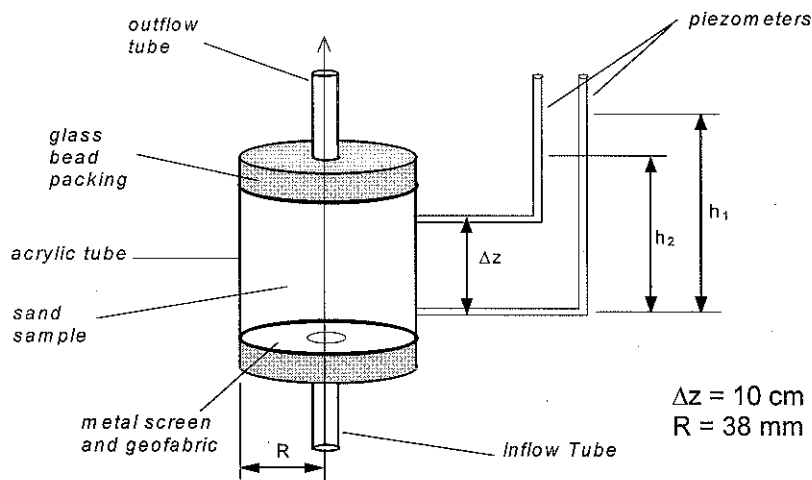
Figure 4-5. A schematic of the constant head permeameter used to test for saturated hydraulic conductivity of sand samples (not to scale).

4.4.1.4 Unsaturated Hydraulic Conductivity

The unsaturated hydraulic conductivity relationship $(K\{\psi\})$ for the silty-sand layer was estimated in the field by experiment, and the unsaturated hydraulic conductivity relationship $(K\{S'\})$ for the sand layer was numerically interpreted from Darcian flow theory and the ten-month-long field record of soil matric potentials shown in Chapter 3. The $K\{S'\}$ of the sand layer was also predicted theoretically for comparison with the numerical results. Each approach is described below.

Theoretical Estimates   The ability to theoretically predict the unsaturated hydraulic conductivity relationship of a soil (either as a function of moisture content, θ, effective saturation, S', or matric potential, ψ) from limited data is immediately useful as the direct measurement of $K\{\theta\}$ in the field or laboratory is generally difficult, time-consuming and expensive (Dirksen, 1991). Theoretical techniques for predicting $K\{\theta\}$ involve either a macroscopic or a statistical approach (Mualem, 1976), with the most appropriate approach depending on the quality and type of data available.

In the macroscopic approach, an analogy is made between simple laminar flow systems and bulk soil-water flow. Kozeny (1927), Averjanov (1950) and others have shown that there exists a theoretical justification for the use of a power function, ie:

$$K\{S'\} = K_s \, S'^{\,\alpha} \qquad\qquad \textbf{(Equation 4-15)}$$

where S'is the effective saturation and α is a soil dependent parameter. Values of α between 2.5 and 24.5 have been reported in the literature for various soil types (Mualem, 1976) whilst sandy soils tend to have an α greater than 4 (eg, Hillel, 1980). S' is defined as follows:

$$S' = (\theta-\theta_r)/(\theta_s-\theta_r) \qquad\qquad \textbf{(Equation 4-16)}$$

where θ_r is the residual moisture content and θ_s is the saturated moisture content.

In the statistical modelling approach, $K\{\theta\}$ is inferred from the soil-water retention characteristic. The three main assumptions of this approach are (Klute, 1986):

1) The interconnected pores of a given radius may be statistically characterised by a relative volume function, assuming that the areal distribution of pore radii is the same for any cross-section of the media.

2) The hydraulic conductivity of each elementary (microscopic) pore unit may be determined theoretically and then combined to provide an estimate of the overall (macroscopic) hydraulic conductivity.

3) The soil-water retention function is analogous to the pore radii distribution function, given that pore radii are uniquely related to capillary head.

Because of the various assumptions required in the above theoretical techniques, the resulting $K\{\theta\}$ would have been too inaccurate for application in the current modelling study. Hence, in preference to methods outlined above, field experiments were devised to quantify $K\{\theta\}$ of Heron Island sand (see below).

Disc Permeameter Test: Silty-Sand Layer *In situ* unsaturated hydraulic conductivity and sorptivity of the silty-sand layer at Heron Island were measured in the field with minimal disturbance to the soil structure using a disc permeameter (see Figure 4-6). The disc permeameter is a device which can supply water to a soil surface over fixed circular

area and at constant applied negative pressure (Sully and White, 1987; White, 1988). The selection of the applied pressure is important as it controls the soil pore-size sequence that participates in the infiltration process. For a theoretical background to the disc permeameter, White and Perroux (1989) and Wooding (1968) should be consulted.

The base of the permeameter was covered by a 63 μm nylon screen that was supported by steel mesh and a porous material which enabled water to pass through under suction. Water in the permeameter was stored in an upright water reservoir located in the centre of the device. A side bubble tower provided air to the central reservoir at a controlled negative head equivalent to $z_2 - z_1$ (see Figure 4-6).

The site was prepared prior to using the permeameter. This involved clearing away of surface mulch and soil until a flat surface at the appropriate depth was achieved. The moisture content and the bulk density of the soil were determined prior to the test (refer Section 5.4.1.1). Physical contact between the membrane and the soil surface was obtained by creating a slight mounding of sand beneath the permeameter base. Two pressure heads and two levels in the soil profile were examined with the permeameter giving a total of four experiments, ie: (1) $\psi = -1$ cm (applied matric potential) and $z = 0$ cm RGL (vertical position in vadose zone), (2) $\psi = -10$ cm and $z = 0$ cm RGL (3) $\psi = -1$ cm and $z = -21$ cm RGL, and (4) $\psi = -10$ cm and -21 cm RGL.

Infiltration was observed to commence when air bubbles first appeared in the water reservoir. Initially, the infiltration process is sorptivity-dominated, but after a period of time the infiltration rate reaches a steady-state and the process is then gravity dominated. The steady-state infiltration rate is used to numerically separate the capillary and gravity components from the total infiltration process. Due to the rather high flowrates involved in these particular experiments, the capacity of the central reservoir of the permeameter was insufficient to achieve steady-state flow conditions. For this reason the experiments were interrupted (for about 10-20 seconds) some time after the sorptivity-dominated

phase so that the reservoir could be refilled with water. Flow rates were recorded until steady-state was finally achieved. At the completion of the experiment soil samples from 2-3 mm beneath the permeameter were quickly taken to determine θ at the point of water entry. The cumulative infiltration, Q, the soil sorptivity, S_o, and the unsaturated hydraulic conductivity of the soil, $K\{\psi\}$, were determined using equations recommended by Sully and White (1987) (see Appendix D):

$$K\{\psi\} = q/\pi r^2 - 4bS_o^2 /[\, \pi r\, (\theta\{\psi\} - \theta_n\,)] \qquad \textbf{(Equation 4-17)}$$

where,

b ≈ 0.55
$K\{\psi\}$ = unsaturated hydraulic conductivity at a matric potential of ψ [L/T]
$\theta\{\psi\}$ = volumetric moisture content at ψ $[L^3/L^3]$
θ_n = volumetric moisture content at initial conditions $[L^3/L^3]$
q   = steady-state infiltration rate $[L^3/T]$
r   = 100, disc permeameter contact radius   (mm)
S_o = sorptivity $[L/T^{0.5}]$

S_o is equivalent to the slope of the linear portion of the Q versus $t^{0.5}$ graph in the early phase of infiltration. The steady-state flow rate (q) was calculated from Q in the late phase of infiltration.

<u>Interpretive Modelling: Sand Layer</u>   The $K\{\theta\}$ of the sand layer (ie, -1 m RGL to 2.5 m LWD) in the study plot was evaluated by numerical optimisation. The optimisation procedure involved matching $\psi'\{z = -145 \text{ cm}, t\}$ and $\psi'\{z = -200 \text{ cm}, t\}$ simulated by the finite-difference soil-water transport model to the 9 am $\psi\{z = -145 \text{ cm}, t\}$ and $\psi\{z = -200 \text{ cm}, t\}$ data recorded by the tensiometers between 1st January and 30th October 1994 (refer Chapter 3). As a first approximation, the power function (Kozeny, 1927; Averjanov 1950; Mualem, 1976; Hillel, 1980) was used to represent the $K\{\psi\}$ relation of Heron Island sand over the range of ψ encountered in the field, ie:.
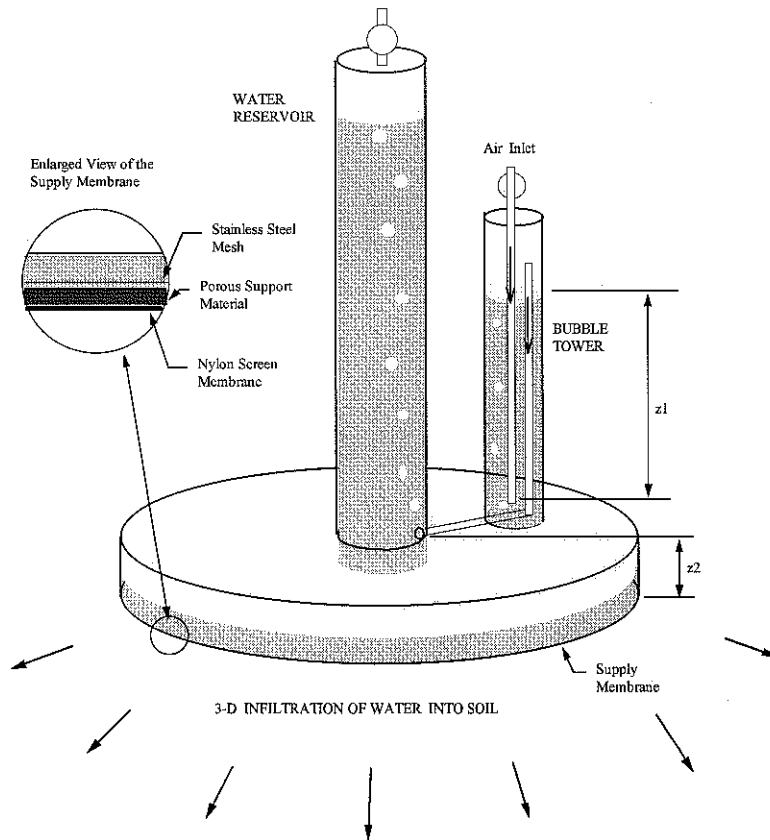
Figure 4-6. The disc permeameter (after Sully and White, 1987)

$$K\{\psi\} = \beta \left| \frac{\psi}{\psi_{ae}} \right|^{\alpha}$$

(Equation 4-18)

where,

β	= optimised parameter	(cm/hr)
α	= optimised parameter	(-)
ψ_{ae}	= -3, soil matric potential at air entry	(cm)

Although more complex empirical formulae have been used in the literature to represent the $K\{\psi\}$ relations of various soil types, the above function is advantageous in that it only has two parameters which require optimisation (ie, α and β). The optimal values for α and β were found on the basis of minimal Φ_{-145} and Φ_{-200} values, where Φ_{-145} and Φ_{-200} are the square-root of the sum-of-errors-squared on a daily basis for tensiometers located at -145 cm and -200 cm, respectively:

$$\Phi_{-145\,cm} = \sqrt{\frac{\sum_{t=1}^{303}\left(\psi_{-145\,cm}\{t\} - \psi'\{z'=-42,t\}\right)^2}{303}}$$

(Equation 4-19)

$$\Phi_{-200\,cm} = \sqrt{\frac{\sum_{t=1}^{303}\left(\psi_{-200\,cm}\{t\} - \psi'\{z'=-97,t\}\right)^2}{303}}$$

(Equation 4-20)

where,

ψ'	= simulated matric potentials	(cm)
ψ_{-145}	= field data from the tensiometer at -145 cm RGL	(cm)
ψ_{-200}	= field data from the tensiometer at -200 cm RGL	(cm)
t	= time	(d)

The finite-difference model used 30 equally sized cells to represent a 3 m deep homogeneous sand layer. The finite-difference model was not required to simulate the silty-sand layer as the tensiometer pressures recorded at -103 cm RGL were employed as the upper boundary condition. Because the top boundary of the model is at -103 cm RGL, the vertical levels used in the numerical simulations were taken relative to -103 cm RGL for convenience, ie:

$z' = z + 103$ cm $: 0 \geq z' \geq -300$ cm   (Equation 4-21)

hence,

$\psi_{-103\,cm}\{t\} = \psi\{z' = 0$ cm, t$\}$ $: 0 < t < 7272$ h   (Equation 4-22)

It is assumed in the optimisation that there were no evapotranspirative losses from the sand layer. This assumption seems reasonable as the roots of *Pisonia grandis* were only found in appreciable quantity in the silty-sand layer. Soil-water redistribution or deep drainage at the lower-boundary (ie, at z' = -300 cm) was assumed due to gravity drainage alone, hence:

$$\frac{\partial \psi \{z' = -300, t\}}{\partial z'} = 0 \qquad \text{(Equation 4-23)}$$

The above equation was approximated numerically in the model by forcing the following condition:

$$\psi\{z' = -295, t\} = \psi\{z' = -285, t - \Delta t\} \qquad : 0 \le t \qquad \text{(Equation 4-24)}$$

For the optimisation strategy to be feasible, a mathematical model of $\psi\{\theta\}$ was required a priori. For this purpose a continuous polygon with 30 straight-line segments (see Figure 4-7) was fitted to the available data describing the main drying curve of Heron Island gravelly-sand (refer Tables D-7, D-8 and D-9) using the method described in Appendix D4 and Table D-18. The initial matric potential profile at the start of the simulations were interpolated and extrapolated from tensiometer pressures recorded on the 1st January 1994 (see Figure 4-8).
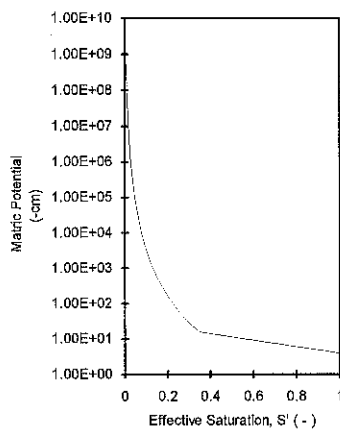
Figure 4-7. The soil-water retention model used in the simulation of unsaturated flow through Heron Island gravelly-sand.
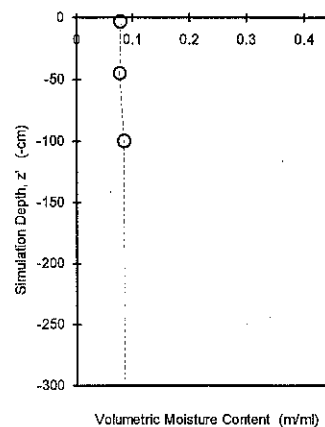
Figure 4-8. The soil-water profile on the 1st January 1994 inferred from tensiometer data (circles).

4.4.2 Results

4.4.2.1 Bulk Dry Density

A coral sand ρ_d of 1.40 ± 0.05 kg l^{-1} was determined from the five *in situ* samples taken from between -0.86 and -1.2 m RGL, and a ρ_d of 1.40 ± 0.07 kg l^{-1} was determined in the laboratory from disturbed sand samples #4.03 and #3.09. The bulk density data and the following empirical $\rho_d\{z\}$ model are displayed in Figure 4-9. From Figure 4-9 it can be seen that the silty-sand layer is less dense and less homogeneous than the clean sand.

$$\rho_d = 1.0 - 0.004\,z \quad : 0 \geq z > \text{-100 cm RGL}$$

$$\rho_d = 1.4 \quad\quad\quad : 250 \text{ cm LWD} \leq z \leq \text{-100 cm RGL} \quad\quad \textbf{(Equation 4-25)}$$

where z has units of cm and ρ_d has units if g cm^{-3}. Under ambient dry conditions the ρ_d of sand sample #7.04 was not affected by compactive force or by vibration under laboratory conditions. However when a subsample of sand sample #7.04 was allowed to settle in water, subsequent reorientation of sand grains resulted in improved grain packing and a 6% increase in ρ_d. With the ρ_d of Heron Island sand equal to 1.40 ± 0.07 g cm^{-3} and ρ_{solid} of CaCO$_3$ taken equal to 2.65 g cm^{-3} (ie, similar to that of marble; Touloukian et al., 1970) the porosity (η) of Heron Island sand is 0.47 ± 0.026.
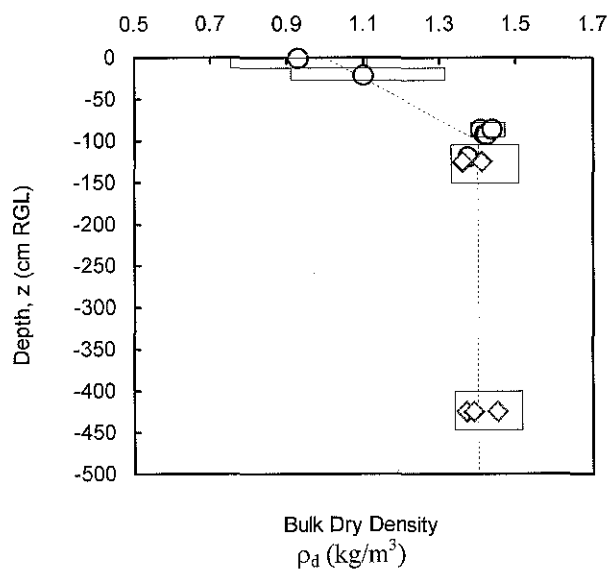
Figure 4-9. The bulk dry density profile of Heron Island soil (dashed lines are the model, cirlces are the field data, diamonds are the laboratory data, and boxes are the approx. 95% confidence intervals).

4.4.2.2 Soil-Water Retention

Theoretical Predictions   The results of Haverkamp and Parlange's (1986) water retention model are shown below in Figure 4-10 to Figure 4-12 for soil samples #7.01 (silty-sand), #7.04 (sand) and #6.08 (sand-and-gravel), respectively.

Hanging Column and Pressure Plates   Heron Island sand moisture content and matric potential data obtained from the hanging column and the pressure plate apparatus are presented in Figures D-3 and D-4 of Appendix D. Gravimetric moisture contents were converted to volumetric moisture contents using a dry bulk density of 1.4 g cm^{-3} for sand samples #7.02, #7.03, #7.04, #7.05, #3.05, #3.07, and #3.09. For the silty-sand sample #3.02, a dry bulk density of 1.3 g cm^{-3} was used.
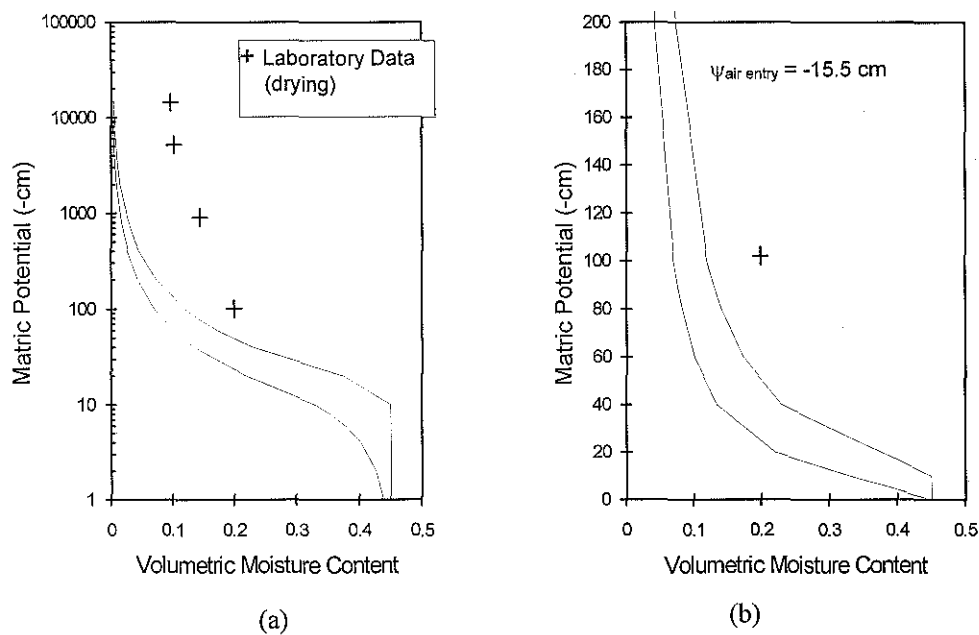
Figure 4-10. The main characteristic curves of Heron Island silty-sand at 5.42m LWD: predicted using the model of Haverkamp and Parlange (1986) and the particle size data of sample #7.01 (a) linear-log (b) linear-linear.
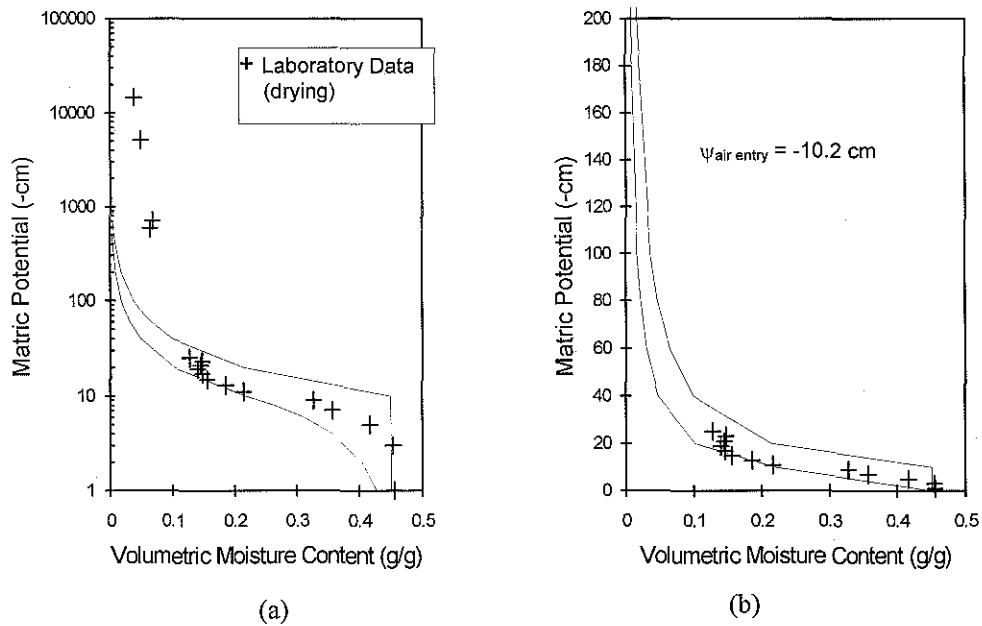
Figure 4-11. The main characteristic curves of Heron Island sand at 2.42 m LWD: obtained theoretically using the model of Haverkamp and Parlange (1986) and the particle size data of sample #7.04 (a) linear-log (b) linear-linear.
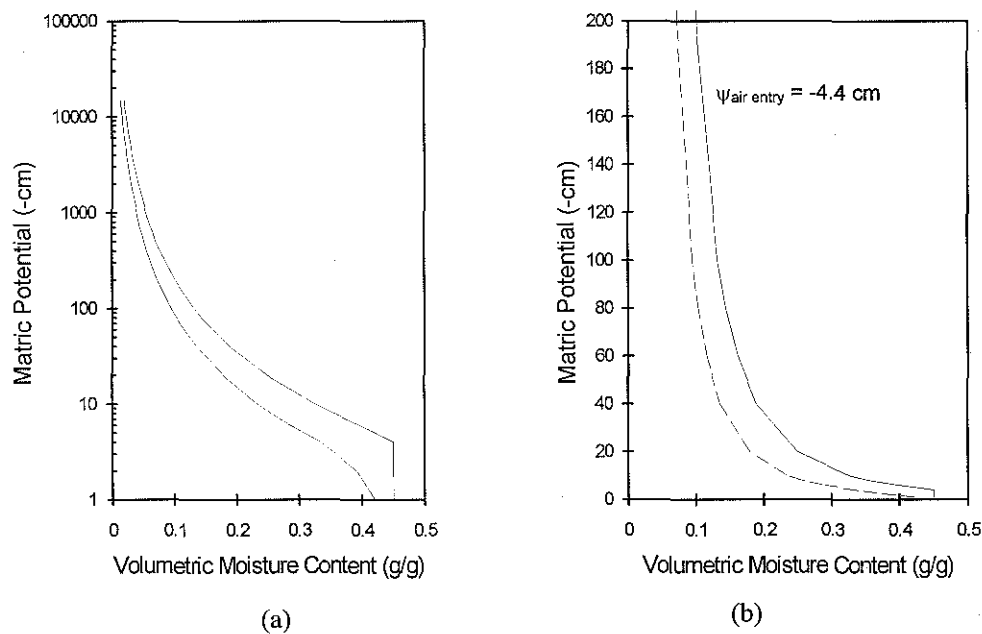
Figure 4-12. The main characteristic curves of Heron Island sand-and-gravel: obtained theoretically using the model of Haverkamp and Parlange (1986) and the particle size data of sample #6.08 (a) linear-log (b) linear-linear.

4.4.2.3 Saturated Hydraulic Conductivity

<u>Constant Head Permeameter</u>   The K_s of Heron Island soil determined by the constant head permeability test are summarised in Table 4-1. The raw data from the experiments are given in Tables D-13 and D-14 of Appendix D.

Table 4-1. Saturated hydraulic conductivities of Heron Island soil: results of constant head permeameter testing.

Sample No.	Sample Mid-depth	Sample Mid-depth	Silt Sized	Sand Sized	Gravel Sized	No. Tests	Mean K_s	Std. Dev. σ_K
(#)	(m RGL)	(m LWD)	(g/g %)	(g/g %)	(g/g %)		(m/d)	(m/d)
7.01	*0.25*	*5.42*	*2.55*	*96.1*	*1.39*	*3*	*7.1*	*0.18*
7.02	*1.25*	*4.42*	*0.11*	*99.4*	*0.54*	*4*	*38.8*	*2.3*
4.03	**1.25**	**4.10**	**0.44**	**96.3**	**3.2**	**2**	**139**	**0.55**
7.04	**3.25**	**2.42**	**0.02**	**97.6**	**2.4**	**4**	**190**	**17**
3.08	**3.75**	**1.63**	**0.05**	**95.0**	**5.0**	**2**	**138**	**0.43**
6.07	3.25	1.42	0.31	74.5	25.2	2	131	1.5
7.05	4.25	1.42	0.00	93.1	6.9	2	250.	6.2
7.09	6.5	-0.83	(no data)	(no data)	(no data)	2	1030	36

Notes:
a) Italicised text denote samples from the silty-sand layer (ie, containing organic material).
b) Bold text denote samples from the sand layer (ie, supra-tidal).
c) Regular text denote samples from the sandy-gravel layer (ie, inter-tidal).
d) Replications were under the same soil packing conditions.
e) Water temperature = 17.5 °C.
f) Sample #7.01 was coffee-coloured and compressible due to organic material.

4.4.2.4 Unsaturated Hydraulic Conductivity

Disc Permeameter: Silty-Sand Layer   The disc permeameter test was only carried out at 0 and -21 cm RGL using water potentials of -1 and-10 cm and no experimental replicates were made because of time limitations. The four resulting unsaturated hydraulic conductivity values for the silty-sand layer are shown in Table 4-2. The final $K\{\psi\}$ model for the silty sand is a power-type function (see Equations 4-18 and 4-26 and Figure 4-13) that was regressed through the data at -21 cm RGL and the laboratory determined K value for fully saturated conditions (refer sample #7.01, Table 4-1). Because the experimental data are rather scant, the $K\{\psi\}$ model derived from the field data should be considered with care (refer Table 4-2 and Figure 4-13).

$$K\{\psi\} = 2.2 \left| \frac{\psi}{-1} \right|^{-1.865}$$ **(Equation 4-26)**

where K has units of m day^{-1} and ψ units of cm.

Table 4-2. Results of the disc permeameter testing.

Code	Depth z (cm RGL)	Suction Head ψ (cm)	Duration of Expt. (hr)	Sorptivity S (mm h$^{-0.5}$)	Steady State Flow Rate q/A (mm h^{-1})	Hydraulic Conductivity K (m day^{-1})	95% Confidence ΔK (m day^{-1})	Final Moisture θ (ml ml^{-1})
A	0	-10	1.633	1.28	1.86	0.044	0.001	0.55±0.03
B	0	-1	1.483	3.61	6.4	0.152	0.003	0.7-1.0[b]
C	-21	-10	1.283	1.11	1.30	0.030	0.001	0.24±0.03
D	-21	-1	0.313	81.5	254	2.2	0.5	0.37±0.035

Notes:
a) Date of experiments was 30/10/93
b) Due to a high organic content.
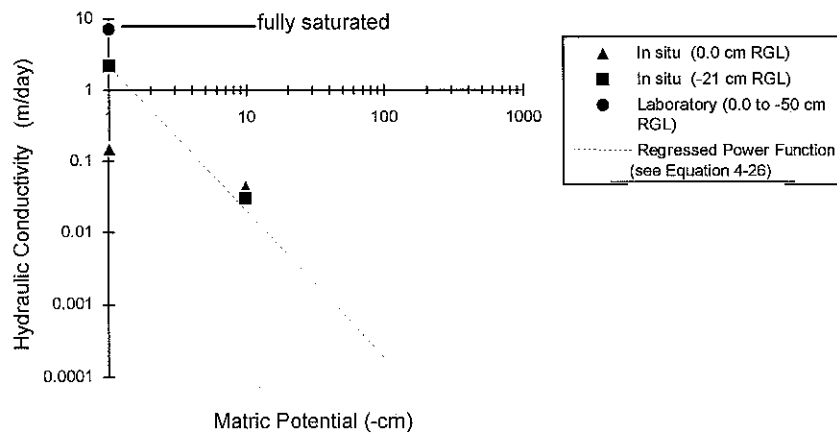
Figure 4-13. Preliminary unsaturated hydraulic conductivity model (dashed line) and experimental data for Heron Island silty-sand (refer main text).

Interpretive Modelling: Sand Layer   Variables α and β in Equation 4-18 were optimised for the sand layer by the trial-and-error matching of simulated matric potentials with field data over a 303 day period of soil-water redistribution. In the optimisation exercise 78 different combinations of α and β were tested. Each simulation using the finite-difference soil-water transport model required approximately 45 minutes of CPU time on a 40 MHz 486 DX personal computer. The error indices, Φ_{-145} and Φ_{-200}, for each of these simulations are presented in Figure 4-14 and Figure 4-15, respectively, as function of α and β. Values of Φ_{-200} in Figure 4-15 show quite clearly that the combination $\alpha = -2.7$ and $\beta = 2.8$ cm h^{-1} is near-optimal. On the other hand, over the range of α and β tested, the resulting Φ_{-145} values do not indicate an optimal solution (see Figure 4-14). Because of the greater sensitivity of Φ_{-200} to α and β, the values $\alpha = -2.7$ and $\beta = 2.8$ cm h^{-1} were selected as the final results of this optimisation exercise. The simulated matric potentials at z = -145 cm and z = -200 cm (assuming α = -2.7 and β = 2.8 cm h^{-1}) are compared in Figure 4-16 with the observed matric potentials at z = -145 cm and z = -200 cm.
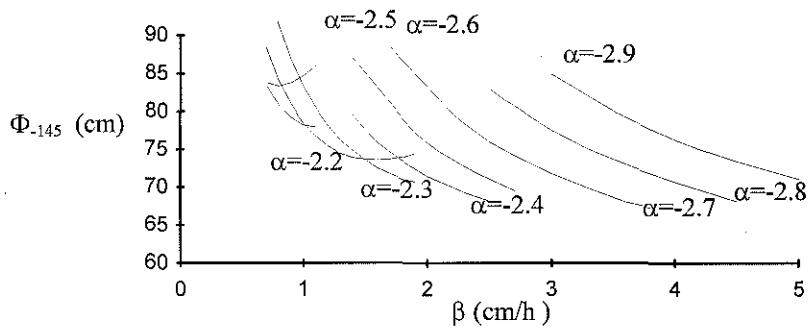
Figure 4-14. Goodness-of-fit of various α and β values in simulating field matric potentials at z=-145 cm for a 303 day study period (refer Equation 4-18).
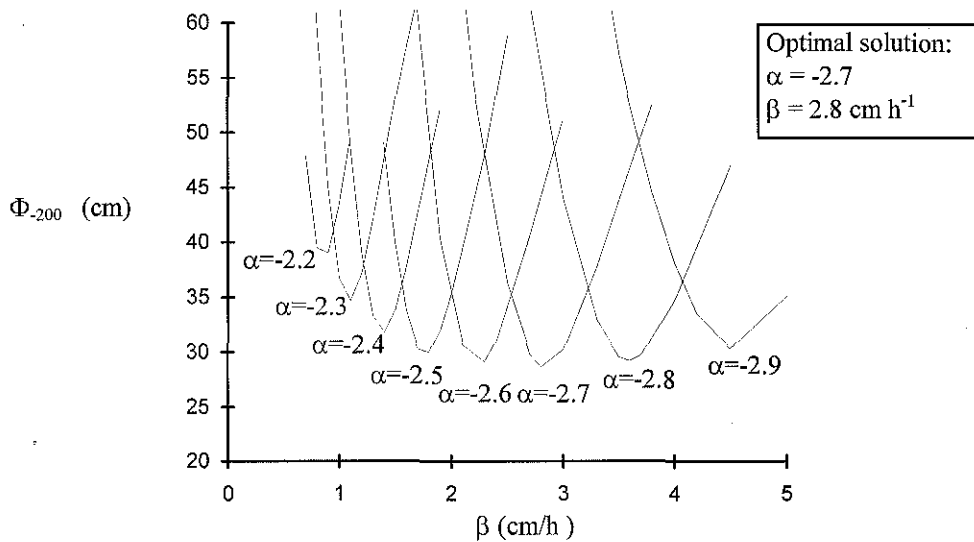
Figure 4-15. Goodness-of-fit of various various α and β values in simulating field matric potentials at z=-200 cm for a 303 day study period (refer Equation 4-18).
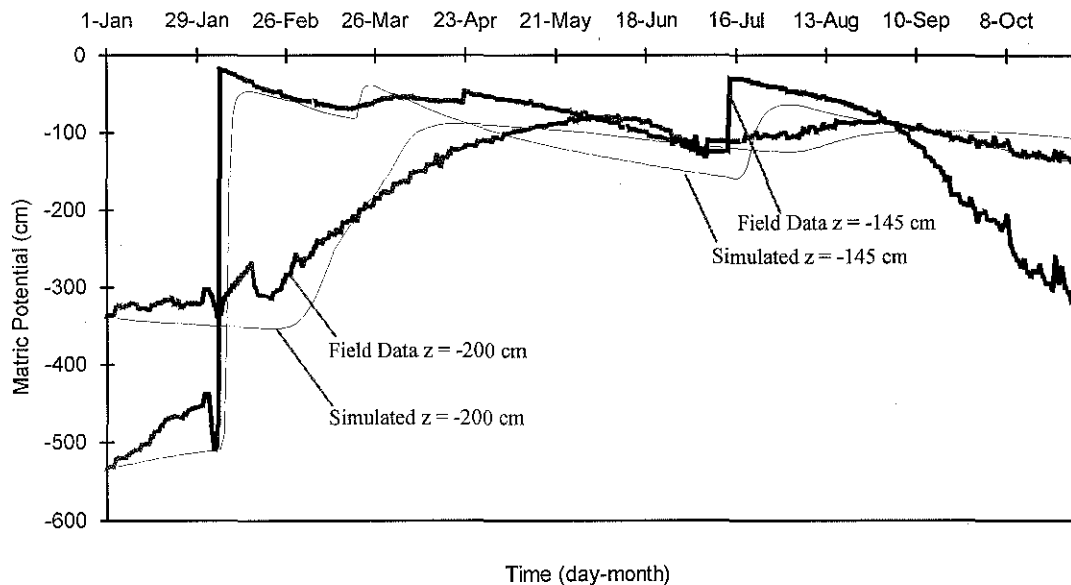
Figure 4-16. A comparison of field and simulated soil matric potentials at the -145 and -200 cm levels: results of the optimisation for $K\{\psi\}$ using the Darcian finite difference model (refer main text).

4.5 DISCUSSION

<u>Soil-Water Retention</u>   The soil-water retention data that were obtained from the hanging column (high moisture levels), the tensiometer nest (intermediate moisture levels) and the pressure plates (low moisture levels) are combined in Figure 4-17 and Figure 4-18 to characterise the water-retentivity of the silty-sand and the coral sand, respectively. The experimentally derived ψ-θ relationship for sand sample #7.04 (see Figure 4-11) shows that ψ reduces to -3 cm (ie, the air-entry pressure) at the first stage of desaturation. With further drying (ie, $0.43 < \theta < 0.15$ ml ml^{-1}) ψ reduces rather gradually until a 'critical' region (ie, $\theta \approx 0.15$ ml ml^{-1}) is reached where further drying results in ψ reducing dramatically. Hence four regions are identified in the $\psi\{\theta\}$ relationship for coral sand: (1) the saturation region, where ψ is first affected by air entering the soil-water matrix, (2) the 'wet' region, where ψ is rather insensitive to changes θ, (4) the 'critical' region, and (4) the 'dry' region, where ψ is sensitive to small

changes in θ. The experimentally derived ψ-θ data for the silty-sand (see Figure 4-18) indicates that its relationship is highly non-linear but without the critical region evident in the ψ-θ data of the coral sand.

The pressure plate data in Figure 4-17 (drying phase only) show a rather consistent water-retention pattern for the gravelly-sand layer. It therefore appears that this layer is reasonably homogeneous and may be modelled with a single characteristic curve. Sample #3.02, which was taken from the silty-sand layer, retained significantly more moisture than did the sand samples and so is modelled with a different characteristic curve (see Figure 4-18).

The ψ-θ data produced by the hanging column apparatus show an anomaly between -22 and -24 cm of matric potential (see Figure D-1). A likely explanation for this anomaly is that moisture near the top of the hanging column was not in hydraulic equilibrium with the soil matrix. Figure D-1 also shows that water-retention in Heron Island soil is hysteretic. Compared to the wetting cycle, matric potentials recorded during the drying cycle are significantly lower due to enhanced imbibition during drying cycle. The hysteretic nature of water-retention in the silty-sand, sand, and gravelly-sand are also illustrated theoretically in Figure 4-10, 4-11 and Figure 4-12, respectively.

A number of closed-form empirical models were fitted to the coral sand water-retention data (refer Appendix D5). It was found that the simple power/exponential function, the exponential function of Simmons et al. (1979) and the power function of Brooks and Corey (1964) provide poor fits to the data, whereas the more complex models of Brutsaert (1966), Haverkamp et al. (1977) and Van Genuchten (1980) were found to perform reasonably well (not shown). Of these, the model of Van Genuchten (1980) gave the best overall fit to the data (see below).

$$\theta\{\psi\} = \frac{(\theta_s - \theta_{wp})}{\left[1 + \left(|\psi|/a\right)^b\right]^c} + \theta_{wp} \qquad \text{(Equation 4-27)}$$

$$S'\{\psi\} = \frac{1}{\left[1 + \left(|\psi|/a\right)^b\right]^c} \qquad \text{(Equation 4-28)}$$

Table 4-3. Parameters describing the dying characteristic of Heron Island sand (refer Equation 4-27).

Soil Type	Wilting Point θ_{wp} [a] $(cm^3\ cm^{-3})$	Saturation θ_s [b] $(cm^3\ cm^{-3})$	a (cm)	b $(-)$	c $(-)$
Heron Island Sand	0.042	0.45	5.5	6	0.11
Heron Island Silty-Sand	0.096	0.45	5.5	6	0.07

Notes:
(a)   The curve-fitting was accomplished with SigmaPlot Scientific Graphing System software (© Jandel Corporation) using the method of least squares with θ as the independent variable.
(b)   Near permanent wilting point moisture contents (obtained from the pressure plate test at -14 bar).
(c)   Obtained from the hanging column test.
(d)   Equation 4-27 is that of Van Genuchten (1980).

The closed-form model of Van Genuchten (1980) was fitted to the ψ-θ data using the method of weighted least squares (see Figure 4-17 and Table 4-3). It was found by the trial-and-error testing of different weighting schemes that the weighting of the ψ data in the intermediate-θ region gave reasonable results for both high-θ and low-θ regions, however despite the careful selection of the weighting scheme the model is unable to provide a close fit to all of the ψ-θ data simultaneously (see Figure 4-17). The greatest deviations occur in the 'critical' region of $0.10 < \theta < 0.20$ ml ml^{-1}. Equation 4-27 was fitted to the ψ-θ data for the silty-sand assuming the same a and b values that were obtained for the coral sand (see Figure 4-18 and Table 4-3). It appears that the silty-sand data are well suited to the model of Van Genuchten (1980), however because the experimental ψ-θ data are rather scant at intermediate and high θ levels the silty-sand $\psi\{\theta\}$ model should be considered with care.
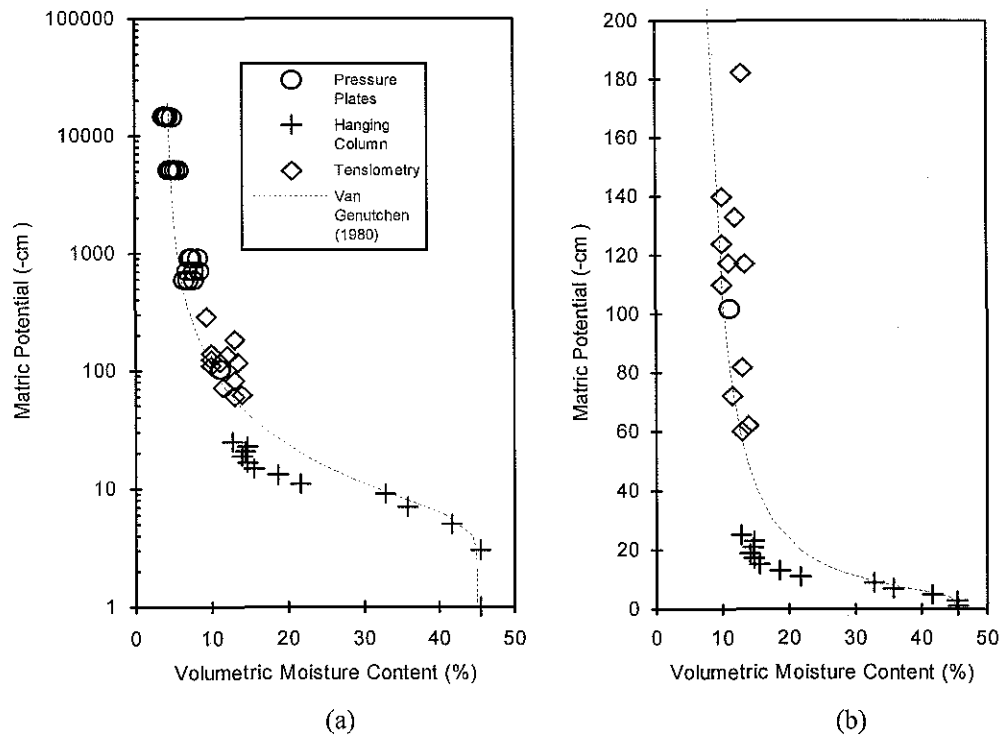
Figure 4-17. A water-retention model for Heron Island gravelly-sand (refer Appendix D for data): (a) log-linear plot, (b) linear-linear plot.
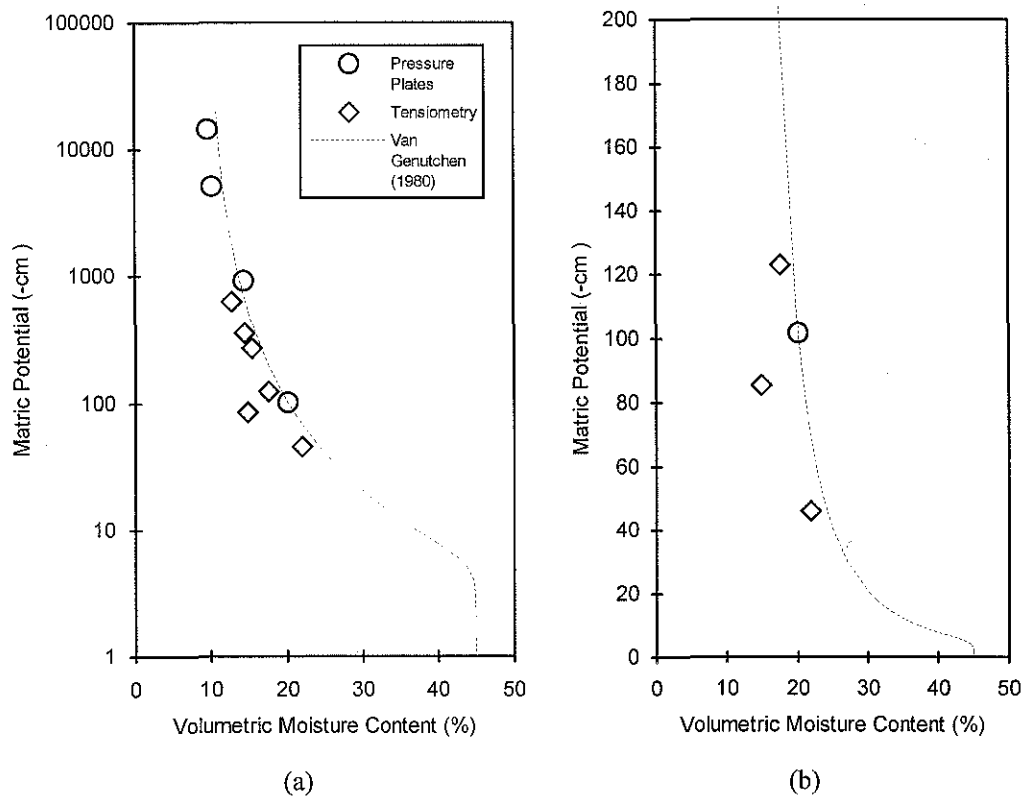
Figure 4-18. A water-retention model for Heron Island silty-sand (refer Appndix D for data): (a) log-linear plot, (b) linear-linear plot.
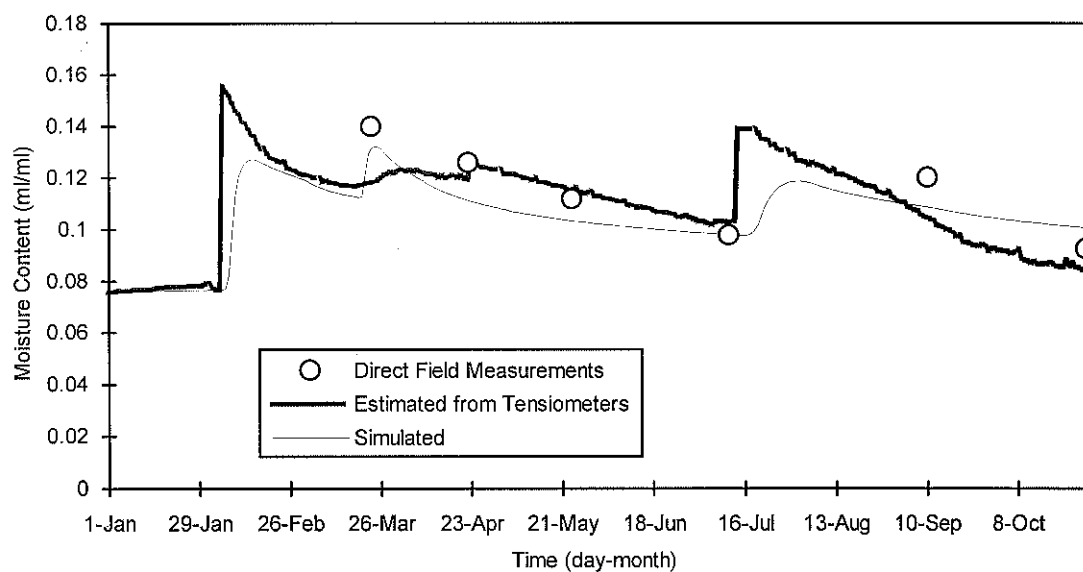
Figure 4-19. A comparison of actual and simulated soil moisture contents at the -145 cm level: results of the optimisation for K{ψ} using the Darcian finite difference model (refer main text).
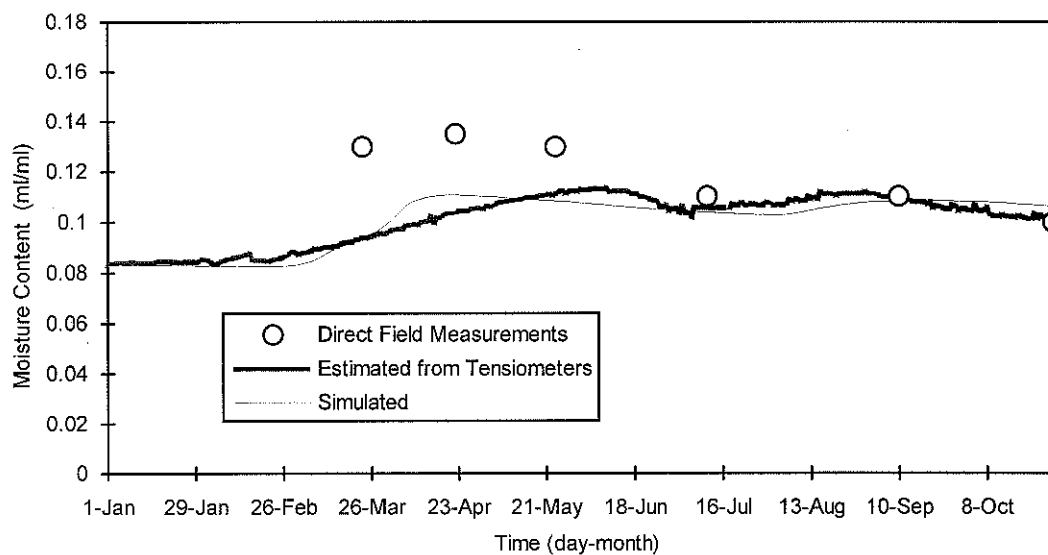
Figure 4-20. A comparison of actual and simulated soil moisture contents at the -200 cm level: results of the optimisation for K{ψ} using the Darcian finite difference model (refer main text).

<u>Saturated Hydraulic Conductivity</u>   The K_s of Heron Island sand was measured in the laboratory to give a mean value of 155 ± 60 m day^{-1} (N=3) which is typical of a coarse sand. The results of constant head permeability experiments also show that the K_s of silty-sand is about one order-of-magnitude smaller than the K_s of sand (see Table 4-1). This difference can be attributed to the organic content of the silty-sand which gives a softer, lighter, less-grainy structure and possibly different physico-chemical properties.

<u>Interpretive Modelling: Sand Layer</u>   The combination of $\alpha = -2.7$ and $\beta = 2.8$ cm h^{-1} appear optimal with regards to Φ_{-200} (refer Figure 4-15). On the other hand the combination $\alpha = -2.7$ and $\beta = 2.8$ cm h^{-1} is not optimal with regards to Φ_{-145} (refer Figure 4-14). This reliance on Φ_{-200} as the optimising criterion seems to have been a reasonable choice given that Φ_{-200} was more sensitive to α and β than was Φ_{-145}, and that the final $\psi\{z,t\}$ simulations are qualitatively and quantitatively similar to the field data over most of the 303 day simulation period (see Figure 4-16). In Figure 4-16 it is observed that the matric potentials simulated at $z = -145$ cm deviate substantially from the observed potentials after the 10th September. Whilst the cause of this deviation is not clear, one possible explanation is that the assumed gravity-drainage lower boundary condition is inappropriate during that period of soil-water redistribution.

To further assess the validity of the interpreted $K\{S'\}$ function, the simulated moisture contents at $z = -145$ cm and $z = -200$ cm are compared with the moisture contents determined by tensiometry and the gravimetric method in Figure 4-19 and Figure 4-20, respectively. The approximate nature of the numeric model has resulted in noticeable differences between the simulated and observed data sets. In over half of the cases STEM underestimated the actual soil moisture contents but followed reasonably closely the soil moisture trends determined by tensiometry. The cause of the differences cannot be explained explicitly but would have been caused in part by the hysteresis in the ψ-θ relationship in the field. The overall qualitative and quantitative matching of simulated to observed matric potentials is encouraging and is believed reasonable given the scope of the study and the experimental and conceptual uncertainties inherent in the numerical model.

5. EVAPOTRANSPIRATION AND SURFACE WATER FLOW: A FIELD APPROXIMATION

5.1 INTRODUCTION

Some of the field and laboratory results described in Chapters 3 and 4 are used in this chapter to estimate the evapotranspiration and surface runoff from the study site during the 10-month-long study period. As mentioned in Chapter 2, the vertical one-dimensional field-water balance for the soil-plant atmosphere continuum (SPAC) can be used to estimate the cumulative evapotranspiration, $\int E_t \, dt$, from a control volume if suitable field data are available (see Equation 5-1 & Figure 5-1a), i.e.:

$$\int P \, dt = \int E_t \, dt + \int D \, dt + \int R \, dt + \Delta S \qquad : t_1 \to t_2$$

$$\Rightarrow \int E_t \, dt = \int P \, dt - \int R \, dt - \int D \, dt - \Delta S \qquad : t_1 \to t_2 \qquad \textbf{(Equation 5-1)}$$

where,

P	= precipitation rate	$(mm \; d^{-1})$
R	= surface runoff rate	$(mm \; d^{-1})$
E_t	= evapotranspiration rate	$(mm \; d^{-1})$
D	= deep drainage rate	$(mm \; d^{-1})$
ΔS	= soil water storage change	(mm)
t	= time	(d)

In this study the application of the above field-water balance formula is not straight-forward due to the absence of field values of deep drainage and surface water ponding and movement. To overcome the absence of deep drainage, surface runoff and ponding data, two approximate sub-models are introduced to allow the indirect estimation of these particular parameters. To further simplify the analysis, canopy interception, a significant component of evapotranspiration, is removed from the balance by substituting rainfall (P) with throughfall (P_c). Also discussed in this chapter is a possible relationship between soil-water potential and forest evapotranspiration rate.
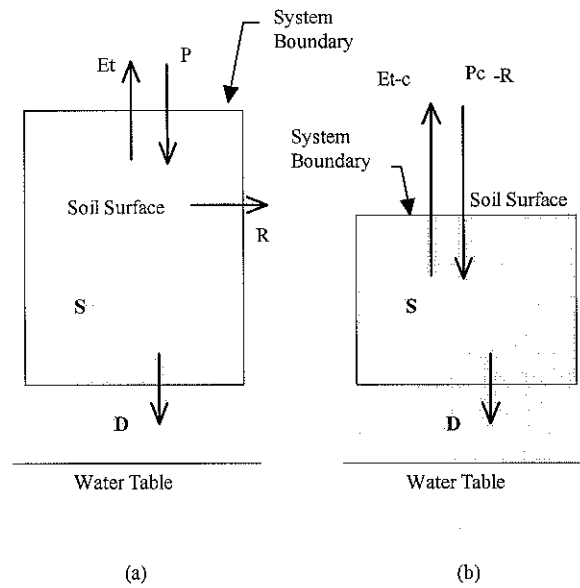
Figure 5-1. System boundaries and flow terms for the estimation of 1-D field-water balance using either: (a) total evapotranspiration, or (b) evapotranspiration-less-interception

5.2 OBJECTIVES

The main objective of this chapter is to estimate the field-water balance for the forested study site at Heron Island for a period of 10 months (ie, the study period). This field-water balance estimate will be used in the following chapter to calibrate a Soil-Water Transport and Evapotranspiration Model (STEM). Other objectives of this chapter are to discuss the likely relationship between actual evapotranspiration rate (E_t) and soil moisture levels in the *Pisonia grandis* forest, and to propose a simple but effective empirical model for this relationship for incorporation with STEM in Chapter 6.

5.3 A FIELD-WATER BALANCE APPROACH

Rather than using the daily rainfall (P) values recorded by the HIRS weather station (recorded about 200 m from the study plot; refer Chapter 3), throughfall (P_c) recorded at the study site was used with Equation 5-2 to evaluate the cumulative evapotranspiration-less-canopy interception, $\int E_{t-c} dt$. Equation 5-2 is derived for a sub-

system within the soil-plant-atmosphere continuum that is defined by Figure 5-1b. This sub-system field-water balance is prefered here because it avoids the estimation of canopy interception: a parameter which is difficult to measure in the field for logistical reasons. The hourly and daily records of P_c and and daily records of $S\{t\}$ were obtained in the field (refer Chapter 3).

$$\int E_{t\text{-}c} \ dt = \int P_c \ dt - \int R \ dt - \int D \ dt + S\{\text{1st Jan. 1994}\} - S\{t\} : t1 \to t2$$

(Equation 5-2)

where,

$E_{t\text{-}c}$ = evapotranspiration-less-interception rate   (mm d^{-1})
P_c = throughfall rate   (mm d^{-1})
S = soil-water storage in system   (mm)

R and D are both required in Equation 5-2 but were not measured in the field. An indirect estimate of deep drainage, D, across the -172.5 cm RGL level in the study plot was evaluated using Darcy's formula for macroscopic water velocity in unsaturated porous media, ie:

$$D = K(\theta)\left(\frac{\partial \psi(\theta)}{\partial z} + 1\right) : \theta \leq \theta_s$$

(Equation 5-3)

where z is +ve upwards and D +ve downwards. By substituting the true matric potential gradient with the tensiometer readings at -145 and -200 cm RGL (refer Chapter 3) the following approximate formula for D at -172.5 cm RGL is obtained, ie:

$$D\{t\} \cong K(\theta_{avg})\left(\frac{\psi_{-200}\{t\} - \psi_{-145}\{t\}}{-200 + 145} + 1\right) \quad : \theta \leq \theta_s$$

(Equation 5-4)

where θ_{avg} is the average of the two moisture contents that are inferred from tensiometer readings as follows;

$$\theta_{avg} = \frac{\theta\{\psi_{-200}\{t\}\} + \theta\{\psi_{-145}\{t\}\}}{2}$$ (Equation 5-5)

The above 'moisture averaging' approach for estimating D{t} employs the K{θ} and ψ{θ} functions for coral sand that were determined in Chapter 4. The D{t} estimate obtained using Equations 5-4 and 5-5 is shown in Figure 5-2. Also shown in Figure 5-2 is D{t} estimated using the moving mean slope (MMS) numerical technique. The MMS technique, which is considered to be more accurate than simple 'moisture averaging' is described in Chapter 4.
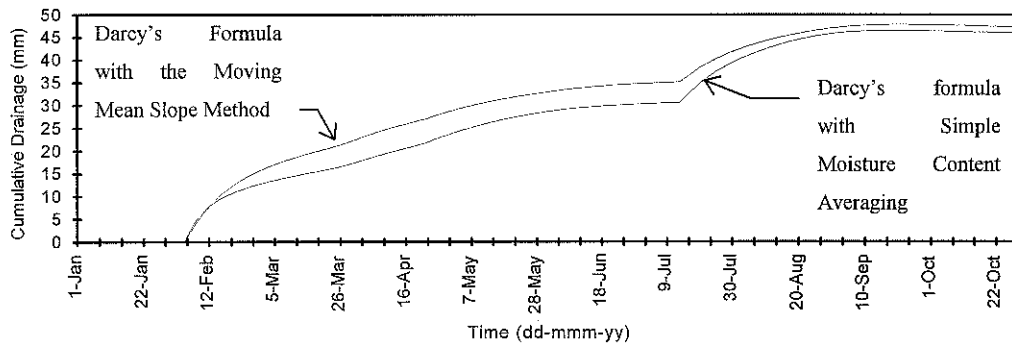
Figure 5-2. Darcian estimates of cumulative drainage at -172.5 cm RGL (refer main text).

Although the study site at Heron Island was relatively flat it appears that small-scale topographic relief and limited surface infiltrability had resulted in significant water movement across the study site on occasions. Because overland flow, R, into and out of the study site was not measured or controlled during the field investigations, some assumptions regarding R are required in the estimation of $\int E_{t-c}dt$ from Equation 5-2. The main assumption is that R is greater than zero only on those days when the hourly rainfall rate exceeded the measured infiltration capacity of the soil (see Equation 5-6). A soil-surface infiltration test conducted in October 1993 indicates that the steady-state infiltration capacity of the soil surface in the study area was about 6 mm h^{-1} at that time (refer Chapter 4). Further, by assuming that E_{t-c} is equal to its potential value during those days of expected runoff, a continuous estimate of E_{t-c} and R was made. This approach is best suited to sites where surface runoff is infrequent. At the Heron Island study site there were only 15 days during the 303 day study period when P_c was greater than 6 mm/hr. These days are the 18th, 19th, and 20th of January, the 3rd, 4th and 23rd of February, the 2nd, 4th, 18th and 30th of March, the 4th of April, the 1st of May, the 15th of June, and the 22nd and 29th of October 1994.

$$E_{t-C} = P_c - d/dt\ S - D \text{ and } R=0 \qquad : P_c \leq 6 \text{ mm/hr} \qquad \textbf{(Equation 5-6)}$$

$$E_{t-C} \cong E_{tP} \text{ and } R = P_c - d/dt\ S - E_{tP} - D \qquad : P_c > 6 \text{ mm/hr}$$

Because E_{tP} is uncertain, arbitrary low (3 mm d^{-1}), medium (5 mm d^{-1}) and high (8 mm d^{-1}) values for E_{tP} were tested with Equation 5-6 in an uncertainty analysis. The results of the analyses for the period 1st January - 30th of October 1994 are shown in Figure 5-3 and Appendix C. The $\int E_{t-c}dt$ estimated for this period is 645-720 mm which implies an average daily E_{t-c} of 2.1-2.4 mm d^{-1} (see Figure 5-3). $\int E_{t-c}dt$ is therefore estimated to be about 70-80% of $\int P_c dt$, $\int R dt$ about 15-25% of $\int P_c dt$, and $\int D dt$ about 5% of $\int P_c dt$ for the study period.

Although the results are lacking a rigorous uncertainty analysis, the figures are realistic in terms of mass balance and the observed throughfall, soil matric potentials and moisture contents for the 10-month-long study period.
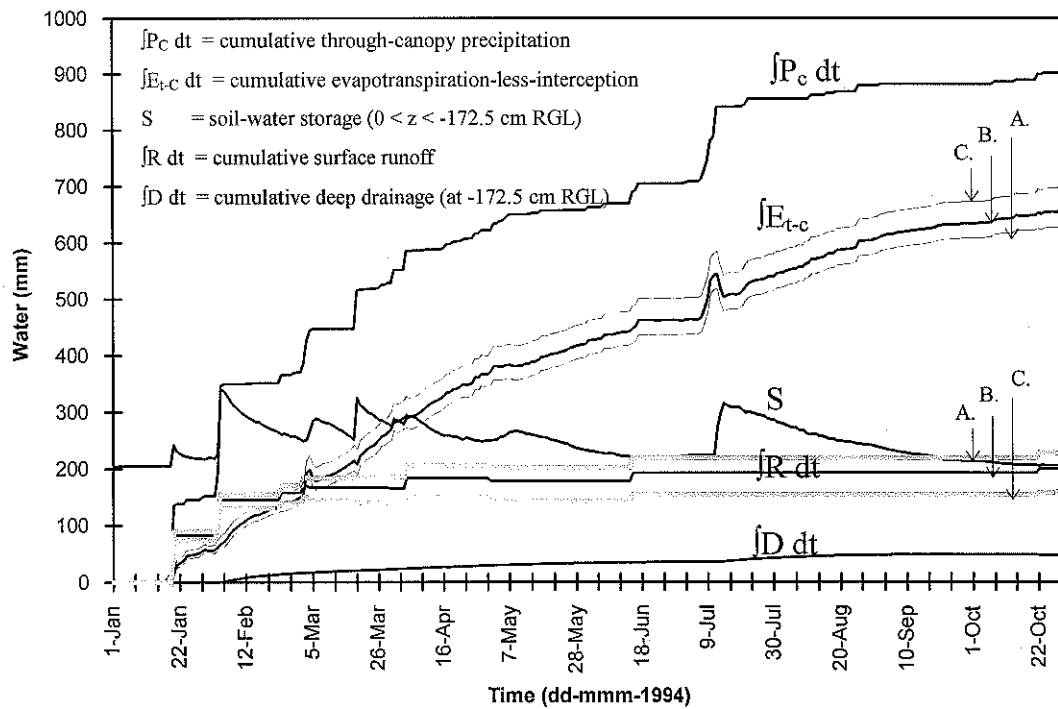
Figure 5-3. A field-water balance estimate of actual evapotranspiration (less canopy interception) and runoff from the study site using Equation 5-6 and assuming (A.) $E_{tP} = 3$ mm d^{-1}, (B.) $E_{tP} = 5$ mm d^{-1} and (C.) $E_{tP} = 8$ mm d^{-1}

Cumulative evapotranspiration, $\int E_t \, dt$, for the study period may now be estimated by adding to $\int E_{t-c} \, dt$ an estimate of cumulative canopy interception, $\int E_c \, dt$. A first approximation of $\int E_c \, dt$ is 210 mm: the measured difference between $\int P \, dt$ and $\int P_c \, dt$ over the period 1 January - 30 October, 1994 (see Figure 3-6). Thus the best available estimate of $\int E_t \, dt$ at Heron Island is 855-930 mm for the entire 303 day study period. This equates to 2.8-3.1 mm d^{-1} on average and extrapolates to 1000-1100 mm a^{-1}.

5.3.1   Uncertainty

The $\int E_{t-c} dt$ and $\int R dt$ curves shown in Figure 5-3 are subject to uncertainty associated with the conversion of tensiometer potentials to soil moisture values (and ΔS) and with the prediction of unsaturated flow velocties (and D). Because ΔS between the 1st

January and the 31st October 1994 is relatively small the absolute error in ΔS is expected to be small. The uncertainty in $\int D dt$ is difficult to rationalise, however, as the current estimates of $\int D dt$ are related to the $K\{\theta\}$ and $\psi\{\theta\}$ functions for the soil: functions which were determined by a combination of approximate experimental and numerical techniques. A major source of uncertainty in the field-water balance for the study period derives from the partitioning of throughfall between the evapotranspiration and surface runoff compartments. Relative errors associated with the evaluation of $\int E_{t-c} dt$ are expected to be greatest when the integration period is smallest. Hence the results shown in Figure 5-3 should be considered with care as confidence limits were not determined due to lack of suitable field data.

5.4 SOIL-WATER POTENTIAL AS AN INDICATOR OF EVAPOTRANSPIRATION RATE

A gradient of water-potential is required to mobilise moisture from surrounding soil to a plant's roots and from its roots to its leaves. Hence the water-potentials within plant foliage (p_L) give an indication as to the transpiration rate, evaporative demand and soil-water availablility (eg, Davie, 1982; Carbon, 1973). Campbell (1977) defines p_L as the sum of the gravitational, osmotic, matric, and hydrostatic potentials.

In general, p_L is usually more negative during the day reaching a minimum at the peak of evaporative demand around midday (see Figure 5-4). When soil-water is plentiful, falling leaf-pressures are usually accompanied by the opening of stomates enabling transpiration. Towards dusk, a plant's stomates tend to close and p_L tends to rise as it equilibrates with the soil-water pressure regime (eg, Carbon, 1973). If soil-water becomes depleted due to a lack of rainfall, soil matric potentials become more negative and daytime leaf-water pressures in the plant must reduce even further if water is to be drawn from the soil into the plant. This water-stressed condition is usually evidenced by lower pre-dawn pressures in the plant. Prolonged water-stress may eventually result in closure of the stomates, overheating, and finally wilting of the plant's leaves.

Allaway et al. (1984) provide some information on the plant-water relations of *Pisonia grandis* at nearby One Tree Island: a small shingle cay 18 km ESE of Heron Island with an area of about 5 ha and a maximum elevation of 3 m. The vegetation at One Tree is more exposed to saltation than at Heron Island. The soil there is a mixture of coral rubble, coral sand and organic material, and is porous and well draining but with an overall water-retaining capacity "...larger than would be expected from its texture" (Allaway et al., 1984 page 452).

Allaway et al. (1984) found that when soil-moisture was plentiful, *Pisonia grandis* at One Tree demonstrated negative predawn p_L and a diurnal decrease in p_L in the range of 0.5 - 1.0 Mpa (see Figure 5-4). Other plant species at One Tree (ie, *Melanthera*, *Argusia* and *Scaerola spp.*) also demonstrated similar diurnal decreases in leaf-water pressure. During drought conditions, predawn p_L of *Pisonia grandis* were significantly lower than for unstressed conditions but smaller daytime pressure differences occurred (Allaway et al., 1984).
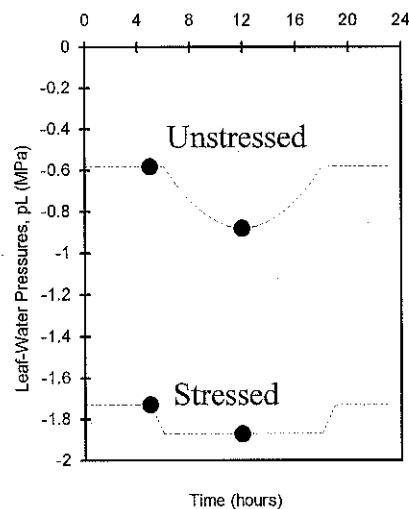
Figure 5-4. Leaf-water pressures in *Pisonia grandis* at One Tree island under stressed and unstressed conditions (reproduced from Allaway et al., 1984; dashed lines are the author's interpretation).

As mentioned in Chapter 2, the rate of transpirative water loss is greatly influenced by total canopy resistance to vapour transfer, r_{vc} (eg, Zhang and Lemeur, 1992; Stewart, 1984). Total canopy resistance to vapour transfer is in turn related to canopy density, plant-water pressure, soil-water status, evaporative demand and other factors (possibly) such as irradiance and biomorphology. The measurement of r_{vc} characterictics of *Pisonia grandis* was beyond the resources of the current study and are currently unknown. None-the-less, empirical equations provided by Campbell (1985) are supposed to describe well the relationship between total canopy resistance to vapour transfer (r_{vc}) and leaf-water pressure (p_L) for various tree species (see Equation 5-7). According to Campbell (1985) the lowering of p_L has little effect on r_{vc} until a critical p_L value is reached. When p_L falls below this critical value r_{vc} increases dramatically (see Figure 5-5). Campbell (1985) claims that broad leafed plant species tend to have n values as high as 20.

$$r_{vs} = r^o_{vs} (1 + (p_L / p_C)^n)$$ **(Equation 5-7)**

where,

r^o_{vs}	= minimum stomatal resistance to vapour diffusion	$(s\,m^{-1})$
r_{vc}	= canopy resistivity to vapour diffusion	$(s\,m^{-1})$
p_C	= critical leaf-water pressure	(MPa)
p_L	= leaf water pressure	(MPa)
n	= constant (3-20 approx.)	(-)

If p_L and average soil-water potentials are coupled, then it can be argued that r_{vc} is coupled to soil matric potentials such that r_{vc} will *increase* dramatically when the average soil-water potential reaches some critical value. Transpiration rate and E_t should therefore *decrease* dramatically when the average soil-water potential reaches a critical value.
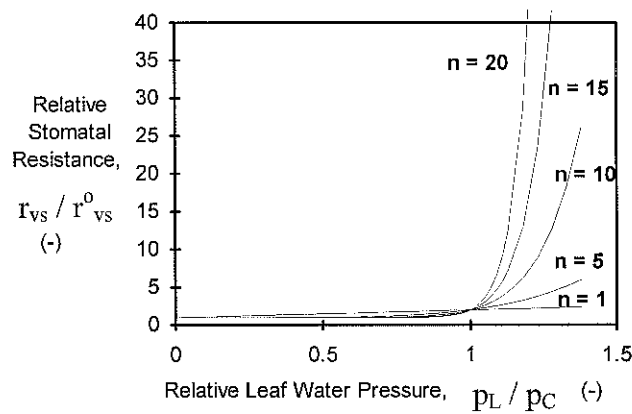
Figure 5-5. Empirical models for stomatal resistance to vapour diffusion (from Campbell (1985); refer Equation 5-7).

Subsurface investigations of this study show that the roots of *Pisonia grandis* at Heron Island are concentrated in the organically rich silty-sand layer (ie, to a depth of about - 1 ± 0.1 m RGL). It seems reasonable, then, that the average matric potential between the soil surface and -1.0 m RGL is a good measure of water-stress experienced by the roots of *Pisonia grandis*. An average matric potential, ψ_{stress}, for the rooting zone was approximated from the tensiometer readings at -20, -50 and -70 cm RGL:

$$\psi_{stress} = (\psi_{-20} + \psi_{-50} + \psi_{-70}) / 3 \qquad \textbf{(Equation 5-8)}$$

where,

ψ_{stress}	= indicator of soil-water stress	(cm)
ψ_{-20}	= matric potential at the -20 cm level	(cm)
ψ_{-50}	= matric potential at the -50 cm level	(cm)
ψ_{-70}	= matric potential at the -70 cm level	(cm)

The tensiometric field data were considered sufficently accurate to be analysed on a monthly basis with Equation 5-8. The monthly soil-water stress values and concurrent rainfall figures and qualitative observations are summarised in Table 5-1 for the extent of the study period. During the dry season (ie, July - November.) the canopy density of

Pisonia was least due to wilting (see Table 5-1). It has also been observed by Ogden (1981) that the *Pisonia grandis* at Heron Island grow quickest during the wet season, and during the dry season of some years produce abundant flowers and seeds.

Table 5-1. Soil-water availability and its qualitative effect on *Pisonia grandis* at Heron Island: summarised from the field data.

Year	Month	Total Monthly Rainfall P (+/-5 mm)	Average Stress Potential ψ_{stress} (cm)	Qualitative Plant-Water Conditions	Qualitative Canopy Density
1993	November	30	no data	Very Stressed	Very Low
1993	December	90	-510	Very Stressed	Very Low
1994	January	130	-480	Stressed	Low
1994	February	230	-140	Unstressed	Moderate
1994	March	230	-110	Unstressed	Moderate
1994	April	130	-90	Unstressed	High
1994	May	50	-150	Unstressed	High
1994	June	50	-380	Moderate Stress	High
1994	July	170	-210	Stressed/Unstressed	High
1994	August	20	-200	Unstressed	High
1994	September	45	-415	Moderate Stress	High
1994	October	30	-620	Stressed	Very High
1994	November	20	-400[$]	Stressed	High
1994	December	70	-450	Moderate Stress	High

Notes:

[$] = based upon $\psi_{-20\ cm}$ and $\psi_{-50\ cm}$ only due to a fault with the tensiometer at $\psi_{-75\ cm}$

5.5 DISCUSSION

The cumulative evapotranspiration-less-canopy-interception, $\int E_{t-c} dt$, which was estimated using a field-water balancing approach, generally increased at an unsteady rate but also decreased on occasions (see Figure 5-3). In reality $\int E_{t-c} dt$ cannot decrease. The negative E_{t-c} rates are believed to be the result of a lagged reponse in the measured $S\{t\}$ and are also believed to be mathematically compensated by higher-than-actual E_{t-c} rates at other times. Two clear examples of the underestimation of E_{t-c} and its subsequent overestimation occur on the 5th March and 9th July 1994 in Figure 5-3. A lagged response in $S\{t\}$ is expected due to the tensiometer nest being unable to detect soil moisture between the soil-surface and the shallowest tensiometer and between tensiometers.

On 15 days throughfall intensities exceeded the approximate infiltration capacity of the soil surface and runoff was assumed to have occurred (refer Equation 5-6). Because P_c and dS/dt are generally much larger than E_{t-c} and D when runoff was likely to have occurred, R is primarily dependent on the difference between P_c and dS/dt. For this reason the uncertainty in R is most heavily dependent on the uncertainty in dS/dt.

Water that ponded in the study site on any given day was categorised as runoff. However, some of the ponded water may have infiltrated the next day (possibly while it was still raining) giving rise to an overestimation of $\int Rdt$. Under such circumstances the computed $S\{t\}$ should have increased marginally the next day due to delayed infiltration. With the current estimation scheme the computed $\int Rdt$ fell slightly at certain times (see Figure 5-3). It is believed that these reductions in $\int R\,dt$ are a mathematical correction associated with the delayed infiltration of ponded water in the field.

The seasonal wilting and regeneration of *Pisonia grandis* is clear evidence that soil-moisture was a major factor in affecting evapotranspiration. It is inferred from the field data that significant wilting of *Pisonia grandis* at Heron Island occurred when ψ_{stress} was less than -500 cm (and $\theta < 10\text{-}15\%$ approx.). Wilting, which causes a reduction in leaf area index (LAI) and r_c, is a coping mechanism of many plant species when

experiencing drought conditions (Campbell, 1977). It is therefore suggested here that a ψ_{stress} in the range -400 to -500 cm delineates a critical region that probably coincides with large changes in average stomatal resistance, LAI and actual E_t.

Whilst the resulting estimates of evapotranspiration and surface water runoff for the study site are without confidence limits, they are used as calibration data in the development of the Soil-Water Transport and Evapotranspiration Model (STEM) as shown in the next chapter (Chapter 6).

6. GROUNDWATER RECHARGE: INTERPRETIVE MODELLING

6.1 INTRODUCTION

Heron Island soil, like that of many small low carbonate islands, is uniform and medium-to-coarse grained in texture. Soils of this type are often perceived as being 'well-draining' (eg, Underwood, 1990; Allaway et al., 1984) and are not expected to 'complicate' the natural recharge process (Underwood, 1990). However the tensiometric field data presented in Chapter 3 give a somewhat different impression of the recharge process at Heron Island. Whilst this data show that initial infiltration and wetting-front propagation in the vadose zone at Heron Island was rapid, the data also show that the bulk of the meteoric water never reached the water-table due to relatively slow redistribution of soil-water and evaporative losses. This slow moisture redistribution may be partly explained by experiments which show that moisture strongly adheres to the coral sand when effective saturation is below about 25% (refer Chapter 4).

In this final chapter of Part I, the natural recharge process is investigated indirectly using a mathematical model called the Soil-Water Transport and Evapotranspiration Model (STEM). This model is to simulate Darcian soil-water redistribution and the field-water balance in the forested study site as a function of daily rainfall. It is based on the general-purpose soil-water transport algorithm that was previously developed in Chapter 4 and approximate empirical expressions for canopy interception, infiltration, evapotanspiration, surface ponding and runoff.

In Chapter 4 an empirical formula for the gravelly-sand's unsaturated hydraulic conductivity relationship was determined by matching matric potentials simulated by the soil-water transport algorithm with those recorded in the field. In Chapter 5 this empirical formula was used with Darcian flow theory, field data and certain assumptions to approximate the 1994 field-water balance: including deep-drainage, surface runoff and evapotranspiration terms. In this chapter STEM is 'calibrated' against the 1994 field-water balance estimate although this estimate is actually dependent on the soil-water transport algorithm. Hence, the proposed calibration of STEM is an empirical measure adopted to ensure that STEM's simulations are in reasonably close agreement

with the observed 1994 soil-matric potentials and the interpreted 1994 field-water balance. The 1994 throughfall record is used as the driving variable of STEM in this calibration procedure.

6.2 OBJECTIVES

The main objective of this chapter is to improve understanding of the timing and intensity of natural recharge at Heron Island by way of mathematical experimentation. To achieve this objective a hydrological model, called STEM, is developed by combining the soil-water transport algorithm of Chapter 4 with empirical sub-models for (a) canopy interception, (b) infiltration, (c) surface ponding, (d) evapotranspiration and (e) surface runoff. The evapotranspiration sub-model is to be calibrated by matching STEM's simulations with the approximate field-water balance figures provided in Chapter 5. Historical rainfall records are then to be used as input into STEM to simulate natural recharge over a period of time that is much greater than the 1994 study period (ie, between 1985-1994). Finally, key parameters used in STEM are to be varied in a sensitivity analysis to examine which of these are critical to the long-term recharge simulations.

6.3 THE SOIL-WATER TRANSPORT & EVAPOTRANSPIRATION MODEL

6.3.1 Rainfall

Daily rainfall depths recorded by the Heron Island Research Station between 1985 and 1994 (refer Chapter 3) are the driving variable in the STEM simulations. For the intermittent periods when rainfall figures are lacking, a zero daily rainfall is assumed.

6.3.2 Canopy Interception

Field records of rainfall and throughfall at Heron Island (refer Chapter 3) highlight the significance of rainfall interception by the *Pisonia* forest. However the interception ratio, *IR*, of the forest at any location is subject to temporal variations in rainfall and evaporative demand and seasonal changes in canopy density. However the accurate characterisation of *IR* was beyond the resources of the current study and a very simple

interception sub-model was adopted, ie:

$$P_c\{t\} \approx (1 - IR)\, P\{t\}$$
$$\approx 0.9\, P\{t\}$$

(Equation 6-1)

The application of Equation 6-1 with actual rainfall data, $P\{t\}$, in reproducing the stochastic nature of throughfall is believed reasonable given that the timing of daily rainfall and throughfall were similar in the field (refer Chapter 3). The average IR at Heron Island is uncertain and 0.10, the average IR of an Amazonian rainforest (Shuttleworth, 1988), is adopted as a rough approximation. Arbitrary average interception ratios of 0.8, 0.10 and 0.12 are also used in a sensitivity analysis to examine its effect on long-term recharge (refer Table 6-2).

6.3.3 Soil-Water Redistribution and Initial Conditions

The most elaborate component of STEM is the general purpose finite-difference soil-water redistribution algorithm that is discussed in Chapter 4. This algorithm approximates isothermal unsaturated fluid flow in porous media and is used here to predict soil infiltration, moisture profiles and deep drainage rates as a function of daily rainfall and time. As mentioned in Chapter 1, the vadose zone at Heron Island has two major layers: a 1-m-thick silty-sand layer and rooting zone, and a 3.5 m (approx.) thick medium- to course-grained sand layer. A finite-difference grid with 45 cells, each 10 cm thick, was used with STEM to approximate this vadose zone (ie, 4.5 m deep).

The $\psi\{\theta\}$ and the $K\{\psi\}$ relationships of the silty-sand are represented by a Van Genuchten-type formula (see Equation 6-2) and a power function (see Equation 6-3) respectively. The $\psi\{\theta\}$ relationship of the gravelly-sand is represented by a continuous polygon (see Appendix D4) and the $K\{\psi\}$ relationships of the gravelly-sand is represented by a power function (see Equation 6-4). These functions, which were determined in Chapter 4, are reproduced below for clarification:

(a) for silty-sand the characteristic equation is

$$\psi\{\theta\} = -0.055 \left[\left(\frac{0.45 - 0.096}{\theta - 0.096} \right)^{\frac{1}{0.07}} - 1.0 \right]^{\frac{1}{6}}$$ **(Equation 6-2)**

(b) for silty-sand the hydraulic conductivity formula is

$$K\{\psi\} = \alpha \left| \frac{\psi}{-0.01} \right|^{\beta} \quad : \alpha = 2.2, \beta = -1.865$$ **(Equation 6-3)**

(c) for gravelly-sand layer the hydraulic conductivity formula is

$$K\{\psi\} = \alpha \left| \frac{\psi}{-0.03} \right|^{\beta} \quad : \alpha = 0.672, \beta = -2.7$$ **(Equation 6-4)**

where K has units of m day^{-1}, ψ has units of metres, and θ is the volumetric moisture content.

Initial moisture contents, which have only a relatively small influence on the long-term recharge predictions, are assigned values approximately equal to those recorded in the study site in January 1994 (see Figure 6-1 and Appendix E).
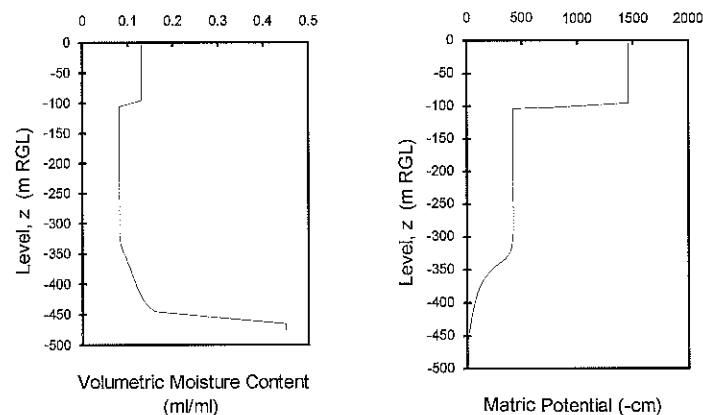
Figure 6-1. The (a) soil moisture contents and (b) soil-matric potentials assumed for the 1st January 1985: initial conditions in the STEM simulations.

6.3.4 Infiltration and Ponding

In STEM the surface infiltration rate over each 24 hour period is taken equal to the daily throughfall rate unless the throughfall rate exceeds the maximum surface infiltration rate (I_{max}) in which case the infiltration rate is set to I_{max} and ponding occurs. The ponded water is the difference between I_{max} and the throughfall rate on a daily basis and is allocated as additional throughfall over the next day. I_{max} is computed as the rate of water adsorption at the current time-step assuming a maximum allowable moisture content of (θ_{max}) at the soil surface. To simplify the model, ponding pressure head is not considered in the calculation of I_{max}. In most of the STEM simulations all of the ponded water eventually infiltrates the soil. The exception is when ponded water is removed numerically to investigate the affect of surface runoff on the water-balance (see Section 6.3.5).

The finite-difference unsaturated flow algorithm employed by STEM generally requires smaller time-steps at higher levels of saturation to avoid numeric instabilities. In the current application of STEM it was found that the cells adjacent to the infiltration boundary were prone to saturation, resulting in rather small time-steps and large CPU times. To circumvent these large CPU times, a θ_{max} of 0.43 (ie, S' $\cong$ 0.95) was used in STEM. With this value of θ_{max}, STEM required about 2.7 minutes of CPU time on a 40 MHz 486 DX personal computer to simulate each 365 days of soil-water redistribution: a CPU time considered manageable. This numeric artifice does not introduce conceptual problems as the natural wetting of field soils usually results in a maximum S' of only about 0.91 due to air entrapment (eg, Peck, 1960).

6.3.5 Surface Runoff

Rainwater ponding, small-scale topographic relief and non-uniform infiltrability of the soil surface at Heron Island guarantees that at least some lateral surface flow occurs at times. Moreover, anecdotal evidence and water-balance in Figure 5-3 show that intra-island surface flow can be significant. However no data on surface water movement was obtained at Heron Island and surface runoff is assumed to be zero in the base-case STEM model. To investigate the sensitivity of long-term natural recharge to surface runoff, surface runoff is taken as 100% of ponded water in a separate simulation.

6.3.6 Water-Table and Groundwater Recharge

The water-table at Heron Island is affected by the ocean tide such that it rises and falls in a tide-like fashion with a semi-diurnal periodicity and a range of about 0.5-1 m (refer Chapter 8). Groundwater recharge, barometric pressure variations and changing groundwater salinity/density gradients may also perturb the water-table although at different time-scales (refer Chapter 9). However the simulation and prediction of water-table movement was considered too detailed in this study of natural recharge and to simplify the model the water-table boundary was initially represented as a constant-moisture node, ie:

$$\theta\{z = -4.5\text{m}, t\} = \theta_s \qquad\qquad \textbf{(Equation 6-5)}$$

With Equation 6-5 the island's water-table, which has strong hydraulic 'connection' with the ocean, is modelled as a fixed-saturation boundary centred at mean sea level. Whilst the laboratory determined moisture content at saturation (0.46) was initially applied to the RHS of Equation 6-5, a moisture content of 0.3 was adopted in the final model as it gave essentially the same results whilst speeding the finite-difference algorithm considerably. Conceptually, this less-than-saturation moisture content represents a point just above the water-table. The position of the lower boundary was varied by ±0.70 m in a sensitivity analysis to examine the effect of vadose zone thickness on long-term recharge.

6.3.7 Evapotranspiration

In the current study evapotranspiration was modelled as two components: canopy interception (refer Section 6.2.3) and evapotranspiration-less-interception (E_{t-c}). As was mentioned in Chapters 2 and 4, evapotranspiration is a function of more variables than can be practically measured and modelled. None-the-less, in modelling studies of other islands, actual evapotranspiration rates (E_t) have been simulated, with reasonable successs, as a two-part linear function of average soil effective saturation (S') and average potential evapotranspiration rate (E_{tP}) (e.g., Falkland, 1991; Lloyd et al., 1980;

Hunt and Peterson, 1980). This type of model has the advantage of coupling E_t to levels of computed soil moisture whilst being relatively simple to implement. In STEM a similar type of model was employed for modelling E_{t-C} as a function of S' (see also Figure 6-2):

$E_{t-C} \{z,t\} = \zeta \ S'\{z,t\}$ $: z \geq -1 \ m; \ \zeta = 8.8 \ mm \ d^{-1}$ **(Equation 6-6)**

$E_{t-C} \{z,t\} \leq E_{tP}$ $: z \geq -1 \ m; \ E_{tP} = 4.1 \ mm \ d^{-1}$ **(Equation 6-7)**

where ζ is a scale factor that was determined by calibration and E_{tP} is the average potential evapotranspiration rate determined using Nullet's (1987) method (Table 2-1). The above equations were only applied to the nodes in STEM that denote the rooting zone of *Pisonia grandis* (ie, the 1-m-deep silty-sand layer). In other words, values of E_{t-C} were computed at each time increment and subtracted from the simulated soil-moisture values of the silty-sand layer on a node-wise basis. The above empirical model is only approximate because it is insensitive to most weather variables that influence evaporative demand and is insensitive to changes in total plant-resistance to vapour diffusion (refer Section 2.2.1).

The calibration of ζ in Equation 6-6 was achieved by the trial-and-error matching of $\int E_{t-C}dt$ simulated by STEM, with $\int E_{t-C}dt$ previously determined for the study site by field-water balancing (refer Section 5.3). The simulations were for the period 1st January - 31st October 1994 (see Figure 6-3). The canopy interception sub-model (Equation 6-1) was not required in the calibration of ζ because the measured daily throughfall data, and not total rainfall data, were used as the driving variable.

Giving confidence to the effectiveness of STEM is a high linear correlation between the simulated and measured values of total soil-moisture (correl. coeff. = 0.94) and reasonably controlled errors in the simulated total soil-moisture (max. error was 65 mm in mid-July 1994) (see Figure 6-3). Due to the effectiveness of the calibrated STEM model, total deep-drainage, soil-water storage and total evapotranspiration simulated by STEM on the 31st October 1994 are very similar to those values approximated by a field-water balancing approach (refer Section 5.3). However, it is important to note that

the calibration data are a function of STEM's soil-water transport algorithm and therefore are not independent of STEM. Moreover, the calibration procedure is essentially an intermediate step to ensure that STEM's simulations are in approximate agreement with (a) observed soil matric potentials (see Figures E-1 to E-3) and (b) the field water balance estimated in Chapter 5 (see Figure 6-3). Due to a lack of suitable field data confidence intervals for STEM's simulated hydrologic balances and other results cannot be provided.
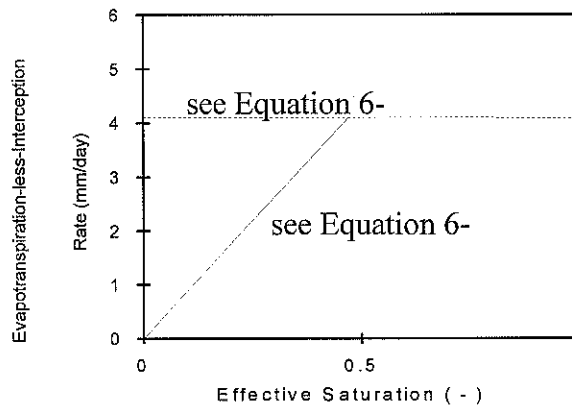
Figure 6-2. The empirical evapotranspiration-less-interception model used with STEM (dashed line is the potential rate)
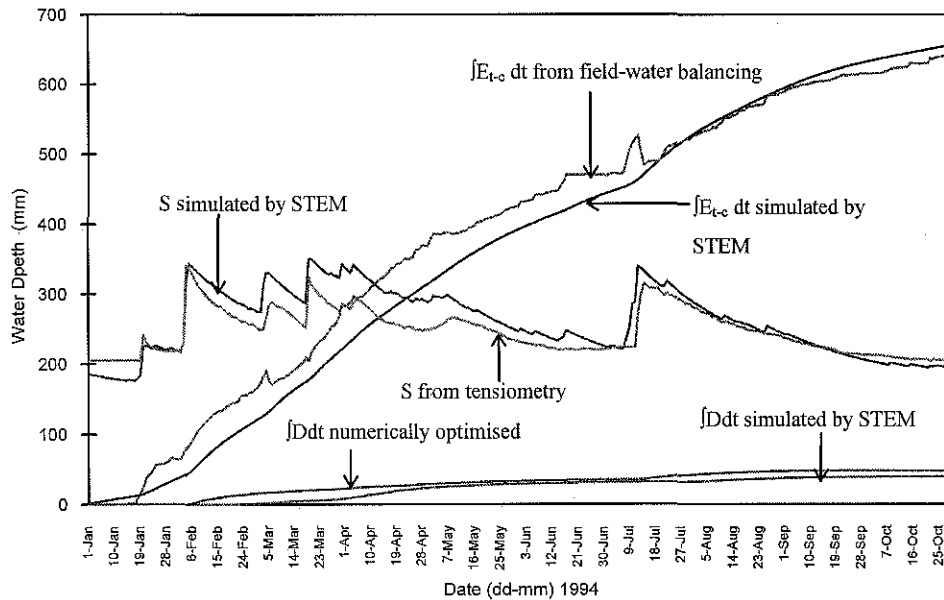
Figure 6-3. Calibration of STEM: predicted and estimated soil-water storage, cumulative deep drainage and cumulative evapotranspiration for the 175-cm-deep study plot (refer main text).

6.4 SIMULATION RESULTS FOR THE PERIOD 1985-1994

STEM was applied to 1985-1994 Heron Island rainfall data to interpret the natural recharge process for this period. For reasons of brevity the rainfall data are only presented as a cumulative plot in Figure 6-5. Output from the model, including predicted recharge, interception, evapotranspiration, soil-water storage and ponded water, are also provided graphically at daily intervals for the 10 year period (see Figures 6-4 and 6-5) and as annual totals in Table 6-1. Rounding-off error in the simulated 10 year water-balance was only 0.4 mm and is considered negligible.

STEM was also programmed to output predicted soil-moisture and soil-matric potentials profiles at times selected by the author. Shown are the simulated soil-moisture profiles that correspond to two major rainfall periods: (i) January 1992 to June 1992 (see Figures 6-6 to 6-8) and (ii) August 1987 to January 1988 (see Figures 6-9 & 6-10). The August 1987 to January 1988 soil-moisture profiles are of interest because they coincide with the groundwater monitoring of Charley et al. (1990), and the January 1992 - June 1992 soil-moisture profiles are of interest because they coincide with the groundwater monitoring of Krol et al. (1992) and this study. The predicted recharge fluxes and the observed groundwater salinities for these two periods are discussed in Chapter 11.

Table 6-1. Approximate annual field-water balance figures for 1985-1994: results of the base-case STEM simulation.

Year	Total Rainfall P (cm)	Groundwater Recharge G (cm)	Recharge to Rainfall Ratio G/P (%)	Total Evapotranspiration E_t (cm)	Evapotranspiration to Rainfall Ratio E_t/P (%)
1985	92	-1	-1	83	90
1986	110	7	6	103	94
1987	99	5	5	94	95
1988	127	16	12	99	78
1989	140	49	35	105	75
1990	156	71	46	88	56
1991	94	15	15	77	82
1992	134	38	29	99	74
1993	98	8	8	87	89
1994	119	23	20	95	80
1985-94	1170	230	20	930	79
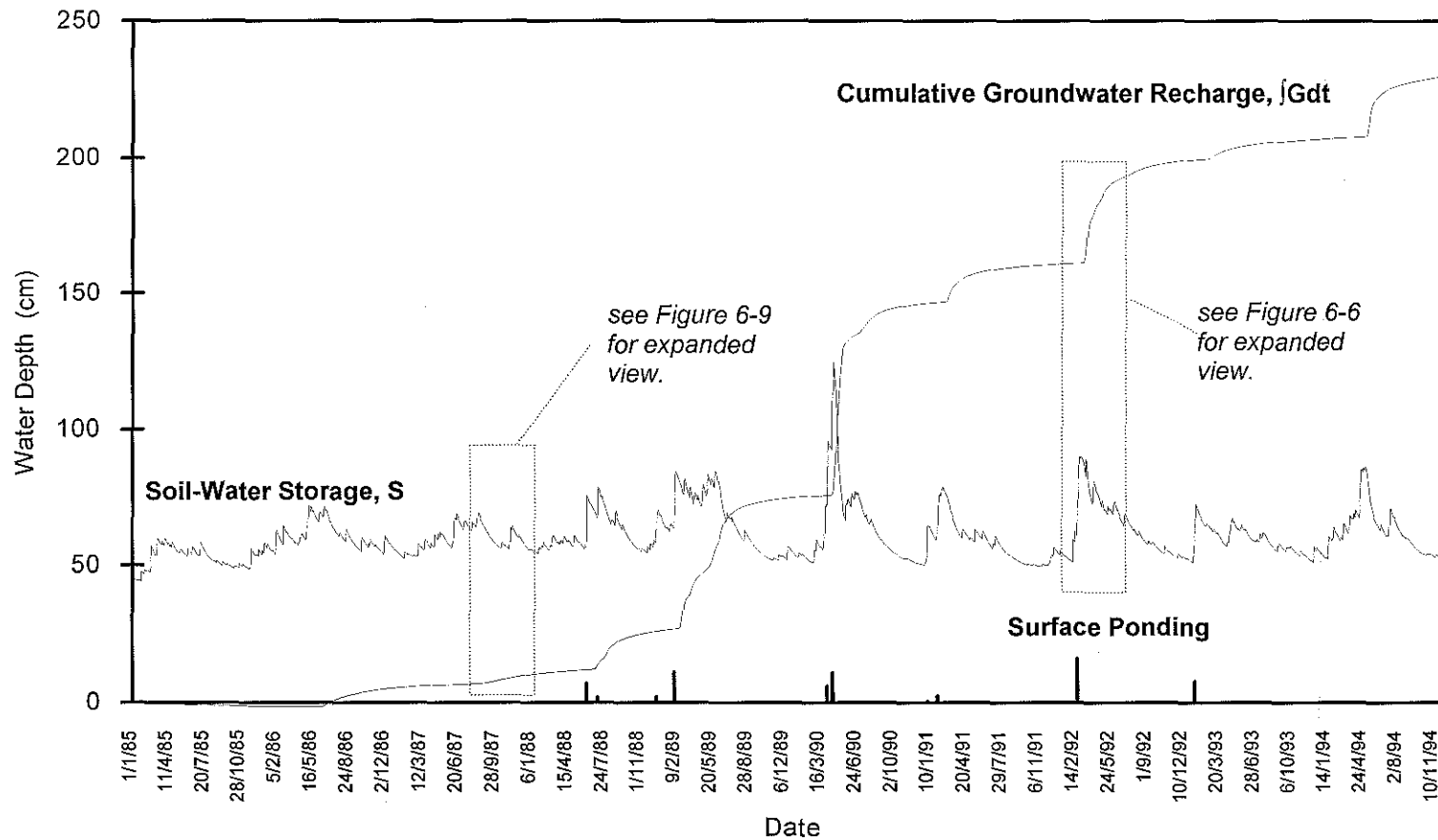
Figure 6-4. STEM predictions for the period 1985-1994: soil-water storage, cumulative groundwater recharge and ponding depth (see also Figure 6-5).
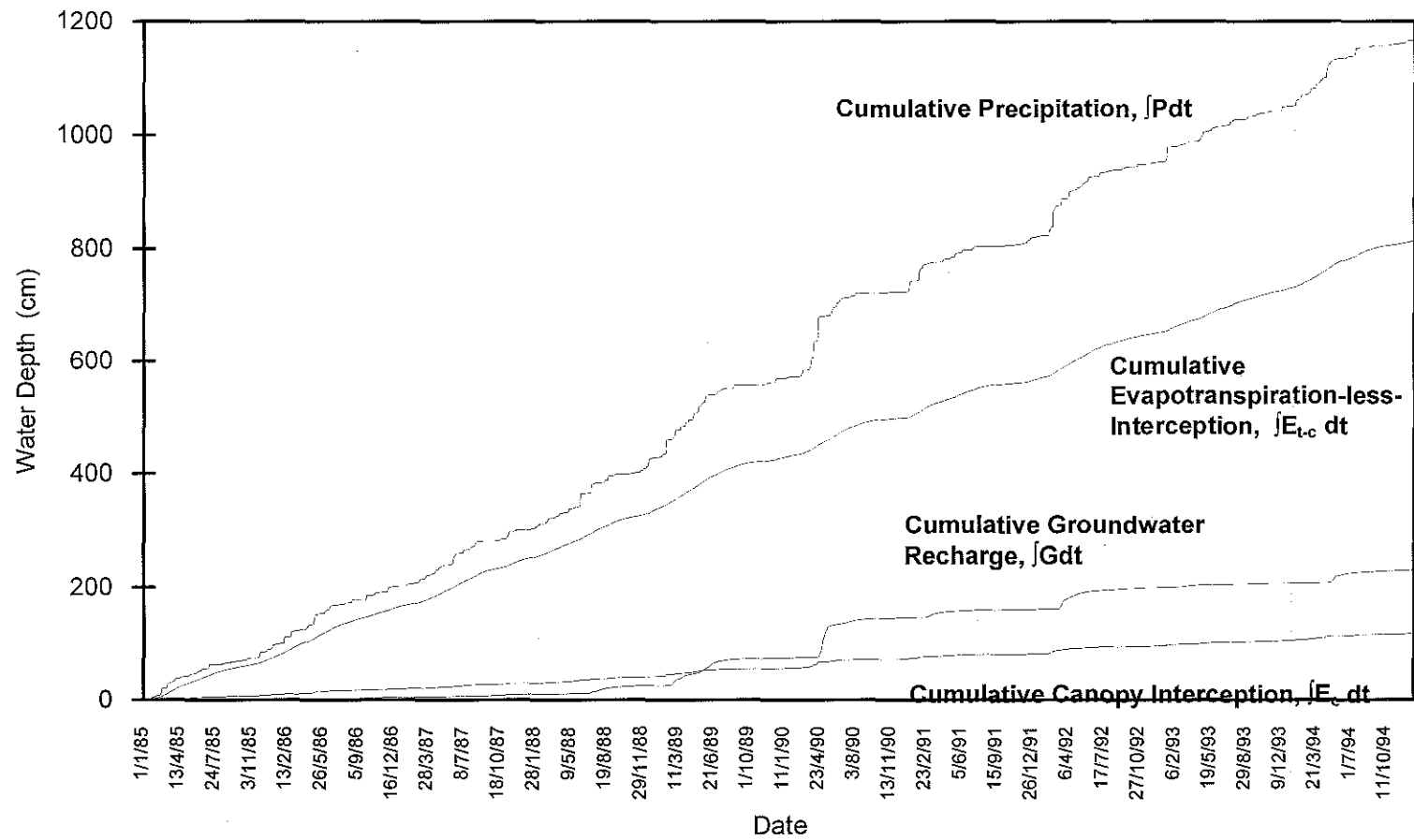
Figure 6-5. STEM predictions for the period 1985-1994: cumulative rainfall, cumulative evapotranspiration-less-interception, cumulative groundwater recharge and cumulative interception (see also Figure 6-4).
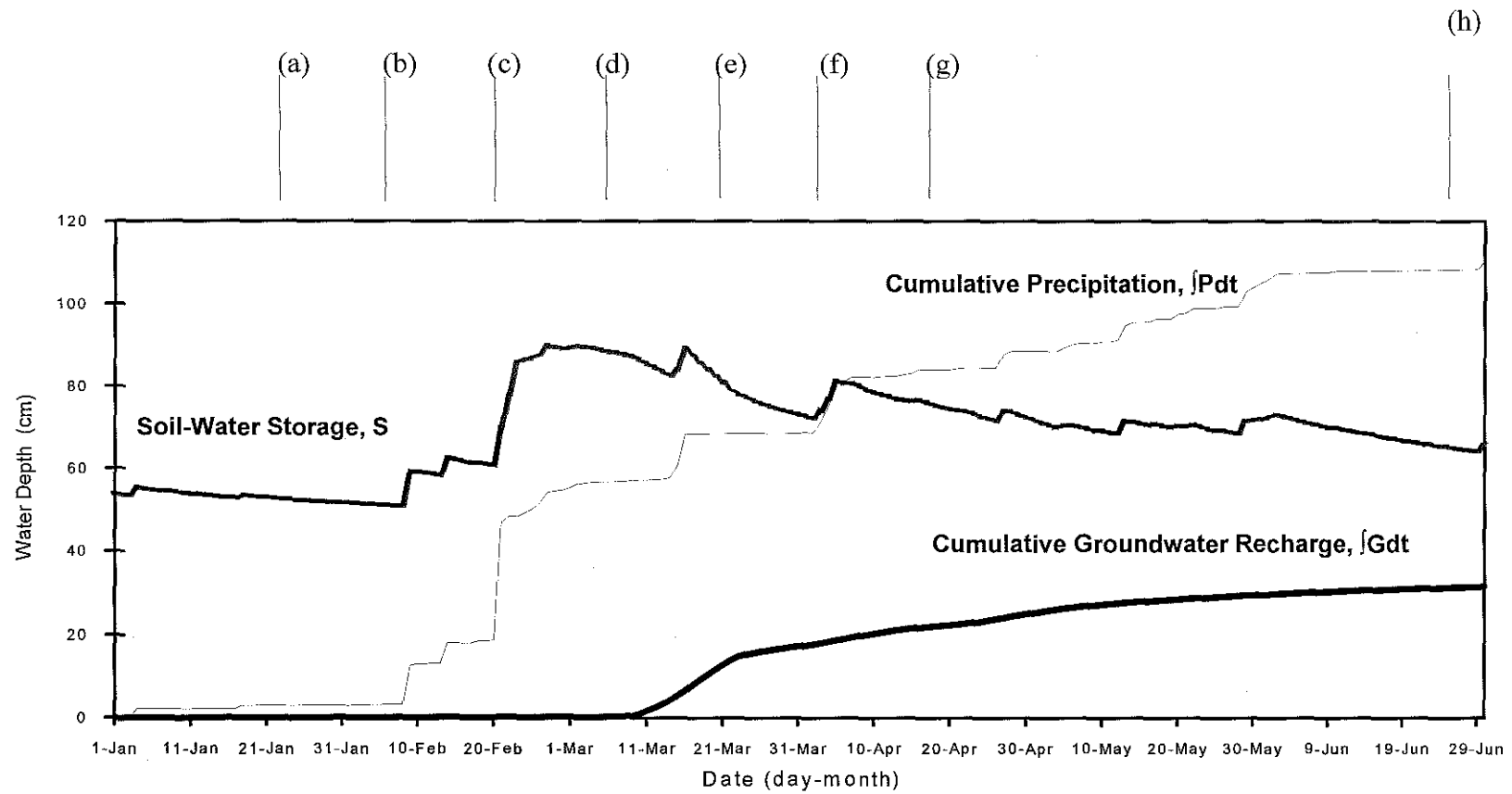
Figure 6-6. Cumulative groundwater recharge predicted by STEM for the first half of 1992 (see also Figures 6-7 and 6-8).
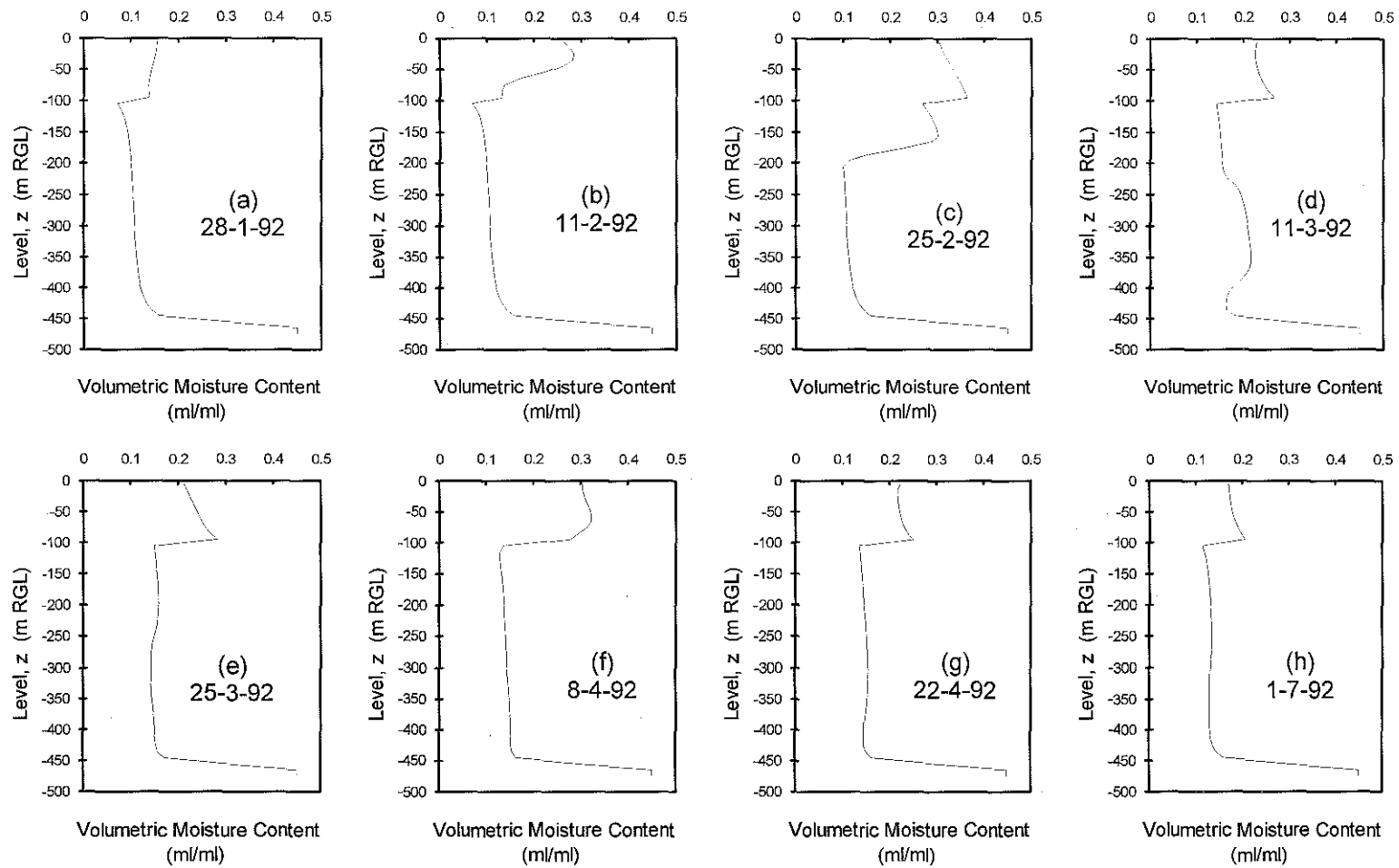
Figure 6-7. Soil moisture profiles predicted by STEM for the first half of 1992 (refer Figure 6-6).
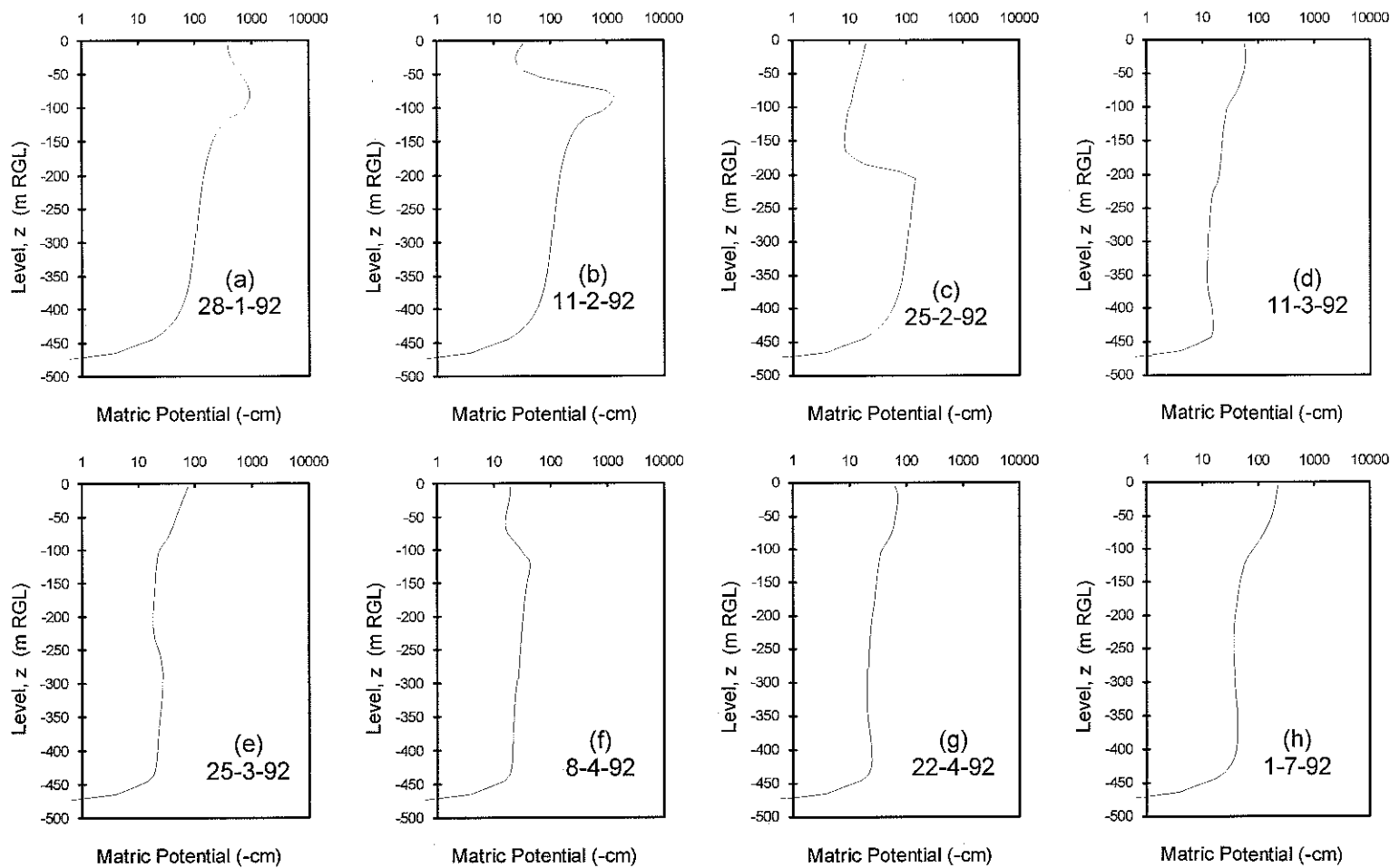
Figure 6-8. Soil matric potential profiles predicted by STEM for the first half of 1992 (refer Figure 6-6).

14
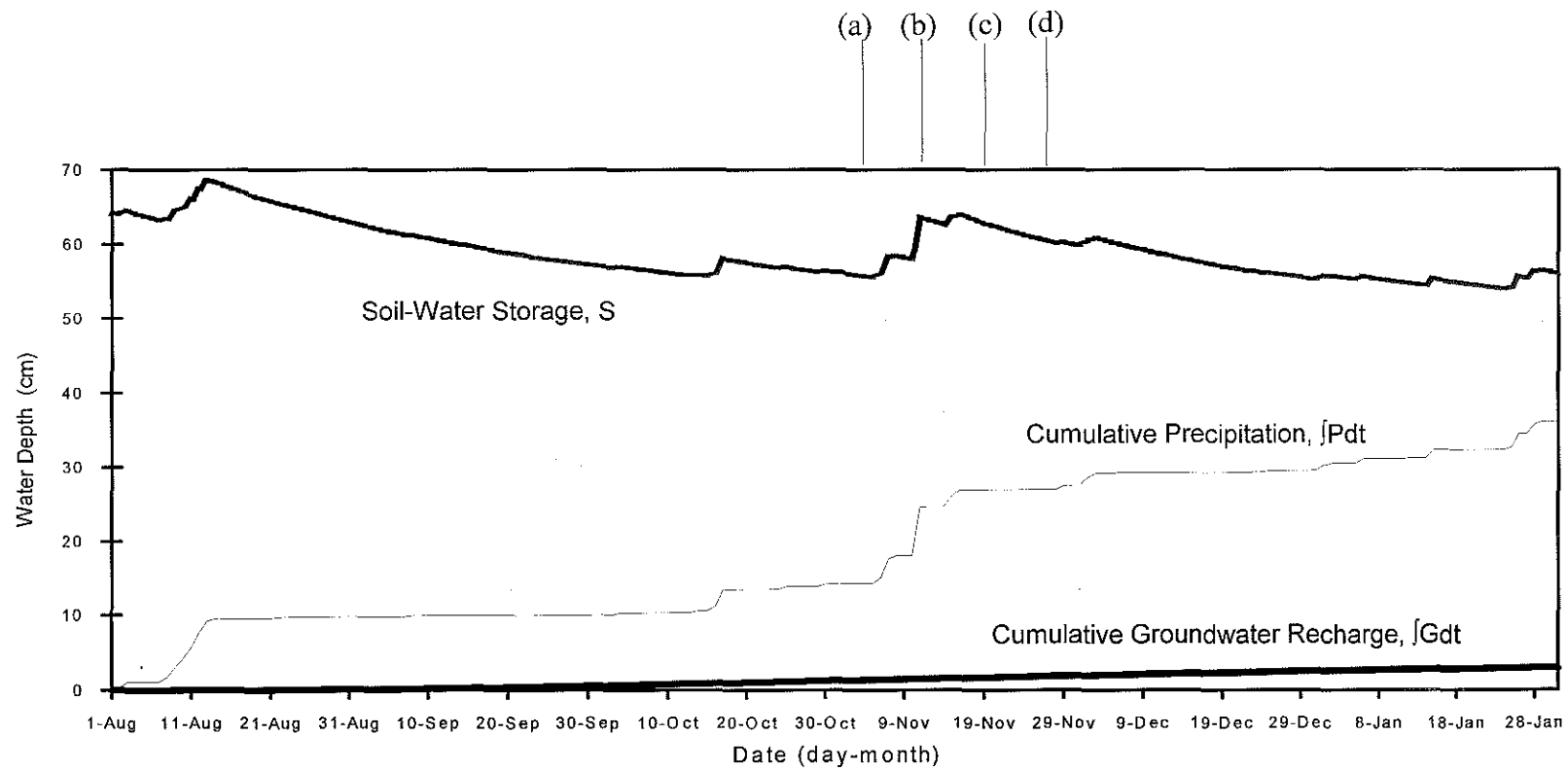
Figure 6-9. Cumulative groundwater recharge predicted by STEM for the second half of 1987 (see also Figure 6-10).

15
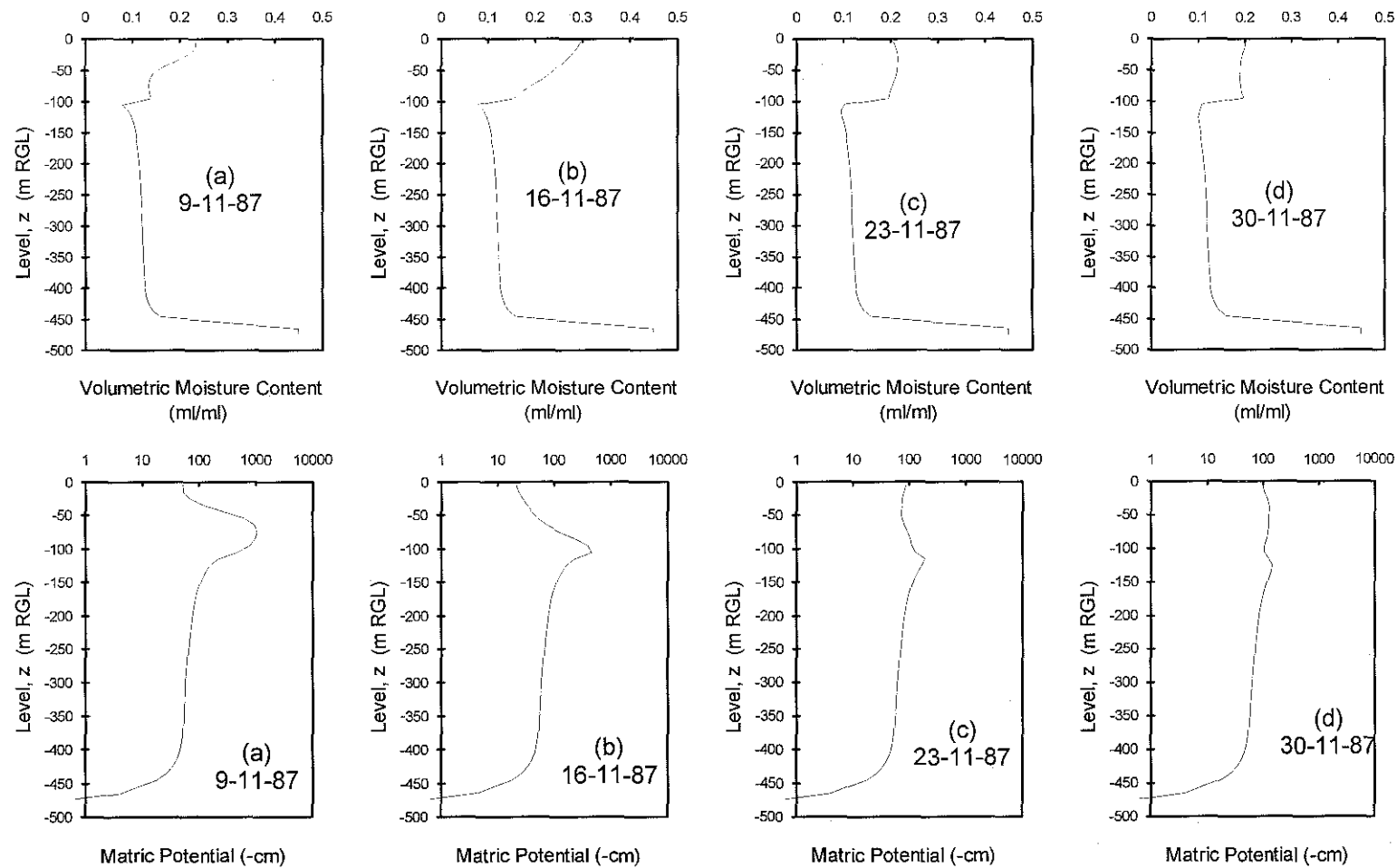
Figure 6-10. Select soil-moisture and soil matric potential profiles predicted by STEM (refer Figure 6-9).

16

6.5 SENSITIVITY ANALYSIS

The sensitivity of the 10-year-long recharge simulations to key parameters is examined in this section. Varied are evapotranspiration-less-interception (by scaling ξ in Equations 6-6 and 6-7), average canopy interception (by scaling *IR* in Equation 6-1), unsaturated hydraulic conductivities of the silty-sand and the gravelly-sand (by scaling α and β in Equations 6-3 and 6-4), effective depth of the gravelly-sand layer, and initial moisture content. The effective depth of the gravelly-sand layer is examined because the vadose zone at Heron Island has a non-uniform thickness. Most parameters are varied by $\pm 20\%$ as described in Table 6-2. A simulation with 100% of ponded-water removed was carried out to examine the potential impact of surface run-off on recharge Simulations with initial moisture content increased by 20% and 40% were carried out to examine the impact of initial conditions on recharge.

6.6 DISCUSSION & CONCLUSIONS

The field-water balance simulated by the calibrated STEM model is in approximate agreement, both qualitatively and quantitatively, with the field estimate of the balance as a result of fine-tuning (see Figure 6-3). Noteworthy in Figure 6-3 is a rather faithful reproduction of the rapid rising and the exponential-type falling of soil-water storage, S, with time, and the similarity between simulated and estimated cumulative deep drainage and cumulative evapotranspiration-less-interception (see Figure 6-3).

Simulated and measured matric potential profiles on the first day of each month between January and October 1994 are compared in Figures E-1 to E-3 (Appendix E) to illustrate the accuracy of the model. The overall result is that STEM estimates the field potentials within about one order-of-magnitude with a generally better result for the gravelly-sand layer compared to the silty-sand layer. STEM's simulations are least reliable in the silty-sand layer probably because (1) the silty-sand layer is prone to more severe moisture fluctuations caused by water infiltration and near-surface evaporation and root-drainage, (2) greater deviations from the assumptions of Richard's equation (discussed below), and (3) the $K\{\psi\}$ relationship of silty-sand was only estimated using limited experimental data whereas the $K\{\psi\}$ relationship of gravelly-sand was calibrated by model optimisation.

Table 6-2. Water totals simulated by STEM for the period 1985-1994: Heron Island groundwater recharge predictions and sensitivity analysis.

Ref No.	Parameter Change	Interception $\int E_c dt$ (cm)	Evapotranspiration-less-Interception $\int E_{c\text{-}t} dt$ (cm)	Surface Runoff $\int R dt$ (cm)	Groundwater Recharge $\int G dt$ (cm)	Relative Change in $\int G dt$ (%)
0	(Base-Case)	117	813	0.0	230	0
1	Evapotranspiration: 20 % increase in ζ	117	867	0.0	177	-23
2	Evapotranspiration: 20 % decrease in ζ	117	733	0.0	309	+34
3	Interception: 20 % increase	140	803	0.0	217	-5.9
4	Interception: 20 % decrease	94	822	0.0	244	+6.0
5	Gravelly-Sand $K\{\psi\}$: 20% increase in α	117	811	0.0	233	+1.1
6	Gravelly-Sand $K\{\psi\}$: 20% decrease in α	117	815	0.0	227	-1.3
7	Gravelly-Sand $K\{\psi\}$: 20% increase in β	117	822	0.0	217	+5.9
8	Gravelly-Sand $K\{\psi\}$: 20% decrease in β	117	797	0.0	251	+8.8
9	Silty-Sand $K\{\psi\}$: 20% increase in α	117	804	0.0	239	+3.8
10	Silty-Sand $K\{\psi\}$: 20% decrease in α	117	824	0.0	219	-4.7
11	Silty-Sand $K\{\psi\}$: 20% increase in β	117	860	0.0	183	-21
12	Silty-Sand $K\{\psi\}$: 20% decrease in β	117	753	0.0	290	+26
13	Sand Layer Depth: 20% increase	117	813	0.0	226	-1.8
14	Sand Layer Depth: 20% decrease	117	813	0.0	234	+1.4
15	Ponding: 100% Lost as Runoff	117	810	68	165	-28
16	Initial Moisture: 20% increase	117	815	0.0	234	+1.4
17	Initial Moisture: 40% increase	117	817	0.0	239	+3.8

Footnotes:
(a) Total rainfall is 1169.5 cm in each simulation.
(b) Simulation time is 10 years (1985-1994) in each case.
(c) The $K\{\psi\}$ formulae for the silty-sand layer and the gravelly-sand layer are Equations 6-3 and 6-4, respectively.
(d) % change in $\int G\, dt$ is relative to 230 cm (the base-case result).
(e) Increasing initial moisture contents by 20% and 40% increased the simulated recharge by 1cm and 6 cm, respectively, in the first year of the simulation.

The error in the simulation of matric potentials may include a combination of random and systematic errors associated with possible deviations from (a) the assumptions of Richard's equation (refer Equation 2-3), (b) the non-hysteretic and approximate $K\{\psi\}$ and $\psi\{\theta\}$ relationships of STEM, and (c) experimental error. A limitation of Richard's equation is that non-ideal soil-water movement could have occurred, particularly in the silty-sand, as a result of non-granular organic material, macropore (pipe) flow through earthworms channels and plant root spaces, and physico-chemically altered capillarity. On the other hand, macropores and organic (plant) material were not found in the well-packed unconsolidated gravelly-sand and as such this material is closer to the idealised porous material described by Richard's equation.

It appears from Figures E-1 to E-3 that STEM is better suited to the prediction of deep drainage (and recharge) than to the prediction of shallow moisture movement in the silty-sand layer where moisture conditions are more variable and random by comparison. The deterministic underpinning's of STEM and its ability to approximate deep matric potentials and trends in the estimated field-water balance (refer Figure 6-3) are believed sufficient to accept the model as an interpretive mathematical tool.

Apparent characteristics of the natural recharge process at Heron Island are interpreted from the STEM past-predictions. The groundwater recharge is evidently highly irregular and infrequent with significant recharge events only being produced by large wet-season rainfall events (see Figure 6-4). These major recharge events (simulated) are trailed by slow recharge that decreases in an exponential fashion as a consequence of soil-water redistribution. The major recharge events are variable in magnitude and occur on average less than once per year and are more common in the wet season (ie, between January and July, approx.).

Figure 6-4 shows that the simulated soil-water storage is a minimum at the start of the simulations (ie, 1st January 1985). Hence a possible under-estimation in the initial moisture contents in conjunction with low rainfall in 1985 may be determining factors in the effectively zero simulated recharge in 1985 (ie, -1 cm). To examine model sensitivity to the initial conditions, simulations were also undertaken with

initial moisture contents increased by (a) 20% and (b) 40% (see Table 6-2). In these simulations, the STEM-predicted 10-year-recharge increased by only 1.4% and 3.8%, respectively. Also, changes in the simulated recharge in the first year (ie, 1985) are only +1 cm and +6 cm, respectively. These results indicate that recharge in 1985 was probably very low despite a possible under-estimation of initial moisture levels in STEM (refer Table 6-1).

Because there appears to be large variations in inter- and intra-annual recharge, it is concluded that the quantification of recharge in terms of a single long-term value could be misleading. For example, the simulated recharge was <10 cm in 1985-87 and 1993 but was as high as 71 cm (ie, 46% of the annual rainfall) in 1990 (see Table 6-1). Also the simulated recharge was insensitive to most of the rainfall events analysed (see Figure 6-4 & 6-5). It appears from the simulations that the vadose zone at Heron Island is a leaky barrier to recharge until tropical storms or cyclones dump relatively large amounts of rainfall over relatively short periods (ie, over hours and days). Although the intra-annual timing of the rainfall is a major control in the evolution of recharge, the annual totals of rainfall correlate quite strongly with annual totals of simulated recharge (correl. coeff. is 0.92) because high-rainfall years were generally associated with storm activity and thus major recharge events, whilst the opposite was the case for low-rainfall years.

In Figure 6-5 it is shown that the simulated evapotranspiration rate, E_t, varied in response to seasonal rainfall patterns (as expected), however this seasonal variation is of small relative significance at the decadal time-scale. Greater changes in E_t are likely to have occurred in the field due to the seasonal wilting and regrowth of *Pisonia grandis* (not simulated) and seasonal and diurnal changes in canopy resistance to vapour transfer (not simulated).

In STEM, a value of 4.1 mm/day is adopted as a first-approximation of the potential evapotranspiration rate, E_{tP} (refer Table 2-1). E_{tP} is the maximum achievable E_t rate in the *Pisonia* forest at any given time. In the field E_{tP} varies in time and space, hence the current model is only approximate. Unfortunately any attempt to develop a more sophisticated E_{tP} model would invite theoretical and practical problems similar to those that plague E_t models. These problems   operate on three fronts: (1) E_{tP} and E_t are

difficult to measure accurately, (2) deterministic models are data intensive and prone to error; and (3) the resources required to develop and accurately calibrate E_t and E_{tP} models are beyond the reach of most studies (refer Section 2.2.1). Hence further refinements to the evapotranspiration sub-model were not pursued.

A smaller interception ratio is expected during high intensity storms when the canopy is wilted (ie, at the onset of the wet season) and a larger interception ratio is expected during low intensity rainfall when the canopy is lush (ie, during the wet season). Hence temporal changes in interception ratio (not simulated) may have also contributed to greater seasonal changes in E_t than was actually simulated by STEM. The simulated canopy interception is equivalent to approximately half of the predicted total recharge for the 10 year period and so represents a significant component of the island's field-water balance. The sensitivity analysis suggests that long-term recharge rate is relatively insensitive to the average canopy interception ratio (see Table 6-2). The sensitivity analysis also shows that the average evapotranspiration rate is critical in the estimation of long-term recharge.

Simulated water ponding events only occurred in some years as a result of 'very' intense rainfall and were mostly accompanied by major recharge events. The simulation with runoff equal to 100% of ponded water suggests that recharge could be overestimated locally by as much as 20-30% if ponded water were to move to another area or completely off the island (see Table 6-2).

The soil-moisture and soil matric potential profiles simulated by STEM (see Figures 6-7, 6-8 & 6-10) indicate that the silty-sand layer has a significant impact on the recharge process by slowing considerably the downward percolation of soil-water and generally maintains a higher level of moisture than the gravelly-sand (ignoring the capillary fringe above the water-table). This would have the effect of improving water-availability to *Pisonia grandis* thus increasing transpiration and reducing long-term groundwater recharge (refer Table 6-2). The sensitivity analysis in also demonstrates that long-term recharge is more sensitive to the α and β parameters of the $K\{\psi\}$ function of the silty-sand layer than to the corresponding parameters of the $K\{\psi\}$ function of the gravelly-sand layer (refer Equations 6-3 & 6-4, respectively).

STEM shows that the gravelly-sand, when well-drained, can have a counter-intuitive influence on recharge by behaving as a 'capillary barrier' to the downward movement of moisture. When saturated, moisture can move quickly through the gravelly-sand, but its large pore spaces tend to fill rapidly with air thus retarding the flow of moisture soon afterwards. For example Figures 6-7c and 6-7d indicate that large wetting fronts (in this case during February-March 1992) can take more than two weeks to reach the water-table. This time-lag between rainfall and recharge is much greater than that previously suggested by Underwood (1990) for atoll islands with similar soils.

7. REEF-ISLAND GROUNDWATER MODELS

7.1 INTRODUCTION

There are three general types of groundwater model (van der Heijde & Elnawawy, 1992): (i) conceptual, (ii) physical, and (iii) mathematical. Conceptual groundwater models are fundamental to any groundwater modelling exercise as they provide a qualitative description of the system under investigation and are the basis of more sophisticated models. A limitation of conceptual models is that they only provide a static description of a system. For describing dynamic systems, either physical or mathematical modelling is required. Physical modelling, which includes scale modelling and analog modelling (such as Hele-Shaw and electrical varieties), is rarely undertaken nowadays because the resulting models are usually expensive and inflexible (Fetter, 1988).

Mathematical modelling, which includes analytical, numerical and stochastic techniques, is the principal means of dynamic simulation in hydrogeology. The objective of mathematical modelling is to obtain a time-series solution to the various governing equations and boundary conditions for fluid flow and possibly heat flow and/or mass transport. Whilst analytical models can be of great utility and provide important benchmark solutions, it is general-purpose numerical models which are currently of greatest utility in hydrogeology due to their ability to give information about the behaviour of complex and dynamic systems.

The success of numerical modelling in hydrogeology is attributable to significant advances in computer technology and numerical techniques over the past 20 to 30 years (Bredehoeft & Hall, 1995; Fetter, 1988). Some noteworthy examples of computer-based general-purpose groundwater models that have previously been used to simulate the groundwater hydraulics of atoll islands are SUTRA (Voss, 1984), FEMWATER (Yeh and Ward, 1980), and HST3D (Kipp, 1987). SUTRA (Saturated Unsaturated TRAnsport) is used in Chapter 10 to simulate the groundwater hydraulics of Heron Island. SUTRA is a 2-dimensional hybrid finite-element and integrated-

finite-difference groundwater model that is capable of simulating two-dimensional saturated or unsaturated density-dependent groundwater flow and solute (or heat) transport and decay in sub-surface environments (Voss, 1984). A discussion of numerical solution techniques for groundwater modelling is beyond the scope of this dissertation and the reader should seek an appropriate text for further information (e.g., Mc Donald and Harbaugh, 1988; Bear & Bachmat, 1990; Bear, 1972).
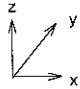
The following section presents the governing differential equations of SUTRA including those for 2-D isothermal fluid flow and mass transport in porous media without reactions, solute decay or sorption. These equations provide a theoretical foundation for modelling groundwater flow and solute transport in 2-D. For reasons of brevity, heat flow terms are not included and the equations are not all identical to their counterparts in Voss (1984).

7.1.1 Governing Differential Equations for Fluid Flow and Mass Transport

The gravitational acceleration vector is described as follows (Voss, 1984):

$$\underline{g} = \left| \underline{g} \right| \underline{\nabla}(z) \qquad \qquad \textbf{(Equation 7-1)}$$

where, $\underline{g}$ is the gravitational acceleration vector, $\underline{\nabla}$ is the grad function vector, and z is vertical distance relative to a fixed datum. By definition, the hydraulic conductivity tensor, $\underline{\underline{K}}$, for an aquifer-groundwater system is (Voss, 1984):

$$\underline{\underline{K}} = \frac{\underline{\underline{k}} \rho \left| \underline{g} \right|}{\mu} \qquad \qquad \textbf{(Equation 7-2)}$$

where, $\underline{\underline{k}}\{x,z\}$ is the solid matrix permeability tensor, μ water viscosity (1.0×10^{-3} kg m^{-1} s^{-1} at 20°C for pure water), and ρ is the fluid density. The hydraulic head, h, of the fluid at any point is (Voss, 1984):

$$h = \frac{p}{\rho|\underline{g}|} + z \qquad\qquad\text{(Equation 7-3)}$$

where p is the fluid pressure.

Darcy's law is the basis to the governing differential equation that describes the average pore-fluid velocity, $\underline{v}$, in porous media. For the vertical x-z case, this equation is (Voss, 1984):

$$\underline{v}\{x,z,t\} = -\left(\frac{\underline{\underline{k}}}{\varepsilon\,\mu}\right) \bullet \left(\nabla p - \rho\underline{g}\right) \qquad\qquad\text{(Equation 7-4)}$$

where, t is time. By combining Equations 7-2, 7-3 and 7-4, a more familiar form of Darcy's law is obtained, ie:

$$\Rightarrow \underline{v}\{x,z,t\} = -\left(\frac{\underline{\underline{k}}\rho|\underline{g}|}{\varepsilon\,\mu}\right) \bullet \left(\nabla\frac{p}{\rho|\underline{g}|} + \nabla z\right) \qquad\qquad\text{(Equation 7-5)}$$

$$\therefore\ \ \underline{v}\{x,z,t\} = -\frac{\underline{\underline{K}}}{\varepsilon} \bullet \nabla h$$

Note also, that the Darcy fluid velocity, $\underline{q}$, is defined as follows:

$$\underline{q}\{x,z,t\} = \varepsilon\underline{v}\{x,z,t\} \qquad\qquad\text{(Equation 7-6)}$$

where ε is the effective porosity of the solid matrix. Consider the equation for fluid mass balance (Voss, 1984):

$$\frac{\partial(\varepsilon\rho)}{\partial t} = -\nabla \bullet \left(\varepsilon\rho\underline{v}\right) + Q_p \qquad\qquad\text{(Equation 7-7)}$$

where, Q_p is the fluid mass flow rate at the system boundary.

A formula describing the relationship between total fluid density and solute concentration, C, may be required to accurately simulate groundwater systems that have solute gradients. The following linear model is commonly applied to freshwater-seawater systems (Voss, 1984):

$$\rho\{C\} \cong \rho_o + \frac{\partial \rho}{\partial C}(C - C_o) \qquad \text{(Equation 7-8)}$$

where, ρ_o is the base fluid density, and C_o is base fluid solute concentration on a mass basis.

The following equation describes single species solute transport and mass conservation in porous media without adsorption, decay or reactions (Voss, 1984):

$$\frac{\partial(\varepsilon \rho C)}{\partial t} = -\underline{\nabla} \bullet (\varepsilon \rho \underline{v} C) + \underline{\nabla} \bullet \left[\varepsilon \rho \left(D_m \underline{\underline{I}} + \underline{\underline{D}}\right) \bullet \underline{\nabla} C\right] + Q_p C^* \qquad \text{(Equation 7-9)}$$

where, D_m is the apparent molecular diffusivity of solute in solution, $\underline{\underline{I}}$ is a 2 by 2 identity tensor, and C^* is the concentration of solute in Q_p. The first term on the RHS of Equation 7-9 accounts for the advective transport of solute, the second term describes the combined dispersion-diffusion transport of solute according to the Fickian model, and the last term describes a solute flux boundary condition which may be present.

The dispersive transport of solute is the result of groundwater velocity deviations from the average advective flux (Voss, 1984). The dispersion tensor, in the x-z plane, is as follows (Voss, 1984):

$$\underline{\underline{D}} = \begin{bmatrix} D_{xx} & D_{xz} \\ D_{zx} & D_{zz} \end{bmatrix} \qquad \text{(Equation 7-10)}$$

$$= \frac{1}{|v|^2} \begin{bmatrix} d_L v_x^2 + d_T v_z^2 & (d_L - d_T)(v_x v_z) \\ (d_L - d_T)(v_x v_z) & d_L v_z^2 + d_T v_x^2 \end{bmatrix}$$

where d_L and d_T are the longitudinal and transverse dispersion terms, respectively. d_L and d_T are assumed proportional to the groundwater speed (Voss, 1984):

$$d_L = \alpha_L |v|$$
$$d_T = \alpha_T |v|$$

(Equation 7-11)

where, α_L and α_T have the dimensions of metres, and are the longitudinal and transverse dispersivities, respectively. If the physical structure of the aquifer is accompanied by direction-dependent physical properties, then anisotropic dispersivity may result. Anisotropic-medium dispersivity requires additional equations to account for significant variations in the actual dispersivity as a function of flow direction. The *ad-hoc* model of Voss(1984) assumes an elliptical function for both α_L and α_T in terms of their maximum and minimum (ie, principle) values and their corresponding (ie, principle) directions (see Equations 7-12 and 7-13). In the model of Voss(1984), the principle directions for dispersivity are aligned with the principle directions for permeability.

$$\frac{1}{\alpha_L} = \frac{\cos^2 \theta_{kv}}{\alpha_{L\max}} + \frac{\sin^2 \theta_{kv}}{\alpha_{L\min}}$$

(Equation 7-12)

$$\frac{1}{\alpha_T} = \frac{\cos^2 \theta_{kv}}{\alpha_{T\max}} + \frac{\sin^2 \theta_{kv}}{\alpha_{T\min}}$$

(Equation 7-13)

where,

α_{Lmax} = maximum longitudinal dispersivity (m)
α_{Lmin} = minimum longitudinal dispersivity (m)
α_{Tmax} = maximum transverse dispersivity (m)
α_{Tmin} = minimum transverse dispersivity (m)
θ_{kv} = angle of fluid flow relative to the principle direction for k (rad)

Cautionary advice is warranted when applying the above equations in groundwater modelling exercises as in most groundwater field studies the actual processes of solute dispersion are rarely investigated in detail. The application of Equations 7-12 and 7-13 should be viewed as an *ad-hoc* adjustment to be applied only when clearly required by the field data (Voss, 1984). For a more detailed account of the theoretical formulation of SUTRA the reader is referred to the original documentation by Voss (1984).

7.1.2 Major Considerations

The following physical characteristics are major considerations when developing conceptual and mathematical models of reef-island groundwater systems and when selecting 'off-the-shelf' computer models (adapted from Reilly and Goodman, 1985):

(i)   Dimensionality (eg, 1-, 2- or 3-D)

(ii)   Flow dynamics (eg, hydrostatic, regional and/or tidal groundwater flow)

(iii)   Flow conditions (eg, hydrostatic, transient, steady-state or pseudo steady-state)

(iv)   Aquifer physical properties, layering and anisotropy

(v)   Boundary conditions (eg, pressures, flows, and phreatic surfaces)

(vi)   Fluid types (eg, miscible or immiscible)

(vii)   Fluid density-solute relationships (eg, freshwater-seawater)

7.2 GROUNDWATER HYDRAULIC MODELS FOR REEF AND ATOLL ISLANDS: A HISTORICAL PERSPECTIVE

Probably one of the first recorded observations concerning reef-island hydrogeology was made by Charles Darwin in 1845 when he wrote (from Davis, 1978):

> "...At first sight it appears not a little remarkable that the fresh water should regularly ebb and flow with the tides... These ebbing wells are common on some of the low islands of the West Indies. The compressed sand, or porous coral rock, is permeated like a sponge with the salt water; but the rain which falls on the surface must accumulate there, displacing an equal bulk of the salt water. As the water in the lower part of the great sponge-like coral mass rises and falls with the tides, so will the water near

the surface; and this will keep fresh, if the mass be sufficiently compact to prevent mechanical admixture; but where the land consists of great loose blocks of coral with open interstices, if a well be dug, the water, as I have seen, is brackish." (Darwin, 1909, p.483)

Darwin (1909) described a reef-island aquifer with tidally dynamic and variable salinity groundwater. It seems reasonable from the above quote that the potable resource beneath the island was the result of freshwater recharge "displacing" salty groundwater (ie, advective displacement), and that "mechanical admixture" (ie, mechanical dispersion) was reducing the freshwater inventory.

During the mid-to-late twentieth century the hydrogeology of numerous reef-islands were studied in considerable detail. Some noteworthy examples include Home Island at Cocos (Jacobson, 1976), Kwaj at Kwajalein (Hunt and Peterson, 1980), Buota Island at Tarawa (Lloyd et al., 1980), Enjebi Island at Enewetak Atoll (Wheatcrat and Buddemeier, 1981), Deke Island at Pingelap Atoll (Ayers and Vacher, 1986), and Laura at Majuro (Anthony, 1987). Most of the relevant literature concerns community requirements for potable groundwater on the larger atoll islands. Unlike atoll islands, however, most coral cays are too small for permanent human settlement and are less likely to have reliable groundwater resources because of their size. For these reasons it is not surprising that hydrogeological studies of coral cays and other types of small reef-island, such as sand and shingle banks, are rare.

During the mid-twentieth century, the formative years of reef-island hydrogeology, it was commonly assumed that in atoll islands (1) the Ghyben-Herzberg model sufficiently explained the presence of fresh groundwater, and (2) that tidal-groundwater phenomena were primarily the result of horizontally propagating tidal signals (Peterson, 1991). Both of these assumptions were later shown to be poorly suited to low carbonate atoll islands (see below). The Ghyben-Herzberg principle and its model derivatives are based upon the following formula which describes the buoyancy of fresh water relative to saline water when the two fluids remain unmixed (ie, immiscible):

$$f\{x.y\} = -\frac{\rho_f \delta\{x,y\}}{\left(\rho_f - \rho_s\right)}$$
$$\cong -40\delta$$

(Equation 7-14)

where f{x,y} is the vertical position of the freshwater-saltwater interface, δ{x,y} is the elevation of the water table above mean sea level, ρ_f is the density of the fresh water (1000 kg m^{-3} at 20°C), and ρ_s is the density of the seawater. Seawater has a density close to 1025 kg m^{-3} at 20°C and a dissolved solids concentration of about 35.7 ppt. Therefore, for hydrostatic equilibrium to occur between a fresh groundwater body and a saline groundwater body that are in contact but remain unmixed, a slight freshwater overheight is required (refer Equation 7-14).

It is widely believed that Equation 7-14 was first formulated independently by Badon Gyhben (1888-9) in the Netherlands and by Herzberg (1901) in Germany (Ghassemi et al, 1993). However, according to Davis (1978), the principle of freshwater buoyancy was reported in the literature at least as early as 1828 by Joseph DuCommun (1828). Qualitative descriptions of the principle have also appeared as early as the first century AD (refer Davis, 1978).

The classic freshwater lens is often depicted as shown in Figure 7-1. The Ghyben-Herzberg school attributes the formation of the lens within an island aquifer to (a) meteoric freshwater recharge, (b) the retardation of fluid mixing by the aquifer solid-matrix, and (c) the buoyancy of freshwater relative to salty water. In some atoll-island groundwater studies the Dupuit assumption has been combined with the Ghyben-Herzberg formula in 2- or 3-dimensions (eg, Chidley and Lloyd, 1977; Lloyd et al., 1980; Falkland, 1983). The resulting Dupuit-Ghyben-Herzberg assumption provides a relatively simple governing differential equation for groundwater flow if it can be assumed that (i) equipotential surfaces are vertical, and (ii) fluid flow is uniform over the depth of flow (Fetter, 1972). For these assumptions to be reasonable, the lens must be thin compared to its lateral extent and the water-table slope should be 'slight' (Fetter, 1972).

Chidley and Lloyd (1977) use the Dupuit-Ghyben-Herzberg assumption to examine well draw-down at Grand Cayman Island, and Lloyd et al. (1980) use the Dupuit-Ghyben-Herzberg assumption to model the groundwater hydraulics of Tarawa Atoll, Gilbert Islands. However the model of Lloyd et al. (1980) reproduced poorly the observed freshwater inventory at Tarawa Atoll: probably because it assumed 2-D horizontal flow and ignored tidal affects. Falkland (1983) studied the groundwater hydraulics of an atoll island, Christmas Island, using the assumptions of no tide, hydrostatic conditions and a sharp transition zone. Falkland (1983) developed a finite-difference model based upon the earlier work of Chidley and Lloyd (1977).
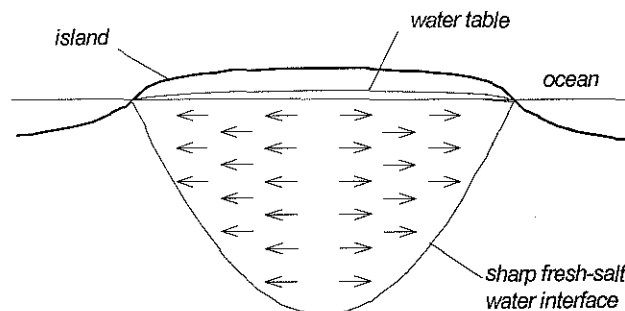
Figure 7-1. A schematic of the classic immiscible freshwater lens in an island aquifer with the Dupuit assumption of horizontal flow (refer Equation 7-14).

Davis (1978) points out that the phrase "Ghyben-Herzberg lens" should not be used, because the Ghyben-Herzberg principle does not in fact explain the existence or shape of a freshwater lens. Furthermore, the immiscible assumption of the Ghyben-Herzberg principle is incorrect and detracts from the actual mechanisms controlling the salinity distribution of a freshwater lens. The freshwater-seawater interface, no matter how 'sharp', always contains a zone of diffusion (Volker, 1980). To account for a thick transition zone in certain reef-island aquifers, some authors (eg, Chidley and Lloyd, 1977) have adopted a Ghyben-Herzberg factor of 20 instead of 40 (refer Equation 7-

14). The thick transition zones and non-horizontal groundwater flow fields found in many reef-island aquifers renders the Ghyben-Herzberg and the Dupuit assumptions untenable in those situations.

Detailed hydrogeological investigations of reef-islands date back to the early 1950's. For example, Cox (1951; 1953) reports on the groundwater tides and chemistry of Arno Atoll, and Arnow (1955) reports on the groundwater hydrology of Ifalik Atoll, Western Caroline Islands. Cox (1951) identified several factors that govern the size and shape of an atoll island freshwater lens, namely sediment permeability, freshwater recharge, and tidal range. He surmised that the damping of tidal signals in the aquifer is greater with larger specific yield, and that the transition zone of the atoll island lens is thickened by tidal groundwater movement and freshwater recharge. These conclusions are a significant departure from the Ghyben-Herzberg school of thought, however Cox (1951) mistakenly assumed that the tidal signals in the aquifer of Arno Atoll propagated mostly horizontally.

Lam (1974) published the results of what may be the first numeric model for tidal groundwater flow within a reef-island. Lam (1974) modelled Swains Island at Swains Atoll in the Tokelau Group using cylindrical coordinates and assuming a homogeneous fluid. Critical to Lam's (1974) model was the use of confining layers within certain portions of the upper aquifer. Lam (1974) concludes that, (i) intermittent beachrock confinement caused spatial variation in the groundwater tide, (ii) lower harmonic frequencies of the ocean tide were less attenuated in the aquifer than higher frequencies, (iii) poor permeability predictions, which spanned three orders of magnitude, account for large discrepancies between the simulated and observed phase lags, and (iv) amplitude is a more reliable parameter than phase lag when calibrating his tidal groundwater model.

Between 1945 and 1958 the US government tested nuclear bombs at Bikini and Enetwetak Atolls in the Marshall Islands (Weatcraft & Buddemeier, 1981). These weapons tests were followed by detailed hydrogeological research in the late 1970's to examine radionuclide mobility in the groundwater, vadose soil and biosphere of the

atoll islands (Weatcraft & Buddemeier, 1981; Peterson, 1991). It appears that Buddemeier and Holloday (1977), who examined Enjebi Island at Enewetak Atoll, were the first researchers to postulate that groundwater tides of an atoll-island may be controlled by vertical coupling between a unconsolidated surficial aquifer and a lower aquifer of permeable limestone. To support their conclusions, Buddemeier and Holloday (1977) present an analytical model which demonstrates that the conventional concept of horizontal propagation of tidal signals does not apply at Enjebi. Wheatcraft and Buddemeier (1981) observed that within the aquifer of Enjebi Island, tidal efficiencies generally increased with depth, tidal lags generally decreased with depth, and relatively strong tidal signals were found close to the shoreline. They suggest that a thin freshwater lens and a thick fresh-saltwater transition zone at Enjebi is also indicative of a highly conductive Pleistocene aquifer and tidal mixing.

Herman and Wheatcraft (1984) and Herman, Buddemeier and Weatcraft (1986) use the finite-element program FEMWATER (Yeh and Ward, 1980) to simulate the tidally affected groundwater flow at Enjebi Island. Their groundwater model was for 2-D, vertical, constant-density fluid flow with tidal-pressure variations at the ocean and lagoon boundaries. Herman, Buddemeier and Weatcraft (1986) propose three major hydrostratigraphic units for Enjebi Island: (1) an unconsolidated sand-and-gravel surficial aquifer of Holocene age (above -15 m MSL), (2) a consolidated karst limestone aquifer of Plio-Pleistocene (-15 to -200 m MSL), and Miocene and Eocene ages (-200 to -1277 m MSL), and (3) an impermeable basalt foundation below -1277 m MSL. A hydraulic conductivity (K) in the order of 60 m d^{-1} for the Holocene aquifer and 6000 m d^{-1} for the Pleistocene aquifer were derived. The relatively high permeability of the Pleistocene limestone was explained by Herman, Buddemeier and Weatcraft (1986) in terms of its geologic history: characterised by periods of glacio-eustatic exposure during which subaerial erosion is believed to have created extensive solution cavities. Solution cavities were most evident at Enewetak Atoll between -20 and -65 m below ground level (Wheatcraft and Buddemeier, 1981). The pseudo steady-state pressure contours produced by FEMWATER show that vertical groundwater flow occurs predominantly within the surficial aquifer at Enjebi Island. Herman, Buddemeier and Weatcraft (1986) also found that computed tidal efficiencies

increase and computed tidal lags decrease with depth below the island. They also claim that the tidal efficiencies and lags computed by their model were in "excellent" agreement with their field data.

Ayers and Vacher (1986) investigated the hydrogeology of Deke Island of Pinglap Atoll in the west Pacific. The conceptual hydrogeological model for Deke has the following important components: (1) an island which is exposed to the hydrologic cycle, (2) a reef-flat plate capping which is indurated and impermeable, (3) a heterogeneous Holocene aquifer composed mostly of unconsolidated sediments, and (4) an underlying, solution-altered and once-emergent Pleistocene limestone aquifer. Evidently Deke straddled the reef-plate and had an asymmetric distribution of sediment. As such, freshwater recharge, groundwater evaporation and tidally affected groundwater flow were found by Ayers and Vacher to be asymmetric across the island.

The numerical simulation of salt transport and mixing in conjunction with groundwater flow requires a higher level of numerical sophistication and greater computer resources. Hogan (1988) used the general-purpose program SUTRA (Voss, 1984) to model a miscible freshwater lens in the tidally-coupled groundwater system of Enjebi Island at Enewtak Atoll. Hogan (1988) calibrated the permeabilities of his model by comparing computed tidal efficiencies with observed. He estimated the hydraulic conductivity of the Pleistocene layer to be two orders-of-magnitude greater than that of the Holocene layer. Dispersivities were adjusted by Hogan on an element-wise basis to achieve numeric stability of the simulated freshwater lens, but according to Underwood (1990), this technique "complicated the interpretation of transport dynamics".

Oberdorfer, Hogan and Buddemeier (1990) also use SUTRA to model the variable-salinity tidally-affected aquifer of Enjebi Island. They calibrated their model against field values of tidal efficiency and average groundwater salinities to arrive at a K of 10 m day^{-1} for the surficial Holocene aquifer, a K of 1000 m day^{-1} for the Pleistocene

aquifer, a porous medium compressibility of 1×10^{-9} m^2 N^{-1}, and a longitudinal dispersivity of 0.02 m. A total simulation time of 3 years, using an hourly time step, was required to reach a stable salinity distribution. Their model results concur with the existence of significant oscillatory vertical flow and an extensive transition zone of brackish water below the Island. The computer-generated flow fields were found to be near-uniform across the island and more variable at the island edges (Oberdorfer, Hogan and Buddemeier, 1990). Oberdorfer, Hogan and Buddemeier (1990) ignore transverse dispersivity, arguing that the large variations in flow velocity at any given point would mask the effects of the "much smaller" transverse dispersivity.

Underwood (1990) and Underwood, Peterson and Voss (1992) present a conceptual hydrogeological model for a generic atoll island subject to freshwater recharge and seawater intrusion. By numeric experimentation, they investigated the processes controlling groundwater tides and the size and shape of freshwater lenses within atoll islands. Underwood (1990) concludes that the principle controls on the groundwater response to the tide are the vertical hydraulic conductivity of the Holocene aquifer (K_{HV}), the vertical and horizontal hydraulic conductivities of the Pleistocene aquifer (K_{PV} and K_{PH}, respectively), and the aquifer specific yield. A general pattern of short-term tidally-affected groundwater flow, similar to that presented in Figure 7-3, was predicted by Underwood (1990) to occur within the generic atoll aquifer.

Underwood (1990) found that the main controls on freshwater-seawater mixing are the dispersion caused by vertical short-term (ie, tidal) groundwater flow and, to a lesser degree, the groundwater flow along the horizontal recharge-discharge path. The position of the 50% seawater isochlor was found by Underwood (1990) to be most sensitive to the recharge rate and the horizontal hydraulic conductivity of the Holocene aquifer (K_{HH}). The potable thickness of the lens was most sensitive to the recharge rate, the discharge rate, and to the dispersive mixing process which in turn is controlled mainly by the vertical longitudinal dispersivity, the tidal range, K_{HV} and K_{PV}.

Underwood, Peterson and Voss (1992) conclude that non-tidal models must use artificially high transverse dispersivities to compensate for the lack of tidally driven vertical mixing. Underwood (1990) claims that non-tidal models, whilst being numerically efficient, are of limited application because they ignore short-term dispersive fluctuations, cannot simulate realistic salinity profiles and cannot be used to calibrate vertical K of an aquifer. Compared to non-tidal models, tidal models are more robust and realistic, are preferable as management tools, but are computationally demanding (Underwood, 1990). The general streamline pattern expected in a hypothetical non-tidal aquifer subject to steady-state freshwater recharge and seawater intrusion is depicted in Figure 7-2.
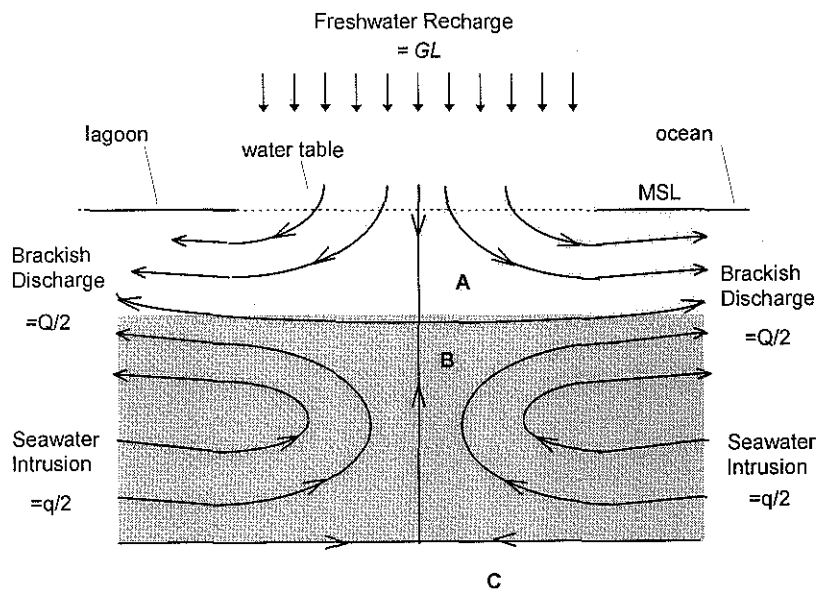
Figure 7-2. A schematic of long-term streamlines in a hypothetical atoll island aquifer without tidal flow and subject to steady-state freshwater recharge and seawater intrusion (adapted from Underwood, 1990): KEY A. Holocene aquifer; B. Pleistocene aquifer; C. basalt foundation.
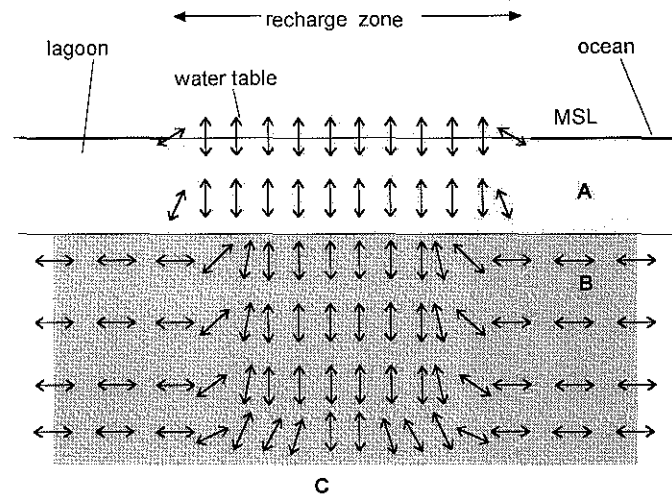
Figure 7-3. A schematic of short-term groundwater flow fields in a hypothetical atoll-island aquifer subject to tidal fluctuations (adapted from Underwood, 1990): KEY A. Holocene aquifer; B. Pleistocene aquifer; C. basalt foundation.

Despite certain inadequacies of non-tidal groundwater models, Griggs (1989) and Griggs and Peterson (1993) numerically simulated the freshwater lens of Laura area, Majuro Atoll, Marshall Islands, using a non-tidal groundwater model. Griggs (1989) and Griggs and Peterson (1993) use SUTRA to simulate freshwater lens dynamics at the atoll scale and to evaluate alternative management options for potable water extraction at Laura. The hydrogeology of Laura is typical of atoll islands, being comprised of an upper stratigraphic unit of layered Holocene sediment and reef plate, a lower unit of highly permeable limestone, and an impermeable foundation of basalt (Griggs and Peterson, 1993). Griggs and Peterson's (1993) non-tidal groundwater model relies on freshwater recharge, rather than tidal fluctuations, to drive groundwater flow. Consequently, dispersivities were treated by Griggs and Peterson (1993) as calibration factors rather than as real physical parameters. Calibration of their model was achieved graphically by matching predicted salinities with field data. They found that the depth of the simulated 50% seawater isochlor was most sensitive to aquifer permeability, and that the thickness of the transition zone was most sensitive to the transverse and horizontal longitudinal components of dispersivity.

Ghassemi, Jakeman and Jacobson (1990) produced a vertical 2-D non-tidal model of the freshwater lens at Nauru, a raised atoll island. Their model was developed using SUTRA, and was calibrated by matching predicted steady-state groundwater salinities with field data. Model results were very sensitive to hydraulic conductivity and recharge, and were also sensitive to porosity, anisotropy, and dispersivity. Ghassemi, Jakeman and Jacobson (1990) examined various freshwater extraction options, and recommend the use of properly designed shallow skimming wells to reduce the risk of groundwater salination and upconing. A 3-D numerical analysis of Nauru's groundwater system was also undertaken by Ghassemi, Jakeman and Jacobson (1990) and Ghassemi et al. (1993) using HST3D (Kipp, 1987). The authors conclude that a 3-D analysis can better reproduce the natural boundary conditions, but is somewhat impractical due to the need for rather fine mesh discretization and substantial 'supercomputing' resources. Ghassemi, Jakeman and Jacobson (1990) found that their application of HST3D failed to produce physically meaningful results.

7.3 STEADY-STATE SEAWATER INTRUSION AND GROUNDWATER RECHARGE-DISCHARGE

The hydrodynamic processes of groundwater advection, salt dispersion and salt diffusion in conjunction with freshwater input (typically recharge) can induce seawater movement in coastal aquifers from the floor of the ocean to the zone of diffusion and back to the ocean again (eg, Cooper, 1959). The net effect of this fluid and salt transport in coastal aquifers is commonly called 'seawater intrusion', and in island aquifers it may be thought of as 'freshwater lens formation'. Whilst a great deal of quantitative analysis has been carried out on the topics of seawater intrusion and freshwater lens formation (Reilly and Goodman, 1985), a general explanation for the steady-state salinity distributions associated with seawater intrusion and freshwater lens formation appears to be lacking in the literature.

To help explain the significance of seawater intrusion in island and coastal aquifers, the following steady-state mass balances for groundwater flow and salt transport are presented. Consider a infinitely long island aquifer with a freshwater lens and subject

to steady-state recharge and seawater intrusion (refer Figure 7-2). The steady-state mass balance per metre length of aquifer is:

$$GL + q = Q \qquad \text{(Equation 7-15)}$$

where G is average freshwater recharge speed (m s^{-1}), L is the island width (m), q is the total seawater intrusion rate (m^2 s^{-1}), and Q is the total groundwater discharge rate (m^2 s^{-1}). Similarly, consider the steady-state mass balance for salt inflows and outflows per metre length of the same aquifer:

$$GLC_f + qC_s = Q\overline{C_d} \qquad \text{(Equation 7-16)}$$

where, C_f is the recharge salinity (kg kg^{-1}), C_s is the seawater salinity (0.0357 kg kg^{-1}), and $\overline{C}_d$ is the average groundwater discharge salinity (kg kg^{-1}). Equations 7-15 and 7-16, when combined, give

$$\Rightarrow \qquad GLC_f + qC_s = (GL+q)\overline{C_d}$$
$$\Leftrightarrow \qquad qC_s - (GL+q)\overline{C_d} = -GLC_f$$
$$\Leftrightarrow \qquad q(C_s - \overline{C_d}) = -GLC_f + GL\overline{C_d} \qquad \text{(Equation 7-17)}$$
$$\therefore \qquad q = GL\frac{(\overline{C_d} - C_f)}{(C_s - \overline{C_d})}$$

When a coastal aquifer undergoes freshwater recharge and groundwater discharge, some freshwater-saltwater mixing will occur. This mixing is commonly attributed to dispersive and diffusive transport of salts across salinity gradients in the groundwater. The net effect of these mixing processes is that the discharging groundwater has a salinity on average greater than that of the recharge fluid (ie, $\overline{C}_d > C_f$). Therefore under steady-state conditions there must be some seawater intrusion to counter the removal of salts from the aquifer (ie, $q > 0$). The mass balance of this phenomena is explained by Equation 7-17 which shows that, for a fixed value of G, increasing the level of salinity in the discharge fluid above C_f results in q being greater than zero.

For example, when $\overline{C}_d$ equals *0.5 C_s,* Q, equals twice *GL*. Furthermore, as $\overline{C}_d \rightarrow C_s$ the computed values of q and Q increase almost exponentially (see Equation 7-17). Hence, relatively large intrusion rates are expected to occur at steady-state if the hydrodynamic-dispersion of solutes is substantial. For example, a $\overline{C}_d$ of 90% seawater at steady-state will cause a total discharge rate 9 times that of the recharge rate when C_f is zero.

7.4 TIDALLY AFFECTED GROUNDWATER FLOW

The affect of ocean tides on groundwater flow can be significant in coastal and island aquifers (eg, Serfes, 1991; Erskine, 1991; Vanek, 1993; Marquis Jr. and Smith, 1994; Millham and Howes, 1995) and marine retaining structures (eg, Farrell, 1994). Tides can also affect solute levels at the aquifer/estuary interface (Yim and Mohsen, 1992), and can induce significant variations in aquifer storativity and groundwater pressure in sub-sea and coastal confined aquifers (eg, Carr and Van der Kamp, 1969; Liu, 1996).

Reef-island aquifers are particularly vulnerable to hydraulic oscillations of tidal origin because of the high permeability of reef-limestones and coralline sediments. Tidal pressure signals in reef-islands originate at the submerged aquifer/ocean boundaries and at the beach/seawater boundaries. To mathematically model these boundaries, the tide may be substituted with a sine-type function (for tidal analysis) or with a constant head equivalent to mean sea level (for non-tidal analysis). In most reef-island groundwater models, laterally propagating tidal signals that originate at the beach-face are assumed negligible. The validity of this assumption may be evaluated using the distance-decay and the periodicity-decay relationships defined by Ferris (1951) and Todd (1980). This simplification of the beach-seawater boundary will, however, introduce some error if wave run-up and/or water-table decoupling results in water-table overheights relative to mean sea level and other distortions of the tidal signal (Urish and Ozbilgin, 1989; Neilsen, 1990; Turner, 1993). Capillarity may also affect the dynamics of the water-table, however this topic is poorly understood at present (Aseervathem, 1992).

Because the water-table in reef-islands can be tidally dynamic, any attempt to numerically simulate a reef-island aquifer will require that variations in saturated thickness of the phreatic aquifer be accounted for. Lam (1974), who numerically modelled 2-D tidal flow within an atoll island, simplified the moving water-table boundary by assuming hydrostatic conditions between the phreatic surface and an arbitrary upper boundary of an unconfined aquifer. Certain computer codes have been developed to simulate a moving water-table (eg, Wang and Anderson, 1972) whilst others can be modified for this purpose (eg, Oberdorfer, Hogan & Buddemeier, 1990).

7.5 TIDALLY AFFECTED SOLUTE MIXING

The processing time needed by a computer to solve tidally-affected variable-salinity groundwater flow problems can be considerable for the following reasons: (i) the processing speeds of computer hardware are finite, (ii) the size of the largest allowable time-step that can be used to simulate a tidal oscillation is typically less than two hours, and (iii) the total simulation time may be in the order of years, decades or longer. One approach to reducing the processing time associated with a tidally-affected variable-salinity groundwater problem is to use a faster computer. Underwood, Peterson and Voss (1992) used super-computing facilities to simulate several years of tidal groundwater flow in an atoll island with a time-step of less than 1.5 hours. Another approach is to replicate the effect of tidal-flow in the model by using regional flow conditions and artificially large dispersivities. This non-tidal approach requires that the model be empirically calibrated against field data that is sufficient to characterise the actual tidally-affected hydrodynamic dispersion process (eg, Griggs and Peterson, 1993; Ghassemi et. al., 1993). The main problem with this non-tidal approach is that it does not simulate the physical system and so cannot be assumed reliable without prior calibration and verification on a case-by-case basis. Underwood, Peterson and Voss (1992) claim that the inaccuracies of this non-tidal approach may result in misleading outcomes.

Cooper (1959), in his study of a tidally affected coastal aquifer, proposed that the net longitudinal dispersion of salts in the tidally affected groundwater was proportional to the mean groundwater speed. Hence, if because the groundwater movement involved sinusoidal variations in speed and was lateral and 1-dimensional, the solute dispersion could be approximated as follows (Cooper, 1959):

$$D_{tide} = 4 \; \alpha_L \, A\{x\}/t_0 \qquad \textbf{(Equation 7-18)}$$

where α_L is the longitudinal dispersivity, t_o is the tidal period and $A\{x\}$ is the tidal amplitude at horizontal distance x relative to the shoreline. Because groundwater flow has been found to be predominantly vertical and sinusoidal below certain reef-island aquifers, the method of Cooper (1959) could have applicability to these islands. The average water-table speed, V_{avg}, can be computed from the average tidal efficiency (η_{avg}), average tidal frequency (ω) and average tidal amplitude (A) by assuming a sinusoidal tide, ie:

$$V_{avg} = 2\omega \, A \, \eta_{avg} / \pi \qquad \textbf{(Equation 7-19)}$$

It follows then that the equivalent vertical long-term dispersivity, D_{tide}, due to the tidal pumping of groundwater in the shallow reef-island aquifer is:

$$D_{tide} = \alpha_L \, V_{avg}$$

$$= 2 \; \alpha_L \; \omega A \; \eta_{avg} / \pi \qquad \textbf{(Equation 7-20)}$$

Oberdorfer, Hogan and Buddemeier (1990), who investigated the salinity distribution in Enjebi Island, used the following data for substitution into Equations 7-19 and 7-20: average water table efficiency, η_{avg}, of 0.09 ± 0.04; average tidal amplitude, A, of 0.9 m; a tidal frequency, ω, of 1/12 cycles h^{-1} (1.454×10^{-4} rad s^{-1}); and a α_L of 0.02 m. Substituting these values into Equations 7-19 and 7-20, V_{avg} is 7.5×10^{-6} m s^{-1} and D_{avg}

is 1.5×10^{-7} m^2 s^{-1}. This value of D_{avg} is two-orders of magnitude greater than the D_m of NaCl in water at 20°C, thus tidally-coupled dispersivity can easily mask diffusive mixing. The approach of Cooper (1959) is, however, limited to 1-dimensional flow problems.

7.6 PREVIOUS STUDIES AT HERON ISLAND

Although there have been some groundwater studies at Heron Island, previous descriptions of the island's hydrogeology have been limited in their scope. The first groundwater investigations at Heron Island were undertaken by Charley et al. (1990, unpublished) in an exploratory fashion. Charley et al. installed seven water-table bores at the eastern half of Heron Island and manually recorded the water-levels in these bores through one tidal cycle. They found that the water-table oscillated in response to the ocean tide and that these oscillations were not uniform over the island. The water-table oscillations observed by Charley et al. (1990, unpublished) were also attenuated and lagged compared to the ocean tide. They speculated that a relationship existed between the efficiency and lag of the groundwater tide at Heron Island and the distance to the nearest unconsolidated beach (ie, Shark Bay; refer Figure 1-3). Their hypothesis was that the tide at Shark Bay affected the water-table inland, whilst beachrock formations on the northern and southern shorelines prevented the tide in those areas from influencing the groundwater (with the benefit of the field data obtained in this study it is shown in Chapters 9 and 10 that this hypothesis is untenable).

In 1991 Krol et al. (1992) installed 13 groundwater investigation wells including a total of 42 working piezometers at Heron Island for the Heron Island Groundwater Project (refer Chapter 1). Groundwater heads were measured in these piezometers over a period of one tidal cycle to investigate patterns of groundwater pressure variation in 3-dimensions. In the deeper piezometers, groundwater pressure variations were more similar to the pressure variations occurring in the ocean. Krol et al. describe these phenomena in terms of two trends: (1) an increasing tidal efficiency with increasing depth in the aquifer, and (2) a decreasing tidal lag with increasing

depth in the aquifer. They suggest that the bulk of the groundwater moved vertically and was coupled to a highly permeable reef rock aquifer beneath the cay. The island's hydrogeology was not described in detail by Krol et al. (1992), although their general observations about Heron Island resemble those made by others studying small low atoll islands (refer Section 7-3).

Charley et al. (1990, unpublished) were also interested in the hydraulics of cay beaches as a possible control on groundwater dynamics. They examined broad patterns of groundwater seepage and water-table movement in the beaches of Heron Island and Price and Frigate cays and concluded that the phreatic surfaces in cay beaches were sloped and generally higher than the tide at low-tide. They found that the surface leakage of groundwater "...usually continued through the low tide..." until being "...overwhelmed by the subsequent flood".

7.7 CONCLUSIONS

From the literature and theoretical analysis in this chapter, it is evident that the transient flow of groundwater in reef islands can be affected by a number of physical processes, ie: (i) fluid density gradients, (ii) short-term advective flows (eg, tidal pumping), (iii) long-term and regional advective flow (eg, recharge and seawater intrusion), (iv) solute advection, dispersion and diffusion, and (v) moveable boundary hydraulics (eg, water-table readjustment, beach-face seepage, and unsaturated flow). The elastic storage of fluid due to compressibility of the fluid and solid matrix is generally insignificant in shallow unconfined aquifers (Domenico & Schwartz, 1990).

Of major consequence in carbonate atoll island aquifers is the propagation of tidal pressure harmonics and the 'dual-aquifer' hydrogeological conceptual model. The time- and space-distortions of tidal harmonics are most conveniently measured in terms of amplitude decay (ie, 'tidal efficiency') and phase lag (ie, 'tidal lag'). In the unconfined portion of the Holocene-age aquifer, the tidal harmonic tends towards least distortion with greater depth below the water-table. This appears to be characteristic of tidally pumped vertically orientated unconfined groundwater flow: the regime of

flow that generally occurs within reef-islands if a 'dual-aquifer' hydrogeology exists. An additional issue for modelling this type of groundwater flow are possible structural heterogeneities in the carbonate aquifer at a scale of metres as a result of, for example, discontinuous reef-plate and beachrock capping (eg, Lam, 1974).

The actual space- and time-distortions of tidal signals and axiomatic water-table movement is currently understood within the context of idealised numerical models that are based upon the governing differential equations for Darcian fluid flow and mass conservation (eg, Herman & Weatcraft, 1984; Herman, Buddemeier & Weatcraft, 1986; Hogan, 1988; Underwood, 1990; Underwood, Peterson & Voss, 1992; Griggs & Peterson, 1993). In such models the fluid and solid matrix are assumed virtually incompressible and tidal influences are usually incorporate as a dynamic boundary condition.

For idealised coastal and island aquifers with steady-state freshwater recharge, seawater intrusion, and discharge, a large-scale circulation of groundwater flow may also occur as a result of dissolved-salt transport and mixing (refer Figure 7-2). Equation 7-17 indicates that when freshwater recharge and saline groundwater become well-mixed under steady-state conditions, total intrusion and total discharge flow rates can far exceed the total recharge flow rate. Whilst potentially important to the understanding of groundwater flow, the development of a regional recharge-discharge groundwater model may prove difficult as steady-state might not be approached in the field (thus adding further complexity) and the cost of collecting the appropriate field data may be inhibitive.

8. PIEZOMETRIC INVESTIGATIONS

8.1 INTRODUCTION

In this chapter the methods and materials that were employed to monitor the ocean tide at Heron Reef and the groundwater piezometric water-levels and salinities at Heron Island are described. The main results of the field study are presented as summary graphs and tables. For reasons of brevity an entire listing of the field data is not given but rather are available in digital format in Appendix J or from the Department of Chemical Engineering, the University of Queensland.

To assist with the hydrogeological interpretations, the field data are analysed to determine the efficiency and lag of tidal signals that were recorded in the groundwater system. Space and time variations in the tidal signal are also interpreted to help elucidate the hydrogeology of the island. More detailed hydrogeological interpretations are made in Chapters 9 and 10 using analytical and numeric techniques.

During the groundwater investigations the opportunity was taken to simultaneously record other physico-chemical parameters and the nutrient content of the groundwater. The resulting water-quality database, which spans April 1992- March 1995 (refer Appendix I) is presented as an adjunct to the current study for future reference. The water-quality database is not discussed in this dissertation in any detail and the reader is referred to Chen and Krol (in press) and Krol et al. (1992) for more information in this respect.

8.1.1 Vertical Water-Levels: Units and Datum

The ocean tide was recorded in metres-of-seawater relative to Low Water Datum (LWD), and groundwater heads were recorded in units of metres-of-groundwater relative to LWD. In the analyses of Chapters 9 and 10, the tide and groundwater heads are given in consistent units: metres-of-equivalent-seawater relative to Mean Sea Level (MSL). As shown in Table 8-1, there exists a small discrepancy in the published MSL at Heron Island due to imperfect analysis of the tide. In this study MSL is taken as 1.61 m above LWD.

Noordink et al. (1992) provide the survey data for well collar heights relative to benchmark PSM 61221 located on the helipad (see Figures 8-1 and Figure 8-2). This survey data allows the piezometer levels to be related to Low Water Datum with a precision of ±1 cm (see Table F-4).

Table 8-1. Tidal planes and datum levels at Heron Reef .

LWD (m)	MHWS (m)	MHWN (m)	MLWN (m)	MLWS (m)	MSL (m)	HAT (m)	LAT (m)	PSM 61221 (m)	Ref.
0.00	2.75	2.15	1.06	0.47	1.61	3.43	0.08	-	Q.D.T. (1992-4)
-0.08	-	-	-	-	1.53	-	0.00	-	Q.D.T (1995)
0.00	-	-	-	-	-	-	0.085	4.511	Hacker (1995)
0.00	-	-	-	-	1.517	-	-	4.511	Q.D.T. (1983)

Notes:
(a) MHWS = Mean High Water Springs
(b) MHWN = Mean High Water Neaps
(c) MLWN = Mean Low Water Neaps
(d) MLWS = Mean Low Water Springs
(e) MSL = Mean Sea Level
(f) HAT = Highest Astronomical Tide
(g) LAT = Lowest Astronomical Tide
(h) Survey benchmark PSM 61221 is located in the centre of the helipad.

8.1.2 Aims and Objectives

The overall aim of the work described in this chapter is to obtain further potentiometric data to allow improved understanding of Heron Island's groundwater system. The specific objectives were:

(1) to measure and record groundwater piezometric levels and the ocean tide over extended periods,

(2) to measure and record the tide over the reef-flat during a low tide,

(3) to measure and record the groundwater salinities before and after the piezometric investigations, and

(4) to use the data from (1), (2) and (3) to determine the efficiencies and lags of the groundwater-pressure signal relative to the ocean tide.
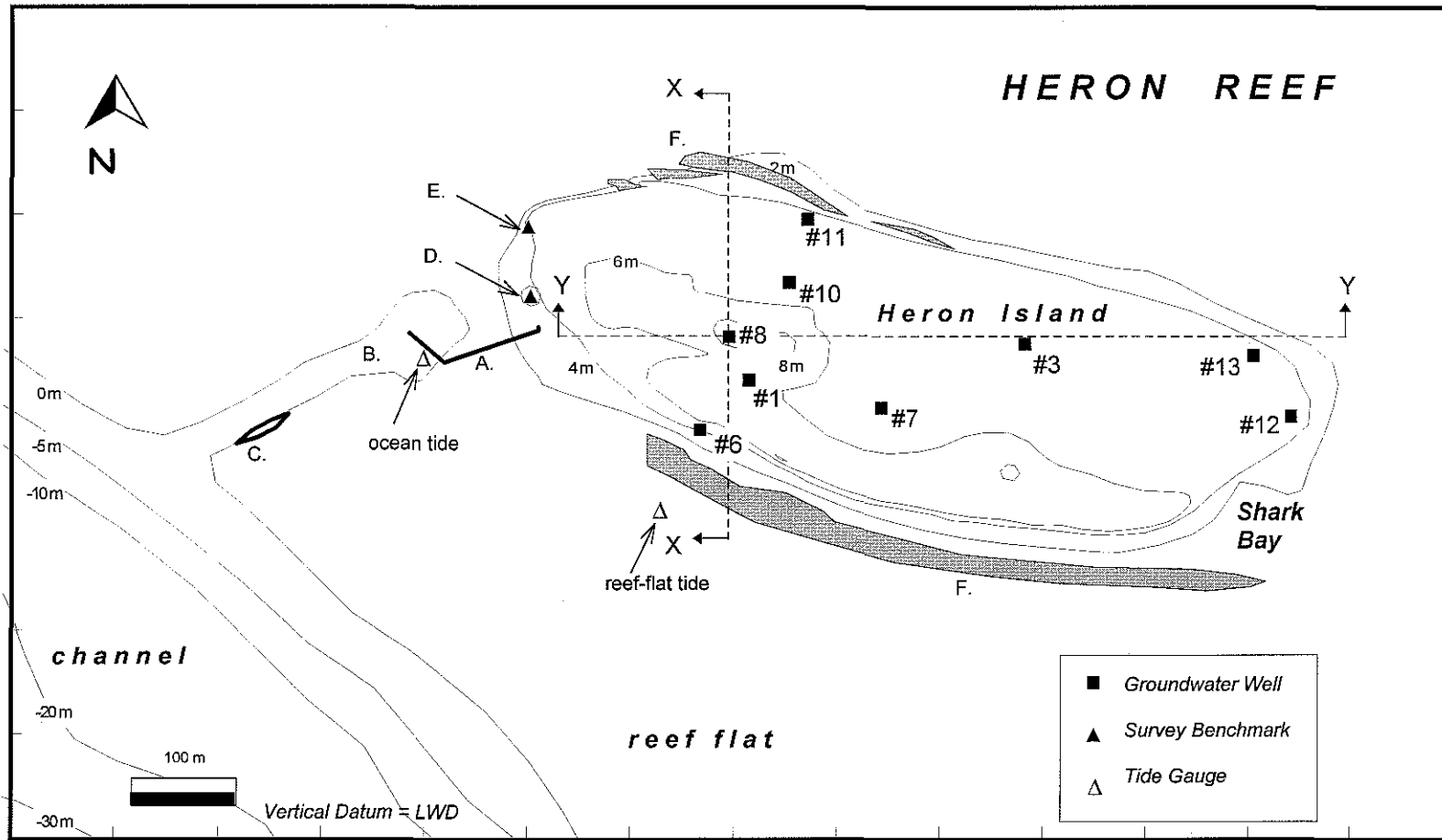
Figure 8-1. A topographic map of Heron Island showing the groundwater investigation wells and tide gauges that were monitored for water-levels during the study (KEY: A, jetty; B, boat harbour; C, shipwreck; D, helipad and survey benchmark PSM61221; E, survey benchmark ; F, beachrock).
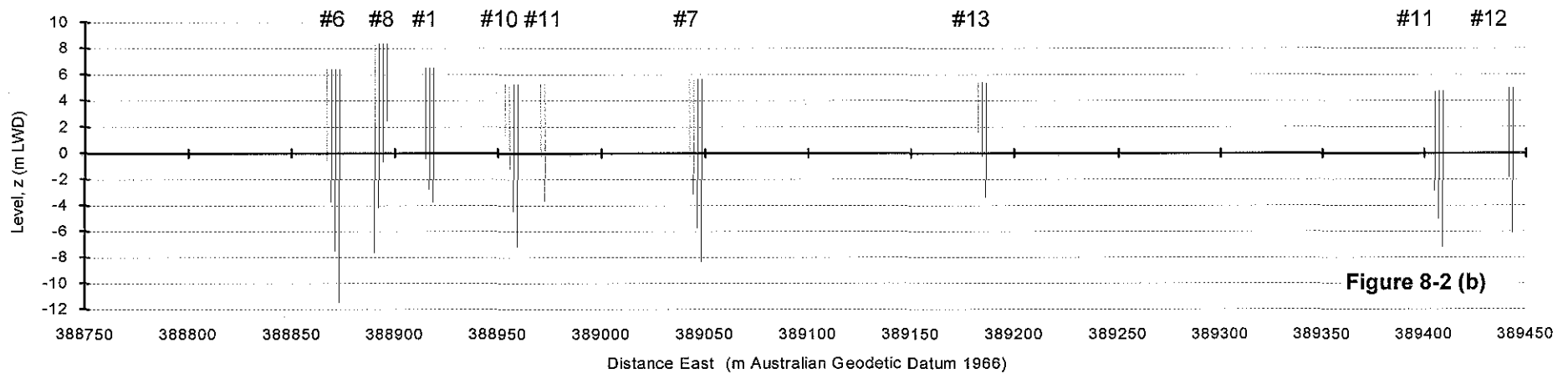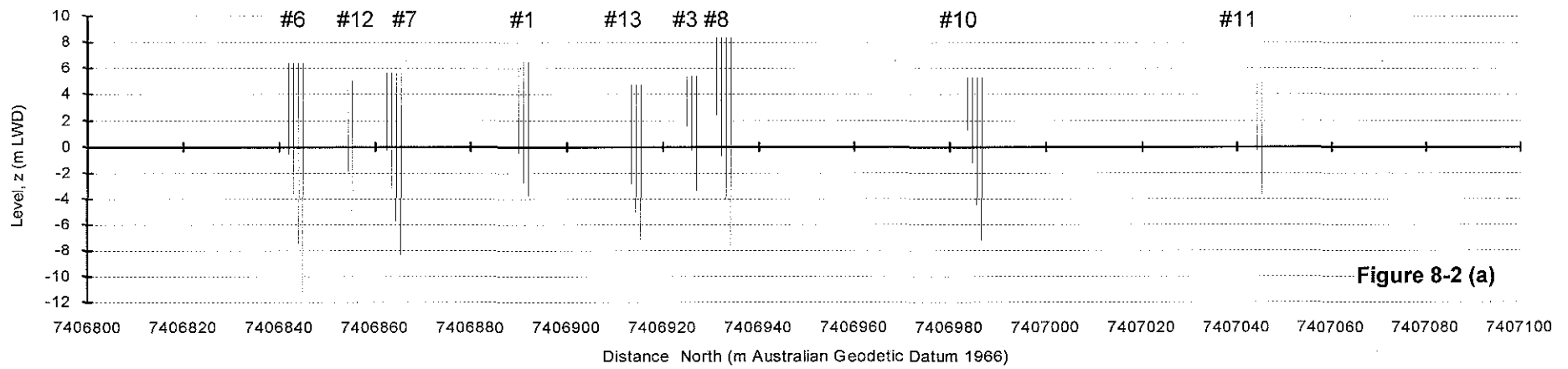
Figure 8-2. The relative positions of the groundwater investigation wells at Heron Island : (a) through section X-X and (b) through section Y-Y (refer Figure 8-1).

With respect to (1), data was to be obtained at 10 minute intervals of over 3-4 weeks. A sample period of 3-4 weeks was chosen so that the most significant features of the lunar and solar tides would be captured, and the 10 minute sample frequency was chosen so that the maxima and the minima (and therefore the efficiencies and the lags) of the pressure signals could be ascertained accurately. The reef-flat tide was compared with the groundwater tides to determine whether these tidal signals could be detected in the Holocene aquifer.

8.2 WATER-LEVELS

8.2.1 Methods and Materials

8.2.1.1 Groundwater-Level Measurements

Eight pressure transducers and three programmable data recorders (Dataflow Systems) were used to record piezometric groundwater-levels for 3-4 week periods (approx.). The main criteria for selecting the equipment were, (i) that it could be left in the field unattended for about 4 weeks, (ii) that the pressure transducers could fit inside the 25 mm diameter piezometers, and (iii) that the data recorders had sufficient memory to record water-levels at 10 minute intervals. Also considered prior to the acquisition of the equipment were the specifications of the equipment relating to cable length, the expected piezometric range, and cost.

Due to resource limitations, it was not feasible to investigate all of the existing piezometers at Heron Island. Rather, the experimental plan was to monitor a total of twenty-two piezometers at wells #1, #3, #6, #7, #8, #10, #11, #12 and #13 (refer Figure 8-1 and 8-2). It was assumed that the data derived from this experimental plan would be sufficient to fulfil the main objectives of the study.

The piezometric monitoring equipment is illustrated in Figure 8-3. Each pressure transducer was constructed from a strain gauge and a temperature sensor cased inside a PVC tube. The temperature compensation of the strain gauges was not undertaken due to the groundwater temperatures being relatively constant during the study. The cables to the pressure transducers were made from 75 ohm air dielectric coaxial cable that allowed air venting and thus eliminated the impact of barometric pressure changes on

instrument readings. Because the pressure gauges were rather light, lead weights were attached to ensure that the gauge cables remained straight when installed (refer Figure 8-3 for details). To prevent algae or fungi growing on the strain gauges, latex rubber sheathes (cut from surgical gloves) were glued to the ends of the gauges and filled with a solution of distilled water and fungicide (pH buffer preservative). The sheathes were effective in protecting the transducers whilst maintaining natural water pressures.

Each data-recorder was stored with silica jell in a weather-proof housing constructed from plastic (see Plate 5). These housings had eight compression glands for accepting the sensor coaxial cables, a port for a computer connection (for programming), and an RS232 interface for the data-recorder. Up to four pressure/temperature gauges could be powered and logged by a single data-recorder. The power requirements of each arrangement included one 9 V and eight 3 V batteries. The plastic housing and associated data recorder were stored inside a lockable outer-housing that was constructed from plywood and perspex, and mounted on a stainless steel tripod (see Plate 4). The tripod was bolted to the relevant well-head casing for the duration of the investigations, and each complete above-ground arrangement was covered by a lockable vinyl cover to keep the equipment clean and dry.

The step-by-step installation procedure for each data recorder and pressure transducer system was as follows (refer Figure 8-3 and Plate 6):-

(i) Water levels in each piezometer, relative to the top of the well casings, were measured using a manual depth gauge (see Plate 5). Levels RGL were reduced to LWD using the survey data of Noordink et al. (1992). The placement depth of each pressure transducer RGL was then calculated so as to ensure that each transducer remained at least 1 m below the lowest expected water level whilst receiving water pressures within the transducer's capacity.

(ii) The tripod stand and outer-housing was bolted to the steel well-casing above the piezometer nest to be monitored (see Plate 4). Each pressure transducer was washed with distilled water prior to its placement into the appropriate piezometer. The length of coaxial cable lowered into each piezometer was recorded from 1m intervals marked on the cables. The position of each transducer was fixed by securing the excess cable to the

tripod with vinyl tape.

(iii) The data recorder was programmed with a lap-top computer to record uncalibrated pressures and temperatures at 10 minute intervals beginning on the hour. The internal clocks of the data recorders and the lap-top computer were set to match Australian Eastern Standard Time to the nearest minute. Over the following 1-2 days, the pressure records were down-loaded to the lap-top computer for calibration purposes. Calibration of the transducers was done by manually recording piezometer water levels (m RGL) and noting the time of the measurements. The uncalibrated transducer responses at the times of the manual records were found by interpolation. The uncalibrated transducer responses and the water levels (m LWD) were linearly regressed to determine two calibration coefficients for each pressure transducer. Temperature compensation of the transducer response was ignored on the basis that groundwater temperatures were relatively constant.

(iv) The calibration procedure was repeated until the calibration curve possessed a 'high' linear correlation. The equipment was then checked, locked and left in position to record levels for the following 3-4 weeks.

(v) After 3-4 weeks of continuous datalogging, the data stored in the data recorder was down-loaded to a lap-top computer.

(vi) The calibration procedure (outlined above) was repeated as a precautionary measure. The new calibration data was used to check that the pressure transducers had not moved nor suffered some electronic 'drift'.

(vii) The equipment was removed from the well collar.
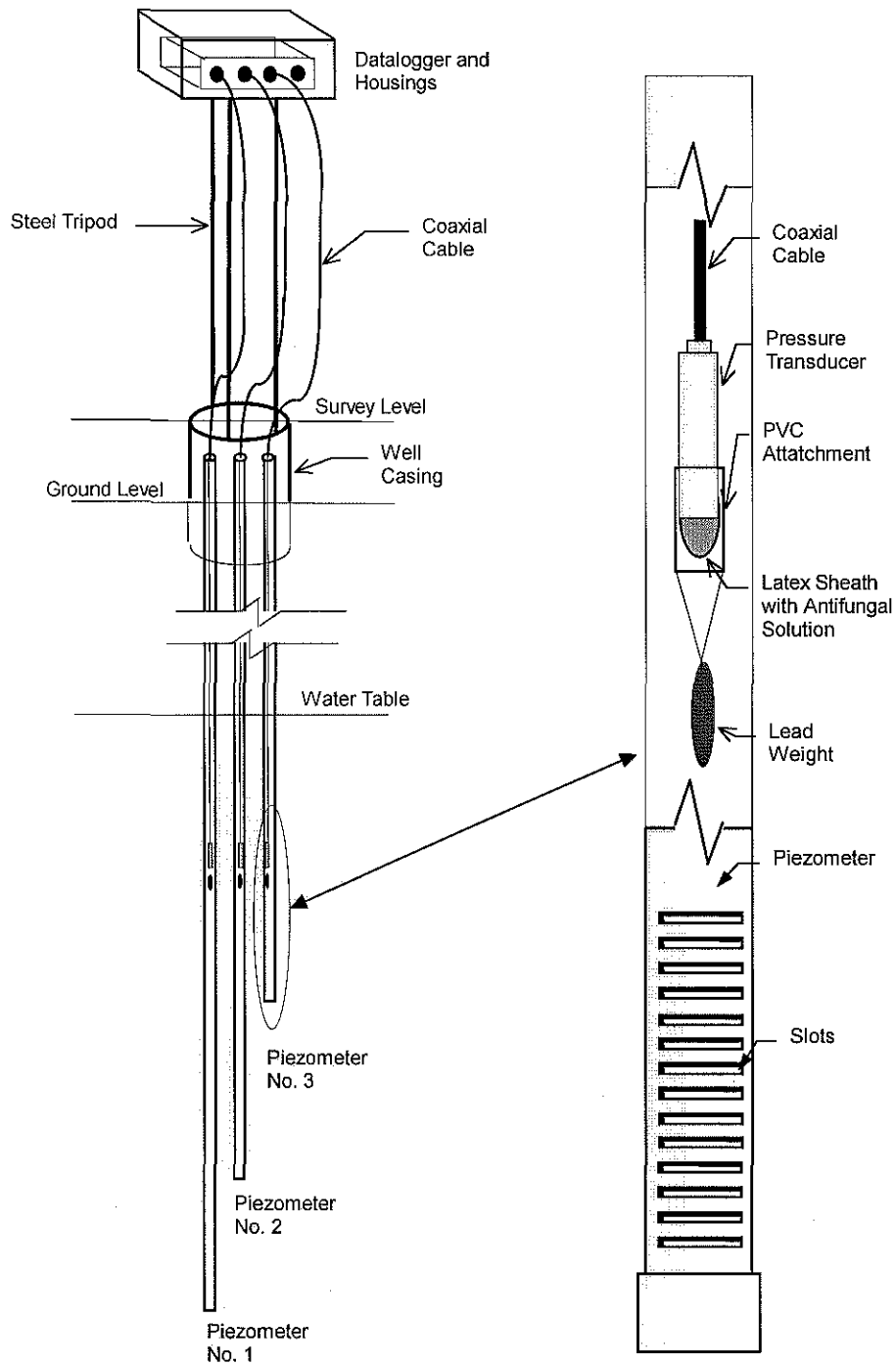
Figure 8-3. Groundwater potentiometric recording equipment (not to scale; see also Plate 6).
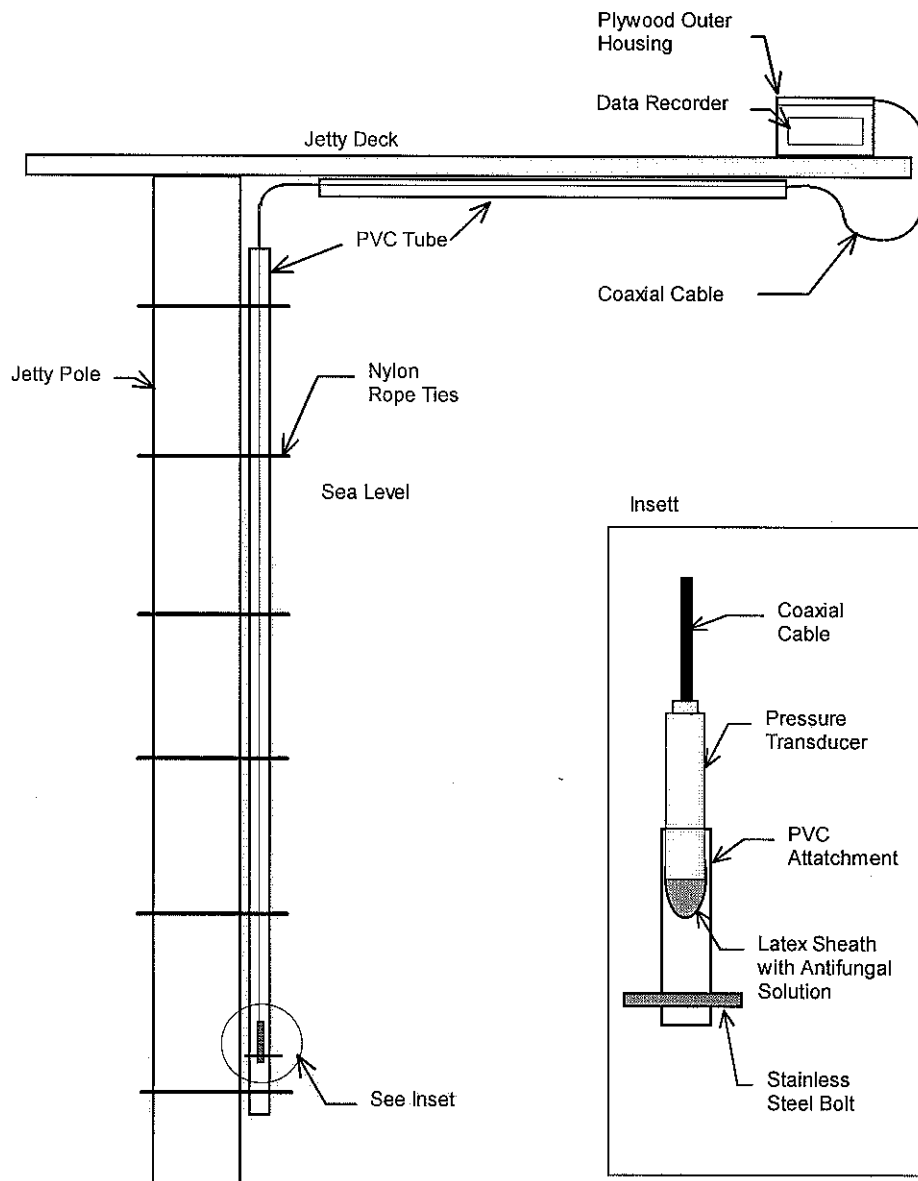
Figure 8-4. Sea level recording equipment (not to scale).

8.2.1.2 Ocean Tide Measurements

A data recorder, a weather-proof plastic housing and a pressure transducer (of the same type mentioned above) were mounted on the harbour jetty to record the ocean tide (see Figure 8-4). A sturdy plywood box lined with foam rubber was used to protect the data recorder and plastic housing from the weather. The end of the pressure transducer was covered with a latex rubber sheath that was filled with anti-fungal solution to protect the transducer from algal growth. The coaxial cable was threaded through a PVC tube which was tied to the jetty so that it could not move. The pressure transducer was bolted to the PVC tubing at about 0.5 m above the harbour floor.

The tide gauge, which was programmed to record at 10 minute intervals, was calibrated in a manner similar to that described in the previous section. During a 12 hour calibration period, the tide was recorded at half-hourly intervals by visually inspecting a graduated staff located on the jetty. When wave action was significant in the harbour, wave mid-heights were used to estimate the tide from the tide staff. The manual readings were reduced to LWD using survey data provided by Hacker (pers. comm., 1994). The jetty was not perfectly fixed in position, however, and Hacker (pers. comm., 1995) found that a part of the jetty had risen by about 3 cm between September 1993 and November 1994. The effect of this shift on the tidal records during the investigations was assumed negligible. The effect of seawater temperature variation on the transducer response was also assumed negligible.

8.2.1.3 Reef-Flat Tide Measurements

The tide over the reef flat during a low tide was recorded manually using a graduated staff accurate to ±0.5 cm. These seawater-levels were measured relative to a submerged temporary benchmark that was surveyed relative to PSM 61221 (refer Figure 8-1).

8.2.2 Results

8.2.2.1 Groundwater Piezometric Levels

A total of 25 piezometers from investigation wells #1, #3, #6, #7, #8, #10, #11, #12 and #13 were monitored for water-levels at certain times between February and July 1994

(see Figure 8-5). Only 68 hours of data were recorded at well #7 because of damage sustained by the equipment when a tree collapsed (see Figure 8-16). For the other wells, observations were made between 27 and 58 tide cycles as indicated in Figure 8-5 and Table F-4. Because the piezometric database is too large to be presented on paper, it is provided in digital format (see Appendix J or the Department of Chemical Engineering, The University of Queensland). For illustrative purposes, the piezometric levels over one week are presented in Figures 8-8 to 8-15.

8.2.2.2 Ocean Tide

The ocean tide was recorded at 10 minute intervals between 10th February and the 19th May 1994 and between the 25th May and the 18th July 1994 (see Appendix J or the Department of Chemical Engineering, The University of Queensland). In that combined period the average tide was 1.607 m LWD, the maximum sea-level was 3.368 m LWD (at 9:10 pm on the 26/4/94) and the minimum sea-level was -0.042 m LWD (at 2:00 pm on the 25/4/94). An excerpt of the tidal database is presented in Figure 8-19 to give an indication of typical tidal patterns at Heron Reef. The 24-hour-average tide is presented for the entire monitoring period in Figure 8-6.

8.2.2.3 Reef-Flat Tide

On the 21st April 1992, the seawater level was recorded periodically during a low tide at a point on the reef flat offshore from well #6 (see Figure 8-1). It was found that the seawater level on the reef flat was higher than the ocean tide when the ocean tide fell below 0.98 m LWD (see Figure 8-7). Once this occurred, the seawater level on the reef flat fell at an average rate of -26 mm per hour (approximately). This gradual fall in the reef-flat tide ended when the ocean tide reconnected at 0.89 m LWD. This result, whilst of a preliminary nature, indicates that the tide on the reef flat near Heron Island is a truncated version of the ocean tide with truncation occurring at about 0.9 m LWD.
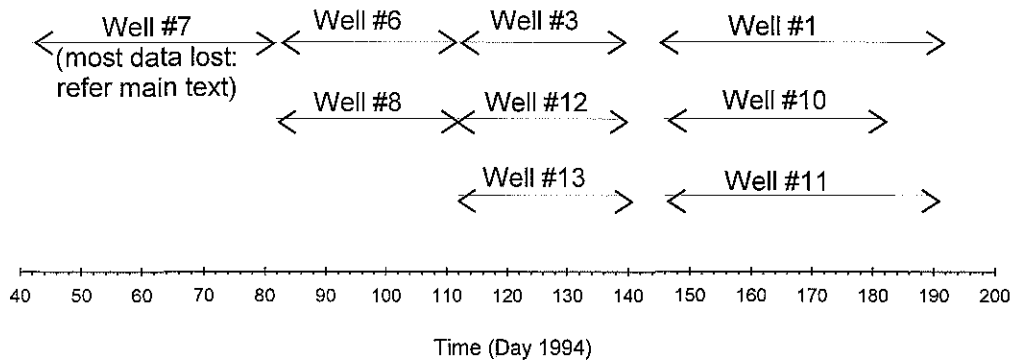
Figure 8-5. The duration of the groundwater piezometric observations at Heron Island.
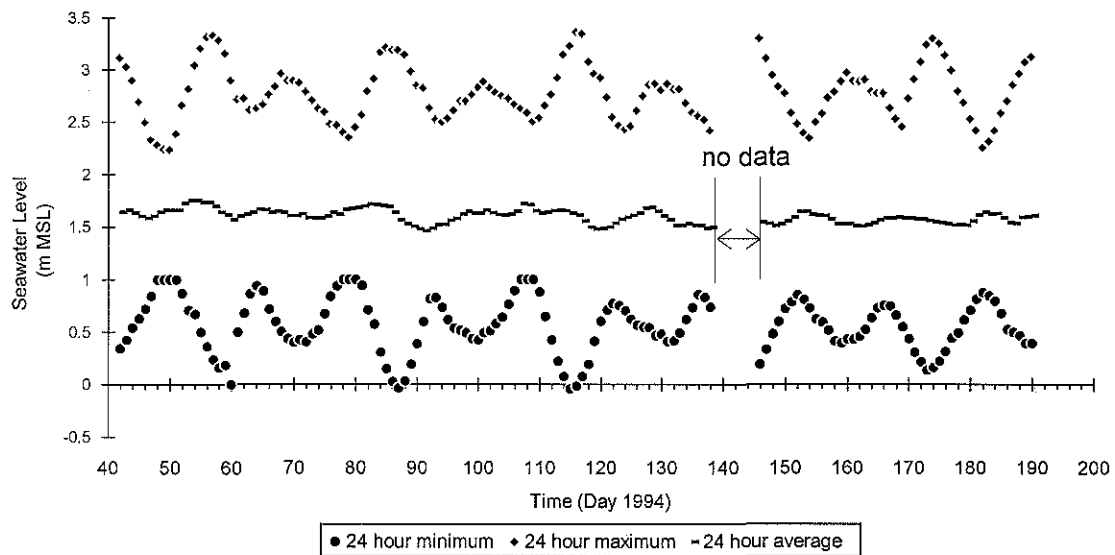
Figure 8-6. Daily recorded maximum, minimum and average tides at Heron Reef.
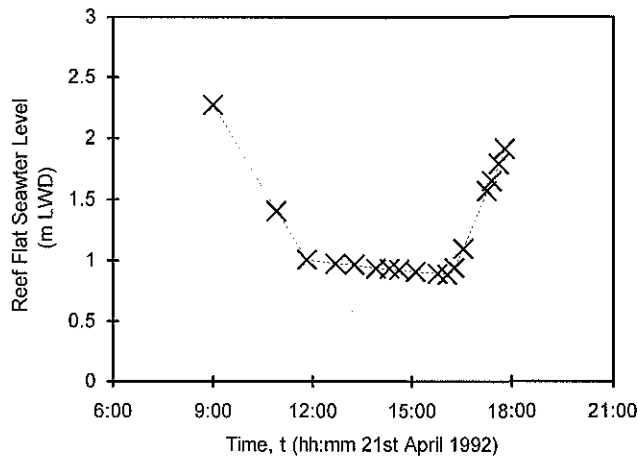
Figure 8-7. The reef flat tide recorded offshore from Heron Island (near well #6).
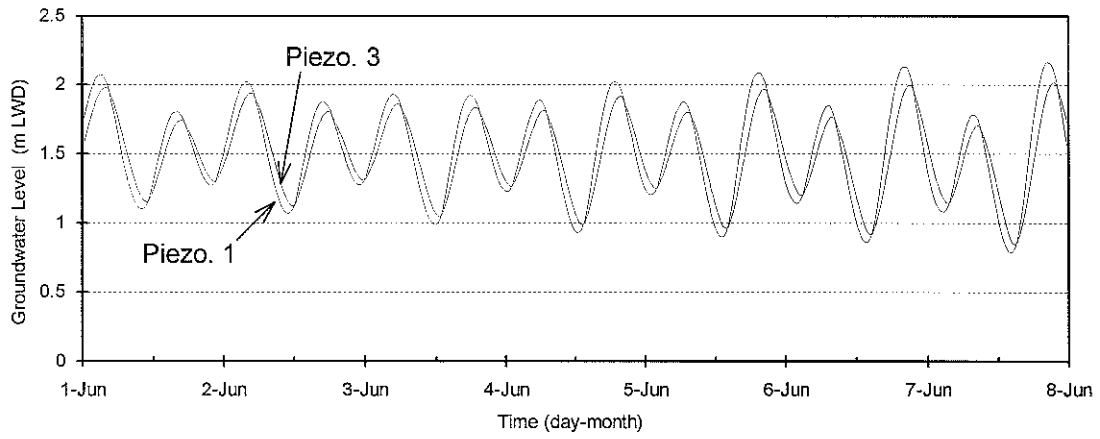
Figure 8-8. Example of groundwater levels recorded in Well 1 during 1994.
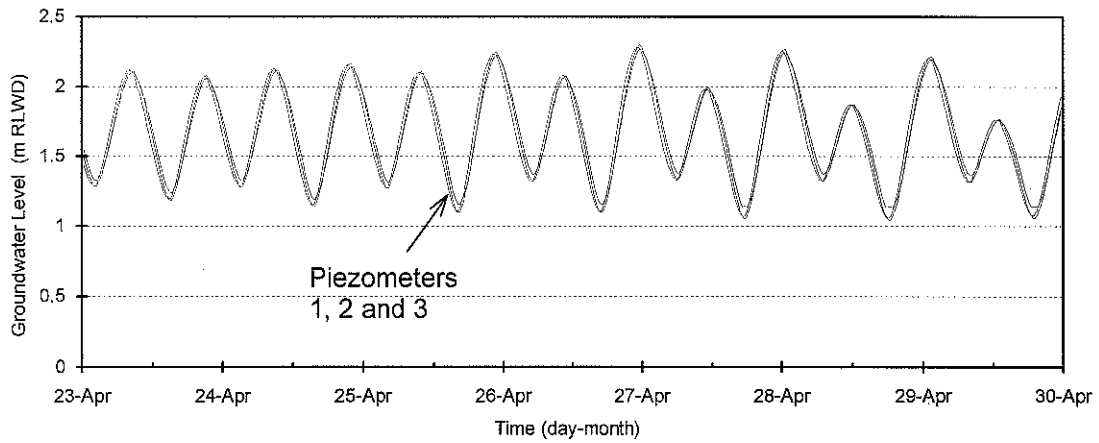
Figure 8-9. Example of groundwater levels recorded in Well 3 during 1994.
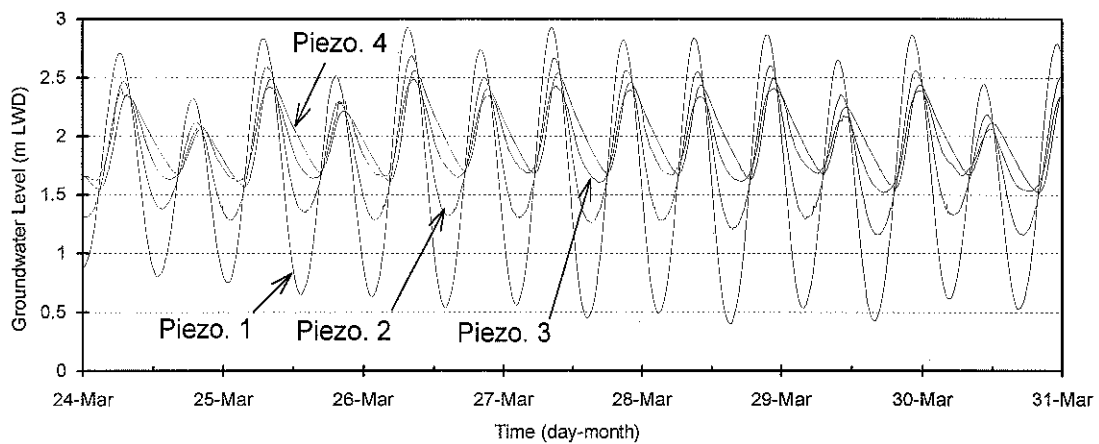
Figure 8-10. Example of groundwater levels recorded in Well 6 during 1994 (the data for Piezo. 3 was rejected due to the malfunction of a pressure transducer at a later time)..
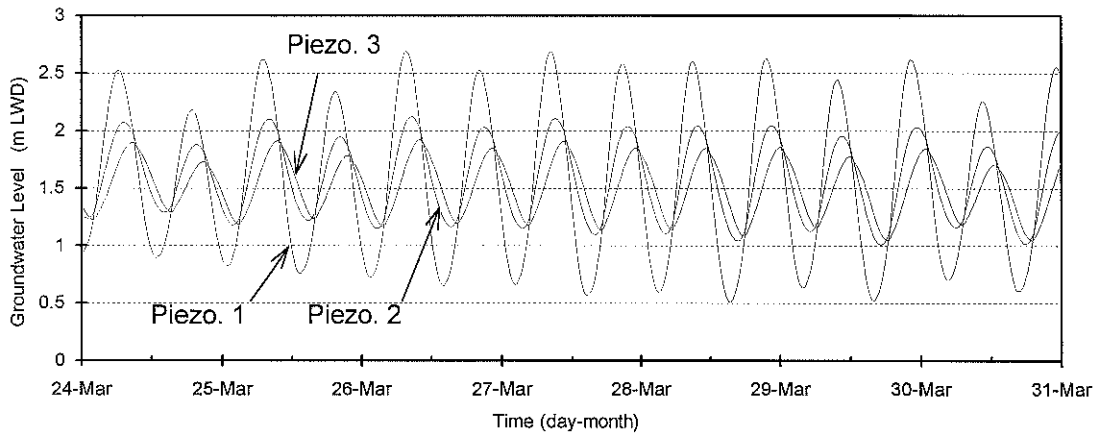
Figure 8-11. Example of groundwater levels recorded in Well 8 during 1994.
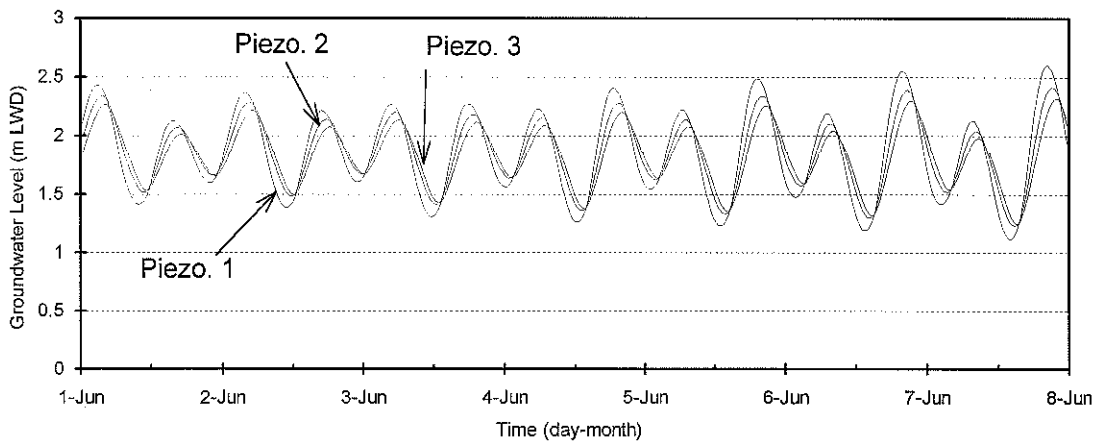
Figure 8-12. Example of groundwater levels recorded in Well 10 during 1994.
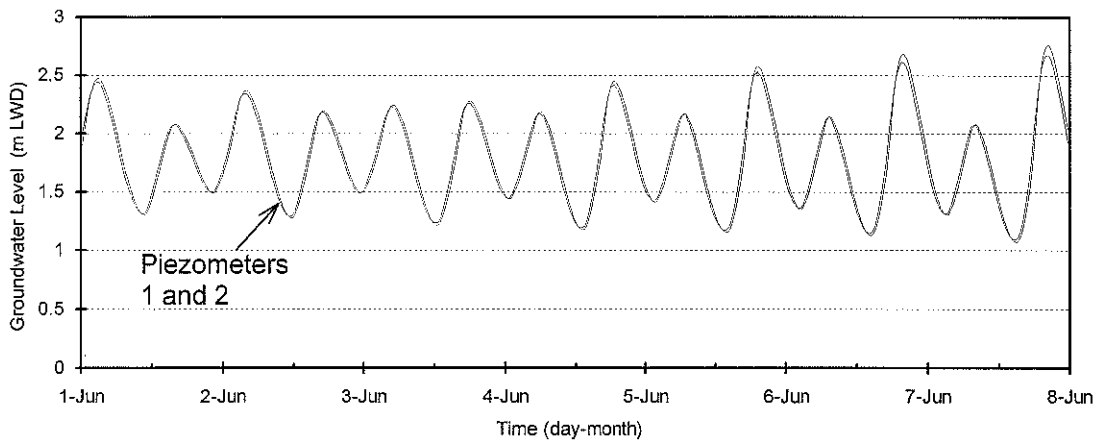
Figure 8-13. Example of groundwater levels recorded in Well 11 during 1994.
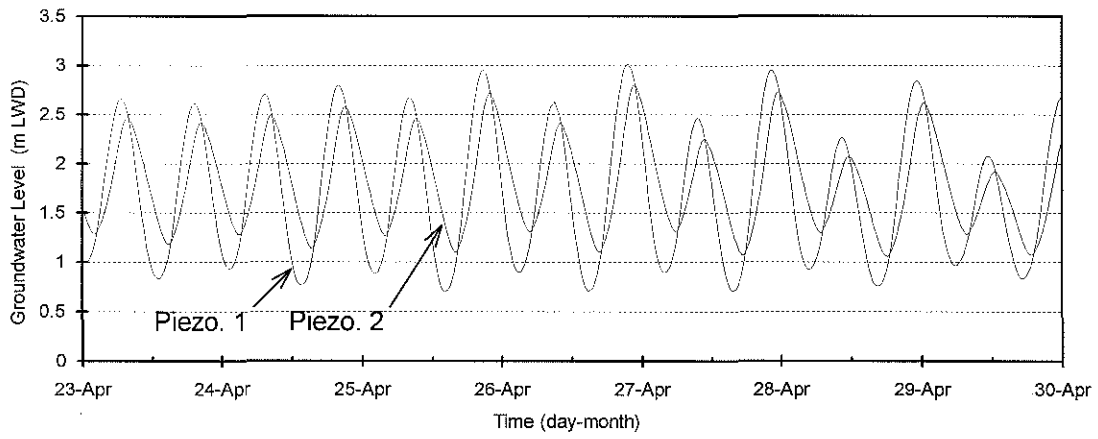
Figure 8-14. Example of groundwater levels recorded in Well 12 during 1994.
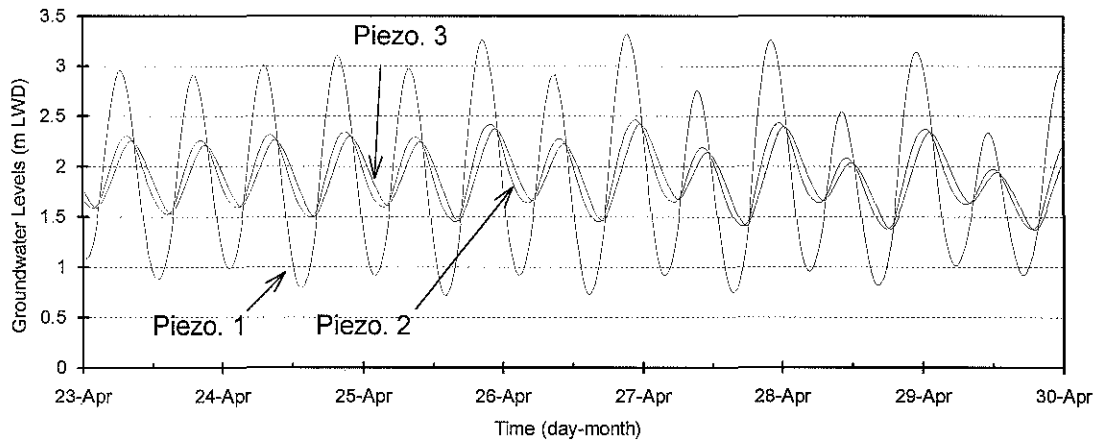
Figure 8-15. Example of groundwater levels recorded in Well 13 during 1994.
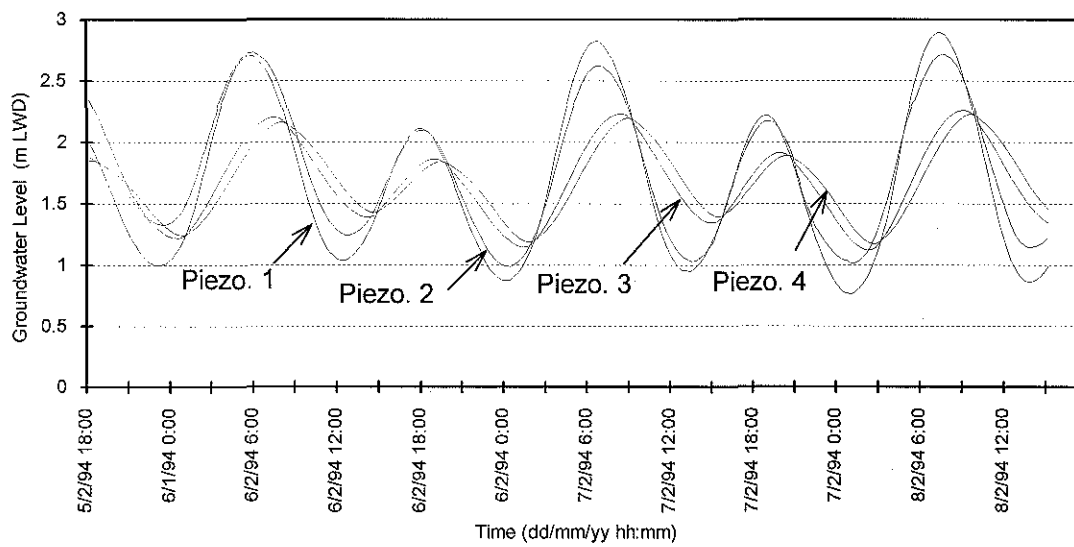
Figure 8-16. Groundwater levels recorded in Well 7 during 1994 (field records are incomplete; refer main text).

8.3 GROUNDWATER SALINITY AND DENSITY

The salinity of the groundwater at Heron Island was measured to assess the importance of fluid density on the potentiometric records and on the efficiency and lag computations. The relevance of groundwater salinity (S_{gw}) to the piezometric records is two-fold. Firstly, variations in S_{gw}, may be produced by freshwater recharge which also tends raise the water-table and alter groundwater pressures and flow patterns. Secondly, S_{gw} should be accounted for when comparing groundwater potentials with tidal potentials (ie, consistent units are required). The salinity records of this study were automatically computed by the field instruments which were used to measure groundwater temperatures (T) and specific conductances (C) (refer Appendix F1).

Other water-quality parameters were also recorded in the field, including pH, redox potential and dissolved oxygen, and concentrations of major dissolved inorganic nutrients, including nitrates (N-NO3), ortho-phosphates (P-PO4), and ammonia (NH3). The entire water-quality database was collected as an adjunct to this study and is provided in Appendix I for future reference.

When considering groundwater potentials in this study, the units 'm-of-groundwater relative to LWD' are converted to 'm-of-equivalent-seawater relative to LWD':

> Let Z be the depth relative to LWD (-ve downwards) where the open end of the piezometer is positioned, and let h_{gw} equal both the water-level in the piezometer relative to LWD and the total head of the groundwater in m-of-groundwater relative to LWD (ie, velocity head is assumed zero). If the pressure head of this groundwater in m-of-groundwater is h_{gw}-Z, then the groundwater pressure relative to atmospheric (p_{gw}) is,

$$p_{gw} = \rho_{gw} g (h_{gw} - Z) \hspace{3cm} \textbf{(Equation 8-1)}$$

> Thus if H is the total head of the groundwater in units of m-of-equivalent-seawater relative to LWD, then H may be computed as follows:

$$H = \frac{p_{gw}}{\rho_s g} + Z$$

$$= \frac{\rho_{gw} g(h_{gw} - Z)}{\rho_s g} + Z \qquad \textbf{(Equation 8-2)}$$

$$= \frac{\rho_{gw}}{\rho_s} h_{gw} + \left(1 - \frac{\rho_{gw}}{\rho_s}\right) Z$$

where ρ_s is the density of seawater (kg m^{-3}).

Thus the density of the groundwater, ρ_{gw}, is required to compute H from h_{gw}. Because S_{gw} were only measured occasionally in this study, S_{gw} between February and July 1994 are assumed equal to the March 1994 values (refer Tables F-5 and I-6). The affect of freshwater recharge on S_{gw} for the entire monitoring period, February-July 1994, is assessed in Section 8.4.3 by sensitivity analysis.

8.3.1 Methods and Materials

The physico-chemistry of Heron Island groundwater was monitored periodically using a Surveyor 3 (SVR3) multiparameter water-quality monitoring apparatus (Hydrolab Corporation ®). The SVR3 includes a H20 ® multiparameter transmitter, a water-resistant SVR3 data recorder/display, a portable battery pack and associated cables and accessories (see Plate 6). The SVR3 had the capacity to monitor groundwater salinity, temperatures, redox potentials, pH, specific conductance, and dissolved oxygen levels. The groundwater salinities that were recorded by the SVR3, were actually computed by the H20 ® multiparameter transmitter using Equations F-1, F-2 and F-3 and the temperature and conductivity values measured with the H20 ® in the field.

The groundwater samples that were tested by the SVR3 were extracted from each piezometer using a manually operated pump that produced a flow rate of approximately one litre per minute. The pump consisted of a teflon tube and an inertial valve attachment (see Plate 6). The above-ground end of the teflon tube was attached to a flow-through chamber that encased the electronic sensors of the H2O ® multiparameter transmitter. This pumping system enabled the groundwater to be monitored during

pumping at pressures near atmospheric (ie, between -8 and 20 kPa approx.) without air contact. The protocol for sampling groundwater at Heron Island is described below.

Step 1.   Once a day, and prior to the sampling of the groundwater, the accuracy of the SVR3 sensors were checked against laboratory standards. Due to the high salinities encountered in this study, a 0.5 M KCl solution (specific conductance = 58.64 mS cm^{-1}; salinity = 37.275 ppt) was used as the salinity standard. The detailed methods of calibrating the SVR3 system are outlined in the manufacturer's operating manual.

Step 2.   The groundwater sampling equipment was set-up over the selected piezometer-nest. One piezometer was sampled at a time.

Step 3.   The water-level in the piezometer to be sampled was measured using a hand held depth gauge accurate to ±3 cm. This water-level was used to compute the approximate volume of groundwater contained in the piezometer given that the diameter and the depth of the piezometer were already known.

Step 4.   A volume of groundwater, approximately three times the computed piezometric water volume, was purged from the piezometer to flush out the stagnant groundwater. This purging process also flushed out any residual groundwater that may have remained in the pumping equipment from the previous sampling episode.

Step 5.   To ensure that the groundwater sample was representative of *in situ* conditions, the groundwater was pumped until the water quality parameters reported by the SVR3 were stable. The water-quality data reported by the SVR3 system were then saved to the data-recorder along with an identification number, time and date.

Step 6.   The groundwater sampling equipment was removed from the piezometer, and a 200 ml sample of groundwater was pumped directly into a 250 ml polyethylene bottle. This sample bottle was marked with a sample number and frozen at the research station laboratory.

Step 7.   The groundwater sampling equipment was placed over the next piezometer, and Steps 2 to 7 were repeated.

The 200 ml groundwater samples were frozen and transported to the Queensland Government Chemical Laboratory (QGCL) in Brisbane for analysis. The QGCL analysed the samples for dissolved nitrate (N-NO$_3$), ortho-phosphate (P-PO$_4$), and ammonia (NH$_3$) concentrations.

Because Heron Island is densely populated by seabirds, including *Puffinus pacificus* and *Anous minutus* (Staunton Smith, 1992), a great deal of bird guano was present on the ground and foliage near the investigation wells. Thus special care had to be taken to avoid accidental contamination of the piezometers, the sampling equipment and the groundwater samples by foreign nutrients. The precautions taken included: (i) use of plastic sheeting on the ground at the sampling site, (ii) use of plastic sheeting to intercept falling guano over the sampling site, (iii) wearing of disposable gloves during sampling, (iv) transportation of the equipment in plastic bags and boxes, and (v) frequent washing of the sampling equipment with distilled water. Further, the sampling equipment was washed with distilled water on site when and if required.

Sampling of groundwater was carried out on seven separate occasions (April 1992, December 1992, April 1993, November 1993, January 1994, March 1994 and March 1995; refer Table I-1).

8.3.2 Results

The full set of results obtained from the groundwater quality investigations are tabulated in Appendix I. To complete the database, the data obtained by Noordink et al. (1992) in February of 1992 are also included in Appendix I. Groundwater salinities recorded during the seven field investigations ranged between a minimum of 5.9 ppt at well # 10 (ie, affected by anthropogenic freshwater derived from unidentified sources) and a maximum of 36.8 ppt at well #6 (ie, at the beach). The overall average from the 255 salinity samples was 27.4 ppt, which represents a seawater-freshwater ratio of approximately 3:1.

A plot of the time-averaged salinities as a function of level shows no clear trend at most of the wells (see Figure 8-17). The exceptions are the wells near the sewage effluent discharge trench (ie, wells #4 and #5) in which there existed a monotonically increasing salinity gradient. Groundwater at wells #6, #11, and #12 had relatively high salinities compared with the groundwater in the other wells. Well #10 demonstrated the greatest disparity in salinity of the all of the groundwater wells that were investigated (see Figure 8-17).
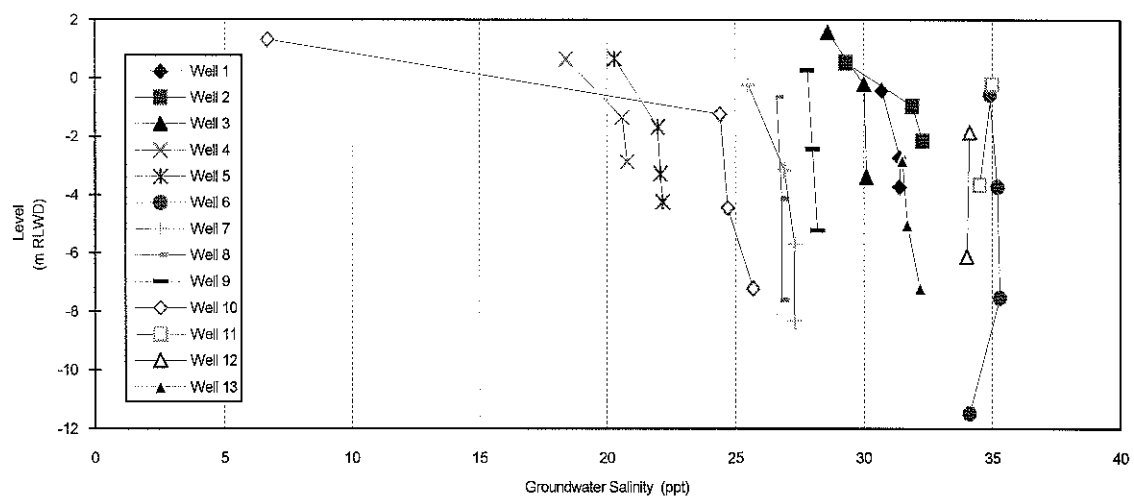
Figure 8-17. Groundwater salinities at Heron Island in March 1994 as a function of piezometer elevation (refer main text and Appendix I)..

8.4 EFFICIENCY AND LAG CALCULATIONS

8.4.1 Methods

The parameters efficiency (η) and lag (γ) are a measure of the attenuation and delay, respectively, of tidal signals in groundwater. In the case of a moving water-table, η is usually taken as the range of the groundwater-tide ($\Delta\delta$) divided by the range of the ocean tide (Δh_{ocean}) for the same tidal half-cycle, and γ is usually taken as the time difference between the high/low of the groundwater-tide and the corresponding high/low of the ocean tide, ie:

$$\eta = \Delta\delta / \Delta h_{ocean}$$
(Equation 8-3)

and

$$\gamma = t_{wt} - t_{ocean}$$
(Equation 8-4)

where,

Δh_{ocean}	= range of the ocean tide.	(m-seawater)
$\Delta\delta$	= range of the water-table variation.	(m-groundwater)
t_{ocean}	= time of a high/low ocean tide.	(hr)
t_{wt}	= time of a high/low water-table.	(hr)

When quantifying η and γ at some fixed point in an aquifer, different definitions of η and γ are required (see Equations 8-5 and 8-6). For any fixed point in the Heron Island aquifer, η and γ are defined in this study in terms of the pressure head of the groundwater (H) and the pressure head of the ocean (h_{ocean}) in units of m-equivalent-seawater relative to LWD (see Equation 8-2 and Figure 8-18). The tidal range and the pressure head range of the ocean are considered equal (ie, effectively hydrostatic). The same does not apply to the groundwater, however, as the groundwater is subject to the vertical pressure gradients that drive the groundwater tide through the porous aquifer.
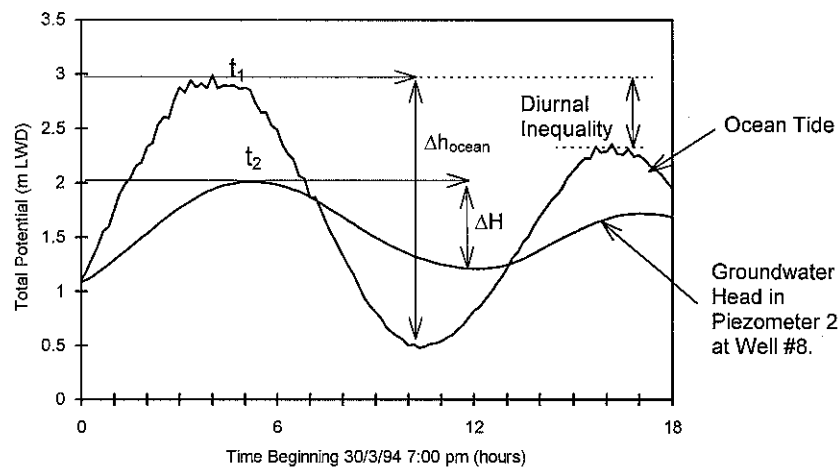
Figure 8-18. Typical time and length measurements used to compute the efficiency and lag of a tidal pressure signal in the aquifer at Heron Island (refer Equations 8-5 and 8-6).

$$\eta = \frac{\Delta H}{\Delta h_{ocean}}$$

$$= \frac{\rho_{gw} \Delta h_{gw}}{\rho_s \Delta h_{ocean}}$$

(Equation 8-5)

and

$$\gamma = t_{gw} - t_{ocean}$$

(Equation 8-6)

where,

ΔH = range of the groundwater pressure-head variation   (m-of-equivalent-seawater)

t_{gw} = time of a high/low groundwater pressure variation   (hr)

The essential difference between the two definitions of η and γ, is that one describes the motion of a water-particle (ie, Equations 8-3 and 8-4), whilst the other describes a pressure signal at a fixed point in the phreatic zone (ie, Equations 8-5 and 8-6). The later definition is intractable when attempting to determine η and γ near the water-table. This is because the portion of aquifer that is within the range of the groundwater-tide will, at times, become unsaturated.

8.4.2 Results

η and γ of the tidal signal were calculated from the piezometric and tidal data using Equations 8-3 to 8-6 as required. The resulting η and γ data for well #8 are shown in Figures 8-20 and 8-21 to illustrate the temporal nature of the results. For brevity, only the time-averaged η and γ for wells #1, #3, #6, #10, #11, #12 and #13 are presented in Figures 8-22 and 8-23 as a function of distance to the nearest shoreline, and in Figures 8-24 and 8-25 as a function of elevation (see also Table F-6).
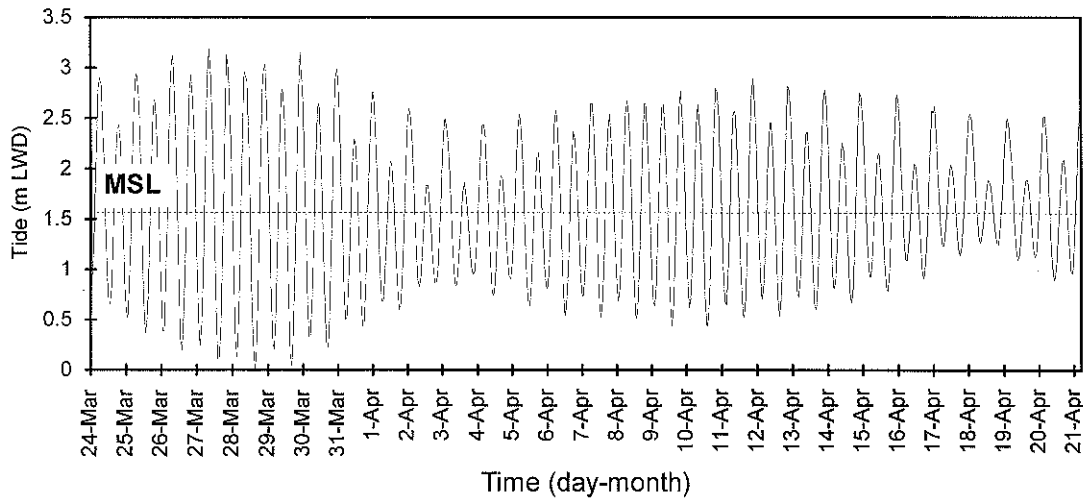
Figure 8-19. The tide at Heron Island: March - April 1994.
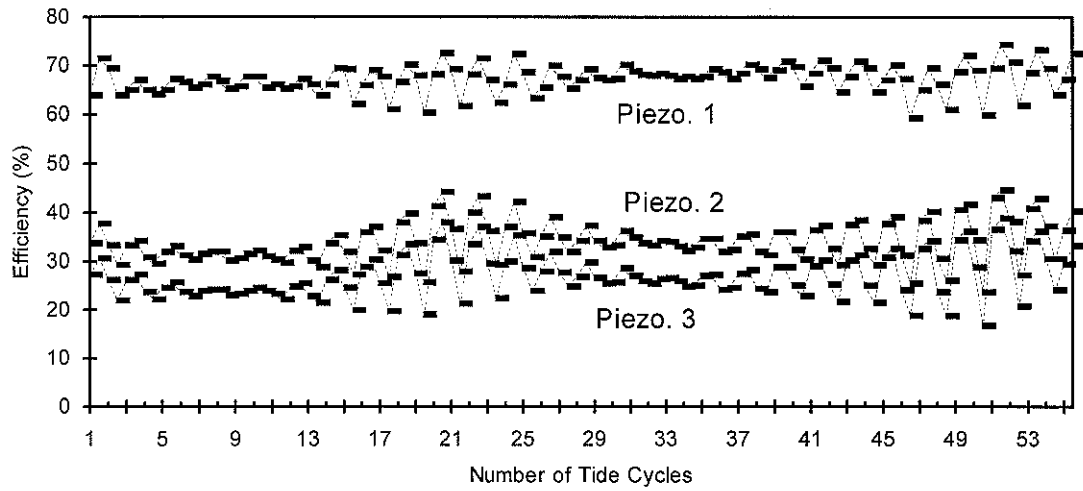
Figure 8-20. Temporal variation in groundwater efficiencies at Well # 8 (concurrent tides are shown in Figure 8-19).
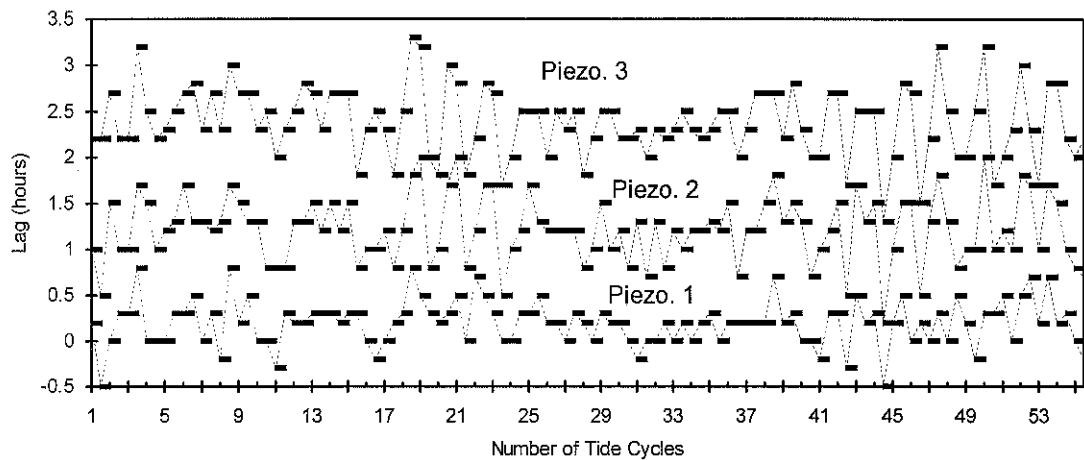
Figure 8-21. Temporal variation in groundwater lags at Well # 8 (concurrent tides are shown in Figure 8-19).

8.4.3 Error Analysis

The 95% probable error associated with the recorded groundwater water-levels, tides, tidal efficiencies and tidal lags are approximated in this section in terms of the following possible sources of experimental error:-

Error Type I.   Pressure transducer movement (systematic/random).

Error Type II.   Pressure transducer electronic drift or malfunction (systematic/random).

Error Type III.   Survey error in well-collar levels relative to LWD (systematic).

Error Type IV.   Pressure transducer calibration error (systematic).

Error Type V.   Deviation of water density from that recorded in March 1994 (random).

Error Type VI.   The effect of waves on the tidal record (random).

Due to the precautions taken in the study it is believed that Error Type I is negligible. Not preventable in some instances, however, was Error Type II, which greatly effected most of the field data at piezometer No. 3 at well #6, a small proportion of the field data at piezometer No. 1 at well #10, and a small proportion of the tidal record (refer Figure 8-6). Any data that was believed to be affected by Error Type II was rejected. Error type III was of the order of ±1 cm (Noordink et al., 1992) and could affect the water-level and tidal records.

Error Type IV is expected to be the main contributor of probable error in the water-level observations. This error type is associated with the calibration data (supplied by the manufacturer) for the pressure transducers. As shown in Table F-3, the sample correlation coefficients computed for each transducer are close to unity, hence a linear calibration model for the transducers was used, ie:

$$h_{fresh} = a + b\,X \hspace{4cm} \textbf{(Equation 8-7)}$$

where X is the transducer response, h_{fresh} is the water-level in metres-of-freshwater relative to atmospheric, and a and b are the regressed intercept and slope respectively (see Table F-3). a and b were corrected for density effects to give h_{gw} at each piezometer in m-of-equivalent-groundwater, ie:

$$h_{gw} = \frac{1000}{\rho_{gw}}(a + b\,X)$$

$$= a' + b'\,X$$

(Equation 8-8)

where ρ_{gw} is the *in situ* groundwater density in kg m^{-3} (see Table F-5). After each transducer was installed in a piezometer, water-levels in those piezometers were recorded a number of times using a manually operated depth gauge. This field data were used with the method of least squares to regress intercepts A and b' of the following calibration curve.

$$h_{gw} = A + b'\,X$$

(Equation 8-9)

where h_{gw} is expressed in units of m-of-groundwater relative to LWD. Inaccuracies in the hand-held depth gauge contributed to the rather high probable errors associated with the A and b' values presented in Table F-2. The regressed A coefficients for the piezometer gauges were statistically accurate within ±6 to ±56 cm (see Table F-2), suggesting that the water-level records presented in this study may be systematically too high or too low by centimetres or even tens-of-centimetres (at the 95% confidence level). The probable relative errors for b' are less than 1.8% for most of the piezometric gauges, with larger probable errors associated with sensors No. 50031, 50038 (ie, about 20%) and 10029 (ie, about 5%; see Table F-3). Unfortunately, the re-calibration of sensors No. 50031, 50038 and 10029 was not possible due to the equipment becoming faulty after the field investigations. The effect of the probable error in A and b' on h_{gw} is found by considering that X were typically between 1500-3500 units and the following equation:

$$error\{h_{gw}\} \cong \pm\sqrt{error\{A'\}^2 + \left(error\{b'\}X\right)^2}$$

(Equation 8-10)

The pressure transducers used in the harbour to record the ocean tide were also calibrated *in situ*, but using a total of 19 and 25 water-level measurements accurate to ±1 cm when surface waves were small, and accurate to ±7 cm when surface waves were large. The probable relative errors for the regressed A and b' coefficients for the tide gauges are about ±10 cm (absolute) and 4% (relative), respectively.

Groundwater densities for the study period were determined from groundwater salinities measured in March 1994 (see Table F-5). Hence temporal variations in groundwater salinity during the monitoring period were ignored in the conversion of piezometric water-levels in metres-of-groundwater, h_{gw}, to groundwater potentials in metres-of-equivalent seawater, H_{gw}, and in the calculation of η (ie, Error Type V). The sensitivity of H and η to variations in groundwater salinity is described analytically in Appendix F-2 and Table F-5. It is evident in Table F-5 that $\partial H / \partial S_{gw}$ is only about -0.001 to 0.009 m ppt^{-1} for each piezometer, and $\partial \eta / \partial S_{gw}$ is only about 0.02 to 0.05 % ppt^{-1} for each piezometer. When these figures and STEM freshwater recharge predictions for the period February-July 1994 (see Figure 6-4) are considered together, it appears that the effect of Error Type V is small enough to be ignored. For example, if the total recharge for the monitoring period was 20 cm and had mixed thoroughly with the top 5 m of groundwater, then a reduction in groundwater salinity of only about -1 ppt would have occurred. Hence, neglecting anthropogenic freshwater, it seems from Table F-5 and Figure 6-4 that natural variations in groundwater salinity contributed rather small errors to H and insignificant errors to η.

The total uncertainty associated with the η data is considerably less than that estimated for h_{gw} and H. This is because η is a function of the pressure range and is independent of the coefficient A (refer Equation 8-9) and Error Type III.

$$\eta = \frac{\rho_{gw} \Delta h_{gw}}{\rho_s \Delta h_{ocean}}$$
$$= \frac{\rho_{gw}}{\rho_s} \frac{b'_{gw}}{b'_{ocean}} \frac{\Delta X_{gw}}{\Delta X_{ocean}}$$

                (Equation 8-11)

The probable relative error in η due to Error Type IV may be approximated as follows:

$$\frac{error\{\eta\}}{\eta} \cong \pm \sqrt{\left(\frac{error\{b'_{gw}\}}{b'_{gw}}\right)^2 + \left(\frac{error\{b'_{ocean}\}}{b'_{ocean}}\right)^2 + \left(\frac{error\{\rho_{gw}\}}{\rho_{gw}}\right)^2}$$

    (Equation 8-12)

Waves appeared in the tidal observations as random fluctuations that were most

conspicuous during the high tide and during windy conditions (eg, see Figure 8-18). Because these fluctuations may have altered the apparent magnitude and timing of each observed high and low tide, some random error would have carried through into each η and γ value. A rough estimate of Error Type VI for each γ sample and for each η sample is ±30 minutes (95% confidence) and ±2 % (95% confidence), respectively. Because Error Type VI is random, it is not expected to significantly affect the central tendency of the time-averaged γ and η values. The approximate combined probable error in each time-averaged η and γ value are presented in Table F-6 and Figures 8-24 and 8-25.

8.5 DISCUSSION AND CONCLUSIONS

The main objectives of the hydrogeological expeditions were satisfied. These include the time-series measurement of piezometric water-levels at a variety of locations at Heron Island, the time-series measurement of the ocean tide, and the discrete measurement of groundwater salinities at the piezometers (see Figure 8-1 for a locality guide). Piezometric water-levels at eight of the thirteen available investigation wells were recorded at ten minute intervals over three-to-four week periods: thus providing the current study with a considerable amount of new hydrogeological data (refer Figures 8-5 and 8-6). The reef-flat tide was measured at one location near Heron Island and was found to be 'truncated' at about -0.71 m MSL (0.9 m LWD) due to seawater capture by the reef surface (see Figure 8-7). This result is typical of the area (Gourlay, 1995). A major implication is that a downward-forcing hydraulic gradient exists within the inter-tidal aquifer when the aquifer is left exposed by the tide.

The standard errors in the water-level measurements are significant particularly in the estimation of h_{ocean}, h_{gw} and H (see Table F-4). These errors are mostly a result of the inaccuracies in the determination of the offset values, A, relating water-levels to LWD (refer Table F-2). However the errors in A are systematic and so cancel out when tidal ranges and tidal efficiencies are computed from the water-level data. Hence most of the standard errors in each tidal efficiency (η) value are a product of wave-action on the ocean tide and error in the slope (b') of the relevant pressure transducer calibration curve. The resulting standard errors in η are believed tolerable (see Table F-6). The error in each tidal lag (γ) measurement is quite high due to random wave-action on the tide, but this effect reduces significantly   in the estimation of the mean γ due to the

large number of samples taken (see Table F-6). The errors introduced to the field data by salinity variations appear to be insignificant (refer Table F-5).

Observed groundwater potentials varied with time and location (see Figures 8-22 to 8-25). The temporal variations were of a tidal nature, and as such are referred to as 'tidal signals'. The tidal signals were attenuated and delayed compared to the ocean tide as indicated by their tidal efficiencies (η) and tidal lags (γ), respectively (see Table F-6). The groundwater dynamics at all locations except wells #3 and #11 were characterised by significant vertical differences in groundwater potential and instantaneous hydrostatic conditions corresponding to the high and low of each water-table oscillation (see Figures 8-8 to 8-16). Hydrostatic or near-hydrostatic conditions occurred locally whenever the vertical component of groundwater flow changed direction: ie, from rising (flooding) to falling (ebbing) or vice versa.

The groundwater hydrographs for wells #3 and #11 show that the groundwater at these wells moved tidally but the vertical differences in groundwater potentials and η were generally smaller than the experimental error (see Figures 8-9 and 8-13, respectively). These results may indicate a high vertical hydraulic conductivity (such as might occur in a karst limestone) and are discussed more fully in Chapter 9 with the analysis of vertical tidal unconfined groundwater flow.

At well #6 the tidal signals nearer the water-table were 'skewed' and had higher centres-of-gravity compared to the signals at lower elevations (see Figure 8-10). Hence the hydrographs for well #6 indicate that there was a net downward-flow of groundwater for the duration of the observations. Because well #6 was only 55-65 m from the shoreline, it may be that the skewing of the tidal signal is somehow related to the reef-flat tide at the beach. The detailed interpretation of Figure 8-10 is deferred to Chapter 10 with the development of two-dimensional conceptual and mathematical models for the aquifer.

The η and γ of the tidal signals varied with time as well as location (eg, see Figure 8-19 to 8-29). The temporal variations in groundwater η at each piezometer almost always followed a pattern of: low η, intermediate η, high η, intermediate η, low η, ... etc. (eg, see Figure 8-20). The outer envelope of η values was also cyclic, having a periodicity of

about 14 days in each case. Most of the η variations are strongly correlated to the diurnal inequality of the ocean tide (corr. coeff.'s are between 0.50 and 0.92) with the greatest changes in η having occurred when alterations in the tidal range were greatest. Temporal variations in γ were less patterned than for η and are poorly correlated to the diurnal inequality of the ocean tide (eg, see Figure 8-21). The detailed interpretation of these results is deferred to Chapter 9 with the analysis of vertical tidal unconfined groundwater flow.

At most of the wells monitored (ie, wells #1, #6, #8, #10, #12, and #13) the time-averaged η increased with depth in the aquifer, whilst at all of the wells monitored the time-averaged γ decreased with depth (see Figures 8-24 and 8-25, respectively). Extrapolation of the η-vs-depth plots and the γ-vs-depth plots for wells #1, #6, #8, #10, #12 and #13 down to the Holocene-Pleistocene contact (-15 m LWD) shows such large efficiencies (>90%) and small lags (effectively 0 h) at that level, that the tidal signal in the Holocene unit can be thought of as having originated in the, obviously, very permeable Pleistocene unit (see Figures 8-24 and 8-25). These trends in η-vs-depth and γ-vs-depth are consistent with earlier observations at Heron Island by Krol et al. (1992). Moreover, the trends are also typical of the tidal signals found in groundwater at small atoll islands that have dual-aquifer structures (eg, Wheatcraft and Buddemeier, 1981). It therefore appears that the dual-aquifer conceptual hydrogeological model for atoll islands is suited to Heron Island although the island is coral cay on a platform reef.
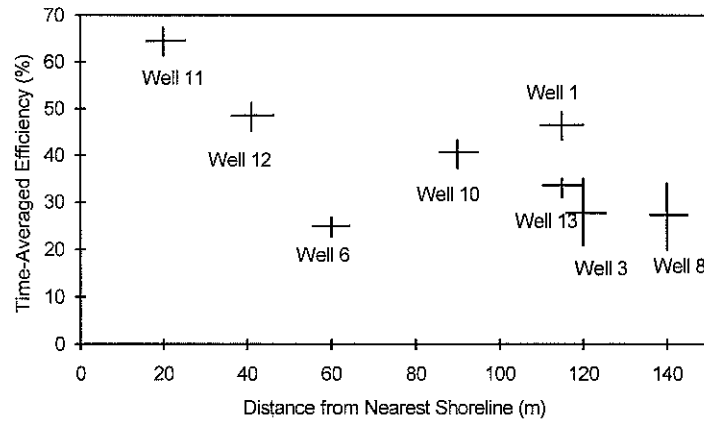
Figure 8-22. Time-averaged water-table efficiency as a function of lateral position.
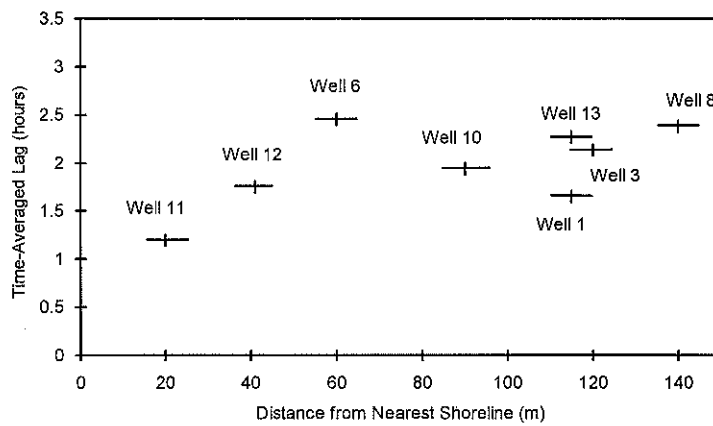
Figure 8-23. Time-averaged water table lag as a function of lateral position.
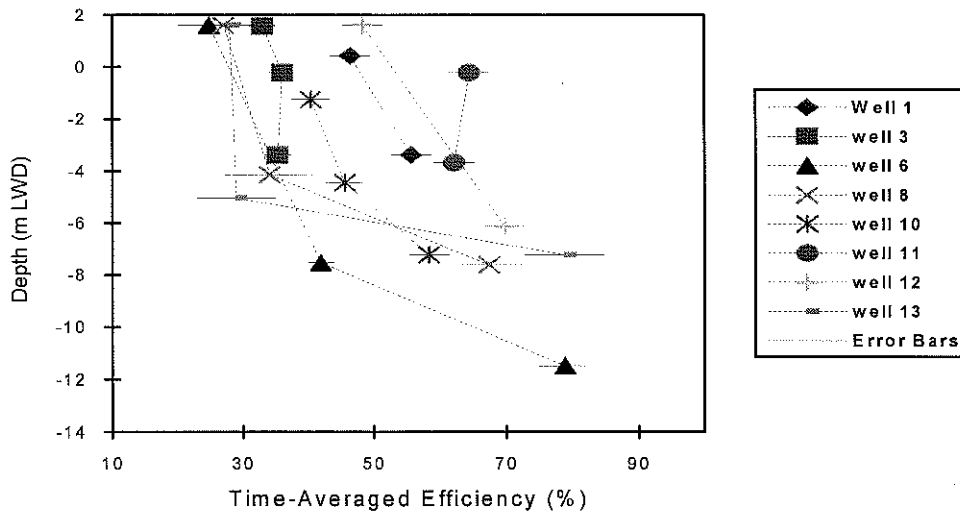
Figure 8-24. Average groundwater efficiencies below Heron Island as a function of level (dashed-lines are interpolated).
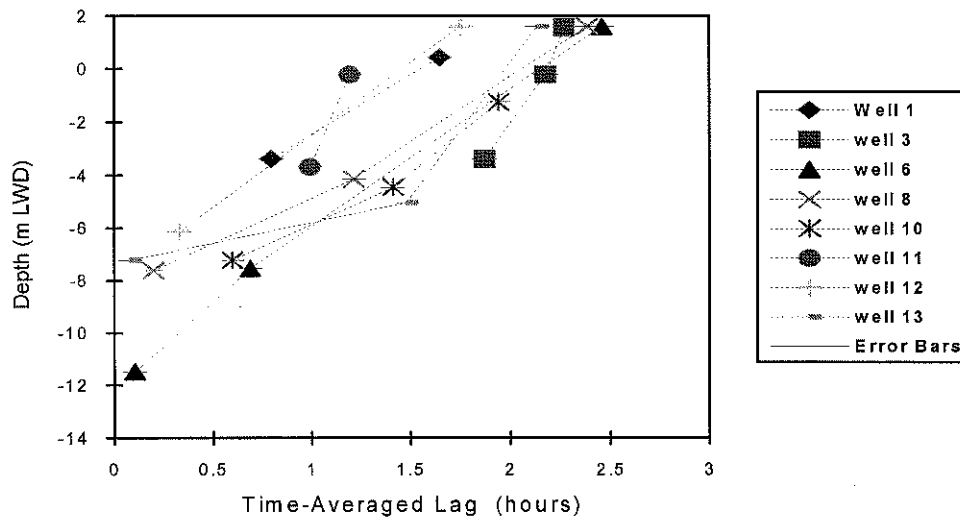
Figure 8-25. Average groundwater lags below Heron Island as a function of level (dashed-lines are interpolated).

Heron Island had its beaches exposed to the reef-flat tide, and so it is conceivable that tidal signals could have propagated laterally through the shoreline and into the aquifer. Tidal signals which propagate laterally through unconfined coastal aquifers tend to decay exponentially with distance travelled (eg, Aseervatham, 1994; Nielsen, 1990). To determine if any such lateral decay relationship had occurred at Heron Island, the time-averaged water-table η and γ were plotted as a function of distance-to-the-nearest-shoreline (see Figures 8-22 and 8-23). As is evident in Figures 8-22 and 8-23, no obvious lateral-distance-decay relationships had occurred. Moreover, it is believed that any lateral distance-decay relationship would have been masked by the much stronger tidal signals propagating upwards from the Pleistocene aquifer: as is typical of the dual-aquifer systems of atoll islands (eg, Weatcraft and Buddemeier, 1981). None-the-less there is some evidence of a shoreline effect given the data obtained at well #11: the closest point to the shoreline. At well #11 the tidal signal was significantly stronger than elsewhere (it had a water-table η of 1.7 standard deviations above the mean, and a water-table γ of 1.9 standard deviations below the mean). However tidal signals propagating inland from the beach were initially expected to show evidence of 'truncation' at about 0.9 m LWD (a likely 'signature' of the reef-flat tide; refer Figure 8-7) but none were. The only tidal signals showing possible influence by the reef-flat tide were recorded at well #6. At well #6 the groundwater hydrographs were 'skewed' (this feature of the data is investigated in Chapter 10). Hence the strengthening of the tidal signal at well #11 was probably not a product of the reef-flat tide. An alternative explanation is that the tidal signal detected at well #11 was enhanced by discontinuous groundwater confinement. This hypothesis seems reasonable as well #11 was located only a few metres inland from exposed beachrock (see Figure 8-1). As mentioned in Chapter 7, Lam (1974) mathematically modelled discontinuous confinement and spatial differences in the efficiency and lag of tidal signals in carbonate aquifers to show that tidal signals are generally stronger nearer areas of confinement. This feature of the data and the confinement hypothesis are discussed further in Chapters 10 and 11.

The reef-flat, reef slopes and ocean floor are aquifer-ocean contact regions where tidal signals may have originated. However, evidence that the reef-flat was a poor conductor of fluid flow and thus a possible barrier to tidal signals include: (i) seawater captured on the reef-flat at low tide drained away slowly indicating that both seawater runoff and through-reef infiltration were minor (refer Figure 8-7); and (ii) none of the tidal signals

observed in the Holocene aquifer were truncated at or near 0.9 m LWD as would be expected if these signals had originated at the reef-flat (compare Figures 8-10 and 8-11 with Figure 8-7). It is therefore hypothesised that a naturally occurring layer of low-permeability material exists immediately below the reef-flat (in contrast to the situation with the cay which which appears to have significant hydraulic connection with the underlying aquifer). A material which fits this description is reef-plate. Reef-plate has been found at numerous other reefs (Hopley, pers. comm. 1996). For example, reef-plate at Davis Reef in the Great Barrier Reef has been described by Buddemeier and Oberdorfer (1986) as a 0.5 - 1.5 m thick layer of cemented corals, coralline algae encrustations and sediments. The reef-plate hypothesis is examined more closely in Chapter 10.

In this discussion some major characteristics of the field data were outlined and some qualitative interpretations were made with regards to the hydrogeology of Heron Island and Reef. To better understand the field data and to validate the hydrogeological interpretations, some tidal-flow theory is developed in Chapters 9 and some quantitative modelling and analyses are undertaken in Chapters 9 and 10. This work is followed by an overview in Chapter 11.

9. VERTICAL TIDAL UNCONFINED GROUNDWATER FLOW: THEORY AND INTERPRETATIONS

9.1 INTRODUCTION

As mentioned in Chapter 7, other small unconfined carbonate island aquifers have been found to have tidally affected groundwater flow that is essentially vertical in orientation (eg, Herman and Weatcraft, 1984; Oberdorfer et al., 1990; Underwood, 1990; Underwood et al. 1992; Peterson and Gingerich, 1995). This regime of flow is termed 'vertical tidal unconfined groundwater flow' or VTUGF for convenience. The basic conditions required for idealised VTUGF to occur are illustrated in Figure 9-1. Flow approaching VTUGF can occur in a carbonate island if it is underlain by a dual-aquifer system: ie, a layer of moderately permeable Holocene limestone and a deeper layer of highly permeable Pleistocene limestone (see Figure 7-3). It is hypothesised that Heron Reef is a dual-aquifer hydrogeological system because the available geologic information is consistent with this model (refer Chapters 1 and 7) and because the groundwater potentials at Heron Island have similar characteristics to those found in other dual-aquifer islands (refer Chapter 8).

To better interpret the Heron Island groundwater potentials of Chapter 8, mathematical models for idealised VTUGF (including analytic and semi-analytic solutions) are developed, verified and validated. The VTUGF models are fitted to the observed groundwater potentials by calibrating unknown parameters (ie, hydraulic diffusivities). The models of VTUGF are derived from Darcy's law and the continuity principle as a function of the fluid pressure at depth and the physical properties of the aquifer and fluid. A major benefit of the VTUGF models is that they obviate the need to simulate more complex two- and three-dimensional flow systems when only the VTUGF is of interest.

In Chapter 10 the validity of the dual-aquifer conceptual model for Heron Island and Reef is examined by combining the current VTUGF-based interpretations with a two-dimensional numeric groundwater model that encapsulates an entire dual-aquifer system.
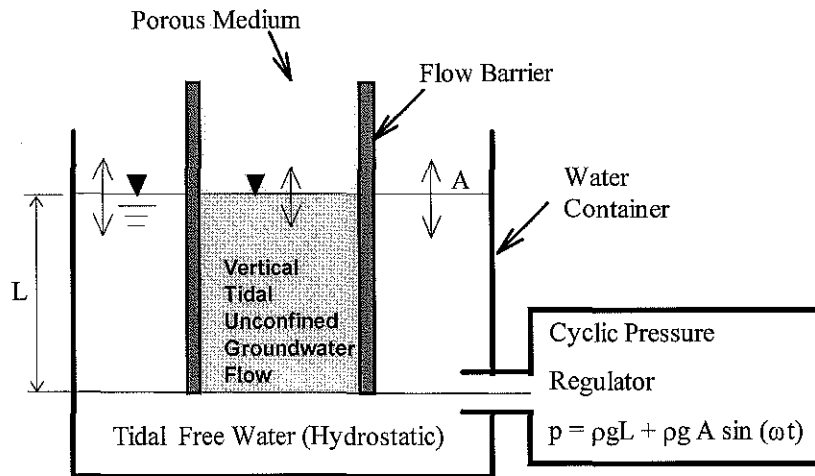
Figure 9-1. A conceptual model for vertical tidal unconfined groundwater flow (the arrows indicate tidal range).

9.1.1 Objectives

The first major objective of this chapter was to develop Darcian-type models for idealised VTUGF in both single- and two-layered aquifers. The models were then to be verified and validated using the most practical means available (time and resource limitations prevented model validation by laboratory experimentation, and mathematical examples and published data were used instead).

The second major objective was to calibrate the VTUGF models to the groundwater potentials observed in wells #1, #6, #8, #10, #12, and #13 (refer Chapter 8). The main parameter to be calibrated was the average vertical hydraulic diffusivity of the aquifer in the locality of the investigation wells.

The third major objective was to discuss the implications of parameter uncertainty and conceptual uncertainty on the VTUGF model and subsequent hydrogeological interpretations.

9.1.2 Previous Studies

It is well known that groundwater heads can fluctuate in response to solid earth tides (eg, Robinson, 1939; Van Der Kamp & Gale, 1983; Hsieh & Bredehoeft, 1987), ocean tides (eg, Jacob, 1940; Carr & Van Der Kamp, 1969; Van Der Kamp, 1972), and river tides (eg, Liu, 1996). The hydraulic diffusivity of the aquifer/fluid complex is an important control on the responsiveness of groundwater to tidal stresses.

Aquifer pressures attributed to transient blanket loading are partitioned between the solids and fluids of an aquifer as a function of the aquifer porosity and the volumetric compressibility of the pore water, solid grains and pore spaces (Domenico & Schwartz, 1990). The fraction of the transient stress carried by the solid matrix is described by the pore pressure coefficient or 'tidal efficiency' (after Jacob, 1940):

$$TE = \frac{C_s}{C_s + nC_w}$$
$$= \frac{\rho_w g n C_w}{S_s}$$

(Equation 9-1)

where,

TE	= tidal efficiency	(-)
C_w	= water compressibility	$(m^2\,N^{-1})$
C_s	= solid pore compressibility	$(m^2\,N^{-1})$
n	= aquifer porosity	(-)
S_s	= specific storativity	(m^{-1})

and

$$S_s = \rho_w\, g(C_s + nC_w)$$

(Equation 9-2)

Barometric efficiency, *BE*, is closely related to *TE* and indicates how faithfully observed heads in an aquifer respond to barometric pressure fluctuations:

$$BE = 1 - TE$$

(Equation 9-3)

Aquifers with a relatively high hydraulic diffusivity respond rapidly to tidal stresses, thereby giving a 'drained response', whereas aquifers with a relatively low hydraulic diffusivity respond slowly, thereby giving an 'undrained response' (Domenico & Schwartz, 1990). Analytic treatments of vertical drained-responses in deformable porous media are commonly based on the following diffusion equation (Domenico and Schwartz, 1990):

$$\frac{\partial^2 h}{\partial z^2} = \frac{S_s}{K}\frac{\partial h}{\partial t}$$

$$= C_v \frac{\partial h}{\partial t}$$

(Equation 9-4)

where,

K	= vertical hydraulic conductivity	$(s\ m^{-1})$
C_v	= vertical hydraulic diffusivity	$(s\ m^{-2})$

Water storage due to fluid and solid compressibility may also occur in unconfined aquifers, "but the water volumes associated with them are negligibly small compared to volumes obtained from drainage of the pores" (Domenico & Schwartz, 1990, p.117). Hence, in unconfined aquifers gravity drainage (ie, specific yield) is generally important whilst elastic storage may usually be ignored. Unlike hydraulic diffusion in deformable porous media, however, hydraulic diffusion in unconfined aquifers is accompanied by temporal changes in effective aquifer dimensions. These temporal changes complicate the theoretical treatment of such problems.

As far as the author is aware, no analytic expressions for VTUGF in either deformable or non-deformable porous media appear in the literature. More attention is given in the literature to 1-D horizontal tidal groundwater flow in idealised confined and unconfined coastal aquifers. Ferris (1951) considered the application of the horizontal diffusion equation with a sinusoidal pressure boundary condition. Ferris's solution and variants of it are frequently used to investigate tidal aquifers (eg, Millham & Howes, 1995), however these formulae provide no information on tidal flows that occur only in the vertical dimension.

At least two analytic expressions for vertical transient groundwater flow have been published. One is the analytic solution for 1-D vertical drainage through a fully saturated porous sample in a falling-head permeameter (refer Section 9.4.2). This solution is most often used to infer K of a soil sample from a laboratory derived hydrograph. The other is less well-known. It is the analytic formula of Polubarinova-Kochina's (1962) which simulates the downward vertical movement of fluid in a previously dry column of porous material subject to a constant operating head applied from above. Neither of these equations address the harmonic boundary conditions associated with VTUGF.

Numerous authors (eg, Herman and Weatcraft, 1984; Oberdorfer et al., 1990; Underwood, 1990; Underwood et al. 1992; Peterson and Gingerich, 1995) have demonstrated that 2-D saturated groundwater flow at atoll islands subject to tidal pumping can be approximated numerically using general-purpose computer programs such as SUTRA (Voss, 1984). Whilst these models demonstrate that VTUGF can occur below some atoll islands, they do not simulate VTUGF independent of non-vertical flows and as such do not explicitly examine the physical relationships that govern tidal efficiency and tidal lag in VTUGF. The results of some of these earlier numeric models are compared in this chapter with the results of the newly derived VTUGF models as a validation exercise.

9.2 VTUGF IN SINGLE-LAYERED AQUIFERS

9.2.1 Assumptions

The assumptions employed in the mathematical models for VTUGF in single-layered aquifers are as follows:

1.   The aquifer is homogeneous.

2.   The groundwater movement is vertical and unconfined.

3.   The fluid, solid grains and solid pore spaces are incompressible.

4.   The capillary zone has negligible impact on the water-table response.

5.   Fluid density gradients do not affect fluid flow.

6.   Tidal (or other) pressure variations originate at a fixed point below the phreatic surface.

7.   Fluid speed is described by Darcy's law.

8.   Barometric pressure variations have negligible affect on water-levels in wells tapping the groundwater.

9.   Inertial effects on groundwater may be assumed negligible.

10.   Groundwater recharge is negligible.

9.2.1.1 The Capillary Zone Assumption

In the VTUGF models to be presented, the time dependent water-table position relative to MSL, $\delta\{t\}$, is defined as the point of zero water pressure relative to atmospheric (see Figure 9-2a). However, the actual boundary between the saturated and the unsaturated zones of an aquifer is not always clear because saturated or near-saturated conditions can occur immediately above the water-table due to capillary suction (see Figure 9-2a). This region of high saturation is often called the capillary zone (Bear, 1972; Gillham, 1984).

If capillary suction acting on pore-water above the water-table is equal and opposite to the pull of gravity, then a hydrostatic or 'equilibrium' pore-water distribution is achieved. The matric potential profile, $\psi\{z\}$, for this equilibrium condition can be determined from Darcy's law for unsaturated flow when the pore-water velocity is set equal to zero, ie:

$$0 = -K\{\Psi\}\left(\frac{\partial\Psi\{z\}}{\partial z}+1\right)$$

$$\Leftrightarrow \quad -1 = \frac{\partial\Psi\{z\}}{\partial z} \qquad\qquad \textbf{(Equation 9-5)}$$

$$\therefore \quad \Psi\{z\} = -z + C \qquad\qquad :z \geq \delta\{t\}$$

where $K\{\psi\}$ is the unsaturated hydraulic conductivity relationship, z is the level above the water table, and C is the constant of integration which, in this case, equals $\delta\{t\}$. Any movement of the water-table will cause unsaturated flow until a new equilibrium $\psi\{z\}$ is achieved (Bear, 1972; Gillham, 1984). As a consequence, $\delta\{t\}$ in VTUGF is affected by both (i) the pressure gradients and groundwater flow in the phreatic zone, and (ii) the

capillary-pressure gradients and pore-water flow in the vadose zone. Gillham (1984) observed that because of the capillary fringe, actual changes in water-table elevation associated with groundwater flow can, in some instances, be much greater than that estimated purely from specific yield.
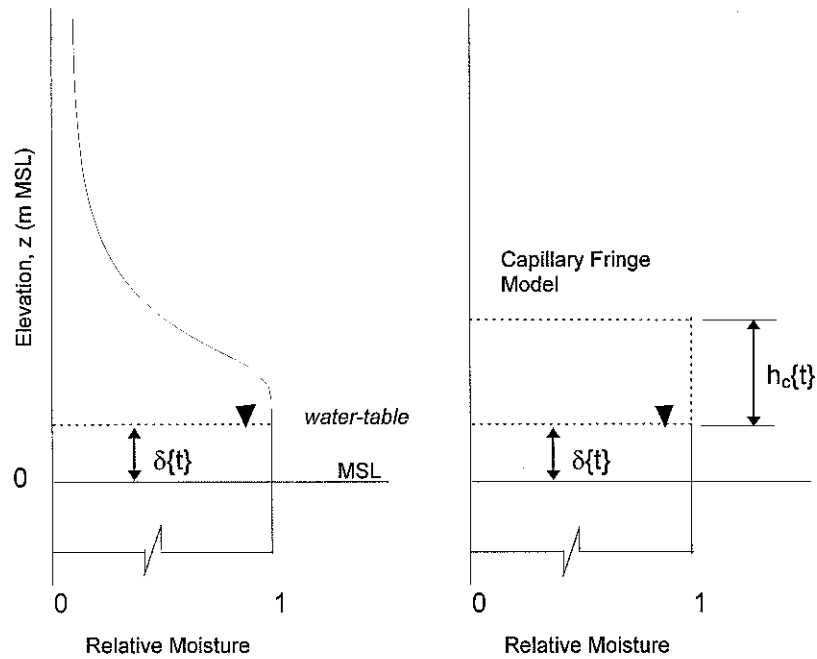
Figure 9-2. Schematic of (a) the water-table and capillary zone at equilibrium, and (b) the idealised capillary fringe model (after Bear, 1972).

To simplify the mathematical treatment of the unsaturated zone, Bear (1972) numerically represents the capillary zone as an idealised fully-saturated capillary 'fringe' with an equilibrium thickness of h_o and a time dependent thickness of $h_c\{t\}$ (see Figure 9-2b). This idealised capillary fringe is considered by Bear (1972) to be an approximate practical concept from which the average hydraulic gradient can be computed, ie:

$$\frac{\partial \Psi\{z,t\}}{\partial z} = \frac{-h_o}{h_c\{t\}} \quad : \; h\{t\} \geq z \geq \delta\{t\} \qquad \textbf{(Equation 9-6)}$$

The above equation assumes that the matric potential at the top of the capillary fringe is always equal to $-h_o$, and that $\psi\{z\}$ is a linear function of z. This simplifying approach is similar to that used by Green and Ampt (1911) to approximate the downward flow of a sharp wetting front in porous media. Equation 9-6, when combined with Darcy's law, approximates the macroscopic pore-water velocity, $v_c\{t\}$, in the idealised capillary fringe at time t, ie (Asseervathem, 1994):

$$v_c\{t\} = -K_c \left\{ \frac{h_c\{t\} - h_o}{h_c\{t\}} \right\}$$ (Equation 9-7)

where K_c is the hydraulic conductivity of the idealised capillary fringe.

Li et al. (1997) examine the impact of the capillary zone on water-table fluctuations within the beach as a result of high frequency fluid-pressure fluctuations caused by wave run-up and run-down and low frequency fluctuations caused by semi-diurnal tides. They developed a numerical model of a rectangular domain (10m long by 1m deep) that incorporates a modified kinematic boundary condition for the beach face and a two-dimensional capillary fringe sub-model that accounts for a linear pressure profile in the capillary zone and mass conservation. Two of the scenarios they examined - with and without capillary effects - show that capillary effects have negligible impact on the water-table position in typical beach sand (ie, K = 50 m d-1 and Sy = 0.4) subject to semi-diurnal tides.

Heron Island's sand has a K at least a large as that of typical continental beach sand (see Table 4-1) and similar specific yield (ie, Sy $\approx$ 0.3) and atoll island sediments generally have a K of in the order of 1 to 1×10^2 m d^{-1} (eg, Underwood, Peterson & Voss, 1992). Therefore, whilst the error introduced by Assumption 4 is not quantified, the work of Li et al. (1997) is strong evidence that the capillary zone assumption of the VTUGF is acceptable at Heron Island and is probably valid for many low atoll islands as well. Hence the modelling of the capillary zone flow in conjunction with VTUGF was, at the time of writing, believed unnecessary. The validity of Assumption 4 with respect to Heron Island is further discussed in Section 9.7.1.

9.2.2 Governing Differential Equations

The total head (H) of the groundwater at any point in the aquifer is the sum of its pressure and elevation components, ie:

$$H(z,t) = p(z,t)/\rho g + z$$ **(Equation 9-8)**

where,

t	= time	(s)
ρ	= fluid density	(kg m^{-3})
g	= gravitational acceleration	(m s^{-1})
p	= pressure	(Pa)
z	= elevation relative to MSL, +ve upwards	(m)

Given Assumptions 2, 3, 4 and 7, the vertically flowing fluid must be described by the continuity principle and by Darcy's law as these apply to the z-dimensional case, ie:

Darcy's Law: $v = -K\dfrac{\partial H}{\partial z}$ **(Equation 9-9)**

Continuity: $\dfrac{\partial v}{\partial z} = 0$ **(Equation 9-10)**

When Equations 9-9 and 9-10 are combined, they give the Laplace equation for z-dimensional fluid flow, ie:

$$\Rightarrow \frac{\partial}{\partial z}\left(-K\frac{\partial H}{\partial z}\right) = 0$$

$$\therefore \frac{\partial^2 H}{\partial z^2} = 0$$ **(Equation 9-11)**

where,

v	= macroscopic vertical fluid speed	$(m\ s^{-1})$
K	= hydraulic conductivity	$(m\ s^{-1})$
H	= total gravitational head	(m)

The Laplace equation shows that $H\{z\}$ is a linear function of elevation, z, between the phreatic surface (at z = 0) and the lower boundary condition (at z = -L) at all times (refer Figure 9-3).

9.2.3 First-Order Analytic Solution

Under conditions of hydrostatic equilibrium with the ocean and with the ocean surface at MSL, the pressure head at any point in the aquifer is the negative of elevation relative to MSL (see Figure 9-3 and Equation 9-11). Hence, under these hydrostatic conditions, the water table height, δ, and $H\{z\}$ must equal zero. If a pressure additional to the hydrostatic pressure, δp, is then applied to the lower boundary (ie, at z = -L), the water table will rise to a height of δp/ρg at which time $H\{z \geq -L\}$ will equal δp/ρg. Hydrostatic equilibrium is therefore represented by any vertical line on the z versus H diagram depicted in Figure 9-3.

However, because the fluid flow and the readjustment of the water table height, δ, are time dependent processes (see Equation 9-9), the groundwater cannot reach hydrostatic conditions instantaneously and a transient pressure boundary condition (such as that induce by the tide) will result in a transient water-table.

In the following analytic treatment, the tidal head in the groundwater at the lower boundary is sinusoidal with an amplitude of A, a frequency of ω, and a periodicity of t_o:

H (-L,t) = A sin (ω t)   (Equation 9-12)

where

$t_o = 2\pi / \omega$ (Equation 9-13)

and

ω	= tidal frequency	$(rad\ s^{-1})$
A	= tidal amplitude	(m)
t_o	= tidal periodicity	(s per cycle)

The pressure at the lower boundary is therefore;

$$p\ (\text{-}L,t) = \rho g\ \{\ L + A \sin (\omega\ t\ )\ \} \qquad\qquad \textbf{(Equation 9-14)}$$

The total head at the water table in Figure 9-3 must equal the water table elevation, $\delta(t)$, since the pressure at the phreatic surface is always zero relative to atmospheric, ie:

$$z\ (\delta,t) = \delta(t) \qquad\qquad \textbf{(Equation 9-15)}$$

$$p\ (\delta,t) = 0 \qquad\qquad \textbf{(Equation 9-16)}$$

$$H\ (\delta,t) = \delta(t) \qquad\qquad \textbf{(Equation 9-17)}$$
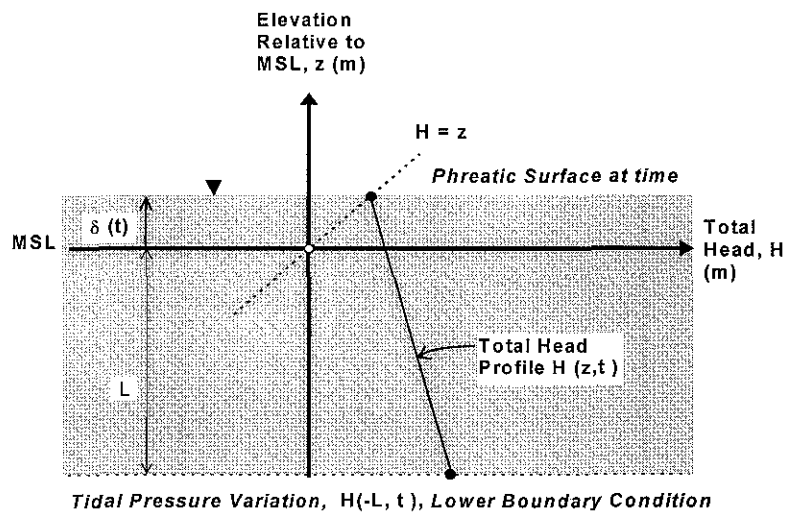
Figure 9-3. The assumed total head profile in an unconfined aquifer with transient groundwater flow and a time varying pressure at the lower boundary.

H{z,t} between the water table and the lower boundary may be obtained by interpolation. Referring to Figure 9-3, the slope of H{z,t} is

$$\frac{\Delta H}{\Delta z} = \frac{\delta(t) - H(-L,t)}{L + \delta(t)}$$

$$= \frac{\partial H}{\partial z}$$

(Equation 9-18)

Darcy's law (Equation 9-9) is combined with Equations 9-12 and 9-18 to give the macroscopic mean speed of groundwater, v, as a function of the head gradient and the saturated hydraulic conductivity, K, of the aquifer, ie:

$$v(t) = -K\frac{\partial H(t)}{\partial z}$$

$$= -K\left\{\frac{\delta(t) - H(-L,t)}{L + \delta(t)}\right\}$$

$$= -K\left\{\frac{\delta(t) - A\sin(\omega t)}{L + \delta(t)}\right\}$$

(Equation 9-19)

For mass to be conserved, any water table variation must be equated with a fluid exchange across the lower boundary. Equation 9-20, which gives the water table height as a function of v and aquifer specific yield (S_y), is correct provided that the unsaturated zone does not affect the flow of groundwater as the water-table rises or falls.

$$\delta(t_o) = \int_0^{t_o} \frac{v(t)}{S_y}dt + \delta(0)$$

(Equation 9-20)

When Equation 9-20 is combined with Equation 9-19, the following integral is obtained which describes the position of the phreatic surface.

$$\delta(t_o) = \int_0^{t_o} \frac{-K}{S_y} \left\{ \frac{\delta(t) - A\sin(\omega t)}{L + \delta(t)} \right\} dt + \delta(0)$$ **(Equation 9-21)**

To simplify the derivation of $\delta\{t\}$, an equation for $\delta\{t\}$ is initially assumed and then tested. For this purpose it is assumed that $\delta(t)$ is a sine function with the same frequency as the lower boundary condition but with a different amplitude, B, and subject to a time lag, γ. Hence, let

$$\delta(t) = B\sin(\omega\{t - \gamma\})$$ **(Equation 9-22)**

where,
ω	= tidal frequency	(rad s^{-1})
B	= water-table amplitude	(m)
γ	= time lag	(s)

Using this assumed formula for $\delta(t)$, a relationship between γ, B, A and ω can be derived. Consider that during each full cycle of the tidal boundary condition, the groundwater flow direction is twice reversed. At such times, t_i, when the groundwater flow direction reverses, $v(t_i)$ must be instantaneously zero throughout the whole profile for the continuity principle to hold. Hence, Equation 9-19 may be rearranged to show that the water-table height is coincident with the total head of the lower boundary condition when fluid speeds are zero, ie:

$$v(t_i) = 0$$

$$\Rightarrow -K \left\{ \frac{\delta(t_i) - A\sin(\omega t_i)}{L + \delta(t_i)} \right\} = 0$$

$$\Leftrightarrow \frac{\delta(t_i) - A\sin(\omega t_i)}{L + \delta(t_i)} = 0$$ **(Equation 9-23)**

$$\therefore \quad \delta(t_i) = A\sin(\omega t_i)$$

For the continuity principle to hold, the rate of change of $\delta(t)$ must also equal zero at time t_i, when fluid speeds are zero:

$$\frac{\partial \delta(t_i)}{\partial t} = \frac{v(t_i)}{S_y}$$

$$\therefore \frac{\partial \delta(t_i)}{\partial t} = 0$$

(Equation 9-24)

Furthermore, for a sine function of the type used to define δ(t), the time differential of δ(t) is zero when δ(t) is a maximum or minimum ie:

$$\frac{\partial \delta(t)}{\partial t} = 0 \quad : t = t_i$$

(Equation 9-25)

where,

$$t_i = i\frac{\pi}{\omega} + \frac{\pi}{2\omega} + \gamma; \quad i = 0,1,2,\dots N$$

(Equation 9-26)

Because Equations 9-22 and 9-23 are equivalent when time is defined by Equation 9-26, the following equality can be used to derive the time lag of the water table:

$$B\sin(\omega\{t_i - \gamma\}) = A\sin(\omega t_i)$$

$$\Leftrightarrow \quad \pm B = A\sin(\omega t_i)$$

$$\Leftrightarrow \quad \pm B = A\sin\left(\omega\left\{i\frac{\pi}{\omega} + \frac{\pi}{2\omega} + \gamma\right\}\right), \quad i = 0,1,2,\dots N$$

$$\Leftrightarrow \quad \pm B = \pm A\sin\left(\frac{\pi}{2} + \omega\gamma\right)$$

(Equation 9-27)

$$\Leftrightarrow \quad \pm B = \pm A\cos(\omega\gamma)$$

$$\therefore \quad \gamma = \frac{1}{\omega}\cos^{-1}\left(B/A\right)$$

The above equation can be expressed in terms of η, the tidal efficiency at the water table, ie:

$$\gamma = \frac{1}{\omega}\cos^{-1}(\eta)$$

(Equation 9-28)

and so

$$\eta = \cos(\omega\gamma)$$ **(Equation 9-29)**

If the equation for $\delta(t)$ is differentiated with respect to time, then the following formula for $v(t)$ is obtained,

$$
\begin{aligned}
v\{t\} &= S_y \frac{\partial}{\partial t}\delta(t) \\
&= S_y \frac{\partial}{\partial t} B\sin(\omega\{t-\gamma\}) \\
&= S_y\,\omega\,B\cos(\omega\{t-\gamma\})
\end{aligned}
$$

(Equation 9-30)

By combining the above equation with Equation 9-19, the following equality is derived.

$$
\begin{aligned}
v(t) &= -K\left\{\frac{\delta(t)-A\sin(\omega t)}{L+\delta(t)}\right\} \\
\Rightarrow S_y\,\omega\,B\cos(\omega\{t-\gamma\}) &= -K\left\{\frac{\delta(t)-A\sin(\omega t)}{L+\delta(t)}\right\}
\end{aligned}
$$

(Equation 9-31)

By considering the simple case of t equal to γ, $\delta\{t\}$ is reduced to zero, and Equation 9-31 is reduced to the following,

$$
\begin{aligned}
\Rightarrow S_y\,\omega\,B\cos(\omega\{\gamma-\gamma\}) &= -K\left\{\frac{-A\sin(\omega\gamma)}{L}\right\} \\
\Leftrightarrow \frac{LS_y\,\omega\,B}{KA} &= \sin(\omega\gamma) \\
\Leftrightarrow \frac{LS_y\,\omega}{K}\eta &= \sin(\omega\gamma) \\
\Leftrightarrow \frac{LS_y\,\omega}{K}\cos(\omega\gamma) &= \sin(\omega\gamma) \\
\Leftrightarrow \frac{LS_y\,\omega}{K} &= \tan(\omega\gamma) \\
\therefore \quad \gamma &= \frac{1}{\omega}\tan^{-1}\left(\frac{LS_y\,\omega}{K}\right)
\end{aligned}
$$

(Equation 9-32)

Given that L, ω, S_y and K are known, the lag of the sinusoidal VTUGF problem can be easily computed from Equation 9-32. By combining Equations 9-29 and 9-32, the following formula for the tidal efficiency at the water table is obtained.

$$\eta = \cos\left\{\tan^{-1}\left(\frac{S_y \, L\omega}{K}\right)\right\}$$

(Equation 9-33)

The following formula is therefore the first-order analytic solution for the current problem when H(-L,t) is a simple sine-type function:

$$\delta(t) = A\cos\left\{\tan^{-1}\left(\frac{S_y \, L\omega}{K}\right)\right\}\sin\left\{\omega t - \tan^{-1}\left(\frac{S_y \, L\omega}{K}\right)\right\}$$

(Equation 9-34)

9.2.4 Semi-Analytic Solution

Finite-differences in time, Δt, are used here to extrapolate $\delta(t)$ into the future. This is achieved in two steps. Firstly, $v(t+\Delta t)$ is estimated from Equation 9-19 assuming that $\delta(t)$ is a reasonable approximation of $\delta(t+\Delta t)$ (see Equation 9-35), and then $\delta(t+\Delta t)$ is approximated as a function of Δt, $v(t+\Delta t)$, and $\delta(t)$ (see Equation 9-36).

$$v(t + \Delta t) = -K\left\{\frac{\delta(t) - A\sin(\omega\{t + \Delta t\})}{L + \delta(t)}\right\} \quad : \Delta t \to 0$$

(Equation 9-35)

$$\delta(t + \Delta t) = \delta(t) + \frac{v(t + \Delta t)\,\Delta t}{S_y} \quad : \Delta t \to 0$$

(Equation 9-36)

This procedure may be repeated to evaluate $\delta(t)$ into the future as long as the lower boundary condition, $H(-L,t)$, is predefined. This implicit finite-difference solution to the VTUGF problem can be handled very easily by computer and is presented numerically as follows,

$$\delta_j = \delta_{j-1} + \frac{-K}{S_y}\left\{\frac{\delta_{j-1} - H(-L,t)_j}{L + \delta_{j-1}}\right\}\Delta t \quad : \Delta t \to 0$$

(Equation 9-37)

$j = 1,2,3,\ldots N; \quad t = j\,\Delta t$.

Solution convergence of the finite difference VTUGF model was investigate by solving

Example Problem 1 with different time-step sizes. Example Problem 1 describes a hypothetical aquifer layer with physical properties and dimensions typical of Holocene-age reef rock (see Appendix G.2 for details). Larger time-step sizes were found to result in larger computed water table elevations and larger computed tidal efficiencies (see Figure 9-4). A time-step size of 10% of the tidal periodicity (ie, 4 320 s) was found to provide a value of η which over-estimates the correct solution by about 10%. A time-step size of 1% of the tidal periodicity provided a value of η which overestimates the correct solution by about 1%, and so on and so forth for time-step sizes of 0.1% and 0.01% etc. of the tidal periodicity.
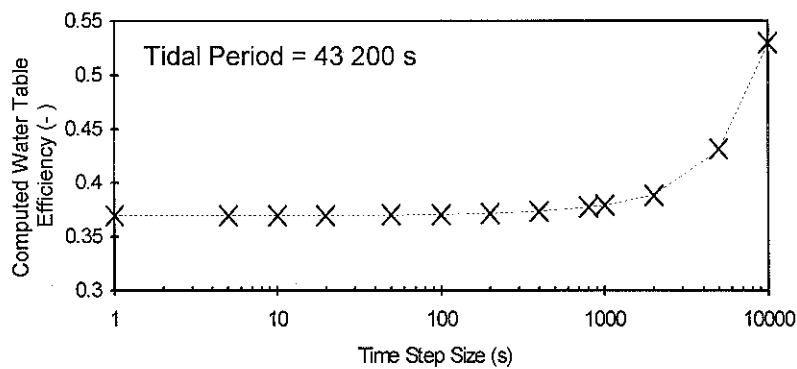
Figure 9-4. The effect of time step size on computed water table efficiencies for Example Problem 1: results of the finite-difference VTUGF model (see Appendix G2 for details)..

9.3 VTUGF IN TWO-LAYERED AQUIFERS

9.3.1 Assumptions and Governing Differential Equations

The assumptions and governing differential equations used in the VTUGF model for a two-layered aquifer are the same as those used in the previous VTUGF model for a single-layer aquifer: the only difference being that a change in aquifer properties occurs at distance l_2 above the lower boundary. The continuity principle requires that macroscopic fluid flow within each layer be the same at all times, hence:

$$v_1(t) = v_2(t)$$
$$= v(t)$$

(Equation 9-38)

where the upper layer (or region) is denoted by subscript 1, and the lower layer (or region) is denoted by subscript 2.

Figure 9-5. The assumed total head profile in a two-layered unconfined aquifer with transient groundwater flow and a time varying pressure at the lower boundary.

According to the Laplace equation (Equation 9-11), the head gradient within each layer of the aquifer will be uniform. Hence, when the upper layer and the lower layer have different hydraulic conductivities (ie, K_1 and K_2), the total head profile is expected to be like that shown in Figure 9-5. Even though the head gradient within each homogeneous region can be different, the head profile is continuous across the region boundary (see Figure 9-5).

9.3.2 First-Order Analytic Solution

A first-order analytic solution to VTUGF in a two-layered aquifer is derived from first principles in Appendix G.1. For brevity, the analytic solution for VTUGF in a two-layered aquifer is found here by expanding the analytic solution for VTUGF in a single-layered aquifer (refer Equation 9-34). This is achieved by replacing L with the total depth of the two-layer aquifer, as follows:

$$L = l_1 + l_2 \qquad \text{(Equation 9-39)}$$

and by replacing K with K_{1+2}, the harmonic mean of the vertical hydraulic conductivities of the two sub-layers (Mc Donald and Harbaugh, 1988):

$$\frac{l_1 + l_2}{K_{1+2}} = \frac{l_1}{K_1} + \frac{l_2}{K_2}$$

(Equation 9-40)

Substitution of Equations 9-39 and 9-40 into Equation 9-34 gives the following,

$$\delta(t) = A\cos\left\{\tan^{-1}\left(S_{y1}\,\omega\frac{l_1 + l_2}{K_{1+2}}\right)\right\}\sin\left\{\omega t - \tan^{-1}\left(S_{y1}\,\omega\frac{l_1 + l_2}{K_{1+2}}\right)\right\}$$

(Equation 9-41)

To confirm the correctness of the above equation, the two-layered problem is also solved in Appendix G.1 using trigonometric principles.

9.3.3 Semi-Analytic Solution

Combining Equations G-5 and G-10 of Appendix G gives:

$$\delta(t_o) = \int_0^{t_o} \frac{v(t)}{S_{y1}}dt + \delta(0)$$

(Equation 9-42)

$$= \int_0^{t_o} \frac{K_1}{S_{y1}}\left[\frac{A\sin(\omega t) - \delta(t)}{l_1 + \delta(t) + l_2\dfrac{K_1}{K_2}}\right]dt + \delta(0)$$

An implicit finite-difference approximation of the above result may be used to solve for the water-table height. This solution, when expressed numerically, is as follows

$$\delta_j = \delta_{j-1} + \frac{-K_1}{S_y}\left\{\frac{\delta_{j-1} - H(-L,t)_j}{l_1 + \delta_{j-1} + l_2\dfrac{K_1}{K_2}}\right\}\Delta t \quad : \Delta t \to 0$$

(Equation 9-43)

$j = 1,2,3,\dots N; \quad t = j\,\Delta t$.

9.4 VERIFICATION AND VALIDATION

9.4.1 Example Problem 1

The validity of the analytic solution was checked by comparing the fluid speeds predicted from the time-differential of Equation 9-34, $d\delta / dt$, with the fluid speeds predicted from Darcy's Law and the head gradient determined from Equation 9-19, $v\{t\}$. Equations for $d\delta / dt$ and $v\{t\}$ are presented below in terms of η, γ, A, L, K and ω:

$$\frac{d\delta}{dt} = \eta A \omega \cos\left(\omega\{t - \gamma\}\right)$$

(Equation 9-44)

and

$$v\{t\} = -K\frac{\partial H\{t\}}{\partial z}$$
$$= -K\left(\frac{\eta A \sin(\omega\{t - \gamma\}) - A\sin(\omega t)}{L + \eta A \sin(\omega\{t - \gamma\})}\right)$$

(Equation 9-45)

The parameters used in Example Problem 1 (see Appendix G2) are typical for coral reefs: the type of aquifer for which the model has been developed. From Equation 9-32, a water-table γ of 2.28 hours and a water-table η of 0.370 were computed. If the analytic result provided by Equation 9-33 is the exact solution to the VTUGF problem, then $d\delta / dt$ should equal $v\{t\}$. Hence, the difference between $d\delta / dt$ and $v\{t\}$ is a measure of absolute error associated with the first-order analytic solution. This absolute error is divided by the maximum fluid speed predicted by Equation 9-44 to give a measure of relative error, ie:

$$\text{Relative Error} = \frac{\left(\dfrac{d\delta}{dt} - v\{t\}\right)}{\dfrac{d\delta}{dt}_{\max}} \times 100\%$$

(Equation 9-46)

$$= \frac{\left(\dfrac{d\delta}{dt} - v\{t\}\right)}{\eta A \omega} \times 100\%$$

The relative errors computed from the above equation over one tidal cycle are shown in Figure 9-6. From Figure 9-6 it is obvious that Equation 9-44 is not the exact solution to the VTUGF problem, however the relative error associated with the first-order analytic solution appears relatively small, being less than 0.1% in this example. Furthermore, the errors in speed are cyclic and have twice the frequency of the tide. Because of this cyclic property of the speed errors, the cumulative error in the solution provided by Equation 9-34 will tend towards zero at the conclusion of each half-cycle of the tide.
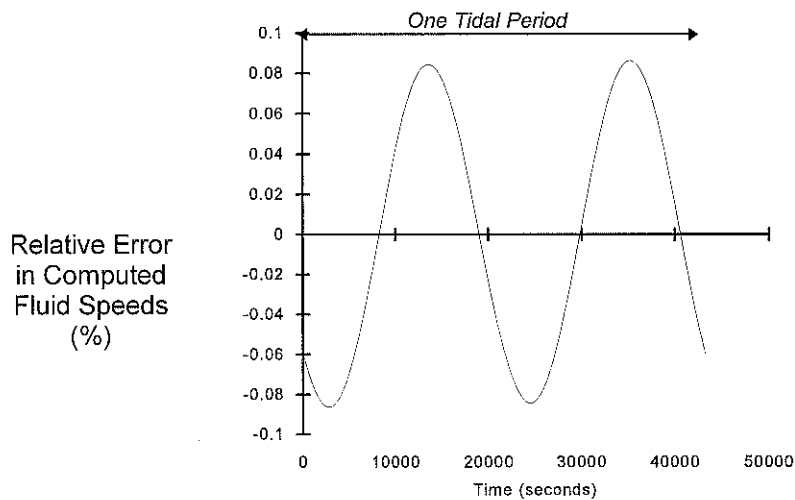
Figure 9-6. The computed relative error in the first-order analytic solution: Example Problem 1 (refer main text).

9.4.2 The Falling-Head Example

To verify the semi-analytic VTUGF model, a hypothetical example problem was solved with Equation 9-43 and the results compared with a well-known formula for determining K from the falling head permeameter experiment (see Equation 9-47). The verification example is of transient water drainage through a saturated porous material

located above a water reservoir (see Figure 9-8). The porous material has a K of 18 m day^{-1}, is 12 m deep, and has a basal elevation coincident with the reservoir surface. The porous material is initially overtopped by 1 m of free-water which drains through the material under gravity. Changes in water level are denoted by $\delta\{t\}$.
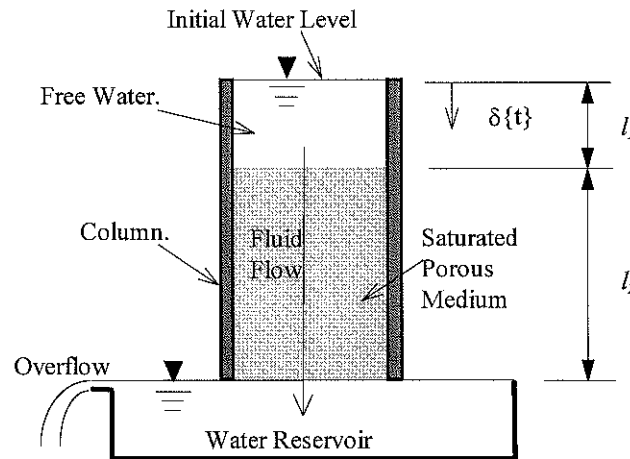
Figure 9-7. A conceptual model of the falling head permeameter verification example.

$\delta\{t\}$ in the falling head permeameter problem may be solved by substituting the following values into Equation 9-43: $K_1 \rightarrow \infty$ m day^{-1}, $K_2 = 18$ m day^{-1}, $l_1 = 1$ m, $l_2 = 12$ m, $H = -13$ m, and $S_y = 1.0$. Time-step sizes of 0.01, 0.1, 1, 10, 100, 1000, 10 000 seconds were tested with Equation 9-43 to examine the significance of time-step size.

The following formula is used to determine the hydraulic conductivity from the falling head permeameter test (adapted from Craig, 1987):

$$K_{fhp} = \frac{l_2}{t} \ln\left(\frac{l_1 + l_2}{l_1 + l_2 + \delta\{t\}}\right)$$

$$= \frac{12}{t} \ln\left(\frac{13}{13 + \delta\{t\}}\right)$$

(Equation 9-47)

The application of Equation 9-47 to the predicted $\delta\{t\}$ levels should give a value of 18 m day^{-1} exactly if the synthetic $\delta\{t\}$ data are perfectly correct. Hence the difference between K_{fhp} and K (18 m day^{-1}) is therefore a measure of the error in Equation 9-43.

This error is made relative by dividing it by K, as follows:

$$\text{Relative Error} = \frac{\left(K_{fhp} - K\right)}{K} 100\% \qquad\qquad \textbf{(Equation 9-48)}$$
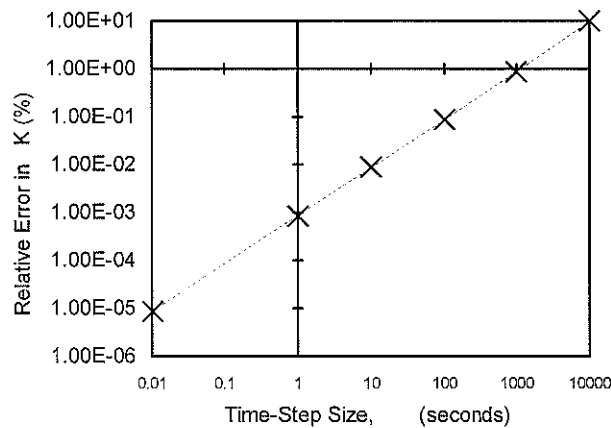
Figure 9-8. Relative differences between the semi-analytic and the exact hydraulic conductivities for a number of different time-step sizes: results of the falling head example (refer text).

Relative errors in K (refer Equation 9-48) were found to decrease when smaller time-step sizes were used, as shown in the log-log plot of relative error versus time-step size (see Figure 9-8). It is therefore believed that the correct $\delta\{t\}$ is approached by Equation 9-48 when the time-step size approaches zero. A relative error in K of only 0.89 % was obtained when a time-step size of 1000 seconds was used.

9.4.3 A Comparison of Analytic and Semi-Analytic Results

For verification of the semi-analytic model, the water-table η predicted by the semi-analytic and the analytic VTUGF models are compared for 350 different hypothetical problems. Each problem has a S_y of 0.3 and a L of either 1, 6.44, 11.89, 17.33, 22.78, 28.22, 33.67, 39.11, 40.56 or 50 metres. Different combinations of tidal periodicity and K are tested, ie: periodicities of 6, 12, 24, 48, 168, 336 and 8766 hours per cycle are tested, and K's of 0.1, 1, 10, 100 and 1000 m d^{-1} are tested. The two sets of predicted η

values are compared in Figure 9-9 and are found to have a correlation coefficient of 0.999995, a linearly regressed slope of 1.00001 and a linearly regressed intercept of 0.0006. This very high linear correlation indicates that the results of two models may be considered to be identical.
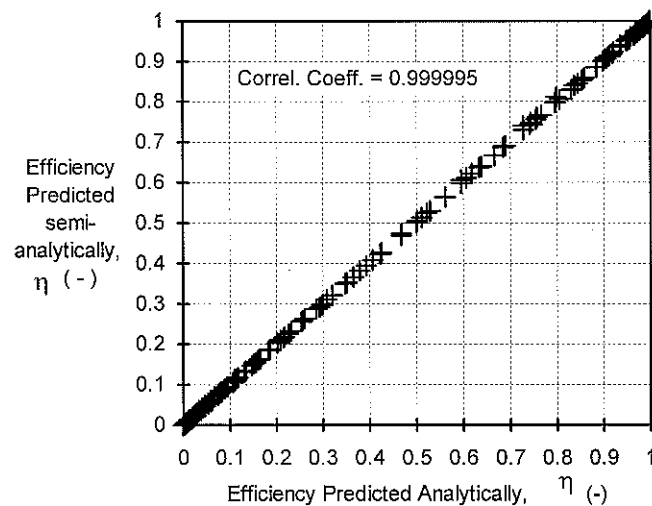
Figure 9-9. Comparison of water table efficiencies predicted by the finite-difference and the analytic VTUGF models: for verification purposes.

9.4.4 Verification with Oberdorfer et al. (1990)

In this section, the independent model of Oberdorfer et al. (1990) is used to verify the analytic single-layer VTUGF solution. Oberdorfer et al. numerically modelled the groundwater flow regime in Enjebi Island: an atoll island subject to two-dimensional tidally affected groundwater flow. They claim that VTUGF occurred near the centre of the island and that their field observations are closely reproduced by using a K of 10 m d^{-1} for the 12 m thick Holocene aquifer, and a K of 1000 m d^{-1} for the Pleistocene aquifer. Using a tidal periodicity of 12 hours and an S_y of 0.3, their model predicted an η of 70% and a γ of 0.25 hours at the Holocene-Pleistocene contact, and an η of 14% and a γ of 2.75 hours at the water table. This implies a relative η change of 20% and a lag shift of 2.5 hours across the Holocene aquifer. Equation 9-34, when used with the above data, gives an η change of 21.6% and a lag shift of 2.58 hours.

Oberdorfer et al. (1990) also examine what affect varying K has on $\eta\{z\}$. Equation 9-

34, when applied to their problem definition with a K of 5, 15, 20, 25 and 50 m d^{-1}, generated the results presented in Figure 9-10a. The results of the VTUGF model and the results of Oberdorfer et al.(1990) are systematically different by only a few percent and are highly correlated (corr. coef. = 0.999). Because of the close agreement between the two sets of results, the VTUGF models are regarded as verified.
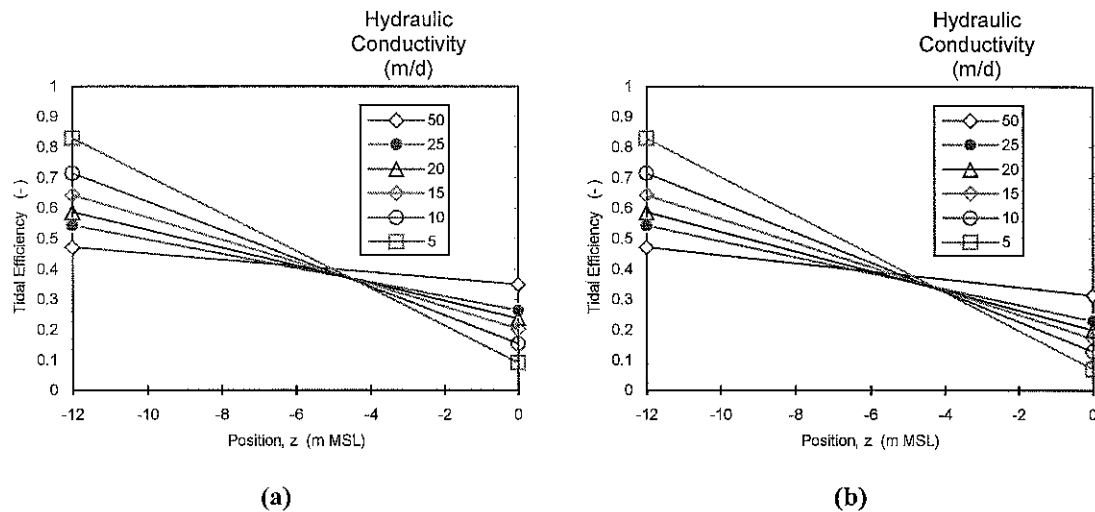
Figure 9-10. Verification of the analytic VTUGF model with published data: (a) VTUGF model results, (b) the tidal efficiencies of Oberdorfer et al. (1990).

9.5 THEORETICAL EFFICIENCY AND LAG PROFILES

The theoretical $\eta\{z\}$ and $\gamma\{z\}$ profiles of a homogeneous aquifer are presented here for ten different values of water-table η (see Figures 9-11a and 9-12a, respectively). The mathematical technique used to compute $\eta\{z\}$ and $\gamma\{z\}$ is presented in Appendix G-4. The efficiency and lag profiles typical of atoll islands (refer Example Problem 1) are also presented for comparative purposes (see Figures 9-11b and 9-12b).
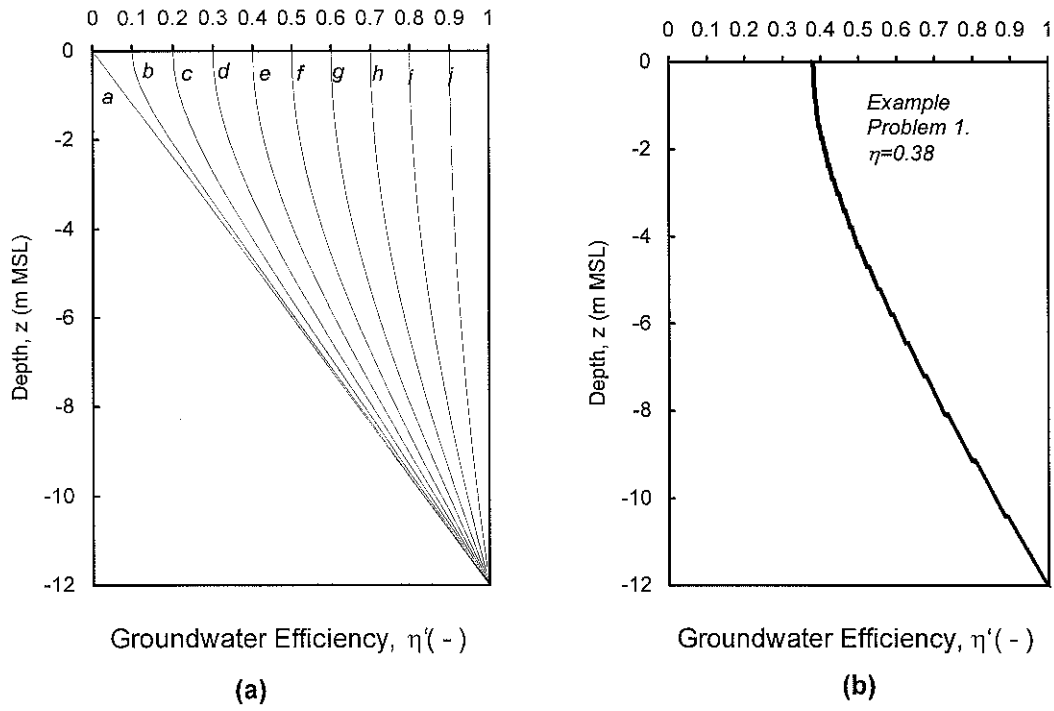
Figure 9-11. Groundwater efficiency profiles in a 1-D homogeneous aquifer with different water table efficiencies (L= 12m, ω=π/6 rad h⁻¹).
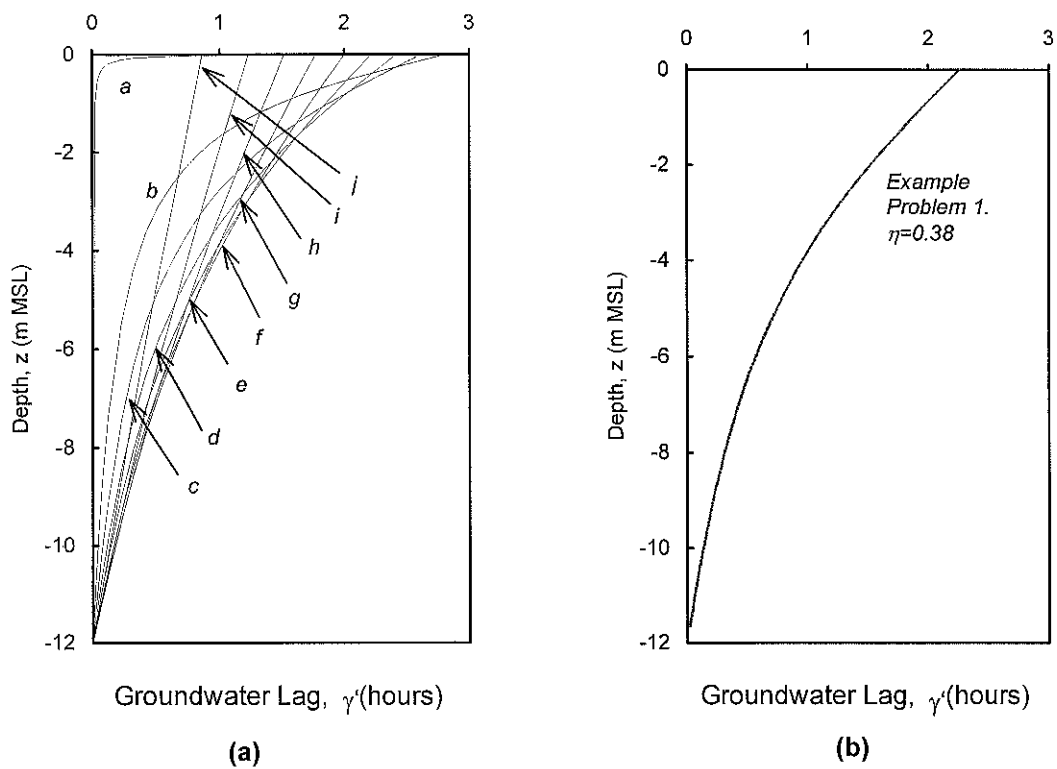
Figure 9-12. Groundwater lag profiles in a 1-D homogeneous aquifer with different water table efficiencies (L= 12m, ω=π/6 rad h⁻¹).

9.6 DIMENSIONAL ANALYSIS

The dimensionless Fourier Number, N_{FO}, for unsteady flow in deformable porous media is defined as follows (Domenico and Schwartz, 1990):

$$N_{FO} = \frac{Kt_e}{S_s L^2} \qquad \textbf{(Equation 9-49)}$$

where K is the hydraulic conductivity, L is some characteristic length, t_e is some characteristic time and S_s is the specific storativity (m^{-1}) of the aquifer. In the case of VTUGF, S_s in the above equation is conveniently replaced with S_y/L and t_e with the periodicity of the tide, t_o, ie:

$$
\begin{aligned}
N_{FO} &= \frac{Kt_o}{S_y L} \\
&= \frac{K2\pi}{S_y L \omega} \qquad \textbf{(Equation 9-50)} \\
&= \frac{2\pi}{\varpi}
\end{aligned}
$$

The term ϖ in Equation 9-50 has the dimensions of radians, and is referred to here as the *characteristic angle,* ie:

$$\varpi = \frac{S_y L \omega}{K} \qquad \textbf{(Equation 9-51)}$$

According to Equations 9-32, 9-33 and 9-50, the η and γ of the water-table are uniquely related to ϖ for any given sinusoidal VTUGF problem. Because ϖ is more readily substituted into Equation 9-33 than is N_{FO}, ϖ is used in Figure 9-13 to illustrate the dimensional properties of the VTUGF problem.
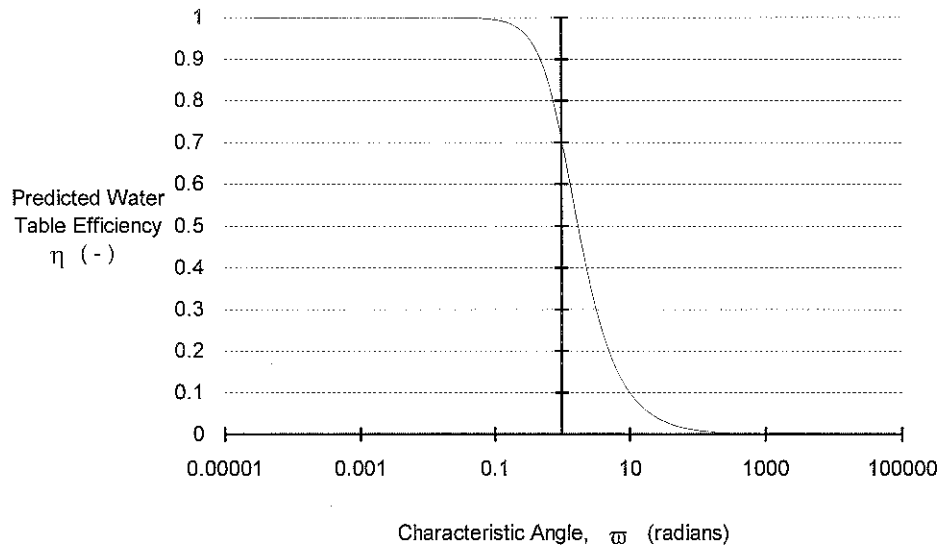
Figure 9-13. Relationship between the tidal efficiency of the water-table and the characteristic angle in vertical tidal unconfined groundwater flow: the first-order analytic solution for a sinusoidal tide (refer Equations 9-33 and 9-50).

9.7 VTUGF AT HERON ISLAND: THE ESTIMATION OF VERTICAL HYDRAULIC CONDUCTIVITY

9.7.1 Assumptions

The VTUGF models can be used to estimate the vertical hydraulic diffusivity, K/S_y, of an aquifer when the aquifer dimensions, the pressure boundary condition, and the groundwater response are known. Further, if S_y is known, then K can be determined explicitly. In the following interpretations of K, S_y is assumed equal to 0.3. This value of S_y seems reasonable as it has been used by Ghassemi, Jakeman & Jacobson (1990) to describe Nauru Island and by Oberdorfer, Hogan & Buddemeier (1990) to describe Enjebi Island. However there exists a degree of uncertainty in the following K values as S_y of between 0.1-0.40 are reported in the literature for various coral reef aquifers (eg, Griggs & Peterson, 1993; Herman, Buddemeier & Wheatcraft, 1986; Underwood, Peterson & Voss, 1992).

Ten assumptions form the basis of the VTUGF models (see Section 9.2.1). In terms of the Heron Island aquifer, Assumption 6 is believed reasonable because groundwater potentials were recorded in the field at fixed positions. Assumptions 3, 8 and 9 are also

believed reasonable because they are rarely invalidated in shallow unconfined aquifers (Domenico and Shwartz, 1990). Closer examination of Assumptions 1, 2, 4, 5, and 7 is warranted:-

Assumption 1: The Homogeneity Assumption

It is apparent that within the water-table range at Heron Island there exists sand- and gravel-sized sediment and irregular layering of limestone with interconnected porosity (see C and D, respectively, of Figure 1-7). Variations in K and S_y within the water-table range are not accounted for by the VTUGF models developed in this study, and so any such variations would reduce model's accuracy.

It is later argued that the aquifer need not be homogeneous with respect to K below the water-table. This is because variations in K within heterogeneous regions are harmonically averaged in the analytic and semi-analytic solutions (see discussion).

Assumption 2: The Vertical Flow Assumption

It was shown in Chapter 8 that Heron Island groundwater potentials and water-table levels vary with time and position. By comparing water-table levels at wells #12 and #13 an order-of-magnitude estimate of lateral gradients in groundwater potential may be obtained, ie:

$$\frac{\partial h}{\partial x} \approx \frac{\Delta h}{\Delta x}$$

$$\approx \frac{h\{Piezo.2, Well\#12\} - h\{Piezo.3, Well\#13\}}{75}$$

(Equation 9-52)

where 75 m is the approximate lateral distance between wells #12 and #13. Vertical potential gradients below the phreatic surface at well #12 were determined from the field potentials presented in Chapter 8 using the following equation:

$$\frac{\partial h}{\partial z} \approx \frac{\Delta h}{\Delta z}$$

$$\approx \frac{h\{Piezo.1, Well\#12\} - h\{Piezo.2, Well\#12\}}{-7.73 + 3.47}$$

(Equation 9-53)

Equations 9-52 and 9-53 were applied to the field data over a two day period to give the results which are shown in Figure 9-14. It is clear that the vertical head gradients at well #12 were about two orders-of-magnitude greater than the lateral head gradients. This suggests that VTUGF is the primary mode of groundwater flow at Heron Island and that Assumption 2 is not unreasonable.
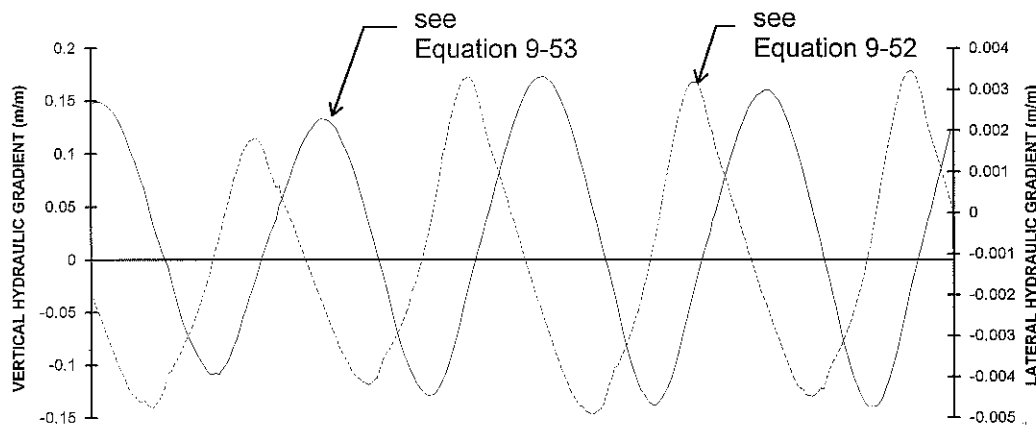
Figure 9-14. A comparison of vertical and lateral hydraulic gradients near well #12 over a two day period beginning 22nd April 1994: solid lines are the vertical gradient; dotted lines are the lateral gradient (refer main text).

Assumption 4: The Capillary Zone Assumption

The impact of the capillary zone on VTUGF was not quantified in this study but the work of Li et al. (1997) indicates the impact is likely to be negligible when groundwater flow oscillations have a semi-diurnal, diurnal or lower frequency (as is the case at Heron Island). The work of Li et al. (1997) also shows that the capillary zone assumption is invalidated when high frequency (e.g., 0.1 Hz) pressure-oscillations occur, but oscillations of such a high frequency are clearly absent from the groundwater hydrographs (refer Figures 8-8 to 8-16).

Assumption 5: Fluid Density Assumption.

Fluid density effects as a result of salinity gradients in the groundwater are assumed to have negligible effect on groundwater flow and are ignored. This assumption appears reasonable given that vertical gradients in salinity were minor at almost every location that was monitored (refer Figure 8-17 and Table I-6).

Assumption 7: The Darcy Assumption

Darcy's law was originally derived for homogeneous sand or rock with intergranular porosity. Unlike these materials the reef rock aquifer at Heron Island is characterised by irregular layering, interconnected porosity, and preferential pathways (refer Chapter 1). An additional assumption/approach, called the 'continuum approach', is therefore required with the application of Darcy's law to the Heron Island aquifer. In the continuum approach it is recognised that the hydraulic properties of some 'fractured' media can be described by Darcy's law at a suitable macroscopic scale even though Darcy's law may fail at smaller scales (Domenico and Schwartz, 1990).

Implicit in the continuum approach is the concept of a macroscopic control volume; a volume which is large compared to individual pore spaces but small at the megascopic scale. At all suitable macroscopic scales aquifer properties should only be a function of position and time and should not vary as a function of the size of the macroscopic control volume (Domenico and Schwartz, 1990). The smallest suitable control volume is the representative elementary volume (REV). Because the REV can be too large for laboratory-scale measurements it is preferable to measure aquifer properties of fractured aquifers at the field-scale. Because the REV's for the Heron Island aquifer are unknown, an advantage of the VTUGF models is that they can be applied to data obtained in the field at the field-scale. For this reason the VTUGF models are considered inherently reliable unless localised heterogeneities in the Heron Reef aquifer, such as megapores, are incompatible with the continuum approach.

Assumption 10: The Recharge Assumption

The application of the VTUGF models was undertaken assuming that recharge is zero or so small as to have negligible effect on groundwater flow (see page 9-5). The validity of this assumption depends on (a) the recharge that actually occurred in the field, and (b) the physical response of groundwater to recharge. As mentioned in Chapter 6, groundwater recharge at Heron Island was not measured but was mathematically interpreted using a approximate model called STEM. STEM provides preliminary information on recharge during the piezometric study (see Figures 6-4 and G-1) including the prediction that recharge peaked on the 14th of May 1994 with a maximum rate of 0.01 m d^{-1} (see Figure G-1a). Hence the results of the recharge study support the nill recharge assumption of the VTUGF analyses for wells #7, #6, #8, #1, #10 and #11

as these wells were monitored at times outside the expected recharge activity (compare Figure 8-5 with Figure G-1a). The supposed recharge peak does, however, coincide with the observations made at wells #3, #12 and #13. By way of example, the water-table hydrographs for well #3 (see Figure G-1d) does not spike and appears to vary due to tidal fluctuations only. Hence the available evidence supports the assumption. The author acknowledges that further research would be required to describe the potential impact of recharge on VTUGF and associated interpretations. Such work may be done by others in the future.

9.7.2 Methods

9.7.2.1 Estimates Based on Average Tidal Efficiency

The analytic and the semi-analytic VTUGF models were used to estimate the average vertical hydraulic diffusivity (K/S_y) of the Holocene aquifer at Heron Island by matching computed groundwater efficiencies with the time-averaged field efficiencies that are given in Chapter 8. In the following interpretations of K, the average groundwater head variations, H{z,t}, at Heron Island are represented by a single frequency sine function (ie, like Equation 9-12).
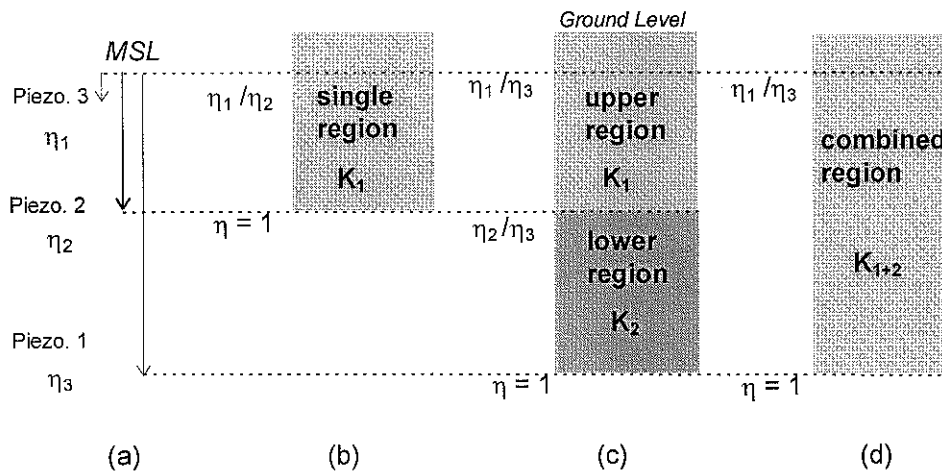
Figure 9-15. Schematic of (a) piezometer levels and field efficiencies, (b) the single-region model , (c) the two-region model, and (d) the combined-region model.

The data used in the interpretation of K are provided in Table G-1. This data consists of piezometer levels relative to MSL, piezometer construction details, and time-averaged groundwater efficiencies and lags. For convenience, field efficiencies were all taken relative to the field efficiency at the lowest point in the simulated aquifer (see Figure 9-15 and Table G-2). The validity of this manipulation is justified by the fact that η is independent of tidal amplitude in the first-order analytic solution for VTUGF (refer Equation 9-33).

The data collected from the two-piezometer nests (ie, wells #1 and #12) were used to obtain average relative η_1/η_2 to solve for the K_1/S_y of a single region (see Figure 9-15b). The data collected from the three-piezometer nests (ie, wells # 6, 8, 10 and #13) were used to obtain pairs of average relative efficiency (ie, η_1/η_3 and η_2/η_3) to solve for K_1/S_y and K_{1+2}/S_y of the upper and the combined regions, respectively (see Figure 9-15c and d). Further, in the three-piezometer nests, K_2 was determined either (i) by substituting K_1 and K_{1+2} into Equation 9-40, or (ii) by modelling the upper and lower regions together in a two-layered finite-difference VTUGF simulation. The analytic VTUGF models are only directly applicable to field data accompanied by water-table efficiencies. For this reason, the estimates of K for wells #1 and #10 were obtained by trial-and-error optimisation using the semi-analytic VTUGF models.

The potentiometric data from well #13 could not be analysed with the VTUGF models because groundwater efficiencies there decreased with increasing depth (thereby invalidating the assumptions implicit in the VTUGF models). The potentiometric data from well # 3 was not analysed either. This is because the data from the piezometers of that well were too similar.

9.7.2.2 *Estimates Based on Recorded Groundwater Potentials*

The semi-analytic VTUGF models were used to estimate the average vertical hydraulic diffusivity (K/S_y) of the Holocene aquifer at Heron Island by matching computed groundwater heads with the time-series $H\{z,t\}$ data recorded in the field. By using actual $H\{z,t\}$ data the various astronomical and random components of the tide were included in the analysis. Hence it is expected that the following estimates of K will be more accurate than those found assuming a sinusoidal $H\{z,t\}$. The K/S_y results are

presented in terms of K assuming S_y equals 0.3.

The groundwater potentials for the deepest piezometers (ie, Piezo. 1) of each well were used as the forcing term, $H\{-L,t\}$, and a time-step size of 600 seconds was used so that the model simulations were synchronised with the field records.

The previous estimates of K (see Table G-2) were improved by trial-and-error until the final results shown in Table G-3 were obtained. The simulated and observed water levels associated with each piezometer are compared in Table G-3 in terms of the slopes (α) and the intercepts (β) of the Equation 9-54 which were found by linear regression. Any value of α different to unity or β different to zero indicates that the simulated water-levels are systematically different to the field data. Two potential factors contributing to a non-zero β are (i) experimental error, and (ii) an average groundwater over-height (for a positive β) or an under-height (for a negative β).

$$H_{field}\{t_i\} = \alpha\, H_{predicted}\{t_i\} + \beta \quad : \alpha \to 1 \qquad \text{(Equation 9-54)}$$

9.7.3 Results

The local vertical hydraulic conductivities, K, of the Heron Island aquifer were estimated from the groundwater potentials observed at wells #1, #6, #8, #10, #12 and #13 using the two calibration methods described above. The results of the first method (ie, based on average tidal efficiencies and a sinusoidal tide) are shown in Table G-2 and Figure 9-16. Table G-2 also outlines the particular methodology used for each well that was analysed.

The results of the second method (ie, based on actual groundwater potentials) are presented in Table G-3 and Figure 9-17. In the second method, between 2000-6419 data points were used for each calibration region. The results of the linear regression analysis (see Table G-3) show that the linear correlation between predicted and recorded potentials is quite high in most cases. The maximum correlation coefficient is 0.997 for Piezo. 3 of well #1 and the minimum is 0.898 for Piezo. 4 of well #6. The predicted,

observed and residual groundwater potentials for Piezo. 3 of well #1 and Piezo. 4 of well #6 are compared in Figures 9-18 and 9-19, respectively. The predicted and observed groundwater potentials for the other piezometers are not shown for reasons of brevity.

Figures 9-16 and 9-17 show the vertical positions of each calibrated region and the approximate 95% error for each K (based on the experimental error; refer Chapter 8). The K values and there respective confidence levels were derived assuming S_y equals 0.3 and that the groundwater flow is ideal VTUGF.
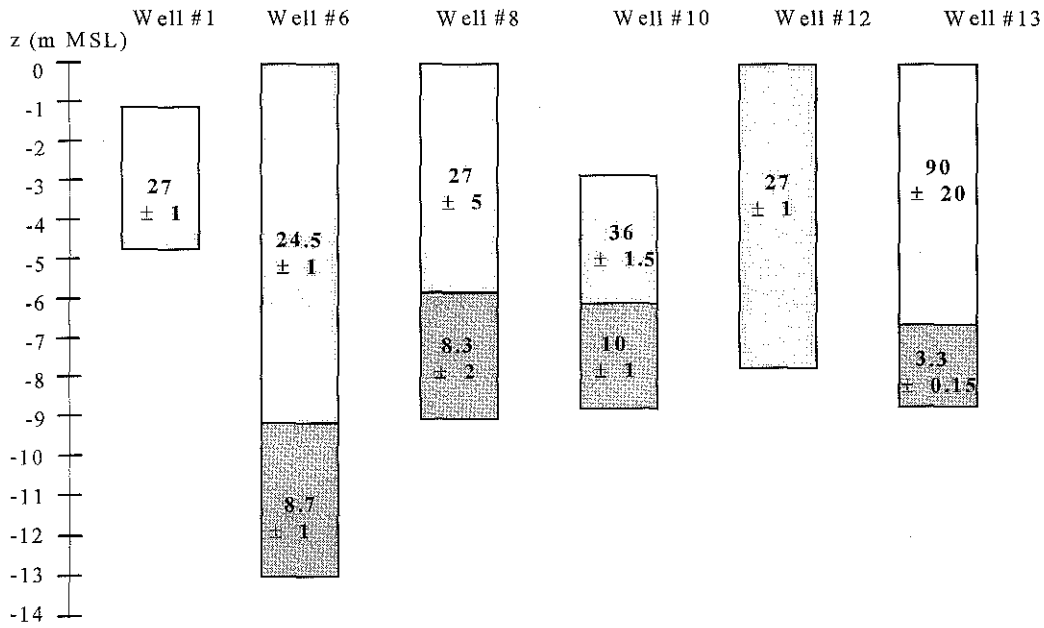
Figure 9-16. Average vertical hydraulic conductivities (m d^{-1}) of the Holocene aquifer at Heron Island: interpreted from average tidal efficiencies using the VTUGF models and $S_y = 0.3$.
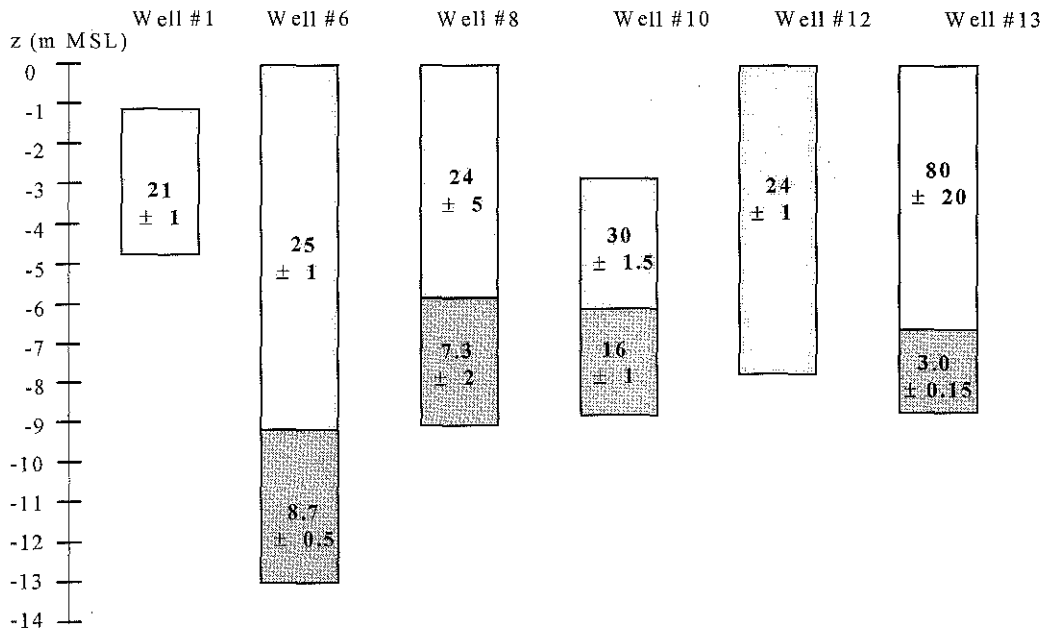
Figure 9-17. Average vertical hydraulic conductivities (m d^{-1}) of the Holocene aquifer at Heron Island: interpreted from the water-level records using the finite-difference VTUGF model and $Sy = 0.3$.
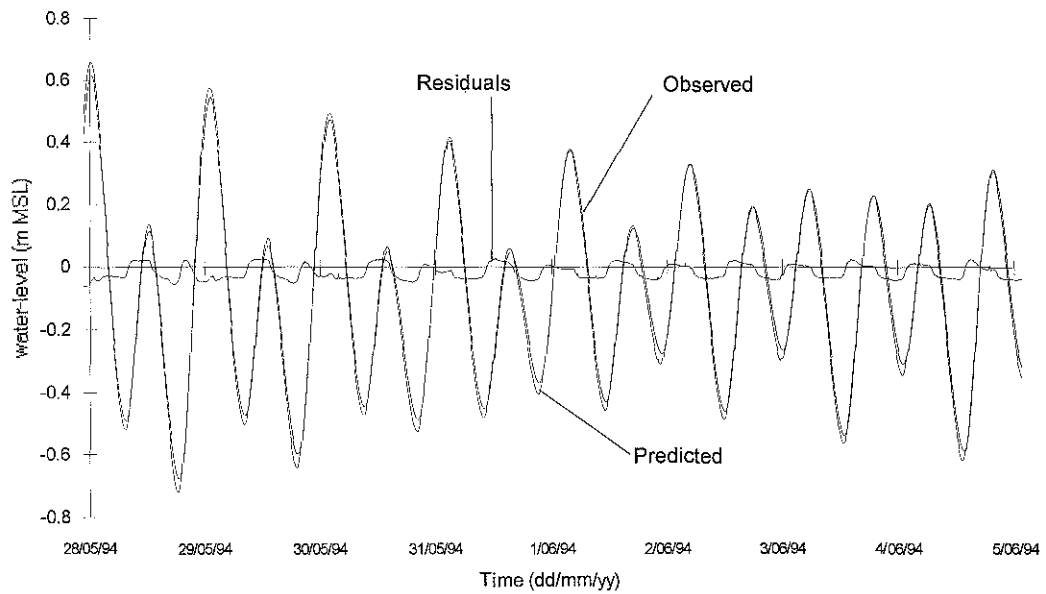
Figure 9-18. A comparison of observed and predicted water levels for Piezo. 2 of well #1 over an eight day period: a very high correlation and small average residual.
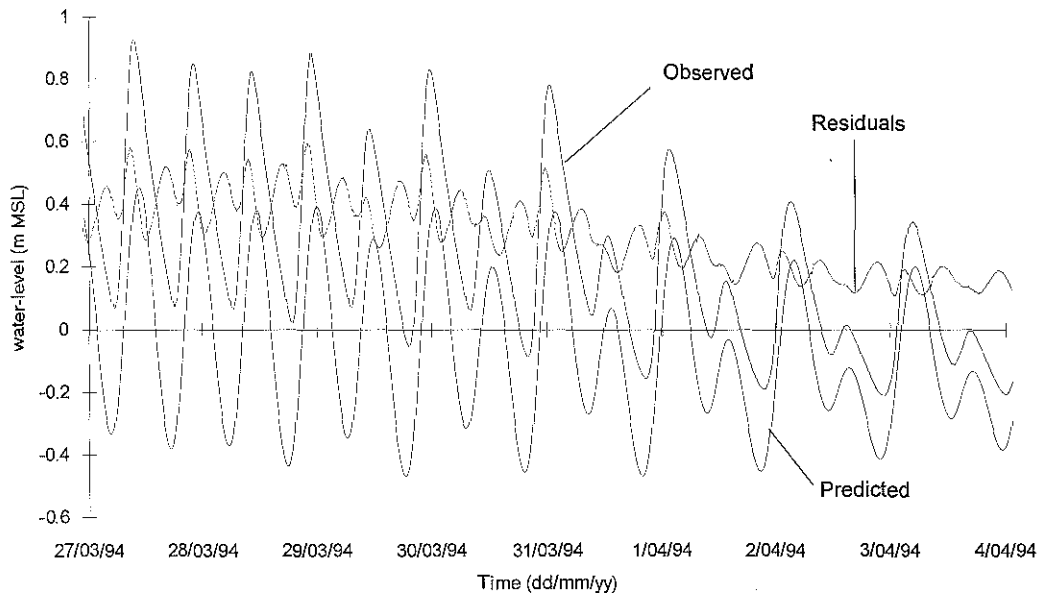
Figure 9-19. A comparison of observed and predicted water levels for Piezo. 4 of well #6 over an eight day period: a moderately high correlation but a large average residual.

9.8 DISCUSSION AND CONCLUSIONS

9.8.1 VTUGF Models

Approximate analytic and semi-analytic solutions to the VTUGF problem were derived in this chapter. Because these solutions are approximate, some mathematical checks were required to determine if they are sufficiently accurate for practical application. It was found that the relative error in the groundwater speeds predicted by the VTUGF models were small (ie, < 0.1%) when state variables and boundary conditions were set to values typical for coral reef aquifers with a semi-diurnal tide. It is believed that errors are inherent in the analytic solutions because a perfectly sinusoidal groundwater tide was assumed when in fact the water-table tide should be asymmetric due to fluctuations in aquifer effective depth (refer Figure 9-3). The errors were cyclic, manifesting at twice the tidal frequency (see Figure 9-8). Mathematical investigations (not shown) indicate that these errors are stable and are smaller when the characteristic angle, ϖ, is larger.

The validity of the semi-analytic VTUGF solution was determined by cross-checking the semi-analytic results with the analytic results for 350 different test problems. This cross-check detected a very high level of similitude (refer Figure 9-9). In practical terms, the two approaches give essentially the same results. The semi-analytic VTUGF solution was also verified with a hypothetical falling-head permeameter example using hydraulic conductivity (K) as the indicator of performance. The relative errors associated with the semi-analytic VTUGF solution were reduced to negligible levels (ie, < 0.001%) by decreasing the time step-size. However this particular test does not relate to the cyclic properties of tidal flow and so is less than ideal.

Oberdorfer et al. (1990), in their study of groundwater at Enjebi Island, describe a system approaching VTUGF. A comparison of their model's results with results of the current VTUGF models shows close agreement (refer Section 9.4.4): further evidence that the current VTUGF models are valid and compatible with the dual-aquifer concept (refer Figure 9-10).

In practice VTUGF will cause some unsaturated flow above the water-table, but in the modelling of VTUGF the capillary zone and unsaturated flow were ignored (refer Section 9.2.1). The full implications of unsaturated flow for VTUGF under a wide

variety of conditions is currently unknown and more research on this topic may be undertaken by others. Further theoretical developments in this area may include the development of a more complete semi-analytic model of VTUGF (ie, with a capillary fringe) and/or the adaptation of existing numeric codes that simulate saturated and unsaturated flow together. Not until such work is carried out can the error introduced in the Heron Island study through model assumptions be quantified.

9.8.2 Physical Relationships and Tidal Filtering

From the sinusoidal VTUGF theory developed in this chapter some important physical relationships were determined, namely:

(i)   the water table lag (γ) is a function of the water-table efficiency (η) and the periodicity of the tide,

(ii) η is independent of tidal amplitude (A), and

(iii) η in a homogeneous aquifer is uniquely related to the characteristic angle, ϖ, which is a function of hydraulic conductivity (K), specific yield (S_y), depth to lower boundary (L) and tidal periodicity (ω).

From the dimensional properties of ϖ, it was shown that lower-frequency signals in sinusoidal VTUGF are transmitted more efficiently than are higher-frequency signals. Hence an unconfined aquifer subject to sinusoidal VTUGF will behave as a 'low-pass filter' to tidal signals (refer Figure 9-20): Lam (1972) originally used this terminology to describe the physical properties of a partially-confined atoll island aquifer subject to tidal flow. It was also shown that $\eta\{z\}$ and $\gamma\{z\}$ are non-linear functions of depth in homogeneous aquifers subject to sinusoidal VTUGF. $\eta\{z\}$ and $\gamma\{z\}$ are uniquely described by η at the water-table, L and ω, and are independent of tidal amplitude (see Figures 9-11a and 9-12a). In some previous studies of tidal groundwater flow, $\eta\{z\}$ has been incorrectly depicted as a linear function of depth in homogeneous aquifers (eg, Oberdorfer et al., 1990).

9.8.3 VTUGF Models for Layered Aquifers

The analytic solution for VTUGF in a two-layered aquifer was derived using two different approaches. In the first approach, the two-layered problem was converted to a single-layer problem by substituting K_1 (ie, of the upper layer) and K_2 (ie, of the lower layer) with their harmonic mean value, K_{1+2}. In the second approach, the two-layered problem was solved from first principles (refer Appendix G-1). Both approaches produce the same result. Harmonic averaging can be applied to aquifers with N layers, in which case the harmonic mean K for flow perpendicular to the stratigraphic layering is determined as follows (Domenico and Schwartz, 1990):

$$K = \frac{\sum_j^N l_j}{\sum_j^N \frac{l_j}{K_j}}$$

            (Equation 9-51)

where l_j is the thickness and K_j is the hydraulic conductivity of the j'th layer. It is interesting to note that harmonic averaging is not just a concept pertaining to idealised layered aquifers, but it is probably inherent in all values of K that describe real-world aquifers. In other words, it is conceivable that the K of any region in a real-world aquifer is actually the harmonic mean of N subregions, where $N \rightarrow \infty$ in a fully heterogeneous region.

A limitation of the first-order analytic solution for VTUGF in a layered aquifer is that it cannot account for differences in S_y or K within the water-table range. Hence, if S_y or K vary significantly in the water-table range then the VTUGF models may not be reliable.

9.8.4 The Average Hydraulic Diffusivity of the Heron Island Aquifer

Two different calibration techniques were employed to estimate the average vertical hydraulic diffusivity, K/S_y, of the Heron Island aquifer. The first technique employed analytic and the semi-analytic solutions to fit the η of a sinusoidal tidal signal to the time-averaged η of the field potentials. Because the first calibration method employed a single-frequency signal (12.4 hour periodicity), it is a 'single frequency calibration' (SFC). The second technique employs the semi-analytic solution to fit predicted

groundwater potentials to the field potentials. Because the second technique calibrated against all of the harmonic and random components of the tide, it is a 'multiple-frequency calibration' (MFC). It is believed that the K/S_y estimates determined by MFC are more reliable than those determined by SFC (see Figures 9-16 and 9-17). MFC in this study involved the matching of between 2000 and 6419 data points in each calibration. With SFC, only one or two average η values were matched in each calibration. In both techniques a value of 0.3 for S_y was assumed to obtain the estimates of K shown in Figures 9-16 and 9-17.

The groundwater potentials predicted by MFC were found to be highly correlated to the field data for wells #1, #8, #10, #12 and #13 (correl. coeff.'s > 0.956; see Table 6-3). Thus the semi-analytic VTUGF model is generally a good model, both quantitatively and qualitatively, for the groundwater hydraulics at these wells (eg, see Figure 9-18). There was, however, some systematic difference between the predicted and the observed potentials for all of the wells examined (refer Equation 9-54). A slope, α, of between 0.986 and 1.023, and an intercept, β, of between -3.8 and 5.3 cm were determined for wells #1, #8, #10, #12 and #13 (see Table G-3). A high correlation coefficient was found for Piezo. 2 of well #6 (ie, 0.981) and a moderately high correlation coefficient was found for Piezo. 4 of well #6 (ie, 0.898). The β values for Piezos. 2 and 4 of Well #6 are the largest: 10.5 and 24.0 cm, respectively.

When the field potentials of Piezo. 4 of well #6 are compared the with the potentials predicted by the semi-analytic VTUGF model (see Figure 9-19), it is apparent that asymmetric pressure signals and significant overheights in the field potentials are not reproduced by VTUGF theory (hence the relatively weak correlations). Asymmetric signals and significant overheights are also apparent in the field data of Piezo. 2 of well #6, however these are not as severe as for Piezo. 4. Hence groundwater movement around well #6 may have deviated significantly from VTUGF. For this reason, the K/S_y values interpreted for well #6 should be considered with care. Further interpretations of this data are made in Chapter 10 in an investigation of groundwater flow within and across the beach zone.

Deviations from perfect linear correlation between the field potentials and the fitted potentials may be attributed to one or more of the following causes: (i) deviations from

Assumptions 1-9 in practice (refer Section 9.3.1), (ii) experimental error in the field data, and (iii) calibration error. The groundwater potentials recorded at wells #3 and #11 were not analysed with the VTUGF models because the differences between the upper and lower potentials recorded at wells #3 and #11 are less than the experimental error (refer Figures 8-9 and 8-13). One possible explanation for the similarity between the upper and lower potentials at wells #3 and #11 is a relatively high K/S_y in the field, however the actual cause of the similarity was not determined.

The average K determined for Heron Island's Holocene aquifer (see Figure 9-17) seems reasonable as it is within range of the published K estimates previously determined for a number of Holocene-age atoll island aquifers: K values in the order of 1 to 1×10^2 m d^{-1} are reported by Underwood, Peterson & Voss (1992). The best estimate of the overall average vertical K of the Holocene aquifer at Heron Island is 15.4 m d^{-1} (the harmonic mean of the ten K values shown in Figure 9-17 assuming a specific yield of 0.3).

In all four instances that K was estimated in two regions of the same vertical profile (ie, wells #6, #8, #10 and #13), K was least in the lower region. The greatest contrast between upper and lower K values were determined for well #13 (ie, 80±20 m d^{-1} for the upper region and 3.0±0.15 m d^{-1} for the lower region). The K value of 80±20 m d^{-1} for the upper region at well #13 is marginally less than the K predicted for unconsolidated sediment of the inter-tidal and supra-tidal zones (refer Chapter 4). In general it appears that there may exist an irregular hydrogeologic transition in the Holocene at Heron Island somewhere between -5 and -10 m MSL (see Figure 9-17). Vertical differences in K/S_y may be related to differences in primary and secondary porosity and inter-connectivity of pores. The rather extreme K values at well #13 could be due to sand-and-gravel overlying a low-permeability layer.

9.8.5 Dimensional Properties of VTUGF

According to the analytic VTUGF models, the efficiency and lag of tidal signals at the water-table is a function of K, S_y, L and ω (see Equation 9-34). Because each astronomical and random component of an ocean tide may be approximated as a simple sine function, the affect of signal frequency on VTUGF at Heron Island may be examined with the analytic model. In this examination, the hydrogeology of well #8 is

the test example. Considered are the diurnal and semi-diurnal solar and lunar components of the tide, the annual solar component of the tide, barometric sea-level variations (1 to 10 day periodicity approx.; Voss, 1974) and wind-induced surface waves (1 to 10 second periodicity assumed). The predicted water-table efficiency for each of these tidal components was determined from Equation 9-33 and is presented in Figure 9-20. The first-order VTUGF solution predicts that the highest frequency signal, the surface waves, are completely damped-out whilst the lowest frequency component of the tide, the annual solar, is entirely transmitted to the water-table (see Figure 9-20). Intermediate between these two extremes are the barometric sea-level variations and diurnal and semi-diurnal tidal components.

The frequency-efficiency relationship depicted in Figure 9-20 shows that signal frequency is important when monitoring and modelling groundwater hydraulics at Heron Island. Moreover, if a single-frequency signal is assumed when calibrating K/S_y in a model of VTUGF, then some error will be introduced to the estimate of K/S_y by the model. Hence it is recommended that mathematical models of VTUGF should be used consistently with either MFC or SFC results. Although SFC is 'artificial', it offers a convenient method of simplifying an otherwise demanding numerical problem.
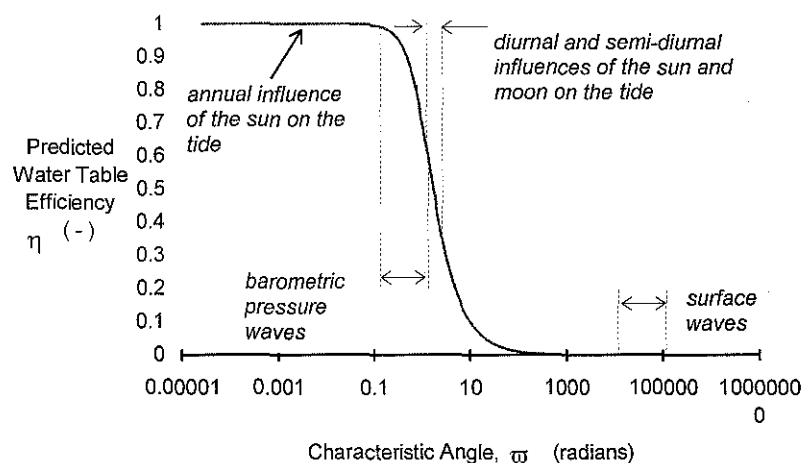
Figure 9-20. Theoretical efficiencies of some astronomical and random components of the tide as defined by vertical-unconfined-groundwater-flow theory and the hydrogeology of the Heron Island aquifer at well #8 (refer main text).

9.8.6 Further Evidence for the Dual-Aquifer Hypothesis

Because the VTUGF model predictions and the field observations are mostly in good-to-excellent agreement, it is concluded that VTUGF is the predominant regime of groundwater flow in the Holocene-age aquifer at Heron Island. Additionally, the presence of VTUGF is consistent with, and therefore supportive of, the dual-aquifer hypothesis for Heron Island and Reef. However, because scant geologic data and no hydraulic data were collected off-shore from the island or deeper than the Holocene-age aquifer, it is recognised that more field investigations are needed to elucidate the hydrostratigraphy of the whole reef-cay. In the next chapter preliminary numerical modelling is undertaken to validate a dual-aquifer hydrogeological model for the reef-cay system.

9.8.7 Further Evidence for the Reef-Plate Hypothesis

From the author's personal observations, it appeared that the drainage of seawater from the reef-flat at Heron Reef was largely a result of seawater flow over the reef edge. However, less obvious is the possibility that some drainage was due to interstitial seepage through the reef-flat surface. A downward forcing hydraulic gradient which exists during tidal separation lends itself to this possibility. But, if it is assumed that the vertical hydraulic conductivity of the Holocene reef rock beneath the reef-flat were moderate (eg, $K_{HV} > 1$ m d^{-1}), then according to VTUGF theory (refer Figure 9-20 with $\varpi < 50$ rad s^{-1}) a discernible tidal signal should be transmitted through to the reef-flat from the Pleistocene aquifer. Given that no discernible tidal signal is evident on the reef-flat during tidal separation (refer Figure 8-7), it appears that the average vertical hydraulic conductivity of the Holocene beneath the reef-flat is not great (ie, less than about 1 m day^{-1}). This reasoning conforms with the hypothesis that the reef near Heron Island is capped by reef plate.

10. LARGE-SCALE TIDAL GROUNDWATER FLOW: INTERPRETIVE MODELLING

10.1 INTRODUCTION

The dual-aquifer conceptual hydrogeological model was originally deduced by hydrogeologists attempting to explain the existence of tidal groundwater fluctuations in small low atoll islands (Buddemeier & Holloday, 1977; refer Chapter 7). The dual-aquifer conceptual model denotes a layered aquifer with (1) a upper layer comprised of 'moderately' permeable Holocene reef rock and unconsolidated sediments (and island), (2) a lower layer of 'highly' permeable and porous Pleistocene reef rock, and (3) a foundation of relatively impermeable basalt. As discussed in Chapter 9, vertically aligned tidal groundwater flow occurs within the unconfined portion of the Holocene layer and tidal non-vertical groundwater flow occurs in most other regions of the Holocene and Pleistocene layers (eg, Underwood, 1990). The tidally affected groundwater movement is significant because the Pleistocene layer has hydraulic connectivity with the ocean and a relatively high hydraulic conductivity; typically in the order of 100 -6000 m d^{-1} (eg, Herman, Buddemeier & Weatcraft, 1986; Oberdorfer, Hogan & Buddemeier, 1990; Underwood, Peterson & Voss, 1992; Griggs & Peterson, 1993).

It was implied in Chapter 9 that the dual-aquifer conceptual hydrogeological model for atoll islands explains the occurrence of VTUGF at Heron Island. This hypothesis is tested by incorporating the geological information of Chapter 1 with the hydrogeologic interpretations presented in Chapters 8 and 9 in a two-dimensional numerical groundwater model. The model represents short-term tidal groundwater flow in a north-south slice through the middle of Heron Island (see Figure 1-1) and as such ignores three-dimensional flow patterns and non-tidal hydrodynamics. The two-dimensional approach is simplistic given the irregular shape of the aquifer, however the current model is only a first-attempt at validating the hydrogeological interpretations and was not intended to provide highly accurate simulations.

The groundwater potentials recorded at well #6 demonstrate that the tidal signal at that locality were 'skewed' and the groundwater somewhat elevated above mean sea level (refer Chapter 8). Because the dual-aquifer model and VTUGF theory seem to explain the bulk of the observed groundwater movement at Heron Island, it appears that this localised 'skewing' of the signal was probably caused by a lateral component of groundwater flow of limited influence and possibly originating at the shoreline. A seawater intrusion model was interpreted from the field data by comparing groundwater potentials with the ocean tide, the reef-flat tide (synthetic) and water-table exit-point elevations at the beach-face (predicted). An important interpretation of the data is that seawater intrusion at Heron Island could be much more than previously envisaged because of a combination of interacting hydraulic processes. An order-of-magnitude estimate of the seawater intrusion rate is provided.

10.2 OBJECTIVES

The main objectives of Chapter 10 are to present a conceptual hydrogeological model for Heron Island and Reef and to validate this model numerically for the two-dimensional case. This numeric model should provide a first-approximation of the large-scale tidal groundwater flow pattern that occurred in the reef-cay aquifer including the vertical tidal unconfined groundwater flow (VTUGF) that was observed beneath the cay (refer Chapters 8 and 9). In this preliminary model recharge and seawater intrusion are not considered.

The hydrogeology of the beach zone is to be interpreted from the available field data in a separate exercise that utilises published models for beach seepage-face hydraulics. Shoreline effects are ignored in the previously mentioned numerical model of large-scale short-term tidal groundwater flow.
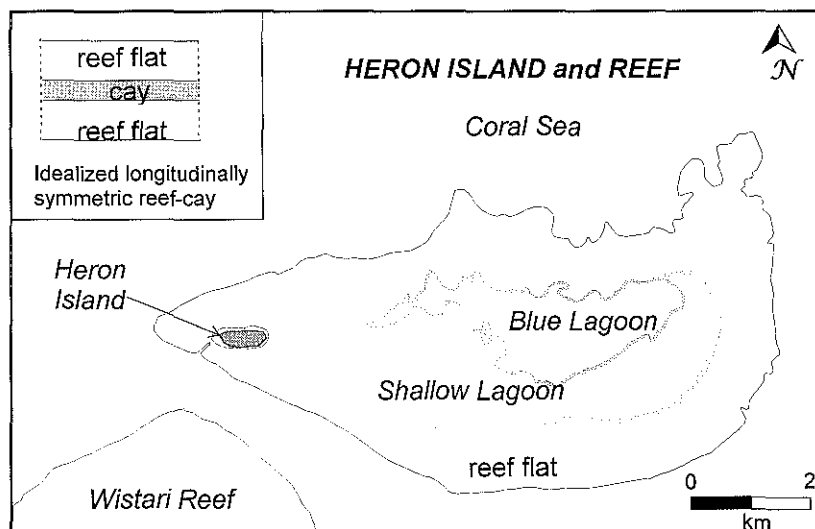
Figure 10-1. Heron Reef and the idealised reef-cay system modelled using SUTRA (see inset).

10.3 TWO-DIMENSIONAL TIDAL REEF-CAY GROUNDWATER MODEL

10.3.1 Introduction

In this section a numerical model of an idealised reef-cay groundwater system is used to reproduce the tidal efficiencies and lags that were observed near the centre of Heron Island (ie, at well #8). The model aquifer is infinitely-long, is symmetric about the vertical axis, and has a hydrostratigraphy based on the dual-aquifer hydrogeological concept. It is comprised of a moderately permeable surficial sand aquifer (ie, the cay), a discontinuous surface-confining layer of reef-plate, a two-layered and moderately permeable Holocene reef rock aquifer, a highly permeable Pleistocene reef rock aquifer, and a relatively impermeable foundation of terrigenous sand (see Figure 10-2).

The main purpose of the model is to validate the dual-aquifer concept for Heron Island and to interpret large-scale tidal groundwater flow patterns without recharge or beach related seawater intrusion. In terms of groundwater flow, the model is not expected to be highly accurate because of the various simplifying assumptions (refer Section 9.7.1) and because calibration data are only available for the Holocene aquifer.

Further, to simplify the calibration procedure a direct comparison is made between tidal efficiencies (η) and lags (γ) produced by the model and observed near the centre of the island (ie, at well #8). This approach is to simplify the calibration procedure and to enable the simulation of η and γ values that were typical of the field situation.

10.3.2 Computer System and Software

The computer code SUTRA[1] (Saturated Unsaturated TRAnsport) Version 690-2D (Voss, 1984) was selected for developing the model because it can reliably approximate complex fluid flow patterns in 2-dimensions as a result of unsteady pressure variations (eg, Hogan, 1988; Oberdorfer, Hogan and Buddemeier, 1990; Underwood, 1990; Underwood Peterson and Voss, 1992; Griggs and Peterson, 1993; Ghassemi, Jakeman and Jacobson, 1990). The governing differential equations of SUTRA are described in Chapter 7. A minor modification to the SUTRA source code was required (see Section 10.3.6).

The SUTRA source code was compiled with Microsoft ® FORTRAN Professional Development System Version 5.1 and executed under Microsoft Windows for Workgroups Version 3.11 with extended memory. The computer system was an American Megatrend 486DX - 40 MHz personal computer with 16Mb of RAM and a 200Mb capacity hard disk.

10.3.3 Hydrostratigraphy

The hydrostratigraphy of the groundwater model was inferred from the geological interpretations of Chapter 1 (see Figure 1-5) and the hydraulic diffusivity interpretations of Chapter 9. It consists of: (1) a moderately permeable upper region of Holocene reef rock, (2) a moderately permeable lower region of Holocene Reef rock, (3) a highly permeable layer of Pleistocene reef rock, and (4) a relatively impermeable foundation of terrigenous sand (see Figure 10-2). The Holocene-Pleistocene contact is

---

[1] Technical support for SUTRA is provided by the International Groundwater Modeling Centre in the USA and Europe.

modelled at -10.5 m MSL and the transition to terrigenous sand is modelled at -150 m MSL; as indicated by drill core information (refer Chapter 1).

The Holocene aquifer is modelled as a two-layered unit with average vertical hydraulic conductivities (K_{HV}) of 27 m d^{-1} for the upper region and 8.3 m d^{-1} for the lower region, respectively, and a transition level corresponding to the level of Piezo. No. 2 at well #8 (ie, at -5.75 m MSL). These conductivities and dimensions correspond to the field results obtained at well #8 (refer Figure 8-16; see Table 10-1) and were incorporated into the model to ensure thta its calibration was straightforward. The field data were considered insufficient to attempt the simulation of greater structural detail (see Table 10-1), however sensitivity of the model to variations in K_{HV1}, K_{HV2}, isotropy and porosity is examined (see Table H-2).

The other parameters which physically describe the fluid and the aquifer are listed in Table 10-1. Most of the parameter values were assumed from published values for other small-low-carbonate-island groundwater models.

10.3.4 Model Geometry

The model aquifer is infinitely-long (ie, a 'strip island') and symmetric about the y-z plane with groundwater flow parallel to the x-z plane (see inset of Figure 10-1). For reasons of numeric expediency only one-half of the symmetric model was actually simulated with SUTRA. An obvious limitation of the model is that it assumes that groundwater flow only occurs in a north-south direction (see section A-A in Figure 1-2). None-the-less, the model geometry is considered sufficiently detailed for a first-attempt at validating the conceptual hydrogeological model and for elucidating tidal groundwater flow patterns. Future researchers may expand the model into three-dimensions if more accurate simulations are required.

Figure 10-2. The idealised longitudinally symmetric reef-cay model in x-section: dimensions, hydrostratigraphic units and boundary conditions.

Table 10-1. Parameters describing the base-case tidal reef-cay groundwater flow model simulated using SUTRA.

Parameter	Symbol	Value	Units	Reference
Aquifer Hydraulic Conductivity				
Upper Holocene Vertical	K_{HV1}	27	m d^{-1}	H.I.
Upper Holocene Horizontal	K_{HH1}	27	m d^{-1}	H.I.
Lower Holocene Vertical	K_{HV2}	8.3	m d^{-1}	H.I.
Lower Holocene Horizontal	K_{HH2}	8.3	m d^{-1}	H.I.
Pleistocene Vertical	K_{PV}	1000	m d^{-1}	H.I. (optimised)
Pleistocene Horizontal	K_{PH}	3000	m d^{-1}	H.I. (optimised)
Aquifer Dimensions				
Total Island Width	B1	300	m	H.I. (approx.)
Total Width of Reef Platform	B2	1140	m	H.I. (approx.)
Total Width of Reef Basement	B3	1980	m	H.I. (nominal.)
Thickness Holocene Upper Layer	T1	5.75	m	H.I. (approx.)
Thickness Holocene Lower Layer	T2	4.75	m	H.I. (approx.)
Thickness Pleistocene Layer	T3	139.5	m	H.I. (approx.)
Solid Properties				
Holocence Aquifer Porosity	n_H	0.30	m^3 m^{-3}	E.I.1, E.I.2
Pleistocene Aquifer Porosity	n_P	0.30	m^3 m^{-3}	E.I.1, E.I.2
Density Solid Grain	ρ_s	2700	kg m^{-3}	R.I.
Compressibility Solid Consolidated	β_{sc}	1.0×10^{-9}	m s^2 kg^{-1}	E.I.1, E.I.2,G.I.
Fluid Properties				
Density Freshwater	ρ_f	1000	kg m^{-3}	V *
Density Seawater	ρ_{sea}	1025	kg m^{-3}	V
Freshwater Salinity	C_f	0.000	kg kg^{-1}	V
Seawater Salinity	C_{sea}	0.0357	kg kg^{-1}	V
Coefficient of Solute-Density Change	$\partial\rho/\partial C$	700.28	kg m^{-3}	V
Fluid Compressibility	β_f	4.47×10^{-10}	m s^2 kg^{-1}	L.I.
Fluid Viscosity	μ	1×10^{-3}	kg m^{-1} s^{-1}	V
Gravity				
Acceleration	g	-9.8	m s^{-2}	V
Ocean Tide				
Average Tidal Amplitude	A	0.87	m	H.I.
Average Tidal Frequency	ω	1.4075×10^{-4}	rad s^{-1}	H.I.
Average Tidal Periodicity	$2\pi/\omega$	44 640	s	H.I.

Notes:
SUTRA   = Saturated Unsaturated TRAnsport (Voss, 1984).
E.I.1   = Enjebi Island   : Herman, Buddemeier, and Wheatcraft (1986).
E.I.2   = Enjebi Island   : Oberdorfer, Hogan, and Buddemeier (1990).
G.I.   = Generic Atoll Island: Underwood (1990).
H.I.   = Heron Island   : this study.
L.I.   = Laura Island   : Griggs and Peterson (1993).
Optimised = Optimised by matching tidal efficiencies (refer main text).
R.I.   = Roi-Namur Island   : Gingerich (1992).
V   = SUTRA manual   : Voss (1984).
*   = recharge is not simulated in the model.

10.3.5 Ocean Tide

Tidal harmonics are important when predicting groundwater responses to tidal-pressure variations as tidal damping generally increases with increasing tidal frequency (refer Chapter 9). Tidal harmonics are created by astronomical forces, are predictable, and are commonly represented as a Fourier series, ie:

$$h_{ocean}\{t\} = h_{MSL} + \sum A_j \sin(\omega_j t - \gamma_j)$$ (Equation 10-1)

where,

$h_{ocean}\{t\}$ = astronomical ocean tide	(m)
h_{MSL} = mean sea level relative to datum	(m)
A_j = tidal amplitude of the j'th harmonic	(m)
ω_j = tidal frequency of the j'th harmonic	(rad s^{-1})
γ_j = time lag of the j'th harmonic	(s)
t = time	(s)

However, a single frequency sine function is used in preference to a Fourier series for modelling the tidal boundary condition for reasons of mathematically expediency. Most other researchers in this field of study use a similar approach (eg, Herman Buddemeier & Wheatcraft, 1986; Oberdorfer & Buddemeier, 1988; Underwood, Peterson & Voss, 1992):

$$h_{ocean}\{t\} = h_{MSL} + A_{avg} \sin(\omega_{avg} t)$$ (Equation 10-2)

where A_{avg} is the average tidal amplitude and ω_{avg} is the average tidal frequency. A value of 0.87 m for A_{avg} and a value of 1.40639×10^{-4} rad s^{-1} for ω_{avg} (ie, periodicity = 12.4 hours) were deduced for Heron Reef from a 30-day-long synthetic record of ocean levels that were generated using Equation 10-1 with the five most significant harmonic components of the ocean tide in the diurnal and semi-diurnal frequency range (refer Table G-4).

The actual tide may also contain unpredictable components associated with waves, currents, ocean salinity gradients and barometric pressure variations (Serfes, 1991). However the unpredictable components of the tide provide no immediate advantages in terms of model calibration and are ignored in this model which simulates the long-term average tide at Heron Reef. The pressure heads, as defined by $h_{ocean}\{t\}$, were applied to the parts of the finite element mesh which denote the ocean floor and the reef-slopes (see C and D of Figure 10-2).

10.3.6 Moving Water-Table Boundary: The Vertical Equilibrium Boundary Approach

A major limitation of SUTRA when attempting to model unconfined flow is that it "...does not, in fact, simulate a moving water table" Voss (1984). Because a moving water-table occurs in atoll island groundwater systems, previous researchers studying such systems with SUTRA have modified SUTRA's governing differential equations to simulate a dynamic water-table (eg, Oberdorfer, Hogan & Buddemeier, 1990). This involved use of a storativity term to replicate the specific yield of the aquifer. In this work an alternative approach to modelling a vertically-moving water-table with SUTRA was used. The current approach had the advantage that only the SUTRA input data files and a 'user-defined' subroutine, UNSAT, required modification. The necessary modifications were:

(i)   fixing of the relative hydraulic conductivity, k_r, to unity for all levels of saturation (in subroutine UNSAT),

(ii)   allocation of a nominally large hydraulic conductivity to the unsaturated zone to effectively remove the time-dependent properties of unsaturated flow (1×10^5 times the K of the saturated aquifer proved sufficiently large),

(iii) arbitrary use of the following Van Genuchten (1980) water-retention relationship to allow the saturation-desaturation of the aquifer immediately above the water-table [subroutine UNSAT in Voss (1980)]:

$$S_w = 0.30 + 0.70 \left[\frac{1}{1 + \left(5.0 \times 10^{-5} p_c\right)^{2.0}} \right]^{0.5}$$

(Equation 10-1)

and,

(iv)   inclusion of a relatively large unsaturated zone in the simulated aquifer to ensure that readjustment of the equilibrium moisture profile caused negligible changes in simulated moisture content at the upper no-flow boundary (a 50 m thick unsaturated region proved to be sufficiently large; see Figure 10-5).

Modifications (i) to (iv) enabled SUTRA to compute the region of saturation and the groundwater pressures without being significantly affected by the unsaturated zone in terms of water mass-balance or time-dependency. In other words, the simulated unsaturated zone reached equilibrium with gravity and the water-table very rapidly whilst contributing only negligibly to the water-balance of the saturated zone. The above ad-hoc method of simulating a moving water-table with SUTRA may be applied to problems in which groundwater near the water-table moves vertically and is termed the Vertical Equilibrium Boundary Approach (VEBA).

Example Problems 1 and 2 (refer Appendix G.2 and G.3, respectively) were solved to verify the current application of SUTRA-VEBA. As can be seen in Figures 10-2 and 10-3, the results of SUTRA-VEBA are almost indistinguishable from the solutions provided by the VTUGF models described in Chapter 9. The correlation coefficients are 0.9990 for Example Problem 1, and 0.9993 and 0.997 for Example Problem 2 (at -5m and 0 m, respectively). For convenience the head predicted by SUTRA at $z = 0$ is taken equal to the water-table position. This approximation was found to introduce negligible error for the types of problems being considered.

The water-table boundary for the 300-m-wide unconfined strip island (see A in Figure 10-2) is represented in the model as a 50-m-high modified unsaturated zone over the full width of the island (see Figure 10-5). The finite-element mesh configuration is shown in Figure 10-5 and is defined by the FORTRAN program listed in Appendix H-2.
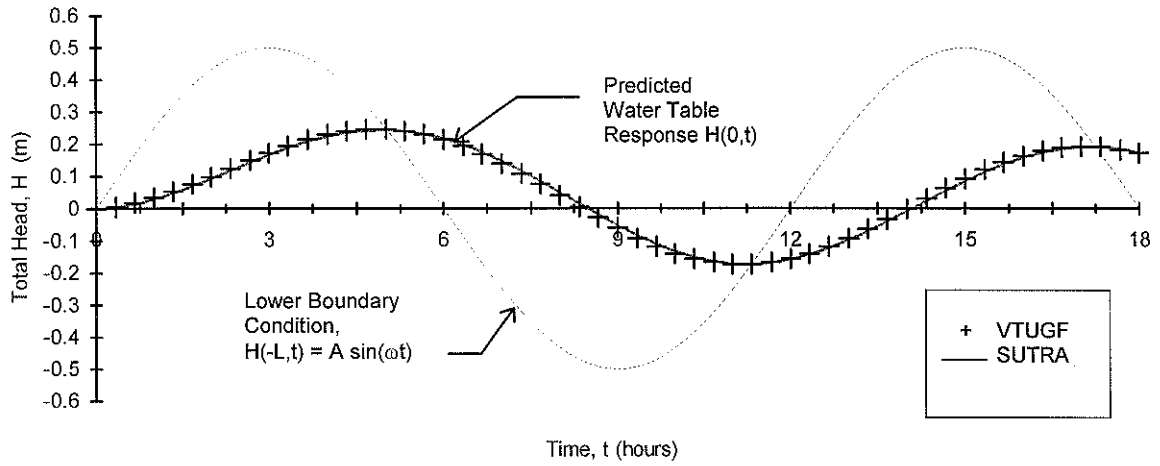
Figure 10-3. A comparison of simulated groundwater heads for Example Problem 1: VTUGF model results (crosses) and SUTRA results (solid line).
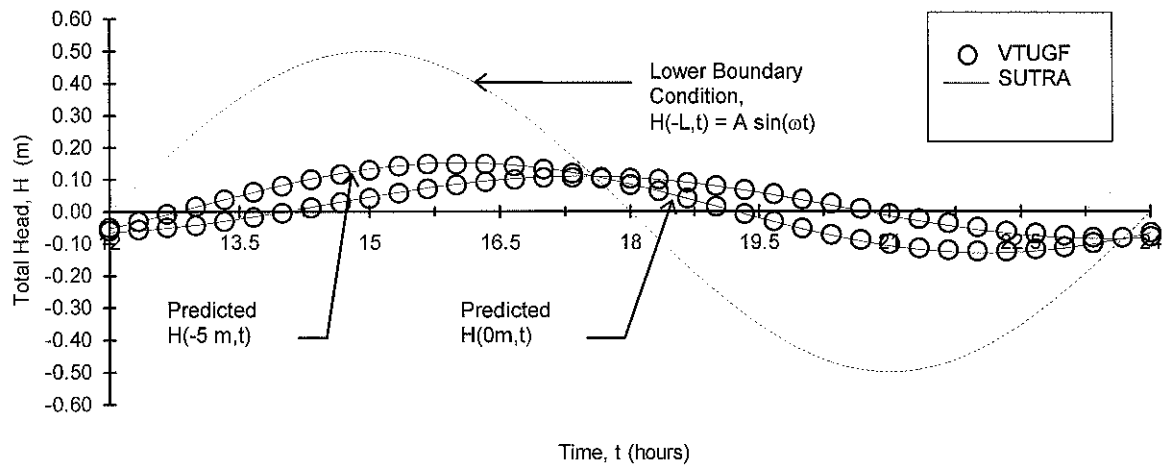
Figure 10-4. A comparison of simulated groundwater heads for Example Problem 2: VTUGF model results (circles) and SUTRA results (solid lines).

10.3.7 No-Flow Boundaries

To provide a first-order approximation of the aquifer's boundaries, no-flow conditions are applied to the top of the reef-flat, the sides and the base of the Pleistocene unit, and the shoreline of the cay (see bounadries B, E, F and G in Figure 10-2, respectively). The no-flow boundary at -150 m MSL is applied under the assumption that the hydraulic conductivity, K, of the terrigenous sand foundation is orders-of-magnitude smaller than that of the Pleistocene reef rock: medium-grained quartz sand typically has a K in the range of of 0.08 - 43 m d^{-1} (Domenico and Schwartz, 1990) whereas the K of porous and karst Pleistocene-age limestone is typically in the range of 100 - 6000 m d^{-1} (eg, Herman, Buddemeier & Weatcraft, 1986; Oberdorfer, Hogan & Buddemeier, 1990; Underwood, Peterson & Voss, 1992; Griggs & Peterson, 1993). The no-flow boundary on the top of the reef-flat is to represent a relatively thin and impermeable layer of reef-plate: an important feature of the current conceptual hydrogeological model (refer Chapters 8 and 9). The no-flow boundaries assigned to the cay shoreline are to avoid the complexity of seawater/groundwater flow across the beach-face: it is believed that beach related flows can be neglected in first-order approximations of groundwater flow within dual-aquifer systems (Buddemeier & Holloday, 1977). Lateral limits are placed on the Pleistocene unit in the form of no-flow boundaries (ie, as if abutting symmetric problems existed). It was found by numerical experimentation (not shown) that a wider model (ie, >2000 m) and/or the use of tidal-pressure boundaries at the sides of the model (ie, at E in Figure 10-2) required greater computational effort but produced negligible differences in simulated groundwater flow within the main area of interest.

10.3.8 Initial Conditions

At time zero the simulated groundwater was in hydrostatic equilibrium with MSL at all points in the aquifer. The salinity and density of the groundwater was made constant and equal to that of seawater everywhere in the model to simplify the simulation exercises. As actual groundwater salinities were generally quite high in the field, density gradients were expected to have insignificant influence on short-term tidal groundwater flow.

10.3.9 Numerical Space- and Time-Discretization

The finite-element (FE) mesh used to represent the reef-cay aquifer is presented in Figure 10-5. The mesh is most finely discretized in the area below the strip island (the area of main interest) and across the Holocene-Pleistocene contact where large changes in aquifer properties occur. It is most coarsely discretized below the ocean boundary where the slowest groundwater flows are expected (the area of least interest). A FORTRAN program (see Appendix H.2) was written to generate the finite-element mesh shown in Figure 10-5, including coordinates, node numbers and connectivity data for input into SUTRA.

The development of the FE mesh and the model was an iterative process (refer figure 1-9). Certain variables, including the lateral dimension of the aquifer, B3 (see Figure 10-2), the level of space-discretization in the finite-element mesh and the time-step size, Δt, were varied to examine their affect on the simulation results. A value of 1980 m for B3 was selected on the basis that larger values did not significantly alter the results of the model. A time-step size, Δt, of 1/80th of the tidal period (ie, 558 seconds) was chosen to provide a 'smooth' tidal signal and to reduce the error caused by time-discretization to negligible levels.

As a guide to numerical stability, the Courant number of the FE mesh should be less than or equal to unity at all elements, ie (van der Heijde & Elnawawy, 1992):

$$C_r = v \frac{\Delta t}{\Delta x}$$
$$\leq 1$$

(Equation 10-2)

The peak tidal groundwater speed, v_{max}, predicted by the model occurred below the cay and is approximated as follows (refer Figure 8-22 and Table 10-1):

$$v_{max} \cong \eta_{avg} A \omega$$
$$\approx 0.4 \times 0.87 \times 1.40639 \times 10^{-4}$$
$$\approx 5 \times 10^{-5} \text{ ms}^{-1}$$

(Equation 10-3)

Substituting v_{max} and Δt into Equation 10-8 gives a maximum allowable dimension of about 35 m for the finite-elements in the high velocity area. According to Equation 10-8, larger elements are allowed in areas where groundwater moves more slowly. The FE mesh shown in Figure 10-5, is therefore finer than that required by Courant number analysis. To examine the affect of spatial discretization on the model's results, a FE mesh with 387 elements and 436 nodes (not shown) and a FE mesh with 492 elements and 548 nodes (see Figure 10-5) were constructed and the simulated tidal efficiencies (η) compared. Although the models gave very similar results, the finer FE mesh was used throughout the remainder of this study.

10.3.10 Model Calibration

The horizontal hydraulic conductivity of the Pleistocence aquifer, K_{PH}, was calibrated by matching the predicted tidal efficiencies (η) to those measured in the field at well #8 whilst assuming K_{PV} equal to 1000 m d^{-1} [the same value of K_{PV} determined by Oberdorfer, Hogan & Buddemeier (1990) for Enjebi Island at Enewetak Atoll]. It was found that a value of 3000 m d^{-1} for K_{PH} gave a close match between the simulated η and the average observed η (see Figure 10-13a): correlation coefficients were 0.9997 and 0.9993 for tidal efficiencies and lags, respectively, for the three piezometers at well #8. A value of 3000 m d^{-1} for K_{PH} was therefore assigned to the base-case model (see Table 10-1).

10.3.11 Sensitivity Analysis

The relationship between the water-table η and hydraulic conductivity of the Holocene and the Pleistocene layers was investigated by sensitivity analysis (see Table H-2 and Figures H-2 and H-3). Investigated were a wide range of parameter values, including: (a) a K_{PH} of 1000 m d^{-1} and 5000 m d^{-1}, (b) 50% of the base-case K_{HV1}, K_{HV2}, K_{HH1} and K_{HH2}, (c) 200% of the base-case K_{HV1}, K_{HV2}, K_{HH1} and K_{HH2}, and (d) a isotropy ratio of 2:1 for $K_{HH}:K_{HV}$ (see Table H-2).

10.3.12 Results

10.3.12.1 Pseudo Steady-State Groundwater Potentials

The real time required to solve 3 tidal cycles (ie, 37.2 hours) with a back-up of the numerical solution at each time step was 1 hour and 12 minutes. The simulated groundwater potentials reached a pseudo steady-state condition by the completion of the second tidal cycle, as shown in Figure 10-10.
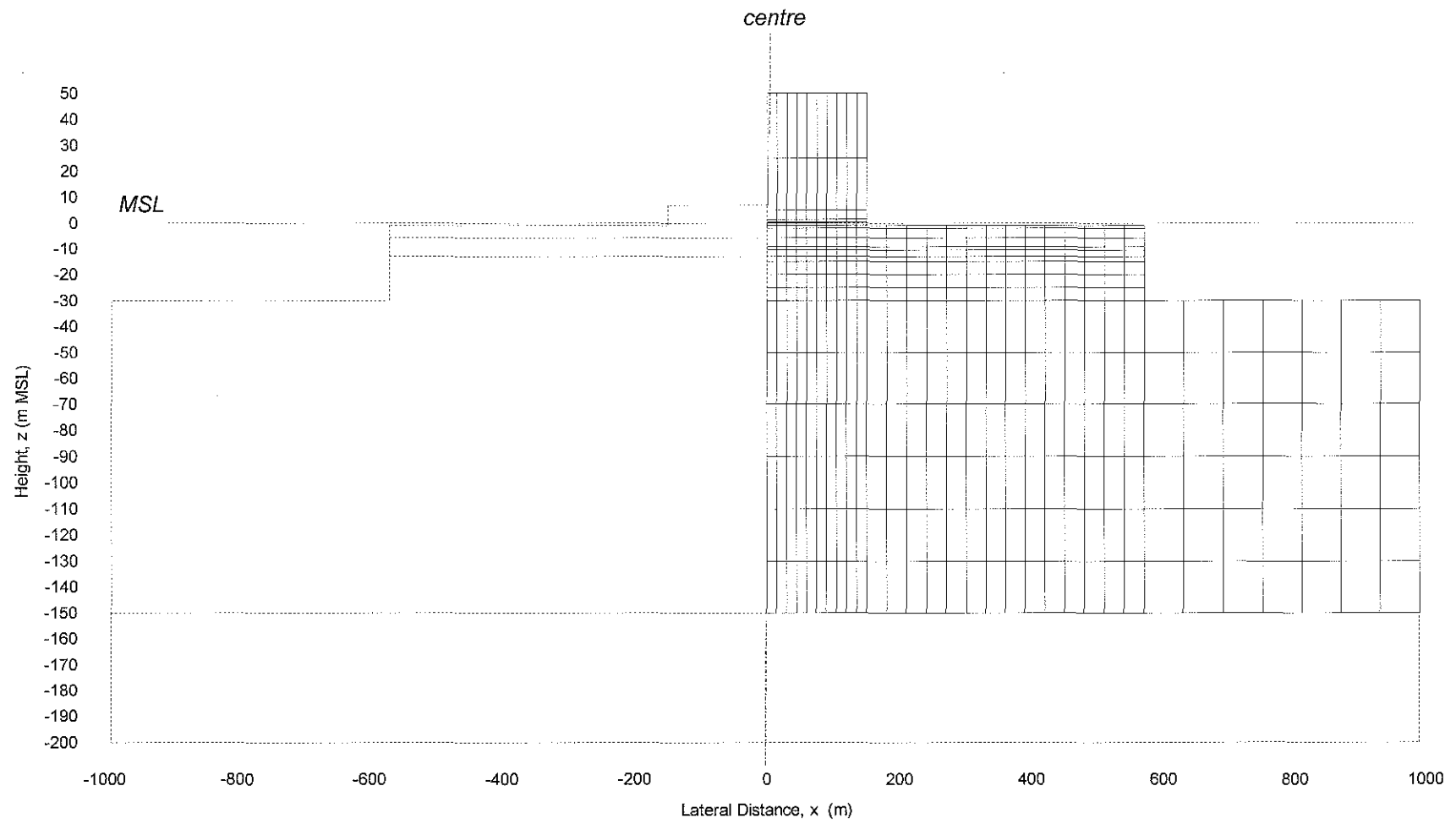
Figure 10-5. Finite-element mesh used in a SUTRA simulation of tidal groundwater flow in the idealised reef-cay model.
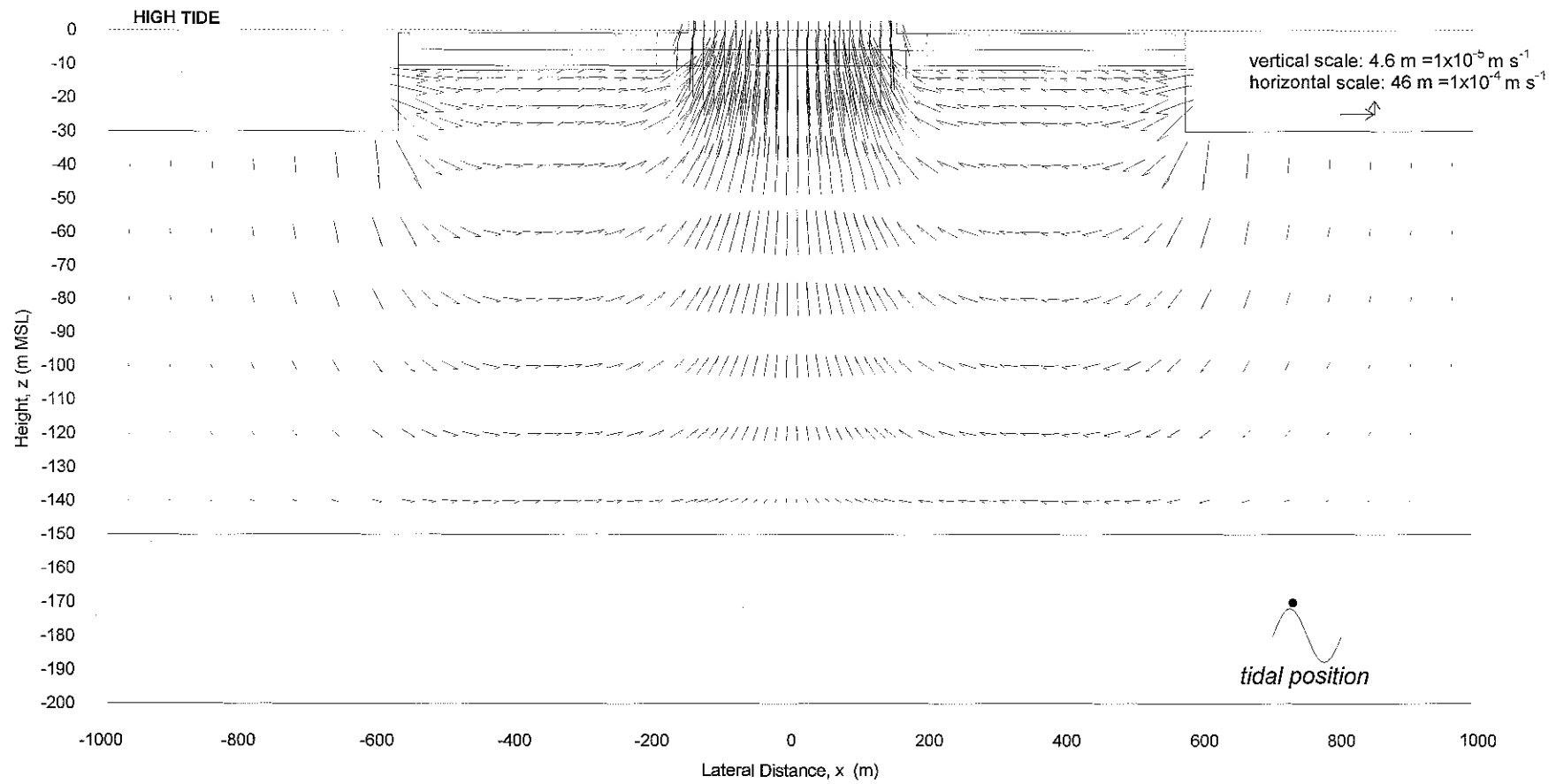
Figure 10-6. Groundwater velocity vectors predicted by SUTRA for each element in the tidal reef-cay groundwater model: results at high tide.
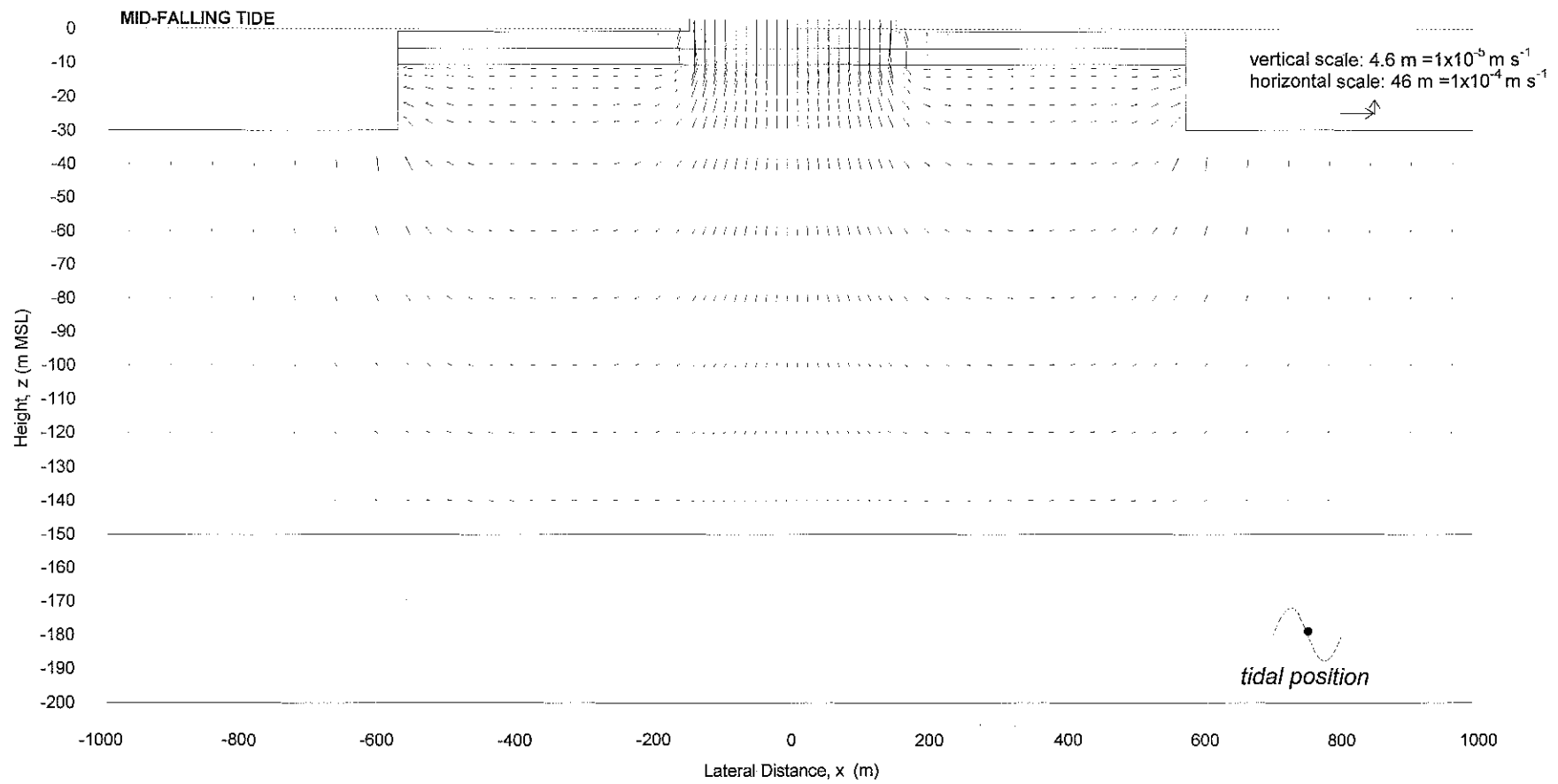
Figure 10-7. Groundwater velocity vectors predicted by SUTRA for each element in the tidal reef-cay groundwater model: results at mid-tide during the fall of the tide.
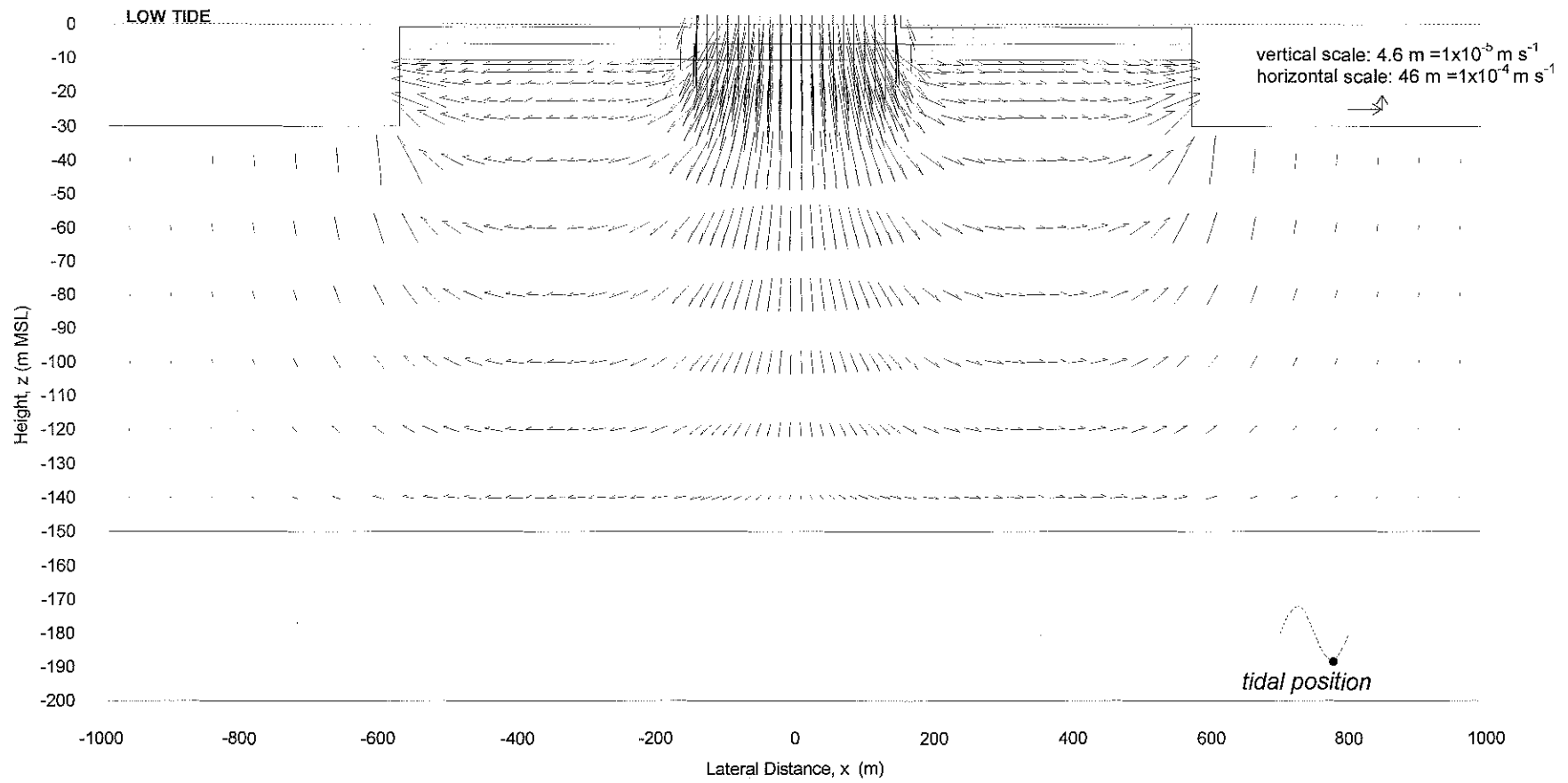
Figure 10-8. Groundwater velocity vectors predicted by SUTRA for each element in the tidal reef-cay groundwater model: results at low tide.
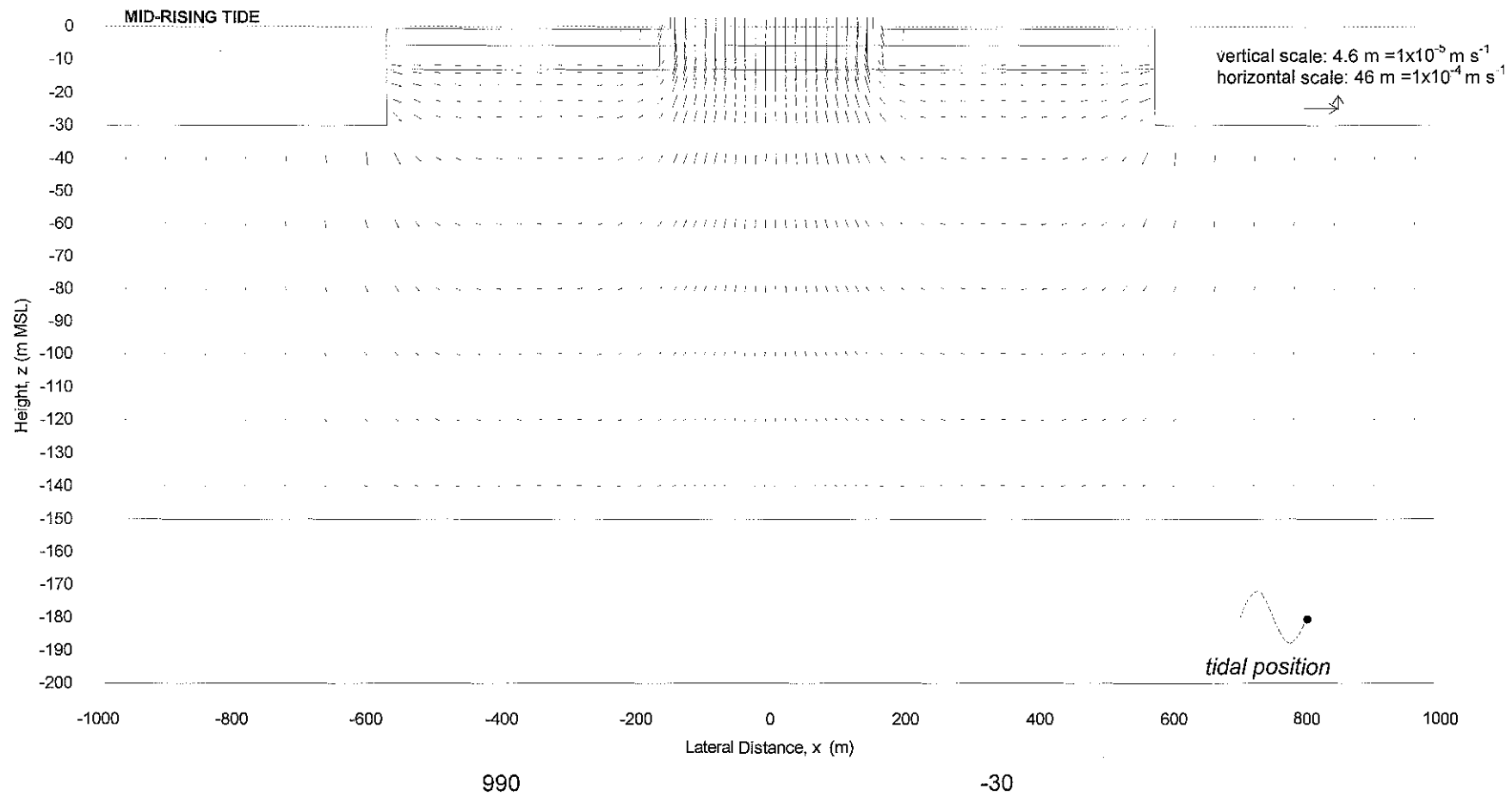
Figure 10-9. Groundwater velocity vectors predicted by SUTRA for each element of the tidal reef-cay groundwater model: results at mid-rising tide.
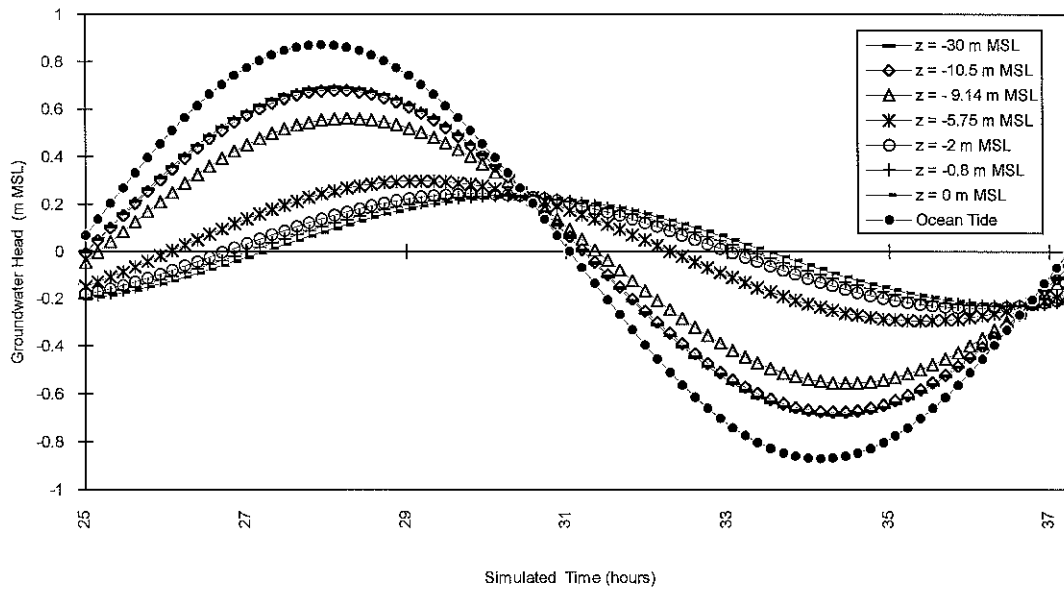
Figure 10-10. Groundwater heads predicted by SUTRA-VEBA for the centre of the tidal reef-cay groundwater model at pseudo steady-state: the results of the base-case simulation with homogeneous fluid.

10.3.12.2 Pseudo Steady-State Groundwater Velocities

The pseudo steady-state groundwater velocities computed at high tide, mid-falling tide, low-tide and mid-rising tide at each element are presented as vectors in Figures 10-6, 10-7, 10-8 and 10-9, respectively. The x-z coordinates of these velocity vectors were computed from the SUTRA output files using a FORTRAN program written by the author. Note that the x- and z- scales of Figures 10-6 to 10-9 differ to allow them to fit on a single page.

10.3.12.3 Tidal Efficiencies and Lags

Tidal efficiencies, η, and tidal lags, γ, at the centre node of the reef-cay model were computed and compared with the time-averaged η and γ observed in the field at well #8 (see Figure 10-12). To give some idea of the uniformity of the water-table response to tidal pumping, the pseudo-steady state η's across the whole cay are presented in Figure 10-11. Notable in Figure 10-11 is that the tidal efficiencies nearest the reef-plate (ie, near the shoreline) are 70% greater than at the centre of the cay suggesting some type of 'edge-effect'.
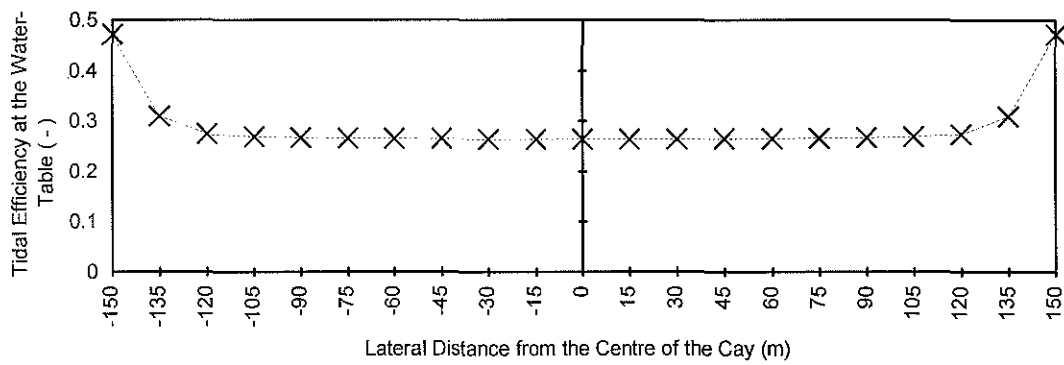
Figure 10-11. Tidal efficiencies at MSL in the base-case tidal reef-cay groundwater model: the results of a SUTRA-VEBA simulation (refer Table 10-1).
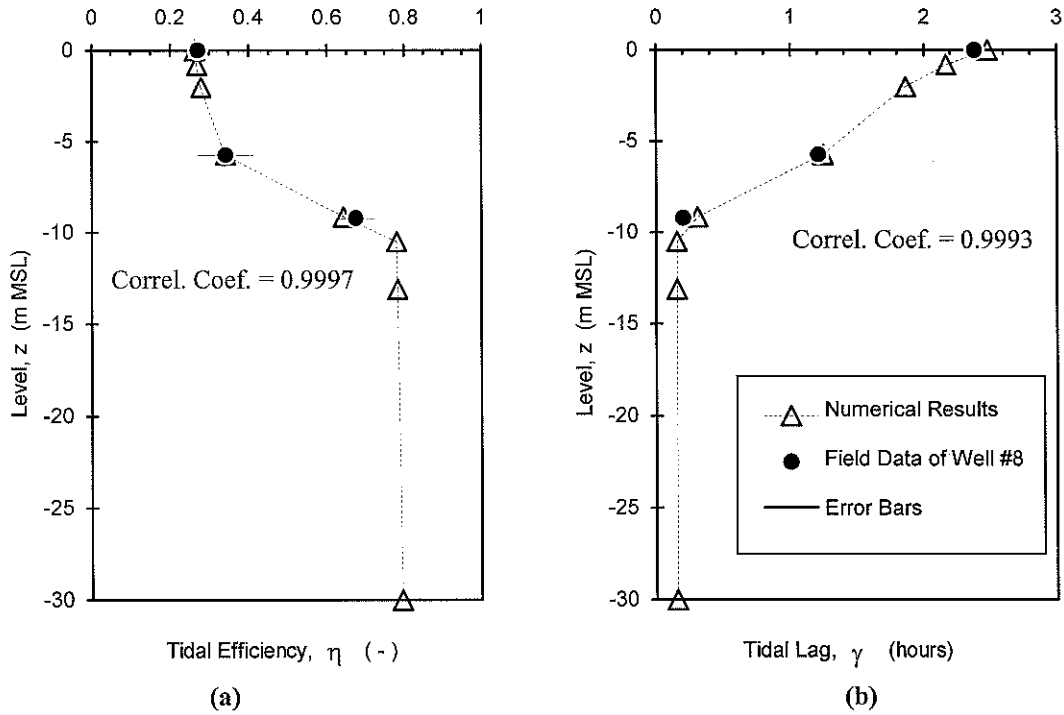
Figure 10-12. The results of the base-case tidal reef-cay groundwater model at pseudo steady-state (refer Table 10-1): (a) tidal efficiencies at centre and (b) tidal lags at centre.
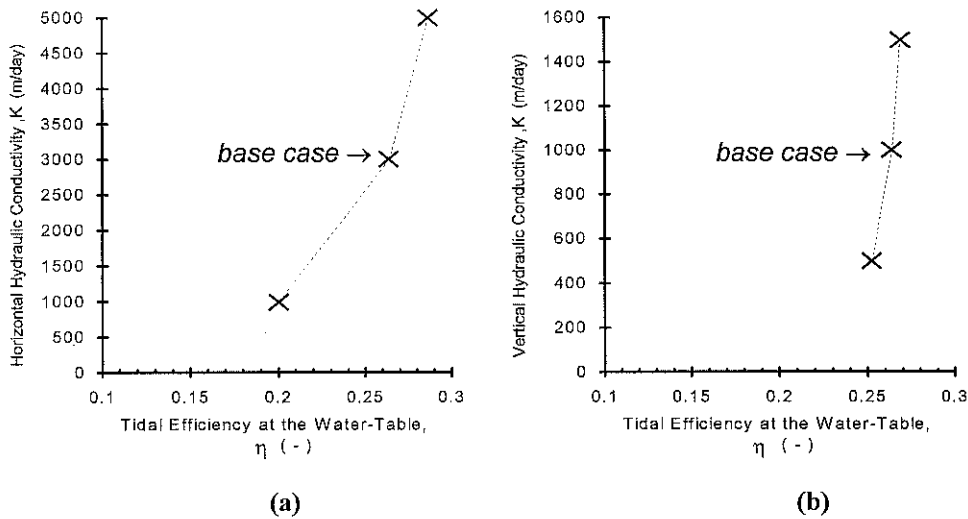
Figure 10-13. Calibration curves for the hydraulic conductivity of the Pleistocene aquifer (refer Table H-2): (a) three different values of K_{PH} with $K_{PV} = 1000$ m d^{-1}, and (b) three different values of K_{PV} with $K_{PH} = 3000$ m d^{-1}.

10.4 GROUNDWATER FLOW IN THE BEACH

Groundwater flow patterns within the beach at Heron Island are potentially complex because of tidal forcing at the beach-face, tidal forcing through the highly conductive Pleistocene aquifer, and structural heterogeneities within the beach due to, for example, discontinuous beachrock and reef-rock. Furthermore, a 'decoupling' of the water-table from the tide (ie, the creation of an exit-point and seepage-face) will occur when and where the water-table at the beach-face falls at a slower rate than the reef-flat tide (see Figure 10-15). To further the interpretations, predictions of the reef-flat tide and exit-point elevations are compared with the potentiometric data that were obtained at the beach at Heron Island (refer wells #11, #12 and #6 in Chapter 8).

10.4.1 Reef-Flat Tide

Gourlay (1995) investigated the reef-flat tide, $h_{reef-flat}\{t\}$, at six points near the western end of Heron Island before and after a harbour bund wall was constructed. Gourlay (1995) found that seawater flow and $h_{reef-flat}\{t\}$ were affected by the ocean tide, the bund wall, and by wind and wave set-up. He also found that the reef-flat tide, $h_{reef-flat}\{t\}$, in the vicinity of Heron Island differed marginally with locality and had a characteristic minimum of 0.7 to 0.9 m LWD (-0.9 to -0.7 m MSL). To simulate the reef-flat tide in this study, the following empirical model was developed:

$$
\begin{aligned}
h_{reef\ flat}\{t\} &= h_{ocean}\{t\} &&: h_{ocean}\{t\} \geq -0.61\,m\,MSL \\
h_{reef\ flat}\{t\} &= -0.61 - 7.2 \times 10^{-6}(t_{sep} - t) &&: h_{ocean}\{t\} < -0.61\,m\,MSL
\end{aligned}
$$

(Equation 10-4)

where t_{sep} is the time when h_{ocean} equals -0.61 m MSL for the most recent tidal half-cycle. The second part of Equation 10-4 was fitted to the data shown in Figure 8-7 and approximates the rather steady fall of the reef-flat tide during tidal separation. Equation 10-4 was used to synthesise reef-flat water levels over a 30 day period (eg, see Figure 10-16 and Table H-3).

10.4.2 Beachrock

Beachrock is found at Heron Island along much of the southern and northern intertidal zone (Coote, 1984; see Figure 1-2). This carbonate rock is consolidated and fissured (Coote, 1984) and so would have behaved as a leaky barrier to groundwater flow. A detailed geological investigation of the beach was beyond the resources of the current study, and so the geomorphology of antecedent beachrock was interpreted from aerial photographs and piezometric responses and is by no means certain (see Section 10.4.4).

10.4.3 Seepage-Face and Exit-Point

Charley et al. (1990) examined seepage-face formation on a few coral cays in the Great Barrier Reef, including Heron Island, Frigate Cay (21° 44' Lat., 152° 25' Long.) and Price Cay (21° 47' Lat., 152° 27' Long.). Charley et al. (1990) found that the seepage-faces, which they called "beach rilling", often formed at low tide. Seepage-faces have been investigated in detail on continental beaches (eg, Nielsen, 1990; Turner, 1993; Aseervatham, 1994), laboratory models (Aseervatham, 1994), and embankments (Dracos, 1963). Dracos (1963) proposed that the top of the seepage-face, called the 'exit point', falls at a terminal velocity (V_{term}) as a consequence of gravity. Dracos (1963) based the following analytical equation for V_{term} upon the dynamics of a falling water particle:

$$V_{term} = -\frac{K}{n}[\sin\beta]^2$$

(Equation 10-5)

where β is the slope of the seepage-face, n is the effective porosity of the sediment and K is the hydraulic conductivity of the sediment. Following the theory of Dracos (1963), Turner (1993) proposed a model similar to the following for the exit-point elevation, $h_{ep}\{t\}$, in a beach as a function of V_{term} and the tide, ie:

$$h_{ep}\{t\} = h_{reef\ flat}\{t\}$$

(Equation 10-6)

when coupled, and

$$h_{ep}\{t\} = h_{ep}\{t_{term}\} + \int_{t_{term}}^{t} V_{term}\{t\} \, dt \qquad \text{(Equation 10-7)}$$

when decoupled, where t_{term} is the time of disconnection during the most recent fall of the tide. The re-coupling of $h_{ep}\{t\}$ with $h_{reef\text{-}flat}\{t\}$ occurs at some time after t_{term} when the tide is rising. Hence, $h_{ep}\{t\}$ at Heron Island will have the same level as the reef-flat tide when coupled and will be higher than the reef-flat tide when decoupled. Turner (1993) applied formulae similar to Equations 10-4, 10-5 and 10-6 to the data of Nielsen (1990) to simulate the exit point positions at North Harbour Beach on the central Queensland coast and at Barrenjoey Beach, Sydney. Turner (1993) found that field observations can be closely matched by the model and that the model results are particularly sensitive to *n* and K.

Average beach slopes at Heron Island were estimated from a 1:2500 scale topographic map (Sunmap, 1979). These beach slopes range between 4-6° along the southern beach, between 3-8° along the eastern beach (Shark Bay), between 6-9° along the northern beach, and between 1.4-6° along the northern shoreline fronting the P&O resort. The north-west corner of the cay is retained at 90° by a concrete wall and therefore has no beach. A hydraulic conductivity in the range of 100-240 m d^{-1} and a porosity of 0.45 were determined for the beach sediments at Heron Island (refer Chapter 5). Using Equations 10-4, 10-5 and 10-6 with a K of 170 m d^{-1}, a *n* of 0.45 and a β of 5°, a 30 day-long synthetic $h_{ep}\{t\}$ record was computed to correspond with the previously mentioned $h_{ocean}\{t\}$ and $h_{ree\text{-}flat}\{t\}$ records (see Figure 10-16 and Table H-3).
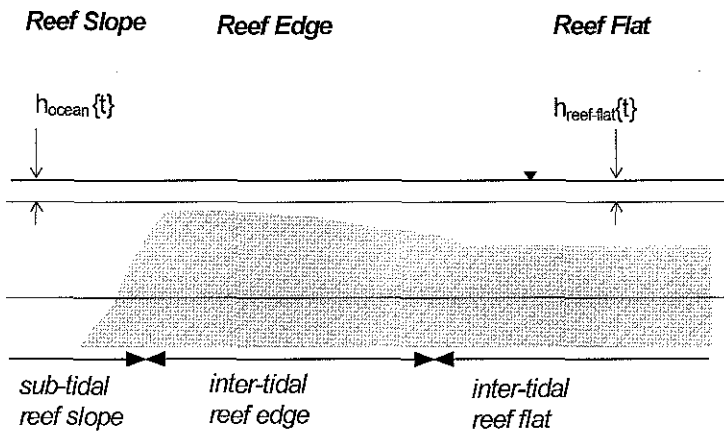
Figure 10-14. Schematic of the ocean tide and the reef-flat tide at Heron Reef (not to scale).
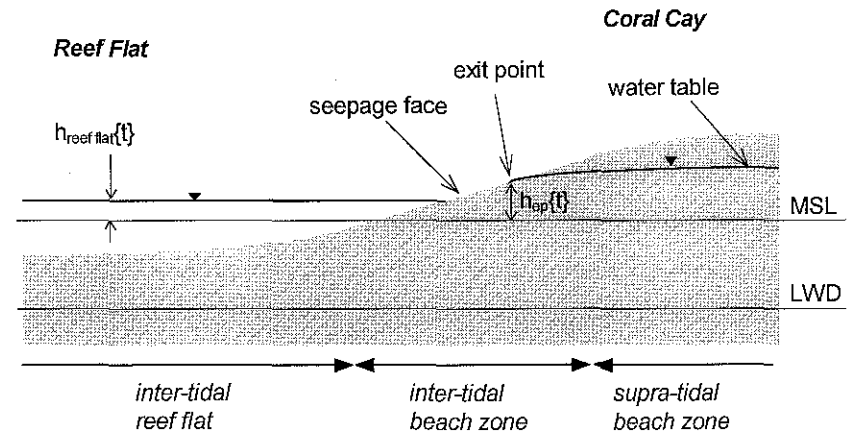
Figure 10-15. Schematic of the reef-flat tide and exit-point position in the beach-face at Heron Island (not to scale).
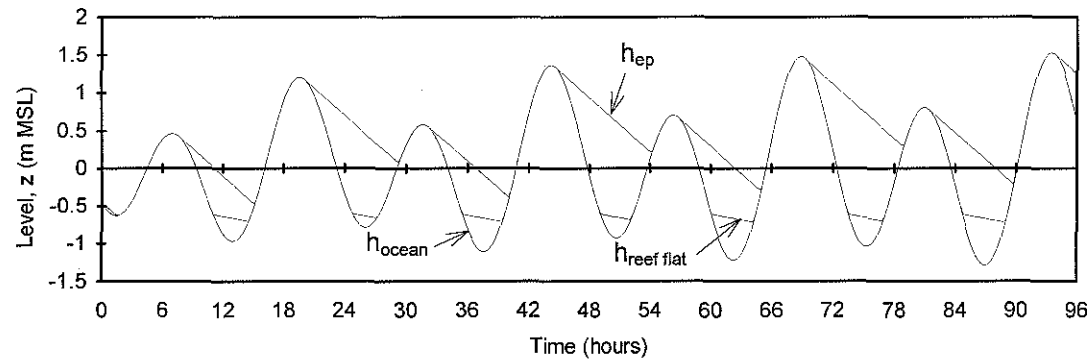
Figure 10-16. An example of the predicted ocean tide (h_{ocean}), predicted reef-flat tide ($h_{reef-flat}$) and the predicted beach exit-point elevation (h_{ep}) for an arbitrary period of time at Heron Island (refer main text for details).

10.4.4 Beach Related Seawater Intrusion

10.4.4.1 The Composite Tidal Signal Hypothesis

It was shown in Chapter 9 that groundwater potentials recorded at well #6 (located on the beach; see Figure 8-1) deviate substantially from those predicted by VTUGF models. In particular, there are asymmetric distortions of the tidal signal in the hydrographs for Piezometers 2 and 4 of well #6 (see D & C in Figure 10-19, respectively). It was also found that the time-averaged groundwater heads recorded near the water-table at well #6 were marginally higher than MSL (see Table F-4).

Urish and Ozbilgin (1989) provide an approximate solution for the effective mean sea level at a sloping beach face at a continental island and claim that the sloping beach face can influence the groundwater flow patterns of barrier beaches and atoll islands. However, the hydrogeology of Heron Island's beach is more complicated than that described by Urish and Ozbilgin (1989) and it is argued that main characteristics of the well #6 hydrographs were caused by (a) tidal-pressures propagating vertically from the Pleistocene, (b) tidal-pressures propagating laterally from the reef -flat, and (c) seepage-face hydrodynamics. For convenience, this hypothesis is called the 'composite tidal signal hypothesis'. Intrinsic to the hypothesis is the presumption that the beach-face is on average less transmissive to discharging groundwater than it is to intruding seawater because of seepage-face formation thus resulting in some mounding of groundwater within the beach.

A 2-dimensional conceptual hydrogeological model for the beach at well #6 is proposed (see Figure 10-17a). The model was inferred from the stratigraphic summary presented in Chapter 1 and the well survey data of Noordink et al. (1992) (refer Figure 8-2). The geomorphology of the subsurface beachrock was assumed from aerial photographs (Sunmap, 1979) and is not known accurately. An important feature of the model is that a hydraulic conduit for seawater intrusion is provided by the unconsolidated beach sediments between the shoreline and well #6 (see Figure 10-17a).

(a)

(b)

(c)
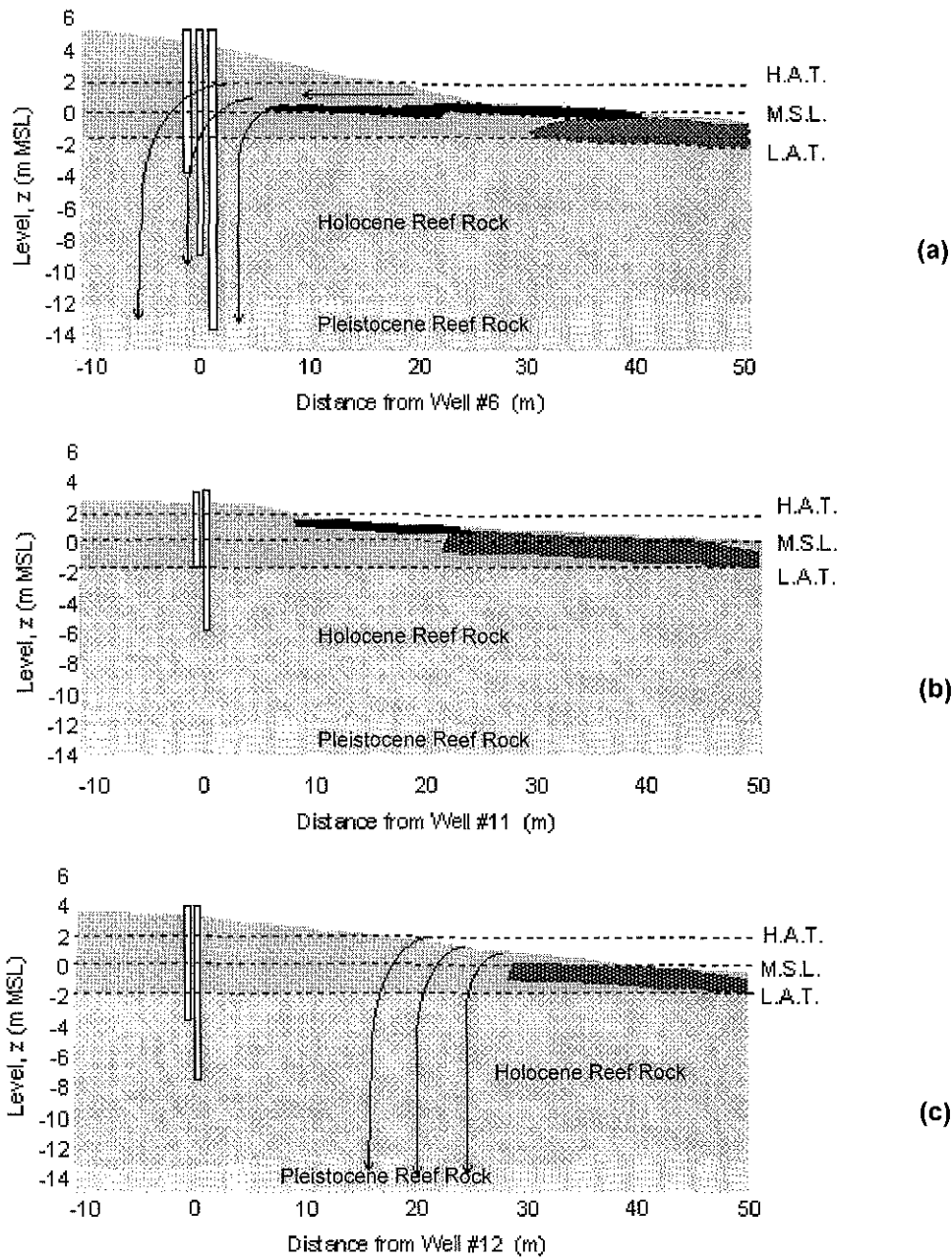
Figure 10-17. A preliminary conceptual hydrogeological model for the beach at Heron Island: (a) near well #6 (arrows indicate net seawater intrusion and seepage face present), (b) near well #11 (seepage-face prevented by beachrock), and (c) near well #12 (arrows indicate net seawater intrusion and seepage-face present).

Legend

unconsolidated coralline sediment (permeable)	reef-plate (impermeable)	beachrock (impermeable)	piezometer	net flow after tidal effects averaged out
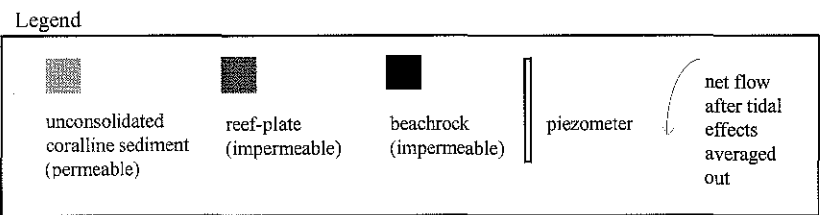
Qualitative similarities between the hydrograph for the exit-point and the water-table at well #6 (see B and C in Figure 10-18, respectively) and qualitative similarities between the hydrographs for Piezo. 1 of well #6 and the ocean tide (see E and A in Figure 10-19, respectively) are the main evidence supporting the composite tidal signal hypothesis. The exit-point hydrograph is 'saw-tooth' shaped and has a time-averaged level higher than MSL. Also evident in Figure 10-19 is that tidal-pressure signals recorded at Piezo's 1 and 2 of well #6 (see E and D in Figure 10-19, respectively) are qualitatively and quantitatively more similar to the ocean tide than is the tidal-pressure signal at the water-table.

It is believed that the ocean tide (A in Figure 10-19; refer Chapter 8) is the main driving force for the groundwater potentials at well #6 (C, D & E in Figure 10-1) however it also appears that shallow groundwater (C in Figure 10-18) was affected by the seepage-face (and exit-point) for the same period (B in Figure 10-18).

10.4.4.2 An Estimate of Daily Net Vertical Seawater Intrusion

For the purpose of investigating possible seawater intrusion through the beach at well #6, the groundwater potentials (at well #6), ocean potentials and predicted exit-point potentials were filtered in the daily and semi-daily frequency range (see Figure 10-20). The filtering of the data was done with a moving 25 hour window over a 29 day sample period using a technique described by Serfes (1991). The raw field data are described in Chapter 8.

As shown in Figure 10-20, the filtered $h_{ep}\{t\}$ for the 29 day period are greatest during the spring tide, when the tidal range is greatest, and are least during the neap tide, when the tidal range is least. In accordance with the composite tidal signal hypothesis, the filtered water-table hydrograph (see C in Figure 10-20) is qualitatively and quantitatively more similar to the filtered $h_{ep}\{t\}$ hydrograph than it is to the filtered hydrograph for the ocean tide (see B & A, respectively, in Figure 10-20), whilst groundwater potentials at Piezo. 1 of well #6 (see E in Figure 10-20) are more similar to the filtered ocean tide.

LEGEND

A. Ocean tide.
B. Predicted exit-point at the shoreline (Equations 10-5, 10-6 & 10-7; $\beta = 5°$, $K = 170$ m d^{-1}, $n = 0.45$).
C. Water-table 25±5 m inland from the shoreline (Piezo. 4, well #6).
D. Groundwater heads 9.14 m below C. (Piezo. 2, well #6).
E. Groundwater heads 13.09 m below C. (Piezo. 1, well #6).
F. Empirical reef-flat tide (Equation 10-4).
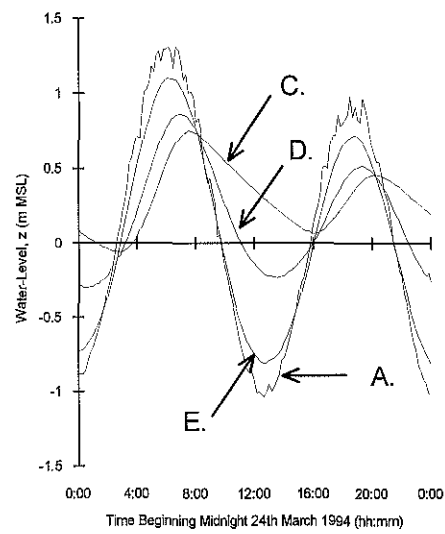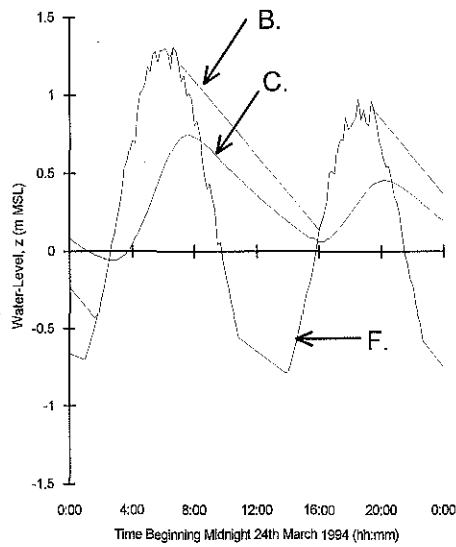
Figure 10-18. A comparison of hydrographs for groundwater and seawater at or near the beach: (B) the predicted exit-point and water-table elevation at the beach-face; (C) water-table position at well #6; and (F) approximate reef-flat tide.

Figure 10-19. A comparison of hydrographs for groundwater and seawater at or near the beach: (A) the ocean tide; and (C, D and E.) groundwater potentials recorded at well #6.

When the groundwater potentials at well #6 are filtered, it becomes apparent that time-averaged groundwater potentials reduced with depth in the Holocene aquifer and approached 0 m MSL near the top of the Holocene-Pleistocene contact (see E in Figure 10-20). Consequently the time-averaged hydraulic gradient would have forced groundwater to flow from the top of the Holocene aquifer to the Pleistocene aquifer. It is believed that the cause of the hydraulic gradient and source of the intruding fluid was seawater intrusion through the beach. The interpreted seawater intrusion process is believed to result from the previously mentioned 'composite tidal signal': ie, one tidal signal originating at the beach seepage-face and the other rising upwards from the highly conductive Pleistocene aquifer.

Groundwater potentials recorded at Well #11 (located 15 m from the shoreline) and at well #12 (located 25 m from the shoreline) are presented in Figures 8-13 and 8-14, respectively. In contrast to the situation at well #6, the groundwater potentials recorded at wells #11 and #12 do not demonstrate the asymmetric distortions found at well #6 and predicted by the seepage-face model. A plausible hypothesis for this inconsistency is given in the form of the two-dimensional conceptual hydrogeological models depicted in Figure 10-17. It is hypothesised in Figure 10-17b that little or no seawater intruded the aquifer near well #11 because beachrock covered most of the inter-tidal zone and prevented the formation of a seepage face at low tide. In Figure 10-17c, it is hypothesised that seawater intruded the aquifer at the shoreline, but was too distant from well #12 to be detected in the hydrographs for that well.

Given that unconsolidated sandy beaches constitute about 50% ($\approx$1 km) of the shoreline at Heron Island, it is possible that seawater intrusion could have been a wide-spread occurrence. An order-of-magnitude estimate of seawater intrusion was obtained from a simple model based on Figure 10-17c and average predicted exit-point elevations for a hypothetical section of beach (see Figure 10-21). The model assumes a beach slope of 5° (typical at Heron Island; see Table H-3), an average vertical conductivity of 15.4 m day^{-1} (the harmonic mean of all K_{HV} values determined in Chapter 9), a 15 m deep Holocene layer (refer Chapter 1), and an average groundwater potential of 0 m MSL in the Pleistocene aquifer.

LEGEND

A. The ocean tide.
B. The predicted exit-point near well #6 (Equations 10-4, 10-5 & 10-6,; β = 5°, K = 170 m d⁻¹, n = 0.45).
C. The water-table 35±5 m inland from the shoreline (Piezo. 4, well #6).
D. Groundwater heads 9.14 m below C. (Piezo. 2, well #6).
E. Groundwater heads 13.09 m below C. (Piezo. 1, well #6).
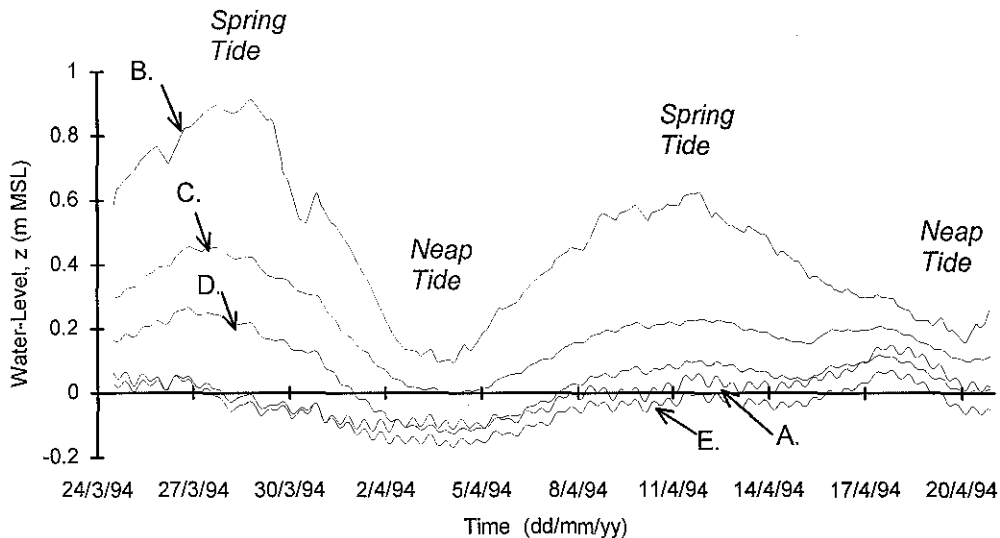
Figure 10-20. Filtered groundwater potentials in the beach at Heron Island (refer legend and main text).

The average predicted exit-point level (see B in Figure 10-21) is 0.40 m MSL, and is believed to be typical for the island (see Table H-3). The model assumes an intrusion width, X, of 5.9 m which is equal to one-half of the predicted average tidal reach (see Table H-3 & Figure 10-21). The computed average flow rate per metre length of coastline was computed from Darcy's law (Equation 9-9) to arrive at a value of 2.4 m³ d⁻¹ (see Table H-4). This corresponds to 2 400 m³ d⁻¹ for 1 km of shoreline: hence an order-of-magnitude estimate of seawater intrusion at Heron Island is 1×10^3 m³ d⁻¹.
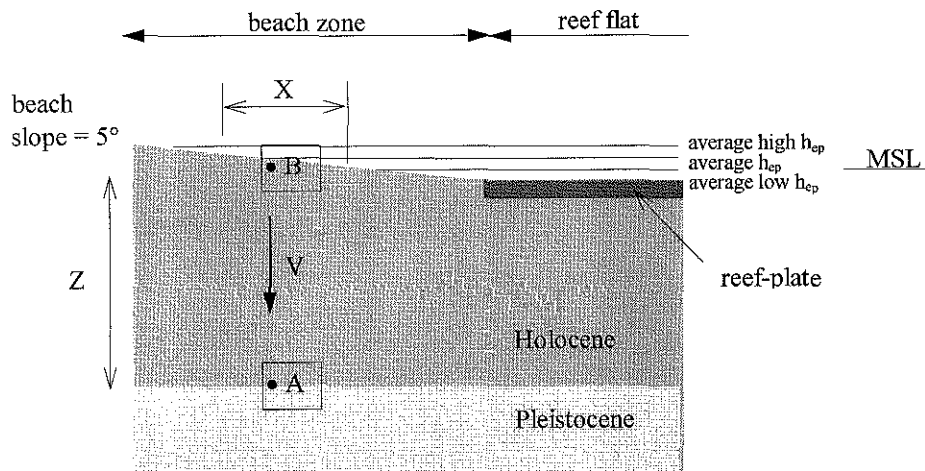
Figure 10-21. A conceptual model for the estimation of net seawater intrusion through the shoreline: (X) width of idealised intrusion surface, (Z) thickness of the Holocene layer, (V) average intrusion speed.

10.5 DISCUSSION

10.5.1 The Tidal Reef-Cay Groundwater Model

A conceptual hydrogeological model for Heron Island and Reef was presented and validated in two-dimensions by finite-element simulations of short-term tidal groundwater movement. The conceptual model is based on the dual-aquifer concept for atoll islands in combination with other geologic interpretations and assumptions; including an impermeable reef-flat (as a consequence of supposed reef-plate capping), permeable reef-slopes and ocean floor, and impermeable sedimentary foundation.

The numeric model, which was developed from a general purpose program called SUTRA (Voss, 1984), closely reproduced the time-averaged tidal efficiencies (η) and lags (γ) that were observed at a central location at Heron Island (ie, at well #8; see Figure 10-12). By reproducing these η and γ values, the model illustrates a broad-scale mechanism by which the ocean tide could have forced groundwater flow through the reef-cay structure. Whilst the observed and simulated values of η and γ are very similar, this result does not imply that the whole model is accurate. It is believed that the simulated vertical tidal unconfined groundwater flow (VTUGF) was amenable to

precise calibration, despite the approximate nature of the model, because η and γ are controlled primarily by (a) the characteristic angle, ω, of the Holocene region which was pre-determined in Chapter 9, and (b) the strength and timing of the simulated tidal signal at the Holocene-Pleistocene contact which was adjusted by trial-and-error calibration (a procedure that, by choice, only involved the permeability tensor of the Pleistocene aquifer).

The model provides a rough approximation of the actual large-scale tidal groundwater movement and demonstrates in basic terms how VTUGF could have evolved within the surficial aquifer (see Figures 10-6 to 10-9). From the simulation results it would also appear that the groundwater flow at Heron Reef has the following features:

(i)   tidal flow within the Pleistocene portion of the reef platform was predominantly horizontal,

(ii)   significant seawater/groundwater exchange occurred across the reef slope and ocean floor, with the later decreasing in magnitude with distance from the reef,

(iii) flow within the confined portion of the Holocene layer (ie, beneath the reef-flat) was minimal compared with flow in the Pleistocene layer and unconfined portion of the Holocene layer.

(iv)   maximum tidal flow speeds occurred beneath the cay at about high and low tide, and

(v)   in the unconfined region, the tidal flow was greater near the edge of the reef-plate capping.

In respect to (v) above, the greatest water-table η (simulated) in the surficial aquifer occurred near the edge of the reef-plate (see Figure 10-11). Although there is relatively scant field data from which to compare this particular result, it appears that significantly higher water-table η did occur near the shoreline (see well #11 in Figures 8-22). This could have been caused by greater fluid pressurisation associated with discontinuous reef-plate and/or beachrock near well #11: as suggested by the model. However, this type of tidal signal enhancement and lateral propagation were not calibrated in the current model. Further theoretical research is required to formally

describe the hydrodynamics of tidal signals passing around discontinuous confinement, to calibrate the current model for such phenomena, and to confirm the current interpretations.

The current model relies on a Pleistocene horizontal hydraulic conductivity (K_{PH}) in the order of 3000 m d^{-1} and vertical hydraulic conductivity (K_{PV}) in the order of 1000 m d^{-1} to provide the necessary tidal signal conductance between the ocean and the surficial aquifer (refer Table H-2). These values are typical of atoll island aquifers (eg, Herman, Buddemeier & Weatcraft, 1986; Oberdorfer, Hogan & Buddemeier, 1990; Underwood, Peterson & Voss, 1992; Griggs & Peterson, 1993). The relevant calibration curves show that the simulated tidal signal at the water-table is rather insensitive to K_{PH} and K_{PV} over the range of values examined (see Figure 10-13). This suggests that K_{PH} and K_{PV} may be prone to inaccurate calibration. Figure 10-13 also shows that K_{PH} is more critical to the model than is K_{PV} (at least for the range of values examined). This is probably because tidal signals in the Pleistocene have much further to travel in the horizontal dimension compared to the vertical dimension and so are likely to be more sensitive to K_{PH} than to K_{PV}.

The sensitivity analysis shows that the simulated groundwater response were rather insensitive to the isotropy and K_{HH} of the Holocene aquifer (see Table H-2). This result is not surprising given that the simulations produced vertical or near-vertical flow in the unconfined Holocene aquifer. For this reason, K_{HV} may also be prone to inaccurate calibration.

The current mathematical model of tidal groundwater hydraulics at Heron Reef may be refined and improved by investigating: (a) beach related seawater intrusion and discontinuous confinement by reef-plate and beach-rock; (b) groundwater flow through the terrigenous sand foundation (which was assumed impermeable in the current study); (c) possible heterogeneity of the Holocene and Pleistocene regions and its effect on tidal signals; and (d) aquifer geometry and groundwater flow in three-dimensions.

10.5.2 Beach Related Seawater Intrusion

This chapter provides conceptual hydrogeological models for three sections of Heron Island's shoreline (see Figure 10-17) and an order-of-magnitude estimate of the total seawater intrusion flow rate at Heron Island (ie, 1×10^3 m^3 d^{-1}). The conceptual models describe a seawater intrusion process that results from a combination of (1) dual-aquifer tidal groundwater flow [after Buddemeier & Holloday (1977)] and (2) seepage-face flow [after Dracos (1963), Urish & Ozbiligin, 1989 and Turner (1993)]. The models ignore fluid pressurization by reef-plate and/or beachrock as a simplifying assumption.

An order-of-magnitude seawater intrusion rate of 1×10^3 m^3 d^{-1} was estimated for Heron Island from the mean theoretical exit-point level (refer Table H-3) which is generally higher than the mean groundwater potentials that occurred within the Holocene aquifer: hence a net downward flow of groundwater had occurred (see Table H-3). Theoretical exit-point levels are related to the beach slope (β) and the permeability and porosity of the beach sediment. The 1×10^3 m^3 d^{-1} seawater intrusion rate for Heron Island is only a rough guide because of conceptual uncertainties and gross simplifications made. None-the-less, it appears that net seawater intrusion could be of the same order-of-magnitude as (and possibly larger than) the total average rainfall for the cay: the cay's mean annual rainfall (1.03 m year^{-1}) when multiplied by the cay's surface area (0.2 km^2) gives a total flow rate of 550 m^3 day^{-1}. Seawater intrusion of this magnitude would greatly affect groundwater movement and chemistry near the shoreline and is much greater and more regular than the predicted natural recharge for the island (which is expected to be <25% of rainfall in the long-term; refer Chapter 6). Further research is needed to quantify with confidence the long-term seawater intrusion rate at Heron Island.

Although Figures 10-17 and 10-21 are a considerable improvement on previous hydrogeological interpretations regarding Heron Island's shoreline, they should be considered with care due to the sparsity of the field data and the possibility that some geomorphological features of the shoreline were mis-interpreted or omitted.

11. OVERVIEW AND CONCLUDING REMARKS

11.1 INTRODUCTION

The main objective of the current study was to provide a reliable hydrodynamic description of Heron Island's vadose and phreatic zones. Examined in detail, and the main focus of the study, were natural recharge and tidal groundwater hydraulics as these processes were thought to have a significant affect on groundwater movement, geochemistry and nutrient dynamics at the island-scale, but were poorly understood previous to the current study.

The interpretations and conclusions provided herein were arrived at by integrating literature information, new field data and the simulation results of a number of mathematical models. Key achievements of this thesis are the development of conceptual and mathematical models for simulating natural recharge (Part I) and tidal groundwater flow (Part II) at Heron Island. The main findings of the thesis are summarised below, together with implications for nutrient transport and future research directions.

11.2 HYDROLOGY (PART I)

Rainfall at Heron Island averages at a moderate 1069 mm a^{-1} but is seasonal and highly variable mainly as a result of tropical storms and cyclones which are most frequent between the months of January and July (refer Table A-2). The estimated hydrologic balance (see Table 2-1) suggests that less than 25% of rainfall becomes natural recharge. The cay is topographically low-lying and has a two-to-six metre deep vadose zone comprised of medium- to coarse-grained sediment; as such it might be expected that meteoric water would readily percolate through the soil and produce a groundwater recharge regime strongly coupled to rainfall. However, empirical methods used in this study have shown this is not the case. The dynamics and magnitude of natural recharge were established through a series of tensiometric and

other experiments, and the development and application of a Soil-Water Transport and Evapotranspiration Model (STEM).

11.2.1 Natural Recharge Simulations and Interpretations

The vadose zone was shown to have two major hydrostratigraphic layers: (1) the silty-sand layer and (2) the gravelly-sand layer. The silty-sand layer was typically 1 m thick and contained organic material and the rooting zone of *Pisonia grandis*. The underlying 1 to 5 m thick gravelly-sand layer extends down to the inter-tidal zone which consists of a mixture of sand-, gravel- and shingle-sized sediment and brackish groundwater.

Tensiometric field investigations conducted in the forest at Heron Island over a ten month period in 1994 show that rainwater infiltration and wetting-front propagation occurred over a time-scale of hours during tropical downpours. However, the redistribution of soil-water was relatively slow and appreciable deep drainage usually took weeks or months (refer Figures 3-11 to 3-13).

Laboratory experiments described in Chapter 4 showed that, for a given matric potential, the silty-sand layer has greater water retentivity and lower permeability than the gravelly-sand. When the moisture content of gravelly-sand falls below a 'critical' moisture content of 0.10-0.20 ml ml^{-1}, the matric potential rises rapidly and the unsaturated hydraulic conductivity decreases dramatically because pore-water inter-connectivity is severely limited. This leads to the phenomenon described above, and as such a large proportion of soil-water is effectively retained by the vadose zone and made available to plant roots for transpiration.

A model - the Soil-Water Transport and Evapotranspiration Model (STEM) - was developed to simulate soil-water dynamics, natural recharge and the field-water balance at Heron Island. STEM simulations indicate that major recharge events only occur when there is very intense rainfall of around 100 mm per week or more; such events are infrequent, occurring less than once per year on average (see Figure 6-4). Groundwater recharge events were shown to be characterised by early peak flows

followed by an exponential decay of flow over a period of many months (refer Figure 6-4). As such, the relationship between rainfall and natural recharge is highly non-linear and there is considerable variation in the annual hydrologic balance (see Table 6-3). A mean annual recharge estimate of 230 mm a^{-1} (1985-94) was provided by the base-case STEM model. Independent empirical estimates support this result, including the rainfall-recharge relationship for small low islands established by Falkland (1991) (refer Figure 2-4) and the empirical estimate found using Nullet's (1987) method (i.e., ≤ 250 mm a^{-1}; refer Table 2-1).

A sensitivity analysis with STEM indicates that the four most critical parameters effecting the long-term recharge simulations were (refer Table 6-3 and Figure 6-5)

- daily rainfall rate (measured);
- average daily evapotranspiration rate (approximated by model calibration);
- hydraulic conductivity function of the uppermost silty-sand layer (experimentally derived); and
- daily surface runoff rate (assumed in this study).

Surface runoff is a factor which probably leads to spatial variations in groundwater recharge and a reduced net recharge rate for the cay as a whole. Analysis of tensiometric field data showed that overland flow at the study site was significant during the heavier rainfall events of 1994 (see Figure 5-3). The lateral movement of minor surface water was probably inhibited by the low-lying topography, vegetation, leaf litter and the ground burrows created by wedgetail shearwaters (*Puffinus pacificus*).
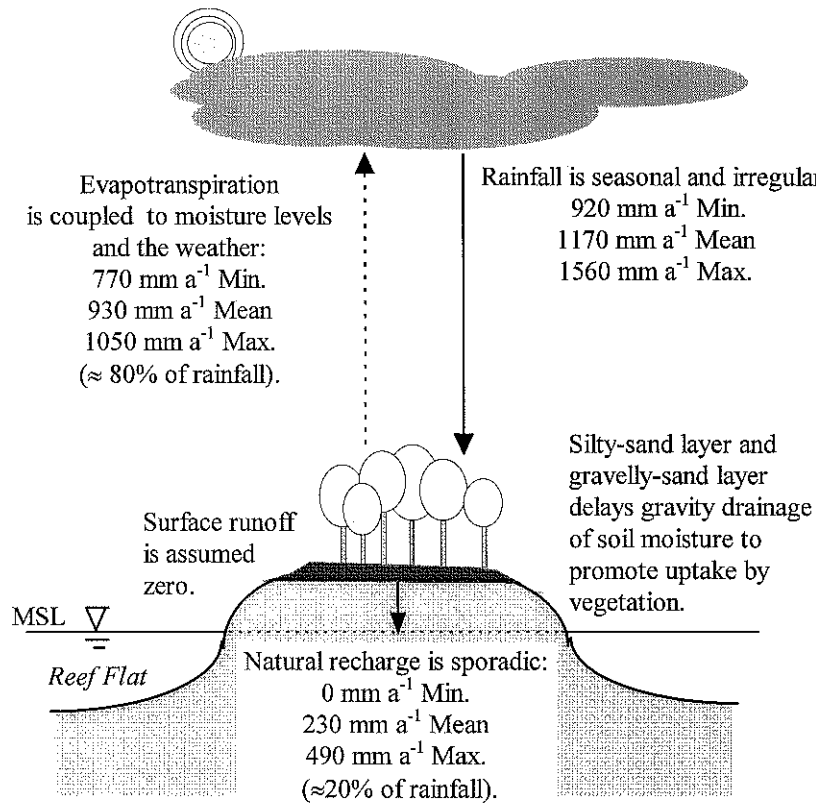
Figure 11-1. The approximate hydrologic balance of Heron Island as simulated by the base-case STEM model: minimum, mean and maximum annual values for the period 1985-1994 (refer Chapter 6).

In summary, tropical downpours at Heron Island with an intensity of about 100 mm per week or more will result in a rapidly moving wetting front and appreciable groundwater recharge. Ponding and possibly surface flow will also occur. STEM simulations suggest that the hypothetical removal of all ponded water could reduce recharge by as much as 30% (see Table 6-3). Hence there exists a significant capacity for lateral variations in natural recharge if ponded water were prone to lateral movement. The net influence of overland flow on the cay's hydrologic balance was not investigated but is probably small.

STEM was able to closely simulate soil-water potentials observed in the field over a wide-range of time-scales using only daily throughfall as the driving variable (refer Figure 6-3). As such, it should be useful for further more detailed studies of the vadose zone. However, such studies need to be cognoscente of the model's main limitations: (a) field calibration against actual groundwater recharge events was not

done; (b) the model does not consider some processes which could be important in more detailed studies (e.g., capillary hysteresis, seasonal variations in forest foliage and evapotranspiration, the effect of different vegetation types, and surface water movement) and (c) the model does not consider anthropogenic influences.

11.3 HYDROGEOLOGY

The large-scale hydrogeology of Heron Island and Reef was interpreted from a combination of geologic information, piezometric data, tidal data, and mathematical models. The developed model uses the 'dual-aquifer' concept first proposed by Buddemeier and Holladay (1977) for Enjebi Island at Enewetak Atoll; this implies a moderately permeable upper region of Holocene-age limestone underlain by a highly permeable lower region of Pleistocene-age limestone. These types of aquifers typically involve a strong component of tidally affected groundwater movement (eg, Underwood, Peterson and Voss, 1992).

At Heron Reef the Holocene-age aquifer extends to a depth of about -15 m MSL and is comprised of porous and poorly consolidated reef rock and unconsolidated sands, gravels and silts. The Pleistocene-age aquifer extends to a depth of about -150 m MSL and is comprised mainly of karst reef rock (refer Section 1.4). The karst features of Pleistocene aquifer are a result of subareal erosion during periods of eustatic regression (eg, Vacher, 1978; Hopely, 1982). Both the Holocene-age and the Pleistocene-age aquifers are structurally heterogeneous as a result of biogeochemical and geological processes particular to coral reefs (refer Chapter 1).

The conceptual model for Heron reef also incorporates the following important features:

(i)   unconfined water-table within the surficial aquifer;

(ii)   impermeable reef-plate capping (a layer of cemented material which is believed to underlie most of the reef-flat surface);

(iii)   permeable reef-slopes and ocean floor (it is assumed that these surfaces have the similar permeability as their parent material);

(iv)   a foundation of relatively impermeable terrigenous sand below about -150 m MSL (ie, relatively impermeability compared to reef-rock); and

(v)   impermeable exposed and antecedent beach-rock in certain sections of the cay's shoreline.

The following evidence was felt to indicate the existence of an impermeable reef-plate capping over the reef-flat:

- the hydrodynamics of the reef is such that a significant depth of seawater is retained on the reef-flat when the sea level falls below the reef rim, and this seawater slowly discharges at a rate which is not tide-related (i.e. suggesting that the principal discharge point is over the reef rim rather than through the reef flat); and

- during low tide, the tidal signals within the island aquifer were related to ocean tides and not the seawater level on the reef-flat.

11.3.1 Large-Scale Tidal Groundwater Flow

During the sampling period, the mean groundwater speeds of between 3.4×10^{-5} m s^{-1} (well #6) and 8.8×10^{-5} m s^{-1} (well #11) occurred at Heron Island as a result of tidal pumping. These are three-to-four orders of magnitude more rapid than the average groundwater recharge rate predicted by empirical methods and STEM ($<8.5 \times 10^{-9}$ m s^{-1} on an annualised basis). Mean observed groundwater speeds are also two orders of magnitude more rapid than peak recharge speeds predicted by STEM (e.g. 3.8×10^{-7} m s^{-1} over 4 days in April 1990 and 1.7×10^{-7} m s^{-1} over 10 days in March 1992; refer Figure 6-6). Hence tidal effects are by far the dominant influence on groundwater flow dynamics at Heron Island.

The measured tidal pressure signals in the groundwater were characterised by an increase in efficiency and a decrease in lag with depth. Extrapolation of the measured

trends down to the Holocene-Pleistocene contact (at about -15 m LWD) showed that large efficiencies (>80%) and small lags (effectively 0 hr) occur there, thus the Pleistocene-age aquifer is the main transmitter of tidal-pressure oscillations to the Holocene-age aquifer. Such a regime of tidal signal propagation is consistent with the dual-aquifer concept and the hypothesis of vertical tidal unconfined groundwater flow (VTUGF) within the surficial aquifer.

The tidal efficiency and lag characteristics measured at field piezometers were interpreted using analytical models to provide estimates of aquifer properties (see Appendix G). The analytical approximations to VTUGF (refer Chapter 9) give tidal efficiency at the water-table (η) and tidal lag at the water-table (γ) as a function of the tidal signal at depth, hydraulic conductivity (K), specific yield (S_y), aquifer thickness (L) and tidal frequency (ω) (see Equations 9-32 & 9-33). Relating these parameters into a single relationship is the characteristic angle, ϖ (see Equation 9-51), which is similar to the dimensionless Fourier number for transient fluid flow in porous media. The derivation and application of these VTUGF analytics is a unique aspect of this study, and offers a more straightforward method of estimating the average vertical hydraulic diffusivity from groundwater piezometric records than numerical approaches.

The VTUGF analysis showed that the damping of the tidal signal by the Holocene aquifer is a function of each of the harmonic components of the tide as well as aquifer properties (Equation 9-33). The superposition of the various out-of-phase astronomical frequencies (lunar, solar, etc.) results in temporal variations in η and γ which were measured in the field to be as large as $\pm10\%$ (absolute) and ±1 hour, respectively. At most of the piezometers that were monitored, η and the diurnal inequality of the tide were strongly correlated.

VTUGF theory proves that an unconfined dual-aquifer system behaves as a 'low-pass filter' to tidal signals as a consequence of the time-dependency of Darcian fluid flow. This is illustrated in Figure 9-20 for well #8 in terms of transmission of the solar-year component of the tide (this is almost entirely transmitted to the water-table), the

barometric, diurnal and semi-diurnal components of the tide (these are partially filtered), and surface waves (these are essentailly filtered out). The term 'low-pass filter' was previously used by Lam (1974) to describe the hydraulic resistance of an atoll island's (Swains Island) aquifer to tidal groundwater flow. Lam's analysis relies only on beachrock capping and so could not be used to explain the groundwater hydraulics at Heron Island where vertical variations in aquifer permeability are vital to the timing and amplitude of the groundwater tide.

11.3.1.1 *Hydraulic Diffusivity Estimates*

The VTUGF analytics were used to estimate the vertical hydraulic diffusivity (K_{HV}/S_y) of the Holocene-age aquifer (expressed in terms of vertical hydraulic conductivities, K_{HV}, assuming a specific yield, S_y, of 0.30 - see Figure 9-17). The harmonic-mean value of all of the K_{HV} estimates is 15.4 m d^{-1} (N=10), with maximum and minimum estimates of 80±20 and 3±0.15 m d^{-1}. The inter-well variation in the K_{HV} estimates indicates that there is significant heterogeneity in the aquifer over lateral distances of <100 m (refer Figure 9-17). The intra-well variation in the K_{HV} estimates is somewhat lower near the Holocene-Pleistocene contact. It should be noted that the K_{HV} values of Figures 9-16 and 9-17 are for vertical regions of the aquifer as defined by piezometer locations and do not imply that there existed sharp transitions in K_{HV}. These K_{HV} estimates should be scaled up or down (as appropriate) if a better estimate of S_y becomes available.

The potentiometric data from wells #3 and #11 (refer Figures 8-9 & 8-13, respectively) could not be analysed because intra-well groundwater potentials were too similar. This could be due to a high K_{HV}/S_y at these wells or to a failure in the bentonite seal between piezometers. The K_{HV}/S_y estimates for well #6 (see Figure 9-17) are the least reliable because of the composite tidal signal in that region of the aquifer (refer Section 10.4).

11.3.1.2 The Two-Dimensional Tidal Groundwater Flow Model

To test the conceptual hydrogeological model proposed above, and further elucidate groundwater flow patterns within the reef, a two-dimensional numeric model was developed using SUTRA (Voss, 1984). The model is believed to be novel in terms of its simulation of tidal groundwater flow in a platform reef.

The model assumes a simplified "strip-island" geometry and, as a simplification, the model was only calibrated against the tidally-impacted groundwater potentials measured near the centre-line of Heron Island (ie, well #8; refer Figure 8-1). The calibration involved using as an input the hydraulic diffusivities of the Holocene aquifer determined by VTUGF analysis at well #8, and then manipulating the hydraulic conductivity tensor of the Pleistocene layer to achieve a "best fit" (see Figure 10-13). The calibrated model's tidal efficiencies (η) and lags (γ) are highly correlated to the field measurements at well #8 (see Figure 10-12). Overall, it is suggested that the model provides a level of sophistication sufficient for the validation of the basic conceptual hydrogeological model for Heron Island. Further model refinements, including lateral heterogeneity of the Holocene layer, may be considered as a topic for future research.

The main interpretations afforded by the groundwater model are:

(i)   groundwater in the Holocene and Pleistocene regions directly below the cay moves predominantly in the vertical direction;

(ii)   groundwater within the confined portion of the reef platform (i.e. below the reef flat) moves predominantly in the horizontal direction in the Pleistocene region, but movement in the Holocene layer is negligible;

(iii)   seawater/groundwater exchange is significant at the reef slope and ocean floor but decreases to negligible levels 1 km from the centre-line of the cay; and

(iv)   attenuation of the tidal-pressure signal occurs mostly in the Holocene-age aquifer beneath the cay.

Model simulations also suggest that the efficiency of the tidal signal in unconfined groundwater near the cay's shoreline is enhanced by the greater fluid pressures

occurring below the reef-plate (Figure 10-11). A similar type of fluid pressurisation was described by Lam (1974) in his study of Swains Island (an atoll). However, this aspect of the current mathematical models was not confirmed by field or laboratory investigations and further research is required to evaluate its implications for actual groundwater flow.

11.3.1.3 Seawater Intrusion at the Cay's Shoreline

Piezometric observations at one well close to the cay's shoreline (i.e., well #6; see Figure 8-10) were unusual in that the tidal signals were skewed and the mean water-table position was greater than mean sea level. It is suggested that this phenomenon resulted from superposition of two different tidal pressure-signals: one propagated vertically from the Pleistocene aquifer as a product of the reef's dual-aquifer hydrogeology, and the other propagated laterally through the beach as a result of the reef-flat tide acting on the beach-face. Importantly, net groundwater discharge across the beach-face is believed to be less than net seawater intrusion due to hydraulic properties of the seepage-face (including a terminal velocity of discharging water particles; refer Section 10.4.3). This superposition of signals is termed the 'composite tidal signal of the dual-aquifer shoreline'. A further possible influence on this process is the 'edge-effect' (mentioned above) as it may enhance the tidal efficiency of the vertically propagated signal in the vicinity of the shoreline.

Seawater intrusion through the beach is a corollary of the composite tidal signal hypothesis. As a rough guide, the net seawater intrusion rate for the whole of Heron Island is expected to be in the order of 1×10^3 m^3 d^{-1} (refer Chapter 10) and an order-of-magnitude greater than the natural recharge for the island. It follows logically that this type of seawater intrusion does not occur along the shoreline where impermeable beachrock or retaining walls prevent the formation of a beach seepage-face.

It is suggested that the above hydrogeological model of Heron Island's shoreline is a significant improvement on the preliminary hydraulic interpretations provided by Charley et al. (1990) (refer Section 10.4). However, further field research is required to confirm the model and better understand the impact of tidal seawater intrusion

through the beach - particularly if investigations are being undertaken into the impact of human activity *immediately* adjacent to a beach.

11.3.2 Groundwater Salinity

The groundwater at Heron Island is of brackish-to-brine salinity and is non-potable (Figure 8-17 and Appendix I). Groundwater closest to the shoreline is generally the most saline (refer wells #6, #11 and #12 in Figure 1-2), a trend which is explicable in terms of VTUGF domination, a freshwater recharge zone encompassing the whole cay, treated sewage discharges near the centre of the cay, and solute transfer with the ocean caused by tidal exchanges and net seawater intrusion through (possibly) large sections of the cay's shoreline (Section 11.2.1.3).

The interpretation of salinity observations is complicated by the impact of anthropogenic inputs, as follows:

- Groundwater wells #2, #4, #5, #7 and #10 were affected by anthropogenic 'freshwater' (Figure 8-17). Measured salinities at wells #4, #5 and #7 were lowered by the treated sewage effluent, which was comprised of about 25% seawater and 75% 'freshwater' (Chen & Krol, 1997). It is suggested (but not proven) that measured salinities at wells #2 and #10 were impacted by freshwater leakages from underground pipes.

- Groundwater wells #1, #3, #6, #8, #9, #11, #12 and #13 are apparently unaffected by anthropogenic "freshwater". The measured salinities for well #9 are believed to reflect 'natural' changes, despite contamination by incidental petrol spills (since addressed by the resort's management) at the fuel depot (Chen and Krol, 1997). The cause of the relatively low salinities observed at well #13 in February 1992 are unknown, but may reflect local hydrogeological conditions and antecedent natural recharge (Table I-6).

A notable depression in salinity in most of the observation wells between February and December, 1992 was matched by STEM's prediction of a natural recharge event of about 40 cm (Table I-6, Figure 6-6). However, a 15 cm recharge event for the period April to May, 1994 did not coincide with a clear measured perturbation in

groundwater salinity. The evaluation of STEM's performance in this respect is limited by the frequency and location of the groundwater salinity measurements and the above mentioned influences on advective and dispersive transport of solutes in the aquifer.

In summary, it appears that the most important factors controlling the spatial and temporal distribution of salts in Heron Island's groundwater are:

- a natural recharge regime that is moderate, sporadic and spatially variable due to (i) a moderate and highly variable rainfall; (ii) heterogeneities in the cay's surface hydrology; and (iii) damping and attenuation of recharge by evapotranspiration and highly non-linear soil-water redistribution;

- seawater intrusion at the shoreline (related to the tidal hydrodynamics and shoreline hydrogeology);

- localised and variable anthropogenic recharge (including treated effluent and pipe leakages); and

- heterogeneity of the cay's aquifer resulting in uneven propagation of the tidal pressure signal, uneven groundwater flow and uneven hydrodynamic dispersion of dissolved salts.

In such a system, it is suggested that evaluation of groundwater dynamics for practical purposes, such as establishing the environmental significance of anthropogenic impacts, must almost inevitably involve reasoned interpretation (supported by conceptual frameworks) of deterministic and/or numerical models which will only provide a partial description of the hydrodynamic system. A more complete analysis would involve a monitoring programme which, for most purposes, will be beyond the bounds of what is reasonable in terms of cost and time.

In this respect the modelling of Heron Island's groundwater salinity is probably more complex than that of the generic atoll island. There are some significant hydrogeological differences between Heron Island and a "generic" atoll island (eg, Peterson and Gingerich, 1995); ie. Heron Island is supported by a senile platform reef and is small compared to the surrounding reef-flat and shallow lagoons (see Figure 1-1), whereas a generic atoll island is somewhat larger, is surrounded by deep lagoons

and deep ocean, receives significantly more rainfall and natural recharge, and has a well-formed freshwater lens system. Consequently some researchers, such as Peterson and Gingerich (1995), have successfully interpreted the groundwater salinities of atoll island's using steady-state and transient groundwater models (refer Chapter 7).

11.4 IMPLICATIONS FOR NUTRIENT DYNAMICS

A thorough description of nutrient dynamics within the vadose and phreatic zones at Heron Reef is beyond the scope of this thesis in that it requires knowledge of significant nutrient sources and sinks, biochemical and geochemical reactions and transformations, and large-scale advective, dispersive and diffusive transport mechanisms. The availability of such information is limited. Nevertheless, the understanding of the cay's hydrodynamics developed by this study, plus the work of Charley et al. (1990) and Chen and Krol (1997), does enable presentation of a broad preliminary view on the role the groundwater system plays with respect to the dynamics of nitrogen and phosphorus compounds. These compounds are important because of their abundance at Heron Island and their role as limiting nutrients in coral reef ecosystems of the Great Barrier Reef (Bell, 1992).

11.4.1 Dissolved Inorganic Nitrogen (natural)

Charley et al. (1990) found that nitrogen (N) was present in high concentrations (0.25 to 9.8 mg g^{-1}) in the organically rich surface soils as a result of guano deposition by seabirds; the deposition pattern also leads to appreciable lateral variation in N concentrations, particularly across vegetation boundaries and below individual plants (i.e. favoured roosting sites). Staunton Smith (1992) showed that during periods of plentiful moisture, bacterial activity causes substantial loss of organic-N from fresh guano to the atmosphere as a result of ammonification (e.g. under controlled experimental conditions, a 58% decrease in guano-N occurred within 4 days, and 87% within 28 days). This can be qualitatively observed in the field by the distinctive ammoniacal smell that follows rain events. However, much of the remnant nitrogen is converted to an inorganic form, mainly nitrates, and as such is readily leached into the soil-water system. Charley et al. note that there is an "exceptionally" high rate of microbial nitrite/nitrate production in these soils.

Dissolved inorganic nitrogen (DIN) is relatively unaffected by adsorption phenomena and solubility limits (eg, D'Elia, Webb and Porter, 1981) and only a very small fraction of the total available is taken up by vegetation (Charley et al., 1990) and, as such, once it enters the soil water system it is primarily influenced by the vagaries of the hydrodynamics associated with that system. This study has shown that most of the soil-water at Heron Island is retained by the vadose zone prior to being returned to the atmosphere by evapotranspiration. The DIN capital of the vadose zone probably increases with time and probably results in high concentrations of DIN in natural recharge (Charley et al., 1990). Chen and Krol (1997) measured DIN concentrations in the groundwater of the Holocene-age aquifer (mean DIN was 28 mg L^{-1} as N and 4.73 mg L^{-1} as N for groundwater further than 60 m from the shoreline and less than 60 m from the shoreline, respectively) to show that it exceed by up to three-orders-of-magnitude the eutrophication threshold level (14 μg L^{-1} as N) proposed by Bell (1990) for coral reefs of the Great Barrier Reef.

Charley et al. (1990) and Chen and Krol (1997) have confirmed that almost all groundwater DIN is nitrate (N-NO$_3$). The groundwater hydrodynamic model developed in this study suggests that nitrate will move down through the Holocene-age aquifer and into the Pleistocene aquifer, and ultimately will be discharged (much diluted) to the marine environment through the reef edge and sea bed (Figure 11-2). Two principal mechanisms will cause this movement:

(i) the previously noted advective net flux of groundwater, driven by a potential gradient resulting from seawater intrusion through the beaches and, to a lesser extent, natural recharge; and

(ii) hydrodynamic dispersion driven by nitrate concentration gradients and enhanced by tidal groundwater movement.
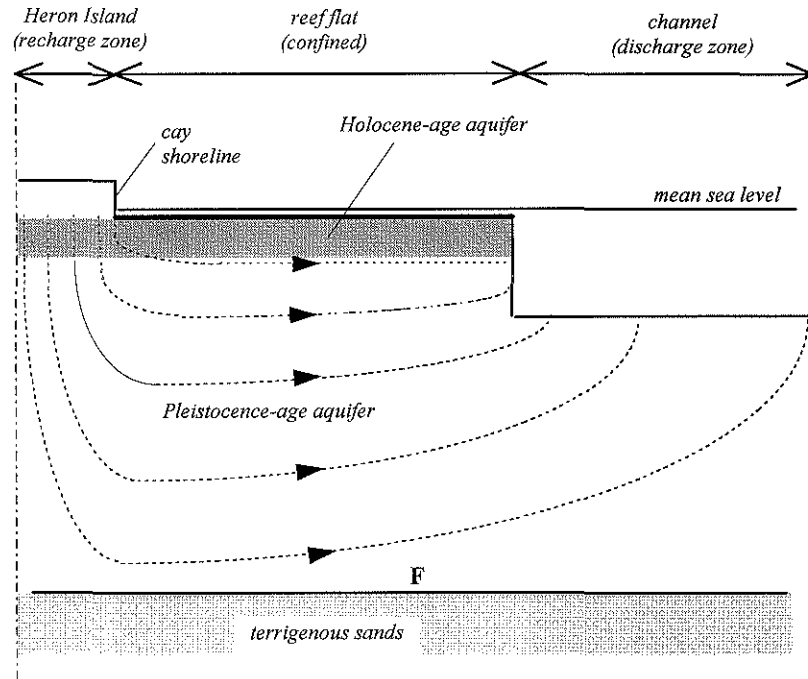
Figure 11-2. Schematic of hypothetical N-NO₃ transport pathway resulting from land-based guano leaching and hydrodynamic dispersion by tidal groundwater flow (not to scale): inferred from computer simulations of tidal groundwater flow only..

Chen and Krol (1997) and Charley et al (1990) found that the lowest N-NO₃ concentrations and greatest salinities occur near the shoreline. This is consistent with the seawater intrusion model described earlier. Other factors that would lead to some heterogeneity in groundwater nitrate concentrations include:

- non-uniform deposition of bird guano;

- areal variations in natural recharge, principally due to variations in soil surface permeability and surface topography;

- spatial differences in advective-dispersion transport of DIN, principally due to tidal groundwater flow patterns; and

- anthropogenic impacts, an issue which is discussed below.

It is currently unknown whether groundwater nitrate concentrations have reached a pseudo steady-state (subject to stochastic variations) or are destined to increase as a

result of continued guano deposition and leaching. The later possibility may have ecological implications for the future.

Brock and Waterhouse (1990) considered monitoring macro-algal abundance and distribution (an indicator of eutrophication) on the reef flat near Heron Island's beaches as a means of indirectly detecting nutrient-rich groundwater seepage. However, from their preliminary investigations, they reasoned that large-scale stochastic events, including sporadic rainfall runoff events and the voiding of guano by seabirds, would probably mask any signal caused by groundwater seepage that may occur at the beach-face. This study suggests that net seawater intrusion across the beach face should lead to negligible fluxing of groundwater $N-NO_3$ to the reef-flat, unless there are atypical hydrodynamic circumstances, e.g. a "piping" effect caused naturally by reef rock or human construction activities.

11.4.2 Dissolved Inorganic Phosphorus (natural)

Dissolved inorganic phosphorus (DIP) is leached from bird guano resulting in high concentrations of total phosphorus (P) in the organic surface soils of Heron Island (eg, in the range 0.54 to 59 mg g^{-1}; Charley et al., 1990). Total P in the soil decreases with depth but approaches a limiting minimum value (about 0.8-1.5 mg g^{-1}; Charley et al., 1990, p.52) a pattern that is consistent with effective immobilisation of P by the soil (due to adsorption phenomena and solubility constraints) and a natural low concentration of P in beach sand. The residence time of P in the vadose zone is unknown, but is probably of the order of the time-scale of the cay's geological stability.

Chen and Krol (1997) showed that the DIP in Heron Island's groundwater is mostly ortho-phosphate ($P-PO_4$) with mean DIP of 0.098 mg L^{-1} (as P) and 0.039 mg L^{-1} (as P) for groundwater further than 60 m from the shoreline and less than 60 m from the shoreline, respectively. These concentrations are not unusual for interstitial waters of coral reefs (Chen and Krol, 1997). Nevertheless, they are high compared to those

typical of oligotrophic seawater and are one order-of-magnitude greater than the eutrophication threshold level (3-6 μg L^{-1} as P) suggested by Bell (1992) for coral reefs of the Great Barrier Reef.

Chen and Krol (1997) found that the lowest concentrations of groundwater DIP and highest groundwater salinities tend to occur near the shoreline. As discussed above for DIN, this is consistent with the hydrodynamic model proposed in this study, i.e. net seawater intrusion near the beaches dilutes groundwater DIP concentrations.

The spatial distribution of DIP in the groundwater will be impacted by a number of other mechanisms, including:

- local variations in geochemistry, and thus adsorption and solubility;

- spatial variations in soil-water and groundwater dynamics; and

- anthropogenic impacts, as discussed below.

11.4.3 Anthropogenic Impacts

Anthropogenic impacts on the groundwater system were not investigated directly in this study, however the discharge of treated sewage effluent (120-240 m^3 d^{-1} approximately and not accounting for evaporative losses) would have been responsible for the salinity depressions observed around wells #4 and #5 (see Figure 8-17). This effluent was discharged via a perforated pipe located in the vadose zone near the centre of the island and appears to have been 1-2 times the total average natural recharge at the island (Table 2-1).

The work of Chen & Krol (1997) showed that the effluent had a DIN concentration of <10 mg L^{-1} and DIP concentration of 12-20 mg L^{-1}. Chen and Krol (1997) found that the impact of treated sewage on the groundwater DIN and DIP was minimal because the background levels of DIN in groundwater were very high and because most of the

DIP contained in the effluent was adsorbed by soil and aquifer matrices. They also found that organic material introduced with the effluent was actively biodegraded in the groundwater causing a localised depletion of oxygen and elevation of ammonia.

The additional nitrate contribution of the sewage to the groundwater will be mobile in a similar manner to that derived from bird guano (Figure 11-2) and, as such, will eventually pass through the aquifer towards the reef edge and sea bottom. The mobility of phosphate sourced from sewage will be restricted by adsorption and solubility phenomena in a similar manner to that sourced from bird guano. In conclusion, the current method of sewage disposal used at Heron Island appears to be environmentally benign in terms of DIN or DIP.

11.5 IMPLICATIONS FOR ATOLL ISLANDS

Certain findings of this study immediately contribute to the broader topic of atoll island hydrogeology. These findings include the improved conceptualisation of the natural recharge process in the vadose zone of atoll islands with soil similar to Heron Island soil (ie, an upper layer of 1-m deep silty-sand and a lower layer of gravelly-sand and comprised mainly of coral sediment). Importantly it was found that the unsaturated zone, although only a few meters thick, will only transmit significant recharge when soil moisture contents at depth exceed a critical level of about 0.10-0.20 ml ml^{-1}. This feature of Heron Island soil is related to the its water-retention and unsaturated hydraulic conductivity relationships and is conceptually more sophisticated than the description provided by Underwood (1990) who suggested that atoll island soils do not 'complicate' groundwater recharge.

Of great significance to atoll island studies is possibility that seawater intrusion through certain beaches could be much greater than previously expected if a hydrographic 'signature' called the 'composite tidal signal at the dual-aquifer shoreline' is present. This signature will develop where a beach seepage-face occurs over a classic dual-aquifer reef structure. Further implications exist for groundwater modelling studies, estimates of aquifer water-budgets, and hydrogeochemical studies.

The third major contribution of this body of work to atoll island research centres around the new analytic and semi-analytic VTUGF models. The VTUGF models contribute to the repertoire of techniques available to hydrogeological field investigators and computer-based modellers. The VTUGF theory will help in the efficient design of groundwater piezometers and water-level monitoring procedures on atoll islands and will assist in the interpretation of field data and the estimation of aquifer hydraulic diffusivity values. Furthermore, the VTUGF models provide a benchmark solution from which more general models of tidally-affected groundwater flow can be verified and validated.

11.6 RECOMMENDATIONS FOR FURTHER STUDY

11.6.1 Hydrology

Further research into groundwater recharge and the hydrologic balance is not recommended until more practical and cost-effective techniques for quantifying natural and anthropogenic recharges, evapotranspiration and overland flow are developed for use at Heron Island. Better estimates of recharge would allow improved interpretation of available nutrient and geochemical data (refer Chen and Krol, 1997; Appendix I).

11.6.2 Hydrogeology

According to the current conceptual hydrogeological model for Heron Island and Reef, the only boundaries through which groundwater can exchange with seawater are the beach-face, the reef-slope and ocean floor. The beach-face is particularly interesting because it is a porous boundary separating nutrient-rich groundwater and the biota on the reef-flat: suggesting a degree of vulnerability for the reef ecosystem. However only three of the groundwater investigation wells that were monitored in this study were actually located on the beach (ie, wells #6, #11 and #12) and at only one of

these was the *composite tidal signal* and associated seawater intrusion detected (ie, well #6).

Further complicating the seawater intrusion process is the reef-plate capping which, according to numerical analysis, could have amplified the tidal signal near the shoreline. The effect of discontinuous confinement on tidal groundwater movement and seawater intrusion at Heron Island have been speculatively deduced in this work, hence uncertainties remain. Further study, including the derivation of a definitive theoretical description, is recommended.

Future field investigations at Heron Island could include the monitoring of groundwater pressures within the beach along two- and three-dimensional grids and the application of Darcian flow theory to interpret tidal groundwater dynamics and the seawater intrusion rates. The resulting flow estimates would lend themselves to the estimation of solute fluxes across the beach zone and other geochemical interpretations.

This study has presented an initial approximation of tidal groundwater flow at Heron Island and Reef. The level of complexity could be increased by further study and incorporation of other hydrodynamic processes such as freshwater recharge, groundwater discharge, seawater intrusion, dissolved-salt transport and density-affected flow. According to Equation 7-17, if regional flow were to approach pseudo steady-state conditions (a simplistic postulate) then regional flows might be substantially greater than that suggested by natural and anthropogenic recharge estimates. However, improving on the current model would present a very significant research effort: careful analytical and numerical analyses and better estimation would be required for tidal flows, natural and anthropogenic recharges (possibly including stochastic components), seawater intrusion, and groundwater discharge. Such an exercise would provide a better overall picture of fluid and nutrient migration in the aquifer, but is not necessarily recommended unless the appropriate allocation of resources can be justified.

11.6.3 Issues for Environmental Management

At the time of writing, the continuation of this hydrological and hydrogeological research at Heron Island was not considered urgent as the island's groundwater was non-potable, was not utilised as a resource, and had not been linked to any detectable degradation of the marine environment. However, the groundwater at Heron Island has been shown by Charley et al. (1990) and Chen and Krol (1997) to have concentrations of DIN and DIP that are extremely high compared to eutrophication threshold levels suggested by Bell (1992) for reef seawater. Therefore, in terms of environmental management, there may be merit in:

- investigating the affects of harbour expansion, coral dredging, spoil dumping and other construction activities on the hydrogeology of the reef flat and the cay shoreline so as to evaluate and prevent man-induced groundwater seepage into the marine environment;

- investigating the benefits of aquifer-disposal of treated sewage at other coral cays that may rely on less effective, more risky or more expensive methods than those employed at Heron Island, and

- investigating the feasibility and benefits of relaxing the sewage effluent standards currently adopted at Heron Island.
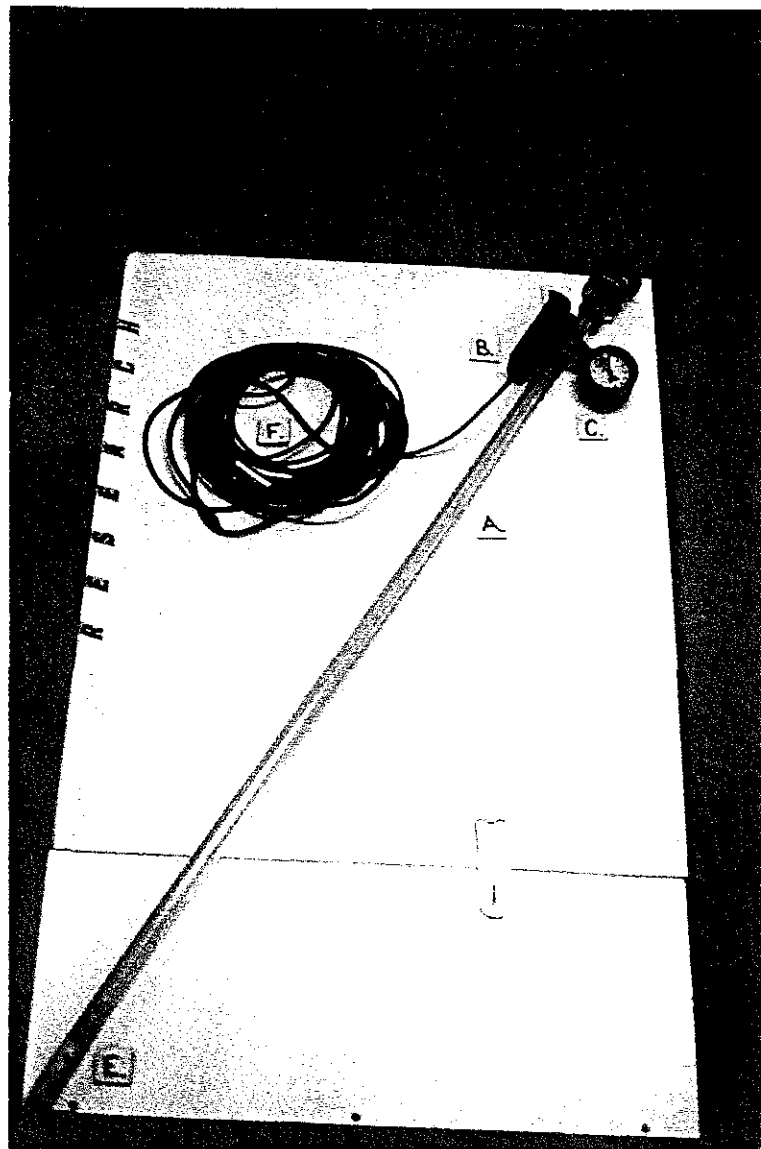
Plate 1. Tensiometer laying on top of the soil-moisture station's outer-housing whilst in the laboratory (KEY: A. 2-m-long tensiometer tube; B. pressure transducer; C. pressure gauge; D. water reservoir; E. ceramic tip; F. cable).

Plate 2. Top-down view of electronic equipment contained in the inner-housing of the soil-moisture station (KEY: A. programmable datalogger with RS232 socket; B. voltage-to-pulse signal converters; C & D. power junction box and plastic container; E. cable input connectors; F. six tensiometer cables and power cable passing through compression glands; G. one raingauge and three temperature cables passing through compression glands).

Plate 3. The soil-moisture station located in the forest at Heron Island: six tensiometers with perforated covers (foreground), wooden outer-housing (white box), tipping-bucket raingauge (on top of outer-housing), and house (background).
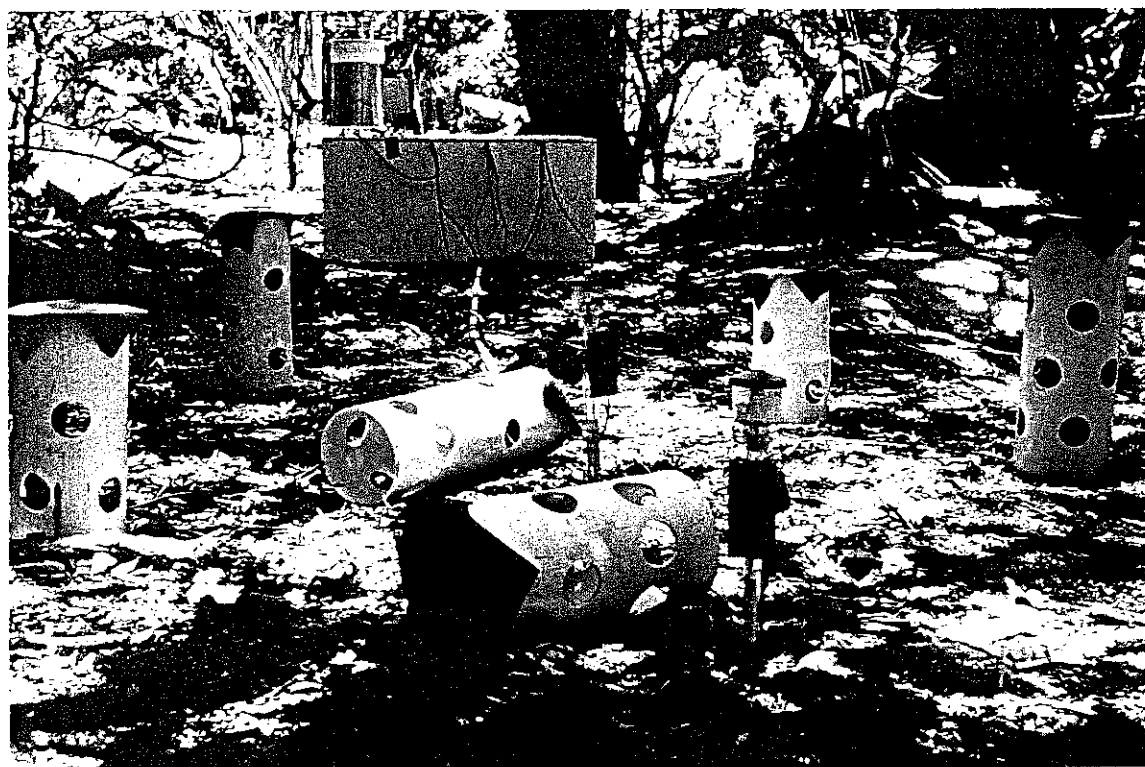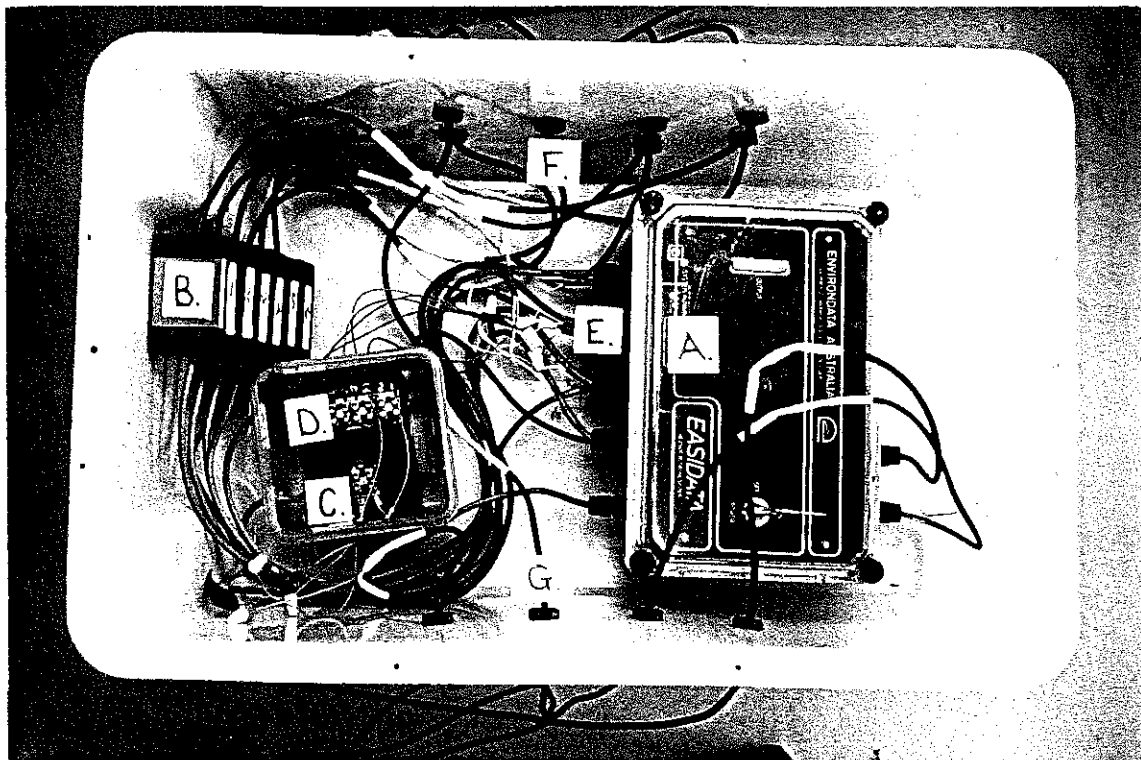
Plate 4. Equipment used at Heron Island to measure piezometric groundwater levels [KEY: hand-held battery powered water-level sensor (top left); coaxial cable and pressure transducer with lead weight and latex cover attached (right); computer cable (centre bottom); weather proof inner-housing with three cables connected (bottom left); laptop computer (centre left); and electronic data recorder (centre)].

Plate 5. Equipment used at Heron Island to measure groundwater physico-chemical parameters [KEY: A. electronic H2O multi-sensor device; B. programmable data recorder; C. portable battery pack; D. hand-held electronic depth gauge; E. flow-through chamber (attaches to A.); F. groundwater sampling tube with inertial valve attached; G. 250 ml polyethylene groundwater sampling bottle; purge bucket (top centre)].
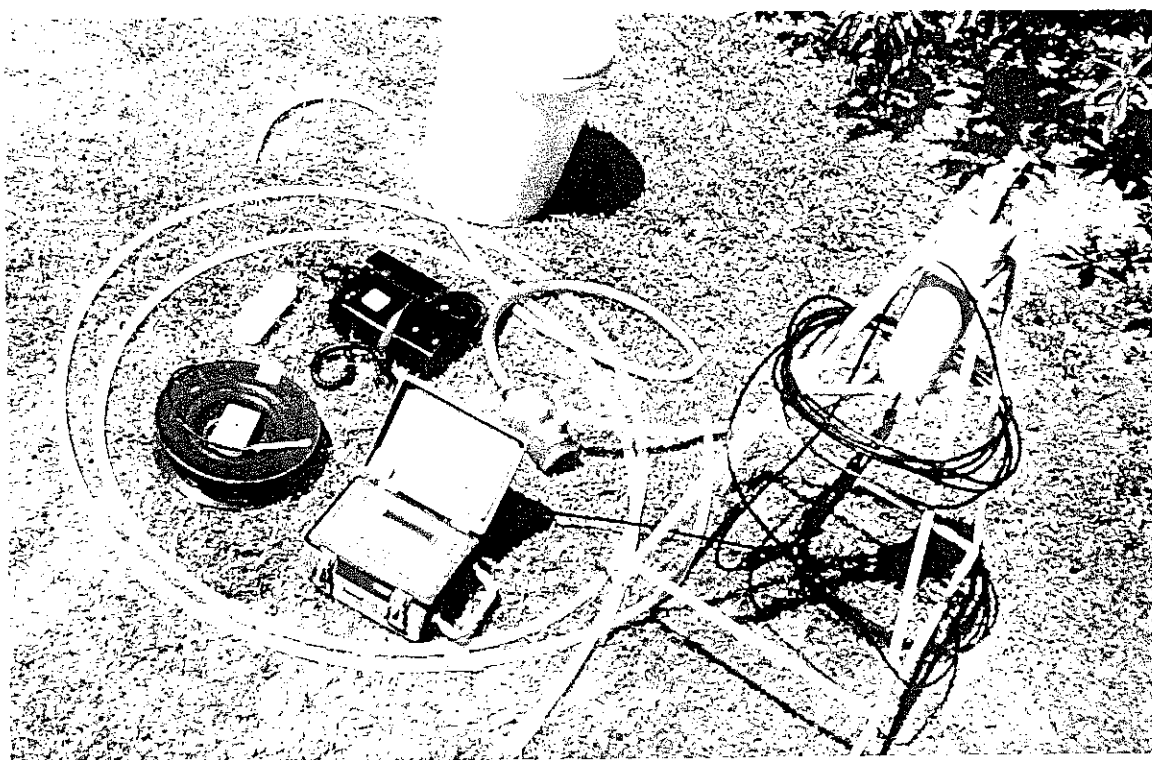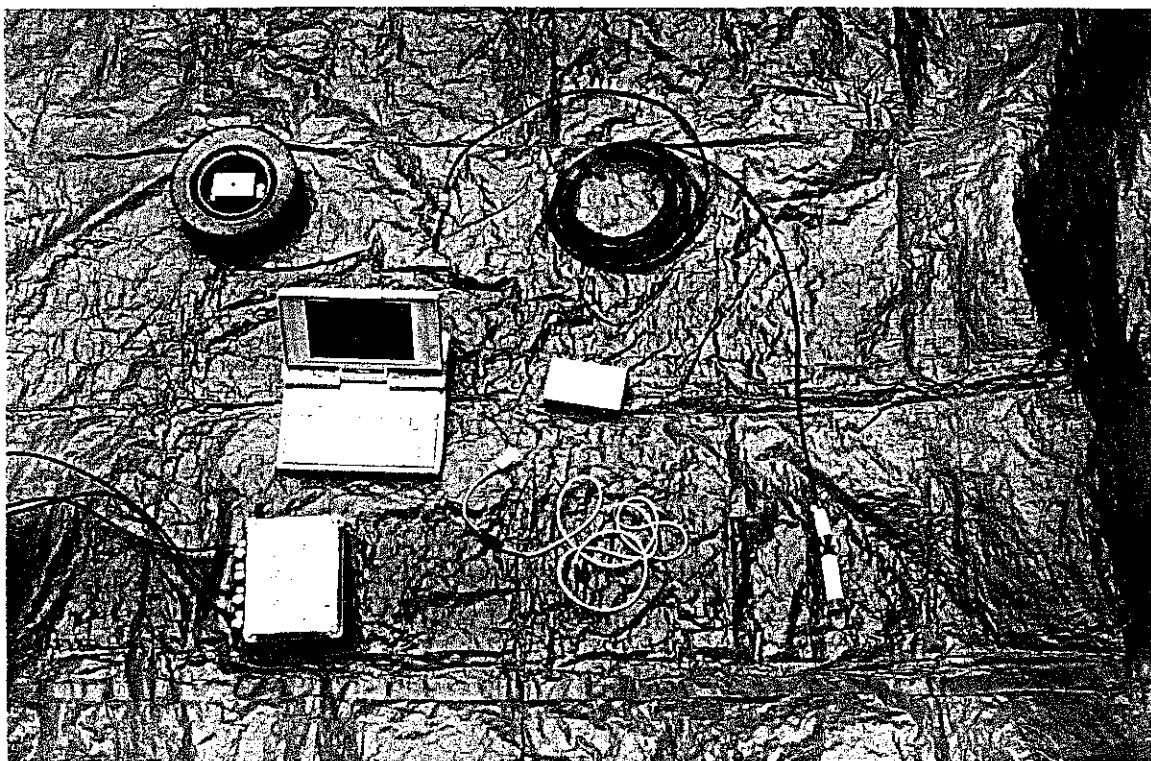
Plate 6. Equipment used to monitor water-levels in the three piezometers located at well #2 at Heron Island: well-head casing and piezometers (centre bottom): stainless steel stand with excess cable attached (centre); wood and perspex outer-housing with three cables passing through compression glands (centre top)].

BIBLIOGRAPHY

Abell, R.S. (1993). Aquifer vulnerability on small volcanic islands in the southwest Pacific region - an example from Norfolk Island. AGSO Journal of Australian Geology and Geophysics, 14 (2/3): 123-133.

Allaway, W.G., M.G.Pitman, R.Storey, S.Tyerman & A.E.Ashford (1984). Water relations of a coral cay vegetation on the Great Barrier Reef: water potentials and osmotic content. Aust. J. Bot., 32: 449-464.

Andrews, J.C. and H. Müller (1983). Space-time variability of nutrients in a lagoonal patch reef. Limnol. Oceanogr., 28(2): 215-227.

Anthony, S.S. (1987). Hydrogeochemistry of a small limestone island: Laura, Majuro Atoll, Marshall Islands. Univeristy of Hawaii, M.S. Thesis, pp.114.

Anthony, S.S. (1992). Electromagnetic methods for mapping freshwater lenses on Micronesian atoll islands. Journal of Hydrology, 137. 99-111.

Anthony, S.S., F.L. Peterson, F.T. Mackenzie and S.N. Hamlin (1989). Geohydrology of the laura fresh-water lens, Majuro Atoll: a hydrogeochemical approach. Geological Society of America Bulletin, 101: 1066-1075.

Arnow, T. (1955). The hydrology of Ifilak Atoll, Western Caroline Islands. Atoll Research Bulletin, 44(1): 1-15.

Aseervatham, A.M. (1994). Tidal dynamics of coastal water tables. Ph.D. Thesis, Dept. of Civil Engineering, Univ. of Queensland, Australia, pp. 253.

Averjanov, S.F. (1950). About permeability of subsurface soils in case of incomplete saturation. In: English Collection, Vol.7, 1950, as quoted by P.Ya. Palubarinoua, 1962 in "Theory of Ground Water Movement" (translated from the Russian by J.M. Roger de Wiest, Princeton Univ. Press, Princeton, New Jersey, 1962).

AWWA (1995). Australian Water & Waste Water Association Inc, PO Box 388, Artarmon, NSW, 2062, Australia.

Ayers, J.F. and H.L. Vacher (1986). Hydrogeology of an atoll island: a conceptual model from detailed study of a Micronesian example. Ground Water, 24: 185-198.

Ayers, J.F. and H.L.Vacher (1986). Hydrogeology of an atoll island: a conceptual model from detailed study of a Micronesian example. Ground Water, V. 24: 185-198.

Bartle, G. A. (1987). Report on the evaluation of the Aokautere thermoelectric heat pulse for measuring transpiration in coconut palms. CSIRO, Division of Water Science. Australian Government.

Baydon-Ghyben, W. (1888-9). Nota in verband met de voorgenomen putboring nabij Amsterdam. Koninklyk Instituut Ingenieurs Tijdschrift (The hague): 8-22.

Bear J. & Y. Bachmat (1990). Introduction to modeling transport phenomena in porous media. Kluwer Academic Publishers, London, pp.553.

Bear J., (1972). Dynamics of fluids in porous media. American Elsevier Publishing Company, New York, 2nd Ed., pp. 764.

Bell, P.R.F. & I. Elmetri (1995). Ecological indicators of large-scale eutrophication in the Great Barrier Reef lagoon. AMBIO, Journal of the Human Environment, 24 (4): 208-215.

Bell, P.R.F. (1991). Must GBR pollution become chronic before management reacts? Search, 22(4): 117-119.

Bell, P.R.F. (1992). Eutrophication and coral reefs-some examples in the Great Barrier Reef Lagoon. Water Res., 26(5): 553-568.

Bell, P.R.F. (pers. commun. 1997). Department of Chemical Engineering, The University of Queensland, St Lucia, Brisbane, Australia.

Belmans, C., J.G. Wesseling & R.A. Feddes (1983). Simulation model of the water balance of a cropped soil: SWATRE. J. Hydrol., 63: 271-286.

Boucher, D.A. (1977). Submarine diagenesis of the corals of Bellairs Reef, Barbados. Unpubl. M.Sc. Thesis, McGill Univ., Montreal (as mentioned in Hopley 1982; original not seen).

Bredehoeft, J. & P. Hall (1995). Ground-water models. Editorial, Ground Water, 33(4): 530-531.

Brock, M. A. & B. M. Waterhouse (1990). Macroalgal abundance and distribution on reef platforms with and without cays. In: Nutrient Dynamics on Coral Cays. Final Report to the Aust. Res. Counc. (unpublished), Proj. No. A18615988, pp. 206 (Charley, J., H. Heatwole and M. Brock, 1990).

Brooks, R.H. & A.T. Corey (1964). Hydraulic properties of porous media. Hydrology
 Paper 3, Colorado State Uni., Fort Collins (original not seen).

Brutsaert, W. (1966). Probability laws for pore-size distributions. Soil Sci. 101: 85-92.

Brutsaert, W. (1982). Evaporation into the atmosphere: theory history and
 applications. D.Reidel Publishing Company, Dordrecht, Holland, pp. 299.

Buddemeier, R.W. & G.L. Holladay (1977). Atoll hydrology: Island ground-water
 characteristics and their relationship to digenesis. Proc. 3rd Int. Coral Reef
 Symp., Miami. Vol.2: 167-174.

Buddemeier, R.W. & J.A. Oberdorfer (1986). Internal hydrology and geochemistry of
 coral reefs and atoll islands: key to diagenetic variations. In: Reef
 Diagenesis.(Edited by Schroede, J.H. and Purser, B.H.), Springer-Verlag,
 Berlin Heildelberg, pp. 455.

Buddemeier, R.W. and J.A. Oberdorfer (1988). Hydrogeology and hydrodynamics of
 coral reef pore waters. Proc. 6th Int. Coral Reef Symp., Aust., 3: 485-490.

Burdine, N.T. (1953). Relative permeability calculation size distribution data. Pet.
 Trans. Am. Inst. Min. Metal. Pet. Eng. 198: 71-78.

Bureau of Meteorology (1995). Bureau of Meteorology, Regional Office, 295 Ann
 Street, Brisbane, Australia.

Butterworth (pers. commun., 1992). Department of Geology, The University of
 Queensland, St Lucia, Brisbane, Australia.

Byrne, G., G. Shorten,F. Bullen, W. Collins and R. Smith (1990). Groundwater in a
 coral cay; water resources, pollutants and their translocation. G.G. Shorten,
 Dept. Applied Geology, QUT. In: SOPAC Miscellaneous Report 105. Coastal
 Engineering in the Pacific. Lecture notes from CIDA-SOPAC Coastal
 Investigations and Engineering Workshop.

Campbell, G.S. (1977). An introduction to environmental biophysics. Springer-
 Verlag, New York, pp. 150.

Campbell, G.S. (1985). Soil physics with basic transport models for soil-plant
 systems. Developments in soil science 14, Elsevier, Amsterdam, pp.150.

Carbon, B.A. (1975). Redistribution of water following precipitation on previously
 dry sandy soils. Aust. J. Soil Res., Vol. 13: 13-19.

Carbon, B.A. & K.A. Galbraith (1975). Simulation of water balance for plants growing on coarse-textured soils. Aust. J. Soil Res., Vol. 13: 21-31.

Carbon, B.A. (1973). Diurnal water stress on plants grown on a coarse soil. Aust. J. Soil Res., 24: 33-42.

Carbon, B.A., F.J. Roberts, P.Farrington & J.D. Beresford (1982). Deep drainage and waer use of forests and pastures grown on deep sands in a mediterranean environment. Journal of Hydrology, 55: 53-64.

Carpenter, R.A. & J.E.Margos (1989). How to assess environmental impacts on tropical island and coastal areas. A training manual prepared for the South Pacific Regional Environment Programme, SPREP. Environment and Policy Institute East-West Center, 1777 East-West Road, Honolulu, Hawaii 96848. October 1989.

Carr, P.A., and G.S. Van Der Kamp, (1969). Determining aquifer characteristics by the tidal method. Wate Resources Research. 5 (5): 1023-1031.

Carrier and Munk (1954). On the diffusion of tides into permeable rock. McGraw Hill, New York, 1954, Proc. Symposia in Applied Math., Vol.5: 89.

Chapman, T.G. (1985, unpublished). The use of water balances for water resource estimation, with special reference to small islands. School of Civil Engineering, Univ. of NSW, Kensington, Australia, August 1995.

Chapman, T.G. (1990). Natural processes of groundwater recharge and discharge. In: Groundwater and the Environment. Proc. 2nd Int. Ground WaterConf., Kota Bahru, June 1990: c1-c30.

Charley, J., H. Heatwole and M. Brock (1990). Nutrient Dynamics on Coral Cays. Final Report to the Aust. Res. Counc. (unpublished), Proj. No. A18615988, pp. 206.

Chen, D. & A. Krol (1997). Hydrogeology of Heron Island, Great Barrier Reef, Australia. In: Geology and Hydrogeology of Carbonate Islands, Developments in Sedimentology, Vol. 54, Chpt. 30 (edited by H.L. Vacher and T.M. Quinn). Elsevier, Amsterdam, 948 pp.

Chidley, T.R.E. & J.W. Lloyd (1977). A mathematical model study of fresh-water lenses. Ground Water, 15(3): 215-222.

Childs, E.C. & Collis-George (1950). The permeability of porous materials. Proc. Roy. Soc., Ser. A, 201: 392-405.

Childs, E.C. and A. Poulovassilis (1962). The moisture profile over a moving water table. Journal of Soil Science, 13 (2): 271-285.

Clothier, B.E., D.R.Scotter & J.P. Kerr (1977). Drainage flux in permeable soil underlain by a coarse-textured layer. Soil Science Society Am. J. (41): 671-676.

Coleman, G. & D.G. DeCoursey (1976). Sensitivity and model variance analysis applied to some evaporation and evapotranspiration models. Water Resources Res., 12(5): 873-879.

Cooper Jr., H.H. (1959). A hypothesis concerning the dynamic balance of freshwater and salt water in a coastal aquifer. Journal of Geophysics Research, 64(4): 461-467.

Coote, S.M., (1984). A study of beachrock on Heron Island Great Barrier Reef, Australia. M.Sc. Thesis, Dept. Geology & Minerology, Univ. Queensland, Brisbane, Australia.

Corey, A.T. (1977). Mechanics of heterogeneous fluids in porous media. Water Res. Publications, P.O. Box 303, Fort Collins Colorado, 80522 USA.

Cox, D.C. (1951) The hydrology of Arno Atoll, Marshall Islands. Atoll Res. Bulletin No.8, Dec. 1951. The Pacific Science Board, National Academy of Sciences - National Research Council, Washington, USA.

Crago, R.D. & W.Brutsaert (1992). A comparison of several evaporation equations. Water Res. Research, Vol. 28 (3): 951-954.

Craig, R.F., (1987). Soil mechanics. 4th Ed., Van Nostrand Reinhold, UK. 410 pp.

Cresswell, H.P. (1992). A sensitivity analysis of the Jackson method of predicting unsaturated hydraulic conductivity. Aust. J. Soil Res., 1992, 30: 285-290.

CSIRO (1988). CSIRO disc permeameter: instruction manual.CSIRO Centre for Environmental Mechanics, Canberra, 1988.

Custodio, E. (1988). Present state of coastal aquifer modelling short review. In: Groundwater flow and quality modelling, NATO series, Vol. 224, pp.785.

D'Elia, C.F., Webb, K.L., and Porter, J.W. (1981). Nitrate-rich groundwater inputs to Discovery Bay, Jamaica: a significant source of N to local coral reefs? Bull. Mar. Sci. 31(4): 903-910.

D'Ella, C.F. & W.J. Wiebe (1990). Biogeochemical nutrient cycles in coral reef ecosystems. In: Ecosystems of the World, Coral Reefs, Vol. 25.

Dalton, F.N., W.N. Herkelrath, D.S.Rawlins & J.D. Rhoades (1984). Time domain reflectometry: simultaneous measurement of soil water content and electrical conductivity with a single probe. Science, Vol. 224: 989-990.

Darwin, C. (1909). The voyage of the Beagle. New York, P.F. Collier & Son, The Harvard Classics. v.29 (Reprint of original edition published in 1845), 547 pp.

Davie, J.D.S. (1982). Pattern and process in the mangrove ecosystems of Moreton Bay, Southeastern Queensland. Ph.D. Dissertation, Dec. 1982. University of Queensland.

Davies, P.J. & D. Hopley (1983). Growth fabrics and growth rates of Holocene reefs in the Great Barrier Reef. BMR J. Aust. Geology Geophysics, 8: 237-251.

Davies, P.J. & D.W. Kinsey (1973). Organic and inorganic factors in recent beachrock formation, Heron Island, Great Barrier Reef. Journal of Sedimentary Petrology, Vol. 43: 59-81.

Davies, P.J. (1974). Cation electrode measurements in the Capricorn Area, Southern Great Barrier Reef Province. Proc. Second Int. Coral reef Symp., Great Barrier Reef Committee, Brisbane, December, 1974: 449-455.

Davies, P.J. (1992). Origins of the Great Barrier Reef. Search, 23: 193-196.

Davies, P.J., (1974). Subsurface solution unconformities at Heron Island, Great Barrier Reef Proc. 2nd Int. Coral Reef Symp. Brisbane: 573-578.

Davis, S.N. (1978). Floatation of freshwater on seawater, a historical note. Ground Water 16 (6) : 444-445.

DeKanel, J. and Morse, J.W., (1978). The chemistry of orthophosphate uptake from seawater on to calcite and aragonite. Geochim. Cosmochim. Acta, 42: 1335-1340.

Domenico, P. A. & F.W. Schwartz (1990). Physical and chemical hydrogeology. John Wiley & Sons, Brisbane, pp. 824.

Dracos, T. (1963). Ebene nichtstationare Grundwasserabflüsse mit freier Oberfläche. Mitt. Versuchsanst. Wasserbau Erdbau, Eidgenoss. Tech. Hochsch., Zürich, Rep., 57, pp.114 (original not seen).

DuCommun J. (1828). On the cause of fresh water springs, fountains, and c. American Journal of Science, 1st ser., vol. 14 (1828): 174-176. As cited in: Flotation of Fresh Water on Sea Water, A Historical Note (author S. N. Davis). Ground Water, 1978, 16(6): 444-45.

Enos, P. & L.H. Sawatsky (1981). Pore networks in Holocene carbonate sediments. Journal of Sedimentary Petrology, 51(3): 961-985.

Erskine, D. (1991). The effect of tidal fluctuations on a coastal aquifer in the UK. Ground Water, 29(4): 556-562.

Falkland, A.C. (1983). Christmas Island water resource study. Vol. 1 of General Report, Australian Dept. Housing and Construction, Canberra, ACT, 1983.

Falkland, A.C. (1991). Hydrology and water resources of small islands: a practical guide. UNESCO 1991, France, pp. 435.

Falkland, A.C. and J.P. Brunel (1989). Regional hydrology and water resource problems of humid tropical islands. Internat. Colloquium on the Development of Hydrologic and Water Management Strategies in the Humid Tropics.Unesco-IHP. James Cook Univ., Townsville, Australia, pp. 38.

Fang, C.S., S.N. Wang and W. Harrison (1972). Groundwater flow in a sandy tidal beach, two-dimensional finite-element analysis. Water Resources Research, 8(1): 121-128.

Farrell, E.R. (1994). Analysis of groundwater flow through leaky retaining marine structures. Géotechnique, 44(2): 255-263.

Ferris, J.G. (1951). Cyclic water level fluctuations as a basis for determining aquifer transmissivity. Assn. Int. Hydrol. Sci., 2: 148-155.

Fetter, C.W. (1988). Applied Hydrogeology 2nd Edition. Macmillan Publishing Company, New York, pp. 592.

Flood, P.G. (1986). Sensitivity of coral cays to climatic variations, southern Great Barrier Reef, Australia. Coral Reefs, 5: 13-18.

Fosberg, F.R.(1957). Description and occurrence of atoll phosphate rock in Micronesia. Am.J.Sci., 255: 584-592.

Frith, C.A. (1983). Some aspects of lagoon sedimentation and circulation at One Tree Reef. BMR Journal of Australian Geology and Geophysics, 8: 211-221.

Froelich, P.N. (1988). Kinetic control of dissolved phosphate in natural rivers and estuaries: a primer on the phosphate buffer mechanism. Limnol. Oceanogr., 33: 649-668.

Gardner, W.R. (1957). Some steady-state solutions of the unsaturated moisture flow equation with applications to evaporation from a water table. Soil Sci., 1958, Vol. 85.

Gersekowski, J. N. (1992). Sewage treatment on Green Island. In Environmental Engineering 1992: The global environment - Australian implications. Reprints of Papers. The Institute of Engineers, Australia, National Conference Publication No 92/5, Gold Coast, 17-19 June 1992.

Ghassemi, F., A.J. Jakeman and G. Jacobson (1990). Mathematical modelling of seawater intrusion, Nauru Island. Hydrological Processes, Vol. 4: 269-281.

Ghassemi, F., T.H. Chen, A.J. Jakeman and G. Jacobson (1993). Two and three-dimensional simulation of seawater intrusion: performances of the "SUTRA" and "HST3D" models. AGSO Journal of Australian Geology and Geophysics, 14 (2/3): 219-226.

Gillham, G. W. (1984). The capillary fringe and its effect on water-table response. Journal of Hydrology, 67: 307-324.

Gingerich, S.B. (1992). Numerical simulation of the freshwater lens on Roi-Namur Island, Kwajalein Atoll, Republic of the Marshall Islands, M.S.Thesis, Dept. of Geology & Geophysics, Univ. of Hawaii, Honolulu, 1992.

Glover, R.E. (1959). The pattern of fresh-water flow in a coastal aquifer.Journal of Geophysical Research, 64(4): 457-459.

Godin, G. (1972). The analysis of tides. The University of Toronto Press, London.

Gourlay, M.R. & C.J.McMonagle (1989). Cyclonic wave prediction in the Capricornia Region, Great Barrier Reef. 9th Australian Conf. on Coastal & Oceanic Engineering, Adelaide, 4-8 Dec., 1989: 112-116.

Gourlay, M.R. & J.S. Jell (1991). Heron Island spoil dump: short term monitoring and environmental effect. Univ. Queensland, Dept. Civil Eng., Report CH 38/91, January 1992.

Gourlay, M.R. (1988). Coral cays: products of wave action and geological processes in a biogenic environment. Proc. 6th Int. Coral Reefs Symp., Aust., 2: 491-496.

Gourlay, M.R. (1993). Impact of Heorn Island boat harbour on its adjoining reef and cay. Reprints: 12th Australiasian Conf. on Coastal and Ocean Engineering, Melbourne, 28 May - 2 June, 1995. Inst. of Eng. Australia.

Gourlay, M.R. (1995). Impact of Heron Island boat harbour upon its adjoining reef and cay. Reprints: 12th Australasian Conf. on Coastal and Ocean Engineering, Melbourne, 28 May - 2 June 1995, Institute of Engineers Australia.

Gourlay, M.R. (pers. commun., 1993). Personal Communication. Department of Civil Engineering, The University Queensland, St Lucia, Brisbane, Australia.

Green, W. H. and G.A. Ampt, (1911). Studies on soil physics: 1. Flow of air and water through soils. Journal of Agricultural Science, 4(1): 1-24.

Green, W.H. & G.A. Ampt (1911). Studies on soil physics: Part I. The flow of air and water through soil. J. Agr. Sci. IV: 1-24.

Green, W.H. & J.C. Corey (1971). Calculation of hydraulic conductivity: a further evaluation of some predictive methods. Division S-1 soil physics. Soil Sci. Soc. Amer. Proc. 35.

Griggs, J.E. & F.L. Peterson (1993). Ground-water flow and development strategies at the atoll scale. Ground Water, 31(2): 209-220.

Griggs, J.E. (1989). Numerical simulation of groundwater development schemes for the Laura area of Majuro Atoll, Marshall Islands. Ph.D. dissertation, Univ. of Hawaii at Manoa, pp. 203.

Hacker, J. (pers. commun., 1995) Personal Communication. Department of Civil Engineering, The University of Queensland, St Lucia, Brisbane, Australia.

Hanshaw, B.B. & W.Back (1979). Major geochemical processes in the evolution of carbonate-aquifer systems. J. hydrol., 43: 287-312.

Haverkamp, R. and Parlange J.Y. (1986). Predicting the water-retention curve from particle-size distribution: 1. sandy soils without organic matter. Soil Science 142(6): 325-339.

Haverkamp, R., M. Vauclin, J. Touma, P.J. Wierenga & G. Vachaud (1977). A comparison of numerical simulation models for one-dimensional infiltration. Soil Sci. Soc. Am. J., Vol. 41: 285-294.

Henry, L. de W. (1989). Legistlation affecting water management on tourist islands. Water, Journal of the Aust. Water and Wastewater association, 15(6): 24-26.

Herman, M.E. & S.W. Weatcraft (1984). Groundwater dynamics investigation of Enjebi Island, Enewetak Atoll: an interpretive computer model simulation. In: Finite elements in water resources (editors: J.P. Laibale, C.A. Brebbia & G. Pinder). Springer-Verlag, New York: 133-142.

Herman, M.E. (1984). Tidal fluctuations and groundwater dynamics in atoll island aquifers. MSc Thesis, University of Nevada-reno, Reno, Nevada.

Herman, M.E., R.W. Buddemeier and S.W. Weatcraft (1986). A layered aquifer model of atoll island hydrology: validation of a computer simulation. Journal of Hydrology, 84: 303-322.

Herzberg, A.(1901). Die Wasserversorgung einiger Nordseebader. Journal Gasbeleuchtung und Wasserversorgung (Munich), 44 (1901); 815-19, 842-44.

Hillel, D. (1980). Fundamentals of soil physics. Academic Press., 1980, New York.

Hillel, D. (1982). Introduction to soil physics. Academic Press., 1982, New York.

Himmelblau, D.M. (1989). basic principles and calculations in chemical engineering, 5th Edition. Prentice Hall International, Inc., London: pp. 735.

Hogan, P. (1988). Modeling of freshwater-seawater interaction on Enjebi Island, Enewetak Atoll. M.Sc. Thesis, San Jose St. Univ., pp. 75.

Hopley, D. (1982). Geomorphology of the Great Barrier Reef: Quarternary development of coral reefs. John Wiley-Interscience, New York, pp. 453.

Hopley, D. (in press). Geology of reef islands of the Great Barrier Reef, Australia. In: Geology and Hydrogeology of Carbonate Islands, Developments in Sedimentology, Vol. 54, Chpt. 29 (edited by H.L. Vacher and T.M. Quinn). Elsevier, Amsterdam, 948 pp.

Hopley, D., A.M. Slocombe, F. Muir and C. Grant (1983). Nearshore fringing reefs in north Queensland. Coral Reefs 1: 151-160.

Hopley, D., K.E. Parnell & P.J. Isdale (1989). The Great Barrier Reef Marine park: dimensions and regional patterns. Aust. Geographical Studies, 27(1): 47-66.

Hornberger, G.M., J.P. Raffensperger, P.L. Wiberg and K.N. Eshleman (1998). Elements of Physical Hydrology. The Johns Hopkins University Press, Baltimore and London, pp. 302.

Howard, K.W.F. & J.W. Lloyd (1979). The sensitivity of parameters in the Penman evaporation equations and direct recharge balance. J. hydrol., 41: 329-344.

Hsieh, P.A. and J. D. Bredehoeft, (1987). Determination of aquifer transmissivity from Earth tide analysis. Water Resources Research, 23 (10): 1824-1832.

Hunt Jr., C.D. (1991). Climate-driven saltwater intrusion in atolls. In: Ground water in the Pacific rim countries. Proc. of the Symp. sponsored by the Irrigation and Drainage Division of the American Society of Civil Engineers (editor H.J. Peters), Honolulu, Hawaii, 23-25 July 1991: 43-49.

Hunt, B. (1979). An analysis of the groundwater resources of Tongatapa Island, Kingdom of Tonga. Journal of Hydrology, 40: 185-196.

Hunt, C.D. and F.L. Peterson (1980). Groundwater resources of Kwajalein Islands, Marshall Islands. Universty of Hawaii, Water Resources Research Centre Tech. Rept. No.126, pp. 91.

Hutchinson, G.E. (1950). Survey of contemporary knowledge of biogeochemistry. 3. The biogeochemistry of vertebrate excretion. Bulletin of the American Museum of Natural History, 96(3): 1-554.

Hydrolab (1991, unpublished). Hydrolab Surveyor 3 Technical Manual, Hydrolab Corporation, USA.

Jacob, C.E. (1940). On the flow of water in an elastic artesian aquifer. Trans. Amer. Geophys. Union, v.22: 575-586.

Jacobson, G. (1976). The freshwater lens on Home Island in the Cocos (Keeling) Islands. BMR Jl. of Aust. Geol. and Geophysics, VI: 335-343.

Jell, J.S. and P.G. Flood (1977). Guide to the geology of reefs of the Capricorn and Bunker Groups, Great Barrier Reef Province, with special attention to Heron Reef. In: Papers Dep.Geol., Univ. Queensland, Aust. Sedimentol. Group, 8(3): 1-85.

Jury, W.A., W.R. Gardener & W.H. Gardener (1972). Soil physics. 5th Ed. John Wiley and Sons, Inc. New York, pp. 328.

Kinsey, D.W. (1991). Can we resolve the nutrient issue for the Reef? Search, 22(4): 119-121.

Kipp, K. L. (1987). HST3D: A computer code for simulation of heat and solute transport in three dimensional ground-water flow systems. US Geological survey. Water resources Investigations, Report 86-4095, pp. 517.

Kirsch, S.W. (1993). A field test of a soil-based measure of evapotranspiration. Soil Science, 156 (6): 396-404.

Klute, A. (1972). The determination of hydraulic conductivity and diffusivity of the unsaturated soils. Soil Science, 113(4): 264-276.

Klute, A. (1986) Methods of Soil Analysis, Part 1, 2nd Edition: Physical and Mineralogical Methods. American Society of Agronomy, Inc. Soil Science of America, Inc., Madison, Wisconsin, USA, pp. 1187.

Kozeny, J. (1927). Uber kapillare leitung des wassers in boden. Sitzungsber Akad. Wiss. Wien., Vol. 136: 271-306.

Krol A., M. Noordink, J. Jell, and D. Chen (1992). The Heron Island Groundwater Project. In: National Conference on Environmental Engineering, Gold Coast, Australia, 17-19 June 1992, Reprints of Papers. The Institute of Engineers Australia, National Conference Publication No 92/5.

Krol, A. (pers. commun. 1996). Personal Communication. Department of Chemical Engineering, University of Queensland, St Lucia, Brisbane, Australia.

Kunze, R.J., G. Uehara, K. Graham (1968). Factors important in the calculation of hydraulic conductivity. Soil Sci. Soc. Amer. Proc., 32: 760-765.

Lam, R.K.(1974). Atoll permeability calculated from tidal diffusion. J. Geophys. Res., 79(21): 3073-3081.

Lee, R. (1980). Forest hydrology. Columbia Univ. Press, New York, 349 pp.

Lerner, D.N., A.S. Issar and I. Simmers (1990). Groundwater recharge: a guide to estimating and understanding natural recharge. International Assoc. of Hydrologists, Vol. 8. Verlag Heinz Heise. pp. 345.

Li, L., D.A. Barry, J.-Y. Parlange & C.B. Pattiaratchi (1997). Beach water table fluctuations due to wave run-up: capillarity effects. Water Res. Research, Vol. 33 (5): 935-945.

Liu, Ko-Fei, (1996). Tide-induced ground-water flow in deep confined aquifer. Journal of Hydraulic Engineering, Feb. 1996: 104-110.

Lloyd, J. W. and J.A. Heathcote (1985). Natural inorganic hydrochemistry in relation to groundwater : an introduction. Oxford University Press, Oxford, pp. 296.

Lloyd, J.W., J.C. Miles, C.R. Chapman & S.F. Bugg (1980). Aground water resource study of a Pacific Ocean atoll - Tarawa, Gilbert Islands. Water Resources Bull., Vol. 16: 646-653.

Lourensz, R.S. (1977). Tropical cyclones in the Australian region July 1909 to June 1975. Australian Government Publishing Service, Canberra, pp. 110.

Mahrer, Y. & G. Rytwo (1991). Modelling and measuring evapotraspiration in a daily drip irrigated crop field. Irrig. Sci., 12:13-20.

Marquis Jr., S.A. & E.A. Smith (1994). Assessment of ground-water flow and chemical transport in a tidally influenced aquifer using geostatistical filtering and hydrocarbon fingerprinting. Ground Water, 32(2): 190-199.

Marsh Jr., J.A. (1977). Terrestrial inputs of nitrogen and phosphorus on fringing reefs of Guam. Proc. 3rd Int. Coral Reef Symp., Miami, 1977: 331-336.

Marshall, J.F. & P.J. Davies (1981). Submarine lithification on windward reef slopes: Capricorn-Bunker Group, Southern Great Barrier Reef. Journal of Sedimentary Petrology, 51(3): 953-960.

Marshall, J.F. (1983). Lithology and diagenesis of the carbonate foundations of modern reefs in the Southern Great Barrier Reef. BMR J. Aust. Geology Geophysics, 8: 253-265.

Marshall, J.F. and P.J. Davies (1982). Internal structure and Holocene evolution of One Tree Reef, Southern Great Barrier Reef. Coral Reefs, 1: 21-28.

Marshall, T.J. (1958). A relation between permeability and size distribution of pores. J. Soil Sci. 9: 1-8.

Massey, B. S. (1984). Mechanics of fluids. 4th Edition. Van Nostrand Reinhold, UK, pp.625.

Maxwell, W.G.H. (1962). Lithification of carbonate sediments, in the Heron Island Reef, Great Barrier Reef. J. Geol.Soc. Aust., 8: 217-238.

Mc Arthur, A.J. (1990). An accurate solution to the Penman equation. Agricultural and Forest Meteorology, 51: 87-92.

Mc Caskill, M.R. (1990). Prediction of solar radiation from rainday information using regionally stable coefficients. Agriculture & Forest Meteorology, 51: 247-255.

Mc Donald and Harbaugh (1988). A modular three-dimensional finite-difference ground-water flow model. U.S. Geological Survey, Book 6, Chapter A1.

Mc Ilroy, I.C. (1984). Terminology and concepts in natural evaporation. Agricultural Water Management, 8: 77-98.

Miller, D.L.R.. & F.T. Mackenzie (1988). Implications of climate change and associated sealevel rise for atolls. Proc. of the 6th Int. Coral Reef Symp., Australia, 1988, Vol.3: 519-522.

Millham, N. P. and B.L. Howes (1995). A comparison of methods to determine K in a shallow coastal aquifer. Ground Water, 33 (1): 49-57.

Millington, R.J., and P.J. Quirk (1961). Permeability of porous solids. Trans. Faraday Soc., 57: 1200-1206.

Moldrup, P., D.E. Rolston & J.A. Hansen (1989). Rapid and numerically stable simulation of one dimensional, transient water flow in unsaturated layered soils. Soil Sci., 148 (3): 219-226.

Moldrup, P., D.E. Rolston, J.A. Hansen & T.Yamaguchi (1992). A simple, mechanistic model for soil resistence to plant water uptake. Soil Sci., 153 (2): 87-93.

Moldrup, P., T.Yamaguchi, J.A. Hansen & D.E. Rolston (1992). An accurate and numerically stable model for one dimensional solute transport in soils. Soil Sci., April 1992, 153 (4): 261-273.

Monteith, J.L. (1965). Evaporation and the environment. Symp. Soc. Expt. Biol., 19: 205-234.

Monteith, J.L. (1975). Vegetation and the atmosphere. Academic press, London, 1975: Vol. 1 Principles, Vol. 2 Case Studies.

Monteith, J.L. (1990). Principles of Environmental Physics, 2nd Edition. Routledge, Chapman & Hall, Inc.

Morel, F. M. M. and J.G. Hering (1993). Principles and applications of aquatic chemistry. John Wiley & Sons, Inc., Brisbane, pp. 588.

Morns, P.H. & D.J.Williams (1991). Sample size for laboratory calibration of subsurface neutron moisture gauges. Geotechnical Testing Journal, GTJODJ, March 1991, Vol. 14 (1): 71-77.

Morrison, R.D. & J.E. Szecsody (1987). A tensiometer pore water sampler for vadose zone monitoring. Soil Science, November 1987, 144 (5): 367-372.

Mualem, Y. (1976). A new model for predicting the hydraulic conductivity of unsaturated porous media. Water Resources Research, 12 (3): 513-522.

Nielsen, D.M. (1991). Ground-Water Monitoring. Lewis Publishers, Chelsea, Michigan, pp. 717.

Nielsen, P. (1990). Tidal dynamics of the water table in beaches. Water Resouces Research, 26 (9): 2127-2134.

Nolan, G.A. & I.R. Cameron (1989). Total water management on resort islands: design, operation and maintenance. Water, Journal of the Aust. Water and Wastewater association, 15(6):28-30.

Noordink, M., A. Krol, and D. Chen (1992, unpublished). Heron Island Groundwater Programme, status report following field trip 31 January - 9 February 1992. Department of Chemical Engineering, The University of Queensland (departmental report).

Nullet, D. (1987). Energy sources for evaporation on trpoical islands. Phys. Geogr. 8; 36-45.

Oberdorfer J.A., P.J. Hogan & R.W. Buddemeier (1990). Atoll island hydrogeology: flow and freshwater occurrence in a tidally dominated system. Journal of Hydrology, 120: 327-340.

Oberdorfer, J.A. and R.W. Buddemeier (1986). Coral-reef hydrology: field studies of water movement within a barrier reef. Coral Reefs, 5: 7-12.

Oberdorfer, J.A. and R.W. Buddemeier (1988). Climate change: effects on reef island resources. Proc. 6th Int. Coral Reef Symp., Australia, 1988, Vol. 3.

Ogden, J. (1981). Dendrochronological studies and the determination of tree ages in the Australian tropics. Journal of Biogeography, 18: 405-420.

Orme, G.R. & B.G. Thom (1977). Diagenesis in a sequence of Holocene-Pleistocene carbonate deposits of the northern region of the Great Barrier Reef. Geology Society of Australia Incorporated Abstracts of the 2nd Australian Geological Convention, Dept. of Earth Sciences, Monash Univ., 2-4 February, 1977.

Paige, G.B. & D. Hillel (1993). Comparison of three methods for assessing soil hydraulic properties. Soil Science, 155(3): 175-189.

Palmer, C.M. (1992). Principles of contaminant hydrogeology. Lewis Publishers, Chelsea, Mich., 1992, pp. 211.

Parnell, K.E. (1986). Water movement within a fringing reef flat, Orpheus Island, North Queensalnd, Australia. Coral Reefs 5: 1-6.

Peck, A.J. (1960). Change of moisture tension with temperature and air pressure: theoretical. Soil Science, Vol. 89 (6): 303-310.

Penman, H.L. (1948). Natural evaporation from open water bare soil and grass. Proc. Roy. Soc. Lond., 193: 120-145.

Peterson, F.L. & S.B. Gingerich (1995). Modeling atoll groundwater systems. In: Groundwater models for resource analysis and management (Chapter 15), CRC Press Inc., 1995.

Peterson, F.L. (1991). Recent advances in atoll hydrogeology. In: Groundwater in the Pacific rim countries. Proc. Sympo. Sponsored by the Irrigation & Drainage Division of the Am. Soc. of Civil Engineers, Honolulu, Hawaii, 23-25 July 1991, pp. 183.

Philip, J. R., (1957). The Theory of infiltration 1. Soil Science, 83:345-357.

Philip, J. R., (1969). Theory of infiltration. Division of Plant Industry, CSIRO, Canberra, Australia. Advances in Hydroscience, 1969, Vol. 5.

Pinder, G.F. & H.H. Cooper Jr. (1970). A numerical technique for calculating the transient position of the saltwater front. Water Resources Research, 6(3): 875-882.

Plummer, L.N. (1975). Mixing of seawater with calcium carbonate seawater. Geological Society of America, Memoir 142.

Polubarinova-Kochina, P. YA. (1962). Theory of ground water movement. Translated from the Russian by J.M. Roger de Wiest, Princeton Univ. Press, Princeton, New Jersey, 1962.

Priestly, C.H.B. & R.J. Taylor (1972). On the assessment of surface heat flux and evaporation using largescale parameters. Mont. Weather Rev., 100: 81-92.

QDT (1992). Queensland Department of Transport. Mineral House 41 George Street, GPO Box 2595, Brisbane 4001.

Raupach, M.R. (pers. commun., 1992). Personal Communication. Senior Principal Research Scientist, CSIRO Division of Environmental Mechanics, Canberra, Australia.

Reilly, T.E. & A.S. Goodman (1985). Quantitative analysis of smaltwater-freshwater relationships in groundwater systems - a historical perspective. J. of Hydrol., 80: 125-160.

Richards, H.C. (1938). Boring operations at Heron Island, Great Barrier Reef (17 May to 13 August 1937). Rep. of The Great Barrier Reef Comm., 4(3): 135-142.

Richards, H.C. and D. Hill (1942). Great Barrier Reef bores, 1926 and 1937: descriptions, analyses and interpretations. Rep. of the Great Barrier Reef Comm., 5: 1-111.

Richter, J. (1980). A simple numerical solution for the vertical flow equation of water through unsaturated soils. Soil Sci., 129 (3).

Risk, M.J. and H.R. Muller (1983). Porewater in coral heads: Evidence for nutrient regereration. Limnol. Oceanogr., 28(5), 1983, 1004-1008.

Robinson, T.W. (1939). Earth tides shown by fluctuations of water levels in wells in New Mexico and Iowa. Trans. Amer. Geophy. Union, v. 20: 656-666.

Rogowski, A.S. (1971). Watershed physics: model of the soil moisture characteristic. Water Resources Research, 7(6): 1575-1582.

Rose, C.W. (1965). Determination of hydraulic conductivity as a function of depth and water content in-situ. Aust. Journal of Soil Res., Vol.3.

Ross, P.J. & J.Y. Parlange (1994). Comparing exact and numerical solutions of Richard's equation for one-dimensional infiltration and drainage. Soil Science, 157 (6): 341-344.

Ross, P.J. (1993). A method for solving hydraulic properties from field water cotents for application in water balance studies. J. Hydrol., 144: 143-153.

Rushton, K.R. & C. Ward (1979). The estimation of groundwater recharge. J.Hydrol. 41: 345-361.

Sansone, F.J. (1985). Methane in the reef flat porewaters of davies Reef, Great Barrier Reef (Australia). Proc. 5th Int. Coral Reef Congress, Tahiti, 1985, Vol.3:415-419.

Sansone, F.J., C.C. Andrews, R.B. Buddemeier & G.W. Tribble (1988b). Well-point sampling of reef interstitial water. Coral Reefs, 7: 19-22.

Sansone, F.J., G.W. Tribble, R.W. Buddemeier, C.C. Andrews (1988a). Time and space scales of anaerobic diagenesis within a coral reef frwmework. Proc. 6th Int. Coral Reef Symp., Australia, 1988, Vol. 3: 367-372.

Schmugge, T.J., T.J. Jackson, and H.L. McKim (1980). Survey of methods for soil moisture determination. Water Resources Research, 6: 961-979.

Serfes, M.E. (1991). Determining the mean hydraulic gradient of ground water affected by the tidal fluctuations. Ground Water, Vol. 29(4): 549-555.

Shaw, E. M. (1985). Hydrology in practice. Van Nostrand Reinhold (UK) Co. Ltd, England, pp. 569.

Shuttleworth, W.J. (1988). Evaporation from Amazonian rainforest. Proc. R. Soc. London, B233: 321-346.

Sophocleous, M., & C.A. Perry (1985). Experimental studies in natural groundwater recharge dynamics: the analysis of observed recharge events. J. Hydrol., 81: 297-332.

Spittlehouse, D.L. & J.A. Black (1981). Measuring and modelling forest evapotranspiration. The Canadian Journal of Chemical Engineering, 59: 173-180.

Staunton Smith, J. (1992). Bird guano and local eutrophication at Heron Island. Univ. of Queensland, Unpublished thesis submitted as partial fulfilment of B.Sc.(Hons.), pp. 79.

Stewart, J.B. (1984). Measurement and prediction of evaporation from forested and agricultural catchments. Agricultural Water Management, 8:1-28.

Stoddart, D.R., P.E. Gibbs & D. Hopley (1981). Natural history of Raine Island, Great Barrier Reef. Atoll Research Bulletin, No. 254. Issued by the Smithsonian Institute, Washington, D.C., USA, July 1981.

Sully, M. & I. White (1987). A rapid in situ method for measuring soil hydraulic properties and structure with the disc permeameter. In: Conference & Workshop Series, Qld Dept. Primary Industries, 1987, No. qc87006: 140-143a. proc (editors: K.J. Coughlan & P.N. Truong). National workshop, Toowoomba, Qld, 7-10 Sept., 1987.

Sunmap (1979). Heron Island, Great Barrier Reef (1:2500 contoured, 1:1000 and 1:25 000). Sunmap, Dept. Mapping & Surveying, Queensland Dept.of Natural Resources, Brisbane, Australia.

Thom, B.G. & P.S. Roy (1985). Relative sealevels and coastal sedimentation in southeast Australia in the Holocene. Journal of Sedimentology and Petrology, 55(2): 257-264.

Todd, D.K., (1980). Ground Water Hydrology, 2nd Edition. John Wiley and Sons, New York, NY, pp. 496.

Touloukian, Y.S., P.E. Liley, S.C. Saxena (1970). Thermal Conductivity. Vol. 3, Nonmetallic Liquids and Gases. IFI/PLENUM, New York, Washington.

Touloukian, Y.S., P.E. Liley, S.C. Saxena (1970). Thermal Conductivity. Vol. 2, Nonmetallic Solids. IFI/PLENUM, New York, Washington.

Tribble, G.W., F.J. Sansone, Y.H. Li, S.V. Smith and R.W. Buddemeier (1988). Material fluxes from a reef framework. Proc. 6th Int. Coral Reef Symp., Townsville, 2: 577-582.

Turc, L. (1954). Calcul du bilan de l'eau evaluation fonction des precipitations at des temperatures. IASH Rome Symp. 111 Pub. No. 38: 188-202.

Turner, I. (1993). Water table outcropping on macro-tidal beaches: a simulation model. Marine Geology, 115: 227-238.

Underwood, M.R. (1990). Atoll island hydrogeology: conceptual and numerical models. Ph.D. Thesis in geology and geophysics, May 1990. University of

Hawaii, 1990.

Underwood, M.R., F.L. Peterson, and C.I. Voss (1992). Groundwater lens dynamics of atoll islands. Water Resour. Res., 28(11): 2889-2902.

Urish, D.W. and M.M. Ozbilgin (1989). The coastal ground-water boundary. Ground Water, 27(3): 310-315.

Vacher, H.L. and T.M. Quinn (Editors) (1997). Geology and Hydrogeology of Carbonate Islands, Developments in Sedimentology, Vol. 54. Elsevier, Amsterdam, 948 pp.

Vacher, H.L. & J.F. Ayers (1980). Hydrology of small oceanic islands - utility of an estimate of recharge inferred from the chloride concentration of the freshwater lenses. Journal of Hydrology, 45: 21-37.

Vacher, H.L. (1978). Hydrology of small oceanic islands - influence of atmospheric pressure on the water table. Ground Water, Vol. 16(6): 417-423.

van der Heijde, P.K.M. & O.A. Elnawawy (1992). Quality assurance and quality control in the development and application of ground-water models. Robert S. Kerr Environmental Research Laboratory, Office of Research and Development, U.S. Environmental Protection Agency, ADA, Oklahoma 74820, EPA/600/R-93/011, Sept. 1992.

van der Kamp and J.E. Gale (1983). Theory of Earth tide and barometric effects in porous formations with compressible grains. Water Resources Res., 19: 538-544.

van der Kamp, (1972). Tidal fluctuations in a confined aquifer extending under the sea. Ottawa, Env. Canada reprint 242: 101-106.

van Genuchten, M. Th. (1980). A closed-form equation for predicting the hydraulic conductivity of unsaturated soils. Soil Sci. Am. J., 44: 892-898.

Vanek, V. (1993). Groundwater regime of a tidally influenced coastal pond. J. of Hydrology, 151: 317-342.

Vogt, R. & L. Jeager (1990). Evaporation form a pine forest - using the aerodynamic method and Bowen ratio method. Agr. Forest Meteor., 50: 39-54.

Volker (1980). Predicting the movemet of seawater into a coastal aquifer. Australian Water Resources Council Technical Paper No. 51, Aust. Govt. Publ. Service,

Canberra, 1980, pp. 72.

Voss, C.I. (1984). SUTRA: A finite element simulation model for saturated-unsaturated, fluid-density dependent ground-water flow with energy transport or chemically reactive single species solute transport. US Geological Survey, National Centre, Reston Virginia.

Walker, T. A. (1991b). The distribution, abundance and dispersal by seabirds of Pisonia grandis. In National Museum of National History, Smithonian Institute, Washington D.C., U.S.A. (Issued by), Pisonia islands of the Great Barrier Reef. Atoll Res. Bull., 350: 1-23.

Walker, T.A. (1991a). Tourism Development and Environmental Limitations at Heron Island, Great Barrier Reef. J. Environ. Manage., 33: 117-122.

Walker, T.A. (1991c). Is the Reef really suffering from chronic pollution? Search, 22(4): 115-117.

Warrick, A.W. (1983). Parameters in infiltration equations. Advances in infiltration. Proc. of the Nat. Conf.on Advances in Infil., December 12-13, 1983, Chicago Illinois. Amer. Soc. of Agric. Engineers: 69-81.

Weeks, W.D. (1982). Evaporation: a case study using data from a lake in Eastern Queensalnd. Hydrology and Water Resources Symposium, 1982, Melbourne, 11-13 May: 189-193.

Wheatcraft, S.W., and Buddemeier, R.W., (1981). Atoll island hydrology. Ground Water, 19(3): 311-320.

White, I. (1988). Measurement of soil physical properties in the field. In: Flow and transport in the natural environment: advances and applications. W.L.Steffen & O.T.Denmead (editors). Springer Verlag, Berlin: 59-85.

White, I. and K.M. Perroux (1989). Estimation of unsaturated hydraulic conductivity from field sorptivity measurements. Soil Sci. Soc. Am. J., 53: 324-329.

Whitehead, D. & F.M. Kelliher (1991). Modeling the radiation balance of a small radiata catchement. Tree Physiology, 9: 17-33.

Whitten, D.G.A., and J.R.V. Brooks (1987). "The Penguin Dictionary of Geology". Penguin Books Ltd, Great Britain, 1987.

Wigley, T.M.L. & L.N. Plummer (1976). Mixing of carbonate waters. Geochimica et Cosmochimica Acta. Pergamon Press., 40: 989-995.

William, R.D., L.R. Ahuja & J.W. Naney (1992). Comparison of methods to estimate soil water characteristics from soil texture, bulk density and limited data. Soil Science, 153(3): 172-184.

Wooding, R.A. (1968). Steady infiltration from a circular pond. Water Resources Research, 4: 1254-1273.

Woodley, S.J. (1989). Management of water quality: Great Barrier Reef Marine Park. Water, Journal of the Aust. Water and Wastewater association, 15(6): 20-22.

Yeh, G.T. and D.S. Ward (1980). FEMWATER: A finite element model of water flow through saturated-unsaturated porous media. rep. ORNL-5567. Oak Ridge National Laboratory, Oak Ridge, Tenn., pp. 153.

Yim, C.S. & M.F.N. Mohsen (1992). Simulation of tidal effects on contaminant transport in porous media. Ground Water, 30 (1): 78-86.

Zhang, L. & R. Lemeur (1992). Effect of aerodynamic resistance on energy balance and Penman-Monteith estimates of evapotranspiration in greenhouse conditions. Agricultural and Forest Meteorology, 58: 209-228.

APPENDIX A

APPENDIX A.

Table A-1. Sieve sizes used in the particle-size analysis of Heron Island soil.

Size Type	Sieve Size (mm)	Sieve Number (#)	Phi (ϕ)
gravel	4	14	-2
gravel	2.80	13	-1.5
gravel	2.00	12	-1.0
very coarse sand	1.40	11	-0.5
very coarse sand	1.00	10	0.0
coarse sand	0.71	9	0.5
coarse sand	0.500	8	1.0
medium sand	0.355	7	1.5
medium sand	0.25	6	2.0
fine sand	0.180	5	2.5
fine sand	0.125	4	3.0
very fine sand	0.090	3	3.5
very fine sand	0.0630	2	4.0
silt and clay size	0	1-PAN	PAN

Notes:
(a) gravel-sized = 2.0 - 60 mm
(b) sand-sized = 0.06 - 2.0 mm
(c) silt-sized = 0.002 - 0.06 mm

Table A-2. Climatic averages for Heron Island (Australian Bureau of Meteorology, 1975).

	Jan	Feb	Mar	Apr	May	Jun	Jul	Aug	Sep	Oct	Nov	Dec	Year
9 am													
Dry Bulb (C)	27.5	27.2	26.3	24.6	22.0	20.1	18.8	19.8	22.1	24.3	26.0	26.7	23.8
Wet Bulb (C)	23.8	23.7	22.9	21.2	18.9	17.1	15.9	16.8	18.2	20.2	22.1	22.8	20.3
Dew Point (C)	22	22	21	19	17	15	14	15	16	18	20	21	18
Rel. Hum. (%)	72	73	73	72	73	72	72	72	67	67	70	70	71
3 pm													
Dry Bulb (C)	28.2	27.9	26.9	25.5	23.0	21.1	20.3	21.3	23.0	24.8	26.4	27.2	24.6
Wet Bulb (C)	24.1	24.0	23.1	21.4	19.1	17.4	16.6	17.3	18.4	20.3	22.2	23.1	20.6
Dew Point (C)	22	22	21	19	17	15	14	14	15	18	20	21	18
Rel. Hum. (%)	70	71	71	68	67	67	67	65	62	64	68	69	67
Daily Max. Temperature													
Mean (C)	29.6	29.4	28.3	26.9	24.3	22.3	21.3	22.4	24.6	26.7	28.1	28.7	26.1
86 Perc. (C)	31.3	31.1	30.0	28.5	26.1	23.9	23.3	24.4	26.1	28.3	29.4	30.5	
14 Perc. (C)	27.8	27.8	26.7	25.0	22.2	20.6	18.9	20.0	22.8	25.0	26.7	27.2	
Daily Min. Temperature													
Mean (C)	23.8	23.8	23.0	21.5	19.4	17.3	16.2	16.9	18.5	20.2	22.1	22.8	20.5
86 Perc. (C)	25.6	25.6	24.6	23.3	21.7	19.4	18.3	19.2	20.6	21.7	23.9	24.4	
14 Perc. (C)	22.2	22.2	21.1	19.4	16.7	15.0	13.9	14.4	16.1	18.3	20.6	21.1	
Rainfall													
Mean (mm)	154	141	102	74	105	131	88	50	20	43	60	101	1069
Median (mm)	146	119	86	68	127	68	65	43	13	26	57	80	
Raindays													
Mean (No.)	14	17	14	13	15	12	17	7	5	6	8	8	136

Notes:
a) Computed from data collected between 1957-1975.
b) Station name is Heron Island, Queensland, Australia.
c) Latitude 23 Deg 26 Min S; Longitude 151 Deg 55 Min E; Elevation 3.7 m.
d) Perc. = percentile.

Table A-3. Heron Island sand particle size distributions and classifications.

No.	Sample Number (#)	Middle Depth of Sample z (m LWD)	Geometric Mean Size by Mass d_{gm} (mm)	Geometric Standard Deviation σ_{gm} (mm)	Mass Fraction Silt-Sized (%)	Mass Fraction Sand-Sized (%)	Mass Fraction Gravel-Sized (%)
1	1.01	6.32	0.53	1.43	4.06	94.81	1.13
2	1.02	6.24	0.59	1.43	0.23	98.91	0.85
3	1.03	5.66	0.59	1.41	1.18	98.32	0.5
4	1.04	5.16	0.60	1.37	0.18	99.77	0.05
5	1.05	4.74	0.57	1.36	0.45	99.48	0.07
6	1.06	4.32	0.56	1.27	0.05	99.89	0.06
7	1.07	3.82	0.55	1.29	0.02	99.91	0.07
8	1.09	3.14	0.57	1.36	0.07	99.86	0.07
9	1.10	2.745	0.57	1.38	0.07	99.67	0.26
10	1.11	2.53	0.59	1.43	0.03	99.63	0.34
11	1.12	2.205	0.63	1.50	0.03	98.73	1.24
12	1.13	1.835	0.61	1.55	0.13	97.89	1.98
13	1.14	1.525	0.68	1.55	0	94.43	5.56
14	1.15	1.08	0.61	1.55	0.08	96.75	3.17
15	1.16	0.7	0.61	1.62	0.04	94.86	5.11
16	1.17	0.455	0.64	1.92	0.06	91.59	8.35
17	2.01	2.23	0.66	2.09	0.26	88.05	11.69
18	2.02	1.79	0.83	1.84	0.93	89.66	9.4
19	2.03	0.68	0.92	2.36	0.27	82.56	17.18
20	2.04	0.29	0.89	2.31	0.7	82.89	16.42
21	2.05	-0.335	0.97	2.98	0.7	76.08	23.22
22	3.01	5.13	0.66	1.50	0.03	96.5	3.47
23	3.02	4.63	0.61	1.53	0.19	97.42	2.39
24	3.03	4.13	0.69	1.55	0.3	94.87	4.83
25	3.04	3.63	0.66	1.51	0.54	94.92	4.54
26	3.05	3.13	0.62	1.48	0.41	98.95	0.65
27	3.06	2.63	0.63	1.47	0.11	99.34	0.55
28	3.07	2.13	0.66	1.57	0.35	96.17	3.48
29	3.08	1.63	0.69	1.61	0.05	94.96	4.99
30	3.09	1.13	0.68	1.74	0.12	93.09	6.78
31	4.01	5.1	1.29	4.02	0.07	55.11	44.82
32	4.02	4.6	0.85	1.49	0.47	97.29	2.24
33	4.03	4.1	0.68	1.46	0.44	96.33	3.23
34	4.04	3.6	0.64	1.52	0.38	97.82	1.8
35	4.05	3.1	0.68	1.89	0.28	89.85	9.87
36	4.06	2.6	0.79	2.55	0.15	83.85	16
37	4.07	2.1	1.01	2.34	0.16	79.36	20.48
38	4.08	1.6	1.05	1.87	0.11	84.98	14.91
39	4.09	1.1	1.07	2.09	0.12	81.43	18.45
40	5.01	4.97	0.79	1.61	0.06	90.63	9.31
41	5.02	3.97	0.74	1.62	0.05	91.27	8.68
42	5.03	2.97	0.79	1.53	0.05	96.19	3.76
43	5.04	1.97	1.09	3.71	0.03	71.26	28.7
44	5.05	0.97	1.02	2.73	0.55	76.47	22.98

(continued next page)

Table A-3. (continued)

No.	Sample Number	Middle Depth of Sample z	Geometric Mean Size by Mass d_{gm}	Geometric Standard Deviation σ_{gm}	Mass Fraction Silt-Sized	Mass Fraction Sand-Sized	Mass Fraction Gravel-Sized
	(#)	(m LWD)	(mm)	(mm)	(%)	(%)	(%)
45	6.01	4.42	0.68	1.44	0.21	97.82	1.98
46	6.02	3.92	0.72	1.56	0.23	94.51	5.25
47	6.03	3.42	0.75	1.64	0.28	91.12	8.6
48	6.04	2.92	0.76	1.67	0.18	91.38	8.44
49	6.05	2.42	0.84	2.04	0.22	86.37	13.4
50	6.06	1.92	0.94	2.14	0.19	83.77	16.03
51	6.07	1.42	1.10	2.78	0.31	74.51	25.18
52	6.08	0.92	1.26	3.11	0.22	65.47	34.3
53	6.09	0.42	1.03	2.68	0.22	76.62	23.16
54	6.10	-0.08	1.15	3.10	0.5	70.26	29.24
55	7.01	5.42	0.58	1.52	2.55	96.06	1.39
56	7.02	4.42	0.63	1.45	0.11	99.34	0.54
57	7.03	3.42	0.65	1.45	0.02	98.95	1.03
58	7.04	2.42	0.68	1.48	0.02	97.59	2.38
59	7.05	1.42	0.89	1.56	0	93.1	6.9
60	8.01	8.1	0.68	1.38	0.02	98.8	1.18
61	8.02	7.1	0.56	1.43	0.67	99.28	0.06
62	8.03	6.1	0.64	1.45	0.42	99.41	0.17
63	8.04	5.1	0.67	1.43	0.21	99.67	0.12
64	8.05	4.1	0.68	1.42	0.1	99.34	0.56
65	9.01	7.62	0.57	1.63	9.41	84.76	5.83
66	9.02	6.62	0.57	1.52	11.63	87.38	0.99
67	9.03	5.62	0.56	1.51	9.74	89.24	1.01
68	9.04	4.62	0.53	1.53	14.32	84.88	0.8
69	9.05	3.62	0.58	1.48	5.6	93.97	0.42
70	9.06	2.62	0.85	1.57	7.77	87.55	4.68
71	9.09	-0.38	2.36	1.84	5.6	34.38	60.01
72	9.12	-3.38	3.89	1.35	10.36	15.27	74.37
73	9.14	-5.18	2.99	1.68	16.07	18.87	65.06
74	10.01	4.04	0.54	1.58	1.69	97.6	0.71
75	10.02	3.04	0.61	1.48	0.47	98.88	0.65
76	10.03	2.04	0.97	1.82	0.31	88.67	11.02
77	11.01	5.03	0.53	1.53	0.43	98.17	1.4
78	11.03	3.03	0.57	1.44	0.06	99.24	0.7
79	11.04	2.03	0.79	1.72	0.05	93.49	6.46
80	12.01	4.75	0.54	1.41	0.19	98.93	0.88
81	12.02	3.75	0.55	1.52	0.12	99	0.88
82	12.03	2.75	0.64	1.51	0.11	97.75	2.14
83	13.01	4.75	0.64	1.52	0.66	93.63	5.72
84	13.02	3.75	0.72	1.42	0.15	95.85	4.01
85	13.03	2.75	0.75	1.59	0.1	96.63	3.28
86	13.04	1.275	0.92	1.94	0.08	87.41	12.51
87	13.05	0.75	0.85	2.23	0.19	85.02	14.79

Notes:
(a) Sieving was carried out by the Department of Geology, The University of Queensland.
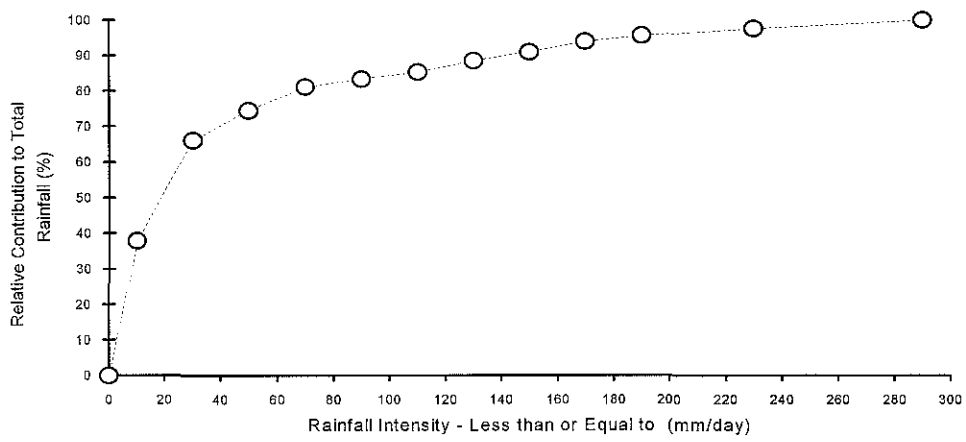
Figure A-1. Proportion of total rainfall at Heron Island as a function of rainfall intensity (calculated from daily rainfall figures for the period 1985-1994).

APPENDIX A1 The Penman and Penman-Monteith Formulae: Notes

The Penman and Penman-Monteith formulae are partially derived below in order to highlight some important features of these formulae and of the evapotranspiration process itself. Firstly, consider the following equation for estimating evapotranspiration, E_t (after Dalton, circa 1800):

$$E_t = \frac{c_{vs} - c_{va}}{r_v}$$

(Equation A-1)

where,

c_{vs}	= water vapour concentration at the surface	$(g\ m^{-3})$
c_{va}	= water vapour concentration of the air	$(g\ m^{-3})$
E_t	= evapotranspiration rate	$(g\ m^{-2}\ s^{-1})$
r_v	= total resistance to water vapour transfer	$(s\ m^{-1})$

The total resistance to vapour transfer (r_v) is comprised of two components, ie:

$$r_v = r_{vc} + r_{va}$$

(Equation A-2)

where r_{va} is the atmospheric boundary layer (ABL) resistance to turbulent water vapour transfer (units are $s\ m^{-1}$) and r_{vc} is the canopy resistance to vapour diffusion (units are $s\ m^{-1}$). Both parameters are empirical and may be averaged in space and time. The canopy resistance, r_{vc}, is a biophysical parameter that is directly related to the stomatal resistance of the vegetation, r_{vs}, and inversely related to the surface area of the vegetation. The following equation for r_{vc} can be used if r_{vs} can be assumed spatially uniform:

$$r_{vc} = r_{vs} / 2\ LAI$$

(Equation A-3)

where

r_{vs}	= stomatal resistance to vapour diffusion	$(s\ m^{-1})$
LAI	= leaf area index	$(m^2\ m^{-2})$

The water vapour deficit between the air and the plant surface (refer Equation A-2) may be closely approximated using the local slope of the saturated water vapour-temperature curve (Campbell, 1977):

$$c_{vs} - c_{va} \cong c'_{va} - c_{va} + s(T_s - T_a)$$ **(Equation A-4)**

where,

c'_{va} = saturated water vapour concentration of the air   (g m^{-3})

s = $\dfrac{\partial c'_{va}}{\partial T_a}$, local slope of the c'_{va} - T_a curve   (g m^{-3} K^{-1})

T_a = air temperature   (°C)

Hence, by substituting Equation A-4 into Equation A-1, the following is obtained,

$$E_t = \frac{c'_{va} - c_{va} + s(T_s - T_a)}{r_v}$$ **(Equation A-5)**

Then by substituting T$_s$-T$_a$ with a heat flow formula (refer Equation 2-8) the following may be obtained:

$$E_t = \frac{c'_{va} - c_{va}}{r_v} + \frac{sHr_h}{C_p \, r_v} .$$ **(Equation A-6)**

The above derivation assumes that the evaporating surface is the same as the surface for convective heat. For an evaporating system involving a soil surface as well as a plant canopy, the primary surface for heat exchange may in fact be quite different to the primary surface for vapour exchange (Campbell, 1977). However, according to Campbell (1977), in dense well-watered crop canopies the heat exchange and the vapour exchange surfaces are essentially the same.

If Equation 2-6 and Equation A-6 are combined, then the well-known Penman formula may be derived after some rearranging:

$$LE_t = \frac{s(R_n - G_H)}{\gamma^* + s} + \frac{C_p/r_h (c'_{va} - c_{va})}{\gamma^* + s}$$

(Equation A-7)

where γ (the psychrometric constant with units of g m^{-3} K^{-1}) and γ^* (the apparent psychrometric constant with units of g m^{-3} K^{-1}) are introduced to simplify the formula, ie:

$$\gamma = \frac{C_p}{L}$$

(Equation A-8)

and

$$\gamma^* = \gamma \frac{r_v}{r_h}$$

(Equation A-9)

The equilibrium evapotranspiration rate (E_{eq}) is the ideal rate of E_t which would occur if E_t were the result of radiation adsorption only and not the result of the atmospheric moisture deficit or turbulence, ie:

$$E_{eq} = \frac{s(R_n - G_H)}{(\gamma^* + s)L}$$

(Equation A-10)

Campbell (1977) argues that the Penman formula is not always useful because of R_n's implicit dependence on T_s (refer Equation 2-7) and the fact that R_n and T_s are rarely measured in the field. To help overcome these problems, Monteith (1965) provides a linearized model for the net long-wave radiation based upon air temperature in what is known as the Penman-Monteith formula (see Equation A-11). The Penman-Monteith formula differs from the Penman formula because (a) net isothermal radiation, R_{ni}, is used instead of R_n, and (b) non-isothermal long-wave radiation conductance and heat conductance are combined in a single conductance term, K_{hr}, ie:

$$E_t = \frac{s}{s+\gamma^*} \frac{R_{ni} - G}{L} + \frac{\gamma^*}{s+\gamma^*} \frac{c'_{va} - c_{va}}{r_{vc} + r_{va}}$$

(Equation A-11)

where,

$$\gamma^* = \frac{r_v K_{hr}}{L},$$

(Equation A-12)

$$K_{hr} = \frac{C_P}{r_h} + K_r$$

(Equation A-13)

and

$$K_r = 4\,\varepsilon_s\,\sigma T_a^{\,3}.$$

(Equation A-14)

The ratio of E_t to E_{tP} is given by the following relationship (Campbell, 1977):

$$\frac{E_t}{E_{tP}} = \frac{(s+\gamma^*_p)}{(s+\gamma^*)}$$

(Equation A-15)

where γ^*_p is the apparent psychrometric constant when r_{vc} is at its minimum value.

In certain situations hydrologists may attempt to estimate actual evapotranspiration by scaling estimates of E_{tP}. But difficulty with measuring plant and aerodynamic resistances has been a major problem with the approach (Campbell, 1977). Another major problem which may render the approach "...futile..." (Campbell, 1977; p141), is that actual E_t can be functionally unrelated to E_{tP} when the soil-plant system is controlling water loss and not the atmospheric boundary layer.

APPENDIX B

APPENDIX B.

Table B-1. Rainfall intensity class frequency analysis for Heron Island 1956-1995 (raw data supplied by the Bureau of Meteorology, 1995).

Lower Limit >	Upper Limit <=	Middle Value	Frequency	Normalised Frequency
(mm d^{-1})	(mm d^{-1})	(mm d^{-1})	(d)	
0	0	0	8406	
0	1	0.5	1401	0.31161
1	2	1.5	595	0.13234
2	3	2.5	386	0.085854
3	4	3.5	255	0.056717
4	5	4.5	225	0.050044
5	10	7.5	645	0.028692
10	15	12.5	323	0.014368
15	20	17.5	163	0.007251
20	25	22.5	135	0.006005
25	30	27.5	87	0.00387
30	35	32.5	54	0.002402
35	40	37.5	55	0.002447
40	45	42.5	25	0.001112
45	50	47.5	28	0.001246
50	55	52.5	22	0.000979
55	60	57.5	15	0.000667
60	65	62.5	10	0.000445
65	70	67.5	11	0.000489
70	75	72.5	7	0.000311
75	80	77.5	10	0.000445
80	85	82.5	9	0.0004
85	90	87.5	4	0.000178
90	95	92.5	3	0.000133
95	100	97.5	1	4.45E-05
100	150	125	13	5.78E-05
150	200	175	10	4.45E-05
200	250	225	2	8.90E-06
250	300	275	2	8.90E-06
300	350	325	0	0
>350			0	0

Table B-2. The micro-climatic parameters recorded at Heron Island during the short-term monitoring exercise.

No.	Data Type	Sensor Type	Instrument Precision	Units	Sample Time	Station Name
1	T_a	Air Temperature	± 0.5	°C	hourly, instantaneous	wind station
2	R.H.	Relative Humidity	± 1	%	hourly, instantaneous	wind station
3	P	Tipping Bucket Raingauge	± 3	mm x 10^{-1}	hourly, cumulative	wind station
4	U	Anemometer	± 1	knots	hourly, 1 minute average	wind station
5	T_c	Canopy Air Temperature	± 0.3	°C	hourly, 1 minute average	soil-moisture station
6	T_{-5}	- 5 cm Soil Temperature	± 0.3	°C	hourly, 1 minute average	soil-moisture station
7	T_{-10}	-10 cm Soil Temperature	± 0.3	°C	hourly, 1 minute average	soil-moisture station
8	P_c	Below Canopy Raingfall	± 0.3	mm h^{-1}	hourly, cumulative	soil-moisture station
9	p_1	Pressure Transducer		-kPa	hourly, 1 minute average	soil-moisture station
10	p_2	Pressure Transducer		-kPa	hourly, 1 minute average	soil-moisture station
11	p_3	Pressure Transducer		-kPa	hourly, 1 minute average	soil-moisture station
12	p_4	Pressure Transducer		-kPa	hourly, 1 minute average	soil-moisture station
13	p_5	Pressure Transducer		-kPa	hourly, 1 minute average	soil-moisture station
14	p_6	Pressure Transducer		-kPa	hourly, 1 minute average	soil-moisture station
15	S_{hu}	Solar Radiation Sensor	0.01 %	uncalibrated	hourly, cumulative	solar station

Notes:
(a) For descriptions of the monitoring stations and equipment refer to the main text.

Table B-3. Parameters contained in the HIRS weather station records.

No.	Sensor Type	Data Type	Units	Precision of Instrument	Timing of Records
18	Raingauge	P	mm/d		Daily at 9 am (H.I.R.S.)
19	Mercury Thermometer	T_{min}	°C		Daily at 9 am (H.I.R.S.)
20	Mercury Thermometer	T_d	°C		Daily at 9 am (H.I.R.S.)
21	Mercury Thermometer	T_w	°C		Daily at 9 am (H.I.R.S.)
22	Mercury Thermometer	T_{max}	°C		Daily at 9 am (H.I.R.S.)

Table B-4. Installation details and calibration data for the electronic equipment used in the soil-moisture station.

Sensor Type	Data Type	Data Recorder Channel Number	Position RGL z (cm)	Calibration Constant (kPa/Hz)	Zero Offset Constant ρgH (kPa)	Date and Time of Installation (dd/mm/yy hh)
Tensiometer	p_1	1	-20	1.659	4.1	19/12/93 2 pm
Tensiometer	p_2	3	-50	1.658	7.9	19/12/93 2 pm
Tensiometer [a]	p_3	6	-70	1.684	8.1	23/3/94 2 pm
Tensiometer	p_4	2	-103	1.686	12.1	19/12/93 2 pm
Tensiometer	p_5	5	-145	1.696	14.9	19/12/93 2 pm
Tensiometer	p_6	4	-200	1.673	21.1	19/12/93 2 pm
Temperature	T_{-5}	8	-5	1/3 [b]	-	19/12/93 2 pm
Temperature	T_{-10}	9	-10	1/3 [b]	-	19/12/93 2 pm
Temperature	T_c	7	308	1/3 [b]	-	19/12/93 2 pm
Rainfall	P_c	10	40	3 [b]	-	19/12/93 2 pm

Notes:
a) Due to a technical fault, this tensiometer was not installed until 2 pm on the 23/3/94.
b) Manufacturer's calibration.

Table B-5. The microclimate database filenames.

Station 1: Hourly Weather Station Records	Station 2: Hourly Soil-moisture Station Records	Station 3: Hourly Solar Station Records	Station 4: Hourly Wet and Dry Bulb Records	Station 5: H.I.R.S. 9 am Meteoro-logical Records
NOV93_S1.TXT	-	-	-	1982_S .TXT
DEC93_S1.TXT	DEC93_S2.TXT	DEC93_S3.TXT	-	1983_S .TXT
JAN94_S1.TXT	JAN94_S2.TXT	JAN94_S3.TXT	-	1984_S .TXT
FEB94_S1.TXT	FEB94_S2.TXT	FEB94_S3.TXT	-	1985_S .TXT
MAR94_S1.TXT	MAR94_S2.TXT	MAR94_S3.TXT	-	1986_S .TXT
APR94_S1.TXT	APR94_S2.TXT	APR94_S3.TXT	-	1987_S .TXT
MAY94_S1.TXT	MAY94_S2.TXT	MAY94_S3.TXT	-	1989_S .TXT
JUN94_S1.TXT	JUN94_S2.TXT	JUN94_S3.TXT	-	1990_S .TXT
JUL94_S1.TXT	JUL94_S2.TXT	JUL94_S3.TXT	JUL94_S1.TXT	1991_S .TXT
AUG94_S1.TXT	AUG94_S2.TXT	AUG94_S3.TXT	AUG94_S1.TXT	1992_S .TXT
SEP94_S1.TXT	SEP94_S2.TXT	SEP94_S3.TXT	SEP94_S1.TXT	?
OCT94_S1.TXT	OCT94_S2.TXT	OCT94_S3.TXT	OCT94_S1.TXT	?
	?	?	?	1993_S5.TXT
	?	?	?	1994_S5.TXT

Notes:
a) The first five alphanumerics of the filenames denote the month and year.
b) The last three alphanumerics denote the monitoring station (" _S1" for weather station, " _S2" for soil-moisture station, " _S3" for solar station, " _S4" for A.B.M. meteorological records, and " _S5" for H.I.R.S. meteorological records).
c) A actual data files may be obtained from the Department of Chemical Engineering, the Univeristy of Queensland if not supplied with this thesis.

Table B-6. Corrections to the H.I.R.S. rainfall records for 1994.

Error Type	Beginning	Ending	Changes Made to the Records
Data missing and incorrectly dated.	31-3-94, 9am	1-4-94, 9 am	26th-30th shifted 1 day later, and the 26th replaced with data from raingauge No. 2.
Data missing.	21-4-94, 9 am	1-6-94, 9 am	Substituted with data from raingauge No.2.
Data wrong.	15-4-94, 9 am	20-4-94, 9 am	Data was divided by 10 to correct.
Data missing.	16-8-94, 9 am	17-8-94, 9 am	Substituted with data from raingauge No.2.

Table B-7. Average morning and afternoon atmospheric moisture levels at Heron Island (raw data from the Bureau of Meteorology, 1975).

Month	9 am Averages				•	3 pm Averages		
	Air Temp.	Rel. Humidity	Vapour Conc.	Satd Vapour Conc.	Air Temp.	Rel. Humidity	Vapour Conc.	Satd Vapour Conc.
	Ta ($^\circ$C)	R.H. (%)	c_{va} (g m^{-3})	c_{vs} (g m^{-3})	Ta ($^\circ$C)	R.H. (%)	c_{va} (g m^{-3})	c_{vs} (g m^{-3})
Jan	27.5	72	19.1	26.5	28.2	70	19.3	27.5
Feb	27.2	73	19.0	26.0	27.9	71	19.2	27.1
Mar	26.3	73	18.1	24.8	26.9	71	18.2	25.6
Apr	24.6	72	16.2	22.5	25.5	68	16.1	23.7
May	22	73	14.2	19.4	23	67	13.8	20.6
Jun	20.1	72	12.5	17.4	21.1	67	12.3	18.4
Jul	18.8	72	11.6	16.1	20.3	67	11.8	17.6
Aug	19.8	72	12.3	17.1	21.3	65	12.1	18.6
Sep	22.1	67	13.1	19.5	23	62	12.7	20.6
Oct	24.3	67	14.8	22.1	24.8	64	14.6	22.8
Nov	26	70	17.0	24.4	26.4	68	16.9	24.9
Dec.	26.7	70	17.7	25.3	27.2	69	18.0	26.0
Year	23.8	71	15.5	21.8	24.6	67	15.4	22.8

Table B-8. Linear regression results for T_c and Δp_i.

		$\Delta p_{-50 cm}$	$\Delta p_{-103 cm}$	$\Delta p_{-145 cm}$	$\Delta p_{-200 cm}$
correlation coefficient		-0.89	-0.93	-0.90	-0.91
slope	($^\circ$C/kPa)	-1.76	-1.85	-2.19	-1.44
intercept ($^\circ$C)		26.9	26.1	25.1	26.2
number of consecutive samples (-)		239	239	239	239

Notes:
(a) The linear regression is based upon the data presented in Figure B-2 and the method of least squares.

Table B-9. Weekly rainfall totals for 1994 from three different rainguages at Heron Island.

Week No.	Date Commencing (dd-mmm-yy)	Raingauge[a] No. 1 (mm)	Raingauge[b] No. 2 (mm)	Raingauge[c] No. 3 (mm)
1	1-Jan-94	0	0	0
2	8-Jan-94	6.6	7	0
3	15-Jan-94	98.1	99.6	138.3
4	22-Jan-94	8.2	5.9	6.9
5	29-Jan-94	217.3	226.4	201.6
6	5-Feb-94	3.6	8.4	2.7
7	12-Feb-94	4.2	4.1	1.8
8	19-Feb-94	21	21	15
9	26-Feb-94	83.4	69.8	77.4
10	5-Mar-94	9.6	11.4	3.9
11	12-Mar-94	1.4	0.3	0
12	19-Mar-94	92.4	40.8	71.4
13	26-Mar-94	49.7	44	33
14	2-Apr-94	39.4	39.9	34.2
15	9-Apr-94	8	7.1	1.8
16	16-Apr-94	28.4	24.9	17.1
17	23-Apr-94	57.5	57.4	17.1
18	30-Apr-94	35.5	26.4	22.8
19	7-May-94	14	8.9	5.1
20	14-May-94	8.8	5.1	7.2
21	21-May-94	0	0	0.9
22	28-May-94	4	4.1	5.1
23	4-Jun-94	11.3	8.0	6.3
24	11-Jun-94	34	33.9	35.1
25	18-Jun-94	0	0.0	0.0
26	25-Jun-94	0	0.0	0.0
27	2-Jul-94	37.2	34.5	6.0
28	9-Jul-94	112.4	99.1	99.1
29	16-Jul-94	14.6	7.8	7.8
30	23-Jul-94	1.4	0.8	0.0
31	30-Jul-94	0.4	0.3	0.0
32	6-Aug-94	1.4	4.0	7.2
33	13-Aug-94	7.2	8.3	5.1
34	20-Aug-94	12.2	13.0	11.7
35	27-Aug-94	40.4	3.3	2.4
36	3-Sep-94	0.2	0.0	0.0
37	10-Sep-94	0.4	0.0	0.0
38	17-Sep-94	0	0.0	0.0
39	24-Sep-94	0.1	0.0	0.0
40	1-Oct-94	0	0.0	0.0
41	8-Oct-94	1.8	4.3	3.6
42	15-Oct-94	3.4	3.8	3.9
43	22-Oct-94	12.2	12.9	12.9
	TOTALS (mm)			

Notes:
(a) Provided by the H.I.R.S. (with amendments).
(b) Weather station raingauage (with amendments).
(c) Soil-moisture station rainguage located beneath the *Pisionia* forest (with amendments).
(d) The weekly rainfall totals begin at 9 am.

Table B-10. Summary data from the soil moisture profiling investigations in the study site at Heron Island.

Time	Day	Month	Year	Depth	Liquid Content	Standard Error	Water per layer	Total Water
				z	w	Δw		
(24 hr)	(day)	(month)	(year)	(cm RGL)	(g/g%)	(g/g%)	(mm)	(mm)
12	12	12	93	-2	50.00	8.38	42.84	
12	12	12	93	-15	8.83	0.13	13.11	
12	12	12	93	-30	8.09	0.46	13.59	
12	12	12	93	-45	8.44	0.65	14.94	
12	12	12	93	-60	7.93	0.13	14.75	
12	12	12	93	-75	7.79	0.20	15.19	
12	12	12	93	-90	4.84	0.31	9.87	
12	12	12	93	-105	5.15	0.30	18.01	
12	12	12	93	-140	4.74	0.20	21.57	
12	12	12	93	-170	4.99	0.18	20.95	
12	12	12	93	-200	5.25	0.15	11.03	195.84
16	15	12	93	-2	15.09	2.22	12.93	
16	15	12	93	-15	11.62	0.54	17.24	
16	15	12	93	-30	13.52	0.33	22.72	
16	15	12	93	-45	14.59	1.05	25.83	
16	15	12	93	-60	12.95	0.27	24.09	
16	15	12	93	-75	10.51	0.81	20.50	
16	15	12	93	-90	3.33	0.23	6.79	
12	12	12	93	-105	5.15	0.30	18.01	
12	12	12	93	-140	4.74	0.20	21.58	
12	12	12	93	-170	4.99	0.18	20.95	
12	12	12	93	-200	5.25	0.15	11.03	201.66
14	23	3	94	0	27.10	6.48	40.65	
14	23	3	94	-30	17.95	1.29	60.31	
14	23	3	94	-60	16.99	1.61	63.21	
14	23	3	94	-90	12.51	0.32	51.05	
14	23	3	94	-120	9.91	0.65	41.62	
14	23	3	94	-150	10.26	1.28	43.10	
14	23	3	94	-180	9.18	1.18	32.12	
14	23	3	94	-200	9.28	0.47	12.99	345.05
16	22	4	94	0	41.68	10.00	62.52	
16	22	4	94	-30	13.37	0.40	44.92	
16	22	4	94	-60	12.43	0.14	46.26	
16	22	4	94	-90	8.75	0.36	35.71	
16	22	4	94	-120	8.46	0.49	35.54	
16	22	4	94	-150	9.08	0.40	38.14	
16	22	4	94	-180	9.98	0.60	34.93	
			interpolated	-200	9.52		13.33	311.34
16	22	4	94	-210	9.29	0.30		
16	22	4	94	-240	9.07	0.12		

Table B-10 continued...

Time	Day	Month	Year	Depth	Liquid Content	Standard Error	Water per layer	Total Water
				z	w	Δw		
(24 hr)	(day)	(month)	(year)	(cm RGL)	(g/g%)	(g/g%)	(mm)	(mm)
15	24	5	94	0	10.00	11.58	32.94	
15	24	5	94	-30	11.92	0.46	40.06	
15	24	5	94	-60	14.44	3.08	53.71	
15	24	5	94	-90	8.81	0.13	35.95	
15	24	5	94	-120	7.83	0.17	34.78	
15	24	5	94	-150	8.10	0.31	38.86	
15	24	5	94	-180	8.25	0.09	35.47	
			interpolated	-200	9.32		12.68	284.45
15	24	5	94	-210	9.86	0.61		
15	24	5	94	-240	10.05	0.79		
16	11	7	94	0	105.53	15.83	organics	
16	11	7	94	-15	31.67	20.20	75.53	
16	11	7	94	-30	18.78	3.06	47.32	
16	11	7	94	-60	11.82	0.90	43.98	
16	11	7	94	-90	7.52	0.16	30.70	
16	11	7	94	-120	6.70	0.47	28.15	
16	11	7	94	-150	7.08	0.64	39.66	
			extrapolated	-200	7.71		26.99	292.33
14	10	9	94	0	41.87	20.78	20.94	
14	10	9	94	-10	14.29	2.06	22.29	
14	10	9	94	-30	10.88	0.19	30.47	
14	10	9	94	-60	11.14	0.36	34.54	
14	10	9	94	-80	9.16	0.43	36.26	
14	10	9	94	-120	8.13	0.23	39.82	
14	10	9	94	-150	8.62	2.77	36.20	
14	10	9	94	-180	8.89	2.23	31.11	
			interpolated	-200	8.04		11.25	262.88
14	10	9	94	-210	7.61	0.11		
14	10	9	94	-240	8.54	0.28		
14	29	10	94	0	29.1	4.9	21.83	
14	29	10	94	-15	7.81	0.54	12.42	
14	29	10	94	-30	8.5	0.28	14.28	
14	29	10	94	-45	8.56	0.38	15.15	
14	29	10	94	-60	8.71	0.099	22.41	
14	29	10	94	-86.5	9.85	0.78	25.19	
14	29	10	94	-98	6.04	0.052	14.08	
14	29	10	94	-120	6.88	0.11	22.64	
14	29	10	94	-145	6.62	0.21	26.18	
14	29	10	94	-176.5	7.54	0.17	27.71	
14	29	10	94	-197.5	7.18	0.15	11.81	
				-200	7.16		13.78	227.48
14	29	10	94	-225	6.99	0.15		

Notes:

(a) The total water in mm was calculated using Equations 3-5.

Table B-11. Raw data from the tensiometer pressure transducer calibration.

Pressure Transducer Number	Applied Suction (in Hg)	Datalogger Response (Uncalibrated)	Applied Suction (kPa)
1	0	0	0
1	4.1	8.4	13.7
1	16.2	32.6	54.2
2	0	0	0
2	4.15	8.3	13.9
2	16.2	32.1	54.2
3	0	0	0
3	4	8.2	13.4
3	8.05	16.3	26.9
3	16	32.2	53.5
4	0	0	0
4	4	8.1	13.4
4	8	16.1	26.7
4	12	24	40.1
4	16	32.1	53.5
4	20	40	66.9
4	24	47.8	80.2
5	0	0	0
5	4.05	7.8	13.5
5	8	15.7	26.7
5	16.2	32	54.2
6	0	0	0
6	4	7.7	13.4
6	8	15.7	26.7
6	16	31.9	53.5

Table B-12. Tensiometer zero-offset calibration data.

Tensiometer Number	Tensiometer Depth (cm)	Bourdon Guage Reading (kPa)	Column Height H (m)	Column Pressure $\rho g H$ (kPa)	Pressure Transducer Reading (kPa)
1	-20	4	0.365	3.58	4.1
3	-50	8	0.825	8.09	7.9
2	-103	13	1.28	12.6	12.1
5	-145	14.5	1.585	15.5	14.9
6	-70	6	0.820	8.04	-
4	-200	20	2.200	21.6	21.2

Notes:
(a) Pressure transducer reading = zero offset value.

Table B-13. Direct estimates of total soil-water in the top 172.5 cm of the soil profile in the study site, compared with indirect estimates of total soil-water.

NUMBER	1	2	3	4	5	6	7	8
Date	12/12/93	15/12/93	23/03/94	22/04/94	24/05/94	11/07/94	10/9/09	29/10/94
Time	12	16	14	16	15	16	14	14
Field estimate of soil-water stored in the top 1.73 m.[a]	176 ± 10 (mm)	182 ± 7 (mm)	310 ± 19 (mm)	274 ± 19 (mm)	238 ± 24 (mm)	263 ± 50 (mm)	230 ± 18 (mm)	187 ± 7 (mm)
Indirect estimate of soil-water stored in the top 2 m.[b]	(No Data)	(No Data)	345	287	282	252	258	228
Conditions	Very Dry	Very Dry	Heavy Rain	Drying Out	Drying Out	Rain	Drying Out	Drying Out

Notes:
(a) Computed from the field data shown in Figures 3-7, 3-8, 3-9 and 3-10.
(b) Computed from average field soil-water retention relationships (Table 3-6), daily 9am tensiometer data (Figures 3-11, 3-12 & 3-13) and Equation 3-5.
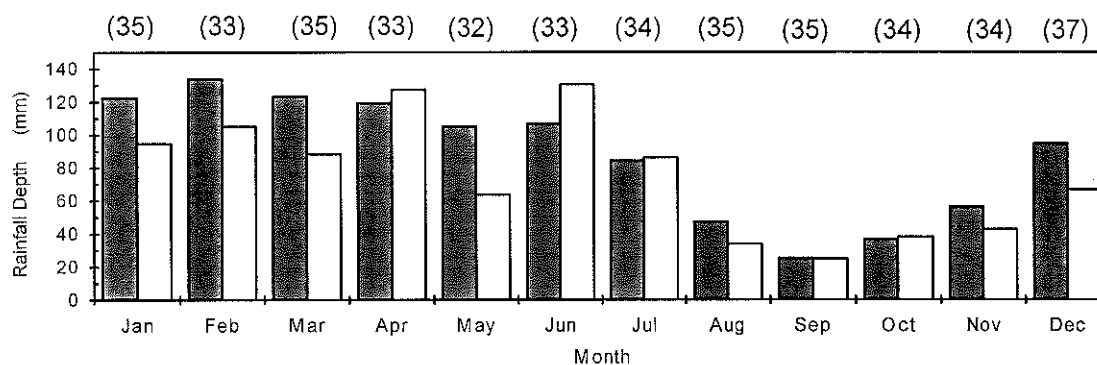
Figure B-1. Averages (grey) and standard deviations (white) of total monthly rainfall figures for Heron Island between 1956-94 (the number of sample months are shown in brackets).

(a)

(b)
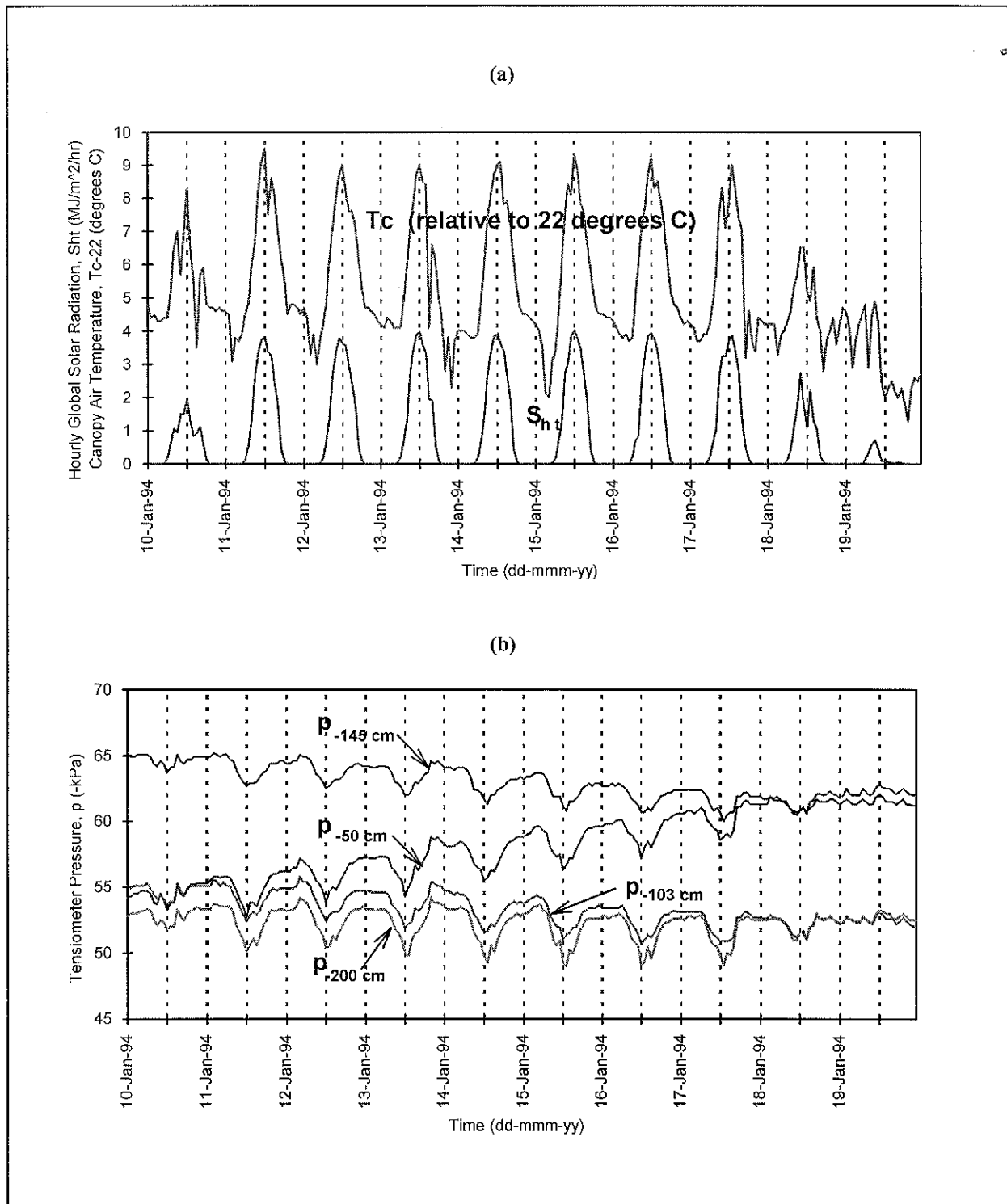
Figure B-2. Canopy air temperatures, solar radiation and tensiometer pressures at Heron Island during ten days of January 1994.

APPENDIX C

APPENDIX C

Table C-1. The computed field-water balance for the study site in the *Pisonia grandis* forest at Heron Island (refer Chapter 5).

Date 1994	Soil-Water Storage S (mm)	Cumulative Throughfall $\int P_c\,dt$ (mm)	Cumulative Deep Drainage [a] D (mm)	Cumulative Runoff $\int R\,dt$ (mm)	Evapotranspiration-less-Interception $\int E_{t-c}\,dt$ (mm)
1-Jan	204.6	0.0	0.0	0.0	0.0
2-Jan	204.6	0.0	0.0	0.0	0.0
3-Jan	204.8	0.0	-0.1	0.0	-0.1
4-Jan	204.7	0.0	-0.1	0.0	0.0
5-Jan	205.3	0.0	-0.1	0.0	-0.6
6-Jan	205.2	0.0	-0.1	0.0	-0.5
7-Jan	205.3	0.0	-0.1	0.0	-0.6
8-Jan	205.2	0.0	-0.2	0.0	-0.4
9-Jan	205.3	0.0	-0.2	0.0	-0.5
10-Jan	204.9	0.0	-0.2	0.0	-0.1
11-Jan	204.8	0.0	-0.2	0.0	0.0
12-Jan	204.8	0.0	-0.2	0.0	0.0
13-Jan	204.9	0.0	-0.2	0.0	-0.1
14-Jan	205.0	0.0	-0.3	0.0	-0.1
15-Jan	205.1	1.8	-0.3	0.0	1.6
16-Jan	204.9	1.8	-0.3	0.0	1.8
17-Jan	205.0	1.8	-0.3	0.0	1.7
18-Jan	204.9	2.7	-0.3	0.0	2.7
19-Jan	204.5	14.4	-0.3	7.2	5.2
20-Jan	241.4	135.3	-0.4	68.6	7.7
21-Jan	231.6	138.3	-0.4	68.6	20.5
22-Jan	227.0	138.3	-0.4	68.6	25.2
23-Jan	223.6	138.3	-0.4	68.6	28.6
24-Jan	221.6	145.2	-0.4	68.6	37.5
25-Jan	220.5	145.2	-0.4	68.6	38.6
26-Jan	219.3	145.2	-0.4	68.6	39.8
27-Jan	218.8	145.2	-0.5	68.6	40.3
28-Jan	217.4	145.2	-0.5	68.6	41.7
29-Jan	217.5	149.7	-0.5	68.6	46.2
30-Jan	216.8	152.1	-0.5	68.6	49.3
31-Jan	219.7	152.1	-0.5	68.6	46.4
1-Feb	219.5	152.1	-0.5	68.6	46.6
2-Feb	218.4	152.4	-0.6	68.6	48.0
3-Feb	228.6	195.6	-0.6	130.7	50.5
4-Feb	340.1	346.8	-0.6	108.5	53.0
5-Feb	337.3	349.5	2.4	108.5	55.6
6-Feb	330.0	349.5	5.2	108.5	60.1
7-Feb	320.6	349.5	7.9	108.5	66.7
8-Feb	313.1	349.5	10.5	108.5	71.6
9-Feb	307.8	349.5	12.8	108.5	74.6
10-Feb	302.1	349.5	15.1	108.5	78.0
11-Feb	297.6	349.5	17.2	108.5	80.4
12-Feb	293.4	350.1	19.2	108.5	83.2
13-Feb	289.4	351.0	21.1	108.5	86.2
14-Feb	286.1	351.3	22.8	108.5	88.1
15-Feb	282.5	351.3	24.5	108.5	90.0
16-Feb	282.4	351.3	25.9	108.5	88.7
17-Feb	278.3	351.3	27.3	108.5	91.4
18-Feb	274.8	351.3	28.7	108.5	93.5
19-Feb	272.3	351.3	30.0	108.5	94.7
20-Feb	268.4	351.3	31.2	108.5	97.4
21-Feb	267.9	351.3	32.4	108.5	96.7
22-Feb	264.9	351.3	33.5	108.5	98.6
23-Feb	261.0	365.4	34.5	117.0	101.1
24-Feb	261.8	366.3	35.6	117.0	100.1
25-Feb	260.1	366.3	36.5	117.0	100.9
26-Feb	257.0	366.3	37.4	117.0	103.1
27-Feb	258.0	368.7	38.3	117.0	103.6
28-Feb	255.1	369.9	39.1	117.0	106.9

(continued next page)

Table C-1 (continued).

Date 1994	Soil -Water Storage S (mm)	Cumulative Throughfall $\int P_c\,dt$ (mm)	Cumulative Deep Drainage [a] D (mm)	Cumulative Runoff $\int R\,dt$ (mm)	Evapotranspiration-less-Interception $\int E_{t-c}\,dt$ (mm)
1-Mar	252.1	369.9	39.9	117.0	109.1
2-Mar	248.8	384.6	40.6	123.4	111.6
3-Mar	250.4	425.4	41.3	148.3	114.1
4-Mar	266.5	443.7	42.1	137.9	116.6
5-Mar	284.3	447.0	42.8	137.9	101.4
6-Mar	288.9	447.0	43.5	137.9	96.1
7-Mar	286.4	447.0	44.1	137.9	98.0
8-Mar	282.7	447.6	44.7	137.9	101.7
9-Mar	281.3	447.6	45.4	137.9	102.4
10-Mar	280.1	447.6	46.0	137.9	103.0
11-Mar	277.0	447.6	46.5	137.9	105.6
12-Mar	274.2	447.6	47.1	137.9	107.8
13-Mar	270.2	447.6	47.7	137.9	111.2
14-Mar	267.3	447.6	48.2	137.9	113.6
15-Mar	263.8	447.6	48.7	137.9	116.6
16-Mar	259.5	447.6	49.2	137.9	120.4
17-Mar	256.2	447.6	49.8	137.9	123.1
18-Mar	251.6	447.6	50.2	137.9	127.3
19-Mar	325.2	514.8	50.7	127.6	129.8
20-Mar	312.7	517.2	51.2	127.6	144.2
21-Mar	307.8	517.8	51.8	127.6	149.1
22-Mar	302.1	517.8	52.3	127.6	154.3
23-Mar	297.8	517.8	52.8	127.6	158.1
24-Mar	296.3	519.0	53.3	127.6	160.3
25-Mar	291.4	519.0	53.9	127.6	164.6
26-Mar	286.3	519.9	54.5	127.6	170.0
27-Mar	284.9	525.6	55.1	127.6	176.5
28-Mar	282.1	525.6	55.7	127.6	178.7
29-Mar	279.9	528.3	56.3	127.6	183.0
30-Mar	275.8	528.3	56.9	127.6	186.5
31-Mar	280.7	552.0	57.6	132.7	189.0
1-Apr	285.1	552.0	58.3	132.7	183.9
2-Apr	282.4	552.0	58.9	132.7	186.0
3-Apr	278.3	552.0	59.6	132.7	189.4
4-Apr	289.1	585.6	60.2	147.9	191.9
5-Apr	291.8	585.6	60.8	147.9	188.6
6-Apr	291.2	586.2	61.5	147.9	189.1
7-Apr	289.1	586.2	62.1	147.9	190.6
8-Apr	284.9	586.2	62.7	147.9	194.2
9-Apr	281.0	586.2	63.2	147.9	197.6
10-Apr	277.3	588.0	63.8	147.9	202.5
11-Apr	273.4	588.0	64.3	147.9	205.9
12-Apr	269.2	588.0	64.8	147.9	209.6
13-Apr	266.0	588.0	65.3	147.9	212.3
14-Apr	263.5	588.0	65.8	147.9	214.3
15-Apr	260.2	588.0	66.3	147.9	217.1
16-Apr	258.8	591.3	66.8	147.9	221.3
17-Apr	259.2	597.6	67.3	147.9	226.7
18-Apr	257.8	597.6	67.7	147.9	227.7
19-Apr	256.0	601.2	68.2	147.9	232.6
20-Apr	256.2	602.4	68.7	147.9	233.1
21-Apr	253.6	602.4	69.1	147.9	235.3
22-Apr	250.9	605.1	69.5	147.9	240.3
23-Apr	254.2	607.2	70.2	147.9	238.4
24-Apr	253.2	607.5	70.9	147.9	239.0
25-Apr	250.8	607.8	71.5	147.9	241.1
26-Apr	248.8	616.2	72.0	147.9	251.0
27-Apr	249.4	616.5	72.6	147.9	250.1
28-Apr	247.7	621.6	73.2	147.9	256.3
29-Apr	248.7	622.2	73.7	147.9	255.4
30-Apr	249.5	622.5	74.2	147.9	254.4
1-May	249.6	622.5	74.8	147.9	253.7
2-May	250.6	633.3	75.3	152.3	256.2
3-May	251.8	634.5	75.8	152.3	255.7
4-May	255.0	637.8	76.2	152.3	255.4
5-May	256.5	639.3	76.7	152.3	254.9

<div align="center">(continued next page)</div>

Table C-1 (continued).

Date 1994	Soil-Water Storage S (mm)	Cumulative Throughfall $\int P_c\, dt$ (mm)	Cumulative Deep Drainage [a] D (mm)	Cumulative Runoff $\int R\, dt$ (mm)	Evapotranspiration-less-Interception $\int E_{t-c}\, dt$ (mm)
6-May	259.6	645.0	77.1	152.3	257.1
7-May	263.9	650.1	77.6	152.3	257.4
8-May	265.4	650.1	78.0	152.3	255.5
9-May	266.4	650.1	78.4	152.3	254.1
10-May	265.4	650.1	78.8	152.3	254.7
11-May	264.1	650.1	79.3	152.3	255.5
12-May	261.8	650.1	79.6	152.3	257.5
13-May	261.2	650.1	80.0	152.3	257.7
14-May	259.8	652.5	80.4	152.3	261.1
15-May	258.8	652.5	80.8	152.3	261.7
16-May	256.8	652.5	81.1	152.3	263.4
17-May	255.4	657.3	81.5	152.3	269.2
18-May	255.0	657.3	81.8	152.3	269.3
19-May	253.7	657.3	82.2	152.3	270.2
20-May	250.5	657.3	82.5	152.3	273.1
21-May	249.4	657.3	82.8	152.3	273.9
22-May	248.5	657.3	83.1	152.3	274.5
23-May	246.4	657.3	83.4	152.3	276.3
24-May	245.0	657.3	83.7	152.3	277.4
25-May	244.0	658.2	84.0	152.3	279.0
26-May	240.2	658.2	84.3	152.3	282.5
27-May	238.1	658.2	84.6	152.3	284.3
28-May	235.7	658.2	84.9	152.3	286.4
29-May	234.4	658.2	85.1	152.3	287.5
30-May	233.2	658.2	85.4	152.3	288.4
31-May	232.5	658.2	85.7	152.3	288.8
1-Jun	231.1	663.3	85.9	152.3	295.1
2-Jun	230.5	663.3	86.2	152.3	295.4
3-Jun	229.5	663.3	86.4	152.3	296.2
4-Jun	228.5	663.3	86.7	152.3	296.9
5-Jun	227.8	663.3	86.9	152.3	297.4
6-Jun	226.4	668.7	87.1	152.3	304.0
7-Jun	226.5	669.6	87.3	152.3	304.6
8-Jun	226.5	669.6	87.6	152.3	304.3
9-Jun	226.0	669.6	87.8	152.3	304.6
10-Jun	224.0	669.6	88.0	152.3	306.4
11-Jun	222.6	669.6	88.2	152.3	307.6
12-Jun	221.9	669.6	88.3	152.3	308.2
13-Jun	221.7	669.6	88.5	152.3	308.2
14-Jun	220.4	669.6	88.7	152.3	309.3
15-Jun	220.5	689.4	88.9	163.3	311.8
16-Jun	220.4	693.6	89.0	163.3	316.0
17-Jun	220.8	704.7	89.2	163.3	326.5
18-Jun	220.6	704.7	89.4	163.3	326.5
19-Jun	220.6	704.7	89.5	163.3	326.4
20-Jun	220.6	704.7	89.6	163.3	326.3
21-Jun	220.2	704.7	89.8	163.3	326.5
22-Jun	220.7	704.7	89.9	163.3	325.9
23-Jun	220.8	704.7	90.0	163.3	325.7
24-Jun	220.6	704.7	90.1	163.3	325.8
25-Jun	220.5	704.7	90.2	163.3	325.8
26-Jun	220.5	704.7	90.3	163.3	325.7
27-Jun	220.4	704.7	90.4	163.3	325.7
28-Jun	219.7	704.7	90.6	163.3	326.2
29-Jun	220.2	704.7	90.7	163.3	325.6
30-Jun	220.2	704.7	90.8	163.3	325.5
1-Jul	221.6	704.7	90.8	163.3	324.1
2-Jul	221.0	706.8	90.9	163.3	326.7
3-Jul	222.8	708.9	91.0	163.3	326.9
4-Jul	222.8	708.9	91.1	163.3	326.8
5-Jul	223.2	708.9	91.2	163.3	326.3
6-Jul	223.4	708.9	91.2	163.3	326.1
7-Jul	223.7	712.9	91.3	163.3	329.7
8-Jul	223.7	728.9	91.4	163.3	345.6
9-Jul	223.7	745.7	91.5	163.3	362.3
10-Jul	223.7	780.8	91.5	163.3	397.4

(continued next page)

Table C-1 (continued).

Date 1994	Soil -Water Storage S (mm)	Cumulative Throughfall ∫P_c d t (mm)	Cumulative Deep Drainage [a] D (mm)	Cumulative Runoff ∫R d t (mm)	Evapotranspiration-less-Interception ∫E_t- c d t (mm)
11-Jul	223.7	787.8	91.6	163.3	404.3
12-Jul	274.0	841.2	91.7	163.3	407.3
13-Jul	298.6	841.3	91.8	163.3	382.7
14-Jul	314.6	841.3	93.0	163.3	365.5
15-Jul	311.5	841.3	94.2	163.3	367.4
16-Jul	308.9	841.3	95.5	163.3	368.7
17-Jul	307.7	841.3	96.7	163.3	368.7
18-Jul	308.4	841.3	97.9	163.3	366.8
19-Jul	307.9	842.1	99.1	163.3	366.9
20-Jul	303.0	842.1	100.0	163.3	370.9
21-Jul	298.0	845.7	101.0	163.3	378.5
22-Jul	300.8	855.9	102.0	163.3	384.9
23-Jul	298.4	855.9	103.0	163.3	386.3
24-Jul	296.6	855.9	104.0	163.3	387.1
25-Jul	294.3	855.9	105.0	163.3	388.4
26-Jul	293.7	855.9	106.0	163.3	388.0
27-Jul	292.2	855.9	107.0	163.3	388.5
28-Jul	288.9	855.9	108.0	163.3	390.8
29-Jul	286.1	855.9	108.0	163.3	393.6
30-Jul	286.7	855.9	109.0	163.3	392.0
31-Jul	281.4	855.9	110.0	163.3	396.3
1-Aug	280.0	855.9	110.0	163.3	397.7
2-Aug	278.6	855.9.	111.0	163.3	398.1
3-Aug	275.5	855.9	112.0	163.3	400.2
4-Aug	273.3	855.9	112.0	163.3	402.4
5-Aug	272.0	855.9	113.0	163.3	402.7
6-Aug	271.6	855.9	114.0	163.3	402.1
7-Aug	266.9	855.9	114.0	163.3	406.8
8-Aug	268.3	855.9	115.0	163.3	404.4
9-Aug	262.8	855.9	115.0	163.3	409.9
10-Aug	259.9	855.9	116.0	163.3	411.8
11-Aug	260.2	863.1	116.0	163.3	418.7
12-Aug	260.8	863.1	117.0	163.3	417.1
13-Aug	258.1	863.1	117.0	163.3	419.8
14-Aug	256.9	863.1	118.0	163.3	420.0
15-Aug	254.9	863.1	118.0	163.3	422.0
16-Aug	252.9	865.5	118.0	163.3	426.4
17-Aug	252.1	866.1	119.0	163.3	426.8
18-Aug	251.1	866.1	119.0	163.3	427.8
19-Aug	248.5	868.2	120.0	163.3	431.5
20-Aug	248.3	868.8	120.0	163.3	432.3
21-Aug	247.9	868.8	120.0	163.3	432.7
22-Aug	246.3	868.8	121.0	163.3	433.3
23-Aug	246.6	868.8	121.0	163.3	433.0
24-Aug	245.5	868.8	121.0	163.3	434.1
25-Aug	243.6	868.8	122.0	163.3	435.0
26-Aug	242.9	879.9	122.0	163.3	446.8
27-Aug	242.7	879.9	122.0	163.3	447.0
28-Aug	241.9	879.9	123.0	163.3	446.8
29-Aug	241.5	879.9	123.0	163.3	447.2
30-Aug	240.9	879.9	123.0	163.3	447.8
31-Aug	238.9	879.9	123.0	163.3	449.8
1-Sep	237.4	879.9	124.0	163.3	450.3
2-Sep	236.2	882.3	124.0	163.3	453.9
3-Sep	234.9	882.3	124.0	163.3	455.2
4-Sep	232.8	882.3	124.0	163.3	457.3
5-Sep	232.3	882.3	124.0	163.3	457.8
6-Sep	231.5	882.3	124.0	163.3	458.6
7-Sep	229.4	882.3	125.0	163.3	459.7
8-Sep	229.0	882.3	125.0	163.3	460.1
9-Sep	228.3	882.3	125.0	163.3	460.8
10-Sep	226.9	882.3	125.0	163.3	462.2
11-Sep	226.4	882.3	125.0	163.3	462.7
12-Sep	225.0	882.3	125.0	163.3	464.1
13-Sep	224.5	882.3	125.0	163.3	464.6
14-Sep	224.2	882.3	125.0	163.3	464.9

(continued next page)

Table C-1 (continued).

Date 1994	Soil -Water Storage S (mm)	Cumulative Throughfall $\int P_o \, dt$ (mm)	Cumulative Deep Drainage [a] D (mm)	Cumulative Runoff $\int R \, dt$ (mm)	Evapotranspiration-less-Interception $\int E_{t-c} \, dt$ (mm)
15-Sep	223.3	882.3	125.0	163.3	465.8
16-Sep	222.8	882.3	125.0	163.3	466.3
17-Sep	221.8	882.3	125.0	163.3	467.3
18-Sep	220.9	882.3	125.0	163.3	468.2
19-Sep	219.8	882.3	125.0	163.3	469.3
20-Sep	217.1	882.3	125.0	163.3	472.0
21-Sep	215.9	882.3	125.0	163.3	473.2
22-Sep	214.7	882.3	125.0	163.3	474.4
23-Sep	215.5	882.3	125.0	163.3	473.6
24-Sep	214.7	882.3	125.0	163.3	474.4
25-Sep	214.5	882.3	125.0	163.3	474.6
26-Sep	214.7	882.3	125.0	163.3	474.4
27-Sep	214.1	882.3	125.0	163.3	475.0
28-Sep	212.4	882.3	125.0	163.3	476.7
29-Sep	212.6	882.3	125.0	163.3	476.5
30-Sep	212.6	882.3	125.0	163.3	476.5
1-Oct	213.0	882.3	125.0	163.3	476.1
2-Oct	212.5	882.3	125.0	163.3	476.6
3-Oct	212.2	882.3	125.0	163.3	476.9
4-Oct	212.3	882.3	125.0	163.3	476.8
5-Oct	212.1	882.3	125.0	163.3	477.0
6-Oct	210.8	882.3	125.0	163.3	478.3
7-Oct	210.6	882.3	125.0	163.3	478.5
8-Oct	210.3	885.9	125.0	163.3	482.4
9-Oct	209.2	885.9	125.0	163.3	483.5
10-Oct	208.6	885.9	125.0	163.3	484.1
11-Oct	208.1	885.9	125.0	163.3	484.6
12-Oct	208.1	885.9	125.0	163.3	484.6
13-Oct	207.4	885.9	125.0	163.3	485.3
14-Oct	206.8	885.9	124.0	163.3	486.9
15-Oct	205.5	889.8	124.0	163.3	492.1
16-Oct	206.3	889.8	124.0	163.3	491.3
17-Oct	206.4	889.8	124.0	163.3	491.2
18-Oct	206.6	889.8	124.0	163.3	491.0
19-Oct	206.3	889.8	124.0	163.3	491.3
20-Oct	206.2	889.8	124.0	163.3	491.4
21-Oct	206.2	889.8	124.0	163.3	491.4
22-Oct	204.2	900.0	124.0	169.7	493.9
23-Oct	206.6	900.0	124.0	169.7	491.5
24-Oct	205.4	902.1	124.0	169.7	494.8
25-Oct	205.6	902.7	124.0	169.7	495.2
26-Oct	205.0	902.7	124.0	169.7	495.8
27-Oct	205.2	902.7	124.0	169.7	495.6
28-Oct	205.5	902.7	123.0	169.7	496.3
29-Oct	204.9	902.7	123.0	169.7	496.9
30-Oct	204.6	918.0	123.0	178.0	499.4

Notes:

(a) The data are shown graphically in Figure 4-10 and described in Section 4.5.2.

APPENDIX D

APPENDIX D

APPENDIX D1 Verification of STEM

Problem A   In this problem, infiltration takes place vertically through a uniform profile of sand. A constant flux of water is supplied to the top of the profile, and drainage is maintained with a constant pressure lower boundary condition. The boundary and initial conditions, expressed mathematically, are as follows:

$\theta = 0.10$ ml/ml $: t < 0 \quad 0 < z < 70$ cm   **(Equation D-1)**

$Q = 13.69$ cm/h $: t \geq 0 \quad z = 0$ **(Equation D-2)**

$\theta = 0.10$ ml/ml $: t \geq 0 \quad z \geq 70$ cm   **(Equation D-3)**

The following hydraulic conductivity and water retention functions were used for the sand:

$$K\{\Psi\} = K_s \frac{A}{A + |\Psi|^\beta}$$ **(Equation D-4)**

where,

K_s = 34   (cm/h)
A = 1.175×10^6 (-)
β = 4.74   (-)

and

$$\theta\{\Psi\} = \frac{\alpha(\theta - \theta_r)}{\alpha + |\Psi|^\beta} + \theta_r$$ **(Equation D-5)**

where,

α = 1.611×10^6 (-)
β = 3.96   (-)
θ_s = 0.287   (cm^3 cm^{-3})
θ_r = 0.075   (cm^3 cm^{-3})

The simulation of Problem A employed 37 nodes with layer thicknesses of 2 cm. For a total simulation time of 0.8 hours, the model required about 30 seconds of CPU time on a 486 DX personal computer. At the end of the simulation, all of the water was accounted for in the water budget. The model solution, which is shown below in Figure 5-2, is in close agreement with the published experimental results and the solutions from six other numeric models shown in Haverkamp et al (1977). The input data file for the execution of Problem A is provided in Appendix E.
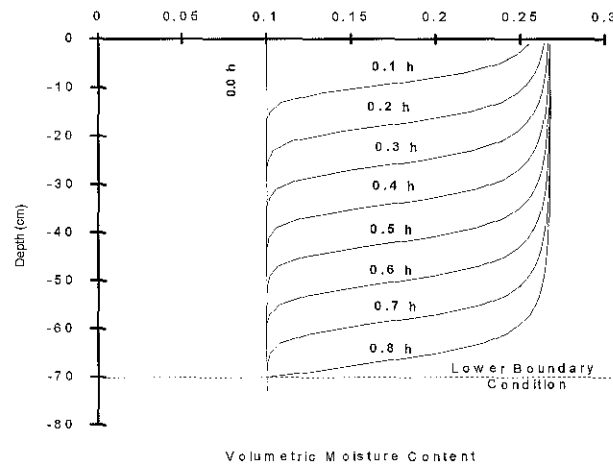
Figure D-1. Water content profiles of Problem A computed by the finite difference Soil-Water Transport Model: constant infiltration into a sand column.

Problem B In Problem B, infiltration takes place vertically through a uniform profile of Yolo Light Clay given the following initial and boundary conditions and unsaturated hydraulic conductivity and water retention functions:

$\theta = 0.2376 \text{ cm}^3 \text{ cm}^{-3}$ $: t < 0 \quad z \geq 0 \text{ cm}$ **(Equation D-6)**

$\theta = 0.4950 \text{ cm}^3 \text{ cm}^{-3}$ $: t \geq 0 \quad z = 0 \text{ cm}$ **(Equation D-7)**

$$K\{\Psi\} = K_s \frac{A}{A + |\Psi|^\beta}$$ **(Equation D-8)**

where,

K_s = 4.428E-2   (cm/h)
A = 124.6   (-)
β = 1.77   (-)

$$\theta\{\Psi\} = \frac{\alpha(\theta - \theta_r)}{\alpha + (\ln|\Psi|)^\beta} + \theta_r \qquad :\psi < -1 \text{ cm}$$ **(Equation D-9)**

$$\theta = \theta_s \qquad :\psi \geq -1 \text{ cm}$$ **(Equation D-10)**

where,

α = 739   (-)
β = 4   (-)
θ_s = 0.495 $(\text{cm}^3 \text{ cm}^{-3})$
θ_r = 0.124 $(\text{cm}^3 \text{ cm}^{-3})$

Fifty-four (54) layers each with a thicknesses of 4 cm were used in the simulation. The moisture content at the surface was set to just-below saturation (ie, 0.4949 $\text{cm}^3 \text{ cm}^{-3}$). The input data file for the execution of Problem B is given in Appendix E. The simulation of 278 hours required approximately 2 minutes and 40 seconds of CPU time, and all water was accounted for in the water budget. The solution to Problem B (see Figure 5-3(a)) agrees very closely with the semi-analytic solution of Philip (1957) as it appears in Haverkamp et al. (1977).

Problem C   In this problem, a semi-infinite column of sand is subject to vertical infiltration due a constant moisture content (or head) boundary condition at the upper surface. The hydraulic properties of the sand are the same as those used in Problem A. The boundary and initial conditions are as follows:

$\theta = 0.100$ ml/ml   : t < 0   z $\geq$ 0 cm   **(Equation D-11)**

$\theta = 0.267$ ml/ml   : t $\geq$ 0   z = 0   **(Equation D-12)**

The simulation used 47 nodes with layer thicknesses of 2 cm. About 40 seconds of CPU time were required on a 486 DX personal computer to solve Problem C. The finite difference solution to Problem C, provided by the Soil-Water Transport Model,

is in close agreement with the semi-analytic and numerical solutions presented by Haverkamp et al. (1977).
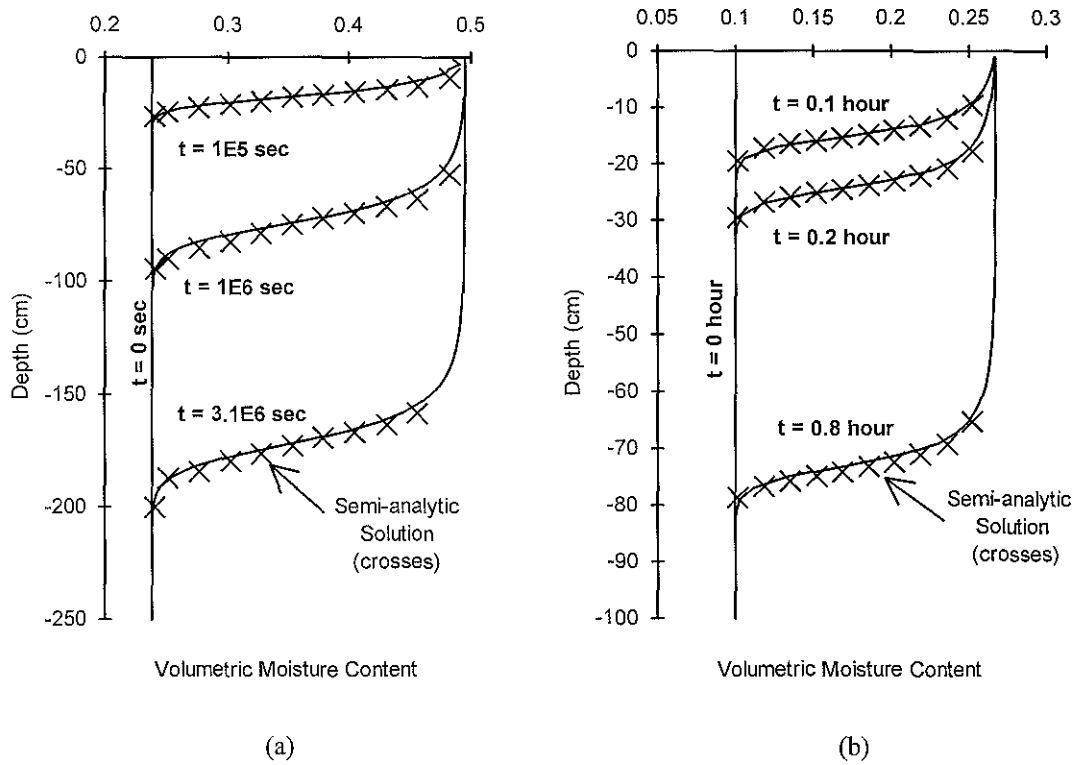
Figure D-2. Water content profiles of (a) Problem B and (b) Problem C computed by the finite difference Soil-Water Transport Model and compared with Philip's semi-analytic solutions (Haverkamp et al., 1977).

APPENDIX D2 The Particle-Size Distribution Model

$$F\{d\} = 1/\{1+(d_g/d)^n\}^m \qquad : m = 1-1/n \qquad \textbf{(Equation D-13)}$$

Table D-1. Cumulative particle size distributions for Heron Island soil samples taken from well #7 (refer Equation D-13).

Sample	Sample Depth z	d_g	n
(#)	(m LWD)	(mm)	(-)
7.01	5.42	0.641	3.69
7.02	4.42	0.676	5.36
7.03	3.42	0.692	5.71
7.04	2.42	0.740	5.21
7.05	1.42	0.980	4.72

APPENDIX D3 Haverkamp and Parlange's (1986) Method of Predicting the Water-Retention Relationship of a Sandy Soil.

Haverkamp and Parlange (1986) present a model for predicting the water retention curve for non-shrinking sandy soils which do not contain organic matter. The model is able to predict the water retention function, $\Psi(\theta)$, for sands, including the effects of air entrapment and hysteresis. The model requires prior knowledge of the sand's particle-size distribution function, $F\{d\}$, dry density, ρ_d, and moisture content at natural saturation, θ_s. To predict the wetting and drying water retention curves for Heron Island sediments, the following parameters were used:

ρ_d	$= 1.400 \pm 0.07$	$(kg\ l^{-1})$
η	$= 0.45 \pm 0.06$, porosity determined experimentally	(cm^3/cm^3)
θ_s	$= 0.45 \pm 0.06$, estimated water content at natural saturation	(cm^3/cm^3)

In the method of Haverkamp and Parlange (1986), m, μ, and d_g are estimated by curve-fitting Equations D-13 of Van Genuchten (1980) to the particle size data of the

soil sample being analysed. The soil index, λ, is then estimated from ρ_d as follows (Haverkamp and Parlange, 1986):

$$\lambda = a_1 \, \mu \, \rho_d^{a2} \qquad : 1.5 \leq \rho_d \leq 1.75 \qquad \textbf{(Equation D-14)}$$

$$a_1 = 0.0723 \pm 0.0084 \qquad \textbf{(Equation D-15)}$$

$$a_2 = 3.8408 \pm 0.42 \qquad \textbf{(Equation D-16)}$$

where, λ is the pore size distribution index value (non-dimensional) and ρ_d is the bulk dry density determined experimentally (g cm^{-3}). The ρ_d of Heron Island coralline sediment is just below the range recommended by Haverkamp and Parlange (1986) for Equation D-14 to be applicable. Despite this short-coming, the anlysis is completed using Equation D-14 with $\rho_d=1.4$ g cm^{-3}. The air entry pressure, Ψ_{ae}, is found iteratively using Equations D-17, D-18 and D-19.

$$\Psi_{ae}/\Psi\{\theta_{ac}\} = \{(1+\lambda)[1- \Psi_{ae}/\Psi\{\theta_{ae}\} \, (1-\theta_{ae}/\eta)]\}^{-1/\lambda} \qquad \textbf{(Equation D-17)}$$

$$\Psi_{ae}/\gamma = 0.149/d_g \, [(\theta_{ae}/\theta_s)^{-1/m} -1]^{(1-m)} \, \Psi_{ae}/\Psi\{\theta_{ae}\} \qquad \textbf{(Equation D-18)}$$

$$\gamma = b_1 + b_2 \lambda + b_3 \lambda^2 \qquad \textbf{(Equation D-19)}$$

where,

Ψ_{ae}	= air entry pressure	(cm)
θ_{ae}	= air entry moisture content	(cm cm^{-3})
γ	= packing coefficient	(-)
η	= porosity	(cm cm^{-3})
b_1	= 17.1736 $\pm$ 0.7	(-)
b_2	= -4.7043 $\pm$ 0.35	(-)
b_3	= 0.1589 $\pm$ 0.009	(-)

The wetting and drying water retention curves are then predicted using Equations D-20 to D-24 (Haverkamp and Parlange, 1986). The main wetting curves are,

$$\theta = \eta/(1 + \lambda) \, (\Psi_{ae}/\Psi)^{\lambda} : \Psi > \Psi_{ae} \qquad \textbf{(Equation D-20)}$$

$$\theta = \eta[1 - \lambda/(1+\lambda)\Psi_{ae}/\Psi] \qquad : \Psi_{we} \leq \Psi \leq \Psi_{ae} \qquad \textbf{(Equation D-21)}$$

$$\theta = \theta_s \qquad : \Psi \leq \Psi_{we} \qquad \textbf{(Equation D-22)}$$

The main drying curve equations are,

$$\theta = \eta \ (\Psi_{ae}/\Psi)^{\lambda} \ [1 - \Psi_{ae}/\Psi(1 - \theta_s/\eta)] \qquad :\Psi > \Psi_{ae} \qquad \textbf{(Equation D-23)}$$

$$\theta = \theta_s \qquad :\Psi \leq \Psi_{ae} \qquad \textbf{(Equation D-24)}$$

where,

$\Psi(\theta_d)$ = drying characteristic curve

$\Psi(\theta_w)$ = wetting characteristic curve

Due to air entrapment, water content at saturation rarely reaches the level of total porosity (Haverkamp and Parlange, 1986). As an approximation, θ_s may be taken equal to 0.9 η (Rogowski, 1971).

APPENDIX D3.1 Physical Properties of Heron Island Sand: Miscellaneous Experimental Results

Table D-2. Some physical properties of Heron Island sand: laboratory results.

Parameter	Symbol	Result	Units	Stand. Error (%)	Sand Sample (#)	Expt. I.D.[c]
dry density	ρ_d	1410	kg m^{-3}	5	4.03	A
dry density	ρ_d	1360	kg m^{-3}	2	4.03	C
dry density	ρ_d	1450	kg m^{-3}	3	3.09	B
dry density	ρ_d	1370	kg m^{-3}	2	3.09	D
dry density	ρ_d	1390	kg m^{-3}	1	3.09	E
porosity	η	0.47	-	9	4.03	G
porosity	η	0.43	-	7	3.09	F
saturated density	ρ_s	3600	kg m^{-3}	2	4.03	H
specific gravity	G_s	2.5	-	5	4.03	G
specific gravity	G_s	2.5	-	6	3.09	F
voids ratio	e	0.90	-	9	4.03	G
voids ratio	e	0.75	-	7	3.09	F

Notes:
a) Sample #4.03 was a dusty, light brown, medium-grained sand with visible organic material.
b) Sample #3.09 was a clean, creamy-white, medium-grained sand.
c) Refer to Table D-3 for experimental details.

Table D-3. Porosity experiments conducted on Heron Island sand.

Expt. I.D.[a]	Sample Number (#)	Replication	Sample Total Volume[b] (ml)	Sample Solid Volume (ml)	Sample Total Mass (g)	Sample Solid Mass (g)	Level of Saturation (-)
A	4.03	0	500±15	-	-	693.4	0.00
A	4.03	1	500±15	-	-	715.1	0.00
B	3.09	0	500±15	-	-	714.5	0.00
B	3.09	1	500±15	-	-	730.4	0.00
C	4.03	0	500±10	-	-	679.5	0.00
D	3.09	0	500±10	-	-	686.6	0.00
E	3.09	0	480±5	-	-	667.0	0.00
F	3.09	0	220±5	126±7	-	313.6	0.00
G	4.09	0	260±5	137±7	-	344.0	0.00
H	4.09	0	255±5	-	911.7	-	1.0

Notes:
a) Experiment I.D. refers to results given in Table D-2.
b) Total volume = solid volume + void volume.
c) Void volume = air volume + moisture volume.

Table D-4. Packing of Heron Island sand sample # 7.04 under dry and saturated conditions.

	Value	Error	Units
Dry Mass	748.6	± 3	g
Total Dry Volume	540	± 1	ml
Dry Density	1466	± 3	kg m^{-3}
Total Wet Volume	510.8	± 1	ml
Volume Difference	-30	± 2	ml
Dry Density Corrected	1552	± 5	kg m^{-3}
Dry Density Correction Factor	1.06		-

Table D-5. In-situ bulk dry density of coral sand at Heron Island.

Soil Type	Sample Depth z (cm)	Dry Density ρ_d (kg l^{-1})	Standard Error $\Delta\rho_d$ (kg l^{-1})	Number of Samples
HISS	0	0.93	0.15	4
HISS	-21 ± 3	1.1	0.2	2
HIGS	-86 ± 3	1.407	0.02	1
HIGS	-86 ± 3	1.436	0.003	1
HIGS	-92 ± 3	1.416	0.003	1
HIGS	-92 ± 3	1.422	0.005	1
HIGS	-120 ± 3	1.372	0.007	1

Notes:
(a) HISS = Heron Island Silty-Sand
(b) HIGS = Heron Island Gravelly-Sand

Table D-6. Sieve data for Heron Island sand sample #7.04.

Sieve Size (mm)	Mass Retained[a] (g)	Mass Passing (%)	Fitted Mass Passing[b] (%)
0.063	0.07	0.02	0.00
0.090	0.07	0.05	0.01
0.125	0.16	0.10	0.06
0.180	0.31	0.20	0.26
0.250	1.05	0.55	1.05
0.355	9.72	3.74	4.49
0.500	35.24	15.34	17.46
0.710	118.14	54.22	52.13
1.000	89.96	83.82	85.79
1.400	33.47	94.84	97.16
2.000	8.45	97.62	99.54
2.800	3.57	98.79	99.92
4.000	1.84	99.40	99.99
6.000	1.83	100.00	100.00

Notes:
(a) Data provided by Marshall (1992, pers. comm.).
(b) Equation 5-26 with d_g=0.740, n=5.2 and m = 0.80769 (Van Genuchten, 1980).

Table D-7. Sand sample #7.04 wetting characteristic data from the hanging column apparatus.

Column Segment No.	Gravity Potential z (cm)	Wt. Dish (g)	Total Wet Wt. (g)	Total Dry Wt. (g)	Wt. Water (g)	Wt. Dry Soil (g)	Moist. Cont. θ (%)	Error ±Δθ (%)
1	1	87.76	134.19	121.96	12.23	34.2	35.8	0.09
2	3	87.98	157.42	141.26	16.16	53.28	30.3	0.05
3	5	88.13	151.57	136.82	14.75	48.69	30.3	0.06
4	7	87.56	144.98	133.01	11.97	45.45	26.3	0.46
5	9	87.45	143.78	134.51	9.27	47.06	19.7	0.06
6	11	86.8	150.66	142.19	8.47	55.39	15.3	0.37
7	13	88.19	148.78	143.21	5.57	55.02	10.1	0.05
8	15	86.89	146.12	141.43	4.69	54.54	8.6	0.05
9	17	87.4	147.65	143.43	4.22	56.03	7.5	0.05
10	19	86.76	145.98	142.41	3.57	55.65	6.4	0.05
11	21	88.25	149.76	146.84	2.92	58.59	5.0	0.05
12	23	88.7	147.48	145.65	1.83	56.95	3.2	0.05
13	25	87.34	132.79	131.82	0.97	44.48	2.2	0.06
14	27	86.96	no soil					

Notes:
a) Duration of the experiment: 12/2/93 to 21/2/93.

Table D-8. Sand sample #7.04 drying characteristic data from the hanging column apparatus

Column Segment No.	Gravity Potential z (cm)	Wt. Dish (g)	Total Wet Wt. (g)	Total Dry Wt. (g)	Wt. Water (g)	Wt. Dry Soil (g)	Moist. Cont. θ (%)	Error ±Δθ (%)
1	1	87.75	154.3	137.97	16.33	50.22	32.5	0.06
2	3	87.99	157.9	140.77	17.13	52.78	32.5	0.20
3	5	88.13	156.9	141.13	15.77	53	29.8	0.06
4	7	88.4	154.38	140.96	13.42	52.56	25.5	0.05
5	9	87.47	156.78	143.62	13.16	56.15	23.4	0.05
6	11	88.09	147.37	139.44	7.93	51.35	15.4	0.06
7	13	88.18	146.81	139.92	6.89	51.74	13.3	0.05
8	15	86.88	147.56	141.49	6.07	54.61	11.1	0.05
9	17	87.41	144.42	139.01	5.41	51.6	10.5	0.05
10	19	86.76	144.36	139.12	5.24	52.36	10.0	0.05
11	21	88.26	154.48	148.27	6.21	60.01	10.3	0.05
12	23	88.73	146.07	140.61	5.46	51.88	10.5	0.05
13	25	87.35	113.07	110.92	2.15	23.57	9.1	0.12

Notes:
a) Duration of the experiment: 3/3/93 to 9/3/93.

Table D-9. Characteristic curves for Heron Island sand sample #7.04.

Suction Head Ψ (-cm)	Moisture Content (drying) θ (% g/g)	Moisture Content (wetting) θ (% g/g)	Effective Saturation (drying) S' (-)	Effective Saturation (wetting) S' (-)	Method
1	32.52	35.76	0.9843	1.0905	hc[a]
3	32.46	30.33	0.9823	0.9125	hc
5	29.75	30.29	0.8934	0.9111	hc
7	25.53	26.34	0.7551	0.7816	hc
9	23.44	19.70	0.6866	0.5639	hc
11	15.44	15.29	0.4243	0.4193	hc
13	13.32	10.12	0.3548	0.2498	hc
15	11.12	8.60	0.2826	0.2000	hc
17	10.48	7.53	0.2616	0.1649	hc
19	10.01	6.42	0.2462	0.1285	hc
21	10.35	4.98	0.2574	0.0813	hc
23	10.52	3.21	0.2630	0.0233	hc
25	9.12	2.18	0.2170	0.0105	hc
713.5	4.85	-	0.0770	-	pp[b]
591.2	4.61	-	0.0692	-	pp
5096	3.42	-	0.0302	-	pp
14780	2.75	-	0.0082	-	pp

Notes:
a) hc = hanging column.
b) pp = pressure plates.

Table D-10. Pressure plate results for Heron Island sand samples from site #7.

	Sample No. (#)	7.02	7.03	7.04	7.05
	Level (m LWD)	1.0-1.5	2.0-2.5	3.0-3.5	4.0-4.5
Pressure (-bar)	Pressure (-cm)	Moisture Content (g/g)	Moisture Content (g/g)	Moisture Content (g/g)	Moisture Content (g/g)
0.7	713.6	6.82	5.54	4.85	5.95
5	5097	4.64	3.23	3.42	3.75
14.5	14781	4.005	2.66	2.75	3.06

Table D-11. Pressure plate results for Heron Island sand samples from site #3.

	Sample No. (#)	3.02	3.05	3.07	3.09
	Level (m LWD)	0.5-1.0	2.0-2.5	3.0-3.55	4.0-4.5
Pressure (-bar)	Pressure (-cm)	Moisture Content (g/g)	Moisture Content (g/g)	Moisture Content (g/g)	Moisture Content (g/g)
0.1	101.9	15.38	7.94	8.01	8.04
0.9	917.4	11.02	5.11	5.25	5.88
5	5096.8	7.91	3.27	3.45	4.13
14	14271	7.41	2.99	3.03	3.50
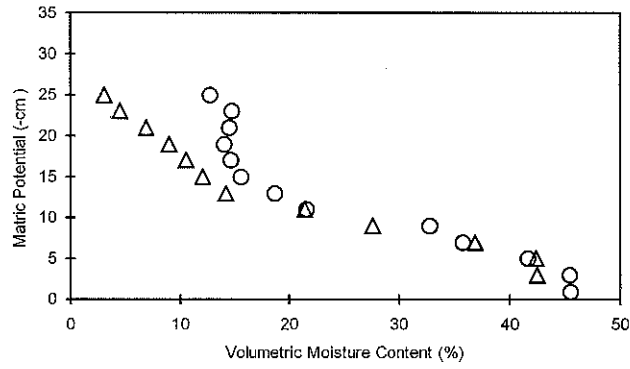
Figure D-3. Water retention data for Heron Island sand sample #7.04 obtained from the hanging column apparatus (circles are the main drying curve, triangles are the main wetting curve).
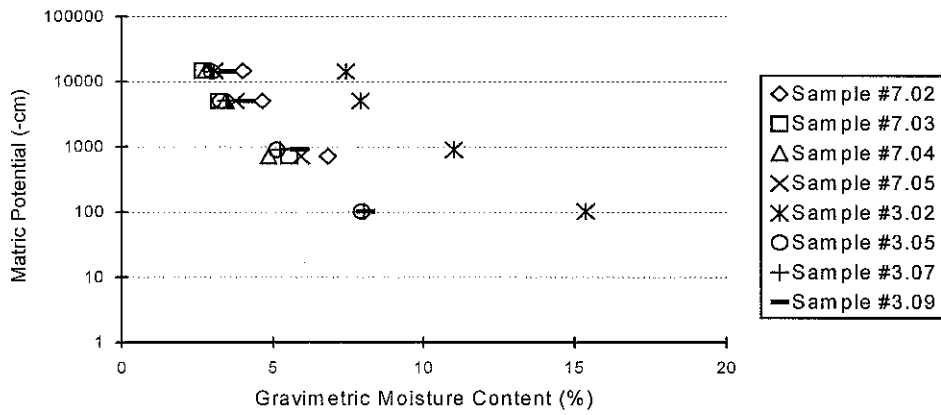
Figure D-4. Pressure plate water-retention data for Heron Island sand samples.

Table D-12. Summary of particle size parameters describing Heron Island sand samples.

Number	Sample Number	Sample Middle Depth z	Geometric Mean Diameter d_{gm}	Uniformity Coeficient U_c
(-)	(#)	(m LWD)	(mm)	(-)
1	1.01	6.32	0.53	2.89
2	1.02	6.24	0.59	2.13
3	1.03	5.66	0.59	1.96
4	1.04	5.16	0.60	1.68
5	1.05	4.74	0.57	1.76
6	1.06	4.32	0.56	1.71
7	1.07	3.82	0.55	1.65
8	1.09	3.14	0.57	1.71
9	1.10	2.745	0.57	1.70
10	1.11	2.53	0.59	1.73
11	1.12	2.205	0.63	1.79
12	1.13	1.835	0.61	1.84
13	1.14	1.525	0.68	1.69
14	1.15	1.08	0.61	1.84
15	1.16	0.7	0.61	1.85
16	1.17	0.455	0.64	1.92
17	2.01	2.23	0.66	1.95
18	2.02	1.79	0.83	2.49
19	2.03	0.68	0.92	2.44
20	2.04	0.29	0.89	2.86
21	2.05	-0.335	0.97	3.05
22	3.01	5.13	0.66	2.07
23	3.02	4.63	0.61	2.31
24	3.03	4.13	0.69	2.14
25	3.04	3.63	0.66	2.06
26	3.05	3.13	0.62	2.00
27	3.06	2.63	0.63	1.91
28	3.07	2.13	0.66	2.16
29	3.08	1.63	0.69	2.07
30	3.09	1.13	0.68	2.15
31	4.01	5.1	1.29	8.90
32	4.02	4.6	0.85	1.98
33	4.03	4.1	0.68	1.97
34	4.04	3.6	0.64	1.93
35	4.05	3.1	0.68	2.08
36	4.06	2.6	0.79	2.40
37	4.07	2.1	1.01	2.93
38	4.08	1.6	1.05	2.59
39	4.09	1.1	1.07	2.54
40	5.01	4.97	0.79	2.07
41	5.02	3.97	0.74	2.09
42	5.03	2.97	0.79	2.11
43	5.04	1.97	1.09	2.63
44	5.05	0.97	1.02	3.13
45	6.01	4.42	0.68	2.00
46	6.02	3.92	0.72	2.03
47	6.03	3.42	0.75	2.03
48	6.04	2.92	0.76	2.12
49	6.05	2.42	0.84	2.15
50	6.06	1.92	0.94	2.17

Table D-12. (continued ...)

Number	Sample Number	Sample Middle Depth	Geometric Mean Diameter	Uniformity Coeficient	
		z	d_{gm}	U_c	
(-)	(#)	(m LWD)	(mm)	(-)	
51	6.07	1.42	1.10	2.43	
52	6.08	0.92	1.26	3.01	
53	6.09	0.42	1.03	2.42	
54	6.10	-0.08	1.15	3.25	
55	7.01	5.42	0.58	3.13	
56	7.02	4.42	0.63	1.82	
57	7.03	3.42	0.65	1.71	
58	7.04	2.42	0.68	1.78	
59	7.05	1.42	0.89	1.79	
60	8.01	8.1	0.68	1.79	
61	8.02	7.1	0.56	1.89	
62	8.03	6.1	0.64	1.87	
63	8.04	5.1	0.67	1.86	
64	8.05	4.1	0.68	1.84	
65	9.01	7.62	0.57	7.15	$
66	9.02	6.62	0.57	64.53	$
67	9.03	5.62	0.56	8.20	$
68	9.04	4.62	0.53	527.14	$
69	9.05	3.62	0.58	2.33	
70	9.06	2.62	0.85	2.69	
71	9.09	-0.38	2.36	4.51	
72	9.12	-3.38	3.89	108.10	$
73	9.14	-5.18	2.99	9173.94	$
74	10.01	4.04	0.54	2.34	
75	10.02	3.04	0.61	2.11	
76	10.03	2.04	0.97	2.89	
77	11.01	5.03	0.53	2.02	
78	11.03	3.03	0.57	1.88	
79	11.04	2.03	0.79	2.22	
80	12.01	4.75	0.54	1.93	
81	12.02	3.75	0.55	2.04	
82	12.03	2.75	0.64	2.08	
83	13.01	4.75	0.64	1.94	
84	13.02	3.75	0.72	1.58	
85	13.03	2.75	0.75	1.86	
86	13.04	1.275	0.92	2.02	
87	13.05	0.75	0.85	2.39	

Notes:
a) $ = poorly conditioned particle size distribution
b) d_{gm} is defined by Equation 4-12
c) $U_c = d_{60} / d_{10}$ (refer p. 4-11)

Table D-13. Constant head permeability test results for Heron Island soil.

Sample	Minimum Sample Depth	Maximum Sample Depth	Water Volume	Time		Head 1	Head 2	Saturated Hydraulic Conductivity	
	z	z	V			h_1	h_2	K_s	
(#)	(m)	(m)	(l)	(min)	(sec)	(cm)	(cm)	(cm s^{-1} x 10^4)	
4.03	1.0	1.5	1.5	3	46	22.0	31.1	1600	
4.03	1.0	1.5	1.4	3	32	22.0	31.0	1609	
3.08	3.5	4.0	1.5	4	5	17.7	26.1	1599	
3.08	· 3.5	4.0	1.5	4	1	17.7	26.1	1592	
6.07	3.0	3.5	1.5	5	43	16.1	22.4	1522	
6.07	3.0	3.5	1.5	5	43	16.1	22.5	1498	
7.01	0	0.5	0.45	4	50	5.8	46.3	84	
7.01	0	0.5	0.30	3	20	5.6	46.1	81	
7.01	0	0.5	0.45	5	5	5.6	46.2	80	
7.02	1.0	1.5	1.20	2	33	26.3	66.2	430	
7.02	1.0	1.5	2.60	4	20	26.5	66.2	423	
7.02	1.0	1.5	0.80	3	00	23.5	44.0	476	
7.02	1.0	1.5	1.40	5	20	23.5	44.0	468	
7.03	2.0	2.5	1.43	5	00	23.8	29.3	1901	$
7.03	2.0	2.5	1.33	3	00	24.9	32.1	2251	$
7.03	2.0	2.5	1.80	4	7	24.9	32.1	2220	$
7.09	?	?	2.00	4	17	22.5	23.9	12194	
7.09	?	?	2.00	3	00	23.6	25.7	11607	
7.04	3.0	3.5	1.0	6	13	19.9	25.4	1069	$
7.04	3.0	3.5	1.5	3	25	23.6	36.3	1263	$
7.04	3.0	3.5	2.0	4	19	24.0	37.1	1293	$
7.05	4.0	4.5	1.5	7	01	21.4	26.2	1628	$
7.05	4.0	4.5	1.0	4	38	21.4	26.3	1610	$
7.04	3.0	3.5	2.0	3	28	25.6	35.1	2220	
7.04	3.0	3.5	2.0	4	28	24.6	31.5	2372	
7.04	3.0	3.5	2.0	5	28	24.4	31.4	1911	
7.04 ·	3.0	3.5	2.0	4	30	24.3	31.4	2289	
7.05	4.0	4.5	2.0	3	47	24.2	31.0	2842	
7.05	4.0	4.5	2.0	4	31	23.6	29.1	2944	

Notes:

a) $ = Sample was not properly saturated (erroneous data).

b) Errors: time +/- 2 sec; Volume +/-15 ml; head +/- 1 mm.

c) d_s = 10 +/- 0.5 cm.

d) Water temperature= 17.5 °C.

e) Radius internal of the cylinder = 38+/-2 mm.

f) Sample #7.1 was a dark brown due to the presence of humic material. This sample was easily compressed by hand. Slight hand compaction was performed on this sample prior to running the test.

Table D-14. Constant head permeameter test results for Heron Island soil.

Sample (#)	Sample Mid-depth z (m RGL)	Sample Mid-depth z (m LWD)	Saturated Hydraulic Conductivity K_s (cm s^{-1} x 10^4)	Saturated Hydraulic Conductivity K_s (m day^{-1})	Average K_s (m day^{-1})	Standard Deviation σ (m day^{-1})
4.03	1.25	4.1	1600	138.2		
4.03	1.25	4.1	1609	139.0	139	0.55
3.08	3.75	1.63	1599	138.2		
3.08	3.75	1.63	1592	137.5	138	0.43
6.07	3.25	1.42	1522	131.5		
6.07	3.25	1.42	1498	129.4	131	1.47
7.01	0.25	5.42	84	7.26		
7.01	0.25	5.42	81	7.00		
7.01	0.25	5.42	80	6.91	7.1	0.18
7.02	1.25	4.42	430	37.2		
7.02	1.25	4.42	423	36.5		
7.02	1.25	4.42	476	41.1		
7.02	1.25	4.42	468	40.4	38.8	2.30
7.03	2.25	3.42	1901	$		
7.03	2.25	3.42	2251	$		
7.03	2.25	3.42	2220	$	184	16.74
7.09	6.5	-0.83	12194	1054		
7.09	6.5	-0.83	11607	1003	1030	35.86
7.04	3.25	2.42	1069	$		
7.04	3.25	2.42	1263	$		
7.04	3.25	2.42	1293	$	104.	10.51
7.05	4.25	1.42	1628	$		
7.05	4.25	1.42	1610	$	140.	1.10
7.04	3.25	2.42	2220	191.8		
7.04	3.25	2.42	2372	204.9		
7.04	3.25	2.42	1911	165.1		
7.04	3.25	2.42	2289	197.8	190.	17.38
7.05	4.25	1.42	2842	245.5		
7.05	4.25	1.42	2944	254.4	250.	6.23

Notes:
a) $ = Sample was not properly saturated (erroneous data).

Table D-15. A summary of the laboratory determined water-retention data for Heron Island sand.

Volumetric Moisture Content θ (cm^3 cm^{-3})	Effective Saturation[a] S' (-)	Matric Potential ψ (-cm)	Laboratory Method[b]	Sample Numbers[c] (#)
0.455	1.00	1	H.C.	7.04
0.454	0.998	3	H.C.	7.04
0.417	0.915	5	H.C.	7.04
0.357	0.781	7	H.C.	7.04
0.328	0.716	9	H.C.	7.04
0.216	0.465	11	H.C.	7.04
0.186	0.398	13	H.C.	7.04
0.156	0.331	15	H.C.	7.04
0.145	0.306[d]	20[d]	H.C.	7.04
0.111	0.230	102	P.P.	3.05, 3.07
0.0726	0.145	816	P.P.	3.05, 3.07, 7.03, 7.04
0.0468	0.0868	5097	P.P.	3.05, 3.07, 7.03, 7.04
0.040	0.0716	14526	P.P.	3.05, 3.07, 7.03, 7.04

Notes:
(a) $\theta_r = 0.008$; $\theta_s = 0.455$
(b) H.C. = Hanging Column; P.P.=Pressure Plates.
(c) Some results are averaged from more than one sample.
(d) Average of results for ψ = -17, -19, -21 and -23 cm.
(e) All data are for the main drying curve.

Table D-16. Heron Island soil moisture and bulk densities for the disc permeameter experiment.

Code	Applied Suctiion Head	Depth RGL	Bulk Dry Density	Standard Error	Initial Moisture Content	Standard Error	Final Moisture Content	Standard Error
	ψ	z	ρ_d	$\Delta\rho_d$	θ_n	$\Delta\theta_n$	$\theta(\psi)$	$\Delta\theta(\psi)$
	(cm)	(cm)	(kg/l)	(kg/l)	(ml/ml)	(ml/ml)	(ml/ml)	(ml/ml)
A	-10	0	0.93	0.15	0.064	0.04	0.55	0.03
B	-1	0	0.93	0.15	0.064	0.04	1.06	0.35
C	-10	-21	1.1	0.2	0.083	0.006	0.24	0.03
D	-1	-21	1.1	0.2	0.083	0.006	0.37	0.035

Notes:
a) Date of experiments was 30/10/93
b) The estimated errors are equal to two times the standard deviation of the data.

Table D-17. Disc permeameter test: regression results.

Code	Correl. Coef. (t vs. q/A)	Number of data points	Steady-State Flow	Standard Error of Regression	Correl. Coef. ($t^{0.5}$ vs. q/A)	Number of data points	Sorptivity	Standard Error of Regression
	r	N	q/A	Δ(q/A)	r	N	S_o	ΔS_o
	(-)	(-)	(mm/hr)	(mm/hr)	(-)	(-)	(mm/hr$^{0.5}$)	(mm/hr$^{0.5}$)
A	0.998	9	1.855	0.035	0.999	14	1.276	0.0054
B	0.998	10	6.422	0.098	0.996	8	3.614	0.014
C	0.999	10	1.296	0.022	0.996	6	1.107	0.0054
D	0.9998	63	253.6	0.16	0.992	10	81.50	0.24

Notes:
a) Date of the experiments was 30/10/93.
b) Sorptivities and steady-state flow rates are taken as equal to the slope of the linear regressions results.

APPENDIX D4   The Continuous Polygon Soil-Water Retention Model for Heron Island Gravelly-Sand.

The soil-water retention characteristic for gravelly-sand used in the Soil-Water Transport Model is defined by the data in Table D-18 and Equations D-25 and D-26.

$$\psi\{S'\} = \psi_i - \frac{(\psi_i - \psi_{i+1})}{(S'_{i+1} - S'_i)}(S' - S'_i) \qquad : S'_i \leq S' < S'_{i+1} \qquad \text{(Equation D-25)}$$

$$S' = \frac{(\theta - \theta_r)}{(\theta_s - \theta_r)} \qquad \text{(Equation D-26)}$$

θ_s = 0.455, saturated moisture content   (ml/ml)
θ_r = 0.008, residual moisture content   (ml/ml)

Table D-18. The soil-water retention model for Heron Island gravelly-sand.

Effective Saturation S'_i (-)	Matric Potential ψ_i (- cm)
1.000	0.00
0.993	3.98
0.938	4.47
0.884	5.01
0.829	5.62
0.775	6.31
0.721	7.08
0.666	7.94
0.612	8.91
0.557	10.0
0.348	15.8
0.307	25.1
0.276	39.8
0.248	63.1
0.223	100
0.201	158
0.181	251
0.162	398
0.146	631
0.131	1000
0.118	1585
0.106	2512
9.57×10^{-2}	3981
8.60×10^{-2}	6310
7.74×10^{-2}	1.00×10^4
4.56×10^{-2}	1.00×10^5
2.68×10^{-2}	1.00×10^6
1.58×10^{-2}	1.00×10^7
9.31×10^{-3}	1.00×10^8
5.48×10^{-3}	1.00×10^9
3.23×10^{-3}	1.00×10^{10}

Notes:
(a) Refer Equations D-25 & D-26.
(b) Refer Figures 4-7 & 4-8.

APPENDIX D5   Some Empirical Water-Retention Formulae

Power Function (Klute, 1986)

$\Psi(\theta) = - a \, \theta^b$ (Equation D-27)

or

$\ln(\Psi(\theta)) = a + b \ln(\theta)$ (Equation D-28)

Simmons et al. (1979)

$\Psi(\theta) = - a \, \{\exp[b/\theta_s(\theta - \theta_s)] - 1\}$ (Equation D-29)

Brooks & Corey (1964)

$\theta(\Psi) = (\theta s - \theta r) \, (a/\Psi)^b + \theta_r$:for $\Psi < a$ (Equation D-30)

$\theta(\Psi) = \theta s$:for $\Psi \geq a$ (Equation D-31)

Brutsaert (1966)

$\theta(\Psi) = a(\theta s - \theta r)/(a + \Psi b) + \theta r$ (Equation D-32)

Haverkamp et al. (1977)

$\theta(\Psi) = a(\theta_s - \theta_r)/(a + \ln|\Psi|)^b) + \theta_r$:for $\Psi < -1$ (Equation D-33)

$\theta(\Psi) = \theta s$:for $\Psi >= -1$ (Equation D-34)

Van Genuchten (1980)

$\theta(\Psi) = (\theta_s - \theta_r)/(1 + (a|\Psi|)^b)^m + \theta_r$:for $\Psi < 0$ (Equation D-35)

$\theta(\Psi) = \theta_s$:for $|\Psi| \leq \Psi_s$ (Equation D-36)

where,

$m = 1 - 1/b$

Rowowski (1971)

$\theta(\Psi) = \theta_e + (\theta_{15} - \theta_e) \ln (\Psi - \Psi_e + 1)/ \ln (\Psi_{15} - \Psi_e + 1)$: $|\Psi| \geq \Psi_s$ (Equation D-37)

$\theta = \theta s$: $|\Psi| \leq \Psi s$ (Equation D-38)

APPENDIX E

APPENDIX E

APPENDIX E1 Soil-Water Transport Model Pseudo Code

MAIN PROGRAM

START
1.   Dimension matrices
2.   Output program limitations
3.   Open data files
4.   Read input data files
5.   Calculate end-of-simulation time and date
6.   Echo problem definition to output devices
7.   Define program parameters
8.   Output controller if time-step > 1 hour

INITIAL COMPUTATIONS
1.   Initialise matrices for moisture, pressure, and conductivity
2.   Determine initial total soil water volume
3.   Surface boundary condition (b.c.) calculations
4.   Constant infiltration or rainfall for b.c. no. 1
5.   Constant moisture content for b.c. no. 2
6.   If an undefined b.c., then output warning message and stop

OUTPUT INITIAL CONDITIONS

PRIMARY DO-LOOP FOR TIME

1.   Read hourly infiltration rate for bc 1
2.   Calculate conductivity for bc 2
3.   Calculate moving mean slopes
4.   Calculate flowrates
5.   Check for numerical stability
6.   Choose maximum stable time step
7.   Choose time step to suit output
8.   Update total infiltration and discharge
9.   Update moisture contents
10.   Apply drainage b.c.
11.   Find new moisture contents
12.   If water budget boundary, then print flow rates
13.   Activate more nodes if needed
14.   Update pressures and conductivities
15.   Calculate pressure at surface for bc 1
16.   Update time
17.   Time simulated to screen
18.   Output controllers
19.   Output times and headers
20.   Update time and date

21.   Output controller
22.   Calculate total soil water
23.   Output information
24.   Output for each activated node
25.   Check time criterion for do-loop
26.   Go to start of do-loop if not complete

CONTINUE DO LOOP

STOP

SUBROUTINE PRESSURE
Calculate soil pressure from moisture
Return to main program

SUBROUTINE CONDUCTIVITY
Calculate soil conductivity from pressure
Return to main program

SUBROUTINE MOISTURE
Calculate soil moisture from pressure
Return to main program

SUBROUTINE CLOCK
Update time and date
Return to main program

APPENDIX E2 Soil-Water Transport Model Program Code

```
        PROGRAM UNSATURATEDFLOW
C===============================================PROGRAM DESCRIPTION
C
C TITLE          :1-D UNSATURATED FLOW FINITE DIFFERENCE PROGRAM
C                 VERSION 15
C PURPOSE        :TO PREDICT TRANSIENT UNSATURATED SOIL WATER MOVEMENT
C                 USING THE MOVING MEAN SLOPE (MMS) METHOD.
C AUTHOR         :DELTON CHEN
C IDENTIFICATION :ENVIRONMENT GROUP, CHEM.ENG.,UofQ
C DATE STARTED   :1/APRIL/1993
C LATEST CHANGE  :25/SEPT/1994
C DATE COMPLETED:
C UNITS          :cm,h,cm^3/cm^3
C REFERENCES     :[52] Moldrup et al (1989)
C                 'Rapid and Numerically Stable Simulation of One
C                 Dimensional, Transient Wtaer Flow in Unsaturated
Layered
C                 Soils', Soil Science Sept.1989, Vol.148,No.3
C ===============================================GLOSSARY
C       AK(L)    K FUNCTION
C       AL(i)    MMS FUNCTION AT NODE i
C       AMC(L)   MC FUNCTION
C       AN(j)    MMS BOUNDARY AT LAYER j
C       BC       BOUNDARY CONDITION (1=RAIN,2=SURFACE M.C.)
C       BK(L)    K FUNCTION
```

```
C          BMC(L)   MC FUNCTION
C          CCHECK   ADVANCES HHDDMMYY BY 1 HOUR (IF=1)
C          CRC      COURANT LIMIT FOR NUMERICAL STABILITY
C          D1 D2    DAY DATE
C          DDEPTH   DEPTH WHERE DRAINAGE OCCURS
C          DHDMC    PARTIAL DIFFERENTIAL dH/dMC
C          DKDH     PARTIAL DIFFERENTIAL dK/dH
C          DKDMC    PARTIAL DIFFERENTIAL dK/dMC
C          DT(i)    COURANT TIME STEP
C          DTMIN    MINIMUM COURANT TIME STEP
C          DZ(j)    DISTANCE BETWEEN NODES AT LAYER j
C          FINISH(8)  AS ABOVE (H1-Y2) BUT FOR Finishing Time
C          H(i)     MATRIC POTENTIAL OF NODE i
C          H1 H2    24 HOUR TIME
C          INFILE   INPUT DATA FILENAME e.g. 'C:\CLAY.DAT'
C          i        NODE NUMBER
C          j        BOUNDARY NUMBER
C          K(i)     UNSATURATED HYDRAULIC CONDUCTIVITY OF NODE i
C          KL(i)    MMS FUNCTION AT NODE i
C          KN(j)    MMS BOUNDARY AT LAYER j
C          L        LAYER TYPE OF NODE i = LAYER(i)
C          LAYER(i) LAYER TYPE ('*' DATA ARE DEPENDANT ON LAYER(i))
C          LNUM     NUMBER OF LAYER TYPES
C          M1 M2    MONTH DATE
C          MC(i,_)  MOISTURE CONTENT NODE i: PRESENT AND NEXT TIME
C          MCBC     MOISTURE CONTENT OF SURFACE BOUNDARY CONDITION
C          NNA      NUMBER NODES ACTIVATED
C          NNMAX    MAXIMUM NUMBER OF NODES DIMENSIONED FOR
C          NNBC     NUMBER NODES TO LOWER BOUNDARY CONDITON
C          OC       OUTPUT CONTROL (SHORT/LONG)
C          Q(j)     FLOW AT LAYER j
C          QBC      SURFACE FLOW BOUNDARY CONDITION (cm/h)
C          RAIN     STORES HOURLY RAINFALL DATA FOR ONE DAY(cm/h)
C          RCHECK   INSTRUCTS READING NEW DAY'S RAINFALL DATA (IF=1)
C          RMC(L)   RESIDUAL MOISTURE CONTENT
C          SK(L)    SATURATED HYDRAULIC CONDUCTIVITY
C          SMC(L)   SATURATED MOISTURE CONTENT
C          t        TIME STEP NUMBER
C          TCHECK   TO CHECK IF TIME STEP FOR OUTPUT (1=YES)
C          TDEPTH   TOTAL DEPTH OF SIMULATION
C          THICK    THICKNESS OF NODES IN SIMULATION
C          TIME     TIME ELAPSED
C          TNN      TOTAL NUMBER OF NODES
C          TSBIG    OUTPUT CONTROLLER IF TSTEP>1 hour
C          TST      TOTAL SIMULATION TIME (hours)
C          TSTEP    TIME STEP FOR OUTPUT
C          WATDIFF  TOTAL WATER UNACCOUNTED FOR IN BUDGET (cm)
C          WATEXIT  TOTAL SOIL WATER DRAINING OUT t>0 (cm)
C          WATRAIN  TOTAL RAINFALL FALLEN t>0 (cm)
C          WATSOIL  TOTAL SOIL WATER IN PROFILE AT TIME t>0 (cm)
C          WATZERO  TOTAL WATER IN SOIL PROFILE AT t=0 (cm)
C          X        H INTERVAL FOR MMS FUNCTION
C          Y1 Y2    YEAR DATE
C          Z(i)     DEPTH TO NODE (MIDDLE OF LAYER)
C          NNTOP    UPPER NODE OF WATER BUDGET COMPUTATIONS
C          NNBOT    LOWER NODE OF WATER BUDGET COMPUTATIONS
C          OCSYS    OUTPUT CONTROL FOR WATER BUDGETING AROUND SYSTEM
C          With the water budgeting I want to print out Q(nntop-1) and
Q(nnbot) with
C          each time step iteration. The moisture profile will be printed
out at the end of
C          each time sub-interval. All other data will not be printed.
C =====================================================PROGRAM
C ------------------------------------------DIMENSIONING STATEMENTS
          DIMENSION H(0:400),Z(0:400),DZ(0:400),Q(0:400),AL(0:400),
     1    KL(0:400),AN(0:400),KN(0:400),DT(0:400),MC(0:400,2),
     2    LAYER(0:400),K(0:400)
          DIMENSION SMC(10),RMC(10),AMC(10),BMC(10),SK(10),
```

```
      1  AK(10),BK(10),FINISH(8),RAIN(24),SOIL(10)
         REAL H,MC,KL,KN,K,MCBC
         DOUBLE PRECISION LOH,HIH,LOK,HIK,LOM,HIM
         INTEGER TNN,t,H1,H2,D1,D2,M1,M2,Y1,Y2,FINISH
         CHARACTER*30 TITLE,POSITION,INFILE,OUTFILE,SOIL
         CHARACTER*6 WORD
         DATA H,Z,DZ,Q,AL,KL/2406*0.0/
         DATA AN,KN,DT,MC,LAYER,K/2807*0.0/
         DATA RAIN,FINISH/32*0.0/
C ------------------------------------OUTPUT PROGRAM LIMITATIONS
         WRITE(*,10)
10       FORMAT(1X,'1D Unsaturated Flow Program'/' ',27('*')/
      1  ' Version 15'/' Delton Chen'/' Chemical Engineering UofQ'//)
         NNMAX=400
         LNUMAX=10
         PRINT*,'MAX. No. OF NODES      :',NNMAX
         PRINT*,'MAX. No. OF LAYER TYPES:',LNUMAX
C-------------------------------------------------OPEN DATA FILES
         PRINT*,'GIVE INPUT FILENAME    :'
         READ(*,*) INFILE
11       PRINT*,'OUTPUT FILE O=OLD N=NEW:'
         READ(*,*) WORD
         IF (WORD.NE.'O'.AND.WORD.NE.'N') GOTO 11
         PRINT*,'GIVE OUTPUT FILENAME   :'
         READ(*,*) OUTFILE
         OC=0
15       PRINT*,'OUTPUT 0=SHORT 1=LONG  :'
         READ(*,*) OC
         IF (OC.NE.0.AND.OC.NE.1) GOTO 15
17       PRINT*,'WATER BUDGET 0=NO 1=YES :'
         READ(*,*) OCSYS
         IF (OCSYS.NE.0.AND.OCSYS.NE.1) GOTO 17
         IF (OCSYS.EQ.1) THEN
                 OC=3
                 PRINT*,'WATER BUDGET - TOP NODE    :'
             READ(*,*) NNTOP
                 PRINT*,'WATER BUDGET - BOTTOM NODE :'
             READ(*,*) NNBOT
         ENDIF
         OPEN(unit=10, file=INFILE, status='OLD')
         IF (WORD.EQ.'O') THEN
            OPEN(unit=11, file=OUTFILE, status= 'OLD')
         ELSE
            OPEN(unit=11, file=OUTFILE, status= 'NEW')
         ENDIF
C-------------------------------------------------READ INPUT DATA
         WRITE(11,10)
         READ(10,20)TITLE
20       FORMAT(A30)
         PRINT*,'PROBLEM TITLE          :',TITLE
         WRITE(11,*) ' ',TITLE
         WRITE(11,*) ' '
         WRITE(11,24) INFILE
24       FORMAT(' INPUT DATA FILE         :',3X,A30,/)
         READ(10,20)POSITION
         PRINT*,'FOUND                  :',POSITION
         READ(10,30)H1,H2,D1,D2,M1,M2,Y1,Y2
         WRITE(11,25) H1,H2,D1,D2,M1,M2,Y1,Y2
         WRITE(*,25) H1,H2,D1,D2,M1,M2,Y1,Y2
25       FORMAT(1X,'STARTING SIMULATION',4X,':',3X,2I1,' HH ',2I1,'-',
      1  2I1,'-',2I1,' DD-MM-YY')
30       FORMAT(8I1)
         FINISH(1)=H1
         FINISH(2)=H2
         FINISH(3)=D1
         FINISH(4)=D2
         FINISH(5)=M1
         FINISH(6)=M2
```

```
            FINISH(7)=Y1
            FINISH(8)=Y2
C.....................................CONTINUE READING INPUT DATA
        READ(10,20)POSITION
        PRINT*,'FOUND                       :',POSITION
        READ(10,*)TSTEP,TST,TDEPTH,DDEPTH,THICK,NNA
        NNBC=INT(DDEPTH/THICK)
C............................CALCULATE END OF SIMULATION TIME
        CALL CLOCK(FINISH(1),FINISH(2),FINISH(3),FINISH(4),FINISH(5),
     1  FINISH(6),FINISH(7),FINISH(8),TST)
        WRITE(*,40) FINISH
        WRITE(11,40) FINISH
40      FORMAT(1X,'STOPPING SIMULATION',4X,':',3X,2I1,' HH ',2I1,'-',
     1  2I1,'-',2I1,' DD-MM-YY')
C.....................................CONTINUE READING INPUT DATA
        READ(10,20)POSITION
        PRINT*,'FOUND                       :',POSITION
        READ(10,*)LNUM
        TNN=INT(TDEPTH/THICK)
        PRINT*,'NUMBER OF NODES           :',TNN
        PRINT*,'NUMBER OF LAYER TYPES   :',LNUM
        IF (TNN.GT.NNMAX) GOTO 3000
        READ(10,20) POSITION
        PRINT*,'FOUND                       :',POSITION
        DO 50 i=1,TNN
                READ(10,*) LAYER(i)
50      CONTINUE
        DO 60 L=1,LNUM
        READ(10,20) SOIL(L)
        PRINT*,'FOUND                       :',SOIL(L)
        WRITE(11,55) L,SOIL(L)
55      FORMAT(' SOIL TYPE ',2X,I2,10X,':',3X,A30)
        READ(10,*)SMC(L),RMC(L),AMC(L),BMC(L),SK(L),AK(L),BK(L)
60      CONTINUE
        READ(10,20)POSITION
        PRINT*,'FOUND                       :',POSITION
        DO 70 i=1,TNN
        READ(10,*)MC(i,1)
70      CONTINUE
        READ(10,20)POSITION
        PRINT*,'FOUND                       :',POSITION
        READ(10,*) BC
        IF (BC.EQ.2) THEN
                READ(10,*) MCBC
        ENDIF
C-------------------ECHO PROBLEM DEFINITION TO OUTPUT DEVICES
        WRITE(11,80) TSTEP,TST,TDEPTH,DDEPTH,THICK,NNA,LNUM,TNN
80      FORMAT(' OUTPUT TIME INTERVALS',3X,':',F7.2,/
     1  ' TOTAL SIMULATION TIME',3X,':',F7.2,/
     2  ' TOTAL DEPTH',13X,':',I5,/
     3  ' DEPTH OF DRAINAGE BC',4X,':',I5,/
     4  ' THICKNESS OF LAYERS',5X,':',F7.2,/
     5  ' NUMBER LAYERS ACTIVATED',1X,':',I5,/
     6  ' NUMBER OF LAYER TYPES',3X,':',I5,/
     7  ' TOTAL NUMBER OF NODES',3X,':',I5,/)
        PAUSE
C------------------------------------------------PARAMETERISATION
        t=0
        TIME=0.0
        WATDIFF=0
        WATZERO=0
        WATSOIL=0
        WATRAIN=0
        WATEXIT=0
        X=0.3
        CCHECK=1.0
        RCHECK=1.0
C...........................OUTPUT CONTROLER IF TSTEP > 1 hour
```

```
        TSBIG=1
        IF (TSTEP.GT.1) THEN
                TSBIG=TSTEP
                TSTEP=1
        ENDIF
C-----------------------------------------INITIALISE SOIL PROFILE
        LAYER(0)=LAYER(1)
        Z(0)=0
        DZ(0)=THICK/2
        DO  100 i=1,TNN
                L=LAYER(i)
                j=i
                MC(i,2)=MC(i,1)
                CALL PRESSURE(L,AMC(L),BMC(L),SMC(L),
     1          RMC(L),MC(i,1),H(i))
                CALL CONDUCTIVITY(L,AK(L),BK(L),SK(L),H(i),K(i))
                DZ(j)=THICK
                Z(i)=Z(i-1)+DZ(j-1)
100     CONTINUE
C....................DETERMINE INITIAL TOTAL SOIL WATER VOLUME
        DO 105 i=1,NNBC
                WATZERO=WATZERO+THICK*MC(i,1)
105     CONTINUE
C---------------------SURFACE BOUNDARY CONDITION CALCULATIONS
        j=0
        i=1
C...................CONSTANT INFILTRATION OR RAINFALL FOR BC 1
        IF (BC.EQ.1) THEN
           L=LAYER(i)
           CALL CONDUCTIVITY(L,AK(L),BK(L),SK(L),H(i),K(i))
           H(j)=DZ(j)*(Q(j)/K(i)-1)+H(i)
        ENDIF
C.........................CONSTANT MOISTURE CONTENT FOR BC 2
C ....ie find pressure that corresponds
        IF (BC.EQ.2) THEN
           MC(0,1)=MCBC
           MC(0,2)=MCBC
           L=LAYER(0)
           CALL PRESSURE(L,AMC(L),BMC(L),SMC(L),RMC(L),MCBC,H(0))
           CALL CONDUCTIVITY(L,AK(L),BK(L),SK(L),H(0),K(0))
        ENDIF
C...................................................FOR UNDEFINED BC
        IF (BC.NE.1.AND.BC.NE.2) THEN
           PRINT*,'BOUNDARY CONDITION DOES NOT EXIST'
           GOTO 3000
        ENDIF
C -----------------------------------OUTPUT INITIAL CONDITIONS
        WRITE(*,110)
        WRITE(11,110)
110     FORMAT(/' INITIAL CONDITIONS'/)
        WRITE(*,740) H1,H2,D1,D2,M1,M2,Y1,Y2
        WRITE(11,740) H1,H2,D1,D2,M1,M2,Y1,Y2
        WRITE(*,781)
        WRITE(11,781)
        WRITE(*,791)
        WRITE(11,791)
        DO 130 i=1,TNN
        j=i
        WRITE(*,811)Z(i),H(i),MC(i,1),Q(j),LAYER(j)
        WRITE(11,811) Z(i),H(i),MC(i,1),Q(j),LAYER(j)
130     CONTINUE
        PRINT*,' '
        PAUSE
C=====================================PRIMARY DO LOOP FOR TIME
        DO 2000 t=1,INT(TST/TSTEP+1)
        TCHECK=0.0
150     DTMIN=10000
C.......................READ HOURLY INFILTRATION RATE FOR BC 1
```

```
        IF (BC.NE.1) GOTO 180
        IF (RCHECK.EQ.1.AND.CCHECK.GT.0) THEN
          IF ((H1*10+H2).EQ.24) THEN
          PRINT*,'READING RAIN'
          READ(10,170)
RAIN(1),RAIN(2),RAIN(3),RAIN(4),RAIN(5),RAIN(6),
     1    RAIN(7),RAIN(8),RAIN(9),RAIN(10),RAIN(11),RAIN(12),RAIN(13),
     2    RAIN(14),RAIN(15),RAIN(16),RAIN(17),RAIN(18),RAIN(19),
     3    RAIN(20),RAIN(21),RAIN(22),RAIN(23),RAIN(24)
170       FORMAT(6X,24F5.2)
          IF (OC.EQ.1) THEN
          PRINT*,RAIN
          PRINT*,' '
          ENDIF
          RCHECK=0.0
          ENDIF
        ENDIF
        CCHECK=0.0
        IF ((H1*10+H2).EQ.23) RCHECK=1.0
        IF ((H1*10+H2).EQ.24) THEN
          QBC=RAIN(1)
        ELSE
          QBC=RAIN(H1*10+H2+1)
        ENDIF
        Q(0)=QBC
C .................................FIND CONDUCTIVITY FOR BC 2
180  ·  IF (BC.NE.2) GOTO 190
          L=LAYER(1)
          CALL CONDUCTIVITY(L,AK(L),BK(L),SK(L),H(1),K(1))
C ----------------------------------CALCULATE MOVING MEAN SLOPES
190     DO 200 i=0,NNA+1
        IF (i.EQ.0) THEN
         L=LAYER(1)
        ELSE
         L=LAYER(i)
        ENDIF
            IF((H(i)+x/2).GE.0) THEN
                TEMP1=H(i)
            ELSE
                TEMP1=H(i)+X/2
            ENDIF
                TEMP2=H(i)-X/2
                CALL CONDUCTIVITY(L,AK(L),BK(L),SK(L),TEMP1,TEMP3)
                CALL CONDUCTIVITY(L,AK(L),BK(L),SK(L),TEMP2,TEMP4)
            IF((H(i)+x/2).GE.0) THEN
                AL(i)=(LOG(TEMP3)-LOG(TEMP4))/X*2
            ELSE
                AL(i)=(LOG(TEMP3)-LOG(TEMP4))/X
            ENDIF
                CALL CONDUCTIVITY(L,AK(L),BK(L),SK(L),H(i),TEMP1)
                KL(i)=TEMP1*EXP(-1*AL(i)*H(i))
200     CONTINUE
        DO 300 j=0,NNA
              i=j
              AN(j)=(AL(i)+AL(i+1))/2
              KN(j)=(KL(i)+KL(i+1))/2
300      CONTINUE
C-----------------------------------------------CALCULATE FLOWRATES
        DO 400 j=0,NNA
              i=j
        IF (i.EQ.0.AND.BC.NE.2) GOTO 400
              Q(j)=-1*(KN(j)*EXP(AN(j)*H(i+1))-KN(j)*EXP(AN(j)*
     1        H(i)))/(EXP(AN(j)*DZ(j))-1)+KN(j)*EXP(AN(j)*H(i))
400      CONTINUE
        QBC=Q(0)
C ------------------------------------CHECK FOR NUMERICAL STABILITY
        DZ(0)=DZ(0)*2
        DO 500 j=0,NNA
```

```
            i=j
            L=LAYER(i)
            if (j.eq.0) L=LAYER(1)
           LOM=MC(i,1)-0.0005
           HIM=MC(i,1)+0.0005
           IF (HIM.GE.SMC(L)) THEN
                 HIM=SMC(L)
           ENDIF
           IF (LOM.LE.RMC(L)) THEN
                 LOM=RMC(L)+.00025
                 HIM=RMC(L)+.0005
           ENDIF
           CALL PREDOUBLE(L,AMC(L),BMC(L),SMC(L),RMC(L),LOM,LOH)
           CALL PREDOUBLE(L,AMC(L),BMC(L),SMC(L),RMC(L),HIM,HIH)
           CALL CONDOUBLE(L,AK(L),BK(L),SK(L),LOH,LOK)
           CALL CONDOUBLE(L,AK(L),BK(L),SK(L),HIH,HIK)
             DKDMC=(HIK-LOK)/(HIM-LOM)
             CRC=(EXP(AN(j)*DZ(j))-1)/(EXP(AN(j)*DZ(j))+1)
             DT(j)=DZ(j)*CRC/DKDMC
C..............................CHOOSE MAXIMUM STABLE TIME STEP
           IF (DT(j).LT.DTMIN) THEN
                 IF (DT(j).EQ.0) PRINT*,'DTMIN=0'
                 DTMIN=DT(j)
           ENDIF
500        CONTINUE
           DZ(0)=DZ(0)/2
C..............................CHOOSE TIME STEP TO SUIT OUTPUT
           IF ((TIME+DTMIN).GE.(t*TSTEP)) THEN
                 DTMIN=t*TSTEP-TIME
                 TCHECK=1
                 IF (INT(t*TSTEP).EQ.t*TSTEP) CCHECK=1
           ENDIF
C.....................UPDATE TOTAL INFILTRATION AND DISCHARGE
           WATRAIN=WATRAIN+Q(0)*DTMIN
           WATEXIT=WATEXIT+Q(NNBC)*DTMIN
C------------------------------------------UPDATE MOISTURE CONTENTS
           DO 600 i=1,NNA
                 j=i
C.......................................APPLY DRAINAGE BC HERE
                 IF (Z(i).GE.DDEPTH) THEN
                       MC(i,2)=MC(i,1)
                 ELSE
C................................FIND NEW MOISTURE CONTENTS
                       MC(i,2)=MC(i,1)+(Q(j-1)-Q(j))*DTMIN/DZ(i)
                 ENDIF
600        CONTINUE
C-------------------------------IF WATER BUDGET BOUNDARY PRINT FLOWS
*
           IF (OCSYS.EQ.1) THEN
           WRITE(*,620) TIME,DTMIN,Q(NNTOP-1),Q(NNBOT)
           WRITE(11,620) TIME,DTMIN,Q(NNTOP-1),Q(NNBOT)
620        FORMAT(1X,F10.5,',',E12.3,',',E12.3,',',E12.3)
           ENDIF
C--------------------------------------ACTIVATE MORE NODES IF NEEDED
           IF(NNA.LT.TNN) THEN
                 IF(MC(NNA,2).NE.MC(NNA,1)) THEN
                       NNA=NNA+1
                 ENDIF
           ENDIF
C----------------------------UPDATE PRESSURES AND CONDUCTIVITIES
650        DO 700 i=1,NNA
                 L=LAYER(i)
                 CALL PRESSURE(L,AMC(L),BMC(L),SMC(L),RMC(L),MC(i,2),H(i))
                 MC(i,1)=MC(i,2)
                 CALL CONDUCTIVITY(L,AK(L),BK(L),SK(L),H(i),K(i))
700        CONTINUE
C....................CALCULATE PRESSURE AT SURFACE FOR BC 1
           IF (BC.EQ.1) THEN
```

```
          j=0
          i=1
          H(j)=DZ(j)*(Q(j)/K(i)-1)+H(i)
          ENDIF
C-----------------------------------------------------------UPDATE TIME
          TIME=TIME+DTMIN
C..........................................TIME SIMULATED TO SCREEN
        IF (OCSYS.EQ.1) GOTO 715
          IF (TSBIG.GT.1) THEN
          WRITE(*,710) TIME,(INT(t/TSBIG+1)*TSBIG)
          ELSE
          WRITE(*,710) TIME,t*TSTEP
          ENDIF
710       FORMAT('+','TIME SIMULATED = ',F7.3,' NEXT OUTPUT = ',F7.3)
C
C==================================================================== OUTPUT DATA
C
C..........................................................OUTPUT CONTROLLERS
C
715       IF (TCHECK.EQ.0.0) GOTO 150
          IF (TSBIG.EQ.1.OR.INT(TIME/TSBIG).EQ.(TIME/TSBIG)) THEN
C
C..........................................OUTPUT TIMES AND HEADERS
C
          WRITE(*,720)INT(TIME),INT((TIME-INT(TIME))*60)
          WRITE(11,720)INT(TIME),INT((TIME-INT(TIME))*60)
720       FORMAT(/,' TIME ELAPSED       =,',I5,',HH, ',I5,',MM'/)
          ENDIF
C
C..........................................................UPDATE TIME AND DATE
C
          CCHECK=0
          IF (INT(TIME).EQ.TIME) CCHECK=1
          IF (TSTEP.GT.1) CCHECK=CCHECK*TSTEP
          CALL CLOCK(H1,H2,D1,D2,M1,M2,Y1,Y2,CCHECK)
C.................................................................OUTPUT CONTROLLER
          IF (TSBIG.EQ.1.OR.INT(TIME/TSBIG).EQ.(TIME/TSBIG)) THEN
C..............................................CALCULATE TOTAL SOIL WATER
          WATSOIL=0
          DO 730 i=1,NNBC
          j=i
          WATSOIL=WATSOIL+THICK*MC(i,1)
730       CONTINUE
C.....................................................OUTPUT INFORMATION
          WRITE(*,740) H1,H2,D1,D2,M1,M2,Y1,Y2
          WRITE(11,740) H1,H2,D1,D2,M1,M2,Y1,Y2
740       FORMAT(' TIME CURRENT       =,',2X,2I1,',HH,',2I1,'-',2I1,
     1    '-',2I1,',DD-MM-YY')
          WATDIFF=WATRAIN-WATEXIT-(WATSOIL-WATZERO)
          WRITE(*,750) WATRAIN,WATZERO,WATSOIL,WATEXIT,WATDIFF
          WRITE(11,750) WATRAIN,WATZERO,WATSOIL,WATEXIT,WATDIFF
750       FORMAT(' TOTAL RAINFALL     =,',2X,F7.3,', (cm)',/
     1    ' INITIAL SOIL WATER =,',2X,F7.3,', (cm)',//,
     2    ' CURRENT SOIL WATER =,',2X,F7.3,', (cm)',//,
     3    ' TOTAL EXITED WATER =,',2X,F7.3,', (cm)',//,
     4    ' UNACCOUNTED WATER  =,',2X,F7.3,', (cm)',/)
          IF (OC.EQ.0) GOTO 1500
          WRITE(*,780)
          WRITE(11,780)
780
FORMAT(3X,'Z(i),',3X,'H(i),',4X,'MC(i),',5X,'Q(j),',4X,'DT(j)')
781       FORMAT(3X,'Z(i),',3X,'H(i),',4X,'MC(i),',5X,'Q(j),',4X,
     1    'TYPE(i)')
          WRITE(*,790)
          WRITE(11,790)
790       FORMAT(4X,'(cm),',4X,'(cm),',2X,'(cm^3/cm^3),',2X,'(cm/h),',
     1    4X,'(h)')
791       FORMAT(4X,'(cm),',4X,'(cm),',2X,'(cm^3/cm^3),',2X,'(cm/h),',
```

```
       1  4X,'(-)')
C
C................................OUTPUT FOR EACH ACTIVATED NODE
C
       DO 1000 i=0,NNA
       j=i
       IF(i.EQ.0) THEN
           IF(QBC.EQ.0) THEN
                  WORD='DRY'
           ELSE
                  WORD='WATER'
           ENDIF
           WRITE(*,800)Z(i),H(i),WORD,Q(j),DT(j)
           WRITE(11,800)Z(i),H(i),WORD,Q(j),DT(j)
800        FORMAT(1X,F6.2,' , ',F7.2,' ,',1X,A6,' , ',E12.3,' ,
',F8.5)
       ELSE
       WRITE(*,810)Z(i),H(i),MC(i,1),Q(j),DT(j)
       WRITE(11,810)Z(i),H(i),MC(i,1),Q(j),DT(j)
810        FORMAT(1X,F6.2,' , ',E11.3,' , ',F6.4,' , ',E12.3,' , ',
     1  F8.5)
811        FORMAT(1X,F6.2,' , ',E11.3,' , ',F6.4,' , ',E12.3,' , ',
     1  I5)
       ENDIF
1000   CONTINUE
       PRINT*,' '
       WRITE(11,*) ' '
       ENDIF
C-------------------------------------TIME CRITERION FOR DO LOOP
1500   IF (TIME.GE.TST) GOTO 2010
2000   CONTINUE
2010   WRITE(*,2020) TIME
2011   WRITE(11,2020) TIME
2020   FORMAT (' STOPPED AT TIME = ',F7.2,'  hours',/,' Thank You.')
3000   END
C===================================================SUBROUTINES
C=============================================================
       SUBROUTINE PRESSURE(L,AMC,BMC,SMC,RMC,MC,H)
       REAL MC
       IF(MC.GE.SMC) THEN
              H=0
              MC=SMC
              RETURN
       ENDIF
C.............................................SOIL TYPE 1
       IF (L.EQ.1) THEN
       IF (MC.LE.RMC) PRINT*,'**WARNING <= RESIDUAL MOISTURE
CONTENT**'
       H=-1*(AMC*(SMC-RMC)/(MC-RMC)-AMC)**(1/BMC)
       ENDIF
C
C.............................................SOIL TYPE 2
C
       IF (L.EQ.2) THEN
       IF (MC.LE.RMC) PRINT*,'**WARNING <= RESIDUAL MOISTURE
CONTENT**'
       H=-1*EXP((AMC*(SMC-MC)/(MC-RMC))**(1/BMC))
       ENDIF
C
C.............................................SOIL TYPE 3
C
       IF (L.EQ.3) THEN
       IF (MC.LE.RMC) PRINT*,'**WARNING <= RESIDUAL MOISTURE
CONTENT**'
       H=-1*EXP((LOG(MC)-AMC)/BMC)
       ENDIF
C
C.............................................SOIL TYPE 4
```

```
C
        IF (L.EQ.4) THEN
        IF (MC.LE.RMC) PRINT*,'**WARNING <= RESIDUAL MOISTURE
CONTENT**'
        S=(MC-RMC)/(SMC-RMC)
        H=-1*BMC*(S**(1/AMC))
        ENDIF
C
        RETURN
        END
C==============================================================================
        SUBROUTINE PREDOUBLE(L,AMC,BMC,SMC,RMC,MC,H)
        DOUBLE PRECISION MC,H
        IF(MC.GE.SMC) THEN
                H=0
                MC=SMC
                RETURN
        ENDIF
C..........................................................SOIL TYPE 1
        IF (L.EQ.1) THEN
        IF (MC.LE.RMC) PRINT*,'**WARNING <= RESIDUAL MOISTURE
CONTENT**'
        H=-1*(AMC*(SMC-RMC)/(MC-RMC)-AMC)**(1/BMC)
        ENDIF
C..........................................................SOIL TYPE 2
        IF (L.EQ.2) THEN
        IF (MC.LE.RMC) PRINT*,'**WARNING <= RESIDUAL MOISTURE
CONTENT**'
        H=-1*EXP((AMC*(SMC-MC)/(MC-RMC))**(1/BMC))
        ENDIF
C..........................................................SOIL TYPE 3
        IF (L.EQ.3) THEN
        IF (MC.LE.RMC) PRINT*,'**WARNING <= RESIDUAL MOISTURE
CONTENT**'
        H=-1*EXP((LOG(MC)-AMC)/BMC)
        ENDIF
C..........................................................SOIL TYPE 4
        IF (L.EQ.4) THEN
        IF (MC.LE.RMC) PRINT*,'**WARNING <= RESIDUAL MOISTURE
CONTENT**'
        S=(MC-RMC)/(SMC-RMC)
        IF (S.LT.1) THEN
        H=-1*BMC*(S**(1/AMC))
        ELSE
        H=0
        ENDIF
        ENDIF
        RETURN
        END
C==============================================================================
        SUBROUTINE CONDUCTIVITY(L,AK,BK,SK,H,UK)
        IF (H.GE.0) THEN
                UK=SK
                RETURN
        ENDIF
C..........................................................SOIL TYPES 1 AND 2
        IF (L.EQ.1.OR.L.EQ.2) THEN
        UK=SK*AK/(AK+(ABS(H))**BK)
        ENDIF
C..........................................................SOIL TYPE 3
        IF (L.EQ.3) THEN
        S=EXP(-1.01627-0.14155*LOG(ABS(H)))
        S=(S-0.05)/(0.46-0.05)
        UK=SK*S**AK
        ENDIF
C..........................................................SOIL TYPE 4
        IF (L.EQ.4) THEN
        IF (H.LT.-3) THEN
```

```
          S=(ABS(H)/3)**(-1*0.61662)
          ELSE
          S=1
          ENDIF
          UK=SK*S**AK
          ENDIF
          RETURN
          END
C=================================================================
          SUBROUTINE CONDOUBLE(L,AK,BK,SK,H,UK)
          DOUBLE PRECISION H,UK
          IF(H.GE.0) THEN
                  UK=SK
                  RETURN
          ENDIF
          IF (L.EQ.1.OR.L.EQ.2) THEN
          UK=SK*AK/(AK+(ABS(H))**BK)
          ENDIF
C.........................................SOIL TYPE 3
          IF (L.EQ.3) THEN
          S=EXP(-1.01627-0.14155*LOG(ABS(H)))
          S=(S-0.05)/(0.46-0.05)
          UK=SK*S**AK
          ENDIF
C
C.........................................SOIL TYPE 4
C
          IF (L.EQ.4) THEN
          IF (H.LT.-3) THEN
          S=(ABS(H)/3)**(-1*0.61662)
          ELSE
          S=1
          ENDIF
          UK=SK*S**AK
          ENDIF
          RETURN
          END
C=================================================================
          SUBROUTINE MOISTURE(L,AMC,BMC,SMC,RMC,H,MC)
          DOUBLE PRECISION H,MC
          IF (H.GE.0) THEN
                  MC=SMC
                  RETURN
          ENDIF
C.........................................SOIL TYPE 1
          IF(L.EQ.1) THEN
          MC=AMC*(SMC-RMC)/(AMC+(ABS(H))**BMC)+RMC
          ENDIF
C.........................................SOIL TYPE 2
          IF(L.EQ.2) THEN
              IF (H.GE.-1.0) THEN
                MC=SMC
              ELSE
                MC=AMC*(SMC-RMC)/(AMC+(LOG(ABS(H)))**BMC)+RMC
              ENDIF
          ENDIF
C.........................................SOIL TYPE 3
          IF (L.EQ.3) THEN
            IF (H.GE.0) THEN
            MC=SMC
            ELSE
            MC=EXP(AMC+BMC*LOG(ABS(H)))
            ENDIF
          ENDIF
C.........................................SOIL TYPE 4
          IF (L.EQ.4) THEN
            IF (H.GE.-3) THEN
            MC=SMC
```

```
          ELSE
          S=(ABS(H)/BMC)**AMC
          MC=(SMC-RMC)*S+RMC
          ENDIF
       ENDIF
       RETURN
       END
C===================================================================
       SUBROUTINE CLOCK(A,B,C,D,E,F,G,H,TIME)
       DIMENSION MONTHSIZE(12)
       INTEGER A,B,C,D,E,F,G,H
       DATA MONTHSIZE/31,28,31,30,31,30,31,31,30,31,30,31/
       IF(INT(TIME).NE.TIME) THEN
              PRINT*,'WARNING CANNOT PROCESS MINUTES'
       ENDIF
       IF (G.NE.9) G=9
       J=INT(TIME)
       DO 100 i=1,J
         B=B+1
         IF(B.GT.9) THEN
            B=0
            A=A+1
         ENDIF
         IF(A.EQ.2.AND.B.GT.4) THEN
            A=0
            B=1
            D=D+1
         ELSE
            GOTO 99
         ENDIF
         IF(D.GT.9) THEN
            D=0
            C=C+1
         ENDIF
         IMONTH=E*10+F
         IF(MONTHSIZE(IMONTH).EQ.31) GOTO 30
         IF(MONTHSIZE(IMONTH).EQ.30) GOTO 20
         IF(MONTHSIZE(IMONTH).EQ.28) GOTO 10
10       IF(C.EQ.2.AND.D.GT.8) THEN
                C=0
                D=1
                F=F+1
         ELSE
                GOTO 99
         ENDIF
         GOTO 40
20       IF(C.EQ.3.AND.D.GT.0) THEN
                C=0
                D=1
                F=F+1
         ELSE
                GOTO 99
         ENDIF
         GOTO 40
30       IF(C.EQ.3.AND.D.GT.1) THEN
                C=0
                D=1
                F=F+1
         ELSE
                GOTO 99
         ENDIF
40       IF(F.GT.9) THEN
                F=0
                E=E+1
         ENDIF
         IF(E.EQ.1.AND.F.GT.2) THEN
                E=0
                F=1
```

```
                H=H+1
          ELSE
                GOTO 99
          ENDIF
99    GOTO 100
100      CONTINUE
         RETURN
         END
C==============================================END OF FILE
```

APPENDIX E3 Input Data File Structure

The follow shows the layout of ASCII input data files for the finite-difference soil-water transport model/program. The italicised text are headers which are read by the program to ensure that the input data is in the correct order. The plain text are the input variables which are described in Table E-1.

TITLE
START TIME-DATE
HHDDMMYY
DEFINITION
TSTEP (MUST BE DIVISIONS OF 1)
TST
TDEPTH
DDEPTH
THICK
NNA
LAYER TYPES
LNUM
LAYERING
LAYER(1)
LAYER(2)
LAYER(3)
.

.

.

LAYER(TNN)
SOIL PROPERTIES
SMC
RMC
AMC
BMC
SK
AK
BK
INITIAL MOISTURE CONTENTS
MC(1)
MC(2)
MC(3)
.

.

.

MC(TNN)
RAINFALL DATA
BC
DDMMYY AAAA BBBB CCCC AAAA BBBB CCCC ... AAAA BBBB CCCC
DDMMYY AAAA BBBB CCCC AAAA BBBB CCCC ... AAAA BBBB CCCC
DDMMYY AAAA BBBB CCCC AAAA BBBB CCCC ... AAAA BBBB CCCC
.

.

.

DDMMYY AAAA BBBB CCCC AAAA BBBB CCCC ... AAAA BBBB CCCC

Table E-1. The input data required by the finite-difference soil-water transport model.

Input Variable	Variable Description	Type
TITLE	Problem title/description	a
HHDDMMYY	Starting hour, day, month and year	i
TSTEP	Time step in hours for output of solutions. Must be either whole numbers if greater than 1 hour, or divisible into 1 if less than 1 hour (ie 0.5, 0.25, 0.1, 2, 10 hours etc)	r
TST	The total simulation time in hours.	r
TDEPTH	The total depth of the profile to be modelled (cm).	r
DDEPTH	The depth below surface at which the drainage boundary condition exists (less deep than the start of the second last node).	r
THICK	The thickness of the all layers in the profile (cm).	r
NNA	The number of nodes activated at the start of the simulation (≤ NN-1)	i
LNUM	The total number of soil types available to the simulation.	i
LAYER(i)	The soil type associated with layer (cell) number i.	i
TNN	The total number of nodes in the soil profile.	i
SMC	Soil property (saturated moisture content as a decimal fraction).	r
RMC	Soil property (residual moisture content as a decimal fraction).	r
AMC	Soil property (constant for the water retention function).	r
BMC	Soil property (constant for the water retention function).	r
SK	Soil property (saturated hydrauklic conductivity in cm/hr).	r
AK	Soil property (constant for the hydraulic conductivity function).	r
BK	Soil property (constant for the hydraulic conductivity function).	r
MC(i)	Initial volumetric moisture content of the soil profile at layer i (decimal fraction).	r
BC	Surface boundary condition type: 1 for a prescribed surface infiltration rate (ie rainfall rate), and 2 for a prescribed surface moisture content.	i
DDMMYY	Date of the rainfall data that follows (optional).	i
AAAAAA	Rainfall in 1/10th mm for each hour beginning at 00 hours.	i

Notes:
a = alpha-numeric
r = real
i = integer

APPENDIX E4   Verification Problem A :Input Data File for STEM.

PROB(A) SAND EXPERIMENTAL	1	SAND PROPERTIES	0.1
START DATE-TIME	1	0.287	0.1
24140993	1	0.075	0.1
PROBLEM DEFINITION	1	1.611E+06	0.1
0.1	1	3.96	0.1
0.8	1	34	0.1
74	1	1.175E+06	0.1
70	1	4.74	0.1
2	1	CLAY PROPERTIES	0.1
10	1	0.495	0.1
LAYER TYPES	1	0.124	0.1
2	1	739.0	0.1
LAYERING	1	4.0	0.1
1	1	4.428E-02	0.1
1	1	124.6	0.1
1	1	1.77	0.1
1	1	INITIAL MOISTURE CONTENT	0.1
1	1	0.1	0.1
1	1	0.1	0.1
1	1	0.1	0.1
1	1	0.1	0.1
1	1	0.1	0.1
1	1	0.1	0.1
1	1	0.1	0.1
(continued above)	*(continued above)*	0.1	0.1
		0.1	RAINFALL DATA
		0.1	1
		(continued above)	150993137 000

APPENDIX E5   Verification Problem B :Input Data File for STEM.

PROB(B) YOLO LIGHT CLAY	2	3.96	0.2376
START DATE-TIME	2	34	0.2376
24311293	2	1.175E+06	0.2376
PROBLEM DEFINITION	2	4.74	0.2376
12	2	CLAY PROPERTIES	0.2376
168	2	0.495	0.2376
154	2	0.124	0.2376
150	2	739.0	0.2376
2	2	4.0	0.2376
5	2	4.428E-02	0.2376
NUMBER OF LAYER TYPES	2	124.6	0.2376
2	2	1.77	0.2376
LAYERING	2	INITIAL MOISTURE CONTENT	0.2376
2	2	0.2376	0.2376
2	2	0.2376	0.2376
2	2	0.2376	0.2376
2	2	0.2376	0.2376
2	2	0.2376	0.2376
2	2	0.2376	0.2376
2	2	0.2376	0.2376
2	2	0.2376	0.2376
2	2	0.2376	0.2376
2	2	0.2376	0.2376
2	2	0.2376	0.2376
2	2	0.2376	0.2376
2	2	0.2376	0.2376
2	2	0.2376	0.2376
2	2	0.2376	0.2376
2	2	0.2376	0.2376
2	2	0.2376	0.2376
2	2	0.2376	0.2376
2	2	0.2376	0.2376
2	2	0.2376	0.2376
2	2	0.2376	0.2376
2	2	0.2376	0.2376
2	2	0.2376	0.2376
2	SAND PROPERTIES	0.2376	0.2376
2	0.287	0.2376	0.2376
2	0.075	*(continued above)*	INFILTRATION DATA
2	1.611E+06		2
(continued above)	*(continued above)*		0.4949

APPENDIX E6 STEM Simulations: Input and Results.

Table E-2. Initial conditions in the STEM simulations: moisture contents and matric potentials at time zero.

Depth z (m RGL)	Moisture Content θ (m³ m⁻³)	Matric Potential ψ (-cm)
-5	0.13	1460
-15	0.13	1460
-25	0.13	1460
-35	0.13	1460
-45	0.13	1460
-55	0.13	1460
-65	0.13	1460
-75	0.13	1460
-85	0.13	1460
-95	0.13	1460
-105	0.08	418
-115	0.08	418
-125	0.08	418
-135	0.08	418
-145	0.08	418
-155	0.08	418
-165	0.08	418
-175	0.08	418
-185	0.08	418
-195	0.08	418
-205	0.08	418
-215	0.08	418
-225	0.08	418
-235	0.08	418
-245	0.08	418
-255	0.08	418
-265	0.08	418
-275	0.08	418
-285	0.08	418
-295	0.08	418
-305	0.0801	414
-315	0.0803	408
-325	0.081	391
-335	0.0835	346
-345	0.0879	266
-355	0.0935	202
-365	0.0985	154
-375	0.1042	121
-385	0.1087	96.9
-395	0.1143	78.4
-405	0.1188	63.5
-415	0.1255	50.7
-425	0.1319	39.2
-435	0.1419	28.5
-445	0.1587	18.3
-455	0.3	8.18
-465	0.45	4.02
-475	0.45	4.02

Footnote: In the simulations time zero is 1st January 1985.
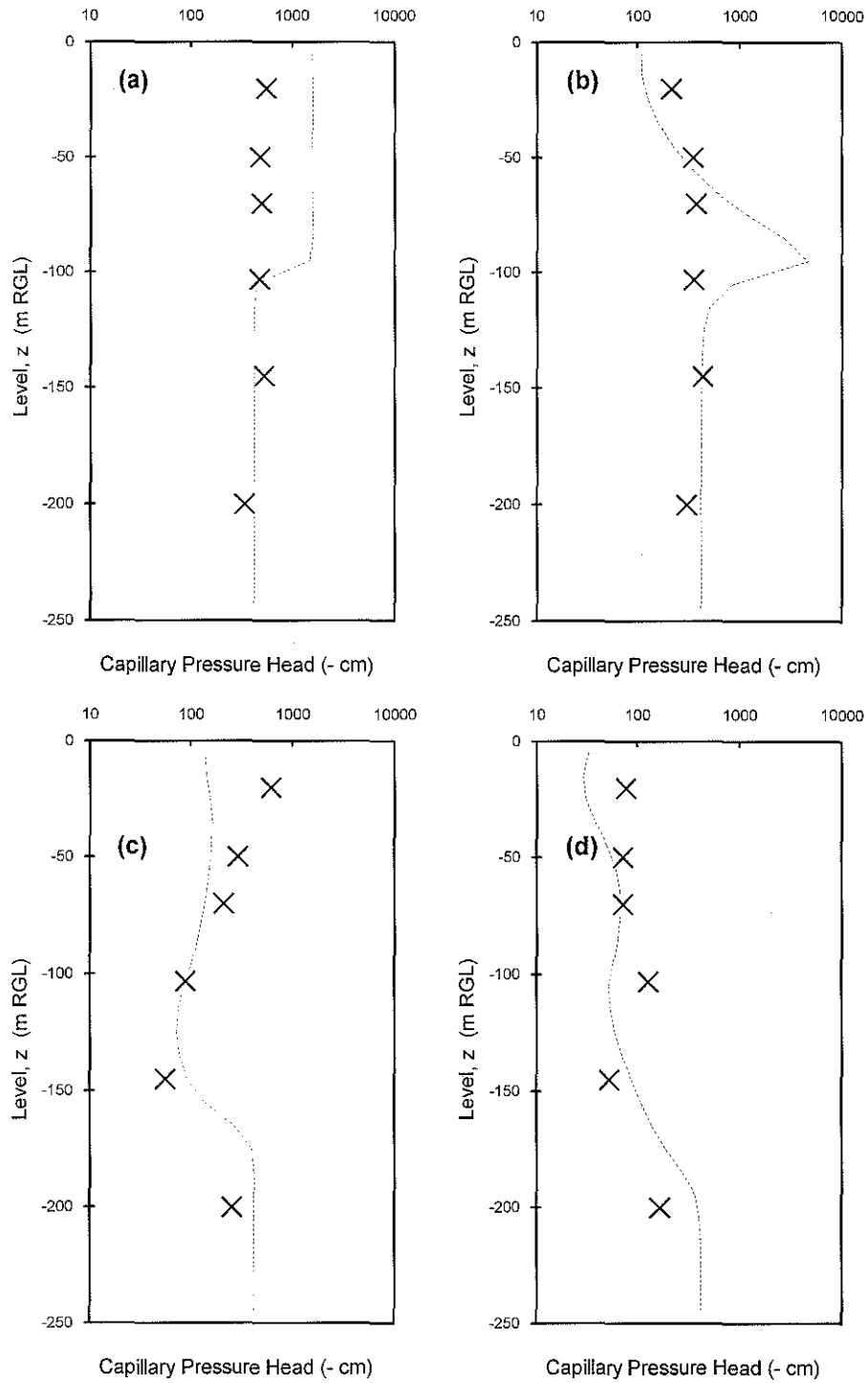
Figure E-1. Comparing soil matric-potentials predicted by STEM (dashed lines) with those recorded in the field using tensiometers (crosses): (a) 1st January 1994, (b) 1st February 1994, (c) 1st March 1994, and (d) 1st April 1994.
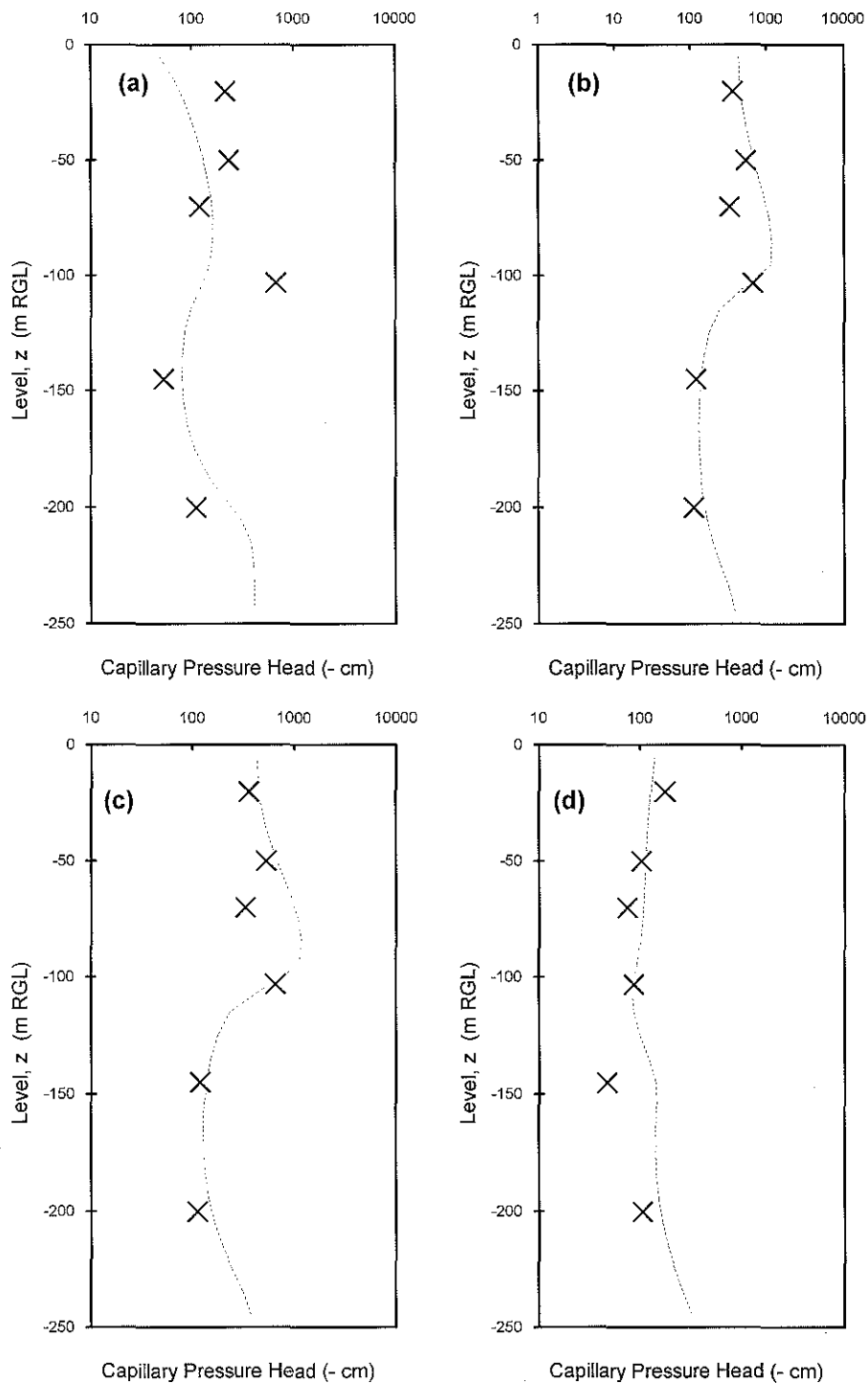
Figure E-2. Comparing soil matric-potentials predicted by STEM (dashed lines) with those recorded in the field using tensiometers (crosses): (a) 1st May 1994, (b) 1st June 1994, (c) 1st July 1994, and (d) 1st August 1994.
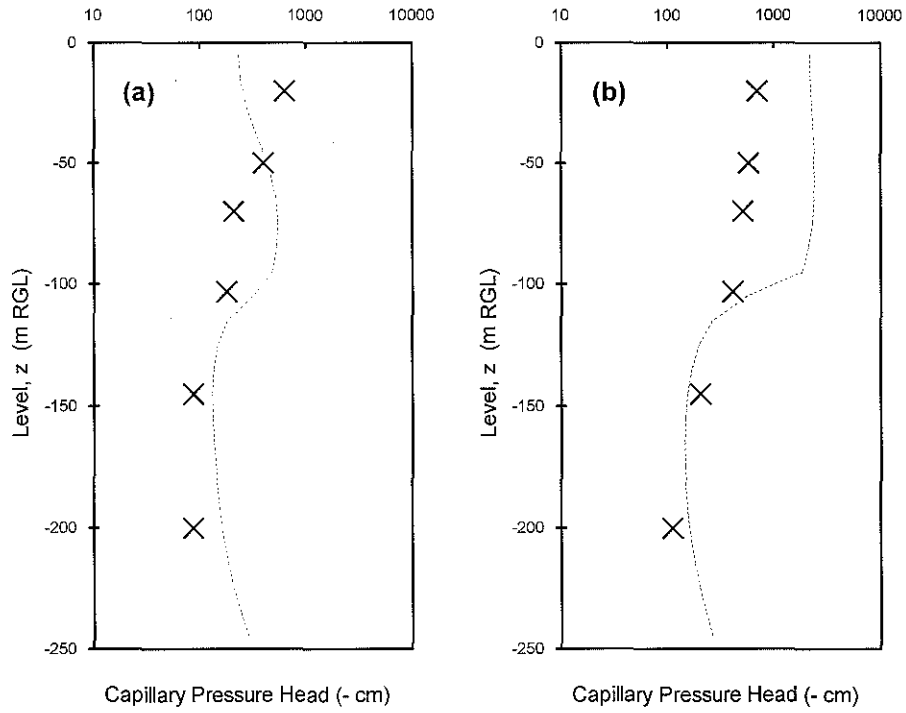
Figure E-3. Comparing soil matric-potentials predicted by STEM (dashed lines) with those recorded in the field using tensiometers (crosses): (a) 1st September 1994, and (b) 1st October 1994.

APPENDIX F

APPENDIX F

APPENDIX F1 Equations For Density, Salinity And Specific Conductance Of Groundwater

The density of Heron Island groundwater (ρ_{gw}) was interpolated between that of pure freshwater and that of typical seawater on the basis of groundwater salinity (S_{wg}):

$$\rho_{gw} = 1000 + \frac{S_{gw}}{36} \times 25 \qquad \text{(Equation F- 1)}$$

Salinity (S) is the mass of major ions in solution per mass of fluid for mild dilutions and for concentrations of seawater, and is expressed in units of ppt. For simplicity, temperature related density variations are assumed negligible. Equation F-1 is considered sufficiently accurate for the purposes of numerically modeling groundwater flow (eg, Voss, 1984). Other possible sources of error in ρ_{gw} estimated from Equation F-1 are: (i) chemical differences between the groundwater and seawater, and (ii) error in S_{gw}.

The S_{gw} data obtained in this study were determined from the following equation which requires that the groundwater's specific conductance (C) and temperature (T) be known (Hydrolab, 1991 unpublished):

$$\begin{aligned} S = &\; 5.9950 \times 10^{-8} C^4 - 2.3120 \times 10^{-5} C^3 + 3.4346 \\ &\times 10^{-3} C^2 + 5.3532 \times 10^{-1} C - 1.5494 \times 10^{-2} \end{aligned} \qquad \text{(Equation F- 2)}$$

C in Equation F-2 was determined by multiplying the measured groundwater conductivity by $F\{T\}$, where $F\{T\}$ is defined as follows (Hydrolab, 1991):

$$\begin{aligned} F\{T\} = &\; 1.2813 \times 10^{-11} T^7 - 2.2129 \times 10^{-9} T^6 + 1.4771 \times 10^{-7} T^5 - 4.6475 \times 10^{-6} T^4 \\ &+ 5.6170 \times 10^{-5} T^3 + 8.7699 \times 10^{-4} T^2 - 6.1736 \times 10^{-2} T + 1.9524 \end{aligned}$$

$$\text{(Equation F- 3)}$$

The multiplier $F\{T\}$ converts seawater conductivity at temperature T to an equivalent seawater conductivity at the standard temperature of 25°C (ie, the specific conductance). Equation F-3 is valid for T between 0-30°C. The specific conductance of natural waters is a function of the ion content and the rate at which ions can move under the influence of an electric potential. The ionic activity and therefore the conductivity of a solution are affected by temperature.

The ion concentration-conductivity relationship is not linear in concentrated ionic solutions (ie, above 0.1 mS cm^{-1}) due to inter-ionic attraction (Lloyd and Heathcote, 1985). According to Lloyd and Heathcote (1985), conductivity measurements cannot be used to obtain "accurate" measurements of ion concentrations or total dissolved solids in groundwater. They also report that sulphate and bicarbonate ions have a particularly poor correlation with conductivity. Any deviation of Equation F-3 from the real-world situation will introduce some error to the groundwater salinity and density records. This error was not investigated and is assumed negligible.

APPENDIX F2 Error Analysis

The sensitivity of groundwater potentials and tidal efficiency values to variations in groundwater salinity are examined in this section using an analytic approach.

Groundwater density is a function of groundwater salinity, as follows:

$$\rho_{gw} = \frac{S_{gw}}{S_s}(\rho_s - \rho_{freshs}) + \rho_{freshs}$$

$$= \frac{S_{gw}}{35.7}25 + 1000$$

(Equation F-4)

where,

ρ_{gw} = groundwater density (kg m^{-3})

ρ_s = seawater density (kg m^{-3})

ρ_{fresh} = 1000, freshwater density (kg m^{-3})

S_{gw} = groundwater salinity (ppt)

S_s = 35.7, seawater salinity (ppt)

Hence the rate in change of groundwater density with groundwater salinity is:

$$\frac{d\rho_{gw}}{dS_{gw}} = \frac{1}{S_s}(\rho_s - \rho_{freshs})$$

$$= \frac{(1025 - 1000)}{35.7}$$

(Equation F-5)

$$= 0.7003 \ \frac{kg}{m^3 ppt}$$

Groundwater potentials relative to LWD in metres-of-equivalent-seawater are defined as follows:

$$H = \frac{p_{gw}}{\rho_s g} + Z$$

$$= \frac{\rho_{gw} g (h_{gw} - Z)}{\rho_s g} + Z$$

$$= \frac{\rho_{gw}}{\rho_s} h_{gw} - \left(\frac{\rho_{gw}}{\rho_s} + 1\right) Z$$

(Equation F-6)

where,

p_{gw} = fluid pressure (kPa)

g = gravitational acceleration (m s^{-2})

Z = piezometer level relative to LWD (m LWD)

Hence the partial differential of groundwater potential with respect to groundwater density is as follows:

$$\frac{\partial H}{\partial \rho_{gw}} = \frac{1}{\rho_s} h_{gw} - \frac{Z}{\rho_s}$$

$$= \frac{1}{\rho_s} (h_{gw} - Z)$$

(Equation F-7)

Further, the rate of change of groundwater potentials with respect to changes in groundwater salinity are derived by combining Equations F-5 and F-7, ie:

$$\frac{\partial H}{\partial S_{gw}} = \frac{\partial H}{\partial \rho_{gw}} \frac{d\rho_{gw}}{dS_{gw}}$$

$$= \frac{0.7003}{\rho_s} (h_{gw} - Z)$$

$$= 0.0006832 (h_{gw} - Z)$$

(Equation F-8)

Tidal efficiency can be expressed as a function of groundwater density (assuming that groundwater density is effectively constant between consecutive tidal cycles) by combining Equations F-6 and 8-5, ie:

$$\eta = \frac{\Delta H}{\Delta h_{ocean}}$$

$$= \frac{H_2 - H_1}{\Delta h_{ocean}}$$

$$= \frac{\dfrac{\rho_{gw}}{\rho_s} h_{gw2} - \left(\dfrac{\rho_{gw}}{\rho_s} + 1\right)Z - \dfrac{\rho_{gw}}{\rho_s} h_{gw1} - \left(\dfrac{\rho_{gw}}{\rho_s} + 1\right)Z}{\Delta h_{ocean}}$$

(Equation F-9)

$$= \frac{\dfrac{\rho_{gw}}{\rho_s} h_{gw2} - \dfrac{\rho_{gw}}{\rho_s} h_{gw1}}{\Delta h_{ocean}}$$

$$= \frac{\rho_{gw}\left(h_{gw2} - h_{gw1}\right)}{\rho_s \Delta h_{ocean}}$$

$$= \frac{\rho_{gw}\Delta h_{gw}}{\rho_s \Delta h_{ocean}}$$

Hence, from Equation F-9 the partial differential of tidal efficiency with respect to groundwater density can be determined:

$$\frac{\partial \eta}{\partial \rho_{gw}} = \frac{\partial}{\partial \rho_{gw}}\left(\frac{\rho_{gw}\Delta h_{gw}}{\rho_s \Delta h_{ocean}}\right)$$

(Equation F-10)

$$= \frac{\Delta h_{gw}}{\rho_s \Delta h_{ocean}}$$

Finally, the partial differential of tidal efficiency with respect to groundwater salinity is as follows:

$$\frac{\partial \eta}{\partial S_{gw}} = \frac{d\rho_{gw}}{dS_{gw}} \frac{\partial \eta}{\partial \rho_{gw}}$$

$$= 0.7003 \frac{\Delta h_{gw}}{\rho_s \Delta h_{ocean}}$$

$$= 0.7003 \frac{\eta}{\rho_{gw}}$$

(Equation F-11)

From the above expression the sensitivity of η to variations in groundwater salinity can be determined, ie:

$$\Delta \eta = \Delta S_{gw} \frac{\partial \eta}{\partial S_{gw}}$$

$$= 0.7003 \frac{\eta}{\rho_{gw}} \Delta S_{gw}$$

(Equation F-12)

The sensitivity of η and H to S_{gw} at the various piezometers at Heron Island is listed in Table F-5.

Table F-1. Calibration results for the tide gauge located on the jetty at Heron Island.

Sensor No.	Day of Year 1994 (d)	No. Samples N (-)	Correl. Coeff. r (-)	Regressed Intercept A (m LWD)	95% Confidence ±δA (m)	Regressed Slope b' (×10⁻³ m unit⁻¹)	95% Confidence ±δb' (%)
50037	111	19	0.9977	-2.027	0.14	1.460	3.9
50031	190	25	0.9969	-1.935	0.10	1.349	3.4

Notes:
(a) Day-of-year 111 is the 21st April 1994 and day-of-year 190 is the 10th July 1994.

Table F-2. Linear regression curves for the pressure transducers used at Heron Island to record water-levels: results of a field calibration exercise.

Transducer Ident. No.	Well No.	Piezo. No.	No. of Samples, N	Regressed Intercept, A	95% Confidence $\pm\delta A$	95% Confidence $\pm\delta A$	Regressed Slope, b'	95% Confidence $\pm\delta b'$	95% Confidence $\pm\delta b'$	Correlation Coefficient r	Transducer Position
(-)	(#)	(-)	(-)	(m LWD)	(m)	(%)	$(\times 10^{-3}\,\text{m/unit})$	$(\times 10^{-3}\,\text{m/unit})$	(%)	(-)	(m RGL)
10029	1	1	6	-4.402	0.123	2.80	1.932	0.0424	2.09	0.99989	-10
50115	1	3	6	-0.433	0.163	37.7	1.518	0.1308	8.27	0.99823	-7.6
10083	10	1	2	-4.918	-	-	2.078	-	-	-	-8.8
10084	10	2	6	-4.670	0.561	12.0	2.130	0.1943	8.56	0.99810	-8.8
50102	10	3	6	-1.815	0.091	5.00	1.457	0.0381	2.44	0.99984	-6.3
50119	11	1	6	-1.759	0.109	6.21	1.535	0.0453	3.02	0.99976	-6.3
50117	11	2	6	-0.794	0.105	13.3	1.553	0.0594	3.84	0.99962	-6.3
10083	6	1	5	-3.407	0.183	5.36	2.066	0.0785	3.67	0.99980	-7
10084	6	2	6	-3.368	0.349	10.4	2.113	0.1485	6.78	0.99881	-7
50101	6	3	6	-0.381	0.480	126	1.413	0.2471	21.4	0.98829	-5
50102	6	4	4	-0.673	0.723	107	1.447	0.3716	27.4	0.99598	-5
10029	8	1	5	-3.096	0.692	22.3	1.937	0.2968	14.8	0.99676	-10.5
50038	8	2	5	-1.620	0.897	55.3	1.306	0.3811	27.8	0.98872	-8.5
50031	8	3	6	-0.748	0.510	68.2	1.317	0.2956	22.0	0.98771	-5.5
10083	3	1	5	-2.514	0.282	11.2	2.072	0.1384	6.68	0.99934	-8
10084	3	2	5	-1.296	0.094	7.26	2.121	0.0695	3.14	0.99985	-.17 m LWD
50102	3	3	-	-	-	-	1.453	-	-	-	1.63 m LWD
10029	13	1	4	-4.406	0.851	19.3	1.930	0.2769	13.40	0.99903	-6.5
50038	13	2	2	-2.912	-	-	1.302	-	-	1.00000	-6.5
50031	13	3	4	-1.774	0.055	3.09	1.313	0.0192	1.46	0.99999	-6
50119	12	1	7	-1.428	0.066	4.62	1.535	0.0304	2.04	0.99984	-5.5
50117	12	2	5	-1.327	0.476	35.9	1.555	0.2253	14.87	0.99674	-5.5

Notes:

(a) The regression curve is $h_{gw} = A + b'$ X where X is the pressure transducer response (uncalibrated) and h_{gw} is the groundwater water-level (units are m-of-groundwater LWD) (refer Equation 8-9).

(b) Confidence intervals are based upon the t-distribution with $\alpha=0.025$.

Table F-3. Linear regression curves for the pressure transducers used at Heron Island to record water-levels: results of a laboratory calibration exercise.

Press. Trans. Ident. No. (-)	Well No. (#)	Piezo. No. (-)	No. of Samples, N (-)	Regressed Intercept, a (m LWD)	95% Confidence ±δa (m)	95% Confidence ±δa (%)	Regressed Slope, b (x10⁻³ m/unit)	95% Confidence ±δb (x10⁻³ m/unit)	95% Confidence ±δb (%)	Correlation Coefficient r (-)	Groundwater Density ρ_{gw} (kg m⁻³)	Density Corrected b' (m/unit)
10029	1	1	4	-0.726	0.334	46.0	1.974	0.1064	5.39	0.99984	1022	1.932
50115	1	3	9	-0.560	0.069	12.3	1.550	0.0275	1.78	0.99980	1021	1.518
10083	10	1	12	-0.992	0.074	7.47	2.115	0.0225	1.07	0.99989	1018	2.078
10084	10	2	12	-0.958	0.080	8.39	2.166	0.0251	1.16	0.99986	1017	2.130
50102	10	3	12	-0.614	0.053	8.70	1.482	0.0216	1.46	0.99979	1017	1.457
50119	11	1	14	-0.672	0.049	7.23	1.572	0.0202	1.28	0.99979	1024	1.535
50117	11	2	13	-0.657	0.057	8.70	1.592	0.0260	1.63	0.99970	1025	1.553
10083	6	1	12	-0.992	0.074	7.47	2.115	0.0225	1.07	0.99989	1024	2.066
10084	6	2	12	-0.958	0.080	8.39	2.166	0.0251	1.16	0.99986	1025	2.113
50101	6	3	12	-0.499	0.028	5.67	1.448	0.0115	0.79	0.99994	1025	1.413
50102	6	4	12	-0.614	0.053	8.70	1.482	0.0216	1.46	0.99979	1024	1.447
10029	8	1	4	-0.726	0.334	46.0	1.974	0.1064	5.39	0.99984	1019	1.937
50038	8	2	3	-0.562	0.746	133	1.330	0.2733	20.54	0.99987	1019	1.306
50031	8	3	3	-0.587	0.831	142	1.342	0.3041	22.66	0.99984	1019	1.317
10083	3	1	12	-0.992	0.074	7.47	2.115	0.0225	1.07	0.99989	1021	2.072
10084	3	2	12	-0.958	0.080	8.39	2.166	0.0251	1.16	0.99986	1021	2.121
50102	3		12	-0.614	0.053	8.70	1.482	0.0216	1.46	0.99979	1020	1.453
10029	13	1	4	-0.726	0.334	46.0	1.974	0.1064	5.39	0.99984	1023	1.930
50038	13	2	3	-0.562	0.746	133	1.330	0.2733	20.54	0.99987	1022	1.302
50031	13	3	3	-0.587	0.831	142	1.342	0.3041	22.66	0.99984	1022	1.313
50119	12	1	14	-0.672	0.049	7.23	1.572	0.0202	1.28	0.99979	1024	1.535
50117	12	2	13	-0.657	0.057	8.70	1.592	0.0260	1.63	0.99970	1024	1.555
50037	-	-	3	-0.617	1.560	253	1.394	0.6112	43.85	0.99941	-	-
10031	-	-	4	-0.820	1.499	183	1.610	0.3846	23.89	0.99693	-	-

(a) The regression curve is y = a + b x, where x = pressure transducer response (uncalibrated) and y = water-level (m LWD).

(b) Confidence intervals are based upon the t-distribution with α=0.025.

(c) Groundwater densities are from field measurements obtained in March 1994 (refer Table F-5).

(d) Raw calibration data provided by Dataflow Systems.

Table F-4. Summary of the piezometer construction details and water-level records.

Well No. (#)	Piezo. No. (-)	Notes	Piezo. Depth Z (m LWD)	Thickness of Sand Infill (m)	Sample Period 1994 (days)	Average Head H_{gw} (m LWD)	Maximum Head H_{gw} (m LWD)	Minimum Head H_{gw} (m LWD)	Standard Errors in H_{gw} (m)	Average Tide h_{ocean} (m LWD)	Maximum Tide h_{ocean} (m LWD)	Minimum Tide h_{ocean} (m LWD)	Standard Errors in h_{ocean} (m)
1	1	t, b	-3.37	0.7	146 -190	1.47	2.48	0.65	0.123	1.568	3.269	0.162	0.10
1	3	t, b	0.43	1.0	146 -190	1.48	2.26	0.75	0.163	1.568	3.269	0.162	0.10
3	1	t	-3.39	2.77	112-139	1.60	2.26	0.98	0.282	1.570	3.325	-0.042	0.14
3	2	t, b	-0.22	1.3	112-139	1.61	2.29	0.96	0.094	1.570	3.325	-0.042	0.14
3	3	w, b	1.58	?	112-139	1.64	2.27	1.14	-	1.570	3.325	-0.042	0.14
6	1	t	-11.48	1.05	83-111	1.56	2.92	0.39	0.183	1.606	3.195	0.020	0.14
6	2	t, b	-7.53	1.2	83-111	1.68	2.69	1.12	0.349	1.606	3.195	0.020	0.14
6	3	f, t, b	-3.73	2.3	83-111	1.79	2.78	1.40	0.480	1.606	3.195	0.020	0.14
6	4	w, b	-0.58	0.5	83-111	1.81	2.56	1.40	0.723	1.606	3.195	0.020	0.14
8	1	t	-7.61	1.52	82-111	1.45	2.63	0.46	0.692	1.606	3.195	0.020	0.14
8	2	t, b	-4.14	1.13	82-111	1.49	2.09	0.98	0.897	1.606	3.195	0.020	0.14
8	3	w, t, b	-0.66	0.96	82-111	1.47	1.91	1.02	0.510	1.606	3.195	0.020	0.14
10	1	t	-7.21	1.3	146-182	1.82	3.24	0.94	-	1.562	3.269	0.162	0.10
10	2	t, b	-4.45	1.04	146-182	1.80	2.67	1.09	0.561	1.562	3.269	0.162	0.10
10	3	t, b	-1.24	1.28	146-182	1.81	2.56	1.14	0.091	1.562	3.269	0.162	0.10
11	1	t	-3.67	1.99	146-190	1.78	3.10	1.00	0.109	1.568	3.269	0.162	0.10
11	2	w, b	-0.22	0.5	146-190	1.79	3.21	0.98	0.105	1.568	3.269	0.162	0.10
12	1	t	-6.12	1.37	112-139	1.64	3.00	0.60	0.066	1.570	3.236	-0.042	0.14
12	2	w, b	-1.86	?	112-139	1.70	2.80	0.95	0.476	1.570	3.236	-0.042	0.14
13	1	t	-7.21	1.16	112-139	1.80	3.30	0.61	0.851	1.570	3.236	-0.042	0.14
13	2	t, b	-5.03	1.91	112-139	1.83	2.44	1.36	-	1.570	3.236	-0.042	0.14
13	3	w, b	-2.83	?	112-139	1.83	2.41	1.30	0.055	1.570	3.236	-0.042	0.14

Notes
(a)   all heads in this table are salinity corrected and expressed in metres-of-equivalent-seawater
(b)   b = a impermeable clay layer was installed below this piezometer
(c)   f = a faulty pressure transducer produced an unsteady signal: it was therefore necessary to "smooth" the data by averaging with a moving window of 9 data points
(d)   t = a impermeable clay layer was installed above this piezometer
(e)   w = water-table levels were recorded by this piezometer
(f)   standard errors are systematic (refer pressure transducer calibrations in Tables F-1 and F-2)

Table F-5. Sensitivity analysis to examine the effect of groundwater salinity variations on groundwater potential and tidal efficiency calculations.

Well No.	Piezo. No.	Piezo. Bottom Level Z	Groundwater Salinity S_{gw}	Groundwater Density ρ_{gw}	Mean Tidal Efficiency η	Sensitivity[d] $\Delta\eta/\Delta S_{gw}$	Average Piezo. Water-Level h_{gw}	Sensitivity[e] $\Delta H/\Delta S_{gw}$
(#)	(-)	(m LWD)	(ppt)	(kg m-3)	(%)	(%/ppt)	(m-LWD)	(m/ppt)
1	1	-3.73	31.4	1022	55.6	0.04	1.47	0.003
1	2	-2.73	31.4	1022	-	-	-	-
1	3	-0.43	30.7	1021	46.4	0.03	1.48	0.001
3	1	-3.39	30.1	1021	35.3	0.02	1.6	0.003
3	2	-0.22	30	1021	36	0.02	1.61	0.001
3	3	1.58	28.6	1020	33	0.02	1.64	0.000
6	1	-11.48	34.1	1024	78.8	0.05	1.56	0.009
6	2	-7.53	35.3	1025	41.9	0.03	1.68	0.006
6	3	-3.73	35.2	1025	-	-	1.79	0.004
6	4	-0.58	34.9	1024	24.8	0.02	1.81	0.002
7	1	-8.33	27.3	1019	-	-	-	-
7	2	-5.7	27.3	1019	-	-	-	-
7	3	-3.16	26.9	1019	-	-	-	-
7	4	-0.23	25.5	1018	-	-	-	-
8	1	-7.61	26.8	1019	67.4	0.05	1.45	0.006
8	2	-4.14	26.8	1019	34.1	0.02	1.49	0.004
8	3	-0.66	26.6	1019	27	0.02	1.47	0.001
10	1	-7.21	25.7	1018	58.3	0.04	1.82	0.006
10	2	-4.45	24.7	1017	45.5	0.03	1.8	0.004
10	3	-1.24	24.4	1017	40.3	0.03	1.81	0.002
11	1	-3.67	34.5	1024	62.1	0.04	1.78	0.004
11	2	-0.22	35	1025	64.4	0.04	1.79	0.001
12	1	-6.12	34	1024	69.7	0.05	1.64	0.005
12	2	-1.86	34.1	1024	48.3	0.03	1.7	0.002
13	1	-7.21	32.2	1023	78.8	0.05	1.8	0.006
13	2	-5.03	31.7	1022	28.9	0.02	1.83	0.005
13	3	-2.83	31.5	1022	27.9	0.02	1.83	0.003

Notes:

(a) groundwater salinities were recorded at Heron Island in March 1994 as described in Chapter 8

(b) hgw = groundwater piezometer water-level (metres-of-equivalent-groundwater).

(c) Hgw = groundwater total-head (metres-of-equivalent-seawater)

(d) refer Equation F-12

(e) refer Equation F-8

Table F-6. Summary of the efficiencies and lags of tidal signals observed in the groundwater at Heron Island.

Well No.	Piezo. No.	Sample Period 1994 (day of year)	Piezo. Bottom Depth z (m LWD)	Mean Efficiency η (%)	Stand. Error ± Δη (%)	Max. Efficiency η (%)	Min. Efficiency η (%)	Stand. Error ± Δη (%)	Mean Lag γ (hours)	Stand. Error ± Δγ (hours)	Max. Lag γ (hours)	Min. Lag γ (hours)	Stand. Error ± Δγ (hours)
1	1	146-190	-3.37	55.6	3	64.7	47	3	0.79	0.06	1.5	0.0	0.5
1	3	146-190	0.43	46.4	3	56.3	37.3	3	1.65	0.06	2.3	0.7	0.5
3	1	112-139	-3.39	35.3	2	47.6	24.4	2	1.87	0.06	2.8	0.7	0.5
3	2	112-139	-0.22	36.0	2	48.8	24.3	2	2.18	0.06	3.2	1.0	0.5
3	3	112-139	1.58	33.0	2	45.	22.2	2	2.27	0.06	3.3	1.5	0.5
6	1	83-111	-11.48	78.8	4	85.6	72.4	4	0.11	0.06	0.8	-0.5	0.5
6	2	83-111	-7.53	41.9	3	54.8	24.2	3	0.69	0.06	1.5	-0.2	0.5
6	3	83-111	-3.73	*	*	*	*	*	*	*	*	*	*
6	4	83-111	-0.58	24.8	2	38.4	8.9	2	2.46	0.06	4.0	0.8	0.5
8	1	82-111	-7.61	67.4	5	74.4	59.4	5	0.20	0.06	0.8	-0.5	0.5
8	2	82-111	-4.14	34.1	7	44.7	23.8	7	1.21	0.06	2.0	0.2	0.5
8	3	82-111	-0.66	27.0	7	38.8	16.9	7	2.38	0.06	3.3	1.3	0.5
10	1	146-182	-7.21	58.3	3	67.6	46.2	3	0.60	0.06	1.3	0.0	0.5
10	2	146-182	-4.45	45.5	3	58.4	35.2	3	1.41	0.06	2.2	0.5	0.5
10	3	146-182	-1.24	40.3	3	51.2	29	3	1.94	0.06	2.8	1.2	0.5
11	1	146-190	-3.67	62.1	3	75.2	50.9	3	0.99	0.06	2.0	0.0	0.5
11	2	146-190	-0.22	64.4	3	78.3	51.7	3	1.19	0.06	2.3	0.2	0.5
12	1	112-139	-6.12	69.7	3	79.3	60.6	3	0.33	0.06	1.2	-0.3	0.5
12	2	112-139	-1.86	48.3	3	61.4	34.8	3	1.75	0.06	2.7	0.8	0.5
13	1	112-139	-7.21	78.8	6	86	72.1	6	0.08	0.06	1.0	-0.7	0.5
13	2	112-139	-5.03	28.9	6	40.1	19.1	6	1.48	0.06	2.5	0.3	0.5
13	3	112-139	-2.83	27.9	7	39.9	16.5	7	2.13	0.06	3.2	1.0	0.5
ALL	ALL			47.8	5	86	8.9	6	1.3	0.06	4	-0.7	0.5

Notes:
(a) * = Due to equipment problems, the field data for Well #6 Piezo. 3 was rejected.
(b) t = top clay layer capping was installed above this piezometer.
(c) b = bottom clay layer capping was installed below this piezometer.
(d) z (m MSL) = z (m LWD) - 1.61 m

APPENDIX G

APPENDIX G

APPENDIX G1   Derivation of the First-Order Analytical Solution for VTUGF in a Two-Layered Aquifer (refer Figure 9-5)

If the total head gradients within regions 1 and 2 are independent of position, then:

$$-\cot(\alpha_1) = \frac{\partial H_1(z,t)}{\partial z} \qquad : \delta(t) \geq z > -l_1$$

$$-\cot(\alpha_2) = \frac{\partial H_2(z,t)}{\partial z} \qquad :-l_1 > z \geq -L$$

(Equation G-1)

where α_1 and α_2 are time dependent angles. The continuity principle requires that macroscopic fluid flow within the entire aquifer be the same at all times, therefore:

$$v_1(t) = v_2(t)$$
$$= v(t)$$

(Equation G-2)

From Darcy's Law,

$$v = -K\frac{\partial H}{\partial z}$$

(Equation G-3)

and Equations G-1 and G-2, the following equality is obtained:

$$K_1 \cot(\alpha_1) = K_2 \cot(\alpha_2)$$

(Equation G-4)

$$or \quad \frac{K_1}{K_2} = \frac{\tan(\alpha_1)}{\tan(\alpha_2)}$$

For mass to be conserved (at saturated conditions and for an incompressible fluid and aquifer), the change in water table height must equate with the total flux of water moving across the lower boundary, hence:

$$\delta(t_o) = \int_0^{t_o} \frac{v(t)}{S_y} dt + \delta(0)$$ **(Equation G-5)**

The above equation holds true as long as the phreatic surface does not move into a region of different S_y or K. To derive values of v(t), it is necessary to model the total head function for the two regions. Using trigonometric principles:

$$H(-l_1,t) = H(-L,t) - l_2 \cot(\alpha_2)$$ **(Equation G-6)**

$$H(-l_1,t) = \delta(t) + \left(l_1 + \delta(t)\right)\cot(\alpha_1)$$ **(Equation G-7)**

By letting

$$H(-L,t) = A\sin(\omega t)$$ **(Equation G-8)**

Equations G-6 and G-7 give:

$$H(-L,t) - l_2\cot(\alpha_2) = \delta(t) + \left(l_1 + \delta(t)\right)\cot(\alpha_1)$$

$$\Leftrightarrow \quad \frac{H(-L,t)}{\cot(\alpha_1)} - l_2\frac{\cot(\alpha_2)}{\cot(\alpha_1)} = \frac{\delta(t)}{\cot(\alpha_1)} + \left(l_1 + \delta(t)\right)$$

$$\Leftrightarrow \quad H(-L,t)\tan(\alpha_1) - l_2\frac{\tan(\alpha_1)}{\tan(\alpha_2)} = \delta(t)\tan(\alpha_1) + l_1 + \delta(t)$$

$$\Rightarrow \quad H(-L,t)\tan(\alpha_1) - l_2\frac{K_1}{K_2} = \delta(t)\tan(\alpha_1) + l_1 + \delta(t)$$ **(Equation G-9)**

$$\Leftrightarrow \quad \left\{H(-L,t) - \delta(t)\right\}\tan(\alpha_1) = l_1 + \delta(t) + l_2\frac{K_1}{K_2}$$

$$\therefore \quad \tan(\alpha_1) = \frac{l_1 + \delta(t) + l_2\dfrac{K_1}{K_2}}{H(-L,t) - \delta(t)}$$

Thus Darcy's law and Equations G-1, G-8, and G-9 combine to give the following:

$$v(t) = K_1 \left[\frac{A\sin(\omega t) - \delta(t)}{l_1 + \delta(t) + l_2 \dfrac{K_1}{K_2}} \right]$$

(Equation G-10)

If the solution to $\delta\{t\}$ is again assumed to be a simple sine function of the form described by Equation 9-22, then the above equation becomes,

$$v(t) = K_1 \left\{ \frac{A\sin(\omega t) - \delta(t)}{l_1 + l_2 \dfrac{K_1}{K_2} + \delta(t)} \right\}$$

(Equation G-11)

$$\Rightarrow S_y\, \omega\, B\cos(\omega\{t - \gamma\}) = K_1 \left\{ \frac{A\sin(\omega t) - \delta(t)}{l_1 + l_2 \dfrac{K_1}{K_2} + \delta(t)} \right\}$$

By considering the above equation with the simple case of $t = \gamma$ (ie, $\delta\{t\} = 0$) a formula for γ is obtained after some rearranging. By using such an expression for γ with Equations 9-29 and 9-22, the following analytic formula is obtained for the two-layered aquifer problem:

$$\delta(t) = A\cos\left\{ \tan^{-1}\left(\frac{S_{y1}\left[l_1 + l_2\,{K_1}/{K_2} \right]\omega}{K_1} \right) \right\}\sin\left\{ \omega t - \tan^{-1}\left(\frac{S_{y1}\left[l_1 + l_2\,{K_1}/{K_2} \right]\omega}{K_1} \right) \right\}$$

$$= A\cos\left\{ \tan^{-1}\left(S_{y1}\left[\frac{l_1}{K_1} + \frac{l_2}{K_2} \right]\omega \right) \right\}\sin\left\{ \omega t - \tan^{-1}\left(S_{y1}\left[\frac{l_1}{K_1} + \frac{l_2}{K_2} \right]\omega \right) \right\}$$

$$= A\cos\left\{ \tan^{-1}\left(S_{y1}\,\omega\frac{l_1 + l_2}{K_{1+2}} \right) \right\}\sin\left\{ \omega t - \tan^{-1}\left(S_{y1}\,\omega\frac{l_1 + l_2}{K_{1+2}} \right) \right\}$$

(Equation G-12)

The above results is the same as that which is obtained in Chapter 9 by computing the harmonic mean of K (refer Section 9.3.2).

APPENDIX G2 Example Problem 1.

Initial Conditions:	$H(z,0) = 0$
Dimensions:	$L = 12$ m
Boundary Condition:	$H(-L,t) = A \sin(\omega t)$
	$\omega = \pi/21600$ rad s^{-1}
	$A = 0.5$ m
Parameters:	$K = 18$ m day^{-1} (2.0833x10-4 m s^{-1})
	$S_y = 0.3$

APPENDIX G3 Example Problem 2.

Initial Conditions:	$H(z,0) = 0$
Dimensions:	$L = 12$ m
	$l1 = 5$ m
	$l2 = 7$ m
Boundary Condition:	$H(-L,t) = A \sin(\omega t)$
	$\omega = \pi/21600$ rad s^{-1}
	$A = 0.5$ m
Parameters:	$K1 = 18$ m day^{-1} (2.0833x10-4 m s^{-1})
	$K2 = 6$ m day^{-1} (6.9444x10-5 m s^{-1})
	$S_{y1} = 0.3$
	$S_{y2} = 0.3$
Time Step Size:	$\Delta t = 600$ s

APPENDIX G4 Tidal-Efficiency and Tidal-Lag Profiles

Step 1. Firstly, use the analytic or the finite difference VTUGF model to determine the tidal efficiency and the lag of the water table given values for S_y, K, L, and ω.

Step 2. Arbitrarily chose a value for lag (ie, γ') which will occur at some depth (z) between the lower boundary and MSL:

$$0 < \gamma' < \gamma \{water\ table\} \quad : \quad -L < z < 0 \qquad \textbf{(Equation G-13)}$$

Step 3. Compute the tidal efficiency (η') which corresponds to a lag of γ':

$$\eta' = \frac{\eta}{\cos[\omega(\gamma - \gamma')]} \qquad \textbf{(Equation G-14)}$$

Step 4. Compute the time, t', at which the tidal signal is peaking, given a lag of γ' and an efficiency of η':

$$t' = \gamma' + \frac{\pi}{2\omega}$$

(Equation G-15)

Step 5. Compute the depth, z, at which the tidal signal is occurring, for given t', γ', and η'.

$$z = L \frac{\eta' - \eta \sin(\omega t' - \omega\gamma)}{\sin(\omega t') - \eta \sin(\omega t' - \omega\gamma)}$$

(Equation G-16)

Table G-1. A summary of the piezometric field data obtained at Heron Island during this study.

Well No.	Piezo. No.	Piezo. Position z (m MSL)	Notes	Sample Period 1994 (Julian days)	Mean Water Level (m MSL)	Max. Water Level (m MSL)	Min. Water Level (m MSL)	Avg. Efficiency η (%)	Avg. Lag γ (hours)
1	1	-4.98	t, b	146 -190	-0.12	0.89	-0.95	55.6	0.79
1	3	-1.18	t, b	146 -190	-0.12	0.66	-0.86	46.4	1.65
3	1	-5.00	t	112-139	0.01	0.67	-0.61	35.3	1.87
3	2	-1.83	t, b	112-139	0.01	0.69	-0.65	36.0	2.18
3	3	-0.03	w,b	112-139	0.03	0.66	-0.47	33.0	2.27
6	1	-13.09	t	83-111	-0.04	1.32	-1.21	78.8	0.11
6	2	-9.14	t, b	83-111	0.07	1.08	-0.49	41.9	0.69
6	3*	-5.34	t, b	83-111	0.18	1.17	-0.21	-	-
6	4	-2.19	w,b	83-111	0.20	0.95	-0.21	24.8	2.46
8	1	-9.22	t	82-111	-0.10	1.09	-1.10	67.4	0.20
8	2	-5.75	t, b	82-111	-0.09	0.51	-0.60	34.1	1.21
8	3	-2.27	w, t, b	82-111	-0.13	0.31	-0.58	27.0	2.38
10	1	-8.82	t	146-182	0.27	1.70	-0.61	58.3	0.60
10	2	-6.06	t, b	146-182	0.24	1.12	-0.48	45.5	1.41
10	3	-2.85	t, b	146-182	0.22	0.98	-0.45	40.3	1.94
11	1	-5.28	t,b	146-190	0.17	1.50	-0.61	62.1	0.99
11	2	-1.83	w,b	146-190	0.18	1.61	-0.63	64.4	1.19
12	1	-7.73	t	112-139	0.04	1.41	-1.01	69.7	0.33
12	2	-3.47	w,b	112-139	0.09	1.20	-0.66	48.3	1.75
13	1	-8.82	t	112-139	0.21	1.72	-0.98	78.8	0.08
13	2	-6.64	t, b	112-139	0.24	0.86	-0.23	28.9	1.48
13	3	-4.44	w, b	112-139	0.23	0.82	-0.29	27.9	2.13

Notes:
(a)   * = due to electronic malfunction with the equipment, this data was rejected.
(b)   t = top clay layer capping was installed above this piezometer.
(c)   b = bottom clay layer capping was installed below this piezometer.
(d)   w = water-table piezometer.
(e)   LWD = MSL + 1.61 m
(f)   Piezo. levels were provided by Noordink et al. (1992)
(g)   Standard errors are provided in Table F-6.

Table G-2. Interpretation of aquifer vertical hydraulic conductivities at Heron Island: VTUGF model results are based on time-averaged efficiencies and sinusoidal pressure signals (refer Figure 9-15 and Table G-1).

Well No.	Regions Simulated[a]	VTUGF Model Type	Boundary Position[f] L (m MSL)	Calibration Level[b] z (m MSL)	Relative Efficiency[c] η (-)	Computed Vertical K (m d^{-1})	Computed Relative γ (m d^{-1})
1	single	(g).	-4.98	-1.18	0.835	26.9 ± 0.2	0.86
6	upper	(i)	-9.14	water-table	0.592	24.5 ± 0.2	2.54
6	combined	(j)	-13.09	water-table	0.315	15.8 ± 0.2	2.58
6	lower	(k)	-	-	-	8.70 ± 0.1	-
8	upper	(i)	-5.75	water-table	0.792	27.2 ± 0.2	2.51
8	combined	(j)	-9.22	water-table	0.401	14.7 ± 0.1	2.49
8	lower	(k)	-	-	-	8.34 ± 0.1	-
10	upper	(g)	-6.06	-2.85	0.886	36.3 ± 0.2	0.50
10	upper+lower	(h)	-8.82	-2.85	0.780 & 0.691	20.3 ± 0.2	0.53 & 1.03
12	single	(i)	-7.73	water-table	0.693	27.1 ± 0.2	1.92
13	upper	(i)	-6.64	water-table	0.965	89.6 ± 0.8	2.00
13	combined	(j)	-8.82	water-table	0.354	12.2 ± 0.1	2.47
13	lower	(k)	-	-	-	3.35 ± 0.03	-

Notes:
(a) Refer Figure 9-15.
(b) Level accuracy = ± 0.05 m (Noordink et al., 1992).
(c) Determined from the field data in Table G-1.
(d) Average tidal periodicity = 12.4 ± 0.1 hours.
(e) S_y = 0.3 (assumed).
(f) LWD = MSL + 1.61 m.
(g) Single-layered semi-analytic model is Equation 9-37.
(h) Two-layered semi-analytic model is Equation 9-43.
(i) Single-layered analytic model is Equations 9-34.
(j) Two-layered analytic model is Equation 9-41.
(k) K of lower region was determined from Equation 9-40.

Table G-3. A comparison of recorded and predicted groundwater piezometric levels: results of the finite-differenceVTUGF model (refer Equation 9-54 and Table G-1).

Well No. (#)	Piezo. No. (#)	Interpreted K (m d^{-1})	Slope a (-)	Intercept b (m MSL)	Correlation Coefficient (-)	Number of Samples[a] (-)
1	3	20.5	0.991	-0.008	0.997	6419
6	2	8.70 (lower)	1.011	0.105	0.981	4062
6	4	24.5 (upper)	0.981	0.240	0.898	4062
8	2	7.33 (lower)	1.010	0.010	0.997	4131
8	3	23.8 (upper)	0.988	-0.038	0.990	4131
10	2	16.3 (lower)	0.991	0.010	0.991	4000[b]
10	3	29.2 (upper)	0.986	-0.033	0.988	4000[b]
12	3	23.6	0.999	0.053	0.994	4680
13	2	2.97 (lower)	1.023	0.007	0.956	2000[b]
13	3	79.5 (upper)	1.002	0.012	0.986	2000[b]

Notes:
(a) Each sample represents a measurement taken at 10 minute intervals.
(b) The entire database was not analysed.

Table G-4. Five most significant diurnal and semi-diurnal harmonic components of the tide at Heron Reef

Tidal Component	Amplitude (m)	Periodicity (hours)	Lag (hours)
O1	0.130	25.81934	116.1
K1	0.2510	23.93447	159.3
N2	0.1820	12.65835	227.3
M2	0.8290	12.4206	252.1
S2	0.2890	12.000	258.6

Notes:
(a) Tidal data provided by QDT (1997).
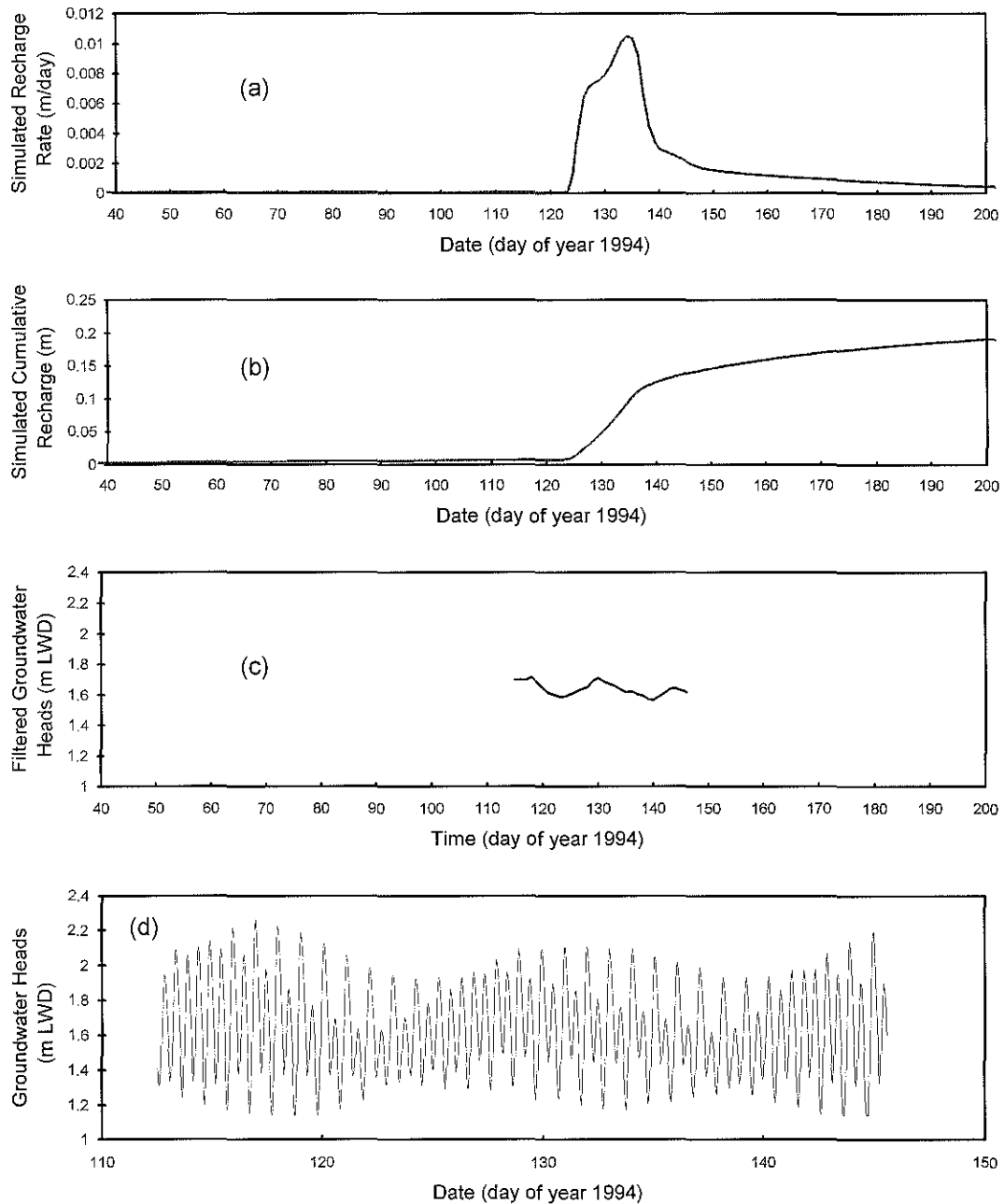
Figure G-1. Comparison of STEM simulated recharge with water-table levels recorded from Piezo. No. 3 at well #3: (a) simulated groundwater recharge rates; (b) simulated cumulative groundwater recharge; (c) 24-hour filtered water-table hydrograph; and (d) water-table hydrograph.

APPENDIX H

APPENDIX H

APPENDIX H1 SUTRA Input Data File For Example Problem 1: The Vertical Equilibrium Boundary Approach

```
SUTRA SOLUTE TRANSPORT   Example Problem 1 (VERT_7.D5) last change 9/2/95
>>>>  Delton Chen, Uo Q Chem. Eng. Heron Island Groundwater Project <<<<
>>> Vertical Column with Transient Head B.C. Below and Free Water Table <<<
      30   14    7    0    2    0    0    0    2 1200
       1    0    0    1    1
     0.00000          0.010          0.010
    1200          100        4.32D+5         144        1.0            600.0    1    1
       1    0    1    0    0    0    0    0
         100     1.0E+2       1000
     0.00D-9          6.6D-6       1025.0  0.000000 · 7.000D+2      1.0D-3
       1.0D-9                       2500.0
NONE
      0.0D-9      0.0D-9      0.0D-9      0.0D-9
         0.0       -9.81
NODE              1.0        1.0        1.0        0.30
       1    2    0.0      -12.0        1.0        1.0
       2    2    1.0      -12.0        1.0        1.0
       3    2    0.0      -0.50        1.0        1.0
       4    2    1.0      -0.50        1.0        1.0
       5    2    0.0      -0.40        1.0        1.0
       6    2    1.0      -0.40        1.0        1.0
       7    2    0.0      -0.30        1.0        1.0
       8    2    1.0      -0.30        1.0        1.0
       9    2    0.0      -0.20        1.0        1.0
      10    2    1.0      -0.20        1.0        1.0
      11    2    0.0      -0.10        1.0        1.0
      12    2    1.0      -0.10        1.0        1.0
      13    2    0.0        0.0        1.0        1.0
      14    2    1.0        0.0        1.0        1.0
      15    2    0.0        0.1        1.0        1.0
      16    2    1.0        0.1        1.0        1.0
      17    2    0.0        0.2        1.0        1.0
      18    2    1.0        0.2        1.0        1.0
      19    2    0.0        0.3        1.0        1.0
      20    2    1.0        0.3        1.0        1.0
      21    2    0.0        0.4        1.0        1.0
      22    2    1.0        0.4        1.0        1.0
      23    2    0.0        1.5        1.0        1.0
      24    2    1.0        1.5        1.0        1.0
      25    2    0.0        5.0        1.0        1.0
      26    2    1.0        5.0        1.0        1.0
      27    2    0.0       25.0        1.0        1.0
      28    2    1.0       25.0        1.0        1.0
      29    2    0.0       50.0        1.0        1.0
      30    2    1.0       50.0        1.0        1.0
ELEMENT   2.0719D-11 2.0719D-11      0.000       0.01       0.01       0.01       0.01
       1    2 1.00D+00  1.00D+00   1.00D+00 ,   1.000      1.000     1.0000     1.0000
       2    2 1.00D+00  1.00D+00   1.00D+00 ·   1.000      1.000     1.0000     1.0000
       3    2 1.00D+00  1.00D+00   1.00D+00     1.000      1.000     1.0000     1.0000
       4    2 1.00D+00  1.00D+00   1.00D+00     1.000      1.000     1.0000     1.0000
       5    2 1.00D+00  1.00D+00   1.00D+00     1.000      1.000     1.0000     1.0000
       6    2 1.00D+00  1.00D+00   1.00D+00     1.000      1.000     1.0000     1.0000
       7    2 1.00D+00  1.00D+00   1.00D+00     1.000      1.000     1.0000     1.0000
       8    2 1.00D+00  1.00D+00   1.00D+00     1.000      1.000     1.0000     1.0000
       9    2 1.00D+00  1.00D+00   1.00D+00     1.000      1.000     1.0000     1.0000
      10    2 1.00D+00  1.00D+00   1.00D+00     1.000      1.000     1.0000     1.0000
      11    2 1.00D+00  1.00D+05   1.00D+00     1.000      1.000     1.0000     1.0000
      12    2 1.00D+00  1.00D+05   1.00D+00     1.000      1.000     1.0000     1.0000
      13    2 1.00D+00  1.00D+05   1.00D+00     1.000      1.000     1.0000     1.0000
      14    2 1.00D+00  1.00D+05   1.00D+00     1.000      1.000     1.0000     1.0000
```

```
        -1
        -2

              6
          1    13
            1      1      2      4      3
            2      3      4      6      5
            3      5      6      8      7
            4      7      8     10      9
            5      9     10     12     11
            6     11     12     14     13
            7     13     14     16     15
            8     15     16     18     17
            9     17     18     20     19
           10     19     20     22     21
           11     21     22     24     23
           12     23     24     26     25
           13     25     26     28     27
           14     27     28     30     29
```

APPENDIX H2   FORTRAN Program That Creates The Finite-Element Mesh For The Reef-Cay Groundwater Model And Input Data For SUTRA.

```
        PROGRAM MAKEMESH
        IMPLICIT REAL (A-H,O-Z)
         DIMENSION XCOORD(30),YCOORD(25)
        .DIMENSION CONNECT(387,4),COORDS(436,2)
         REAL KH,KV
         INTEGER XNODES,YNODES,XELEM,YELEM,NNODE,CONNECT
         OPEN(UNIT=10,FILE='MAKE-7.D5')
         OPEN(UNIT=11,FILE='MESH-7.CSV')C
         DATA YCOORD/-150.0,-130.0,-110.0,-90.0,-70.0,-50.0,
     1   -30.0,-25.0,-20.0,-15.0,-13.1,-10.5,-9.14,
     2   -5.75,-2.0,-0.8,0.0,0.1,0.2,0.3,0.4,1.5,5.0,25.0,50.0/
         DATA XCOORD/30*0.0/
C
C=======EMBEDDED PARAMETERS
C
C.......DIMENSION CONNECT
         TNELEM=387
C
C=======REGION 1 (BELOW CAY)
C
         XLENGTH=150.0
         XNODES=11
         YNODES=25
         XELEM=XNODES-1
         YELEM=YNODES-1
C
C=======REGION 2 (BELOW REEF FLAT)
C
         XLENGTH2=420.0
         XNODES2=7
         YNODES2=16
         XELEM2=XNODES2
         YELEM2=YNODES2-1
C
C=======REGION 3 (BELOW CHANNEL)
C
         XLENGTH3=420.0
         XNODES3=7
         YNODES3=7
         XELEM3=XNODES3
         YELEM3=YNODES3-1
C
C=======CALCULATE X-COORDS
```

```
C
          DO 10 I=1,(XNODES+XNODES2+XNODES3)
          IF (I.LE.XNODES) XCOORD(I)=(I-1)*XLENGTH/XELEM
          IF (I.GT.XNODES.AND.I.LE.(XNODES+XNODES2)) THEN
          XCOORD(I)=XLENGTH+(I-XNODES)*XLENGTH2/XELEM2
          ENDIF
          IF (I.GT.(XNODES+XNODES2)) THEN
          XCOORD(I)=XLENGTH+XLENGTH2+(I-XNODES-XNODES2)*XLENGTH3/XELEM3
          ENDIF
10        CONTINUE
C
C===================OUTPUT NODES X Y COORDS THICK POROSITY
C
C.......REGION 1
C
          NNODE=0
          DO 25 I=1,XNODES
          DO 20 J=1,YNODES
          NNODE=NNODE+1
        thick=1.0
          COORDS(NNODE,1)=XCOORD(I)
          COORDS(NNODE,2)=YCOORD(J)
          WRITE (10,15) NNODE,2,XCOORD(I),YCOORD(J),THICK,1.0
15        FORMAT(I5,I5,4(1X,1E9.3))
20        CONTINUE
25        CONTINUE
C
C.......REGION 2
C
          DO 28 I=(XNODES+1),(XNODES+XNODES2)
          DO 27 J=1,YNODES2
          NNODE=NNODE+1
          THICK=1.0
        COORDS(NNODE,1)=XCOORD(I)
          COORDS(NNODE,2)=YCOORD(J)
          WRITE (10,15) NNODE,2,XCOORD(I),YCOORD(J),THICK,1.0
27        CONTINUE
28        CONTINUE
C
C.......REGION 3
C
          DO 31 I=(XNODES+XNODES2+1),(XNODES+XNODES2+XNODES3)
          DO 30 J=1,YNODES3
          NNODE=NNODE+1
          THICK=1.0
          COORDS(NNODE,1)=XCOORD(I)
          COORDS(NNODE,2)=YCOORD(J)
          WRITE (10,15) NNODE,2,XCOORD(I),YCOORD(J),THICK,1.0
30        CONTINUE
31        CONTINUE
C
C
C===================OUTPUT ELEMENT KH KV ANGLE DISPERSIVITIES
C
C.......REGION 1 (K related to the level of the element bottom node)
C
          NELEM=0
          DO 36 J=1,XELEM
          DO 34 I=1,YELEM
          NELEM=NELEM+1
          IF (YCOORD(I).LE.50.0) KH=1.0000
          IF (YCOORD(I).LE.50.0) KV=1.0E+05
          IF (YCOORD(I).LE.0.3) KH=27.8
          IF (YCOORD(I).LE.0.3) KV=27.8
          IF (YCOORD(I).LE.-8.0) KH=8.56
          IF (YCOORD(I).LE.-8.0) KV=8.56
          IF (YCOORD(I).LE.-12.6) KH=3000.0
          IF (YCOORD(I).LE.-12.6) KV=1000.0
          WRITE(10,33) NELEM,2.0,KH,KV,1.0,1.0,1.0,1.0,1.0
33        FORMAT(I5,I5,7(1X,1E9.3))
34        CONTINUE
36        CONTINUE
```

```
C
C.......REGION 2
C
        DO 38 J=(XELEM+1),(XELEM+XELEM2)
        DO 37 I=1,YELEM2
        NELEM=NELEM+1
        IF (YCOORD(I).LE.-0.8) KH=27.8
        IF (YCOORD(I).LE.-0.8) KV=27.8
        IF (YCOORD(I).LE.-8.0) KH=8.56
        IF (YCOORD(I).LE.-8.0) KV=8.56
        IF (YCOORD(I).LE.-12.6) KH=8000.0
        IF (YCOORD(I).LE.-12.6) KV=1000.0
        WRITE(10,33) NELEM,2.0,KH,KV,1.0,1.0,1.0,1.0,1.0
37      CONTINUE
38      CONTINUE
C
C.......REGION 3
C
        DO 43 J=(XELEM+XELEM2+1),(XELEM+XELEM2+XELEM3)
        DO 42 I=1,YELEM3
        NELEM=NELEM+1
        IF (YCOORD(I).LE.-30.0) KH=8000.0
        IF (YCOORD(I).LE.-30.0) KV=1000.0
        WRITE(10,33) NELEM,2.0,KH,KV,1.0,1.0,1.0,1.0,1.0
42      CONTINUE
43      CONTINUE
C
C================OUTPUT ELEMENT CONNECTIVITY DATA
C
C.......REGION 1
C
        NELEM=0
        DO 50 J=1,XELEM
        DO 45 I=1,YELEM
        NELEM=NELEM+1
        N1=(J-1)*YNODES+I
        N4=(J-1)*YNODES+I+1
        N2=J*YNODES+I
        N3=J*YNODES+I+1
        CONNECT(NELEM,1)=N1
        CONNECT(NELEM,2)=N2
        CONNECT(NELEM,3)=N3
        CONNECT(NELEM,4)=N4
        WRITE(10,60)NELEM,N1,N2,N3,N4
45      CONTINUE
50      CONTINUE
60      FORMAT(I6,I6,I6,I6,I6)
        M1=N1
        M2=N2
        M3=N3
        M4=N4
C
C.......REGION 2
C
        DO 80 J=1,XELEM2
        DO 70 I=1,YELEM2
        NELEM=NELEM+1
        N1=(J-1)*YNODES2+I+1+M1
        N4=(J-1)*YNODES2+I+1+M4
        N2=(J-1)*YNODES2+I+1+M2
        N3=(J-1)*YNODES2+I+1+M3
        IF (J.GT.1) N1=N1+(YNODES-YNODES2)
      IF (J.GT.1) N4=N4+(YNODES-YNODES2)
        CONNECT(NELEM,1)=N1
        CONNECT(NELEM,2)=N2
        CONNECT(NELEM,3)=N3
        CONNECT(NELEM,4)=N4
        WRITE(10,60)NELEM,N1,N2,N3,N4
70      CONTINUE
80      CONTINUE
        M1=N1
        M2=N2
```

```
        M3=N3
        M4=N4
C
C.......REGION 3
C
        DO 100 J=1,XELEM3
        DO 90 I=1,YELEM3
        NELEM=NELEM+1
        N1=(J-1)*YNODES3+I+1+M1
        N4=(J-1)*YNODES3+I+1+M4
        N2=(J-1)*YNODES3+I+1+M2
        N3=(J-1)*YNODES3+I+1+M3
        IF (J.GT.1) N1=N1+(YNODES2-YNODES3)
        IF (J.GT.1) N4=N4+(YNODES2-YNODES3)
        CONNECT(NELEM,1)=N1
        CONNECT(NELEM,2)=N2
        CONNECT(NELEM,3)=N3
        CONNECT(NELEM,4)=N4
        WRITE(10,60)NELEM,N1,N2,N3,N4
90      CONTINUE
100      CONTINUE
C
C.......PRODUCE AN OUTPUT FILE FOR MESH PLOTTING IN EXCELL
C
        DO 110 I=1,TNELEM
        DO 105 J=1,4
        X=COORDS(CONNECT(I,J),1)
        Y=COORDS(CONNECT(I,J),2)
        WRITE(11,120) I,X,Y
105      CONTINUE
        X=COORDS(CONNECT(I,1),1)
        Y=COORDS(CONNECT(I,1),2)
        WRITE(11,120) I,X,Y
        WRITE(11,*)
110     CONTINUE
120     FORMAT (I4,',',E10.3,',',E10.3)
C
        END
```

Table H-1. Details of the SUTRA finite-element mesh used to solve Example Problem 1.

Element Number	Element Upper Level z (m MSL)	Element Lower Level z (m MSL)	Hydraulic Conductivity K_v (m day^{-1})	Specific Yield S_y (-)
14	50	25	1.8×10^6	0.3
13	25	5	1.8×10^6	0.3
12	5	1.5	1.8×10^6	0.3
11	1.5	0.4	1.8×10^6	0.3
10	0.4	0.3	18	0.3
9	0.3	0.2	18	0.3
8	0.2	0.1	18	0.3
7	0.1	0	18	0.3
6	0	-0.1	18	0.3
5	-0.1	-0.2	18	0.3
4	-0.2	-0.3	18	0.3
3	-0.3	-0.4	18	0.3
2	-0.4	-0.5	18	0.3
1	-0.5	-12	18	0.3

Notes:
(a) Example Problems 1 and 2 are described in Appendix G.2 and G.3.

Table H-2. The tidal reef-cay groundwater flow model: the results of a SUTRA sensitivity analysis.

Model Name	Parameter Tested	Value	Tidal Efficiency at Centre η (-)	Tidal Lag at Centre γ (hours)
REEF-CAY-0	(Base Case)		0.264	2.48
REEF-CAY-1	K_{HV1}	19.7 m d^{-1}	0.210	2.48
REEF-CAY-1	K_{HH1}	19.7 m d^{-1}	.	.
REEF-CAY-1	K_{HV2}	6.04 m d^{-1}	.	.
REEF-CAY-1	K_{HH2}	6.04 m d^{-1}	.	.
REEF-CAY-2	K_{HV1}	55.6 m d^{-1}	0.421	2.17
REEF-CAY-2	K_{HH1}	55.6 m d^{-1}	.	.
REEF-CAY-2	K_{HV2}	17.1 m d^{-1}	.	.
REEF-CAY-2	K_{HH2}	17.1 m d^{-1}	.	.
REEF-CAY-3	K_{HV1}	27 m d^{-1}	0.264	2.48
REEF-CAY-3	K_{HH1}	54 m d^{-1}	.	.
REEF-CAY-3	K_{HV2}	8.3 m d^{-1}	.	.
REEF-CAY-3	K_{HH2}	16.6 m d^{-1}	.	.
REEF-CAY-4	K_{PH}	1000 m d^{-1}	0.200	2.64
REEF-CAY-5	K_{PH}	5000 m d^{-1}	0.287	2.33
REEF-CAY-6	K_{PV}	500 m d^{-1}	0.253	2.48
REEF-CAY-7	K_{PV}	1500 m d^{-1}	0.269	2.48

Notes:
(a) For other parameter values, see Table H-2.

Table H-3. Tidal boundary conditions for Heron Reef: mean low-tides, average water levels, mean high-tides, and periodicities based upon 30 days of synthetic tidal data.

Tidal Boundary Condition	30 Day Average Low-Tide (m MSL)	30 Day Average Level (m MSL)	30 Day Average High-Tide (m MSL)	30 Day Average Periodicity (h cycle^{-1})	Hydraulic Conduct. K (m d^{-1})	Beach Slope β (degrees)	Porosity n (m^3 m^{-3})
Ocean [a]	-0.864	0.000	0.870	12.41	-	-	-
Reef Flat[b]	-0.683	0.049	0.870	12.41	-	-	-
Beach[c]	-0.160	0.402	0.870	12.41	170	5	0.45
Beach	0.173	0.556	0.870	12.41	100	5	0.45
Beach	-0.073	0.443	0.870	12.41	150	5	0.45
Beach	-0.240	0.367	0.870	12.41	190	5	0.45
Beach	-0.411	0.286	0.870	12.41	240	5	0.45
Beach	0.364	0.875	0.870	12.41	170	2	0.45
Beach	0.126	0.534	0.870	12.41	170	4	0.45
Beach	-0.424	0.279	0.870	12.41	170	6	0.45
Beach	-0.663	0.092	0.870	12.41	170	8	0.45
Beach	-0.245	0.364	0.870	12.41	170	5	0.40
Beach	-0.175	0.396	0.870	12.41	170	5	0.44
Beach	-0.144	0.410	0.870	12.41	170	5	0.46
Beach	-0.086	0.437	0.870	12.41	170	5	0.50

Notes:
(a) determined from Equation 10-1 using a 9 minute time step and 58 tidal cycles
(b) determined Equation 10-4 and (a) using a 9 minute time step and 58 tidal cycles
(c) determined Equations 10-5, 10-6 and 10-7, and (b) using a 9 minute time step and 58 tidal cycles
(d) K, β and n are approximate ranges (refer main text).
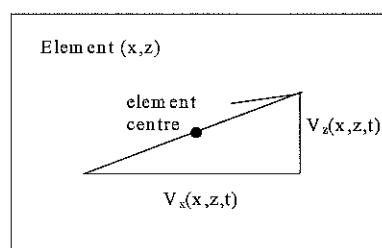
Figure H-1 Schematic of a typical groundwater velocity vector showing the magnitude and direction of groundwater flow at position (x, z) and time t.
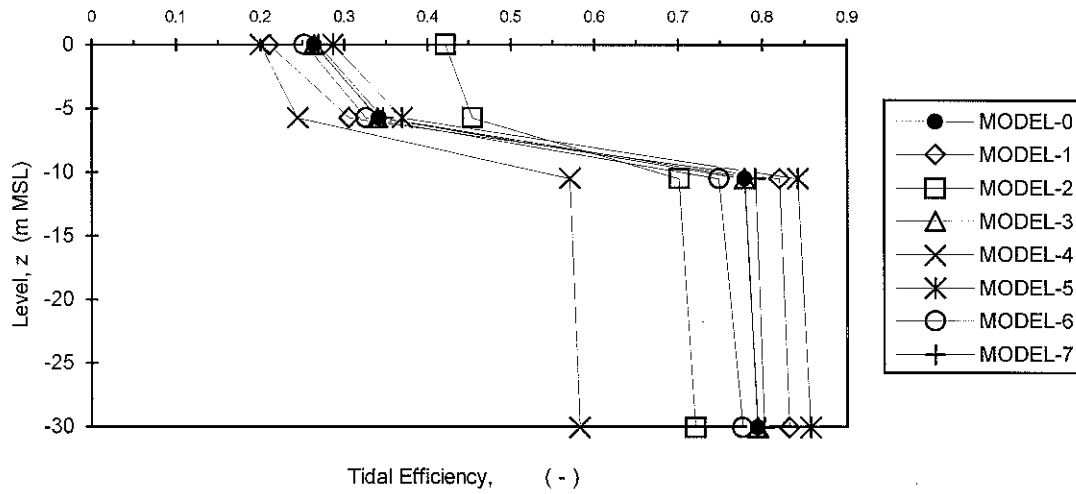
Figure H-2. Tidal efficiencies predicted by SUTRA for the centre of the tidal reef-cay groundwater model at pseudo steady-state (refer Table H-3).
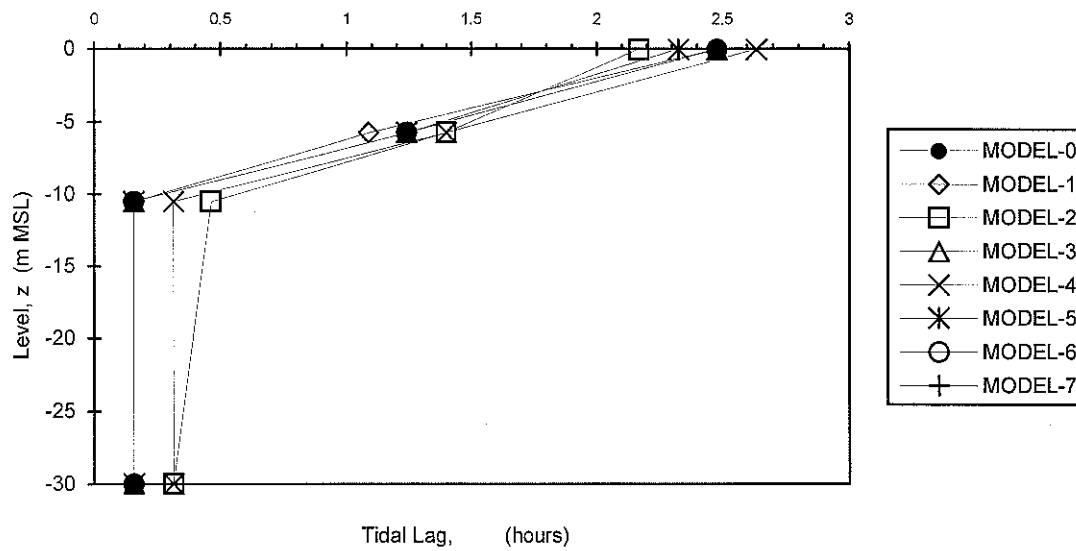
Figure H-3. Tidal lags predicted by SUTRA for the centre of the tidal reef-cay groundwater model at pseudo steady-state (refer Table H-3).

APPENDIX I

**Heron Island
Groundwater-Quality Database
(Adjunct to Thesis)**

APPENDIX I

Table I-1. Sampling dates for the Heron Island groundwater investigations.

Well No.	Piezo No.	Sample 1 Feb-92	Sample 2 Apr-92	Sample 3 Dec-92	Sample 4 Apr-93	Sample 5 Nov-93	Sample 6 Jan-94	Sample 7 Mar-94	Sample 8 Mar-95
1	1	5/02/92		16/12/92	14/4/93	23/11/93		22/03/94	16/03/95
1	2	5/02/92		16/12/92	14/4/93	23/11/93		22/03/94	16/03/95
1	3	5/02/92		16/12/92	14/4/93	23/11/93		22/03/94	16/03/95
2	1	5/02/92	21/4/92	16/12/92	7/04/89	23/11/93		22/03/94	15/03/95
2	2	5/02/92	21/4/92	16/12/92	7/04/89	23/11/93		22/03/94	15/03/95
2	3	5/02/92		16/12/92	7/04/89	23/11/93		22/03/94	15/03/95
3	1	6/02/92		17/12/92	17/4/93	27/11/93	31/01/94	20/03/94	16/03/95
3	2	6/02/92		17/12/92	17/4/93	27/11/93	31/01/94	20/03/94	16/03/95
3	3	6/02/92		17/12/92	17/4/93	27/11/93	31/01/94	20/03/94	16/03/95
4	1	6/02/92		17/12/92	16/4/93	26/11/93		21/03/94	15/03/95
4	2	6/02/92		17/12/92	16/4/93	26/11/93		21/03/94	15/03/95
4	3	6/02/92		17/12/92	16/4/93	26/11/93		21/03/94	15/03/95
4	4			17/12/92	16/4/93				
5	1	6/02/92		16/12/92	17/4/93	27/11/93		21/03/94	
5	2	6/02/92		16/12/92	17/4/93	27/11/93		21/03/94	
5	3	6/02/92		16/12/92	17/4/93	27/11/93		21/03/94	
5	4	6/02/92		16/12/92	17/4/93	27/11/93		21/03/94	
6	1	5/02/92		18/12/92	14/4/93	23/11/93		20/03/94	15/03/95
6	2	5/02/92		18/12/92	14/4/93	23/11/93		20/03/94	15/03/95
6	3	5/02/92		18/12/92	14/4/93	23/11/93		20/03/94	15/03/95
6	4	5/02/92		18/12/92	14/4/93	23/11/93		20/03/94	15/03/95
7	1	6/02/92	24/4/92	17/12/92	14/4/93	26/11/93	1/02/94	21/03/94	15/03/95
7	2	6/02/92		17/12/92	14/4/93	26/11/93	1/02/94	21/03/94	15/03/95
7	3	6/02/92		17/12/92	14/4/93	26/11/93	1/02/94	21/03/94	15/03/95
7	4	6/02/92	24/4/92	17/12/92	14/4/93	26/11/93	1/02/94	21/03/94	15/03/95
8	1	7/02/92		18/12/92	15/4/93	25/11/93		20/03/94	
8	2	7/02/92		18/12/92	15/4/93	25/11/93		20/03/94	
8	3	7/02/92		18/12/92	15/4/93	25/11/93		20/03/94	
8	4	7/02/92		18/12/92	15/4/93	25/11/93			
9	1	5/02/92	24/4/92	19/12/92	16/4/93	28/11/93		22/03/94	16/03/95
9	2	5/02/92		19/12/92	16/4/93	28/11/93		22/03/94	16/03/95
9	3	5/02/92	24/4/92	19/12/92	16/4/93	28/11/93		22/03/94	16/03/95
9	4	5/02/92		19/12/92	16/4/93				
10	1	5/02/92	24/4/92	19/12/92	15/4/93	25/11/93		20/03/94	16/03/95
10	2	5/02/92		19/12/92	15/4/93	25/11/93		20/03/94	16/03/95
10	3	5/02/92	24/4/92	19/12/92	15/4/93	25/11/93		20/03/94	16/03/95
10	4	5/02/92	24/4/92	19/12/92	15/4/93	25/11/93		20/03/94	
11	1	6/02/92		19/12/92	15/4/93	25/11/93		20/03/94	16/03/95
11	2	6/02/92		19/12/92	15/4/93	25/11/93		20/03/94	16/03/95
12	1	6/02/92	24/4/92	17/12/92	17/4/93	26/11/93	2/02/94	19/03/94	16/03/95
12	2	6/02/92	24/4/92	17/12/92	17/4/93	26/11/93	2/02/94	19/03/94	16/03/95
13	1	6/02/92	22/4/92	17/12/92	13/4/93	26/11/93	2/02/94	19/03/94	16/03/95
13	2	6/02/92	22/4/92	17/12/92	13/4/93	26/11/93	2/02/94	19/03/94	16/03/95
13	3	6/02/92	22/4/92	17/12/92	13/4/93	26/11/93	2/02/94	19/03/94	16/03/95

Notes: (a) February 1992 field data are from Noordink et al. (1992).

Table I-2. Heron Island groundwater temperatures (degrees C).

Well No.	Piezo No.	Sample 1 Feb-92	Sample 2 Apr-92	Sample 3 Dec-92	Sample 4 Apr-93	Sample 5 Nov-93	Sample 6 Jan-94	Sample 7 Mar-94	Sample 8 Mar-95
1	1	24.71		24.98	24.72	24.59		24.77	24.56
1	2	24.87		24.83	24.81	24.63		24.71	24.66
1	3	25.48		25.30	24.95	25.25		25.07	24.67
2	1	24.41	25.02	24.60	24.71	24.06		24.29	23.97
2	2	24.79	24.57	25.08	24.60	24.21		24.32	23.92
2	3	25.08		26.84	24.84	24.54		24.47	24.14
3	1	24.62		24.85	24.58	24.71	24.53	24.43	24.58
3	2	24.70		24.99	24.87	24.50	24.69	24.46	24.56
3	3	24.97		26.01		24.83	25.17	24.91	
4	1	25.75		26.24	25.75	25.91		26.46	
4	2	25.89		26.24	25.86	26.30		26.86	27.21
4	3	26.35		26.80	26.34	28.78		28.68	
4	4								
5	1	26.46		26.11	26.70	26.11		26.19	
5	2	26.71		26.21		26.25		26.17	
5	3	27.58		26.32	27.24	26.23		26.37	
5	4	30.84		27.19		26.57		27.43	
6	1	23.90		23.69	23.82	23.31		23.67	23.99
6	2	23.98		23.54		23.05		23.89	23.47
6	3	25.43		23.36		22.76		24.72	24.78
6	4	26.79		24.23	24.54	23.78		25.62	25.30
7	1	25.79	25.53	25.66	25.49	25.43	25.50	25.51	25.77
7	2	25.67		25.57	25.57	25.51	25.54	25.67	26.10
7	3	26.09		26.06	26.26	25.78	26.10	26.22	26.60
7	4	26.79	26.79	26.27	26.58	26.19	26.65	27.13	26.81
8	1	24.95		25.09	24.92	24.58		24.59	
8	2	26.15		25.00	24.63	24.56		24.66	
8	3	27.62		25.18	24.78	24.56		24.65	
8	4								
9	1	28.10	27.43	27.53	27.65	27.63		27.75	28.11
9	2	28.69		27.63	27.89	29.04		28.01	28.63
9	3	28.75	28.22	28.10	28.62	28.90		27.23	30.12
9	4								
10	1	24.68	24.66	24.67	24.69	24.45		24.56	24.58
10	2	24.71		24.82	24.67	24.48		24.65	24.67
10	3	24.70	25.03	24.84	24.70	24.30		24.97	24.59
10	4		25.54	24.73	25.24	24.17		26.15	
11	1	27.18		25.28	25.29	24.06		26.33	25.93
11	2	27.52		25.90	25.67	24.22		26.45	26.15
12	1	25.27	25.51	23.55	25.18	23.04	24.94	25.33	25.25
12	2	26.24	25.41	23.68	25.43	22.83	26.04	25.69	25.84
13	1	25.84	24.93	24.83	24.52	24.31	24.45	24.44	24.36
13	2	25.54	25.02	24.95	24.61	24.36	24.39	24.42	24.50
13	3	25.76	25.06	24.93	24.69	24.35	24.32	24.55	24.31

Notes:
(a) Refer Table I-1 for sampling dates.
(b) Refer Figure 1-2 for well locations.
(c) Refer Appendix F for piezometer levels.
(d) February 1992 field data are from Noordink et al. (1992).

Table I-3. Heron Island groundwater acidity (pH units).

Well No.	Piezo No.	Sample 1 Feb-92	Sample 2 Apr-92	Sample 3 Dec-92	Sample 4 Apr-93	Sample 5 Nov-93	Sample 6 Jan-94	Sample 7 Mar-94	Sample 8 Mar-95
1	1	7.06		7.56	7.38	7.26		7.13	7.36
1	2	7.13		7.49	7.36	7.26		7.13	7.35
1	3	7.07		7.52	7.34	7.28		7.18	7.31
2	1	7.15	7.23	7.52	7.46	7.27		7.21	7.47
2	2	7.15	7.30	7.49	7.42	7.30		7.16	7.47
2	3	7.15		7.46	7.53	7.26		7.14	7.44
3	1	7.18		7.48	7.45	7.36	7.34	7.24	7.34
3	2	7.20		7.53	7.44	7.35	7.36	7.25	7.33
3	3	7.20		7.45		7.37	7.36	7.15	
4	1	7.05		7.36	7.26	7.37		7.16	
4	2	7.03		7.26	7.13	6.97		7.16	7.45
4	3	7.03		7.39	7.18	6.99		7.15	
4	4								
5	1	7.00		7.32	7.34	7.16		7.03	
5	2	6.99		7.27		7.15		7.03	
5	3	6.99		7.34	7.27	7.14		7.04	
5	4	6.76		7.23		7.07		6.98	
6	1	7.21		7.66	7.62	7.53		7.53	7.72
6	2	7.26		7.63		7.62		7.55	7.73
6	3	7.27		7.61		7.62		7.57	7.76
6	4	7.48		7.65	7.70	7.70		7.63	7.81
7	1	7.08	6.92	7.42	7.20	7.13	7.23	7.23	7.41
7	2	7.08		7.42	7.33	7.14	7.23	7.25	7.41
7	3	7.06		7.49	7.30	7.14	7.25	7.24	7.44
7	4	7.01	6.87	7.37	7.39	7.13	7.22	7.23	7.40
8	1	7.10		7.31	7.27	7.25		7.16	
8	2	7.09		7.32	7.33	7.26		7.17	
8	3	7.06		7.39	7.33	7.27		7.18	
8	4								
9	1	6.68	6.58	7.09	6.85	6.74		6.79	6.85
9	2	6.72		7.03	6.84	6.77		6.80	6.86
9	3	6.73	6.63	7.14	7.11	6.78		6.83	6.85
9	4								
10	1	7.10	7.05	7.41	7.42	7.37		7.37	7.39
10	2	7.09		7.39	7.42	7.39		7.39	7.41
10	3	7.11	6.97	7.43	7.32	7.41		7.40	7.37
10	4		6.88	7.44	7.53	7.80		7.62	
11	1	7.50		7.80	7.63	7.62		7.51	7.66
11	2	7.50		7.87	7.78	7.71		7.64	7.74
12	1	7.36	7.29	7.54		7.34	7.47	7.17	7.45
12	2	7.38	7.30	7.57		7.38	7.48	7.19	7.49
13	1	7.24	7.26	7.45	7.43	7.24	7.43	7.04	7.35
13	2	7.20	7.23	7.46	7.45	7.26	7.46	7.06	7.37
13	3	7.10	7.21	7.45	7.45	7.26	7.47	6.95	7.37

Notes:
(a) Refer Table I-1 for sampling dates.
(b) Refer Figure 1-2 for well locations.
(c) Refer Appendix F for piezometer levels.
(d) February 1992 field data are from Noordink et al. (1992).

Table I-4. Heron Island groundwater redox potentials (mV)

Well No.	Piezo No.	Sample 1 Feb-92	Sample 2 Apr-92	Sample 3 Dec-92	Sample 4 Apr-93	Sample 5 Nov-93	Sample 6 Jan-94	Sample 7 Mar-94	Sample 8 Mar-95
1	1	455		221	413	436		419	464
1	2	414		222	410	440		414	467
1	3	401		220	411	443		411	470
2	1	395	382	223	447	447		426	603
2	2	392	400	220	443	438		418	603
2	3	390		222	446	433		414	599
3	1	405		428	433	419	397	432	532
3	2	376		427	426	416	390	422	535
3	3	362		428		412	386	417	
4	1	39		413	417	434		408	
4	2	35		410	393	415		399	485
4	3	110		406	377	398		388	
4	4								
5	1	10		417	504	408		399	
5	2	-19		411		396		391	
5	3	-30		412	473	395		385	
5	4	-104		411		391		380	
6	1	103		388	469	425		410	692
6	2	62		392		425		373	668
6	3	40		399		427		331	645
6	4	200		400	464	429		353	623
7	1	105	230	417	427	418	396	406	484
7	2	139		418	424	415	388	366	492
7	3	194		418	424	414	384	354	493
7	4	197	212	419	424	414	383	368	491
8	1	308		421	509	425		415	
8	2	303		425	500	424		407	
8	3	301		427	496	425		403	
8	4								
9	1	15	-7	-48	-45	-4		-39	-79
9	2	66		-2	-38	-18		-35	-69
9	3	218	367	-1 6.2	-50	-28		-36	-88
9	4								
10	1	206	376	425	459	432		398	477
10	2	133		430	466	421		396	475
10	3	165	393	432	466	419		395	475
10	4		319	435	460	401		376	
11	1	124		419	454	428		405	534
11	2	162		415	441	421		401	498
12	1	239	280	418	525	417	400	414	720
12	2	251	280	417	504	420	395	410	697
13	1	151	364	419	476	426	426	434	583
13	2	172	364	420	464	428	420	425	581
13	3	111	379	417	460	430	417	419	578

Notes:
(a) Refer Table I-1 for sampling dates.
(b) Refer Figure 1-2 for well locations.
(c) Refer Appendix F for piezometer levels.
(d) February 1992 field data are from Noordink et al. (1992).

Table I-5. Heron Island groundwater dissolved oxygen levels (mg/L).

Well No.	Piezo No.	Sample 1 Feb-92	Sample 2 Apr-92	Sample 3 Dec-92	Sample 4 Apr-93	Sample 5 Nov-93	Sample 6 Jan-94	Sample 7 Mar-94	Sample 8 Mar-95
1	1	5.50		6.02	5.91	5.31		5.34	6.06
1	2	5.06		5.72	5.91	5.32		5.19	6.03
1	3	4.49		5.38	6.50	5.46		5.05	5.98
2	1	4.38		6.23	6.53	5.27		4.63	5.45
2	2	4.28		5.71	6.24	5.51		4.77	5.25
2	3	4.54		6.15	7.30	5.79		5.57	5.71
3	1	4.78		5.23	5.55	5.19	5.14	5.16	5.63
3	2	4.05		5.91	5.47	5.05	5.46	5.16	6.13
3	3	6.59		7.01		6.62	6.56	6.08	
4	1	0.32		0.77	0.83	0.58		0.45	
4	2	0.29		0.78	0.79	0.43		0.36	1.28
4	3	0.33		2.00	1.33	0.71		0.67	
4	4								
5	1	0.37		0.41	1.41	0.75		0.50	
5	2	0.34		0.47		0.51		0.52	
5	3	0.30		0.49	1.05	0.63		0.49	
5	4	0.29		1.48		0.67		0.65	
6	1	1.83		3.89	3.66	4.02		4.08	4.98
6	2	0.48		2.75		4.68		4.49	4.68
6	3	0.63		5.22		5.77		5.44	5.91
6	4	3.31		5.66	5.80	6.00		5.44	6.24
7	1	1.53	1.87	3.08	3.38	3.06	3.00	2.66	3.97
7	2	1.19		3.01	3.46	3.00	3.31	2.79	3.69
7	3	0.91		3.59	3.74	2.61	3.25	2.81	3.58
7	4	1.08	1.30	3.27	4.65	2.25	2.94	2.40	0.73
8	1	2.94		4.99	4.93	4.93		4.85	
8	2	2.32		4.66	4.95	4.60		4.82	
8	3	3.71		5.73	5.39	5.11		5.31	
8	4								
9	1	1.30	0.36	1.17	0.62	0.83		0.42	0.74
9	2	1.90		4.55	0.92	0.31		0.41	0.76
9	3	1.46	0.60	5.10	1.43	0.44		0.45	0.53
9	4								
10	1	1.91	1.94	4.29	4.60	5.04		4.86	5.40
10	2	1.85		4.28	4.61	5.10		4.84	5.68
10	3	1.31	1.88	4.72	5.10	5.17		4.88	6.12
10	4			7.59	6.97	8.01		6.84	
11	1	5.32		6.94	6.61	6.87		6.23	6.66
11	2	5.92		7.17	6.93	6.97		6.32	6.87
12	1	5.12	5.20	5.74	5.71	5.92	6.08	5.67	5.96
12	2	5.20	5.20	5.80	5.88	5.76	6.18	5.72	5.98
13	1	4.15		5.54	5.07	5.38	5.36	4.85	5.50
13	2	3.17		4.97	4.62	4.70	4.81	4.65	5.51
13	3	2.53		4.72	4.56	4.71	4.68	5.27	5.03

Notes:
(a) Refer Table I-1 for sampling dates.
(b) Refer Figure 1-2 for well locations.
(c) Refer Appendix F for piezometer levels.
(d) February 1992 field data are from Noordink et al. (1992).

Table I-6. Heron Island groundwater salinities (ppt).

Well No.	Piezo No.	Sample 1 Feb-92	Sample 2 Apr-92	Sample 3 Dec-92	Sample 4 Apr-93	Sample 5 Nov-93	Sample 6 Jan-94	Sample 7 Mar-94	Sample 8 Mar-95
1	1	32.2		24.6	31.2	32		31.4	30.7
1	2	32.0		31.2	31.2	32		31.4	30.5
1	3	31.6		29.9	30.3	31		30.7	29.6
2	1	32.8	27.6	11.6	11.6	32.7		32.3	32.4
2	2	32.8	26.2	14.0	23.4	32.6		31.9	32.0
2	3	32.5		9.3	9.3	32		29.3	30.1
3	1	29.3		26.7	28.6	30	30.3	30.1	30.8
3	2	29.1		12.9	28.5	29.7	30	30	30.4
3	3	28.8		19.5		29.3	29.5	28.6	
4	1	24.6		21.1	24.1	23.5		20.8	
4	2	24.6		15.9	24.0	22.9		20.6	19.2
4	3	23.8		15.7	23.3	17		18.4	
4	4								
5	1	19.5		17.8	18.8	21.4		22.2	
5	2	19.5		17.1		21.2		22.1	
5	3	18.9		17.0	18.5	20.9		22	
5	4	12.6		15.0		20.4		20.3	
6	1	35.9		22.7	35.9	36.6		34.1	35.6
6	2	36.0		33.2		36.3		35.3	35.7
6	3	36.0		26.2		36.8		35.2	35.2
6	4	35.9		31.3	35.5	36.2		34.9	34.9
7	1	18.1	27.0	26.2	27.3	27.5	27.4	27.3	26.5
7	2	26.7		26.0	27.1	27.4	28	27.3	26.3
7	3	28.0		10.2	26.9	26.8	27.4	26.9	25.7
7	4	27.3	25.3	24.0	26.0	25.5	26.6	25.5	20.1
8	1	27.1		15.2	26.1	26.8		26.8	
8	2	26.4		22.8	26.0	26.6		26.8	
8	3	26.1		23.7	25.7	26.6		26.6	
8	4								
9	1	28.5	27.9	21.7	27.5	28.1		28.2	27.9
9	2	28.1		22.6	26.9	27.9		28	27.8
9	3	25.9	24.8	9.5	25.9	27.7		27.8	27.6
9	4								
10	1	28.3	27.1	26.5	28.8	26.1		25.7	27.4
10	2	27.9		20.6	28.5	25.1		24.7	26.6
10	3	28.9	26.2	27.4	29.0	24.5		24.4	26.9
10	4		18.0	16.6	28.5	5.9		6.7	
11	1	36.2		32.7	35.7	35.5		34.5	34.4
11	2	36.1		31.9	36.0	35.8		35	34.5
12	1	34.8	32.4	32.2	33.1	34.2	34.8	34	33.2
12	2	34.9	32.4	29.6	33.5	34.2	34.8	34.1	33.2
13	1	20.3	29.5	24.2	32.2	32.2	33.1	32.2	32.2
13	2	21.5	29.0	29.4	31.5	31.9	32.9	31.7	31.5
13	3	21.2	27.9	28.4	31.4	31.9	33	31.5	31.4

Notes:
(a) Refer Table I-1 for sampling dates.
(b) Refer Figure 1-2 for well locations.
(c) Refer Appendix F for piezometer levels.
(d) February 1992 field data are from Noordink et al. (1992).

Table I-7. Heron Island groundwater orthophosphate concentrations (mg/L as P)

Well No.	Piezo No.	Sample 1 Feb-92	Sample 2 Apr-92	Sample 3 Dec-92	Sample 4 Apr-93	Sample 5 Nov-93	Sample 6 Jan-94	Sample 7 Mar-94	Sample 8 Mar-95
1	1	0.061		0.046	0.061	0.066		0.067	0.045
1	2			0.052	0.066	0.063		0.064	0.061
1	3	0.078		0.070	0.065	0.066		0.067	0.069
2	1	0.067		0.083	0.072	0.066		0.067	0.060
2	2			0.054	0.067	0.070		0.066	0.060
2	3	0.069		0.059	0.064	0.056		0.065	0.068
3	1	0.044		0.042	0.046	0.040	0.036	0.042	0.057
3	2			0.051	0.053	0.042	0.043	0.045	0.043
3	3	0.130		0.069		0.078	0.066	0.066	
4	1	0.078		0.072	0.064	0.066		0.067	0.054
4	2			0.089	0.070	0.067		0.064	0.071
4	3			0.062	0.083	0.069		1.200[d]	
4	4								
5	1	0.059		0.045		0.063		0.077	
5	2			0.051		0.067		0.074	
5	3	0.043		0.055		0.078		0.077	
5	4	0.180		0.082		0.210		0.120	
6	1	0.060		0.031	0.034	0.040		0.037	0.033
6	2	0.060		0.046		0.047		0.046	0.034
6	3			0.039		0.036		0.037	0.028
6	4	0.041		0.025	0.042	0.028		0.023	0.024
7	1	0.081		0.066	0.072	0.066	0.043	0.066	0.057
7	2			0.059	0.083	0.066	0.057	0.064	0.054
7	3			0.085	0.070	0.067	0.041	0.068	0.051
7	4	0.089		0.050	0.069	0.068	0.055	0.069	0.053
8	1	0.085		0.058	0.075	0.079		0.073	
8	2			0.083	0.090	0.088		0.063	
8	3	0.088		0.052	0.084	0.088		0.085	
8	4								
9	1	0.150		0.074	0.120	0.100		0.110	0.120
9	2			0.097	0.130	0.120		0.100	0.120
9	3	0.037		0.100	0.200	0.220		0.250	0.180
9	4								
10	1	0.073		0.063	0.078	0.064		0.057	0.061
10	2			0.059	0.090	0.074		0.066	0.086
10	3			0.200	0.230	0.150		0.120	0.180
10	4			0.440	0.640	0.240		0.190	
11	1	0.024		0.032	0.038	0.033		0.026	0.047
11	2	0.037		0.026	0.051	0.041		0.040	0.029
12	1	0.040		0.031		0.043	0.039	0.037	0.035
12	2	0.044		0.029		0.041	0.036	0.036	0.036
13	1	0.053		0.031	0.053	0.054	0.046	0.051	0.060
13	2			0.055	0.059	0.054	0.046	0.052	0.051
13	3	0.068		0.063	0.054	0.055	0.044	0.050	0.049

Notes:
(a) Refer Table I-1 for sampling dates.
(b) Refer Figure I-2 for well locations.
(c) Refer Appendix F for piezometer levels.
(d) Erroneous data.
(e) February 1992 field data are from Noordink et al. (1992).

Table I-8. Heron Island groundwater nitrous oxides concentrations (mg/L as N)

Well No.	Piezo No.	Sample 1 Feb-92	Sample 2 Apr-92	Sample 3 Dec-92	Sample 4 Apr-93	Sample 5 Nov-93	Sample 6 Jan-94	Sample 7 Mar-94	Sample 8 Mar-95
1	1	21.000		13.000	22.000	18.000		1.100	27.000
1	2			17.000	21.000	19.000		1.200	29.000
1	3	23.000		27.000	19.000	20.000		1.300	39.000
2	1	14.000		15.000	13.000	12.000		11.000	12.000
2	2			16.000	12.000	12.000		11.000	12.000
2	3	14.000		16.000	15.000	8.500		12.000	14.000
3	1	56.000		49.000	51.000	37.000	34.000	34.000	26.000
3	2			60.000	54.000	39.000	36.000	35.000	25.000
3	3	55.000		58.000		41.000	37.000	40.000	
4	1	55.000		50.000	47.000	31.000		30.000	27.000
4	2			48.000	46.000	32.000		30.000	26.000
4	3			36.000	45.000	23.000		29.000	
4	4								
5	1	12.000		13.000		19.000		24.000	
5	2			14.000		19.000		24.000	
5	3	3.700		20.000		18.000		26.000	
5	4	0.002		20.000		20.000		27.000	
6	1	0.130		0.340	0.170	2.200		0.180	0.210
6	2	0.051		0.220		0.160		0.190	0.210
6	3			0.160		0.180		0.190	0.230
6	4	0.260		0.200	0.200	0.170		0.180	0.220
7	1	33.000		26.000	28.000	18.000	17.000	17.000	29.000
7	2			20.000	25.000	19.000	17.000	18.000	18.000
7	3			31.000	27.000	18.000	17.000	19.000	18.000
7	4	33.000		27.000	27.000	17.000	16.000	20.000	20.000
8	1	57.000		41.000	56.000	45.000		46.000	
8	2			58.000	55.000	49.000		48.000	
8	3	61.000		34.000	57.000	49.000		50.000	
8	4								
9	1	0.002		0.011	0.018	0.006		0.004	0.019
9	2			0.015	0.005	0.014		0.026	0.005
9	3	5.300		0.002	0.027	0.011		<0.002	0.007
9	4								
10	1	22.000		25.000	24.000	16.000		17.000	16.000
10	2			23.000	26.000	17.000		14.000	16.000
10	3			23.000	25.000	15.000		15.000	19.000
10	4			21.000	20.000	5.500		5.700	
11	1	1.100		0.760	1.800	1.900		2.500	3.400
11	2	2.500		0.520	1.900	0.720		0.790	2.200
12	1	11.000		17.000		8.600	6.700	6.200	5.300
12	2	9.500		16.000		8.900	5.900	5.600	4.900
13	1	26.000		21.000	24.000	18.000	17.000	18.000	17.000
13	2			29.000	25.000	19.000	16.000	19.000	18.000
13	3	22.000		27.000	25.000	19.000	15.000	20.000	22.000

Notes:
(a) Refer Table I-1 for sampling dates.
(b) Refer Figure I-2 for well locations.
(c) Refer Appendix F for piezometer levels.
(d) February 1992 field data are from Noordink et al. (1992).

Table I-9. Heron Island groundwater ammonia concentrations (mg/L as N).

Well No.	Piezo No.	Sample 1 Feb-92	Sample 2 Apr-92	Sample 3 Dec-92	Sample 4 Apr-93	Sample 5 Nov-93	Sample 6 Jan-94	Sample 7 Mar-94	Sample 8 Mar-95
1	1	0.008		0.012	0.011	0.069		0.012	0.045
1	2			0.013	0.015	0.027		0.013	0.019
1	3	0.005		0.017	0.012	0.037		0.013	0.013
2	1	0.006		0.023	0.010	0.025		0.011	0.006
2	2			0.012	0.006	0.021		0.012	0.009
2	3	0.004		0.008	0.008	0.023		0.012	0.011
3	1	0.009		0.016	0.008	0.021	0.012	0.015	0.025
3	2			0.011	0.008	0.052	0.012	0.012	0.006
3	3	0.032		0.030		0.028	0.013	0.012	
4	1	0.006		0.009	0.005	0.084		0.012	0.006
4	2			0.004	0.009	0.100		0.012	0.012
4	3			0.005	0.030	0.320		0.012	
5	1	9.700		0.170		0.022		0.014	
5	2			0.190		0.021		0.012	
5	3	10.000		0.240		0.019		0.011	
5	4	26.000		0.062		0.017		0.013	
6	1	0.036		0.018	0.010	0.019		0.012	0.010
6	2	0.038		0.007		0.019		0.012	0.012
6	3			0.012		0.019		0.012	0.014
6	4	0.020		0.016	0.022	0.022		0.012	0.012
7	1	0.006		0.009	0.015	0.023	0.014	0.012	0.024
7	2			0.007	0.008	0.021	0.013	0.027	0.009
7	3			0.013	0.010	0.023	0.014	0.013	0.014
7	4	0.005		0.011	0.012	0.018	0.012	0.012	0.014
8	1	0.004		0.016	0.006	0.020		0.013	
8	2			0.011	0.011	0.025		0.012	
8	3	0.002		0.009	0.008	0.019		0.013	
8	4								
9	1	0.390		0.180	0.510	0.260		0.370	0.450
9	2			0.150	0.430	0.250		0.370	0.440
9	3	0.013		0.260	0.670	0.300		0.430	0.400
9	4								
10	1	0.024		0.010	0.008	0.021		0.017	0.012
10	2			0.012	0.006	0.020		0.013	0.020
10	3			0.007	0.015	0.020		0.013	0.007
10	4			0.009	0.016	0.010		0.010	
11	1	0.004		0.007	0.024	0.020		0.012	0.013
11	2	0.005		0.008	0.011	0.019		0.011	0.009
12	1	0.003		0.007		0.020	0.012	0.012	0.007
12	2	0.003		0.008		0.018	0.012	0.011	0.007
13	1	0.002		0.007	0.011	0.018	0.012	0.011	0.018
13	2			0.006	0.015	0.021	0.012	0.012	0.026
13	3	0.074		0.008	0.011	0.022	0.015	0.011	0.013

Notes:
(a) Refer Table I-1 for sampling dates.
(b) Refer Figure 1-2 for well locations.
(c) Refer Appendix F for piezometer levels.
(d) February 1992 field data are from Noordink et al. (1992).

APPENDIX J

CD-ROM

APPENDIX J1 Summary of ASCII Data Files Provided on CD-ROM

Table J-1. Hydrometeorological field data: ASCII files provided on CD-ROM (see directory C:\APPENDIX\WEATHER).

Filename	File Size (kbytes)
1993_S5.TXT	12.782
1994_S5.TXT	13.467
APR94_S1.TXT	20.796
APR94_S2.TXT	41.390
AUG94_S1.TXT	19.21
AUG94_S2.TXT	43.75
DEC93_S1.TXT	21.558
DEC93_S2.TXT	16.983
DEC94_S2.TXT	43.558
FEB94_S1.TXT	18.279
FEB94_S2.TXT	37.278
JAN94_S1.TXT	19.400
JAN94_S2.TXT	42.335
JUL94_S1.TXT	20.327
JUL94_S2.TXT	48.913
JUN94_S1.TXT	20.527
JUN94_S2.TXT	41.452
MAR94_S1.TXT	22.723
MAR94_S2.TXT	41.618
MAY94_S1.TXT	21.021
MAY94_S2.TXT	42.267
NOV93_S1.TXT	20.332
NOV94_S2.TXT	42.126
OCT93_S1.TXT	1.926
OCT94_S1.TXT	21.077
OCT94_S2.TXT	44.945
SEP94_S1.TXT	18.284
SEP94_S2.TXT	42.295

Notes:
(a) 28 file(s) and 800,630 bytes total
(b) File descriptions are provided in Table B-5 of Appendix B.
(c) Refer Chapter 3.

Table J-2. Gladstone pan evaporation and Heron Island rainfall data: ASCII files provided on CD-ROM (see directory C:\APPENDIX\METEOR).

Filename	File Size (kbytes)	Description
LETTER.TXT	1.157	Receipt
PAN_60.TXT	17.412	Gladstone pan depths (mm) 1960-69
PAN_70.TXT	56.947	Gladstone pan depths (mm) 1960-69
PAN_80.TXT	53.039	Gladstone pan depths (mm) 1960-69
PAN_90.TXT	18.053	Gladstone pan depths (mm) 1960-69
RAIN_50.TXT	21.515	Heron Island rainfall 1950-59
RAIN_60.TXT	57.560	Gladstone pan depths (mm) 1960-69
RAIN_70.TXT	53.584	Heron Island rainfall 1970-79
RAIN_80.TXT	58.361	Heron Island rainfall 1980-89
RAIN_90.TXT	29.982	Heron Island rainfall 1990-97

Notes:
(a) 10 file(s) and 367,610 bytes total
(b) The data contained in these files were originally
provided by the Bureau of Meteorology, Brisbane, Australia,
and should not be used without their permission.
(c) Refer Chapter 3.

Table J-3. Piezometric water-levels recorded at Heron Island: ASCII files provided on CD-ROM (see directory C:\APPENDIX\PIEZO).

Filename	File Size (kbytes)	Description
WELL6.LWD	139.618	groundwater potentials well #6
WELL8.LWD	115.191	groundwater potentials well #8
WELL_1.LWD	144.208	groundwater potentials well #1
WELL_10.LWD	177.357	groundwater potentials well #10
WELL_11.LWD	144.379	groundwater potentials well #11
WELL_12.LWD	105.253	groundwater potentials well #12
WELL_13.LWD	127.427	groundwater potentials well #13
WELL_3.LWD	135.468	groundwater potentials well #3

Notes:
(a) 8 file(s) and 1,088,901 bytes total.
(b) Refer Chapter 8.
(c) Low Water Datum (LWD) = Mean Sea Level (MSL) + 1.607 m .
(d) Units are m (LWD).

Table J-4. Ocean tide recorded at the harbour jetty: ASCII files provided on CD-ROM (see directory C:\APPENDIX\TIDE).

Filename	File Size (kbytes)	Description
ALL94_TD.LWD	68.435	hourly Heron Reef tide 1994

Notes:
(a) 1 file(s) and 68,435 bytes total
(b) Refer Chapter 8.
(c) Low Water Datum (LWD) = Mean Sea Level (MSL) + 1.607 m .
(d) Units are m (MSL) and m (LWD).

Table J-5. Tidal lags and efficiencies recorded at Heron Island: ASCII files provided on CD-ROM (see directory C:\APPENDIX\EFF&LAG).

Filename	File Size (kbytes)	Description
WELL_1.LAG	10.323	Well #1
WELL_10.LAG	12.788	Well #10
WELL_11.LAG	10.382	Well #11
WELL_12.LAG	6.589	Well #12
WELL_13.LAG	8.289	Well #13
WELL_3.LAG	9.618	Well #3
WELL_6.LAG	9.837	Well #6
WELL_8.LAG	9.988	Well #8

Notes:
(a) 8 file(s) and 77,814 bytes total.
(b) Refer Chapter 8.
(c) Units and data types are listed in the files.